THE UNIVERSITY
of ADELAIDE

Tectonic geography of Mesoproterozoic Wilton package, north Australia

Bo Yang

Department of Earth Sciences

School of Physical Sciences

The University of Adelaide

July 2019

Table of Contents

Abstract

The Mesoproterozoic is an important but relatively poorly explored interval in Earth history. It is a complicated system with dynamic interactions among tectonic, biosphere, atmospheric composition and ocean chemistry. One of the best sedimentary archives for probing the Mesoproterozoic Earth's system is the Wilton package, greater McArthur Basin, north Australia. It covers the North Australia Craton in thousands kilometre-scale, forms temporal depositional records spanning over 600 million years, from ca. 0.9 Ga to 1.5 Ga. New constraints on this basin, therefore, contribute to a better understanding of the evolution of the Earth's system during this period. In this thesis, we apply a multiproxy isotopic provenance approach to provide new constraints on the age of deposition, basin provenance, spatial intra basin correlation, and further, the paleogeography and tectonic evolution of the Mesoproterozoic North Australia Craton.

Sedimentary rocks of the Wilton package were preserved in several geographically separated basins. The Roper Group of the Beetaloo Sub-basin, the depocentre of the Wilton package, is primarily focused. Data suggest that the Collara Subgroup (lower Roper Group) was sourced from southeast-southern sources. Whereas, the overlying Maiwok Subgroup (upper Roper Group) received more detritus from the eastern sources. This provenance change is interpreted to relate to exhumation of these eastern sources. They were uplifted as rift-shoulder highs, formed by contemporaneous extension between Proterozoic Australia and Laurentia, during the period of ca. 1.45 to 1.4 Ga. After that, progressively younger formations within the Maiwok Subgroup record another provenance shift to southern sources. This provenance change is interpreted to relate to closure of an ocean basin at ca. 1.35 to 1.32 Ga, which resulted in uplift of the southern margin of the North Australia Craton. The deposition of the Roper Group was punctuated by the intrusion of the ca. 1.31 Ga Derim Derim–Galiwinku LIP. The emplacement of Derim Derim–Galiwinku LIP progressively uplifted the basin from the north. Simultaneously, the increased weathering of Derim Derim–Galiwinku basaltic rocks increased nutrient (e.g. phosphorus) supply to the basin and presumably enhanced the primary production in the shallow marine settings, resulting in high organic carbon contents (TOC) that is seen in the top section of the Roper Group.

Provenance consistence between the South Nicholson Group and the Roper Group indicates correlations between the Beetaloo-McArthur and the South Nicholson basins. The successions within the Birrindudu Basin, however, exhibit little similarities to the Roper Group. The Bulita Group of the Birrindudu Basin received detritus from northeast and northern sources, whereas, the younger Tijuna Group records a swamping of the basin by detritus from southerly sources. The Bulita and Tijuna groups demonstrate a provenance change to southern source regions, which is consistent with that is seen in the upper Maiwok Subgroup. These consistent southward provenance changes are interpreted to be related to the same ocean closure event at ca. 1.35 to 1.32 Ga. Despite the provenance dissimilarities in spatial scale, the co-evolution of provenance correlated the Beetaloo and Birrindudu basins temporally. Whereas, the inconsistency of their detrital zircon compositions is interpreted to relate to underwater bathymetries that blocked transportation of sediment.

The supra-Wilton package successions is characterized by a series of unnamed sandstone and mudstone sedimentary units. These unnamed sedimentary units were deposited at least 300 million years after the deposition of the Wilton package, and are interpreted to be sourced from the Musgrave and the Arunta regions. Their significant provenance consistency with other early Neoproterozoic strata/groups indicates an extensive super basin with multiple depocentres.

Declaration

I certify that this work contains no material which has been accepted for the award of any other degree or diploma in my name, in any university or other tertiary institution and, to the best of my knowledge and belief, contains no material previously published or written by another person, except where due reference has been made in the text. In addition, I certify that no part of this work will, in the future, be used in a submission in my name, for any other degree or diploma in any university or other tertiary institution without the prior approval of the University of Adelaide and where applicable, any partner institution responsible for the joint-award of this degree.

I acknowledge that copyright of published works contained within this thesis resides with the copyright holder(s) of those works.

I also give permission for the digital version of my thesis to be made available on the web, via the University's digital research repository, the Library Search and also through web search engines, unless permission has been granted by the University to restrict access for a period of time.

I acknowledge the support I have received for my research through the provision of an Australian Government Research Training Program Scholarship.

Bo Yang

24/06/2019

Acknowledgements

I must first of all thank my supervisor Alan Collins for providing me the valuable opportunity to undertake this PhD project. It has been a wonderful journey and an incredible life experience that makes me a better geologist and also a better person. None of this would have been achievable without Alan's support, inspiration and motivation. I am also thankful for the enthusiastic and relax research atmosphere Alan has fostered in our group, giving us an enjoyable environment to exchange opinions and ideas.

I would like to thank my co-supervisors, Stijn Glorie and Juraj Farkas, for their insight, support and guidance, from sample preparation, to manuscript reviewing, and the final thesis composing. They always come up with constructive ideas and encourage me to think from different perspectives, which greatly improved the quality of this research.

I also gratefully acknowledge the laboratory staffs, Ben Wade, Aoife McFadden, Justin Payne, Sarah Gilbert, David Bruce and Tony Hall, for their immense technique assistance in acquiring and interpreting data. I would also like to thank Tim Munson, a respectful geologist from the Northern Territory Geological Survey, who contributed to this research with his extensive knowledge of Northern Territory and in-depth understanding of sedimentary geology.

Thank you Morgan, for being a lab demonstrator teaching me data collection, a co-author reviewing my manuscripts, a fieldworking mate in the NT and a wonderful friend throughout the last three and half years. Thank you my officemates, Romana, Sheree, Brandon, Pavan, Jarred, Georgie and Dongfang, for all the support and company that makes my entire PhD journey full of joys and memories. My thanks go to my "McArthur mates", Angus, Darwin, Todd, Billy, Nic and Max, for making all my NT field trips being wonderful.

Lastly, I would like to thank my mum and dad and my girlfriend Mengyu. Thank you for your love and encouragements. You are always being there when I need support. This work would have never been done without any of you.

Publications arising from this PhD research

Journal articles

Yang, B., Smith, T.M., Collins, A.S., Munson, T.J., Schoemaker, B., Nicholls, D., Cox, G., Farkaš, J., Glorie, S. (2018). Spatial and temporal detrital zircon U–Pb provenance of the hydrocarbon-bearing upper Roper Group, Beetaloo Sub-Basin, Northern Territory, Australia. *Precambrian Research*, **304**, 140-155.

Yang, B., Collins, A.S., Blades, M.L., Capogreco, N., Payne, J.L., Munson, T.J., Cox, G.M., Glorie, S., (2019). Middle-late Mesoproterozoic tectonic geography of the North Australia Craton: U–Pb and Hf isotopes of detrital zircons in the Beetaloo Sub-basin, Northern Territory, Australia. *Journal of the Geological Society, London*, **176**, 771-784. https://doi.org/10.1144/jgs2018-159.

Yang, B., Collins, A.S., Cox, G.M., Jarrett, A.J.M., Denyszyn, S., Blades, M.L., Farkaš, J., Glorie, S. *In prep*. Sedimentary geochemical record of the middle Mesoproterozoic—early Neoproterozoic tectonic geography of Northern Australia.

Yang, B., Collins, A.S., Munson, T.J., Payne, J.L., Blades, M.L., Glorie, S., Farkaš, J. *in prep*. Intra basin correlations and tectonic geography of the Mesoproterozoic North Australia Craton: detrital zircon U–Pb age and Hf isotope provenance analysis.

Conference abstracts

Yang, B., Smith, T.M., Collins, A.S., Munson, T.J. (2016). Spatial and temporal provenance analysis of the upper part of the Roper Group, Beetaloo Sub-basin, North Australia,13th International Conference on Gondwana to Asia, Kerala, India.

Yang, B., Collins, A.S., Munson, T.J., Smith, T.M. (2017). Spatial and temporal detrital zircon U-Pb provenance of the hydrocarbon-bearing upper Roper Group, Beetaloo Sub-basin, North Australia, Rodinia Conference, Townsville, Australia.

Yang, B., Collins, A.S., Cox, G.M., Munson, T.J., Smith, T.M. (2017). Multi-proxy provenance analysis of the upper Beetaloo Sub-basin, North Australia, Puzzling out Gondwana, Bangkok, Thailand.

Yang, B., Collins, A.S., Munson, T.J., Smith, T.M., Cox, G.M., Payne, J. (2018). Detrital Zircon Provenance Analysis of the Hydrocarbon-bearing Upper Roper Group, Beetaloo Subbasin, North Australia, European Geosciences Union General Assembly, Vienna, Austria.

Yang, B., Cox, G.M., Collins, A.S., Jarrett, A.J.M., Denyszen, S. (2018). Sedimentary provenance and tectonic palaeogeography of the upper Beetaloo Sub-basin, greater McArthur Basin, Australian Geoscience Council Convention, Adelaide, Australia.

Yang, B., Collins, A.S., Farkas, J., Payne, J. (2019). Intra basin correlations and tectonic geography of the Mesoproterozoic North Australia Craton, Gabfest 2019, Darwin, Australia.

Chapter 1

Introduction and thesis outline

Chapter 1

Introduction and thesis outline

1. Introduction

Sedimentary rocks of cratonic basins, which formed during hundreds of millions of years of subsidence (*Bradley, 2008; Allen & Armitage, 2012*), provide unique geological records of tectonic and biological history on our plant (*Ingersoll, 1988; Allen, 2008; Kuiper et al., 2008*). Evolving plate-tectonic processes, such as super-continental break-up, dispersal, plate subduction and amalgamation have an overall control on tectonic geography and thus on the basin's shape and architecture, modifying the local sedimentation and drainage system within the basin, and resulting in variable sediments build-up through time (*Allen 2008; Bradley 2008; Kuiper et al., 2008*). Deciphering these long lived Earth's sedimentary archives, therefore, is essential to probe the ancient tectonic geography framework and its evolution through Earth's history (*Allen & Armitage, 2012; Allen et al., 2015*).

The Mesoproterozoic was a time that saw the dynamic evolution of Earth's plate framework, from the purported break-up of the supercontinent Nuna (*Evans & Mitchell, 2011; Pisarevsky et al., 2014; Zhang et al., 2017; Kirscher et al., 2018*) to the amalgamating Rodinia (*Li et al., 2008; Merdith et al., 2017, 2019*). Paleomagnetic methods have been frequently used for the Mesoproterozoic geography reconstructions and paleocontinent reconfiguration (e.g. *Evans & Mitchell, 2011; Zhang et al., 2012; Pisarevsky et al., 2014; Kirscher et al., 2018*), however, such approaches are typically insufficient to for deeper understanding of local sedimentary basins histories.

One of the more studied and most accessible Mesoproterozoic cratonic basins in the southern hemisphere is the informally named "greater McArthur Basin" of northern Australia (*Close, 2014*). The greater McArthur Basin covers the North Australia Craton (NAC) in 1000-km scale, and spans nearly a billion years of Earth history; from ca. 1.82 Ga to 0.9 Ga (*Rawlings, 1999; Ahmad & Munson, 2013; Cox et al., 2016; Munson, 2016; Munson et al., 2018; Chapters 1 & 2*). In the latest paleomagnetic configuration (*Kirscher et al., 2018*), the NAC has been placed in mid to low latitudes at ca. 1.3 Ga, juxtaposing against Laurentia and the North China Craton (Figure 1; *Kirscher et al., 2018*), whilst the successions within the greater McArthur Basin has been interpreted as a main component of the recently proposed McArthur-Yanliao Gulf, or the Great McArthur Gulf, illustrated in Figure 1. Sedimentary successions of the greater McArthur Basin

thus recorded the detailed tectonic and sedimentation history of the Mesoproterozoic NAC (*Rawlings, 1999; Ahmad & Munson, 2013; Cox et al., 2016; Munson, 2016; Munson et al., 2018; Chapters 1 & 2*). New constraints on the Mesoproterozoic NAC therefore contribute to a better understanding of the Mesoproterozoic Earth's tectonic framework and earth system evolution during this important but relatively poorly explored interval in Earth history.

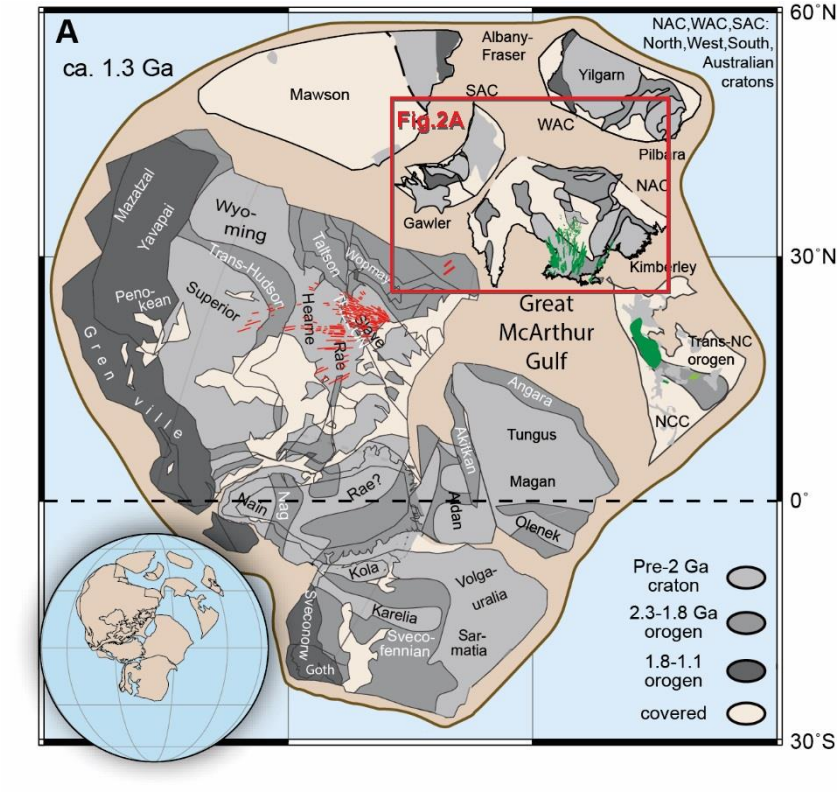

Figure 1 Paleogeography configuration at ca.1.3 Ga after *Kirscher et al. (2018).* Green lines are dykes and sills associated with the Derim Derim – Galiwinku and the Yanliao Large Igneous Province, dated at ca. 1.3 Ga. Red lines are the ca. 1.27 Ga Mackenzie dykes.

2. Geological background

The greater McArthur Basin is a regionally extensive depositional system that is presently surrounded by a series of exhumed NAC basement terrains (Figure 2; *Rawlings, 1999; Ahmad & Munson, 2013; Close, 2014*). The original extent of the basin is poorly constrained due to younger tectonic uplift and eroding of basin sequence. The northern boundary of the basin is currently uncertain and unconstrained due to the fact that it extends present-day coastline of Australia, and thus is overlain by waters of the Gulf of Carpentaria and Arafura Sea. The greater McArthur Basin unconformably overlies the Archaean to Palaeoproterozoic aged crystalline basements/orogens and contains several coherent lithostratigraphic components that has been sub-divided into five sedimentary packages, including the Redbank package, the Goyder package, the Glyde package, the Favenc package and the Wilton package (*Rawlings, 1999; Ahmad*

& Munson, 2013; Munson, 2016; Munson et al., 2018). The uppermost Mesoproterozoic Wilton package is the primary focus of this PhD research.

The Wilton package successions is characterized by a group of siliciclastic successions that exhibit significant subsurface continuity but might have been deposited in several geographically separated sub-basins, including the McArthur Basin and the Beetaloo Sub-basin (Roper Group), the Tomkinson Province (Renner Group), the Birrindudu Basin (Tijuna group), and potentially also the South Nicholson Basin (South Nicholson Group) (Figure 2; *Rawlings, 1999; Ahmad & Munson, 2013; Close, 2014; Munson, 2016; Munson et al., 2018*).

Sedimentary rocks of the Roper Group are largely exposed in the McArthur Basin but are buried in the Beetaloo Sub-basin which represent the main depocentre of this complex and presumably inter-connected Proterozoic depositional system (Figure 2; *Ahmad & Munson, 2013; Munson, 2016*).

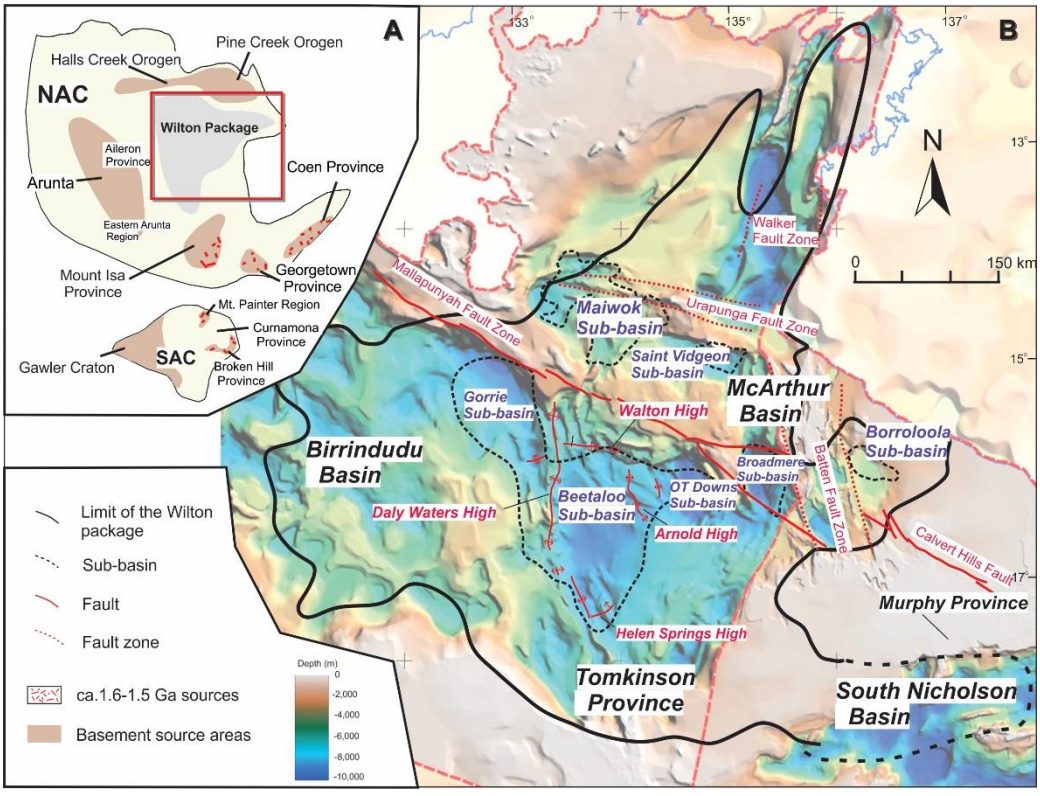

Figure 2 Extent of the Wilton Package (SEEBASE™ basement surface image after *Frogtech Geoscience (2018)*) modified after *Munson (2016)* and *Chapters 2 & 3*.

In terms of paleo-depositional environment, the Roper Group is interpreted to be deposited in a stable shelf coastal/marine settings and is sub-divided into two subgroups—the lower Collara Subgroup and the upper Maiwok Subgroup (Figure 3; *Rawlings, 1999; Abbott & Sweet, 2000; Ahmad & Munson, 2013*). As to age constraints of the deposition, two detrital zircon Sensitive

High Resolution Ion Microprobe (SHRIMP) U–Pb ages from lower formations yielded 1492 ± 29 Ma (2SD; *Jackson et al., 1999*) and 1492 ± 4 Ma (2SD; *Southgate et al., 2000*), which thus provide the maximum depositional age constraints of the Roper Group. Whereas the minimum depositional age is constrained by the Derim Derim Dolerite intrusions that intruded the Roper Group up to the top formations. A secondary ionization mass spectrometry (SIMS) U–Pb age of baddeleyite of the Derim Derim intrusion yielded 1324 ± 4 Ma, reported by *Abbott et al. (2001)* from the Urapunga Region; and a younger U–Pb age of baddeleyite from the northern Beetaloo Sub-basin, acquired by an isotope dilution thermal ionization mass spectrometry (ID-TIMS), yielded an age of 1312.9 ± 0.9 Ma (2SD; *Chapter 4*).

The Birrindudu Basin is located in the western part of the greater McArthur Basin (Figure 2). Two sedimentary groups in the top are the Bulita Group and the Tijuna Group (Figure 3). The Bulita Group is unconformably overlain by the Tijuna Group and deposited in shoaling, shallow-marine platform depositional environments (*Ahmad & Munson, 2013*). The youngest detrital zircon analyse from the underlying Wattie Group (1550 ± 48 Ma (2SD); *Krositcin & Carson, 2017*) might provide a maximum depositional age constraint for this group. The Tijuna Group contains a set of siliciclastic sedimentary rocks that are divided into two formations—the Wondoan Hill Formation in the lower and the Stubb Formation in the upper (*Ahmad & Munson, 2013; Munson, 2016*). The youngest detrital zircon with a $^{207}Pb/^{206}Pb$ age of 1452 ± 48 Ma (2SD; *Munson et al., 2018*), obtained from the Wondoan Hill Formation, might provide the maximum deposition age constraint for this group.

The South Nicholson Group of the South Nicholson Basin is located on the southeast of the Beetaloo-McArthur basins (Figure 2). It unconformably overlies the Murphy Province and the Western Fold Belt of the Mt Isa Province, and underlies a series of Neoproterozoic to Cambrian successions, such as the Georgina Basin and the Helen Spring Volcanics (Figure 3; *Ahmad & Munson, 2013*). The South Nicholson Group is dominated by quartz sandstone interstratified with siltstone and shale, indicating a range of depositional environments from fluvial to coastal and shallow-marine shelf settings (*Ahmad & Munson, 2013*). The South Nicholson Group is poorly age constrained. A recently published $^{207}Pb/^{206}Pb$ age of 1483 ± 12 Ma (weighted mean age of the youngest group, 95% confidence, n=43, MWSD=1.38) from the Crow Formation has been suggested to be used as the maximum depositional constraint for this formation (*Kositcin & Carson, 2019*). Whereas, the youngest analysed zircon grain from the Crow Formation yielded a $^{207}Pb/^{206}Pb$ age of 1371 ± 94 Ma (2SD, *Kositcin & Carson, 2019*).

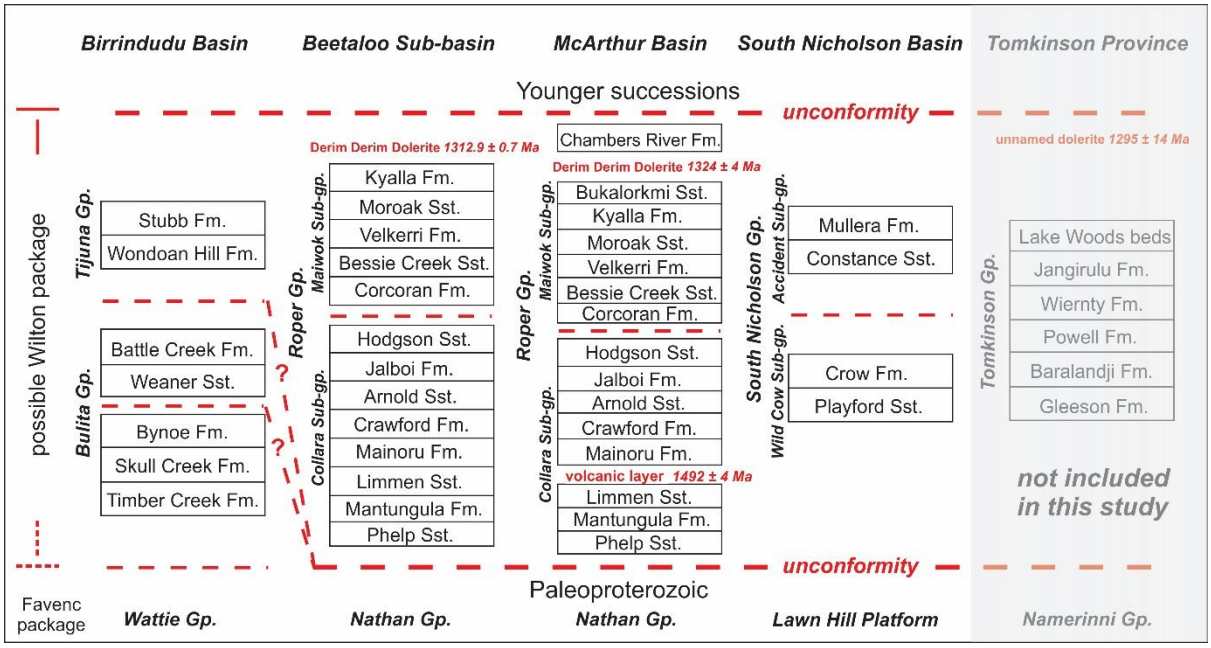

Figure 3 Stratigraphic chart of the Wilton package and its potential correlatives in other inter-connected depositional systems or sub-basins, after *Ahamd & Munson (2013), Munson (2016)* and *Munson et al. (2018)*. Note that the classification of the Bulita Group remains uncertain and unconstrained yet.

A set of latest Mesoproterozoic to Neoproterozoic successions, which unconformably overly various upper Roper Group formations, are informally named the lower and upper Jamison sandstones and Hayfield mudstone, and these are also a focus of this study. These sedimentary units deposited in high-energy shoreline to shallow-marine settings (*Munson, 2016*), and their detrital zircon U–Pb age analysis suggests that the lower Jamison sandstone was deposited after 1092 ± 16 Ma (2SD; *Chapter 2*), whereas the depositional age of the upper Jamison and Hayfield mudstone has been constrained to be after 959 ± 18 Ma (2SD; *Chapter 2*).

3. Thesis outline

The overall aim of this thesis is to apply a multiproxy isotopic provenance approach to (i) investigate the sediment pathways from source to sink of the Wilton package, (ii) get new constraints on the spatial and temporal basin provenance evolution, and (iii) reconstruct the dynamic tectono-sedimentation interactions and processes within the Mesoproterozoic North Australia Craton. This in turn helps to provide an improved understanding of the tectonic evolution of the North Australia Craton that contributes to the Mesoproterozoic paleogeography reconfiguration. Except the Introduction (*Chapter 1*) and Summary (*Chapter 6*), this thesis consists of four thematic chapters, where each applies different methodologies and analytical tools to specific study areas and sedimentary archives (see below),

Chapter 2 focuses on the Beetaloo Sub-basin and presents detrital zircon U–Pb chronology constraints for each formations of the upper Roper Group as well as the unnamed latest Mesoproterozoic to Neoproterozoic successions. Overall, the temporal provenance variation suggests a dynamic tectonic evolution of the North Australia Craton. The spatial comparison of the data reveals sediment drainage patterns and basin geography. This chapter is published as: Yang, B., Smith, T.M., Collins, A.S., Munson, T.J., Schoemaker, B., Nicholls, D., Cox, G., Farkaš, J., Glorie, S. (2018). Spatial and temporal detrital zircon U–Pb provenance of the hydrocarbon-bearing upper Roper Group, Beetaloo Sub-Basin, Northern Territory, Australia. *Precambrian Research*, **304**, 140-155.

Chapter 3 also focuses on the Beetaloo Sub-basin, however, in this chapter, detrital zircon hafnium isotopes, complemented by U–Pb dating, provided an integral assessment on the basin provenance and tectonic geography. This chapter is published as: Yang, B., Collins, A.S., Blades, M.L., Capogreco, N., Payne, J.L., Munson, T.J., Cox, G.M., Glorie, S. (2019). Middle-late Mesoproterozoic tectonic geography of the North Australia Craton: U–Pb and Hf isotopes of detrital zircons in the Beetaloo Sub-basin, Northern Territory, Australia. *Journal of the Geological Society, London,* **176**, 771-784.

Chapter 4 focuses on the upper formation of the Roper Group and the above unnamed latest Mesoproterozoic to early Neoproterozoic successions. A new Isotope dilution thermal ionization mass spectrometry (ID-TIMS) U–Pb baddeleyite geochronology provides tighter age constraints on the dolerite intrusion as well as the termination of the deposition of the Roper Group. Coupled shale whole-rock Sm-Nd and Pb isotope reveals dynamic tectono-sedimentation interactions of North Australia Craton from ca. 1.33 to 0.85 Ga. This chapter is submitted to the journal of *Basin Research* as: Yang, B., Collins, A.S., Cox, G.M., Jarrett, A.J.M., Denyszyn, S., Blades, M.L., Farkaš, J., Glorie, S. Sedimentary geochemical record of the middle Mesoproterozoic—early Neoproterozoic tectonic geography of Northern Australia.

Chapter 5 expends the study focus to the wider Wilton package, and provides coupled detrital zircon U–Pb age and Hf isotope data collected from the potential equivalent successions of the Roper Group. These data are used to test the intra basin correlations within the Wilton package, and further assess the tectonic geography of the Mesoproterozoic North Australia Craton in a boarder scale. This chapter is in preparation for submission as: Yang, B., Collins, A.S., Munson, T.J., Payne, J.L., Blades, M.L., Glorie, S., Farkaš, J. *in prep*. Intra basin correlations and tectonic geography of the Mesoproterozoic North Australia Craton: detrital zircon U–Pb age and Hf isotope provenance analysis.

Chapter 6 is the summary of this thesis. This chapter integrates and summarises the main findings and interpretations from individual chapters to get an overall understanding of the tectonic geography of Wilton package as well as the Mesoproterozoic North Australia Craton.

References

Abbott, S.T. & Sweet, I.P. (2000). Tectonic control on third-order sequences in a siliciclastic ramp-style basin: An example from the Roper Superbasin (Mesoproterozoic), northern Australia. *Australian Journal of Earth Sciences* **47(3)**, 637-657.

Abbott, S.T., Sweet, I.P., Plumb, K.A., Young, D.N., Cutovinos, A., Ferenczi, P.A. & Pietsch, B.A. (2001). Roper Region: Urapunga and Roper River Special, Northern Territory (Second Edition). 1:250 000 geological map series explanatory notes, SD 53-10, 11. Northern Territory Geological Survey and Geoscience Australia (National Geoscience Mapping Accord).

Ahmad, M. & Munson, T.J. (2013). Northern Territory Geological Survey, Geology and mineral resources of the Northern Territory, Special Publication 5. Northern Territory Geological Survey.

Allen, P.A. (2008). From landscapes into geological history. *Nature*, **451(7176)**, 274-276.

Allen, P.A. & Armitage, J.J. (2012). Cratonic Basins. Tectonics of Sedimentary Basins: Recent Advances. John Wiley & Sons, Ltd.

Allen, P.A., Eriksson, P.G., Alkmim, F.F., Betts, P.G., Catuneanu, O., Mazumder, R., Memg, Q. & Young, G.M. (2015). Classification of basins, with special reference to Proterozoic examples. *Geological Society, London, Memoirs*, **43(1)**, 5-28.

Bradley, D.C. (2008). Passive margins through earth history. *Earth-Science Reviews*, **91(1-4)**, 1-26.

Close D.F. (2014). The McArthur Basin: NTGS ' approach to a frontier petroleum basin with known base metal prospectivity. *Annual Geoscience Exploration Seminar (AGES) Proceedings, Alice Springs, Northern Territory 15–16 March 2016.* Northern Territory Geological Survey, Darwin. pp. 85–89.

Cox, G.M., Jarrett, A., Edwards, D., Crockford, P.W., Halverson, G.P., Collins, A.S., Poirier, A. & Li, Z.X. (2016). Basin redox and primary productivity within the Mesoproterozoic Roper Seaway. *Chemical Geology*, **440**, 101-114.

Evans, D.A.D. & Mitchell, R.N. (2011). Assembly and breakup of the core of Paleoproterozoic-Mesoproterozoic supercontinent Nuna. *Geology,* **39(5)**, 443-446.

Frogtech Geoscience. (2018). SEEBASE® study and GIS for greater McArthur Basin. *Northern Territory Geological Survey, Digital Information Package DIP 017*.

Ingersoll, R.V. (2018). Tectonic of sedimentary basins. *Geological Society of America Bulletin,* **100**, 1704-1719.

Jackson, M.J., Sweet, I.P., Page, R.W. & Bradshaw, B.E. (1999). The South Nicholson and Roper Groups: evidence for the early Mesoproterozoic Roper Superbasin. Integrated Basin Analysis of the Isa Superbasin using Seismic, Well-log, and Geopotential Data: An Evaluation of the Economic Potential of the Northern Lawn Hill Platform: Canberra, Australia, *Australian Geological Survey Organisation Record*, *19.*

Kirscher, U., Mitchell, R., Liu, Y., Li, Z.X., Cox, G.M., Nordsvan, A., Wang, C., Pisarevsky, S., 2018. Long lived supercontinent Nuna - updated paleomagnetic constraints from Australia. *2018, AGU Fall Meeting*, abstract #GP21B-0647.

Kositcin, N. & Carson, C.J. (2017). New SHRIMP U–Pb zircon ages from the Birrindudu and Victoria Basins, Northern Territory: July 2016–June 2017. *Geoscience Australia, Canberra. Record 2017/16.* http://dx.doi.org/10.11636/Record.2017.016

Kuiper, K.F., Deino, A., Hilgen, F.J., Krijgsman, W., Renne, P.R. & Wijbrans, J.R. (2008). Synchronizing rock clocks of earth history. *Science*, **320(5875)**, 500-504.

Li, Z.X., Bogdanova, S.V., Collins, A.S., Davidson, A., Waele, B.D., Ernst, R.E., Fitzsimons, I.C.W., Fuck, R.A., Gladkochub, D.P., Jacobs, J., Karlstrom, K.E., Lu, S., Natapov, L.M., Pease, V., Pisarevsky, S.A., Thrane, K. & Vernikovsky, V. (2008). Assembly, configuration, and break-up history of Rodinia: a synthesis. *Precambrian Research, **160**(**1**)*, 179-210.

Merdith, A.S., Collins, A.S., Williams, S.E., Pisarevsky, S., Foden, J.F., Archibald, D., Blades, M.L., Alessio, B.L., Armistead, S., Plavsa, D., Clark, C. & Müller, R.D. (2017). A full-plate global reconstruction of the Neoproterozoic. *Gondwana Research*, **50**, 84-134.

Merdith, A.S., Williams, S.E., Brune, S., Collins, A.S. & Müller, R.D. (2019). Rift and plate boundary evolution across two supercontinent cycles. *Global and Planetary Change*, **173**, 1-14.

Munson, T.J. (2016). Sedimentary characterisation of the Wilton package, greater McArthur Basin. Northern Territory. *Northern Territory Geological Survey, Record 2016-003*.

Munson, T.J, Thompson, J.M, Zhukova, I., Meffre, S., Beyer, E.E., Woodhead, J.D. & Whelan, J.A. (2018). Summary of results. NTGS laser ablation ICP-MS U–Pb and Lu–Hf geochronology project: Roper Group and overlying ungrouped units (McArthur Basin), Renner Group (Tomkinson Province), Tijunna Group (Birrindudu Basin). *Northern Territory Geological Survey, Record* 2018-007.

Pisarevsky, S.A., Elming, S.Å., Pesonen, L.J. & Li, Z.X. (2014). Mesoproterozoic paleogeography: supercontinent and beyond. *Precambrian Research,* **244(1)**, 207-225.

Rawlings, D.J. (1999). Stratigraphic resolution of a multiphase intracratonic basin system: The McArthur Basin, northern Australia. *Australian Journal of Earth Sciences*, **46(5)**, 703-723.

Southgate, P.N., Bradshaw, B.E., Domagala, J., Jackson, M.J., Idnurm, M., Krassay, A.A., Page, R.W., Sami, T.T., Scott, D.L., Lindsay, J.F. & McConachie, B. A. (2000). Chronostratigraphic basin framework for Palaeoproterozoic rocks (1730–1575 Ma) in northern Australia and implications for base-metal mineralisation. *Australian Journal of Earth Sciences*, **47(3)**, 461-483.

Zhang, S., Li, Z. X., Evans, D.A.D., Wu, H., Li, H. & Dong, J. (2012). Pre-Rodinia supercontinent Nuna shaping up: a global synthesis with new paleomagnetic results from north China. *Earth & Planetary Science Letters*, **353-354**, 145-155.

Zhang, S.H., Zhao, Y., Li, X.H., Ernst, R.E. & Yang, Z.Y. (2017). The 1.33–1.30 Ga Yanliao large igneous province in the North China Craton: implications for reconstruction of the Nuna (Columbia) supercontinent, and specifically with the North Australian Craton. *Earth & Planetary Science Letters,* **465**, 112-125.

Chapter 2

Spatial and temporal variation in detrital zircon age provenance of the hydrocarbon-bearing upper Roper Group, Beetaloo Sub-basin, Northern Territory, Australia

Published as:

Yang, B., Smith, T.M., Collins, A.S., Munson, T.J., Schoemaker, B., Nicholls, D., Cox, G., Farkas, J., Glorie, S. (2018). Spatial and temporal detrital zircon U–Pb provenance of the hydrocarbon-bearing upper Roper Group, Beetaloo Sub-Basin, Northern Territory, Australia. *Precambrian Research*, **304**, 140-155.

https://doi.org/10.1016/j.precamres.2017.10.025

Statement of Authorship

Title of Paper	Spatial and temporal variation in detrital zircon age provenance of the hydrocarbon-bearing upper Roper Group, Beetaloo Sub-basin, Northern Territory, Australia
Publication Status	☑ Published ☐ Accepted for Publication ☐ Submitted for Publication ☐ Unpublished and Unsubmitted w ork w ritten in manuscript style
Publication Details	Yang, B., Smith, T.M., Collins, A.S., Munson, T.J., Schoemaker, B., Nicholls, D., Cox, G., Farkas, J., Glorie, S. (2018). Spatial and temporal detrital zircon U–Pb provenance of the hydrocarbon-bearing upper Roper Group, Beetaloo Sub-Basin, Northern Territory, Australia. *Precambrian Research*, **304**, 140-155.

Principal Author

Name of Principal Author (Candidate)	Bo Yang		
Contribution to the Paper	Field work, sample preparation, data collection and processing, data interpretation, manuscript composition.		
Overall percentage (%)	80%		
Certification:	This paper reports on original research I conducted during the period of my Higher Degree by Research candidature and is not subject to any obligations or contractual agreements with a third party that would constrain its inclusion in this thesis. I am the primary author of this paper.		
Signature		Date	10/06/2019

Co-Author Contributions

By signing the Statement of Authorship, each author certifies that:

i. the candidate's stated contribution to the publication is accurate (as detailed above);
ii. permission is granted for the candidate in include the publication in the thesis; and
iii. the sum of all co-author contributions is equal to 100% less the candidate's stated contribution.

Name of Co-Author	Todd M. Smith		
Contribution to the Paper	Field work, sample preparation, data collection and processing, manuscript review.		
Signature		Date	11/06/2019

Name of Co-Author	Alan S. Collins		
Contribution to the Paper	Field work, guidance on data interpretation, manuscript composition and review.		
Signature		Date	11/06/2019

Name of Co-Author	Munson, J. Tim		
Contribution to the Paper	Guidance on data analysis and interpretation, manuscript review.		
Signature		Date	11/06/2019

Name of Co-Author	Brenton Schoemaker		
Contribution to the Paper	Guidance on field work and sample preparation.		
Signature		Date	11/06/2019

Name of Co-Author	De Nicholls		
Contribution to the Paper	Guidance on field work and sample preparation.		
Signature		Date	11/06/2019

Name of Co-Author	Grant M. Cox		
Contribution to the Paper	Manuscript review.		
Signature		Date	11/06/2019

Name of Co-Author	Juraj Farkaš		
Contribution to the Paper	Manuscript review.		
Signature		Date	11/06/2019

Name of Co-Author	Stijn Glorie		
Contribution to the Paper	Manuscript review.		
Signature		Date	11/06/2019

Chapter 2

Spatial and temporal variation in detrital zircon age provenance of the hydrocarbon-bearing upper Roper Group, Beetaloo Sub-basin, Northern Territory, Australia

Abstract

The subsurface Beetaloo Sub-basin of the McArthur Basin, Northern Territory, Australia, comprises a succession of shallow-water, dominantly marine, clastic sedimentary rocks that formed in the main depocentre of the Mesoproterozoic Roper Group. This group contains the oldest commercial hydrocarbons known whose presence has been linked to changing nutrient flux controlled by a changing provenance. LA-ICP-MS detrital zircon U–Pb age data presented here provide new age constraints on the upper Roper Group and reveal spatial and temporal provenance variations illustrating the evolution of the basin and its margins that are linked to a major provenance change caused by the coeval collision of the combined South Australian Craton/North Australian Craton with the Western Australian Craton.

The maximum depositional ages of the Bessie Creek Sandstone and the Velkerri Formation of the Roper Group are constrained to 1386 ± 13 Ma and 1308 ± 41 Ma, respectively, whereas the overlying Moroak Sandstone has no younger detrital zircons, so its maximum depositional age is also constrained as 1308 ± 41 Ma. The Kyalla Formation was deposited after 1313 ± 47 Ma, and two, as yet, informally defined and ungrouped latest Mesoproterozoic to Neoproterozoic sedimentary units, the lower and upper Jamison sandstone, have maximum depositional ages of 1092 ± 16 Ma and 959 ± 18 Ma, respectively. Large detrital zircon age datasets (of 1204 near-concordant analyses) indicate that zircons from the Maiwok Subgroup were originally sourced from Palaeoproterozoic and earliest Mesoproterozoic rocks. These are consistent with derivation from the surrounding exposed basement. Detrital zircon age variations up-section suggest a systematic temporal change in provenance. The oldest formation analysed (Bessie Creek Sandstone) has a major source dated at ca. 1823 Ma. Rocks of this age are common in northern basement exposures. Samples from the overlying Velkerri Formation, show derivation from a ca.

1590 Ma source, consistent with rocks exposed in Queensland, or the Musgrave Province. The Moroak Sandstone and the Kyalla Formation show progressively more ca. 1740 Ma detritus, which we suggest likely reflects new sources in the Arunta Region to the south.

We suggest that the provenance variation initially records exposure and denudation of western Queensland rocks at ca. 1400 Ma due to rifting between Laurentia and the Northern Australian Craton. From then until at least ca. 1320 Ma, the increased ca. 1740 Ma detritus suggests uplift of the Arunta Region that we interpret as reflecting collision between the southern North Australian Craton and the Western Australian Craton as ca. 1300-1400 Ma. This tectonically-controlled provenance change is interpreted to have included erosion of nutrient rich arc-rocks that may have caused a bacterial bloom in the Roper Seaway. The Jamison sandstone and overlying Hayfield mudstone represent a marked change in provenance and were deposited after the Musgrave Orogeny, representing a newly-recognised siliciclastic basin that may have formed a shallow, long wavelength foreland basin to areas uplifted during the Musgrave Orogeny.

1. Introduction

The occurrence and formation processes of vast Proterozoic supra-continental basins throughout the world (e.g. the Cuddapah, Chhattisgarh and Vindhyan basins of India, Athabasca Basin of North America and Centralian Superbasin of Australia, amongst many others) have long been the subject of speculation. It is specifically unclear how such basins remained depocentres for periods of time that span supercontinent cycles, albeit punctuated by periods of uplift and non-deposition (e.g. *Sandiford et al., 2001; Allen et al., 2015; Saha et al., 2016*). Much of this uncertainty is due to the incomplete preservation of many of the basinal successions and subsequent modification of the basin by continent dispersal or orogenesis. In recent years, the volume and quality of detrital isotopic data has begun to provide key constraints on the evolving provenance of these basins and has assisted in unravelling the tectonic setting of their formation and subsequent evolution (e.g., Cuddapah Basin; *Collins et al., 2015*).

The informally named greater McArthur Basin (*Close, 2014*) is a Proterozoic basin system that extends over large parts of northern Australia (Figure 1a). It contains a thick sedimentary pile that was deposited over a time span of up to a billion years of Earth history from the Palaeoproterozoic to the Neoproterozoic (*Rawlings, 1999; Ahmad & Munson, 2013; Munson, 2016a, b*). The upper part of this basin contains the Mesoproterozoic Roper Group, which is the focus of this study. This is a siliciclastic succession characterised by alternating mudrock-rich and cross-bedded sandstone formations that are lithologically laterally continuous over extensive areas. The upper part of the group is notably rich in high organic carbon shales and is of

considerable economic interest for unconventional petroleum (*Cox et al., 2016; Revie, 2017*); one shale interval (Velkerri Formation) has recently been demonstrated to host a major shale-gas resource (*Close et al., 2017*)—the oldest commercial hydrocarbons yet known. Moreover, *Cox et al. (2016)* demonstrated that the organic carbon correlated with phosphorous (P) contents that they suggested were a) a limitation for bacterial growth (see also *Horton, 2015*) and b) were derived from mafic igneous sources, i.e. from a changed provenance.

Detrital zircon grains contain valuable information about the sources region of clastic sedmentary formations as they are incredibly resilient and preserve their radiometric clocks and chemical properties through metamorphic deformation and erosional processes, making them one of the most powerful tools for provenance analysis (*Dickinson & Gehrels, 2009; Cawood et al., 2012; Gehrels, 2014*). With the use of laser ablation inductively coupled plasma mass spectrometry (LA-ICP-MS), the U–Pb age of detrital zircon grains can be obtained rapidly (*Machado & Gauthier, 1996; Gehrels, 2014*). Moreover, the increasing magnitude of datasets enable the use of new statistical techniques to identify and study trends in the temporal and spatial evolution of a basinal successions and their provenance (e.g. *Cawood et al., 2012; Vermeesch, 2013, 2014; Shaanan & Rosenbaum, 2016; Spencer & Kirkland, 2016*).

In this contribution, we present new detrital zircon U–Pb data from the Beetaloo Sub-basin, providing new constraints on basin age and provenance. Samples were collected from core samples drilled throughout the Beetaloo Sub-basin. Several formations of the Maiwok Subgroup (Bessie Creek Sandstone, Velkerri Formation, Moroak Sandstone, and Kyalla Formation) were sampled as well as the overlying, informally named Jamison sandstone, which has previously been correlated with the Bukalorkmi Formation found in the Urapunga region (*Gorter & Gray, 2012*), approximately 180 km to the north of the Beetaloo Sub-basin (*Abbott et al., 2001*; Figures 1a and b). Data are compared with that from outcropping Maiwok Subgroup formations preserved in the Urapunga region (Figure 1a; *Munson, 2016a, b*). The wide stratigraphic and areal extent of sampling, coupled with the amount of data collected (1204 individual zircon analyses), allows an assessment of both the temporal and spatial variation of provenance in this key subgroup. We then use the data to constrain the age and correlation of formations across the basin, to test the tectonic setting of the basin during its evolution and to examine the hypothesis of a provenance control on organic carbon development and preservation in the Roper Group.

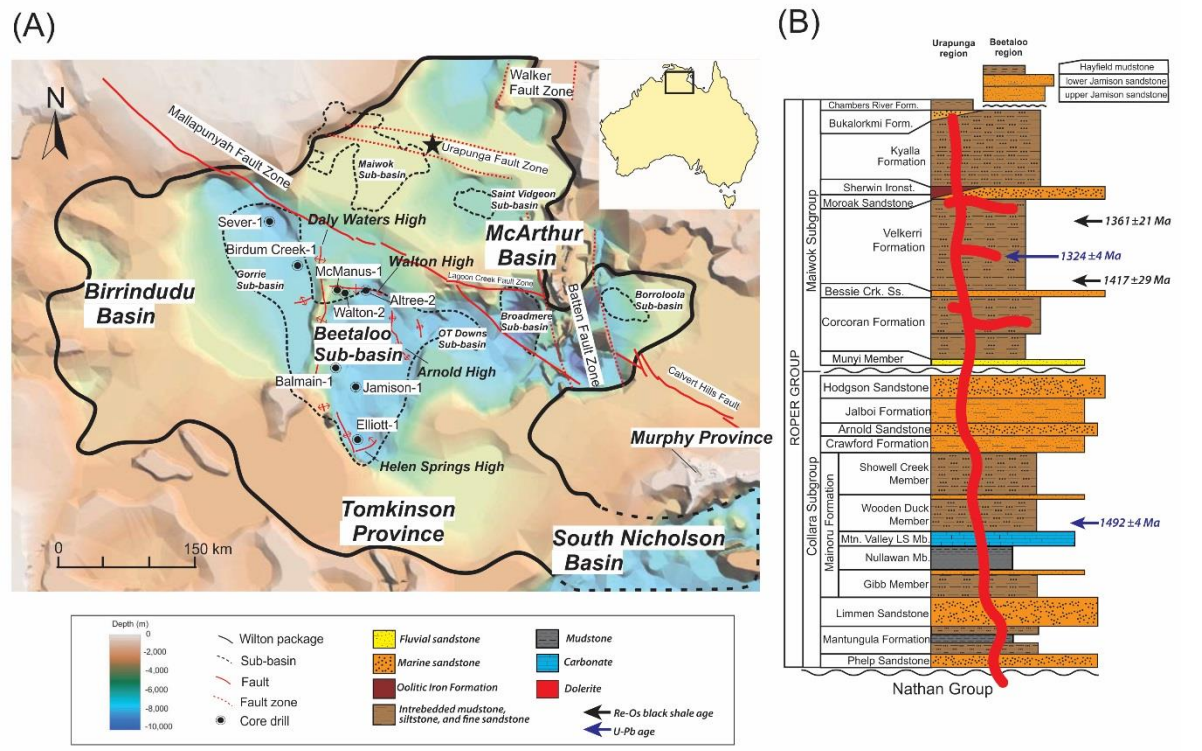

Figure 1 (A) Extent of Wilton package based on Proterozoic SEEBASE™ basement surface, showing the locations of drillholes and major structural highs. SEEBASE™ image after *De Vries et al. (2006)*; black star represents outcrop samples from Urapunga region from *Munson (2016b)*. (B) Stratigraphic column of upper Roper Group modified after *Cox et al. (2016)*. SHRIMP U–Pb zircon ages from *Abbott et al. (2001)* and *Jackson et al. (1999)*. Re–Os ages for the Velkerri Formation from *Kendall et al. (2009)*. Dolerite (Derim Derim Dolerite) U–Pb SHRIMP baddeleyite age reported in *Abbott et al. (2001)*.

2. Geological Setting

2.1. The Wilton package and the Roper Group

The informally named Wilton package (*Rawlings, 1999*) forms a significant portion of the Mesoproterozoic succession near the top of the basin, and is widespread throughout northern Australia, stretching from Queensland to Western Australia and covering an area of over 145,000 km^2 (Figure 1a; *Rawlings, 1999; Jackson et al., 2000; Abbott et al., 2001; Ahmad & Munson, 2013; Betts et al., 2015; Munson, 2016a, b*). The Wilton package comprises several shallow-water siliciclastic-dominated geographically separated successions. These include the Roper Group of the McArthur Basin and the subsurface Beetaloo Sub-basin, the Renner Group of the Tomkinson Province and the Tijunna Group of the Birrindudu Basin (Figure 1a). The South Nicholson Group of the South Nicholson Basin is another possible component of the Wilton package, although connection between it and the rest of the package has not been demonstrated. Because of the remarkable sedimentary lateral continuity, and the lack of evidence for basin-margin facies, the

extent of the Wilton package is likely to be larger than its preserved distribution (*Abbott & Sweet, 2000; Ahmad & Munson, 2013; Munson, 2016a*).

The Roper Group is a sequence of dominantly marine siliciclastic sedimentary rocks, containing six upward-coarsening cyclic sequences (*Jackson et al., 1988; Abbott & Sweet, 2000*), and can be divided into two subgroups - the lower Collara Subgroup and the upper Maiwok Subgroup (*Abbott et al., 2001*). The Collara Subgroup is dominated by sandstone and lesser mudrocks, indicating a range of depositional environments from shoreline to shallow-marine shelf (*Abbott & Sweet, 2000; Abbott et al., 2001*). The Maiwok Subgroup disconformably overlies the Collara Subgroup and is dominated by mudrock sequences with less voluminous sandstones, deposited in a similar range of environments (*Abbott & Sweet, 2000; Abbott et al., 2001; Munson, 2016a, b*). Syn- and post depositional faults are distributed throughout the basin and influenced its shape and depositional history, and the subsequent exhumation of the basin (*Rawlings et al., 2004; Betts et al., 2015*).

The Roper Group overlies the Mesoproterozoic Nathan Group with a regional unconformity that is interpreted to be related to the ca 1580–1500 Ma Isan Orogeny (*Jackson, 1999; Ahmad & Munson, 2013*). The tectonic background of the Roper Group remains controversial. *Jackson et al. (1987)* suggested that the Roper Group formed in an epicontinental environment, distinct from older McArthur Basin successions. *Abbott & Sweet (2000)*, however, argued that the Roper Group was deposited in a broad flexural basin caused by the orogenic load of the Isan Orogeny in the east. *Foster & Ehlers (1998)* suggested that eastern Proterozoic Australia underwent cooling and exhumation during the same period that the Roper Group developed (1470—1370 Ma). *Munson (2016a, b)* and *Revie (2017)* suggested that the Roper Group (and wider Wilton package) formed in an epicontinental setting and invoked an enclosed marine basin, analogous to the modern Black Sea, as demonstrated by periodic redox stratification, intermittent euxinia and fluctuating salinity levels through the succession (*Donnelly & Crick, 1988; Mukherjee and Large, 2016; Cox et al. 2016*).

Age constraints for the Wilton package are limited. Two detrital zircon Sensitive High Resolution Ion Microprobe (SHRIMP) U–Pb overlapping ages of 1492 Ma, from the lower Mainoru Formation, (1492 ± 4 Ma *Jackson et al., 1999* and 1492 ± 29 Ma *Southgate et al., 2000*), are constraining deposition to being younger than these ages. Two Re-Os ages were given by *Kendall et al. (2009)* from the base (1417 ± 29 Ma) and the top (1361 ± 21 Ma) of the Velkerri Formation constraining the deposition of this key formation. Finally, a U–Pb SHRIMP baddeleyite age of 1324 ± 4 Ma (the standard deviation level is unclear) for a dolerite suite (Derim Derim Dolerite) that is mapped as intruding all formations of the Maiwok Subgroup in the Urapunga region,

except the Chambers River Formation (Figure 1b) is reported in the map explanatory notes for the Roper River area (*Abbott et al., 2001*). This age, therefore, provides an upper age constraint on the timing of deposition of this subgroup (*Abbott et al., 2001*).

2.2. Beetaloo Sub-basin

The Beetaloo Sub-basin is in the centre of the interpreted Wilton package distribution, linking the outcropping McArthur Basin in the northeast, Birrindudu Basin in the west, Tomkinson Province in the south and possibly the South Nicholson Basin in the southeast (Figure 1a). It is also where the Roper Group is stratigraphically thickest (in excess of 3,500 m) and is interpreted to be the most significant depocentre of the basin (*Plumb & Wellman, 1987; Lanigan et al., 1994; Ahmad & Munson, 2013; Munson, 2016a, b*). The term 'Beetaloo Sub-basin' is here used in a general sense to refer to several contiguous smaller depocentres that are separated by local basement highs (Figure 1a). These smaller depocentres are the Gorrie Sub-basin in the west, separated by the north–south-trending Daly Waters High from the Beetaloo Sub-basin *sensu stricto*, which is in turn separated by the Arnold High from the smaller OT Downs and Broadmere sub-basins to the east. The southern boundary of the Beetaloo sub-basin is considered to be the Helen Springs High, whereas the northern boundary is marked by the Walton High and northwest-trending Mallapunyah Fault Zone (Figure 1a) (*Silverman et al, 2007, 2011; Hoffman, 2015; Betts et al., 2015*). Geophysics data show that these basement highs are fault-related (*Betts et al., 2015*). But it is unclear whether these basement highs formed topographic/bathymetric features during deposition, as the existence and degree of post-deposition fault reactivation remains unknown. Thickness variations within the Velkerri Formation are seen on 2-D seismic images (*Silverman & Ahlbrandt, 2011*), suggesting that the fault bounding the southern margin of the Walton High, at least, may have been active during deposition.

The Maiwok Subgroup in the Beetaloo Sub-basin consists of five formations; from base to top these are the Corcoran Formation, Bessie Creek Sandstone, Velkerri Formation, Moroak Sandstone and Kyalla Formation (Figure 1b; *Abbott et al., 2001*). Two ungrouped, subsurface siliciclastic successions consisting of the informally named Jamison sandstone and Hayfield mudstone (*Lanigan et al., 1994*) unconformably overlie variously the Kyalla Formation, Moroak Sandstone and Velkerri Formation, and form the top of the McArthur Basin succession in the Beetaloo Sub-basin. In the Urapunga region, to the north of the Beetaloo Sub-basin, three additional formations are recognised; these are the Sherwin Formation between the Moroak Sandstone and Kyalla Formation, the Bukalorkmi Sandstone, overlying the Kyalla Formation, and the Chambers River Formation, which caps the succession (Figure 1b). It is possible that the

undated Chambers River Formation is a correlative of the ungrouped units at the top of the Beetaloo Sub-basin succession, rather than a part of the Roper Group (*Munson 2016a, b*).

The Corcoran Formation is a mudstone and siltstone succession with minor interbedded quartz arenites, deposited mainly in a storm-dominated shallow-marine shelf setting, mostly under relatively low-energy, subtidal conditions (*Abbott et al., 2001*). The Bessie Creek Sandstone is characterised by highly mature quartz sandstones, indicative of a high-energy tide-dominated shoreline to shallow shelf setting (*Abbott et al., 2001*). The Velkerri Formation conformably overlies the Bessie Creek Sandstone, and is a black mudrock succession with minor sandstone, deposited in a marine, subtidal, sub-wave base and generally quiet environment, affected by regular current activity (*Abbott et al., 2001*). Both trace element concentration increases, and the ε_{Nd} values of shales initially increase and then decrease up-section within the Velkerri Formation, suggesting a progressive increase then decrease in basaltic weathering into the basin (*Cox et al., 2016*). The Moroak Sandstone, conformably overlying the Velkerri Formation, is a sequence of fine to medium quartz sandstones, deposited in a high-energy tide-dominated shoreline to shallow shelf setting similar to that of the Bessie Creek Sandstone (*Abbott et al., 2001*). The Kyalla Formation consists of interbedded siltstone, sandstone and mudstone, suggesting a storm-dominated shallow-marine shelf environment (*Abbott et al., 2001*). This formation is disconformably to unconformably overlain by a set of medium to coarse quartz sandstones, deposited in a high-energy shoreline to shallow-marine inner shelf setting; these form the Jamison sandstone (*Lanigan et al., 1994*). *Abbott et al. (2001)* suggested that the Jamison sandstone in the Beetaloo Sub-basin may be equivalent to the Bukalorkmi Sandstone of the exposed McArthur Basin, where it forms the topmost formation of the Roper Group. However, *Gorter & Grey (2012)* suggested that the Bukalorkmi Sandstone and the Jamison sandstone both developed in the Beetaloo Sub-basin and can be separated by gamma ray spectrometry. *Munson (2016a, b)* subsequently demonstrated that the Jamison sandstone is considerably younger than the preceding Roper Group and is probably Neoproterozoic, as was originally suggested by *Lanigan et al. (1994)*; he, therefore, concluded that the Jamison sandstone and the Bukalorkmi Sandstone are not correlatives. *Munson (2016a, b)* suggested that the Jamison sandstone can be divided into informal lower and upper intervals, based on detrital zircon geochronology analysis and the gamma-ray stratigraphy reported by *Gorter & Grey (2012)*. Capping the Jamison sandstone succession is the, also informally named, Hayfield mudstone (*Lanigan et al., 1994*), which is a mudrock-rich succession with minor sandstone, deposited in a subtidal shallow-marine shelf setting. This formation is unconformably overlain by Neoproterozoic (?) to Cambrian sedimentary and volcanic rocks of the Georgina Basin and Kalkarindji Province.

3. Samples and Methods

A total of seventeen drill core sandstone and siltstone samples were collected (Figure 2 and Table 1). The samples were collected from seven wells (Elliott-1, Jamison-1. McManus-1, Walton-2, Sever-1, Altree-2 and Birdum Creek-1) that are widely distributed throughout the Beetaloo Sub-basin (Figure 1a).

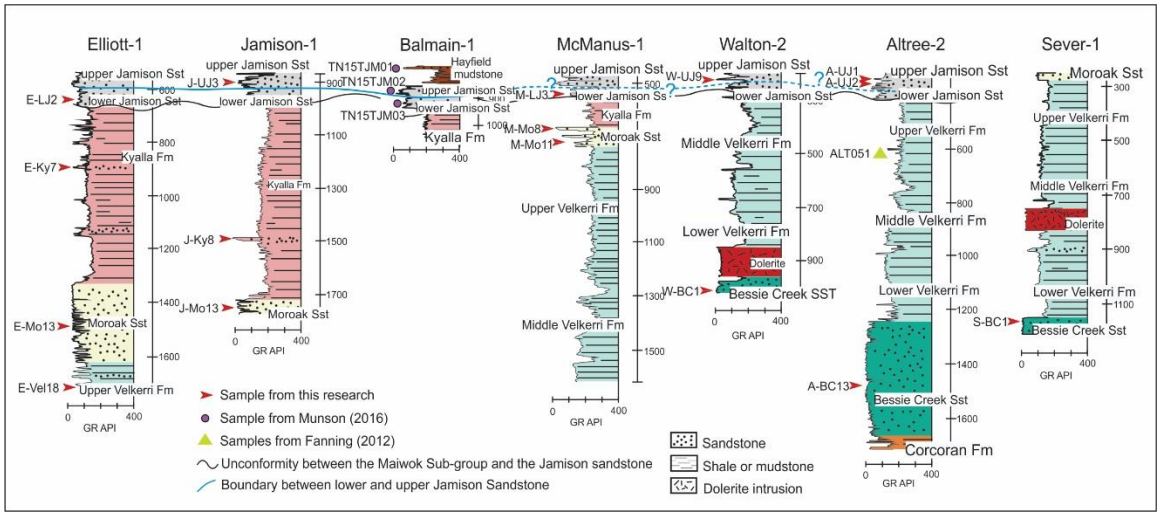

Figure 2 Lithostratigraphic columns as interpreted from gamma-ray spectrometry of drillholes within Beetaloo Sub-basin, showing depth and representative formation for each sample. All drillholes are in same scale. Boundary between unofficially named upper and lower Jamison sandstone follows interpretation of *Gorter & Grey (2013)*. Column colours are used to clarify different formations.

Detrital zircon grains were seperated from crushed samples by conventional magnetic and heavy liquid techniques. Individual zircons were then handpicked and mounted in epoxy resin. Zircon grains were handpicked without preference to size, colour, or shape, and mounted is non-reactive epoxy resin. Cathodoluminescence (CL) images were obtained using a Phillips XL20 scanning electron microscope with attached Gatan CL (working distance: 15 mm; accelerating voltage: 12 kV) at Adelaide Microscopy, The University of Adelaide, for the purpose of analysing zircon internal structures and targeting laser spots.

LA-ICP-MS analysis was conducted on a New Wave 213 nm Nd-YAG laser coupled with the Agilent 7500cs inductively coupled plasma–mass spectrometer (ICP-MS) at Adelaide Microscopy. A 30 µm spot size and a 5 Hz laser frequent were used for the analyses. Full details of the analytical conditions are followed *Payne et al. (2006)* and can be found in the supplementary file.

Instrumental fractionation was corrected using the zircon standard GEMOC GJ-1 with $^{207}Pb/^{206}Pb$ age of 607.7 ± 4.3 Ma, $^{206}Pb/^{238}U$ age of 600.7 ± 1.1 Ma and $^{207}Pb/^{235}U$ age of 602.0 ± 1.0 Ma (*Jackson et al., 2004*), and accuracy was controlled using the Plešovice zircon standard

with $^{206}Pb/^{238}U$ age of 337.13 ± 0.37 Ma (*Sláma et al., 2008*). A total of 252 Plešovice internal standards were analysed yielded weighted average ages of $^{206}Pb/^{238}U$ = 337.15 ± 0.69 Ma (95% confidence, MSWD = 1.2) and $^{206}Pb/^{207}Pb$ = 335.0 ± 3.4 Ma (95% confidence, MSWD = 1.4). Data were reduced using Iolite (*Paton et al., 2011*) and plotted using the Excel add-in Isoplot (*Ludwig, 2003*).

Core drill	Coordinate	Sample	Formation	Lithology
Elliott-1	E: 133.7551° S:17.4025°	E-LJ2	lower Jamison sst.	coarse grained sandstone
		E-Ky7	Kyalla Fm	medium grained sandstone
		E-Mo13	Moroak Sst.	coarse grained sandstone
		E-Vel18	Velkerri Fm.	fine grained siltstone
Jamison-1	E: 133.7672° S: 16.7749°	J-UJ3	upper Jamison sst.	coarse grained sandstone
		J-Ky8	Kyalla Fm	fine to medium grained sandstone
		J-Mo13	Moroak Sst.	coarse grained sandstone
Walton-2	E: 133.6388° S: 15.9051°	W-UJ9	upper Jamison sst.	coarse grained sandstone
		W-BC1	Bessie Creek Sst.	coarse grained arenite
McManus-1	E: 133.6242° S: 15.919°	M-LJ3	lower Jamison sst.	coarse grained sandstone
		M-Mo8	Moroak Sst.	medium grained sandstone
		M-Mo11	Moroak Sst.	medium grained sandstone
Altree-2	E: 133.786592° S:15.923645°	A-UJ1	upper Jamison sst.	coarse grained sandstone
		A-UJ2	upper Jamison sst.	coarse grained sandstone
		A-BC13	Bessie Creek Sst.	coarse grained arenite
Sever-1	E: 132.843963° S:15.24646°	S-BC1	Bessie Creek Sst.	coarse grained arenite
Birdum Creek-1	E: 133.1395° S: 15.625°	BirC-Ky1	Kyalla Fm	fine to medium grained siltstone

Table 1. List of samples collected from Beetaloo Sub-basin drill cores.

Samples were grouped according the formation they were sourced form. Representative internal textures of analysed zircon grains are shown in CL images (Figure 3). Zircon U–Pb cordance was calculated by dividing the $^{206}Pb/^{238}U$ age by the $^{207}Pb/^{206}Pb$ age and multiplying by 100. Only analyses that are under 10% discordant are shown in the U–Pb concordia Wetherill plots and discussed further (Figure 3; Table 2).

In this research, for the best estimate of the 'age' of the detrital grains we chose to use the $^{206}Pb/^{238}U$ age for zircons younger than 1.0 Ga and $^{207}Pb/^{206}Pb$ age for zircons older than 1.2 Ga following *Gehrels et al. (2006, 2008)* and *Gehrels (2014)*. Whereas for analyses within the "controversial age range", between 1.0 Ga and 1.2 Ga, the more precise of the ages was used, in line with the approach of *Nemchin & Cawood (2005)*. The exception to this is for the maximum depositional age of each grain. These 'ages' are of considerable importance due to their implications on the depositional age. We have followed *Spencer & Kirkland (2016)* here in using

single grain ages due to there being no *a priori* reason that any two zircon grains should have the same age in any sandstone (but we have included mean ages of populations in Figure 5 for comparison). For youngest near-concordant zircon ages >1.2 Ga, we have used only analyses that are within 5% of concordance, and have used the older of the $^{207}Pb/^{206}Pb$ or $^{206}Pb/^{238}U$ ages (the $^{207}Pb/^{206}Pb$ age in normally discordant analyses) for all formations, so as to be as conservative as possible. For grains younger than 1.2 Ga, the decrease in $^{207}Pb/^{206}Pb$ age means that we have used the $^{206}Pb/^{238}U$ age, as is usual.

Multidimensional Scaling (MDS) is used in this study. It is a new provenance analysis technique proposed by *Vermeesch (2013)* to visualise sample similarities. This technique is conducted on the Provenance package in R (*Vermeesch, 2013*). By using the Kolmogorov-Smirnov (K-S) test, the dissimilarity (D-value) between two age distributions can be quantified (Figure 6a). The technique then uses these D-values to generate a n-dimensional matrix (where 'n' is the number of samples being compared) and projects this matrix in a two dimensional plane, which is the MDS plot. The MDS plot shows the similarity or dissimilarity among data sets in the proximity of the points to each other. In this plot, the least dissimilar samples will plot closest together and are connected by a solid line (the second least dissimilar samples are connected by a dotted line). It is a relatively objective technique that has been successfully used in provenance analysis (e.g. *Arboit et al., 2016; Johnson et al., 2016; Spencer & Kirkland, 2016*). This method was used to test all the Beetaloo Sub-basin and Urapunga region samples.

4. Results

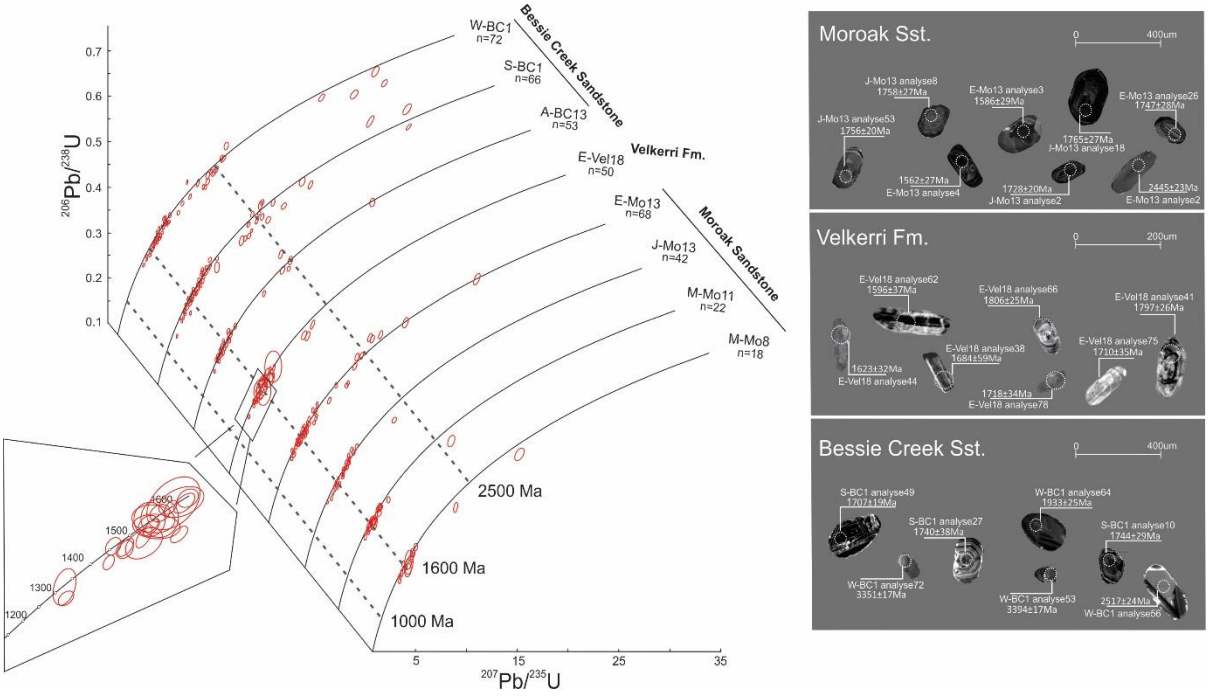

Figure 3 Cathodoluminescence images and U–Pb Wetherill concordia plots of detrital zircon grains (within 10% Concordia) from Beetaloo Sub-basin drill cores. Inset shows magnified youngest analyses from the Velkerri and Kyalla formations. Dash lines are lines of equivalent concordia age.

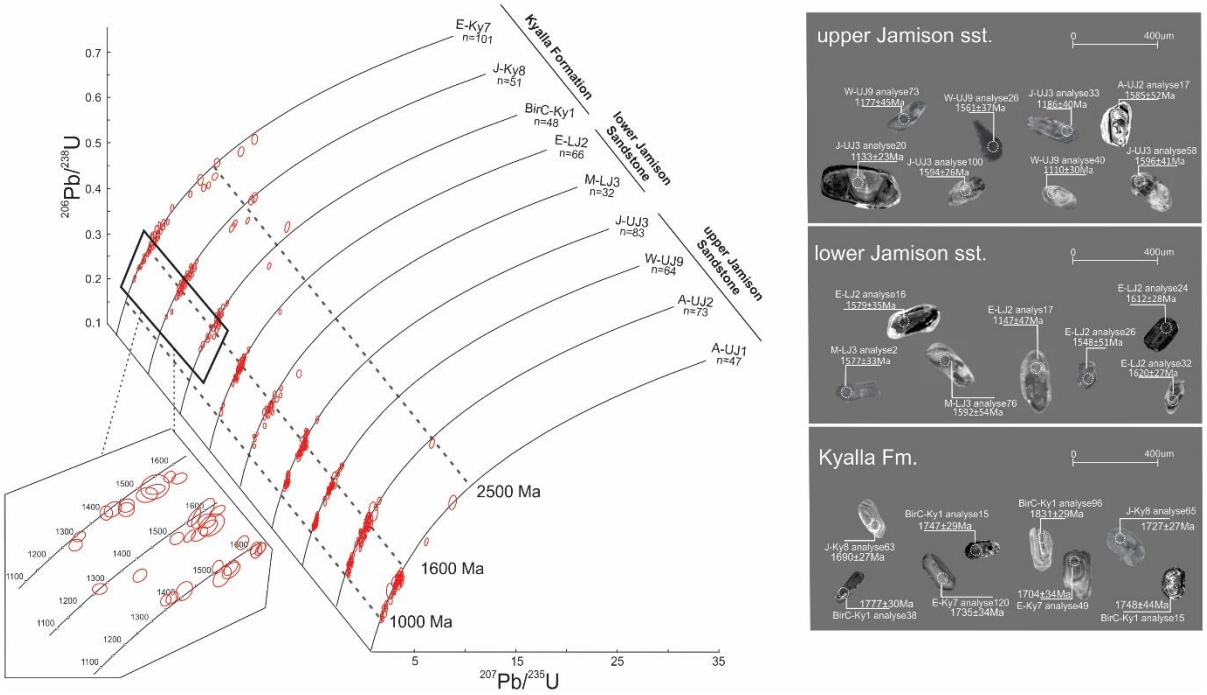

Figure 3 Continued.

Bessie Creek Sandstone

The three samples of the Bessie Creek Sandstone are all white, coarse to medium grained, quartz arenite with prominent cross-beds. Zircon grains from this formation are mostly elongated with both sector and oscillatory zonation (Figure 3). Three samples (W-BC1, S-BC1 and A-BC13) of this formation yielded 191 near-concordant ages (combined) ranging from 3505 Ma to 1354 Ma. In sample W-BC1, seventy-four near-concordant analyses form a broad range from 3505 Ma to 1539 Ma. Seventy grains yielded $^{207}Pb/^{206}Pb$ ages in the range 2539 Ma to 1539 Ma and formed three age peaks clustering at ca. 1735 Ma, ca. 1835 Ma and ca. 2480 Ma (Figure 4). Four isolated Mesoarchaean to Palaeoarchaean grains have ages between 3505 and 3158 Ma. Sample S-BC1 yielded $^{207}Pb/^{206}Pb$ ages, from >90% concordant analysis, ranging from 3443 to 1354 Ma, with one major peak at ca. 1730 Ma and three minor peaks clustered at ca. 1530 Ma, ca. 1840 Ma and ca. 2490 Ma. The majority of analyses of zircons from sample A-BC13 yielded $^{207}Pb/^{206}Pb$ ages between 1850 Ma and 1409 Ma with three peaks at ca. 1530 Ma, ca. 1640 Ma and ca. 1705 Ma, respectively (Figure 4). Six early Palaeoproterozoic to Archaean analyses are broadly spread between 2987 Ma to 2255 Ma. The youngest near-concordant zircon analysis from this formation yielded an age of 1354 ± 14 Ma ($^{207}Pb/^{206}Pb$) from Sever-1.

Velkerri Formation

The sample E-Vel18, from the upper Velkerri Formation in drill hole Elliott-1, is grey fine grained siltstone. Zircon grains from this sample are elongate and variable in size. Most zircon grains show oscillatory or sector-zoned internal textures (Figure 3). Fifty concordant $^{207}Pb/^{206}Pb$ ages show a broad age range between 2345 and 1295 Ma with two distinct age groups: 1886—1414 Ma (n=46) and 2435—2340 Ma (n=3) (Figure 3). A major age peak in kernel density estimate plots is centred on ca. 1600 Ma and two minor peaks are clustered around ca. 1693 Ma and ca. 1795 Ma (Figure 4). Two analyses from the youngest near-concordant zircon yielded $^{207}Pb/^{206}Pb$ ages of 1298 ± 47 Ma and 1348 ± 95 Ma. The mean of these analyses is 1308 ± 41 Ma, which we use as the maximum age constraint for deposition of the Velkerri Formation.

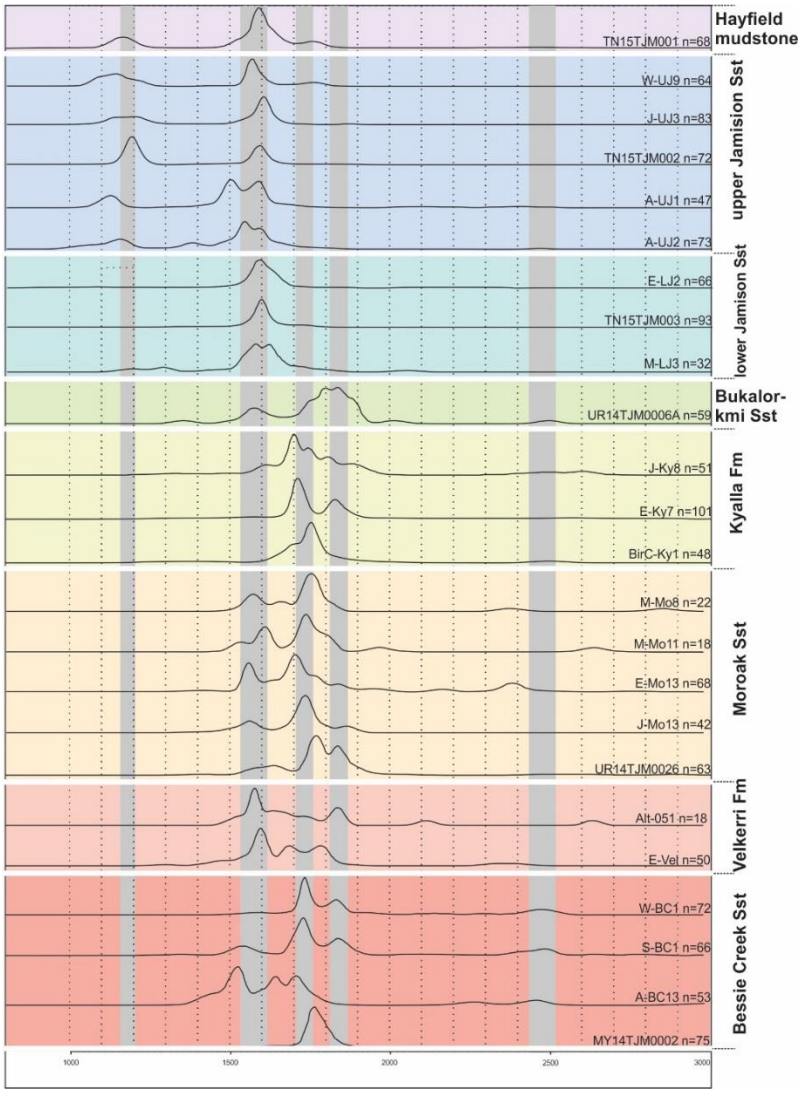

Figure 4 Kernel density estimation (KDE) plots detrital zircons ages from each pooled formation of the upper Roper Group samples collected for this study from Beetaloo Sub-basin drill cores. Samples prefixed by MY, UR and TN are from *Munson (2018)*). Grey columns are bands of equivalent concordia age range. Background colours are used to clarify different formations.

Moroak Sandstone

The four samples of the Moroak Sandstone are all white to yellow medium to coarse grained quartz sandstone. Zircons from this formation are elongated to well rounded, abraded and fractured. Most grains are non-luminescent or sector-zoned (Figure 3). Four samples (E-Mo13, J-Mo13, M-Mo8 and M-Mo11) from this formation contain mainly mid-Palaeoproterozoic to early Mesoproterozoic detritus with minor Archaean to early Palaeoproterozoic grains. In the drill hole of McManus-1, sample M-Mo8 yielded ages with clusters at ca. 1580 Ma and ca. 1750 Ma, whereas sample M-Mo11 clustered around ca. 1610 Ma and ca. 1735 Ma (Figure 4). Sample E-Mo13 from drill hole Elliott-1, showed two peaks at ca. 1560 Ma and ca. 1710 Ma. Sample J-Mo13 from drill hole Jamison-1 shows one major peak at ca. 1735 Ma and a minor peak at ca. 1560 Ma (Figure 4). The youngest near-concordant analyse of the Moroak Sandstone formation yielded an age of 1383 ± 18 Ma ($^{207}Pb/^{206}Pb$) from drill hole Elliott-1.

Kyalla Formation

Samples from the Kyalla Formation are all grey to black fine grained siltstone or shale. Detrital zircons from these samples are elongated to well-rounded with oscillatory, sector-zoned, patchy or cloudy internal patterns. Three samples (BirC-Ky1, J-Ky8 and E-Ky7) from this formation contain mainly mid-Palaeo- detritus with minor Archaean to early Palaeoproterozoic grains. Forty-eight near-concordant zircons from sample BirC-Ky1 yielded ages in the range 2491—1280 Ma with a majority in the range 1890—1617 Ma. There is a major age peak cluster at ca. 1745 Ma and a minor peak at ca. 1696 Ma (Figure 4). Most zircons from sample J-Ky8 yield ages in the range 1932-1324 Ma, with a major peak at ca. 1705 Ma and two minor peaks at ca. 1745 Ma and ca. 1810 Ma (Figure 4). Five late Archaean to early Palaeoproterozoic grains show a spread of ages between 2611 and 2415 Ma. One hundred and one concordant analyses from sample E-Ky7 yield a broad age range between 2817 and 1313 Ma, while the majority are mid- to late Palaeoproterozoic with two peaks at ca. 1705 Ma and ca. 1824 Ma (Figure 4). One zircon with an age of 1280 ± 45 Ma ($^{207}Pb/^{206}Pb$) from drill hole Birdum Creek-1 is the youngest near-concordant analysis from this formation.

Jamison sandstone

Six samples from the Jamison Sandstone (both lower and upper Jamison sandstone) are all yellow to white, trough cross-stratified, coarse grained sandstone. Zircons from both the informally named upper and lower Jamison sandstone are larger than those preserved in the underlying formations. Most of them are sector- or oscillatory-zoned, although non-luminescent grains exist (Figure 3). Two lower Jamison sandstone samples show equivalent late Palaeoproterozoic to late

Mesoproterozoic age distributions. The zircons from sample M-LJ3 yield mainly ages in the range 1799–1087 Ma with one isolated older Palaeoproterozoic zircon yielding a $^{207}Pb/^{206}Pb$ age of 2044 ± 46 Ma. There are two main age peaks in this sample centred at ca. 1580 Ma and ca. 1614 Ma (Figure 4). Sample E-LJ2 yielded zircons with a similar age range of between 1731 and 1050 Ma; one older Palaeoproterozoic grain has an age of 2186 ± 24 Ma. The major age peak of zircons from this sample is centred at ca. 1590 Ma (Figure 4). The youngest near-concordant zircon from the lower part of Jamison sandstone yielded an age of 1050 ± 34 Ma ($^{206}Pb/^{238}U$) from drill hole Elliott-1.

Formation	Sample Name	Drillhole	Number of near concordant Analyses	Age peak (Ma)
upper Jamison sst.	W-UJ9	Walton-2	64	1143, 1580
	A-UJ1	Altree-2	47	1120, 1500, 1593
	A-UJ2	Altree-2	73	1151, 1540, 1600
	J-UJ3	Jamison-1	83	1198, 1600
lower Jamison sst.	E-LJ2	Elliott-1	66	1592
	M-LJ3	McManus-1	32	1590, 1613
Kyalla Fm.	BirC-Ky1	Birdum Creek-1	48	1748
	J-Ky8	Jamison-1	51	1705, 1740, 1810
	E-Ky7	Elliott-1	102	1710, 1813
Moroak Sst.	E-Mo13	Elliott-1	83	1552, 1703, 2386
	J-Mo13	Jamison-1	43	1573, 1720
	M-Mo8	McManus-1	22	1576, 1750
	M-Mo11	McManus-1	18	1604, 1735
Velkerri Fm.	E-Vel18	Elliott-1	50	1600, 1690, 1796
Bessie Creek Sst.	S-BC1	Sever-1	90	1719, 1830
	W-BC1	Walton-2	74	1725,1826
	A-BC13	Altree-2	53	1510, 1617, 1706

Table 2. Summary of results for samples collected for this study from Beetaloo Sub-basin drill cores.

Four samples from the upper Jamison sandstone show equivalent age distributions. Eighty-three near-concordant analyses of sample J-UJ3 yielded an age spread in the range 1866—1066 Ma, with a major peak at ca. 1602 Ma and a board minor cluster from 1210 Ma to 1100 Ma (Figure 4). Sample W-UJ9 also yielded a broad age spread in the range 1778—1051 Ma, with a kernel density distribution age peaks at ca. 1563 Ma and ca. 1160 Ma (Figure 4). Forty-seven concordant analyses from sample A-UJ1 range from 2402 Ma to 1068 Ma with maxima at ca. 1133 Ma, ca. 1503 Ma and ca. 1585 Ma (Figure 4). Sample A-UJ2, collected from ten metres below A-UJ1, yielded a spread of ages in the range 2455—959 Ma with three age maxima at ca. 1155 Ma, ca.

1543 Ma and ca. 1600 Ma (Figure 4). In terms of the upper Jamison sandstone, the youngest near-concordant zircon yielded an age of 959 ± 18 Ma ($^{206}Pb/^{238}U$) from drill hole Altree-2.

5. Discussion

5.1. Constraints on Deposition

The Derim Derim Dolerite, which has a SHRIMP U–Pb baddeleyite age of 1324 ± 4 Ma, is reported to intrude all Maiwok Subgroup formations in the Urapunga region (except the Chambers River Formation, Figures1B and 5), which provides a minimum constraint for the time of depositional of the Bessie Creek Sandstone, Velkerri Formation, Moroak Sandstone and the Kyalla Formation (*Abbott et al., 2001*), although cautioning that the age is not from the Beetaloo Sub-basin and the standard deviation level of the error is uncertain. *Whelan et al (2016)* reported a similar SIMS U–Pb baddeleyite age of 1325 ± 36 Ma (2σ) for the Galiwinku Dolerite in the northern margin of McArthur Basin. An additional dolerite intrusion with a younger SHRIMP U–Pb baddeleyite age of 1294 ± 14 Ma has also been reported from the Tomkinson Province in the Tennant Creek region (*Melville, 2010*), suggesting that there may be a range of ages of dolerite intrusions through the region.

Three Bessie Creek Sandstone samples were analysed. A single, youngest, 98% concordant analysis with a $^{206}Pb/^{238}U$ age of 1386 ± 13 Ma constitutes a maximum age constraint for the time of deposition of this formation (Figure 5). This age overlaps (in 2 sigma error) with the youngest near-concordant U–Pb zircon analysis (1385 ± 116 Ma, $^{207}Pb/^{206}Pb$ age, 100% concordant) from the Urapunga region sample (*Munson, 2016b*).

The maximum depositional age for the Velkerri Formation is 1308 ± 41 Ma, which is within error of the Derim Derim Dolerite (1324 ± 4 Ma; Abbott et al., 2001). This constrains the Velkerri Formation to have been deposited between 1349 Ma and 1320 Ma (Figure 5). This age range also overlaps the Re-Os age of 1361 ± 21 Ma from the upper Velkerri Formation (*Kendall et al., 2009*) (Figure 5).

The youngest >95% concordant analysis of Moroak Sandstone from sample J-Mo13 has a $^{207}Pb/^{206}Pb$ age of 1404 ± 28 Ma (98% concordant). However, this age is older than the maximum age constraint for the time of deposition of the Velkerri Formation, so the Moroak Sandstone Formation is stratigraphically constrained to being deposited between 1345 Ma and 1320 Ma (Figure 5).

The three Kyalla Formation samples are dominated by zircons of late Palaeoproterozoic ages. The youngest near-concordant $^{207}Pb/^{206}Pb$ ages of each of the samples E-Ky7, J-Ky8 and BirC-Ky1, are

of 1313 ± 47 Ma (99% concordant), 1324 ± 59 Ma (96% concordant), and 1400 ± 43 Ma (100% concordant), respectively. The 1313 ± 47 Ma (99% concordant), the youngest with >95% concordance, is used as the maximum age constraint of this formation (Figure 5).

Two samples from the lower Jamison sandstone, E-LJ2 and M-LJ3, yield a youngest >95% concordant $^{206}Pb/^{238}U$ age of 1092 ± 16 Ma (96% concordant), which is used to constrain the maximum age constraint for the time of deposition of this formation (Figure 5). The upper Jamison sandstone samples have relatively abundant 1000–1200 Ma detritus. A single grain, with the youngest >95% concordant $^{206}Pb/^{238}U$ age of 959 ± 18 Ma (97% concordant), from the sample A-UJ2, is used as the maximum age constraint for the time of deposition of this formation (Figure 5).

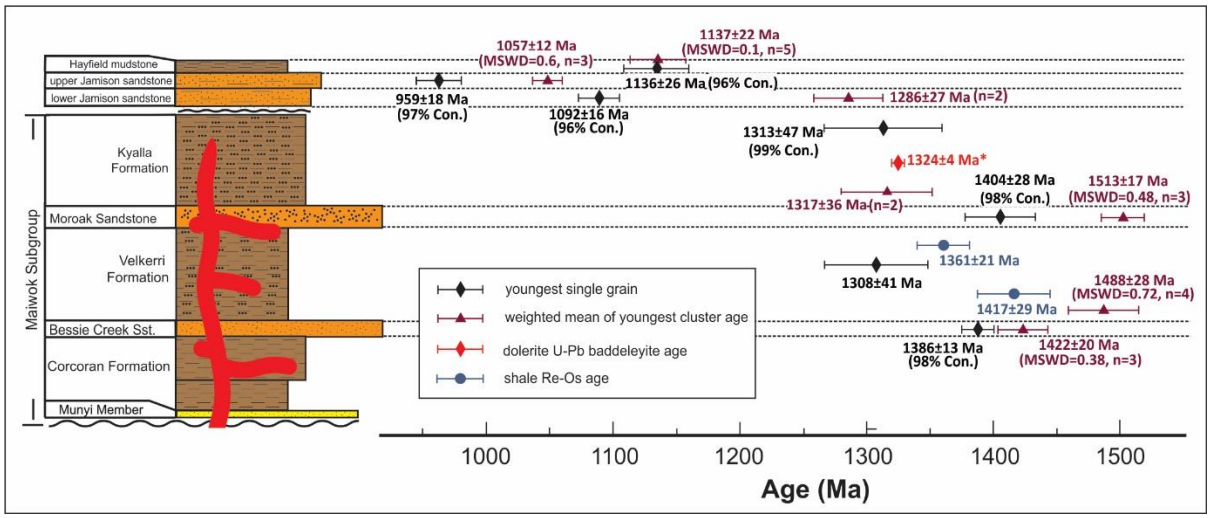

Figure 5 Age constraints for the stratigraphy of the study area (error bars are of 2 sigma error). Dolerite U–Pb SHRIMP baddeleyite age from *Abbott et al. (2001)*. Re-Os ages for the Velkerri Formation from *Kendall et al. (2009)*.

5.2. Multidimensional Scaling and Sample Comparison

In Figure 6a, seventeen samples from this research, and additional seven after *Fanning (2012)* and *Munson et al. (2016)*, are plotted together. Three distinct groups are identified, comprising all the Maiwok Subgroup samples (both the Beetaloo Sub-basin and Urapunga region samples), a lower Jamison sandstone group and an upper Jamison sandstone—Hayfield mudstone group.

Samples from the same formation are grouped together, except the Bessie Creek Sandstone samples and samples from the Urapunga region, which suggests that spatial variation exists. This regionalism is shown by the similar location of the three Urapunga samples, one from each of the Bessie Creek Sandstone sample (MY14TJM0002), the Moroak Sandstone (UR14TJM0026) and the Bukalorkmi Sandstone (UR14TJM0006A), on the MDS plot (Figure 6a). The Moroak Sandstone sample from the Urapunga region (UR14TJM0026) shows little similarity with the

Beetaloo Sub-basin Moroak Sandstone samples (M-Mo18, M-Mo11, J-Mo13 and E-Mo13; Figure 6a). This variation suggests that the Urapunga and Beetaloo Sub-basin depositional areas were likely to have been separated prior to, and during, deposition of the Moroak Sandstone, perhaps by the intervening fault-related Walton High and/or Mallapunyah Fault Zone forming a bathymetric/topographic high at the time, resulting in separate source areas and sediment pathways for these two depositional areas. The different Bessie Creek Sandstone age distributions may also be related to the Walton High (as a bathymetric boundary), the southern margin of which is close to both the Walton-2 and Altree-2 wells (Figure 1a). The Walton-2 Bessie Creek Sandstone sample (W-BC1) is similar to the 'northern' samples (from the Urapunga region and drill hole Sever-1: sample MY14TJM0002 and S-BC1), whereas the Altree-2 sample (A-BC13) forms an 'end-member' of a Beetaloo Sub-basin trend that forms a progression in stratigraphic order, through the Velkerri Formation, the Moroak Sandstone Formation and the Kyalla Formation, suggesting a gradual evolution in age provenance up-section. This stops with the unconformably overlying Jamison sandstone and Hayfield mudstone, which have a distinctly different provenance that marks a major change in the basin evolution, as discussed in the next section.

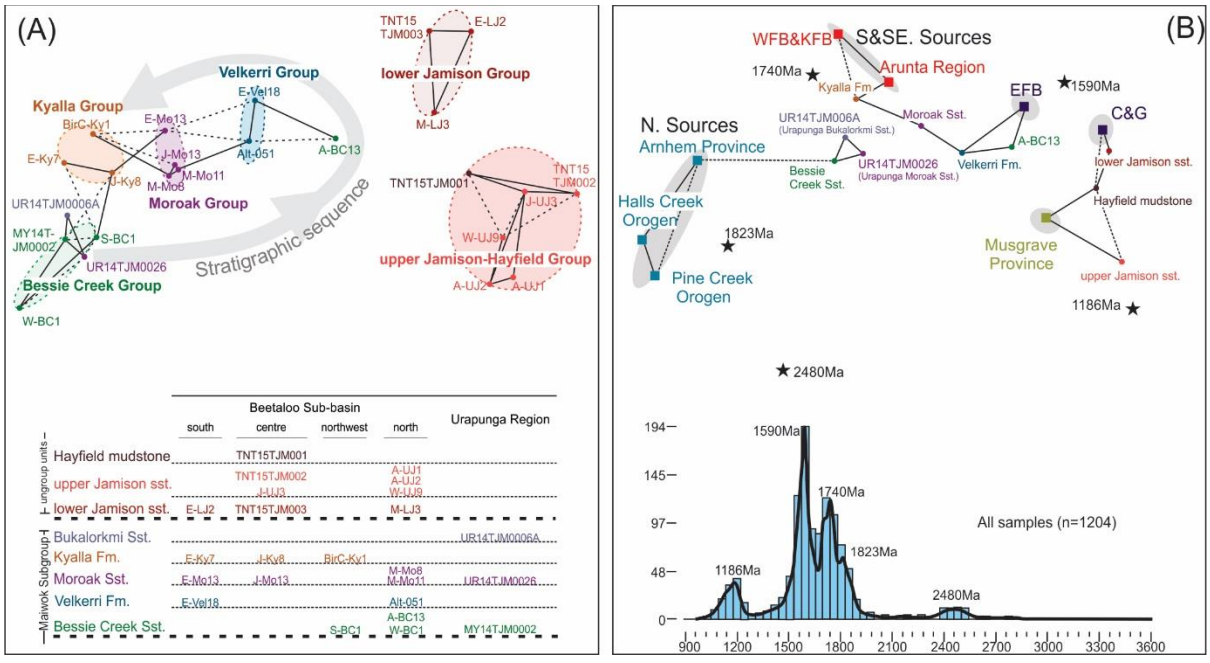

Figure 6 (A) Multidimensional scaling (MDS) plot of sedimentary samples from Beetaloo Sub-basin (this study; *Fanning, 2012*) and Urapunga region (*Munson, (2018)*). Samples with lowest dissimilarity values are plotted closest to one another; solid lines and dashed lines indicate closest and second-closest neighbours respectively (see *Vermeesch, 2013*). Maiwok Subgroup samples cluster together; Velkerri Formation, Moroak Sandstone and Kyalla Formation samples show a progression (arrows) in stratigraphic order. Lower and upper Jamison sandstone and Hayfield mudstone samples are separated into two clusters and show a considerable difference from Maiwok

Subgroup. (B) Multidimensional scaling (MDS) plot of sedimentary samples and potential source areas (shaded), and Kernel distribution estimate (KDE) of combined samples of this research. Dark stars represent detrital zircon age peaks revealed by the combined KDE. Maiwok Subgroup samples show mixed detrital ages of ca. 1590 Ma, 1740 Ma and 1823 Ma and plot between southern–southeastern sources, eastern sources and northern sources. Lower and upper Jamison sandstone samples plots between ca. 1186 Ma and 1590 Ma sources; both share similarities with Musgrave Province. WFB – Western Fold Belt; KFB – Kathleen Fold Belt; EFB – Eastern Fold Belt; C&G – Coen and Georgetown provinces. Published potential source areas data are collected from the Arnhem Province (*Kositcin et al., 2015a*); Pine Creek Orogen (*Worden et al., 2006a, b, 2008; Carson et al., 2009; Hollis et al., 2010; Kositcin et al., 2013a; Beyer et al., 2013*); Halls Creek Orogen (*Worden et al., 2008; Hollis et al., 2014*); the Arunta Region (*Cross et al., 2005a, b, c ; Worden et al., 2006a, b, 2008; Carson et al., 2009; Hollis et al., 2010; Bodorkos et al., 2013; Kositcin et al., 2013a, b; 2014a, b; 2015b; Beyer et al., 2013, 2015, 2016*); Mount Isa Province (*Page & Sun 1998; Neumann et al, 2006, 2009; Cross et al., 2015*); the Coen and Georgetown Provinces (*Blewett et al., 1998; Hoskin & Black 2000; Kositcin et al., 2009*); the Musgrave Province (*Wade, 2006; Smits et al., 2014*).

5.3. Provenance Analysis

Although the upper Jamison sandstone samples and lower Jamison sandstone analyses form two distinct clusters in Figure 6a, there are considerable distances between the individual analyses in the MDS plot. This is because that the K-S test is very sensitive to young age, small volume age cluster. A small variation of the younger age proportion can cause large changes in the cumulative curve plot then lead to large D-Values in the K-S test (this can be visualised in Figure 7b). In order to minimise this bias, samples from the same formation are merged and plotted in figures 6B and 8. The geographically isolated samples (sample A-BC13, UR14TJM0026), separated by bathymetric/topographic highs, are kept separate to illustrate the spatial provenance variation.

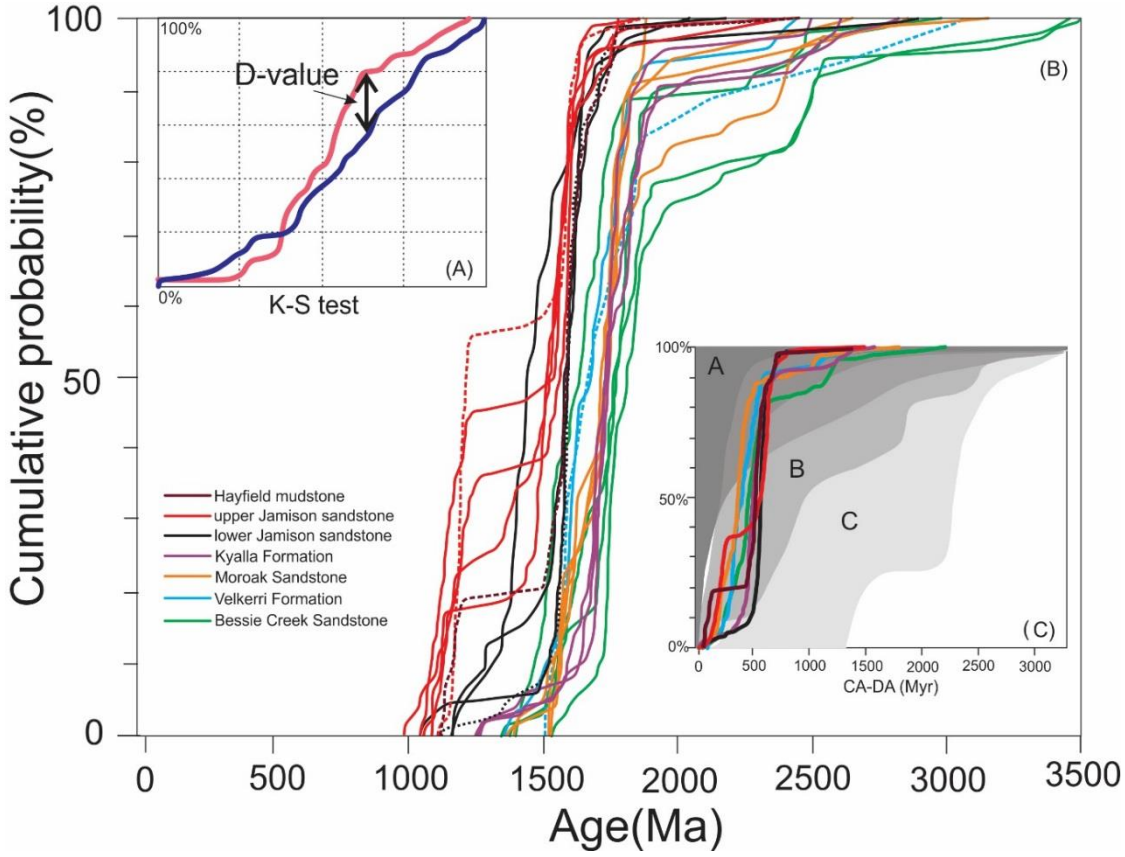

Figure 7: Cumulative frequency curves. (A) Example showing how D-value (dissimilarity between two age distributions) is measured based on Kolmogorov-Smirnov test (K-S test; *Vermeesh, 2013*). (B) Cumulative frequency curves for all upper Roper Group and Jamison sandstone samples from the Beetaloo Sub-basin. (C) Cumulative frequency curves for each formation, normalised to their interpreted depositional age (the time span of zircon from crystallisation to deposition), following *Cawood et al. (2012)*. A-convergent setting filed; B-collisional setting field; C-extensional setting field; CA-crystallisation age; DA-depositional age. Dash lines are Beetaloo Sub-basin samples from *Munson (2018)* and *Fanning (2012)*.

In this study, coupled Multidimensional Scaling (MDS) and Kernel Distribution Estimate (KDE) plots are used in conjunction, in order to limit inaccuracy caused by the MDS and enhance spatial analysis beyond the KDE method (Figures 6b and 8). Published igneous zircon U–Pb ages (LA-ICP-MS and SHRIMP data) from potential source regions that surround the Beetaloo Sub-basin were also collected and used in the MDS analysis (Figures 6b and 8). These potential source areas are the Arnhem Province, Pine Creek Orogen and Halls Creek Orogen in the north, the Arunta Region and Mount Isa Province in the south and southeast, the Coen and Georgetown provinces in the far-east and the Musgrave Province in the far south. Note that the Eastern Fold Belt (EFB), and the Western Fold Belt and Kathleen Fold Belt (WFB&KFB) from the Mount Isa Province are treated as two individual units, as they have different tectonic histories and age distributions (Figures 8 and 9; e.g. *Page & Sun, 1998; Betts & Giles, 2006; Neumann et al, 2006, 2009; Duncan et al, 2006; Bierlein et al, 2011*). This approach examines different regions as sources for different

parts of the basin and at different times. To look at provenance slightly differently, we also wanted to examine possible variations in age-sources in space and time. To do this, we followed *Spencer & Kirkland (2016)*, by plotting the main age peaks from a kernel distribution estimate (KDE) of all samples in the MDS plot (Figure 6b).

In figure 6B, all Maiwok Subgroup formations (and samples), including samples from the Urapunga region (*Munson et al., 2016*), plotted between the Arunta Region, Mount Isa Province, Coen Province, Georgetown Province, Halls Creek Orogen, Arnhem Province and Pine Creek Orogen, which demonstrates that they consist of mixed detrital ages that cluster at ca. 1590 Ma, ca. 1740 Ma and ca. 1823 Ma. These suggest that multiple source areas contributed to the sedimentary succession. Specifically, the northern (and western) samples (Bessie Creek Sandstone sample group, UR14TJM0026 and UR14TJM006A) plotted closer to the northern and western source areas including the Halls Creek Orogen, Arnhem Province and Pine Creek Orogen, and particularly showed considerable influence of the ca. 1823 Ma, and to a lesser extent, the ca. 2480 Ma, sources (Figures 6b and 8). The remaining Maiwok Subgroup samples from the Beetaloo Sub-basin show a distinct trend of changing provenance with time. Samples from older units plot in areas that indicate derivation from ca. 1590 Ma sources consistent with the Eastern Fold Belt of Mount Isa, but up-section, the influence of these sources is lessened and more ca. 1740 Ma detritus is seen, consistent with sources in the Western and Kathleen Fold Belts (Figures 6b and 8), but more particularly, with sources from the southern Arunta Region. The lower and upper Jamison sandstone and Hayfield mudstone sample group are plotted between the ca. 1186 Ma and ca. 1590 Ma sources and both share similarities with the Musgrave Province; the upper Jamison sandstone and the Hayfield mudstone are particularly rich in late Mesoproterozoic detritus (Figures 6b and 8).

Of the four main sandstone-dominated formations examined, the Bessie Creek Sandstone demonstrated a variable age provenance that appears to be strongly controlled by where the sample was collected; with Beetaloo Sub-basin samples preserving very different spectra from the Urapunga, Gorrie Sub-basin and Walton High samples (Figures 4 and 6a). The Moroak Sandstone preserves very similar age spectra in all the Beetaloo Sub-basin samples (Figures 4 and 6A), suggesting that uniform or low bathymetric relief was present in the sub-basin at the time of its formation. The lower Jamison sandstone lies unconformable on the Kyalla Formation at various stratigraphic levels except in Altree-2 and Walton-2, where it is unconformable on the Velkerri Formation (*Silverman & Ahlbrandt, 2011; Gorter & Grey, 2012; Munson, 2016a, b*). This is well reflected in the >200 Ma difference in the maximum depositional age between the Maiwok Subgroup samples and the lower Jamison sandstone. The overlying upper Jamison sandstone and

the Hayfield mudstone probably represent a gradual evolution of this latest Mesoproterozoic/earliest Neoproterozoic basin with increased Musgrave Province-derived sources.

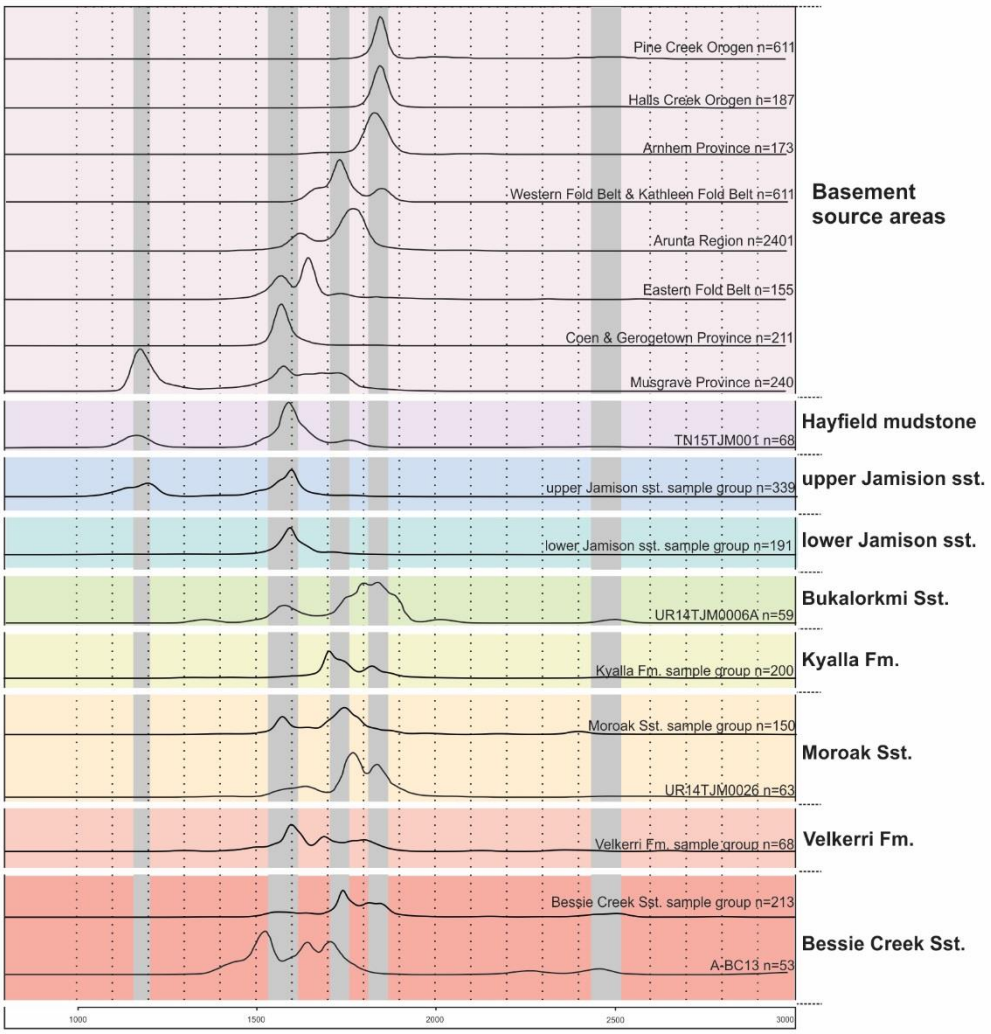

Figure 8 Kernel density estimation (KDE) plots of igneous zircon ages from potential source areas and detrital zircons ages from each pooled formation of the upper Roper Group and isolated samples collected for this study from Beetaloo Sub-basin drill cores. Samples prefixed by MY, UR and TN are from *Munson (2018)*. Grey columns are bands of equivalent concordia age range. Background colours are used to clarify different formations.

Cox et al. (2016) and *Muhkerjee & Large (2016)* both suggested that elemental and isotopic variations in the middle–upper Velkerri Formation represented increased nutrient input due to changing provenance up-section within the shale-dominated formation. *Cox et al. (2016)* used whole-rock major and trace elements along with Nd isotopes to suggest that this provenance change reflected a greater contribution of mafic material up-section, which reached a maximum in the middle Velkerri Formation. The coincident nutrient influx was suggested to have fed a bloom in bacteria that ultimately increased the total organic carbon content of the middle Velkerri Formation (*Cox et al., 2016*). Our data suggest show that the Velkerri Formation was

being deposited as zircon provenance changed from ca. 1590 Ma dominant sources to ca. 1740 Ma dominant sources between ca. 1400-1350 Ma. We suggest that this reflects the uplift and erosion of the Arunta region to the south as bathymetric variations were buried.

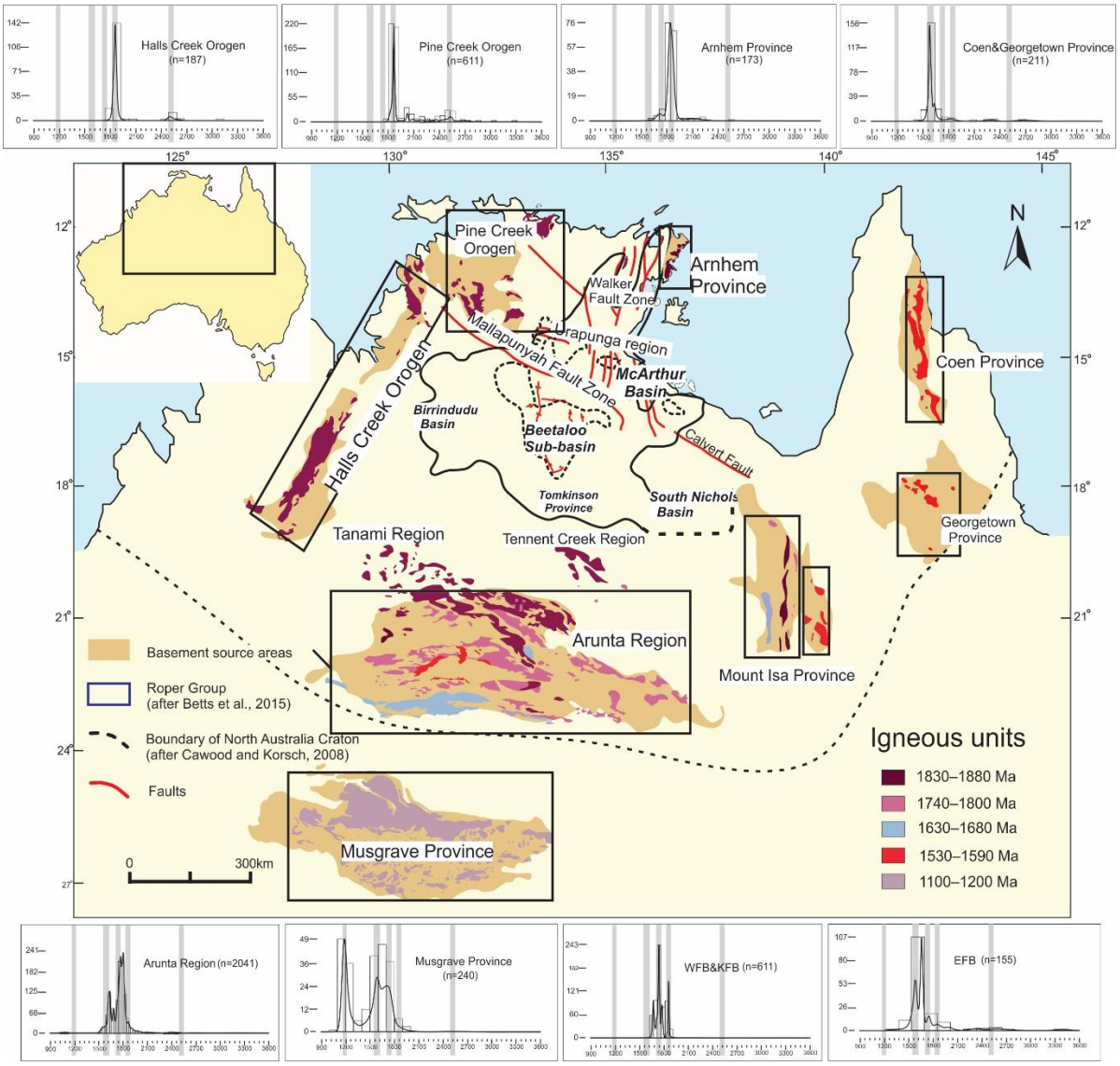

Figure 9 Distribution of igneous units and kernel density estimation (KDE) plots for potential source areas.

5.4. Tectonic Implications and Palaeogeography

The siliciclastic Roper Group was deposited in a stable shelf environment (*Abbott & Sweet, 2000; Betts & Giles, 2006; Munson, 2016b*), but different models exist as to the tectonic setting of the basin (*Jackson et al., 1999; Abbott & Sweet, 2000; Abbott et al., 2001; Munson 2016a, b; Revie, 2017*). Cumulative frequency plots of the time span between the age of detrital zircon crystallization and the inferred time of deposition (e.g. time from source to sink), were demonstrated by *Cawood et al. (2012)* to have characteristic patterns for different tectonic settings. In a plot of this type, the Maiwok Subgroup samples and the lower and upper Jamison

sandstone plot in a 'collisional setting' field (Figure 7c), with all Maiwok Subgroup samples initially trending in the 'extensional setting' field for the youngest 5-10% of data (Figure 7c). The upper Jamison sandstone and Hayfield mudstone have a noticeable population of near-depositional age zircon grains that make them approach the 'convergent setting' field (Figure 7c). This plot emphasises that all but the upper Jamison sandstone samples are dominated by detritus that derived from primary sources that are significantly older than formation of the basin (>>100 Myr). These data suggest that basin formation postdates active convergent tectonism in all cases except for the upper Jamison sandstone (Figure 7c). The provenance analysis in the previous section suggests that the Maiwok Subgroup detritus in the Beetaloo Sub-basin is mainly sourced from the south and east; from the Mount Isa Province and the Arunta Region (Figure 10). *Spikings et al. (2001, 2002)*, reported that post-orogenic exhumation of the Mount Isa Province happened between 1460 and 1390 Ma. This exhumation was fast (average cooling rate was ca. 4°C/My) and heterogeneous (regional cooling rate could reach up to 18°C/My in the Eastern Fold Belt). *Spikings et al. (2001, 2002)* also suggested that this event generated abundant detritus that filled the South Nicholson Basin. Similarly, *Foster & Ehlers (1998)* suggested that the eastern Gawler Craton also exhumed rapidly at about 1420 Ma, which was interpreted to be due to lithospheric extension. This exhumation also coincides with cooling after the ca. 1590–1560 Ma Chewings Orogeny of central Australia (*Shaw & Black, 1991*). *Mulder et al. (2015)* postulated that basin formation in the Rocky Cape Group of northwest Tasmania is associated with widespread rifting throughout eastern Proterozoic Australia. The timing of formation of the Maiwok Subgroup is broadly coeval with the constraints on deposition of the Rocky Cape Group (*Mulder et al., 2015*) and the Cariewerloo Basin of the Gawler Craton (*Flint, 1993*) and, when reconstructed on a palaeogeographic reconstruction using the rotated northern Australia model of *Li and Evans (2011)*, these depositional areas lie along the margin of Proterozoic Australia (Figure 10). We follow *Mulder et al. (2015)* and suggest that Mesoproterozoic basin formation occurred due to rifting between Proterozoic Australia and Laurentia. In this model, the lower Maiwok Subgroup (and presumably also the underlying Collara Subgroup) formed continent-ward of maximum rifting, which would be to the (present-day) east of Mount Isa, in an epicontinental setting.

The transition from dominantly ca. 1590 Ma sources to dominantly ca. 1740 Ma sources seen in the Maiwok Subgroup is interpreted here to be a transition from Mount Isa sources to Arunta sources from ca. 1400-1350 Ma. We suggest that this is due to the subduction of the Mesoproterozoic ocean that separated the West Australian Craton from the combined North Australian Craton and South Australian Craton (recently named the Mirning Ocean by *Kirkland*

et al., 2017; Figure 10). Previous workers have suggested that this collision occurred at ca. 1830-1765 Ma and is represented by the Yapungku Orogeny that is seen in the far east of the Pilbara, in the Rudall River region (*Bagas, 2004; Cawood & Korsch, 2008*). However, magmatism within the Tabletop Terrane, that forms the furthest east basement terrane in this region is dated between 1410-1350 Ma and is distinct from the more west terranes (*Kirkland et al., 2013*), and the Yapungku peak metamorphism has recently been redated at 1380-1275 Ma (*Anderson et al., 2016*), slightly older than the 1280-1250 Ma Mutherbukin Event in the Capricorn Orogen (*Johnson et al., 2013*). In the Western Musgraves, continental arc magmatism and subsequent deformation are dated at 1345-1293 Ma (the Mount West Orogeny) and further south, the newly reported Haig Cave Supersuite, buried beneath the Nullarbor Plain, and the Recherche Supersuite of the Fraser Range both represent subduction-related magmatism between 1415 and 1280 Ma (*Spaggiari et al., 2015; Kirkland et al., 2015; Kirkland et al., 2017*).The unconformity between the Kyalla Formation and the lower Jamison sandstone occurs after late Mesoproterozoic orogenesis in the Musgrave Province (*Kirkland et al., 2012*), after the subsequent emplacement of the ca. 1075 Ma Warakurna Large Igneous Province (*Wingate et al., 2004*) and coeval with voluminous exhumation of the Musgrave Province, the age of which has been determined from apatite fission track data to be in the range 1075–1025 Ma (*Glorie et al., 2017*). We suggest that the Jamison sandstone represents a long-wavelength foreland basin continent-ward of highlands generated after the amalgamation of the Australian part of the supercontinent Rodinia (*Merdith et al., 2017*) and as the Musgrave Province was exhumed (Figure 10c).

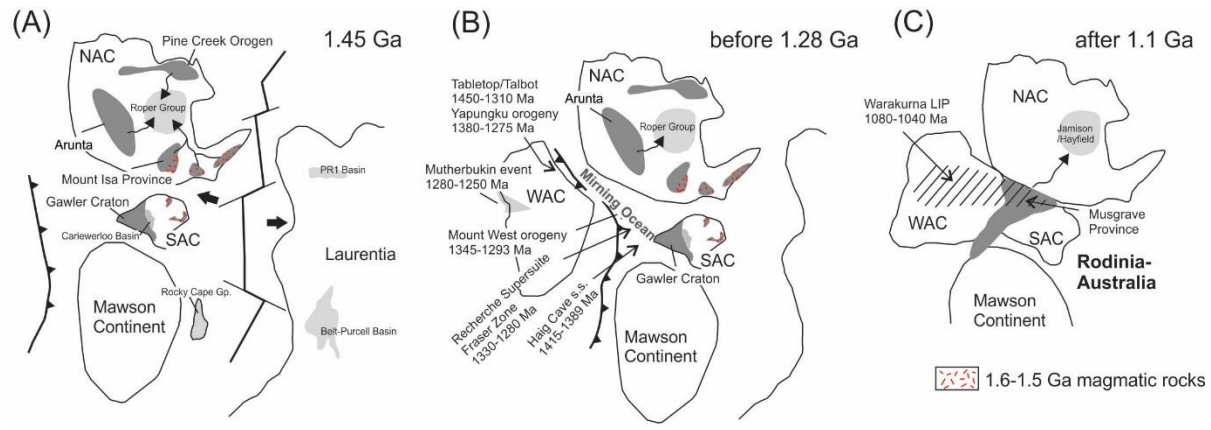

Figure 10 Tectonic scenario sketch showing deposition history of upper Roper Group and Jamison sandstone between ca. 1.45 Ga and after 1.1 Ga. (A) Separation of North Australia Craton and Laurentia, forming a series of extensional basins on both sides (modified after *Mulder et al., 2015*). (B) Collision between the West Australia Craton (WAC) and an already combined North Australia Craton (NAC) and South Australia Craton (SAC), uplifting and exposing the Arunta Region and allowing it to become a source for sands in Moroak and Kyalla Formations (modified after *Smits et al., 2014*). (C) Exhumation of the Musgrave Province after final amalgamation of the Australian part of Rodinia and emplacement of the Warakurna large igneous province (modified after *Li & Evans, 2011*).

Munson (2016a, b) and *Revie (2017)* suggested that the Wilton package was deposited in an enclosed marine environment. The basin was restricted or partly restricted by land or by chains of islands while retaining some connection with the open sea (*Munson, 2016a, b*). This model, to some extent, is consistent with the palaeography suggested by the results of this work, which shows that the Roper Group, at least from ca. 1450 Ma to 1320 Ma, was restricted by multiple sources to the south, east, and possibly west, whereas how far the basin extended in the open sea direction remains unknown (Figure 10a).

6. Conclusions

New detrital zircon data presented in this research provides constraints on the age, provenance and tectonic geography of the hydrocarbon-bearing upper Roper Group (Maiwok Subgroup). Coupled techniques of Multidimensional Scaling (MDS) and Kernel Distribution Estimate (KDE) enable a detailed spatial and temporal provenance analysis of the Beetaloo Sub-basin. This improves our understanding of the palaeotectonic geography and evolution history of the North Australia Craton through the late Mesoproterozoic and into the early Neoproterozoic. The main conclusions and suggestions of this research are:

1) The maximum depositional age of the Bessie Creek Sandstone is constrained at 1386 ± 13 Ma. The Velkerri Formation and overlying Moroak Sandstone are now constrained to being deposited between 1349 Ma and 1320 Ma, based on the youngest detrital zircon grains and assuming that the 1324 ± 4 Ma age for Derim Derim Dolerite is representative of the age of the sills in the Beetaloo Sub-basin. The maximum depositional age of the Kyalla Formation is constrained to 1313 ± 47 Ma by the youngest detrital zircon (taken from drill core Jamison-1). The maximum depositional age of the two ungrouped formations, the lower and upper Jamison sandstones, are constrained to 1092± 16 Ma and 959 ± 18 Ma, respectively.
2) Although spatial variation exists, the Bessie Creek Sandstone most likely consists of detritus that was sourced from the Mount Isa Province. The progressive increase in ca. 1740 Ma detritus from the Bessie Creek Formation through the Velkerri Formation and Moroak Formation to the Kyalla Formation is used to suggest the progressive influx of southern derived detritus from the Arunta region as subduction of the Mirning Ocean occurred in the middle Mesoproterozoic. Late Mesoproterozoic- to early Neoproterozoic-aged detritus of the lower and upper Jamison sandstone and the Hayfield mudstone, is interpreted to have been sourced from the Musgrave Province, as that region was exhumed after emplacement of the Warakurna Large Igneous Province,

suggesting a newly-recognised sandstone-rich basin that may have formed a shallow, long wavelength foreland basin to the Musgrave Orogeny.

3) Three provenance-changing events are recognised in the Maiwok Subgroup and Jamison sandstone. The first happened before deposition of the upper Velkerri Formation, possibly as the result of heterogeneous exhumation of the southern and southeastern regions of the North Australia Craton, due to rifting between Proterozoic Australia and Laurentia. The second event is interpreted to have been caused by the exhumation of the southern and southeastern margins of the North Australia Craton, resulting in uplifting of the Arunta Region, which swamped Mount Isa Province sources and became the major source for the Kyalla Formation. The last provenance shift happened during the late Mesoproterozoic to Tonian exhumation of the Musgrave Province.
4) U–Pb detrital zircon spectra suggest that the early part of the Maiwok Subgroup (at least) was deposited in a basin with significant bathymetry that caused spatial variation in the Bessie Creek Sandstone provenance. The Walton High, and/or the Mallapunyah Fault Zone, in particular, appear to have been a bathymetric high suggesting that these structures were active prior to, or during deposition of the lower Mawiok Subgroup.

Acknowledgements

This research was funded by the Northern Territory Geological Survey, SANTOS Ltd and an Australian Research Council Linkage Project LP160101353, which is partnered by the aforementioned organisations and Origin Energy. Todd Hoffman and Joel Alnes from Pangaea Resources Pty Ltd are thanked for allowing us to sample core from Birdum Creek-1 whilst the hole was still closed file. Jo Whelan and Eloise Beyer are thanked for their suggestions, which improved the manuscript. Uri Shaanan is acknowledged and thanked for the constructive comments that greatly improved the manuscript. The authors thank staff at Adelaide Microscopy for assisting with U–Pb data collection. ASC was funded by an ARC Future Fellowship FT120100340. This paper forms TRaX Record #391 and is a contribution to IGCP projects #628 and 648. TJM publishes with permission of the Executive Director, Northern Territory Geological Survey.

References

Abbott, S.T., Sweet, I.P., 2000. Tectonic control on third-order sequences in a siliciclastic ramp-style basin: An example from the Roper Superbasin (Mesoproterozoic), northern Australia. *Australian Journal of Earth Sciences* **47(3)**, 637-657.

Abbott, S.T., Sweet, I.P., Plumb, K. A., Young, D.N., Cutovinos, A., Ferenczi, P.A., Pietsch, B.A., 2001. Roper Region: Urapunga and Roper River Special, Northern Territory (Second Edition). 1:250 000 geological map series

explanatory notes, SD 53-10, 11. Northern Territory Geological Survey and Geoscience Australia (National Geoscience Mapping Accord).

Ahamad, M., Munson, T.J., 2013. Northern Territory Geological Survey, Geology and mineral resources of the Northern Territory, Special Publication 5. Northern Territory Geological Survey.

Allen, P.A., Eriksson, P.G., Alkmim, F.F., Betts, P.G., Catuneanu, O., Mazumder, R., Meng, Q, Young, G.M., 2015. Classification of basins, with special reference to Proterozoic examples. *Geological Society, London, Memoirs*, **43(1)**, 5-28.

Anderson, J.R., Kelsey, D.E., Hand, M., Collins, W.J., 2016. Mesoproterozoic metamorphism in the Rudall Province: revising the timeline of the Yapungku Orogeny and implications for cratonic Australia assembly. *AESC 2016 – Australian Earth Sciences Convention abstract volume*, 227.

Arboit, F., Collins, A.S., Morley, C.K., King, R., Amrouch, K., 2016. Detrital zircon analysis of the southwest Indochina terrane, central Thailand: Unravelling the Indosinian orogeny. *Geological Society of America Bulletin*, **128(5-6)**, 1024-1043.

Bagas, L., 2004. Proterozoic evolution and tectonic setting of the northwest Paterson Orogen, Western Australia. *Precambrian Research*, **128**, 475–496.

Betts, P.G., Giles, D., 2006. The 1800–1100 Ma tectonic evolution of Australia. *Precambrian Research*, **144(1)**, 92-125.

Betts, P.G., Armit, R.J, Ailleres, L., 2015. Potential-field interpretation mapping of the greater McArthur Basin. PGN Geoscience Report 15/2014: in 'Geophysical and structural interpretation of the greater McArthur Basin'. *Northern Territory Geological Survey, Digital Information Package DIP 015*.

Beyer, E.E., Hollis, J.A., Whelan, J.A., Glass, L.M., Donnellan, N., Yaxley, G., Armstrong, R., Allen, C., Scherstén, A., 2013. Summary of results. NTGS laser ablation ICPMS and SHRIMP U-Pb, Hf and O geochronology project: Pine Creek Orogen, Arunta Region, Georgina Basin and McArthur Basin, July 2008–May 2011. *Northern Territory Geological Survey, Record 2012-007*.

Beyer, E.E., Allen, C.M., Armstrong, R., Woodhead, J.D., 2015. Summary of results. NTGS laser ablation ICPMS U-Pb and Hf geochronology project: selected samples from NAPPERBY 1:250 000 mapsheet area, Arunta Region, July 2010–January 2012. *Northern Territory Geological Survey, Record 2015-009*.

Beyer, E.E., Donnellan, N., Meffre, S., Thompson, J.M., 2016. Summary of results. NTGS laser ablation ICP-MS in situ zircon and baddeleyite geochronology project: Mount Peake Gabbro, Arunta Region. *Northern Territory Geological Survey, Record 2016-002*.

Bierlein, F.P., Maas, R., Woodhead, J., 2011. Pre-1.8 Ga tectono-magmatic evolution of the Kalkadoon–Leichhardt Belt: implications for the crustal architecture and metallogeny of the Mount Isa Inlier, northwest Queensland, Australia. *Australian Journal of Earth Sciences*, **58(8)**, 887-915.

Blewett, R.S., Black, L.P., Sun, S.S., Knutson, J., Hutton, L.J., Bain, J.H.C., 1998. "U-Pb zircon and Sm-Nd geochronology of the Mesoproterozoic of North Queensland: implications for a Rodinian connection with the Belt supergroup of North America." *Precambrian Research*, **89**, 101-127.

Bodorkos, S., Beyer, E.E., Edgoose, C.J., Whelan, J.A., Webb, G., Vandenberg, L.C., Hallett, L., 2013. Summary of results. Joint NTGS–GA geochronology project: Central and eastern Arunta Region, January 2008 – June 2011. *Northern Territory Geological Survey, Record 2013-003*.

Carson, C.J., Claoué-Long, J., Stern, R., Close, D.F., Scrimgeour, I.R., Glass, L.M., 2009. Summary of results. Joint NTGS-GA geochronology project: Central and eastern Arunta Region and Pine Creek Orogen, July 2006–May 2007. *Northern Territory Geological Survey, Record 2009-001*.

Cawood, P.A., Korsch, R.J., 2008. Assembling Australia: Proterozoic building of a continent. *Precambrian Research*, **166(1)**, 1-35.

Cawood, P.A., Hawksworth, C.J., Dhuime, B., 2012. Detrital zircon record and tectonic setting. *Geology*, **40(10)**, 875-878.

Close, D.F., 2014. The McArthur Basin: NTGS ' approach to a frontier petroleum basin with known base metal prospectivity. *Annual Geoscience Exploration Seminar (AGES) Proceedings, Alice Springs, Northern Territory 15–16 March 2016*. Northern Territory Geological Survey, Darwin. pp. 85–89.

Close, D.I., Cote, A.J., Baruch, E.T., Altmann, C.M., Mohinudeen, F.M., Richards, B., Ilett, R., 2017. Proterozoic shale gas plays in the Beetaloo Basin and the Amungee NW-1H discovery. *Annual Geoscience Exploration Seminar (AGES) Proceedings, Alice Springs, Northern Territory 28–29 March 2017*. Northern Territory Geological Survey, Darwin. pp. 91-97.

Collins, A.S., Patranabis-Deb, S., Alexander, E., Bertram, C.N., Falster, G.M., Gore, R.J., Jourdan, F., 2015. Detrital mineral age, radiogenic isotopic stratigraphy and tectonic significance of the Cuddapah Basin, India. *Gondwana Research*, ***28*(4)**, 1294-1309.

Cox, G.M., Jarrett, A., Edwards, D., Crockford, P.W., Halverson, G.P., Collins, A.S., Li, Z.X., 2016. Basin redox and primary productivity within the Mesoproterozoic Roper Seaway. *Chemical Geology*, **440**, 101-114.

Cross, A.J., Claoué-Long, J.C., Scrimgeour, I.R., Close, D.F., Edgoose, C.J., 2005. Summary of results. Joint NTGS-GA geochronology project: southern Arunta Region. *Northern Territory Geological Survey, Record 2004-003*.

Cross, A.J., Claoué-Long, J.C., Scrimgeour, I.R., Crispe, A., Donnellan, N., 2005. Summary of results. Joint NTGS-GA geochronology project: northern Arunta and Tanami regions, 2000–2003. *Northern Territory Geological Survey, Record 2005-003*.

Cross, A.J., Claoué-Long, J.C., Scrimgeour, I.R., Ahmad, M., Kruse, P.D., 2005. Summary of results. Joint NTGS-GA geochronology project: Rum Jungle, basement to southern Georgina Basin and eastern Arunta Region 2001–2003. *Northern Territory Geological Survey, Record 2005-006*.

Cross, A.J., Purdy, D.J., Bultitude, R.J., Brown, D.D., Carr, P.A., 2015. Summary of results. Joint GSQ–GA geochronology project: Thomson Orogen, New England Orogen, Mossman Orogen and Mount Isa region, 2011–2013. *Queensland Geological Record 2016/03*.

De Vries, S.T., Fry, N., Pryer, L.L., 2006. OZ SEEBASE™ Proterozoic basins study. Report to Geoscience Australia and consortium partners by FrOG Tech Pty Ltd. Public domain GIS and report.

Dickinson, W.R., Gehrels, G.E., 2009. Use of U–Pb ages of detrital zircons to infer maximum depositional ages of strata: a test against a Colorado Plateau Mesozoic database. *Earth and Planetary Science Letters*, **288(1)**, 115-125.

Donnelly, T.H., Crick, I.H., 1988. Depositional environment of the middle Proterozoic Velkerri Formation in northern Australia: geochemical evidence. *Precambrian research*, **42(1-2)**, 165-172.

Duncan, R.J., Wilde, A.R., Bassano, K., Maas, R., 2006. Geochronological constraints on tourmaline formation in the Western Fold Belt of the Mount Isa Inlier, Australia: Evidence for large-scale metamorphism at 1.57 Ga?. *Precambrian Research*, **146(3)**, 120-137.

Fanning, C.M., 2012. SHRIMP U-Pb zircon age determinations on detrital zircons from drill core sample ALT-051. ANU Research School of Earth Sciences, PRISE Report 12-260. Esso Australia. *Northern Territory Geological Survey, Core Sampling Report CSR0211*.

Flint, R.B., 1993. Mesoproterozoic. In: DREXEL, J.F., PREISS, W.V., PARKER A.J. (eds.). The Geology of South Australia, Volume 1, The Precambrian. Bulletin – Geological Survey of South Australia, Adelaide, pp. 107-169.

Foster, D.A., Ehlers, K., 1998. ^{40}Ar-^{39}Ar thermochronology of the southern Gawler Craton, Australia: Implications for Mesoproterozoic and Neoproterozoic tectonics of East Gondwana and Rodinia. *Journal of Geophysical Research: Solid Earth*, **103(B5)**, 10177-10193.

Gehrels, G., Valencia, V., Pullen, A., 2006. Detrital zircon geochronology by laser-ablation multicollector ICPMS at the Arizona LaserChron Center. *Paleontological Society Papers*, **12**, 67.

Gehrels, G., Valencia, V., Ruiz, J., 2008. Enhanced precision, accuracy, efficiency, and spatial resolution of U-Pb ages by laser ablation–multicollector–inductively coupled plasma–mass spectrometry. *Geochemistry, Geophysics, Geosystems*, **9(3)**.

Gehrels, G., 2014. Detrital zircon U-Pb geochronology applied to tectonics. *Annual Review of Earth and Planetary Sciences*, **42**, 127-149.

Glorie, S., Agostino, K., Dutch, R., Pawley, M., Hall, J., Danišik, M., Evans, N.J., Collins, A.S., 2017. Thermal history and differential exhumation across the Eastern Musgrave Province, South Australia: Insights from low-temperature thermochronology. *Tectonophysics*, in press.

Gorter, J.D., Grey, K., 2012. Middle Proterozoic biostratigraphy and log correlations of the Kyalla and Chambers River Formations Beetaloo Sub-basin, Northern Territory, Australia. Central Australian Basins Symposium (CABS) III. Poster. *Petroleum Exploration Society of Australia*.

Hollis, J.A., Beyer, E.E., Whelan, J.A., Kemp, A.I.S., Scherstén, A., Greig, A., 2010. Summary of results. NTGS laser U-Pb and Hf geochronology project: Pine Creek Orogen, Murphy Inlier, McArthur Basin and Arunta Region, July 2007–June 2008. *Northern Territory Geological Survey, Record 2010-001*.

Hoffman, T.W., 2015. Recent drilling results provide new insights into the western Palaeoproterozoic to Mesoproterozoic McArthur Basin. in 'Annual Geoscience Exploration Seminar (AGES) 2015. Record of abstracts'. *Northern Territory Geological Survey, Record (Vol. 2, pp. 50-55)*.

Horton, F., 2015. Did phosphorus derived from the weathering of large igneous provinces fertilize the Neoproterozoic ocean? *Geochemistry, Geophysics, Geosystems*, **16**, 1723–1738.

Hoskin, P.W.O., Black, L.P., 2000. Metamorphic zircon formation by solid-state recrystallization of protolith igneous zircon. *Journal of metamorphic Geology*, **18(4)**, 423-439.

Jackson, M.J., Muir, M.D., Plumb, K.A., 1987. Geology of the southern McArthur Basin, Northern Territory (Vol. 220). *Australian Government Publishing Service*.

Jackson, M.J., Sweet, I.P., Powell, T.G., 1988. Studies on petroleum geology and geochemistry, middle Proterozoic, McArthur Basin Northern Australia I: Petroleum potential. *APEA J*, **28(1)**, 283-302.

Jackson, M.J., Sweet, I.P., Page, R.W., Bradshaw, B.E., 1999. The South Nicholson and Roper Groups: evidence for the early Mesoproterozoic Roper Superbasin. *Integrated Basin Analysis of the Isa Superbasin using Seismic, Well-log, and Geopotential Data: An Evaluation of the Economic Potential of the Northern Lawn Hill Platform: Canberra, Australia, Australian Geological Survey Organisation Record, 19*.

Jackson, M.J., Southgate, P.N., 2000. Evolution of three unconformity-bounded sandy carbonate successions in the McArthur River region of northern Australia: the Lawn, Wide and Doom Supersequences in a proximal part of the Isa Basin. In: Cockbain A. E. ed. Carpentaria-Mt Isa Zinc Belt: basement framework, chronostratigraphy and geodynamic evolution of Proterozoic successions (thematic issue). *Australian Journal of Earth Sciences*, **47**, 625-635.

Jackson, S.E., Pearson, N.J., Griffin, W.L., Belousova, E.A., 2004. The application of laser ablation-inductively coupled plasma-mass spectrometry to in situ U–Pb zircon geochronology. *Chemical Geology*, **211(1)**, 47-69.

Johnson, S.P., Thorne, A.M., Tyler, I.M., Korsch, R.J., Kennett, B.L.N., Cutten, H.N., Goodwin, J., Blay, O., Blewett, R.S., Joly, A., Dentith, M.C., Aitken, A.R.A., Holzschuh, J., Salmon, M., Reading, A., Heinson, G., Boren, G., Ross, J., Costelloe, R.D., Fomin, T., 2013. Crustal architecture of the Capricorn Orogen, Western Australia and associated metallogeny. *Australian Journal of Earth Sciences*, **60**, 681–705.

Johnson, T.E., Kirkland, C.L., Reddy, S.M., Evans, N.J., Mcdonald, B.J., 2016. The source of Dalradian detritus in the Buchan Block, NE Scotland: application of new tools to detrital datasets. *Journal of the Geological Society*, jgs2016-019.

Kendall, B., Creaser, R.A., Gordon, G.W., Anbar, A.D., 2009. Re–Os and Mo isotope systematics of black shales from the Middle Proterozoic Velkerri and Wollogorang formations, McArthur Basin, northern Australia. *Geochimica et Cosmochimica Acta*, **73(9)**, 2534-2558.

Kirkland, C.L., Smithies, R.H., Woodhouse, A., Wingate, M., Howard, H.M., Belousova, E., 2012. A multi-isotopic approach to the crustal evolution of the west Musgrave Province. *In GSWA 2012 Extended Abstracts: promoting the prospectivity of Western Australia, 30-31: Geological Survey of Western Australia.*

Kirkland, C.L., Johnson, S.P., Smithies, R.H., Hollis, J.A., Wingate, M.T.D., Tyler, I.M., Hickman, A.H., Cliff, J.B., Tessalina, S., Belousova, E.A., Murphy, R.C., 2013. Not-so-suspect terrane: Constraints on the crustal evolution of the Rudall Province. *Precambrian Research*, **235**, 131-149.

Kirkland, C.L., Smithies, R.H., Spaggiari, C.V., 2015. Foreign contemporaries – Unravelling disparate isotopic signatures from Mesoproterozoic Central and Western Australia. *Precambrian Research*, **265**, 218-231.

Kirkland, C.L., Smithies, R.H., Spaggiari, C.V., Wingate, M.T.D., Quentin de Gromard, R., Clark, C., Gardiner, N.J., Belousova, E.A., 2017. Proterozoic crustal evolution of the Eucla basement, Australia: Implications for destruction of oceanic crust during emergence of Nuna. *Lithos*, **278-281**, 427-444.

Kositcin, N., Champion, D.C., Huston, D.L., 2009. Geodynamic Synthesis of the North Queensland Region and Implications for Metallogeny. *Geoscience Australia Record 2009/30*, pp 196.

Kositcin, N., Carson, C.J., Hollis, J.A., Glass, L.M., Close, D.F., Whelan, J.A., Webb, G., Donnellan, N., 2013. Summary of results. Joint NTGS–GA geochronology project: Arunta Region, Davenport Province and Pine Creek Orogen July 2009 – June 2011. *Northern Territory Geological Survey, Record 2012-008*.

Kositcin, N., Beyer, E.E., Whelan, J.A., Close, D.F., Hallett, L., Dunkley, D.J., 2013. Summary of results. Joint NTGS–GA geochronology project: Arunta Region, Ngalia Basin, Tanami Region and Murphy Province, July 2011–June 2012. *Northern Territory Geological Survey, Record 2013-004*.

Kositcin, N., Whelan, J.A., Hallett, L., Beyer, E.E., 2014. Summary of results. Joint NTGS–GA geochronology project: Amadeus Basin, Arunta Region and Murphy Province, July 2012–June 2013. *Northern Territory Geological Survey, Record 2014-005*.

Kositcin, N., Beyer, E.E., Whelan, J.A., 2014. Summary of results. Joint NTGS–GA SHRIMP geochronology project: Arunta Region, July 2013–June 2014. *Northern Territory Geological Survey, Record 2014 -008*.

Kositcin, N., Kraus, S., Whelan, J.A., 2015. Summary of results. Joint NTGS–GA SHRIMP geochronology project: Arnhem Province, July 2014–June 2015. *Northern Territory Geological Survey, Record 2015-010.*

Kositcin, N., Reno, B.L., Whelan, J.A., 2015. Summary of results. Joint NTGS–GA geochronology project: Arunta Region, July 2014–June 2015. *Northern Territory Geological Survey, Record 2015-007*.

Lanigan, K., Hibbird, S., Menpes, S., Torkington, J., 1994. Petroleum exploration in the Proterozoic Beetaloo sub-basin, Northern Territory. *APEA JOURNAL*, **34**, 674-674.

Li, Z.X., Evans, D.A.D., 2011. Late Neoproterozoic 40° intraplate rotation within Australia allows for a tighter-fi tting and longer-lasting Rodinia. *Geology*, **39**, 39-42.

Ludwig, K.R., 2003. User's manual for Isoplot 3.00: a geochronological toolkit for Microsoft Excel (No. 4). Kenneth R. Ludwig.

Machado, N., Gauthier, G., 1996. Determination of 207 Pb/206 Pb ages on zircon and monazite by laser-ablation ICPMS and application to a study of sedimentary provenance and metamorphism in southeastern Brazil. *Geochimica et Cosmochimica Acta*, **60(24)**, 5063-5073.

Merdith, A.S., Collins, A.S., Williams, S.E., Pisarevsky, S., Foden, J.F., Archibald, D., Blades, M.L., Alessio, B.L., Armistead, S., Plavsa, D., Clark, C., Muller, R.D., 2017. A Full-Plate Global Reconstruction of the Neoproterozoic. *Gondwana Research*, in press.

Melville, P.M., 2010. Geophysics and drilling collaboration final report for drilling program, Lake Woods Project, EL23687, EL24520, EL25631, EL27317, EL27318. *Northern Territory Geological Survey, Open File Report CR2010-0226*.

Mulder, J.A., Halpin, J.A., DACZKO, N.R., 2015. Mesoproterozoic Tasmania: Witness to the East Antarctica–Laurentia connection within Nuna. *Geology*, **43**, 759-769.

Mukherjee, I., Large, R.R., 2016. Pyrite trace element chemistry of the Velkerri Formation, Roper Group, McArthur Basin: Evidence for atmospheric oxygenation during the Boring Billion. *Precambrian Research*, **281**, 13-26.

Munson, T.J., 2016. Sedimentary characterisation of the Wilton package, greater McArthur Basin. Northern Territory. *Northern Territory Geological Survey, Record* **2016-003**.

Munson TJ, Thompson JM, Zhukova I, Meffre S, Beyer EE, Woodhead JD and Whelan JA, in prep. Summary of results. NTGS laser ablation ICP-MS U–Pb and Lu–Hf geochronology project: Roper Group and overlying ungrouped units (McArthur Basin), Renner Group (Tomkinson Province), Tijunna Group (Birrindudu Basin). *Northern Territory Geological Survey, Record*.

Nemchin, A.A., Cawood, P.A., 2005. Discordance of the U–Pb system in detrital zircons: Implication for provenance studies of sedimentary rocks, *Sedimentary Geology*, **182**, 143-162.

Neumann, N.L., Southgate, P.N., Gibson, G.M., McIntyre, A., 2006. New SHRIMP geochronology for the Western Fold Belt of the Mt Isa Inlier: developing a 1800 – 1650 Ma event framework. *Australian Journal of Earth Sciences*, **53(6)**, 1023-1039.

Neumann, N.L., Gibson, G.M., Southgate, P.N., 2009. New SHRIMP age constraints on the timing and duration of magmatism and sedimentation in the Mary Kathleen Fold Belt, Mt Isa Inlier, Australia. *Australian Journal of Earth Sciences*, **56(7)**, 965-983.

Page, R.W., Sun, S.-S., 1998. Aspects of geochronology and crustal evolution in the Eastern Fold Belt, Mt Isa Inlier. *Australian Journal of Earth Sciences*, **45(3)**, 343-361.

Payne, J.L., Barovich, K.M., Hand, M., 2006. Provenance of metasedimentary rocks in the northern Gawler Craton, Australia: implications for Palaeoproterozoic reconstructions. *Precambrian Research*, **148(3)**, pp.275-291.

Paton, C., Hellstrom, J., Paul, B., Woodhead, J., Hergt, J., 2011. Iolite: Freeware for the visualisation and processing of mass spectrometric data. *Journal of Analytical Atomic Spectrometry*, **26(12)**, 2508-2518

Plumb, K.A., Wellman, P., 1987. McArthur Basin, Northern Territory: mapping of deep troughs using gravity and magnetic anomalies. *BMR Journal of Australian Geology & Geophysics,* **10**, 243-251.

Rawlings, D.J., 1999. Stratigraphic resolution of a multiphase intracratonic basin system: The McArthur Basin, northern Australia. *Australian Journal of Earth Sciences*, **46(5)**, 703-723.

Rawlings, D.J., Korsch, R.J., Goleby, B.R., Gibson, G.M., Johnstone, D.W., Barlow, M., 2004. The 2002 southern McArthur Basin seismic reflection survey. *Geoscience Australia Record*, 17, 78.

Revie, D., 2017. Volumetric resource assessment of the lower Kyalla and middle Velkerri formations of the McArthur Basin. *Annual Geoscience Exploration Seminar (AGES) Proceedings, Alice Springs, Northern Territory 28–29 March 2017*. Northern Territory Geological Survey, Darwin. pp. 86-90.

Saha, D., 2017. Proterozoic tectonics and trans-Indian mobile belts: a status report. *Proceedings of the Indian National Science Academy*, ***82(3)***, 445-460.

Sandiford, M., Hand, M., McLaren, S., 2001. Tectonic feedback, intraplate orogeny and the geochemical structure of the crust: a central Australian perspective. *Geological Society, London, Special Publications*, ***184*(1)**, 195-218.

Shaanan, U., Rosenbaum, G., 2016. Detrital zircons as palaeodrainage indicators: insights into southeastern Gondwana from Permian basins in eastern Australia. *Basin Research*.

Shaw, R.D., Black, L.P., 1991. The history and tectonic implications of the Redbank Thrust Zone, central Australia, based on structural, metamorphic and Rb-Sr isotopic evidence. *Australian Journal of Earth Sciences*, **38(3)**, 307-332

Silverman, M.R., Landon, S.M., Leaver, J.S., Mather, T.J., Berg, E., 2007. No fuel like an old fuel: Proterozoic oil and gas potential in the Beetaloo Basin, Northern Territory, Australia: in Munson TJ and Ambrose GJ (editors)'. In Proceedings of the Central Australian Basins Symposium (CABS), Alice Springs, Northern Territory, 16–18 August, 2005.*'Northern Territory Geological Survey, Special Publication (Vol. 2).*

Silverman, M., Ahlbrandt, T., 2011. Mesoproterozoic Unconventional Plays in the Beetaloo Basin, Australia: The World's Oldest Petroleum Systems. *AAPG International Conference and Exhibition, Calgary, Alberta, 2011,* 1-41.

Slama, J., Kosler, J., Condon, D.J., Crowley, J.L., Gerdes, A., Hanchar, J.M., Schaltegger, U., 2008. Plešovice zircon—a new natural reference material for U–Pb and Hf isotopic microanalysis. *Chemical Geology*, **249(1)**, 1-35.

Smiths, R.G., Collins, W.J., Hand, M., Dutch, R., Payne, J., 2014. A Proterozoic Wilson cycle identified by Hf isotopes in central Australia: implications for the assembly of Proterozoic Australia and Rodinia. *Geology*, **42(3)**, 231-234.

Southgate, P.N., Bradshaw, B.E., Domagala, J., Jackson, M.J., Idnurm, M., Krassay, A.A., Page, R.W., Sami, T.T., Scott, D.L., Lindsay, J.F., McConachie, B.A., 2000.Chronostratigraphic basin framework for Palaeoproterozoic rocks (1730–1575 Ma) in northern Australia and implications for base-metal mineralisation. *Australian Journal of Earth Sciences*, **47(3)**, 461-483.

Spaggiari, C.V., Kirkland, C.L., Smithies, R.H., Wingate, M.T.D., Belousova, E.A., 2015. Transformation of an Archean craton margin during Proterozoic basin formation and magmatism: The Albany–Fraser Orogen, Western Australia. *Precambrian Research*, **226**, 440-466.

Spencer, C.J., Kirkland, C.L., 2016. Visualizing the sedimentary response through the orogenic cycle: A multidimensional scaling approach. *Lithosphere*, ***8*(1)**, 29-37.

Spikings, R.A., Foster, D.A., Kohn, B.P., Lister, G.S., 2001. Post-orogenic (< 1500 Ma) thermal history of the Proterozoic Eastern Fold Belt, Mount Isa Inlier, Australia. *Precambrian Research*, **109(1)**, 103-144.

Spikings, R.A., Foster, D.A., Kohn, B.P., Lister, G.S., 2002. Post-orogenic (< 1500 Ma) thermal history of the Palaeo-Mesoproterozoic, Mt. Isa province, NE Australia. *Tectonophysics*, **349(1)**, 327-365.

Vermeesch, P., 2013. Multi-sample comparison of detrital age distributions. *Chemical Geology*, **341**, 140-146.

Vermeesch, P., 2014. Corrigendum to "Multi-sample comparison of detrital age distributions" [Chem. Geol. 341 (11 March 2013)—140-146]. *Chemical Geology*, **380**, 191.

Wade, B.P., 2006. Unravelling the tectonic framework of the Musgrave Province, central Australia. PhD Thesis. University of Adelaide.

Whelan, J.A., Beyer, E.E., Donnellan, N., Bleeker, W., Chamberlin, K.R., Soderlund, U., Ernst, R.E., 2016. 1.4 billion years of Northern Territory geology: Insights from collaborative U-Pb zircon and baddeleyite dating. *Annual Geoscience Exploration Seminar (AGES) Proceedings, Alice Springs, Northern Territory 15–16 March 2016.* Northern Territory Geological Survey, Darwin. pp. 115–123.

Wingate, M.T.D., Pirajno, F., Morris, P.A., 2004. Warakurna large igneous province: a new Mesoproterozoic large igneous province in west-central Australia. *Geology* **32** (2), 105–108.

Worden, K.E., Claoué-Long, J.C., Scrmgeour, I.R., Doyle, N., 2006 Summary of results. Joint NTGS-GA geochronology project: Pine Creek Orogen and Arunta Region, January–June 2004. *Northern Territory Geological Survey, Record 2006-005*.

Worden, K.E., Claoué-Long, J.C., Scrimgeour, I.R., 2006. Summary of results. Joint NTGS-GA geochronology project: Pine Creek Orogen, Tanami Region, Arunta Region and Amadeus Basin, July–December 2004. *Northern Territory Geological Survey, Record 2006-006.*

Worden, K.E., Carsou, C.J., Close, D.F., Donnellan, N., Scrimgeour, I.R., 2008. Summary of results. Joint NTGS-GA geochronology project: Tanami Region, Arunta Region, Pine Creek Orogen and Halls Creek January 2005–March 2007. *Northern Territory Geological Survey, Record 2008-003*.

Chapter 3

Middle-late Mesoproterozoic tectonic geography of the North Australia Craton: U–Pb and Hf isotopes of detrital zircon grains in the Beetaloo Sub-basin, Northern Territory, Australia

Published as:

Yang, B., Collins, A.S., Blades, M.L., Capogreco, N., Payne, J.L., Munson, T.J., Cox, G.M., Glorie, S. (2019). Middle-late Mesoproterozoic tectonic geography of the North Australia Craton: U–Pb and Hf isotopes of detrital zircons in the Beetaloo Sub-basin, Northern Territory, Australia. Journal of the Geological Society, London.

https://doi.org/10.1144/jgs2018-159

Statement of Authorship

Title of Paper	Middle–late Mesoproterozoic tectonic geography of the North Australia Craton: U–Pb and Hf isotopes of detrital zircon grains in the Beetaloo Sub-basin, Northern Territory, Australia
Publication Status	☑ Published ☐ Accepted for Publication ☐ Submitted for Publication ☐ Unpublished and Unsubmitted w ork w ritten in manuscript style
Publication Details	Yang, B., Collins, A.S., Blades, M.L., Capogreco, N., Payne, J.L., Munson, T.J., Cox, G.M., Glorie, S., 2019. Middle-late Mesoproterozoic tectonic geography of the North Australia Craton: U–Pb and Hf isotopes of detrital zircons in the Beetaloo Sub-basin, Northern Territory, Australia. Journal of the Geological Society, London. https://doi.org/10.1144/jgs2018-159.

Principal Author

Name of Principal Author (Candidate)	Bo Yang		
Contribution to the Paper	Field work, sample preparation, data collection and processing, data interpretation, manuscript composition.		
Overall percentage (%)	80		
Certification:	This paper reports on original research I conducted during the period of my Higher Degree by Research candidature and is not subject to any obligations or contractual agreements with a third party that would constrain its inclusion in this thesis. I am the primary author of this paper.		
Signature		Date	13/06/2013

Co-Author Contributions

By signing the Statement of Authorship, each author certifies that:

i. the candidate's stated contribution to the publication is accurate (as detailed above);

ii. permission is granted for the candidate in include the publication in the thesis; and

iii. the sum of all co-author contributions is equal to 100% less the candidate's stated contribution.

Name of Co-Author	Alan S. Collins		
Contribution to the Paper	Guidance on data interpretation, manuscript composition and review.		
Signature		Date	13/06/2019

Name of Co-Author	Morgan L. Blades		
Contribution to the Paper	Data processing, manuscript review.		
Signature		Date	13/06/2019

Name of Co-Author	Nicholas Capogreco		
Contribution to the Paper	Field work, sample preparation, data collection and processing.		
Signature		Date	04/06/2019

Name of Co-Author	Justin L. Payne		
Contribution to the Paper	Data collection and processing, data interpretation, manuscript review.		
Signature		Date	10/06/2019

Name of Co-Author	Tim J. Munson		
Contribution to the Paper	Data interpretation, manuscript review.		
Signature		Date	09/06/2019

Name of Co-Author	Grant M. Cox		
Contribution to the Paper	Field work, manuscript review.		
Signature		Date	14/06/2019

Name of Co-Author	Stijn Glorie		
Contribution to the Paper	Manuscript review.		
Signature		Date	14/06/2019

Chapter 3

Middle-late Mesoproterozoic tectonic geography of the North Australia Craton: U–Pb and Hf isotopes of detrital zircon grains in the Beetaloo Sub-basin, Northern Territory, Australia

Abstract

The upper Beetaloo Sub-basin of the McArthur Basin, Northern Territory, Australia, records over 500 million years of tectonic history of the North Australian Craton from ca. 1.45 to 0.9 Ga. The basin sequences include shallow-water clastic sedimentary rocks that preserve the oldest global commercial hydrocarbon reserves. New detrital zircon U–Pb age and Lu–Hf isotopes, compiled with published data, provide constraints on the basin provenance and reveal the dynamic tectonic evolution of Mesoproterozoic northern Australia.

Data from the oldest formation examined, the ca. 1.4 Ga Bessie Creek Sandstone, suggest provenance from (present-day) eastern sources (e.g. the Mount Isa Province and the palinspastically adjacent Curnamona and Georgetown provinces) with considerable spatial heterogeneity. These eastern source regions are interpreted as uplifted rift-shoulder highs, formed by contemporaneous extension between Proterozoic Australia and Laurentia. Progressively younger formations (the Velkerri Formation, the Moroak Sandstone and the Kyalla Formation) demonstrate a rapid swamping of the basin by detritus from southerly sources (e.g. the Arunta Region) that occurred at ca. 1.4–1.3 Ga. This is particularly characterised by the up-section reduction of ca. 1.6 to 1.5 Ga detrital zircon grains. This change in provenance is interpreted to relate to closure of an ocean basin during the period 1.35 to 1.25 Ga, which resulted in uplift of the southern margin of North Australia Craton. Three ungrouped latest Mesoproterozoic to Neoproterozoic sedimentary units, the lower and upper Jamison sandstone and the Hayfield mudstone, were deposited after the emplacement of the Warakurna Large Igneous Province and are sourced from the Musgrave Province.

Detrital zircon U–Pb and Hf isotope affinities between the lower and upper Jamison sandstone and the Hayfield mudstone, and the latest Mesoproterozoic to early Neoproterozoic successions

along the eastern margin of the North China Craton, suggest that they share a similar provenance. This supports correlations between the Mesoproterozoic of the North China Yanshan Basin and the greater McArthur Basin.

1. Introduction

The Mesoproterozoic has fast become a frontier in our understanding of the evolution of the Earth system. It was a time of poorly constrained atmospheric and ocean oxygen levels that lay somewhere between the low Archean values and modern values (*Holland, 2006; Lyons et al., 2014; Planavsky et al., 2014; Cox et al., 2016; Zhang et al., 2018; Mukherjee et al., 2018*) and during which eukaryote cells first developed (*Knoll et al., 2006; Rassmussen et al., 2008*). It was a time of (partial?) break-up of the supercontinent Nuna (*Evans & Mitchell, 2011; Pisarevsky et al., 2014*) and a continental reconfiguration towards the amalgamating Rodinia (*Li et al. 2008; Merdith et al., 2017*). The evidence for this ancient nascent Earth system is found within sedimentary rocks in intra-continental basins found above Archean and Paleoproterozoic terranes. One of the more studied and most accessible of these basins is the informally named "greater McArthur Basin" of northern Australia (*Close, 2014*), which spans nearly a billion years of Earth history; from ca. 1.82 Ga to ca. 0.9 Ga (*Rawlings, 1999; Ahmad & Munson, 2013; Munson, 2016; Munson et al., 2018; Chapter 2*). The greater McArthur Basin overlies the North Australia Craton (NAC) and is presently surrounded by a series of exhumed NAC basement terrains on all but the northern side of the basin (Figure 1). The original extent of the basin is poorly constrained as most of the current basin boundaries are the result of younger tectonic uplift completely eroding the basin sequences. The northern basin boundary is unconstrained due to the present day coastline of Australia, but the Yanshan Basin of the North China Craton may well have been contiguous with the region at the time (*Chu et al., 2007; Meng et al., 2011*).

A middle Mesoproterozoic shallow-marine siliciclastic-dominated sequence forms the upper part of the greater McArthur Basin succession; it is thickest in the Beetaloo Sub-basin (Figures 1 and 2), where the succession is called the Roper Group, and these rocks are the focus of this study. The Roper Group contains shales that host a major gas resource with considerable economic interest (*Cox et al., 2016, 2019; Revie, 2017; Close et al., 2017*).

Cratonic basins are characterized by prolonged, predominantly continental shallow-water sedimentation and a gross layer-cake stratigraphy that formed during hundreds of millions of years of subsidence (*Allen & Armitage, 2012*). The occurrence, formation and spatial distribution of these long-lived basins are strongly linked to the geodynamic framework of plates, including multiple phases of super-continental break-up, dispersal, plate subduction and amalgamation

(*Sandiford et al., 2001; Allen & Armitage, 2012; Allen et al., 2015; Saha et al., 2016*). Evolving plate tectonic forces over a basin's history re-shape the palaeogeography, and modify the sedimentation and drainage system within the basin, resulting in variable sediment build-up through time. Here, we demonstrate that the evolving tectonic geography of Mesoproterozoic northern Australia can be linked with changing sediment provenance within the upper Roper Group. This is demonstrated by the spatial and stratigraphic variation in age and chemistry of detrital zircon grains (e.g. *Chapter 2*). New detrital zircon Lu–Hf isotope data were collected from core samples drilled through the Beetaloo Sub-basin, the principal depocentre of the Roper Group. These data, complemented by new and previously published U–Pb age data, are used to identify possible source regions. The dynamic temporal provenance variation provides new clues on the basin's tectonic setting and its evolution from ca. 1.45 to 0.9 Ga. These new data also provide constraints on the palaeo-position of the North Australia Craton and yield a positive test for the palaeomagnetically permissive connection with the North China Craton within Nuna/Columbia and Rodinia.

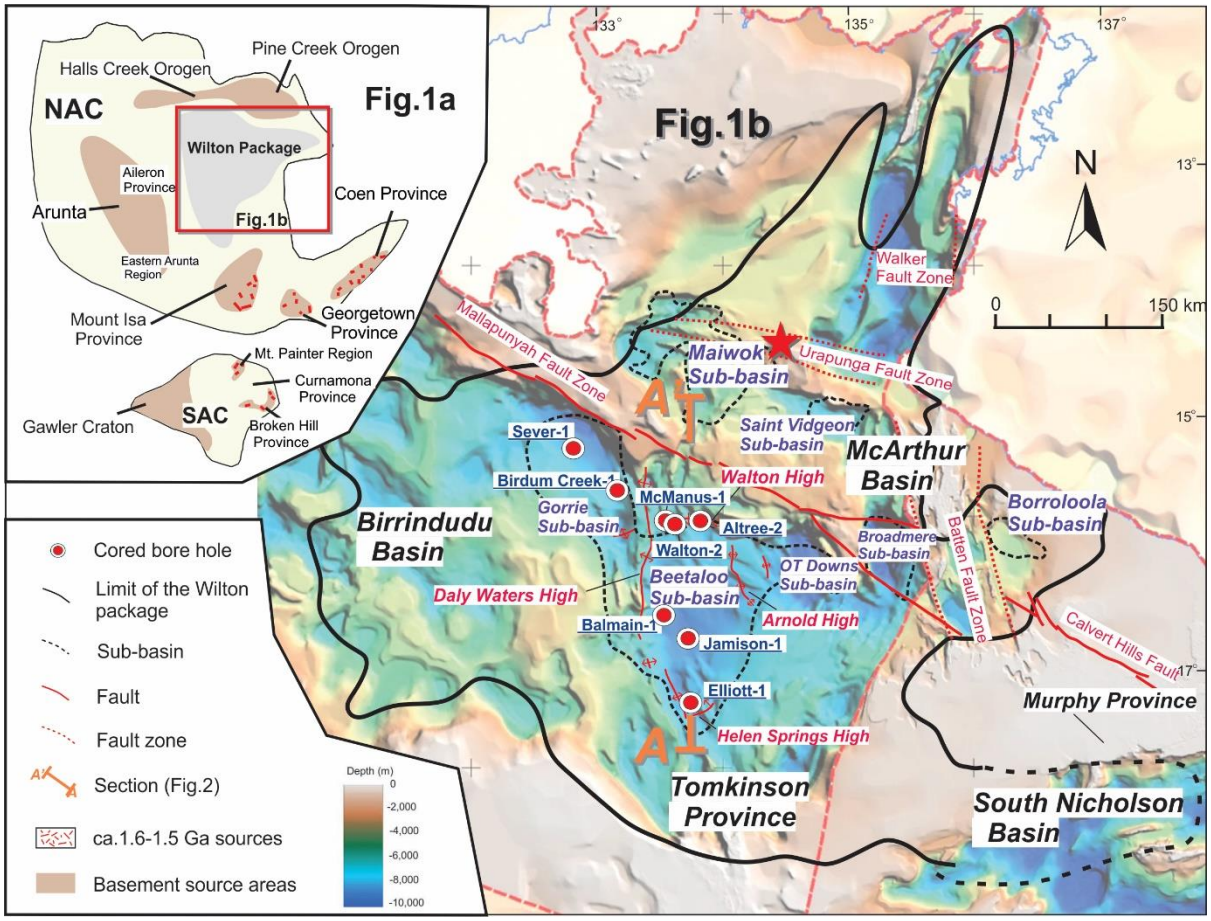

Figure 1. (a) Map showing the broad relationship between the Proterozoic North Australia Craton (NAC) and the South Australia Craton (SAC), using the reconstruction of *Li & Evans (2011)*. (b) Location map of the Wilton Package, showing the top-to-basement (SEEBASE™ basement surface image after *Frogtech Geoscience 2018*), and location of drillholes used in this study. Red star shows the outcrop sampling location of *Munson et al., 2018)*.

2. Geological background

2.1 Wilton package and Roper Group

The informally named greater McArthur Basin (*Close, 2014*) is a regionally extensive multiphase Proterozoic basin located in the North Australia Craton (Figure 1a; *Rawlings, 1999; Ahmad & Munson, 2013*). It comprises five recognised coherent basin phases that have been divided into five stratigraphic 'packages' (*Rawlings, 1999*). The basin overlies crystalline basement rocks of inferred Archean to Paleoproterozoic age, and is overlain by Neoproterozoic and Phanerozoic sedimentary successions that are referred to as the Centralian Superbasin (*Walter et al., 1995*) and other younger basins. The middle Mesoproterozoic Wilton package, at the top of the greater McArthur Basin, mainly contains shallow-water siliciclastic sedimentary rocks (*Abbott & Sweet, 2000; Ahmad & Munson, 2013; Munson, 2016, Munson & Revie, 2018*). The Wilton package is widespread throughout northern Australia, covering an area of over 145,000 km^2, and is geographically separated into correlated groups and basins, including the Roper Group of the McArthur Basin and the subsurface Beetaloo Sub-basin, the Renner Group of the Tomkinson Province and the Tijunna Group of the Birrindudu Basin (Figure 1b; *Jackson et al., 2000; Ahmad & Munson, 2013; Munson, 2016; Munson et al., 2018*). The South Nicholson Group of the South Nicholson Basin is also likely to be a component, but no direct connection has yet been demonstrated (*Ahmad & Munson, 2013*).

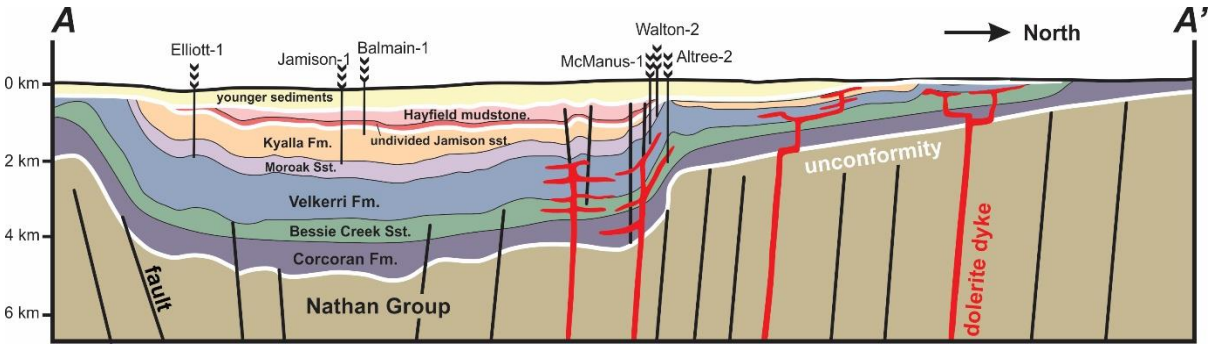

Figure 2. Cross-section through the Beetaloo Sub-basin (modified after *Close et al., 2017*)

The Roper Group was deposited in a stable shelf environment that is often envisaged as an enclosed marine basin, analogous to the modern Black Sea (*Abbott & Sweet, 2000; Mukherjee & Large, 2016; Cox et al., 2016; Munson 2016, Revie, 2017; Munson & Revie, 2018; Chapter 2*). This succession contains six upward-coarsening cyclic sequences and is divided into two subgroups: the lower Collara Subgroup, dominated by sandstones (some glauconitic) with less voluminous mudrocks, deposited in a range of depositional environments from shoreline to shallow-marine shelf; and the upper Maiwok Subgroup that is more shale-rich with less abundant sandstone

formations, and generally deposited in deeper shelf environments (*Jackson et al., 1988; Abbott & Sweet, 2000; Abbott et al., 2001; Ahmad & Munson, 2013*).

2.2 Beetaloo Sub-basin

The Beetaloo Sub-basin extends over an area of approximately 15,000 km^2 and is located in the approximate centre of the present distribution of the Wilton package. This sub-basin is covered by younger sediments and forms a subsurface link with the other components of the Wilton package (*Ahmad & Munson, 2013; Munson, 2016; Munson et al., 2018*). It also preserves the thickest stratigraphic succession, and therefore has been interpreted as the basin's main depocentre (*Plumb & Wellman, 1987; Lanigan et al., 1994; Ahmad & Munson, 2013; Munson, 2016, Frogtech Geoscience, 2018*). Faults, or fault-related basement highs, mark the present margins of the sub-basin (Figure 1b; *Silverman et al., 2007, 2011; Hoffman, 2015; Betts et al., 2015, Frogtech Geoscience, 2018*). Chapter 2 recently demonstrated that they also formed bathymetric barriers to sedimentation in early Maiwok Subgroup times (ca. 1.4 Ga).

Four sandstone/mudrock formations that make up the Maiwok Subgroup are the focus of this study. These include, from base to top, the Bessie Creek Sandstone, Velkerri Formation, Moroak Sandstone and Kyalla Formation. The Bessie Creek Sandstone is a highly mature quartz arenite, deposited in a high-energy tide-dominated shoreline to shallow shelf setting (*Pietsch et al., 1991; Abbott et al., 2001, Munson, 2016*). The youngest single detrital zircon grain analysed from this formation yielded an age of 1386 ± 13 Ma, which constrains the maximum age of deposition of this formation (*Chapter 2*). The Bessie Creek Sandstone is conformably overlain by a set of black shales and minor sandstone/siltstones that make up the Velkerri Formation. This formation was deposited in a marine, subtidal, sub-wave base and generally quiet environment, affected by regular current activity (*Powell et al., 1987; Abbott et al., 2001; Munson, 2016; Sheridan et al., 2018*), and has been demonstrated to host a significant shale-gas resource (*Revie, 2017; Close et al., 2017*). The maximum depositional age of this formation is constrained at 1308 ± 41 Ma (*Chapter 2*). This age overlaps a Re–Os age of 1361 ± 21 Ma from the upper Velkerri Formation (*Kendall et al., 2009*). The Moroak Sandstone was deposited in a similar depositional environment to the Bessie Creek Sandstone and is characterised by fine to medium quartz sandstones (*Jackson et al., 1986; Abbott et al., 2001; Munson, 2016*). The Kyalla Formation comprises interbedded sandstones and mudrocks, and is interpreted to have been deposited in a storm-dominated shallow-marine shelf environment (*Powell et al., 1987; Abbott et al., 2001; Munson, 2016*). It conformably overlies the Moroak Sandstone and is the topmost unit of the Roper Group in the Beetaloo Sub-basin. A dolerite suite (Derim Derim Dolerite) intrudes all

formations of the upper Roper Group, and provides a minimum age constraint on the timing of deposition. *Abbott et al. (2001)* reported a U–Pb Secondary Ion Mass-Spectrometry (SIMS) baddeleyite age of 1324 ± 4 Ma (the standard deviation level was not stated) from this dolerite intrusion, whereas a younger U–Pb Thermal Ionization Mass-Spectrometry (TIMS) baddeleyite age of 1312.9 ± 0.7 Ma (2SD) was recently obtained (*Collins et al., 2018*).

The informally named, latest Mesoproterozoic to Neoproterozoic, lower and upper Jamison sandstone and Hayfield mudstone overlie the Kyalla Formation. The lower and upper Jamison sandstones both contain fine- to coarse-grained quartz sandstone with thin mudrock interbeds, deposited in a high-energy shoreline to shallow-marine setting (*Munson, 2016*). The Hayfield mudstone conformably overlies the upper Jamison sandstone and is a mudstone dominated unit with sandstone interlayers, indicating a subtidal shallow-marine shelf depositional setting (*Munson, 2016*). These three units unconformably overlie various upper Roper Group formations and are unconformably overlain by Neoproterozoic and Phanerozoic successions (*Munson, 2016*). Detrital zircon U–Pb age analysis suggests that the lower Jamison sandstone was deposited after 1092 ± 16 Ma, whereas the deposition of the upper Jamison and Hayfield mudstone has been constrained to be after 959 ± 18 Ma (*Chapter 2*).

3. Analytical methods

In this study, *in situ* hafnium isotope data were collected from detrital zircon samples previously dated using U–Pb techniques by *Chapter 2*. Three new sandstone samples, including one Moroak Sandstone and two Kyalla Formation samples, were collected for detrital zircon U–Pb analysis. Details of samples are presented in Appendix 2.

3.1 U–Pb dating

Sandstone core samples were crushed and milled, and the zircon grains were separated using panning, conventional magnetic methods and heavy liquids (LST 2.85 ± 0.02 g/mL). Individual zircon grains were handpicked without preference to size, colour, or shape, and mounted in non-reactive epoxy resin. Cathodoluminescence (CL) images, showing zircon internal structures, were obtained using a FEI Quanta 600 SEM Scanning Electron Microscope (SEM) with attached Gatan CL detector to determine suitable domains for analysis (working distance: 15 mm; accelerating voltage: 12 kV).

Zircon U–Pb geochronological data were obtained using a New Wave 213 nm Nd-YAG laser coupled with an Agilent 7900cs inductively-coupled-plasma–mass-spectrometer (ICP–MS) at Adelaide Microscopy, the University of Adelaide. A spot size of 30 µm and frequency of 5 Hz was used for all analyses. Laser intensity was set to 70% with fluence varying from ~5 to 7 J/cm^2.

Zircon cores were mainly targeted with background recorded for 30 seconds and ablation recorded for 30 seconds. GEMOC GJ-1 zircon ($^{207}Pb/^{206}Pb$ age of 607.7 ± 4.3 Ma, $^{206}Pb/^{238}U$ age of 600.7 ± 1.1 Ma and $^{207}Pb/^{235}U$ age of 602.0 ± 1.0 Ma; *Jackson et al. 2004*) was used to correct for instrumental fractionation, and the Plešovice zircon standard with a $^{206}Pb/^{238}U$ age of 337.13 ± 0.37 Ma (*Sláma et al., 2008*) was used to monitor accuracy. A total of 66 Plešovice standard analyses were obtained and yielded a weighted average $^{206}Pb/^{238}U$ age of 339.3 ± 1.3 Ma (2SD, MSWD = 2.4) and $^{207}Pb/^{206}Pb$ age of 332.5 ± 9.3 Ma (2SD, MSWD = 1.5). Data were processed using Iolite (*Paton et al., 2011*).

3.2 Hafnium isotope analysis

Hafnium isotope analyses were conducted at the University of Adelaide using a New Wave UP-193 ArF excimer laser attached to a Thermo-Scientific Neptune Multi-Collector ICP–MS. The analytical procedure follows *Payne et al. (2013)*. Zircon grains with less than 10% age discordance were selected for Hf isotope measurement. Zircon grains were ablated using a spot size of 50 µm or 35 µm, frequency of 5 Hz, 4 ns pulse length and an intensity of ~4.5 J/cm^2, and the length of the each analysis was about 1.5 minutes including 20 seconds of background measurement. Zircon Hf data were processed using the HfTRAX Excel macro (*Payne et al., 2013*) and mass bias was corrected using an exponential fractionation law with a stable $^{179}Hf/^{177}Hf$ ratio of 0.7325. Yb and Lu isobaric interferences on ^{176}Hf were corrected by using the methods of *Woodhead et al. (2004)*. The Mudtank zircon and Plešovice zircon were used as primary and secondary standards before and during the analysis to assess instrument stability and monitor data quality. Repeated Mudtank zircon analyses yielded a mean $^{176}Hf/^{177}Hf$ ratio of 0.282494 ± 0.000036 (n=27, 2SD), which is in accordance with the published value of 0.282507 ± 0.000006 (*Woodhead & Hergt, 2005*). Twenty analyses of Plešovice yielded a mean $^{176}Hf/^{177}Hf$ ratio of 0.282462 ± 0.000031 (2SD), which is within uncertainty of the published value (0.282482 ± 0.000013, *Sláma et al., 2008)*. The initial $^{176}Hf/^{177}Hf$ values were calculated using a ^{176}Lu decay constant of 1.865×10^{-11} year^{-1} after *Scherer et al. (2001)* and epsilon hafnium values were calculated using Chondrite reservoir (CHUR) values of $^{176}Hf/^{177}Hf = 0.282785$ and $^{176}Lu/^{177}Hf = 0.0336$ after *Bouvier et al. (2008)*.

4. Results

4.1 U–Pb age data

Sample descriptions and U–Pb data are provided in Appendix 2. Only analyses that are less than 10% discordant are presented (Figures 3 and 4) and discussed further. Uncertainties reported on

individual analyses are a combination of measured uncertainties from internal and external sources. All uncertainties are reported as 2 standard deviation level.

The Moroak Sandstone sample (Sample EN-Mo8), collected from drillhole Elliott-1, yields a dominant age peak at ca. 1700 Ma and a minor peak at ca. 1560 Ma (Figure 3).

Two Kyalla Formation samples, JN-Ky6 and EN-Ky4, collected from Jamison-1 and Elliott-1 drill-cores respectively, both yield dominant peaks at ca. 1735 Ma and a minor peak at ca. 1790 Ma (Figures 3 and 4), which is consistent with other published Kyalla Formation samples (*Chapter 2*).

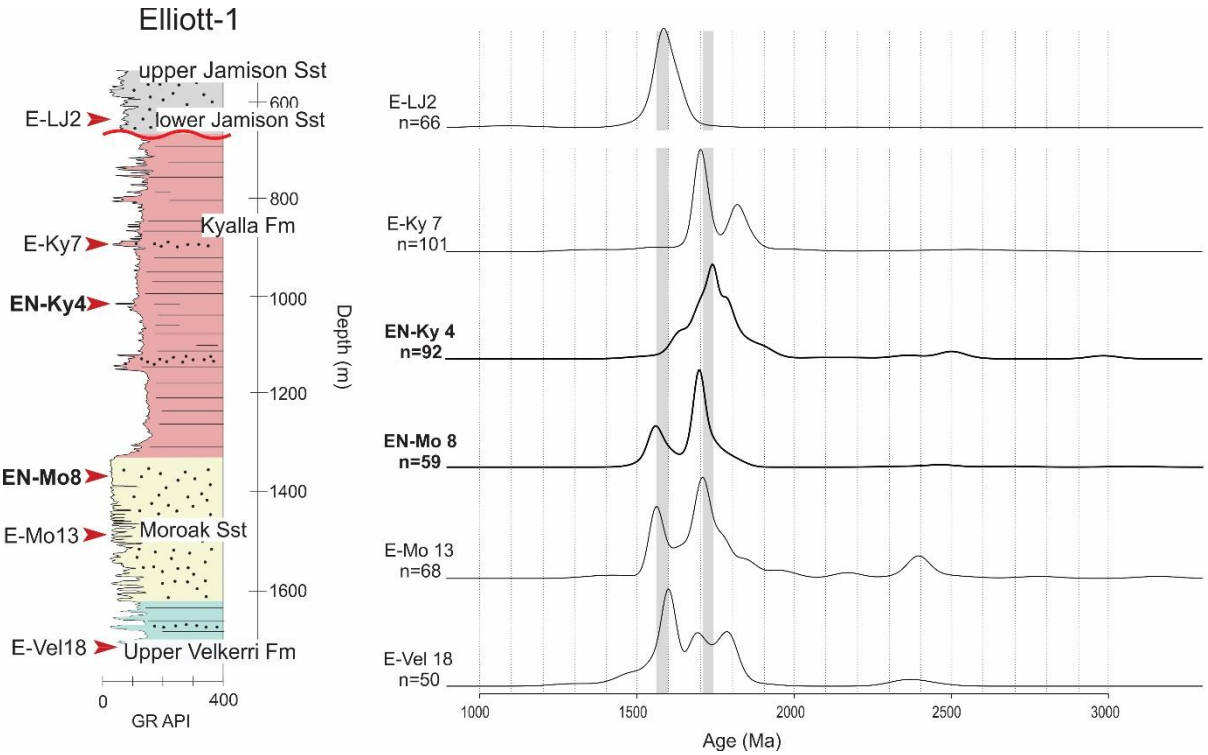

Figure 3. Kernel Distribution Estimates (KDE) of detrital zircon $^{207}Pb/^{206}Pb$ age spectra of samples collected from core from drillhole Elliott-1. Analysed samples reported by *Chapter 2* are in plain text. Additional samples analysed in this study are highlighted in bold. GR API: gamma ray log recorded in API units. Drillhole location shown in Figure 1. Detailed data and concordia plots are present in Appendix 2.

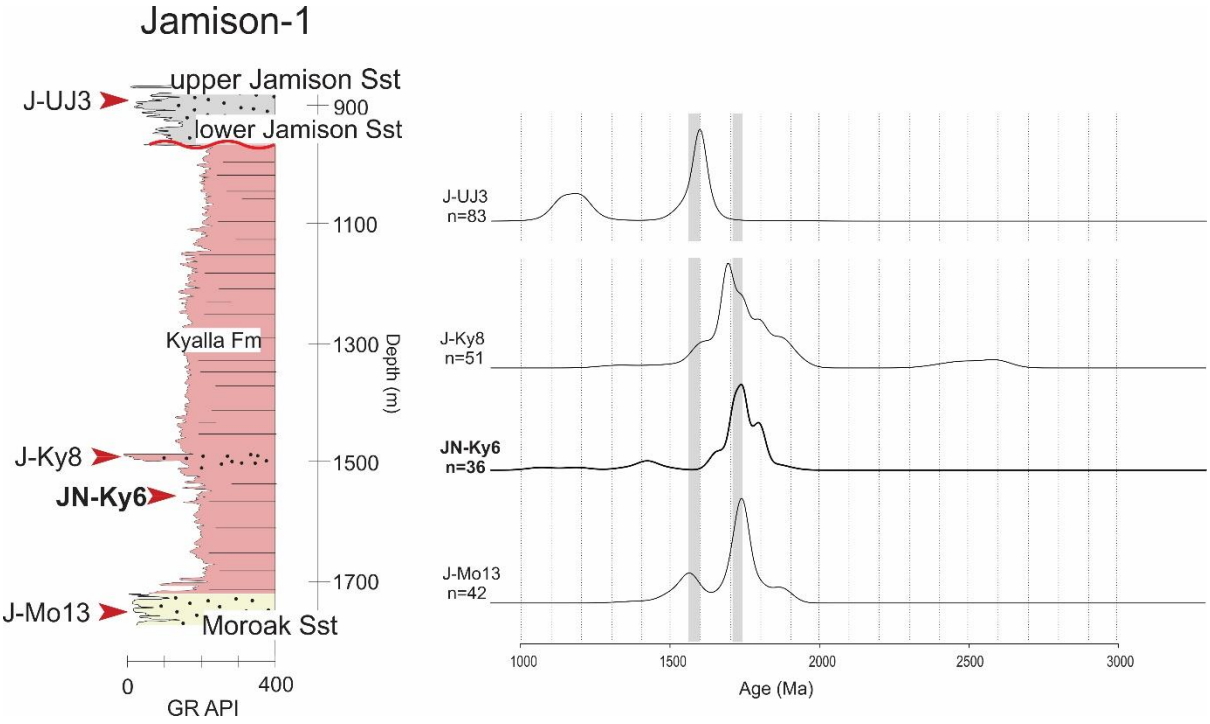

Figure 4. Kernel Distribution Estimates (KDE) of detrital zircon $^{207}Pb/^{206}Pb$ age spectra of samples collected from core from drillhole Jamison-1. Analysed samples reported by *Chapter 2* are in plain text. Additional samples analysed in this study are highlighted in bold. GR API: gamma ray log recorded in API units. Drillhole location shown in Figure 1. Detailed data and concordia plots are present in Appendix 2.

4.2 Lu–Hf isotope data

A total of 221 analyses were collected from 14 samples; the results are given in Appendix 2 and presented in Figures 5 and 6.

Forty-seven analyses were collected from three Bessie Creek Sandstone samples. Samples S-BC1 and W-BC1 yielded a range of Hf isotopic compositions ($^{176}Hf/^{177}Hf_i$=0.280550–0.282051). A single Mesoarchean zircon grain with a $^{207}Pb/^{206}Pb$ age of 3443 Ma yielded an $\varepsilon_{Hf}(t)$ value of -0.2 (Figure 5). Zircon grains dated between ca. 2534 and 2444 Ma yielded $\varepsilon_{Hf}(t)$ values between -5.3 and +2.8, whereas 1860 to 1805 Ma zircon grains have $\varepsilon_{Hf}(t)$ values clustered tightly around -6 to -2 (Figure 5). Zircon grains with $^{207}Pb/^{206}Pb$ ages between ca. 1760 and 1651 Ma yielded $\varepsilon_{Hf}(t)$ values between -8.8 and +2.1. Three early Mesoproterozic analyses dated between ca. 1535 to 1513 Ma returned $\varepsilon_{Hf}(t)$ values between -7.5 and +8.1. Sample A-BC13, however, yielded contrasting Hf isotopic data with $^{176}Hf/^{177}Hf_i$ ratios from 0.280785 to 0.281993. One Mesoarchean zircon grain yielded $\varepsilon_{Hf}(t)$ values of -3.6 and one early Paleoproterozoic zircon grain yielded $\varepsilon_{Hf}(t)$ value of -8.7. A middle Paleoproterozoic zircon grain with a $^{207}Pb/^{206}Pb$ age of 2255 Ma returned a positive $\varepsilon_{Hf}(t)$ value of +1.5, and two late Paleoproterozoic zircon grains (with $^{207}Pb/^{206}Pb$ ages of 1650 Ma and 1648 Ma) both returned negative $\varepsilon_{Hf}(t)$ values of -4.2 and -2.8, respectively (Figure 5). Zircon grains dated between ca. 1555 and 1421 Ma are dominated by

positive $\varepsilon_{Hf}(t)$ values ranging from +1.8 to +6.6, with one analyse yielding a negative $\varepsilon_{Hf}(t)$ value of -5.1 (Figure 5).

Hf isotopic detrital zircon data from the Velkerri Formation were collected from grains dated in *Chapter 2*. Seventeen analyses returned $^{176}Hf/^{177}Hf_i$ ratios from 0.281151 to 0.281766. Of these analyses, two grains with early Paleoproterozoic ages yielded $\varepsilon_{Hf}(t)$ values of -2.6 and -0.2. Zircon grains dated between ca. 1806 Ma and 1674 Ma have $\varepsilon_{Hf}(t)$ values ranging from -7.2 to -1.0, indicating relative radiogenically depleted crystallization environments, similar to the zircon grains dated between ca. 1631 Ma and 1596 Ma, which also yielded dominantly negative $\varepsilon_{Hf}(t)$ values (-9.8 to +0.7; Figure 5).

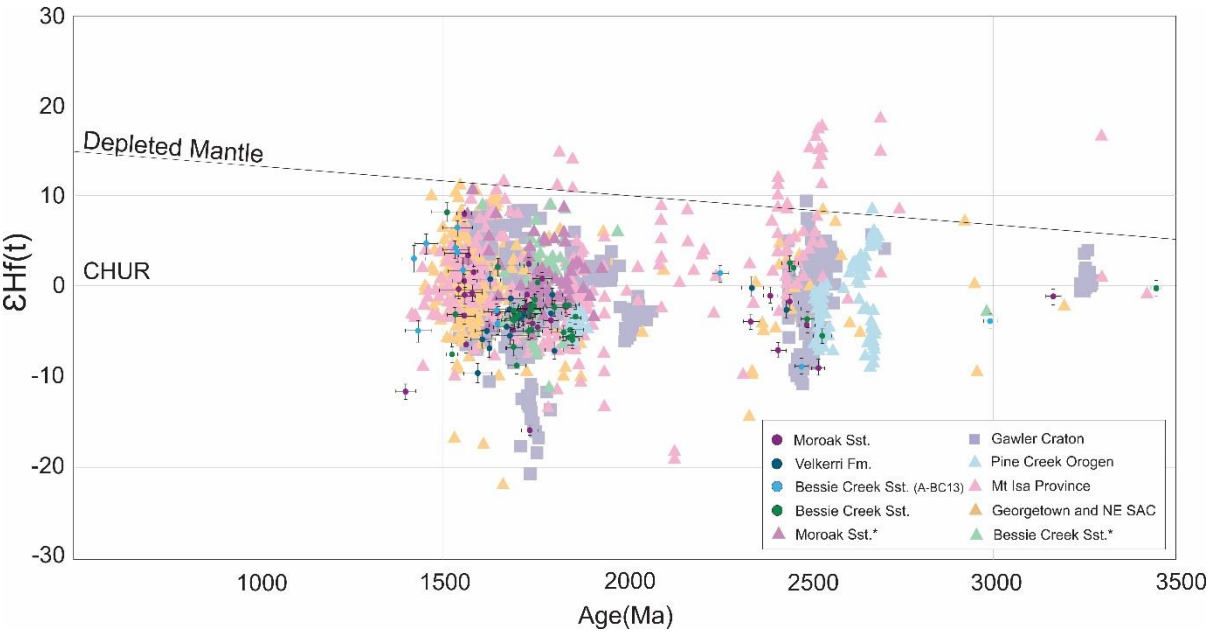

Figure 5 Epsilon Hf values of the lower Maiwok Subgroup plotted against the corresponding analysed $^{207}Pb/^{206}Pb$ spot age. CHUR: chondrite reservoir. *data from *Munson et al. (2018)*. Published data are potential sources, including Gawler Craton (*Nebel et al., 2007; Howard et al., 2011; Szpunar et al., 2011; Reid & Payne, 2017*); Mt Isa Province (*Condie et al., 2005; Griffin et al., 2006; Bierlein et al., 2008*); Pine Creek Orogen (*Worden et al., 2006a, 2006b; Worden et al., 2008; Carson et al., 2009; Hollis et al., 2010; Beyer et al., 2013*); Georgetown Province (*Murgulov et al., 2007*); and northeast South Australia Craton (NE SAC; *Kromkhun et al., 2013; Armit et al., 2014*).

The $^{176}Hf/^{177}Hf_i$ ratios of Moroak Sandstone zircon grains range from 0.280712 to 0.282013. Six Archean to early Paleoproterozoic (dated between ca. 3159 Ma to 2340 Ma) analyses yielded negative $\varepsilon_{Hf}(t)$ values ranging from -8.8 to -0.9. Twelve of fifteen late Paleoproterozoic zircon grains (aged between ca. 1837 and 1655 Ma) returned $\varepsilon_{Hf}(t)$ in the range of -3 to -0.9, with two analyses giving more radiogenic (more juvenile) values ($\varepsilon_{Hf}(t)$ values of +0.74 and +2.34) and one outlier with a significant negative $\varepsilon_{Hf}(t)$ signature of -17.7 (Figure 5). Nine zircon grains with $^{207}Pb/^{206}Pb$ ages of ca. 1586 to 1550 Ma define a vertical array with $\varepsilon_{Hf}(t)$ values between -6.5 and +7.9 (Figure 5). One zircon grain, with a $^{207}Pb/^{206}Pb$ age of ca. 1404 Ma, yielded a negative $\varepsilon_{Hf}(t)$ value of -11.7 (Figure 5).

Fifty-six hafnium analyses from the Kyalla Formation show $^{176}Hf/^{177}Hf_i$ ratios ranging from 0.28093 to 0.281762. Six grains with $^{207}Pb/^{206}Pb$ ages of ca. 2573 Ma to 2264 Ma yielded $\varepsilon_{Hf}(t)$ values ranging from -8.5 to +3.8. The hafnium isotope signature of zircon grains aged between ca. 1833 Ma and 1804 Ma returned negative $\varepsilon_{Hf}(t)$ values (-4.4 to -1.5). Zircon grains dated between ca. 1777 Ma and 1690 Ma are characterized by predominantly negative $\varepsilon_{Hf}(t)$ values (-6.1 to -0.7) with several positive analyses ranging from +0.1 to +2.9 (Figure 6).

The hafnium isotope profiles of the lower and upper Jamison sandstone are similar to one another and are discussed together here (Figure 6). A total of seventy-one analyses, comprising twenty-four from the lower Jamison sandstone and forty-seven from the upper Jamison sandstone, exhibit $^{176}Hf/^{177}Hf_i$ ratios ranging from 0.281133 to 0.282108. Two Paleoproterozoic-aged zircon grains yielded negative $\varepsilon_{Hf}(t)$ values of -5.6 and -4 (Figure 6). Most of the zircon grains aged between ca. 1620 Ma and 1438 Ma yielded positive $\varepsilon_{Hf}(t)$ values, indicating that they crystallized from isotopically depleted magmas, whereas several analyses also returned negative $\varepsilon_{Hf}(t)$ values (-2.8 to -0.48), suggesting slightly enriched crystallization environments (Figure 6). Late Mesoproterozoic zircon grains (ca. 1220 Ma to 1050 Ma) yielded $\varepsilon_{Hf}(t)$ values ranging from -4.9 to +2.7 (Figure 6).

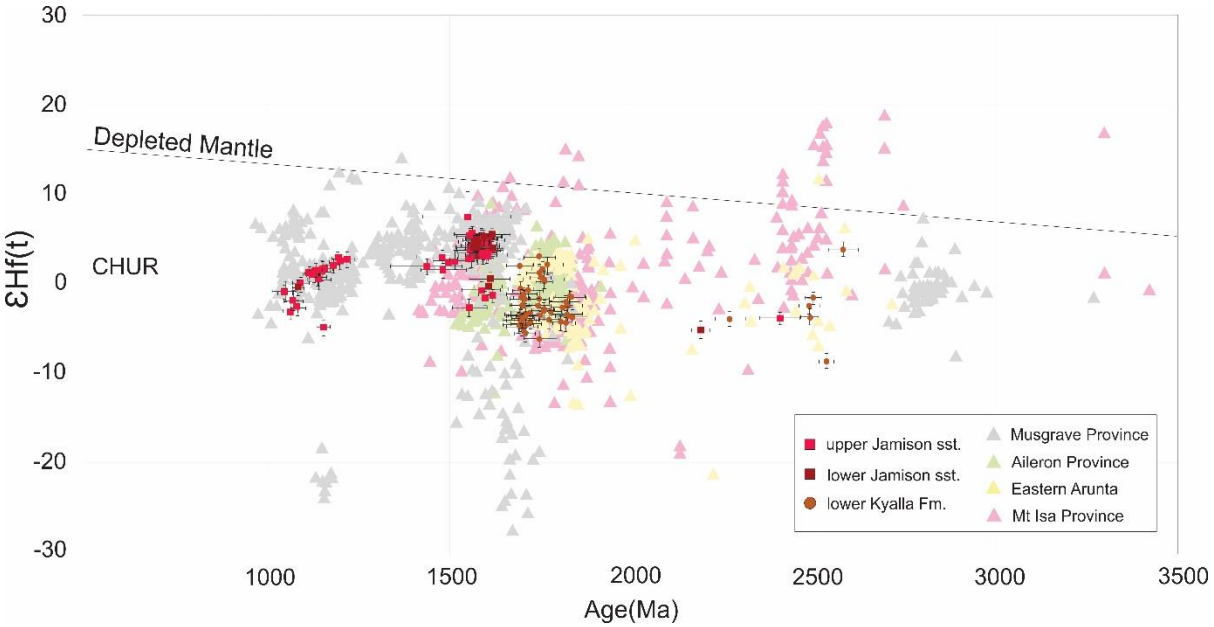

Figure 6. Epsilon Hf values of the Kyalla Formation, lower and upper Jamison sandstone plotted against the corresponding analysed $^{207}Pb/^{206}Pb$ spot age. CHUR: chondrite reservoir. Hayfield mudstone data are from Munson *et al.* 2018. Published data are from potential sources, including Musgrave Province (*Wade, 2006; Smits et al., 2014*); Aileron Province (*Beyer et al., 2013, 2015*); Eastern Arunta (*Beyer et al., 2013, 2015*); Mt Isa Province (*Condie et al., 2005; Griffin et al., 2006; Bierlein et al., 2008*).

5. Discussion

5.1 Provenance and tectonic evolution

Compiled detrital zircon U–Pb age data from this research, and other publications (e.g. *Fanning, 2012; Munson et al., 2018; Chapter 2*), are coupled with hafnium isotope data in order to better identify the source–sink relationships of the sedimentary rocks. These data demonstrate significant provenance variation during deposition of the Maiwok Subgroup and overlying latest Mesoproterozoic/Tonian sequences; this variation is both temporal and spatial.

Chapter 2 suggested that samples analysed from the Bessie Creek Sandstone in the northern and western regions show derivation from northern and western sources (e.g. Pine Creek Orogen and Halls Creek Orogen). However, hafnium isotopes collected within in this study allow for alternative interpretations. The two northern and western samples (S-BC1 and W-BC1) contain detrital zircon grains dated between ca. 1830 Ma and 1700 Ma, with moderately enriched hafnium isotope signatures ($\varepsilon_{Hf}(t)$: -9 to +0.3), suggesting that they were originally derived from reworked crust. Zircon grains with U–Pb ages of ca. 1600 to 1580 Ma are rare in these samples, but three were analysed for hafnium and form a vertical $\varepsilon_{Hf}(t)$ array from -8 to +9 (Figure 5). This characteristic array is seen in the Mount Isa Province, as well as in regions that were adjacent to Mount Isa at that time (Georgetown Province, Curnamona Province and Mount Painter area;

Figure 1; *Blewett et al., 1998; Page & Sun, 1998; Hoskin & Black, 2000; Condie et al., 2005; Griffin et al., 2006; Neumann et al., 2006, 2009; Murgulov et al., 2007; Bierlein et al., 2008; Kositcin et al., 2009; Armit et al., 2014; Cross et al., 2015*).

The other Bessie Creek Sandstone sample, A-BC13, however, shows a distinctive hafnium profile that is characterised by the presence of detrital zircon grains dated between ca. 1600 and 1400 Ma with depleted hafnium isotope signatures and the absence of older zircon grains (ca. 1830 to 1720 Ma) with enriched hafnium isotope signatures, compared to the other two samples (Figure 5). Although A-BC13 exhibits a different signature from other Bessie Creek Sandstone samples, the hafnium isotopes of this sample still overlap with data from Mount Isa (Figure 5; *Condie et al., 2005; Griffin et al., 2006; Murgulov et al., 2007; Bierlein et al., 2008; Armit et al., 2014*). Combined Hf isotopes and U–Pb ages suggest that the Bessie Creek Sandstone samples represent a mix of sources from the north (e.g. Pine Creek Orogen) where ca. 1830 Ma and ca. 2500 Ma magmatic rocks are largely exposed (*Worden et al., 2006a, 2006b; Worden et al., 2008; Carson et al., 2009; Hollis et al., 2010; Kositcin et al., 2013a; Beyer et al., 2013*)and east/southeast (e.g. Mount Isa and adjacent terranes) where ca. 1740 Ma and ca. 1600 Ma magmatism has been frequently reported (*Condie et al., 2005; Griffin et al., 2006; Murgulov et al., 2007; Bierlein et al., 2008; Kromkhun et al., 2013; Armit et al., 2014*). The heterogeneous mixture of detritus form these sources, varying with the samples' locality within the basin, resulted in spatial provenance variations.

The shale-rich Velkerri Formation stratigraphically overlies the Bessie Creek Sandstone and is sub-divided into the lower Kalala Member, middle Amungee Member and upper Wyworrie Member (*Munson & Revie, 2018*), based on lithology, total organic carbon content, chemostratigraphy and wireline logs (*Lanigan et al., 1994; Warren et al., 1998; Cox et al., 2016, 2019; Munson & Revie, 2018*). The combined age spectra of two Wyworrie Member samples (*Fanning, 2012; Chapter 2*), is characterised by a dominant peak at ca. 1600 Ma and two minor peaks centred at ca. 1820 Ma and ca. 1690 Ma (Figure 7). These age clusters are similar to the peaks in the sandstones that underlie and overlie the formation, but they differ in relative magnitude. Although care needs to be taken in assigning too much weight to the relative magnitudes of data, *Chapter 2* suggested that the much higher proportion of ca. 1600 Ma zircon grains in the upper Velkerri Formation could indicate that this formation was sourced from the Eastern Fold Belt of the Mount Isa Province (*Griffin et al., 2006*), or the palinspastically adjacent Georgetown Province (*Condie et al., 2005; Murgulov et al., 2007*), or the eastern Gawler/Curnamona terranes (*Kromkhun et al., 2013; Armit et al., 2014*; Figure 7). The Hf isotope profile of detrital zircon grains from the Velkerri Formation exhibits moderately enriched

hafnium isotope signatures (ε_{Hf}(t): -9 to +0.7; Figure 5). This is consistent with the southeast sources (e.g. Mount Isa Province, Georgetown Province, Coen Province and northeast South Australia Craton) which were subjected to both ca. 1600 to 1500 Ma arc-related and late orogenic granitoids (*Betts & Giles, 2006; Mark & Pollard, 2006; Kromkhum et al., 2013; Nordsvan et al., 2018; Pourteau et al., 2018*). The absence of ca. 1600 Ma analyses with depleted hafnium isotope compositions in the Velkerri Formation may be because it received detritus mainly from orogenic related magmatic sources.

The detrital zircon age spectra of combined Moroak Sandstone samples lacks the older age populations of ca. 1840 Ma and ca. 2500 Ma that are present in the Bessie Creek Sandstone samples (Figure 7). In addition, this formation preserves a detrital zircon age distribution and hafnium isotopic signature similar to those of the Mount Isa Province and Gawler Craton (*Condie et al., 2005; Murgulov et al., 2007; Bierlein et al., 2008; Kromkhun et al., 2013; Armit et al., 2014; Reid & Payne, 2017*) that were located to the east to southeast of the basin (Figures 5 and 7). *Munson et al. (2018)* presented Bessie Creek and Moroak Sandstone hafnium isotopic data from samples collected in the more northern Urupunga Fault Zone area (Figure 1). These data differ from the Beetaloo Sub-basin data in that the ca. 1800–1700 Ma analyses show a vertical ε_{Hf}(t) spread to much more depleted hafnium isotope signatures than seen in the Beetaloo Sub-basin (Figure 5). This suggests different sources for these two regions at Bessie Creek and Moroak times and may indicate that the Walton High, or the Mallapunyah Fault, which separates the regions, was a bathymetric high during deposition.

Two new Kyalla Formation samples described here have age components similar to those of three samples of this formation documented by *Chapter 2* (Figure 7). The combined age spectra of these samples is characterised by a major peak at ca. 1740 Ma and a minor peak at ca. 1800 Ma (Figure 7). The complete absence of ca. 1590 Ma zircon grains in this formation suggests that it received less detritus from the southeast sources (e.g. Mount Isa Province, Georgetown Province, Coen Province and northeast South Australia Craton), and the dominant ca. 1740 Ma age peak is consistent with the crystallization age of magmatic rocks exposed in the eastern Arunta Region (*Hollis et al., 2010*; Figure 7). This is further supported by the hafnium isotope data, which show overlapped ε_{Hf}(t) values of the Kyalla Formation and the eastern Arunta Region (*Hollis et al., 2010*; Figure 6).

Further, the U–Pb data demonstrate an up-section stratigraphic trend of decreasing 1600–1500 Ma sources that are replaced by 1800–1700 Ma sources; these start with the Bessie Creek Sandstone sample from drillhole Altree-2, and evolve through the Velkerri Formation and Moroak Sandstone to the Kyalla Formation at the top of the Roper Group in the Beetaloo Sub-

basin (Figure 8). This was argued to represent a gradual change from eastern sources to southern sources (e.g. the Arunta Region) for upper Roper Group sediments in the Beetaloo Sub-basin (*Chapter 2*), and is consistent with the hafnium isotope data (Figure 5).

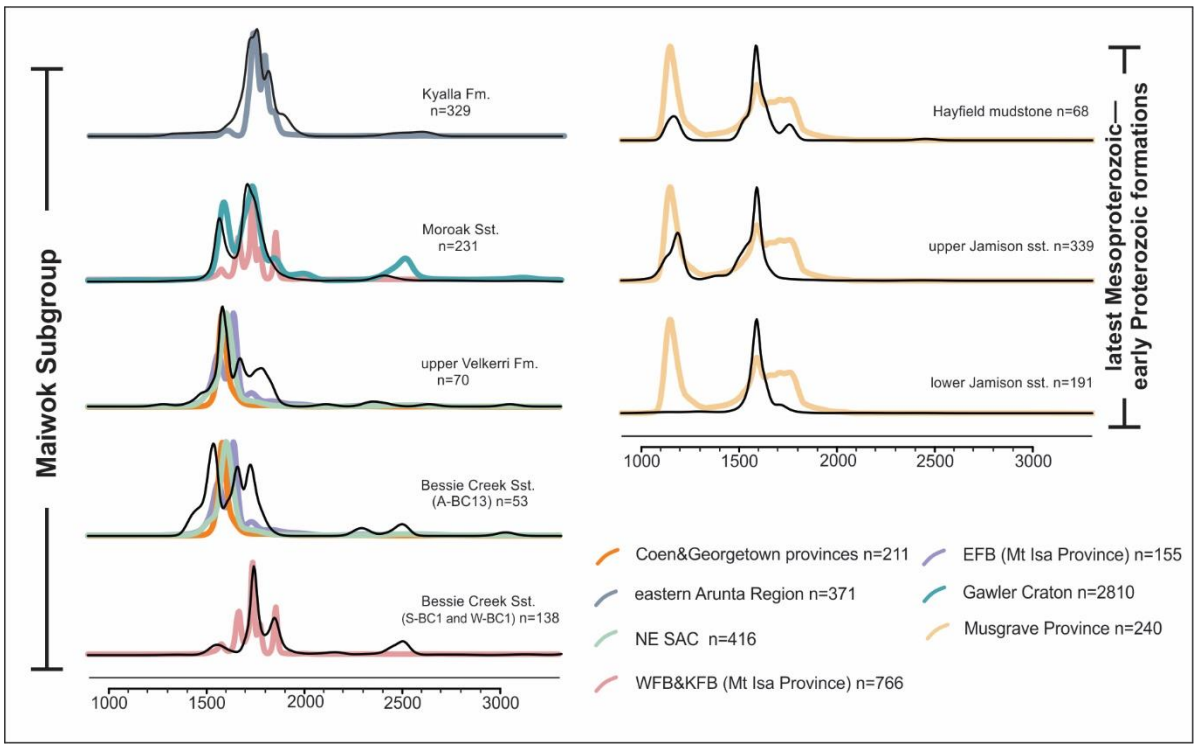

Figure 7 Kernel Distribution Estimates (KDE) of compiled samples from the same formations, and their interpreted sources. Sst: sandstone; SAC: South Australia Craton; WFB: Western Fold Belt (Mt Isa Province); KFB: Kathleen Fold Belt (Mt Isa Province); EFB: Eastern Fold Belt (Mt Isa Province). Published $^{207}Pb/^{206}Pb$ ages from both magmatic and detrital zircon grains are included from potential source areas, including Arunta Region (*Cross et al., 2005a, b, c ; Carson et al., 2009; Bodorkos et al., 2013; Kositcin et al., 2013a, b; 2014a, b; 2015b; Beyer et al., 2013, 2015, 2016*); Gawler Craton (*Nebel et al., 2007; Howard et al., 2011; Szpunar et al., 2011*); Mount Isa Province (*Page & Sun 1998; Neumann et al, 2006, 2009; Cross et al., 2015*); NE SAC (*Kromkhun et al. 2013; Armit et al. 2014*); Coen and Georgetown Provinces (*Blewett et al., 1998; Hoskin & Black 2000; Kositcin et al., 2009*); Musgrave Province (*Wade, 2006; Smits et al., 2014*).

Three late Mesoproterozoic to early Neoproterozoic sedimentary units, deposited after 1092 ± 16 Ma, have markedly contrasting detrital zircon U–Pb ages and hafnium isotopes to those of the underlying Maiwok Subgroup (Figures 6, 7 and 9; *Chapter 2*). These data demonstrate that there was a significant provenance change associated with the deposition of these rocks (Figure 9). *Chapter 2* present detrital zircon chronological data and suggest that these formations all received detritus from the Musgrave Province to the present-day south. This is consistent with the zircon hafnium isotope data that show significant overlap between the three late Mesoproterozoic to early Neoproterozoic formations and the Musgrave Province (Figure 6; *Wade,*

2006; Smits et al., 2014; Munson et al., 2018). In addition, the negative trend of the Hf isotopic array from ca. 1.2 to 1.05 Ga is interpreted to represent the remelting of previously isotopically depleted crust as arc magmas, with a significant mantle source, evolving to collisional magmatism (e.g. see *Spencer et al., 2015*). This is consistent with the ca. 1.2 to 1.1 Ga Musgrave Orogeny and subsequent ca. 1.0 Ga exhumation (*Smithies et al., 2011; Glorie et al., 2017*) of the region after emplacement of the ca. 1.08–1.04 Ga Warakurna Large Igneous Province (*Wingate et al., 2004; Kirkland et al., 2013; Smits et al., 2014; Smithies et al., 2015*). Another possible source for the ca. 1.2 to 1.1 Ga zircon grains is the southern margin of the Arunta Region, where ca. 1.2 to 1.1 Ga magmatism has been reported (*Black & Shaw, 1995; Scrimgeour et al., 2005; Wong et al., 2015*).

5.2 Tectonic geography of northern Australia

Detrital zircon age and hafnium isotopic data indicate variations in exposure and erosion of basement terrains that are related to evolving tectonic events in the source areas to the Beetaloo Sub-basin.

The Bessie Creek Sandstone was deposited after 1386 ± 13 Ma (*Chapter 2*), based on the youngest near-concordant detrital zircon. The deposition of the Bessie Creek Sandstone and the Velkerri Formation are coeval with both post-orogenic exhumation of the Mount Isa Province (ca. 1460 and 1390 Ma, *Spikings et al., 2001, 2002*), newly reported magmatism and high-grade metamorphism (ca. 1450 Ma) in the northern Gawler Craton (*Morrissey et al., 2018*) and exhumation of the eastern Gawler Craton (ca. 1420 Ma, *Foster & Ehlers, 1998*). *Foster & Ehlers (1998)* suggested that widespread Mesoproterozoic extension and exhumation throughout eastern Australia was a result of lithospheric extension related to the rifting of Proterozoic Australia and Laurentia. During this rifting event, a series of basins/sedimentary units formed along the eastern margin of Proterozoic Australia-Antarctica (e.g. Rocky Cape Group of northwest Tasmania—*Mulder et al., 2015*—and the South Nicholson Basin and the Inorunie Group of North Australia Craton—*Betts & Giles, 2006; Aikten, et al., 2016; Nordsvan et al., 2018*—and the Cariewerloo Basin of the Gawler Craton—*Flint, 1993*), and along the western margin of Laurentia (e.g. Belt Supergroup; *Ross & Villeneuve, 2003; Jones et al., 2015*). The lower Maiwok Subgroup, and possibly the underlying Collara Subgroup, are interpreted to have received detritus from the Mount Isa Province (and its adjacent areas) as it was exhumed as a rift-shoulder during this Laurentian–Australian rifting event (Figure 10).

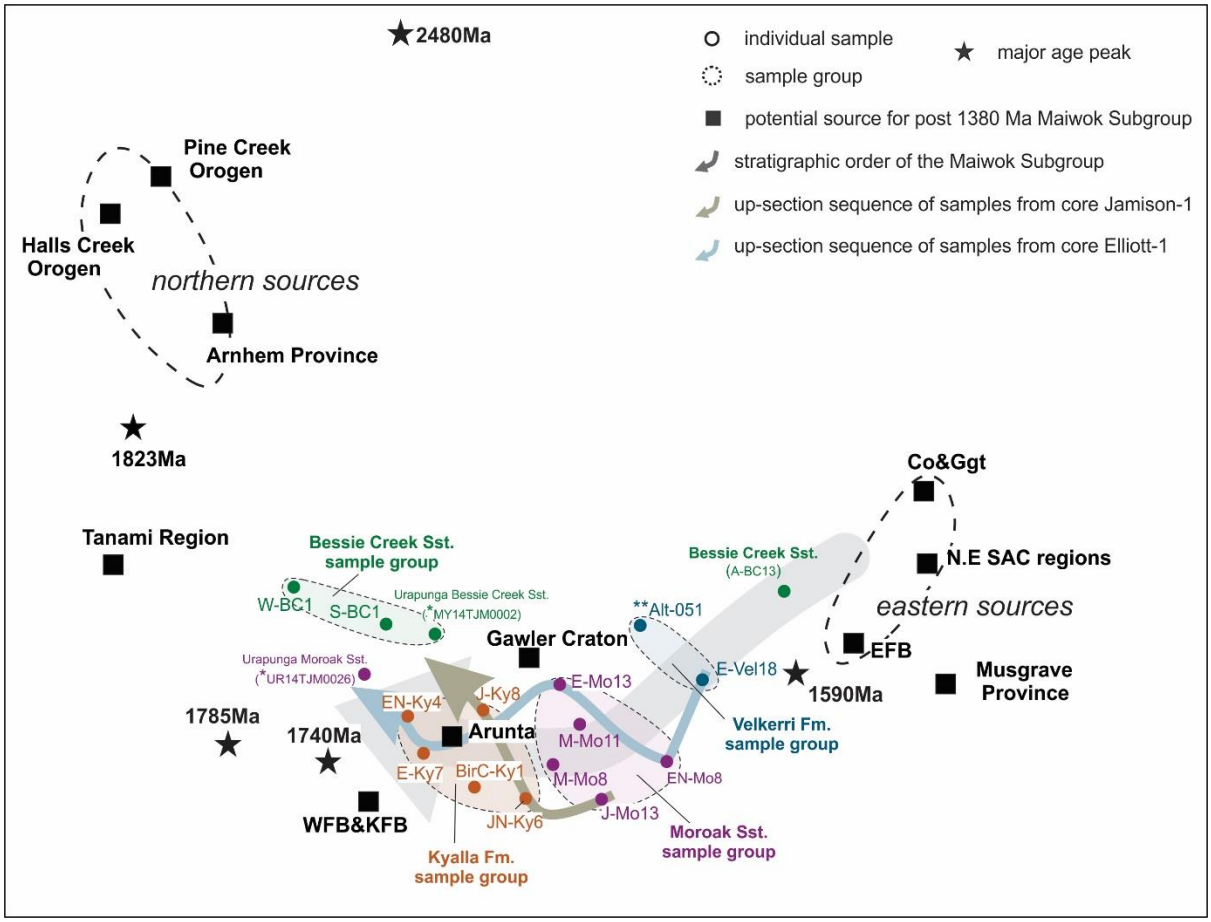

Figure 8 Joint non-parametric Multidimensional Scaling plot (after *Vermeesch, 2013, 2014*) of Maiwok Subgroup detrital zircon $^{207}Pb/^{206}Pb$ age data from *Chapter 2*, this study, (*) *Munson et al. (2018)* and (**) *Fanning (2012)*. SAC: South Australia Craton; WFB: Western Fold Belt (Mt Isa Province); KFB: Kathleen Fold Belt (Mt Isa Province); EFB: Eastern Fold Belt (Mt Isa Province); Co&Ggt: Coen and Georgetown provinces. Published data for potential source comparison are from igneous and sedimentary rocks older than 1380 Ma.

The provenance changes within the upper part of the Maiwok Subgroup are characterized by an up-section decrease in ca. 1590 Ma zircon grains. This begins with the Velkerri Formation, then evolves through the Moroak Sandstone to the lower Kyalla Formation (Figures 3 and 4). The provenance variation is reflected in a Multidimensional Scaling (MDS) plot, in which these formations show a temporal trend from being dominated by ca. 1590 Ma-aged sources through to ca. 1780–1740 Ma-aged sources (Figure 8). Detrital zircon U–Pb *and* hafnium isotope analyses suggest that the dominant source areas shifted from the Mount Isa Province (and adjacent regions) to the Arunta Region during the deposition of the Kyalla Formation. The Moroak Sandstone and Kyalla Formation are constrained to having been deposited between ca. 1350 Ma and ca. 1313 Ma (*Collins et al., 2018; Chapter 2*). The deposition of these two formations was coeval with subduction-related magmatism (*Kirkland et al., 2015; Spaggiari et al., 2015; Morrissey et al., 2017*), orogeny (*Howard et al., 2011; Johnson et al., 2013*) and metamorphism

(*Anderson et al., 2016*) along the boundary separating the West Australian Craton and the combined North and South Australian cratons. The Mesoproterozoic ocean that is interpreted to have separated these continents has been recently called the Mirning Ocean (*Kirkland et al., 2017*). *Smits et al. (2014)* suggested that the West Australian Craton did not assemble with the North Australian and South Australian cratons until at least ca. 1.2 Ga, and that the period ca. 1.35–1.25 Ga signalled ocean closure involving subduction and arc accretion, and the formation of subduction-related basins (e.g. Arid Basin; *Morrissey et al., 2017*). This ca. 1.35 Ga arc-volcanism is temporally consistent with the more radiogenic Nd isotope provenance excursion within the Velkerri Formation reported by *Cox et al. (2016, 2019),* indicating the erosion products of the arc volcanism probably have been transported to the Beetaloo Sub-basin by north-flowing river systems. The delivery of the arc volcanic detritus is argued to have resulted in high nutrient supply to the Beetaloo Sub-basin that caused high bacteria productivity and subsequent high organic carbon burial within the Amungee Member of the Velkerri Formation (*Cox et al., 2016, 2019*).

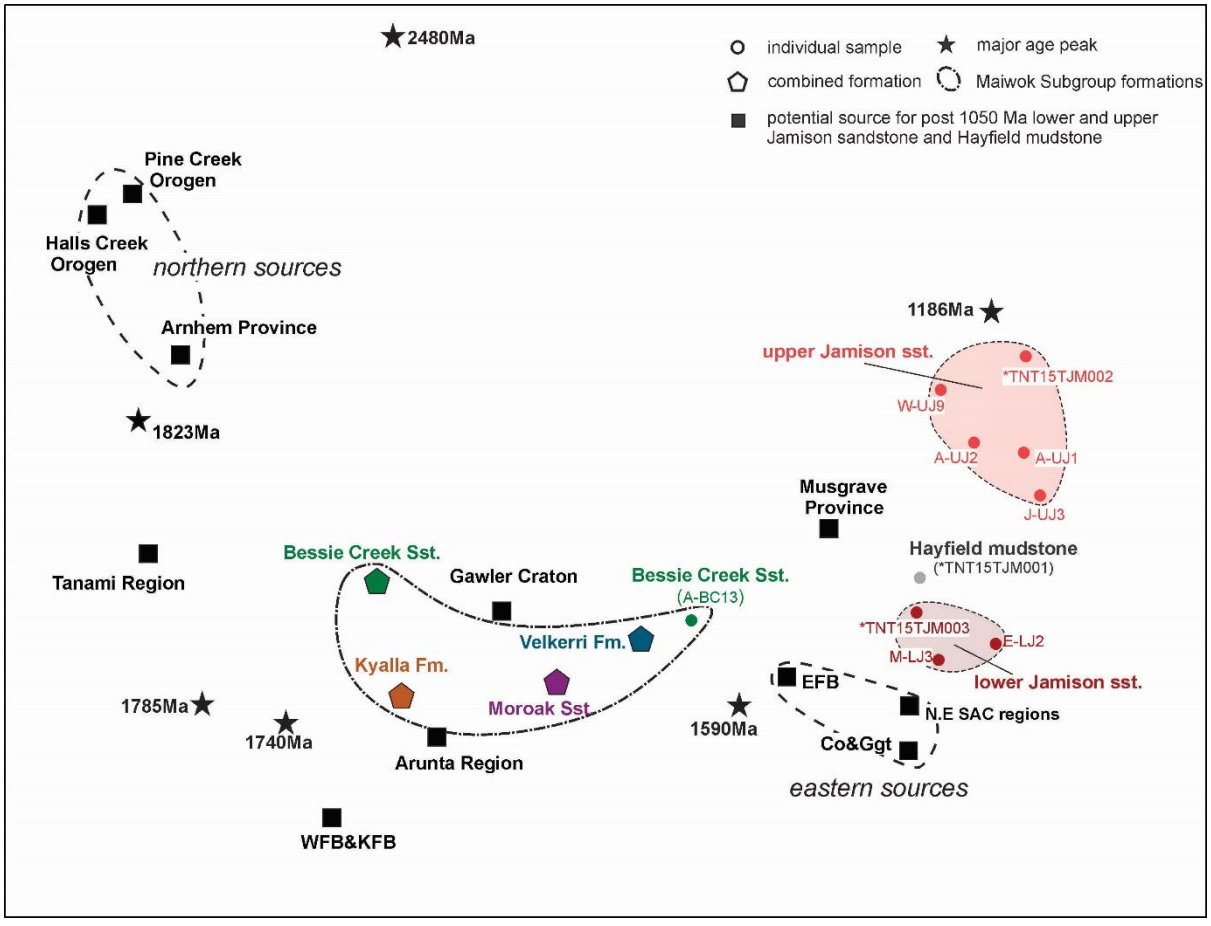

Figure 9 Joint non-parametric Multidimensional Scaling plot (after *Vermeesch, 2013, 2014*) of upper Beetaloo Sub-basin detrital zircon $^{207}Pb/^{206}Pb$ age data from *Chapter 2*, this study, (*) *Munson et al. (2018)* and (**) *Fanning (2012)*. SAC: South Australia Craton; WFB: Western Fold Belt (Mt Isa Province); KFB: Kathleen Fold Belt (Mt Isa Province);

EFB: Eastern Fold Belt (Mt Isa Province); Co&Ggt: Coen and Georgetown provinces. Published data for potential source comparison are from igneous and sedimentary rocks older than 1050 Ma.

The progressive provenance shift through time, from ca. 1600 Ma sources in the east/southeast (e.g. Mount Isa Province, Georgetown Provinces and northeast South Australia Craton sources) to ca. 1780 sources in the south (e.g. Arunta Region) recorded in the upper Maiwok Subgroup is interpreted as the far-field response of plate margin activity on the current-day southern margin of the Musgrave Province. During these continent-forming events, the south margin of the North Australian Craton was uplifted and sources in the Arunta Region then replaced sediment from the Mount Isa Province, becoming the dominant source for the Kyalla Formation, at least in the Beetaloo Sub-basin (Figure 10).

The regional unconformity between the Maiwok Subgroup and three late Mesoproterozoic to early Neoproterozoic formations, the lower and upper Jamison sandstone and the Hayfield mudstone, indicates that basin evolution was punctuated by a long period (over 300 Myr) of uplift and non-deposition. This followed extensive ca. 1313 Ma (*Collins et al., 2018*) dyke/sill intrusion in the northern Beetaloo Sub-basin and was coeval with orogenesis (ca. 1200–1100 Ma; *Kirkland et al., 2013*) and large igneous province magmatism (ca. 1.08–1.04 Ga, *Wingate et al., 2004; Evins et al., 2010*) in the Musgrave Province. Renewal of deposition in the Beetaloo Sub-basin, sourced from the Musgrave Province (Figure 10), is consistent with apatite U–Pb dates (ca. 1075 to 1025 Ma) from that region (*Glorie et al., 2017*).

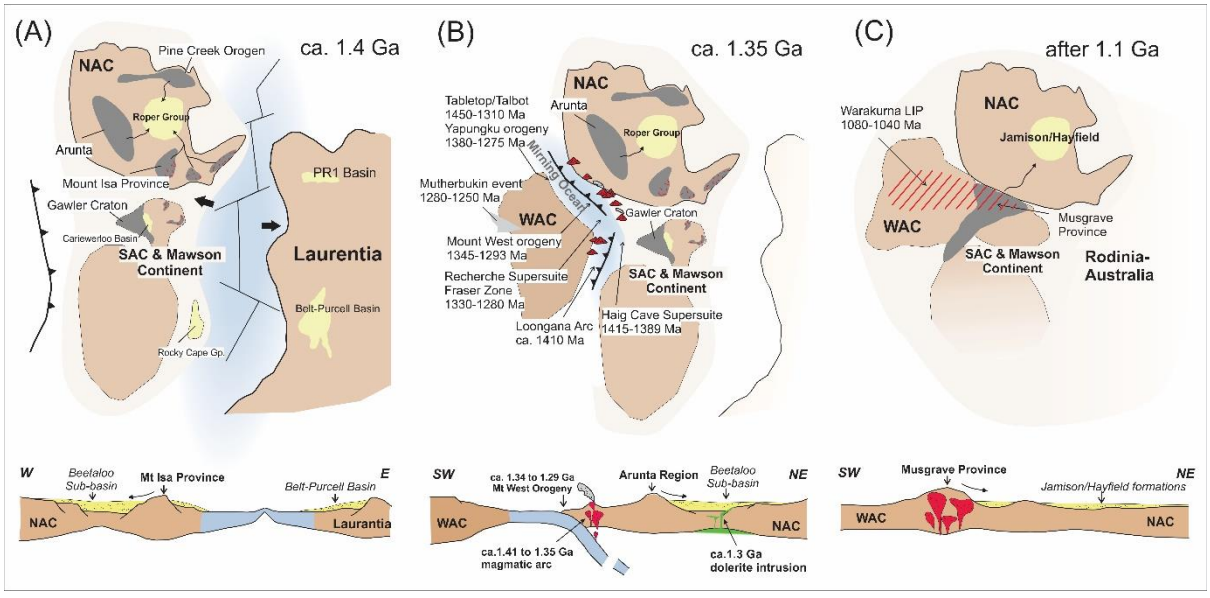

Figure 10. Tectonic and deposition history of the Maiwok Subgroup and Jamison/Hayfield sequences (after *Chapter 2*). NAC: North Australia Craton; WAC: West Australia Craton; SAC: South Australia Craton. Note that there is uncertainty in the polarity of subduction of the south Mirning Ocean (cf. *Spaggiari et al., 2015* & *Morrissey et al., 2017*).

5.3 Palaeogeography and configuration

The Roper Group is interpreted to have been deposited in an enclosed marine basin (*Munson, 2016; Cox et al., 2016; Revie, 2017; Munson & Revie, 2018*). However, the location of the basin's depositional margins are unknown, especially to the present-day north. It is palaeomagnetically feasible to position the North China Craton adjacent to northern Australia from the Mesoproterozoic right through the Neoproterozoic (Figure 11; *Evans & Mitchell, 2011; Zhang et al., 2009; Merdith et al., 2019*), and geologically, this reconstruction is validated. The succession of the Yanshan Basin, which covers much of the North China Craton, is a potential corollary of the Roper Group (*Zhang et al., 2012; Xu et al., 2014*). *Zhang et al. (2009, 2017)* described the 1.33–1.3 Ga Yanliao mafic dyke swarm in the North China Craton, which is broadly coeval with Derim Derim–Galiwinku mafic magmatism in the northern North Australia Craton. Both northern Australia and the North China Craton were uplifted during and/or after this magmatism, suggesting that a mantle plume was located close to these two basins, and supporting the juxtaposition of the two regions at ca. 1300 Ma (*Zhang et al., 2017*). In addition, there are striking stratigraphic and geochemical similarities between the Yanshan Basin succession and the Roper Group (e.g. the Xiamaling Formation and the Velkerri Formation; *Chu et al., 2007; Luo et al., 2015*).

A series of latest Mesoproterozoic to early Neoproterozoic strata are preserved and sporadically exposed in a few locations along the eastern margin of the North China Craton, including the Xihe Group in southern Liaoning Province, the Suxian and Tumen groups in northern Jiangsu Province, the Penglai Group in Shandong and the Sangwon Group in North Korea (Figure 11). These successions unconformably overlie Archean and Paleoproterozoic–Mesoproterozoic basement and share stratigraphic similarities with one another (*Hu et al., 2012*). Previous geochronological work shows that these units all contain concentrations of detrital zircon grains dated between ca. 1.2 to 1.05 Ga (*Li et al., 2007; Yang et al., 2012; Hu et al., 2012; Yang et al., 2016; Park et al., 2016*). Hafnium isotopes of these zircon grains yield $\varepsilon_{Hf}(t)$ values from +10 to -8.3 and plot along a reworking array, similar to that observed in the Jamison–Hayfield succession in the Beetaloo Sub-basin (Figure 11). There are no obvious sources for these zircon grains in the vicinity of the North China Craton. This suggests that ca. 1.2 to 1.05 Ga zircon grains are exotic to that terrane and *Hu et al. (2012)* suggested that they might have been sourced from areas to the present-day east of the North China Craton. In our preferred reconstruction (Figure 11), northern Australia is located east of modern North China and a potential source for both these zircon grains and those of the probably correlative Jamison–Hayfield succession is interpreted to be the Musgrave Orogen of central Australia.

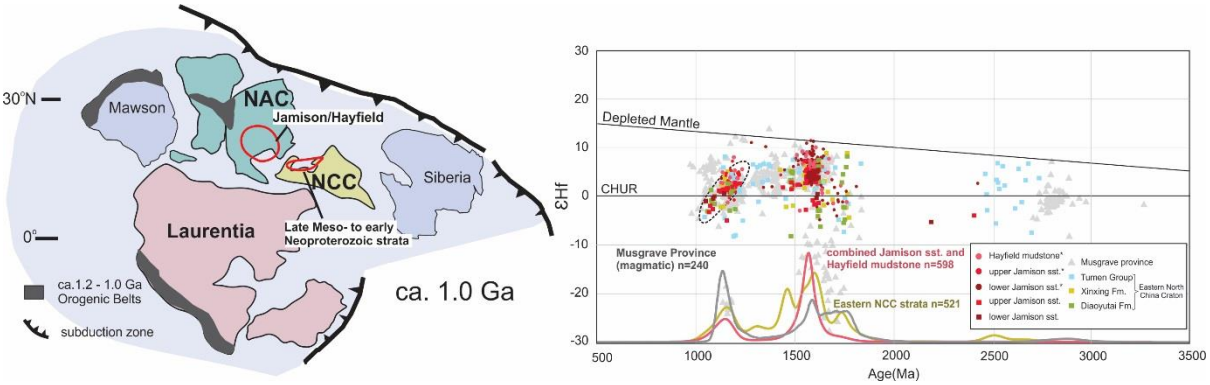

Figure 11. Plate reconstruction at 1.0 Ga (modified after *Spencer et al., 2015* and *Merdith et al., 2018, 2019*) and Hf profile-kernel distribution estimate showing similarities between Jamison/Hayfield formations and the sedimentary rocks in Eastern North China Craton (NCC). *data from *Munson et al. (2018)*. Eastern North China Craton data from *Li et al. (2007), Yang et al. (2012), Hu et al. (2012), Yang et al. (2016) and Park et al. (2016)*.

6. Conclusions

Coupled detrital zircon U–Pb age and Hf isotope data presented in this research indicate that the lower Maiwok Subgroup was mainly derived from the Mount Isa Province to the (present-day) east and palinspastically adjacent terranes. In contrast, the upper Maiwok Subgroup was sourced from the Arunta Region in the south with a gradual decline of easterly sources and increasing prominence of southerly sources from ca. 1.4–1.3 Ga. Three late Mesoproterozoic to early Neoproterozoic sedimentary units, the lower and upper Jamison sandstone and Hayfield mudstone were sourced from the Musgrave Province in the present-day far south. This provenance variation, as recorded within the Beetaloo Sub-basin, is consistent with the interpreted tectonic evolution of the North Australia Craton during the period ca. 1.45 to <0.95 Ga. The first provenance-changing event is related to ca. 1.45–1.4 Ga rifting between Proterozoic Australia and Laurentia, which is interpreted to have exhumed the eastern sources as rift-shoulders. The transition to southern sources is interpreted to represent ca. 1.35 to 1.3 Ga subduction and closure of the Mirning Ocean, uplifting and exhuming the Arunta Region. A period of erosion and/or non-deposition between ca. 1.3 Ga and 1.05 Ga may represent denudation after plume-related magmatism. Subsequent ca. 1.05 to 0.9 Ga exhumation and denudation of the Musgrave Province resulted in a renewal of sedimentation, which is reflected in the deposition of the lower and upper Jamison sandstone and Hayfield mudstone; this might correlate with the early stages of deposition in the Centralian Superbasin (*Walter et al., 1995; Munson et al., 2012*).

Detrital zircon geochronological affinities can be identified between latest Mesoproterozoic to early Neoproterozoic successions in the eastern margin of the North China Craton and the Jamison–Hayfield succession in the North Australian Craton. They both show source–sink

signatures that suggest a Musgrave Province provenance, indicating a potential connection or near-neighbour relationship between these two continents in the Tonian, and probably before.

Acknowledgement

This research was funded by an Australian Research Council Linkage Project LP160101353, which is partnered by the Northern Territory Geological Survey, SANTOS Ltd., Origin Energy and Imperial Oil and Gas. Dr Sarah Gilbert is acknowledged for assistance collecting zircon U–Pb data. Christopher Spencer, Peter Betts and Ian Fitzsimons are acknowledged and thanked for their constructive comments that greatly improved the manuscript.

References

Abbott, S.T. & Sweet, I.P. (2000). Tectonic control on third-order sequences in a siliciclastic ramp-style basin: An example from the Roper Superbasin (Mesoproterozoic), northern Australia. *Australian Journal of Earth Sciences* **47(3)**, 637-657.

Abbott, S.T., Sweet, I.P., Plumb, K.A., Young, D.N., Cutovinos, A., Ferenczi, P.A. & Pietsch, B.A. (2001). Roper Region: Urapunga and Roper River Special, Northern Territory (Second Edition). 1:250 000 geological map series explanatory notes, SD 53-10, 11. Northern Territory Geological Survey and Geoscience Australia (National Geoscience Mapping Accord).

Ahmad, M. & Munson, T.J. (2013). Northern Territory Geological Survey, Geology and mineral resources of the Northern Territory, Special Publication 5. Northern Territory Geological Survey.

Allen, P.A. & Armitage, J.J. (2012). Cratonic Basins. Tectonics of Sedimentary Basins: Recent Advances. John Wiley & Sons, Ltd.

Aitken, A.R.A., Betts, P.G., Young, D.A., Blankenship, D.D., Roberts, J.L. & Siegert, M.J. (2014). The Australo-Antarctic Columbia to Gondwana transition. *Gondwana Research*, 29(1), 136-152.

Allen, P.A., Eriksson, P.G., Alkmim, F.F., Betts, P.G., Catuneanu, O., Mazumder, R., Memg, Q. & Young, G.M. (2015). Classification of basins, with special reference to Proterozoic examples. *Geological Society, London, Memoirs*, **43(1)**, 5-28.

Anderson, J.R., Kelsey, D.E., Hand, M. & Collins, W.J. (2016). Mesoproterozoic metamorphism in the Rudall Province: revising the timeline of the Yapungku Orogeny and implications for cratonic Australia assembly. *AESC 2016 – Australian Earth Sciences Convention abstract volume*, 227.

Armit, R.J., Betts, P.G., Schaefer, B.F., Pankhurst, M.J. & Giles, D. (2014). Provenance of the early Mesoproterozoic Radium Creek Group in the northern Mount Painter Inlier: correlating isotopic signatures to inform tectonic reconstructions. *Precambrian Research,* **243(4)**, 63-87.

Betts, P.G. & Giles, D. (2006). The 1800–1100 Ma tectonic evolution of Australia. *Precambrian Research*, **144(1)**, 92-125.

Betts, P.G., Armit, R.J. & Ailleres, L. (2015). Potential-field interpretation mapping of the greater McArthur Basin. PGN Geoscience Report 15/2014: in 'Geophysical and structural interpretation of the greater McArthur Basin'. *Northern Territory Geological Survey, Digital Information Package DIP 015*.

Beyer, E.E., Hollis, J.A., Whelan, J.A., Glass, L.M., Donnellan, N., Yaxley, G., Armstrong, R., Allen, C. & Scherstén, A., (2013). Summary of results. NTGS laser ablation ICPMS and SHRIMP U-Pb, Hf and O geochronology project: Pine Creek Orogen, Arunta Region, Georgina Basin and McArthur Basin, July 2008–May 2011. *Northern Territory Geological Survey, Record 2012-007*.

Beyer, E.E., Allen, C.M., Armstrong, R. & Woodhead, J.D. (2015). Summary of results. NTGS laser ablation ICPMS U-Pb and Hf geochronology project: selected samples from NAPPERBY 1:250 000 mapsheet area, Arunta Region, July 2010–January 2012. *Northern Territory Geological Survey, Record 2015-009.*

Beyer, E.E., Donnellan, N., Meffre, S. & Thompson, J.M. (2016). Summary of results. NTGS laser ablation ICP-MS in situ zircon and baddeleyite geochronology project: Mount Peake Gabbro, Arunta Region. *Northern Territory Geological Survey, Record 2016-002*.

Blewett, R.S., Black, L.P., Sun, S.S., Knutson, J., Hutton, L.J. & Bain, J.H.C. (1998). U-Pb zircon and Sm-Nd geochronology of the Mesoproterozoic of North Queensland: implications for a Rodinian connection with the Belt Supergroup of North America. *Precambrian Research*, **89**, 101-127.

Bierlein, F.P., Black, L.P., Hergt, J. & Mark, G. (2008). Evolution of pre-1.8 Ga basement rocks in the Western Mt Isa Inlier, northeastern Australia—insights from SHRIMP U—Pb dating and in-situ, Lu—Hf analysis of zircons. *Precambrian Research*, **163(1)**, 159-173.

Bodorkos, S., Beyer, E.E., Edgoose, C.J., Whelan, J.A., Webb, G., Vandenberg, L.C. & Hallett, L. (2013). Summary of results. Joint NTGS–GA geochronology project: Central and eastern Arunta Region, January 2008 – June 2011. *Northern Territory Geological Survey, Record 2013-003*.

Bouvier, A., Vervoort, J.D. & Patchett, P.J. (2008). The Lu—Hf and Sm—Nd isotopic composition of CHUR: constraints from unequilibrated chondrites and implications for the bulk composition of terrestrial planets. *Earth and Planetary Science Letters*, **273(1-2)**, 0-57.

Carson, C.J., Claoué-Long, J., Stern, R., Close, D.F., Scrimgeour, I.R. & Glass, L.M. (2009). Summary of results. Joint NTGS-GA geochronology project: Central and eastern Arunta Region and Pine Creek Orogen, July 2006–May 2007. *Northern Territory Geological Survey, Record 2009-001*.

Chu, X., Zhang, T., Zhang, Q. & Lyons, T.W. (2007). Sulfur and carbon isotope records from 1700 to 800 Ma carbonates of the Jixian section, northern China: implications for secular isotope variations in Proterozoic seawater and relationships to global supercontinental events. *Geochimica Et Cosmochimica Acta, **71**(**19**)*, 4668-4692.

Close D.F. (2014). The McArthur Basin: NTGS ' approach to a frontier petroleum basin with known base metal prospectivity. *Annual Geoscience Exploration Seminar (AGES) Proceedings, Alice Springs, Northern Territory 15–16 March 2016.* Northern Territory Geological Survey, Darwin. pp. 85–89.

Close, D.I., Cote, A.J., Baruch, E.T., Altmann, C.M., Mohinudeen, F.M., Richards, B. & Ilett, R. (2017). Proterozoic shale gas plays in the Beetaloo Basin and the Amungee NW-1H discovery. *Annual Geoscience Exploration Seminar (AGES) Proceedings, Alice Springs, Northern Territory 28–29 March 2017*. Northern Territory Geological Survey, Darwin. pp. 91-97.

Collins, A., Farkas, J., Glorie, S., Cox, G., Blades, M.L., Yang, B., Nixon, A., Bullen, M., Foden, J., Dosseto, A., Payne, J.L., Denyszyn, S., Edgoose, C.J., Close, D., Munson, T.J., Menpes, S., Spagnuolo, S., Gusterhuber, J., Sheridan,

M., Baruch-Jurado, E. & Close, D., 2018. Orogens to oil: government–industry–academia collaboration to better understand the greater McArthur Basin: in *Annual Geoscience Exploration Seminar (AGES) Proceedings, Alice Springs, Northern Territory, 20–21 March 2018.* Northern Territory Geological Survey, Darwin. 49–51.

Condie, K.C., Beyer, E., Belousova, E., Griffin, W.L. & O'Reilly, S.Y. (2005). U–Pb isotopic ages and Hf isotopic composition of single zircons: the search for juvenile Precambrian continental crust. *Precambrian Research,* **139(1–2)**, 42-100.

Cox, G.M., Jarrett, A., Edwards, D., Crockford, P.W., Halverson, G.P., Collins, A.S., Poirier, A. & Li, Z.X. (2016). Basin redox and primary productivity within the Mesoproterozoic Roper Seaway. *Chemical Geology*, **440**, 101-114.

Cox, G.M., Sansjofre, P., Blades, M.L., Collins, A.S. & Farkas, J. (2019). Dynamic interaction between basin redox and the biogeochemical nitrogen cycle in an unconventional Proterozoic petroleum system. *Nature Scientific Reports*. In press.

Cross, A.J., Claoué-Long, J.C., Scrimgeour, I.R., Close, D.F. & Edgoose, C.J. (2005a). Summary of results. Joint NTGS-GA geochronology project: southern Arunta Region. *Northern Territory Geological Survey, Record 2004-003*.

Cross, A.J., Claoué-Long, J.C., Scrimgeour, I.R., Crispe, A. & Donnellan, N. (2005b). Summary of results. Joint NTGS-GA geochronology project: northern Arunta and Tanami regions, 2000–2003. *Northern Territory Geological Survey, Record 2005-003*.

Cross, A.J., Claoué-Long, J.C., Scrimgeour, I.R., Ahmad, M. & Kruse, P.D. (2005c). Summary of results. Joint NTGS-GA geochronology project: Rum Jungle, basement to southern Georgina Basin and eastern Arunta Region 2001–2003. *Northern Territory Geological Survey, Record 2005-006*.

Cross, A.J., Purdy, D.J., Bultitude, R.J., Brown, D.D. & Carr, P.A., (2015). Summary of results. Joint GSQ–GA geochronology project: Thomson Orogen, New England Orogen, Mossman Orogen and Mount Isa region, 2011–2013. *Queensland Geological Record 2016/03*.

Evans, D.A.D. & Mitchell, R.N. (2011). Assembly and breakup of the core of Paleoproterozoic-Mesoproterozoic supercontinent Nuna. *Geology,* **39(5)**, 443-446.

Evins, P.M., Smithies, R.H., Howard, H.M., Kirkland, C.L., Wingate, M.T.D. & Bodorkos, S. (2010). Devil in the detail; the 1150–1000 Ma magmatic and structural evolution of the Ngaanyatjarra Rift, west Musgrave Province, Central Australia. *Precambrian Research*, **183(3)**, 572–588.

Fanning, C.M. (2012). SHRIMP U–Pb zircon age determinations on detrital zircons from drill core sample ALT-051. ANU Research School of Earth Sciences, PRISE Report 12-260. Esso Australia. *Northern Territory Geological Survey, Core Sampling Report CSR0211*.

Flint, R.B. (1993). Mesoproterozoic. In: DREXEL, J.F., PREISS, W.V., PARKER A.J. (eds.). The Geology of South Australia, Volume 1, The Precambrian. Bulletin–Geological Survey of South Australia, Adelaide, pp. 107-169.

Foster, D.A. & Ehlers, K. (1998). ^{40}Ar-^{39}Ar thermochronology of the southern Gawler Craton, Australia: implications for Mesoproterozoic and Neoproterozoic tectonics of East Gondwana and Rodinia. *Journal of Geophysical Research: Solid Earth*, **103(B5)**, 10177-10193.

Frogtech Geoscience, 2018. SEEBASE® study and GIS for greater McArthur Basin. *Northern Territory Geological Survey, Digital Information Package DIP 017*.

Glorie, S., Agostino, K., Dutch, R., Pawley, M., Hall, J., Danišík, M., Evans, N.J. & Collins, A.S. (2017). Thermal history and differential exhumation across the eastern Musgrave Province, South Australia: insights from low-temperature thermochronology. *Tectonophysics,* **703–704**, 23-41.

Griffin, W.L., Belousova, E.A., Walters, S.G. & O''Reilly, S.Y. (2006). Archaean and Proterozoic crustal evolution in the eastern succession of the Mt Isa district, Australia: U–Pb and Hf–isotope studies of detrital zircons. *Journal of the Geological Society of Australia,* **53(1)**, 125-149.

Hoffman, T.W. (2015). Recent drilling results provide new insights into the western Palaeoproterozoic to Mesoproterozoic McArthur Basin. in 'Annual Geoscience Exploration Seminar (AGES) 2015. Record of abstracts'. *Northern Territory Geological Survey, Record (Vol. 2, pp. 50-55).*

Holland, H.D. (2006). The oxygenation of the atmosphere and oceans. *Philosophical Transactions of the Royal Society of London, 361*(1470), 903-915.

Hollis, J.A., Beyer, E.E., Whelan, J.A., Kemp, A.I.S., Scherstén, A. & Greig, A. (2010). Summary of results. NTGS laser U–Pb and Hf geochronology project: Pine Creek Orogen, Murphy Inlier, McArthur Basin and Arunta Region, July 2007–June 2008. *Northern Territory Geological Survey, Record 2010-001*.

Hoskin, P.W.O. & Black, L.P. (2000). Metamorphic zircon formation by solid-state recrystallization of protolith igneous zircon. *Journal of metamorphic Geology*, **18(4)**, 423-439.

Howard, H.M., Werner, M., Smithies, R.H., Kirkland, C.L., Kelsey, D.E., Hand, M., Collins, A., Pirajno, F., Wingate, M.T.D., Maier, W.D. & Raimondo, Y. (2011). The geology of the west Musgrave Province and the Bentley Supergroup–a field guide. *Geological Survey of Western Australia, Record 2011/4*, pp.116.

Hu, B., Zhai, M., Li, T., Li, Z., Peng, P., Guo, J. & Kusky, T.M. (2012). Mesoproterozoic magmatic events in the eastern north China craton and their tectonic implications: geochronological evidence from detrital zircons in the Shandong Peninsula and North Korea. *Gondwana Research, 22***(3–4)**, 828-842.

Jackson, M.J., Muir, M.D. & Sweet, I.P., 1986. Sedimentology of the Middle Proterozoic McArthur Basin, northern Australia. Field excursion guide, 12th International Sedimentological Congress. *Bureau of Mineral Resources, Australia, Canberra*.

Jackson, M.J., Sweet, I.P. & Powell, T.G. (1988). Studies on petroleum geology and geochemistry, middle Proterozoic, McArthur Basin Northern Australia I: Petroleum potential. *APEA J*, **28(1)**, 283-302.

Jackson, M.J. & Southgate, P.N. (2000). Evolution of three unconformity-bounded sandy carbonate successions in the McArthur River region of northern Australia: the Lawn, Wide and Doom Supersequences in a proximal part of the Isa Basin. In: Cockbain A. E. ed. Carpentaria-Mt Isa Zinc Belt: basement framework, chronostratigraphy and geodynamic evolution of Proterozoic successions (thematic issue). *Australian Journal of Earth Sciences*, **47**, 625-635.

Jackson, S.E., Pearson, N.J., Griffin, W.L. & Belousova, E.A. (2004). The application of laser ablation-inductively coupled plasma-mass spectrometry to in situ U–Pb zircon geochronology. *Chemical Geology*, **211(1)**, 47-69.

Johnson, S.P., Thorne, A.M., Tyler, I.M., Korsch, R.J., Kennett, B.L. N., Cutten, H.N., Goodwin, J., Blay, O., Blewett, R.S., Joly, A., Dentith, M.C., Aitken, A.R.A., Holzschuh, J., Salmom, M., Reading, A., Heinson, G., Boren, G., Ross, J., Costelloe, R.D. & Fomim, T. (2013). Crustal architecture of the Capricorn Orogen, Western Australia and associated metallogeny. *Australian Journal of Earth Sciences*, **60**, 681–705.

Jones, J.V.I., Daniel, C.G. & Doe, M.F. (2015). Tectonic and sedimentary linkages between the Belt-Purcell basin and southwestern Laurentia during the Mesoproterozoic, ca. 1.60-1.40 Ga. *Lithosphere,* **7(4)**, 685–700.

Kendall, B., Creaser, R.A., Gordon, G.W. & Anbar, A.D. (2009). Re–Os and Mo isotope systematics of black shales from the middle Proterozoic Velkerri and Wollogorang formations, McArthur Basin, Northern Australia. *Geochimica Et Cosmochimica Acta,* **73(9)**, 2534-2558.

Kirkland, C.L., Smithies, R.H., Woodhouse, A., Howard, H.M., Wingate, M., Belousova, E., Cliff, J.B., Murphy, R.C. & Spaggiari, C.V. (2013). Constraints and deception in the isotopic record; the crustal evolution of the west Musgrave Province, central Australia *Gondwana Research,* **23(2),** 759-781.

Kirkland, C.L., Smithies, R.H. & Spaggiari, C.V. (2015). Foreign contemporaries–Unravelling disparate isotopic signatures from Mesoproterozoic Central and Western Australia. *Precambrian Research*, **265**, 218-231.

Kirkland, C. L., Smithies, R. H., Spaggiari, C.V., Wingate, M., Quentin De Gromard, R., Clark, C., Gardiner, N.J., Belousova, E.A. (2017). Proterozoic crustal evolution of the Eucla basement, Australia: Implications for destruction of oceanic crust during emergence of Nuna. *Lithos*, **278-281**, 427-444.

Knoll, A.H., Javaux, E.J., Hewitt, D. & Cohen, P. (2006). Eukaryotic organisms in Proterozoic oceans. *Philosophical Transactions Biological Sciences,* **361(1470)**, 1023-1038.

Kositcin, N., Champion, D.C. & Huston, D.L. (2009). Geodynamic synthesis of the North Queensland Region and implications for metallogeny. *Geoscience Australia Record 2009/30*, pp 196.

Kositcin, N., Carson, C.J., Hollis, J.A., Glass, L.M., Close, D.F., Whelan, J.A., Webb, G. & Donnellan, N. (2013a). Summary of results. Joint NTGS–GA geochronology project: Arunta Region, Davenport Province and Pine Creek Orogen July 2009–June 2011. *Northern Territory Geological Survey, Record 2012-008*.

Kositcin, N., Beyer, E.E., Whelan, J.A., Close, D.F., Hallett, L. & Dunkley, D.J. (2013b). Summary of results. Joint NTGS–GA geochronology project: Arunta Region, Ngalia Basin, Tanami Region and Murphy Province, July 2011–June 2012. *Northern Territory Geological Survey, Record 2013-004*.

Kositcin, N., Whelan, J.A., Hallett, L. & Beyer, E.E., (2014a). Summary of results. Joint NTGS–GA geochronology project: Amadeus Basin, Arunta Region and Murphy Province, July 2012–June 2013. *Northern Territory Geological Survey, Record 2014-005*.

Kositcin, N., Beyer, E.E. & Whelan, J.A., (2014b). Summary of results. Joint NTGS–GA SHRIMP geochronology project: Arunta Region, July 2013–June 2014. *Northern Territory Geological Survey, Record 2014 -008*.

Kositcin, N., Kraus, S. & Whelan, J.A. (2015a). Summary of results. Joint NTGS–GA SHRIMP geochronology project: Arnhem Province, July 2014–June 2015. *Northern Territory Geological Survey, Record 2015-010.*

Kositcin, N., Reno, B.L. & Whelan, J.A. (2015b). Summary of results. Joint NTGS–GA geochronology project: Arunta Region, July 2014–June 2015. *Northern Territory Geological Survey, Record 2015-007*.

Kromkhun, K., Foden, J., Hore, S. & Baines, G. (2013). Geochronology and Hf isotopes of the bimodal mafic–felsic high heat producing igneous suite from Mt Painter Province, south Australia. *Gondwana Research*, **24(3-4)**, 1067-1079.

Lanigan, K., Hibbird, S., Menpes, S. & Torkinton, J. (1994). Petroleum exploration in the Proterozoic Beetaloo sub-basin, Northern Territory. *APEA JOURNAL*, **34**, 674-674.

Li, X.H., Chen, F., Guo, J.H., Li, Q.L., Xie, L.W. & Siebel, W. (2007). South China provenance of the lower-grade Penglai Group north of the Sulu UHP orogenic belt, eastern China: Evidence from detrital zircon ages and Nd–Hf isotopic composition. *Geochemical Journal*, **41**, 29-45 (in Chinese with English abstract).

Li, Z.X., Bogdanova, S.V., Collins, A.S., Davidson, A., Waele, B.D., Ernst, R.E., Fitzsimons, I.C.W., Fuck, R.A., Gladkochub, D.P., Jacobs, J., Karlstrom, K.E., Lu, S., Natapov, L.M., Pease, V., Pisarevsky, S.A., Thrane, K. & Vernikovsky, V. (2008). Assembly, configuration, and break-up history of Rodinia: a synthesis. *Precambrian Research, **160*(1)**, 179-210.

Li, Z.X. & Evans, D.A.D. (2011). Late Neoproterozoic 40°, intraplate rotation within Australia allows for a tighter-fitting and longer-lasting Rodinia. *Geology,* **39(1)**, 39-42.

Luo, G., Junium, C.K., Kump, L.R., Huang, J., Li, C., Feng, Q., Shi, X., Bai, X. & Xie, S. (2014). Shallow stratification prevailed for ~1700 to ~1300 Ma ocean: evidence from organic carbon isotopes in the North China Craton. *Earth & Planetary Science Letters*, **400**, 219-232.

Lyons, T.W., Reinhard, C.T. & Planavsky, N.J. (2014). The rise of oxygen in earth's early ocean and atmosphere. *Nature,* **506(7488)**, 307-315.

Mark, G. & Pollard, P. (2006). Episodic, potassic, 'A-type' Mesoproterozoic magmatism in the Mount Isa Inlier, NE Australia: a syn-tectonic origin?. *Geochimica Et Cosmochimica Acta,* **70(18)**, A393-A393.

Meng, Q.R., Ma, S.X., Wei, H.H. & Qu, Y.Q. (2011). Stratigraphic and sedimentary records of the rift to drift evolution of the northern North China Craton at the Paleo- to Mesoproterozoic transition. *Gondwana Research,* **20(1)**, 205-218.

Merdith, A.S., Collins, A.S., Williams, S.E., Pisarevsky, S., Foden, J.F., Archibald, D., Blades, M.L., Alessio, B.L., Armistead, S., Plavsa, D., Clark, C. & Müller, R.D. (2017). A full-plate global reconstruction of the Neoproterozoic. *Gondwana Research*, **50**, 84-134.

Merdith, A.S., Williams, S.E., Brune, S., Collins, A.S. & Müller, R.D. (2019). Rift and plate boundary evolution across two supercontinent cycles. *Global and Planetary Change*, **173**, 1-14.

Morrissey, L.J., Payne, J.L., Hand, M., Clark, C., Taylor, R., Kirkland, C.L. & Kylander-Clark, A. (2017). Linking the Windmill Islands, east Antarctica and the Albany–Fraser Orogen: insights from U–Pb zircon geochronology and Hf isotopes. *Precambrian Research,* **293,** 131–149.

Morrissey, L.J., Barovich, K.M., Hand, M., Howard, K.E. & Payne, J.L. (2018). Magmatism and metamorphism at c. 1.45 Ga in the northern Gawler Craton: the Australian record of rifting within Nuna (Columbia). *Geoscience Frontiers.* **10(1)**, 175-194.

Mulder, J.A., Halpin, J.A. & Daczko. N.R. (2015). Mesoproterozoic Tasmania: Witness to the East Antarctica–Laurentia connection within Nuna. *Geology*, **43**, 759-769.

Mukherjee, I. & Large, R.R. (2016). Pyrite trace element chemistry of the Velkerri Formation, Roper Group, McArthur Basin: Evidence for atmospheric oxygenation during the Boring Billion. *Precambrian Research*, **281**, 13-26.

Mukherjee, I., Large, R.R., Corkrey, R. & Danyushevsky, L.V. (2018). The boring billion, a slingshot for complex life on earth. *Scientific Reports*, **8(1)**, 4432.

Munson, T.J., Kruse, P.D. & Ahmad, M. (2012). Chapter 22: Centralian Superbasin. In M. Ahmad and T.J. Munson (eds), Geology and Mineral Resources of the Northern Territory. 22:1, 22:19

Munson, T.J. (2016). Sedimentary characterisation of the Wilton package, greater McArthur Basin. Northern Territory. *Northern Territory Geological Survey, Record 2016-003*.

Munson T.J. & Revie, D. (2018). Stratigraphic subdivision of Velkerri Formation, Roper Group, McArthur Basin, Northern Territory. *Northern Territory Geological Survey, Record 2018-006***.**

Munson, T.J, Thompson, J.M, Zhukova, I., Meffre, S., Beyer, E.E., Woodhead, J.D. & Whelan, J.A. (2018). Summary of results. NTGS laser ablation ICP-MS U–Pb and Lu–Hf geochronology project: Roper Group and overlying ungrouped units (McArthur Basin), Renner Group (Tomkinson Province), Tijunna Group (Birrindudu Basin). *Northern Territory Geological Survey, Record* 2018-007.

Murgulov, V., Beyer, E., Griffin, W.L., O'Reilly, S.Y., Walters, S.G. & Stephens, D. (2007). Crustal evolution in the Georgetown Inlier, north Queensland, Australia: a detrital zircon grain study. *Chemical Geology,* **245(3)**, 198-218.

Nebel, O., Nebel-Jacobsen, Y., Mezger, K., and Berndt, J. (2007), Initial Hf isotope compositions in magmatic zircon from early Proterozoic rocks from the Gawler Craton, Australia: a test for zircon model ages. *Chemical Geology*, **241**, 23-37.

Neumann, N.L., Southgate, P.N., Gibson, G.M. & McIntyre, A. (2006). New SHRIMP geochronology for the Western Fold Belt of the Mt Isa Inlier: developing a 1800–1650 Ma event framework. *Australian Journal of Earth Sciences*, **53(6)**, 1023-1039.

Neumann, N.L., Gibson, G.M. & Southgate, P.N. (2009). New SHRIMP age constraints on the timing and duration of magmatism and sedimentation in the Mary Kathleen Fold Belt, Mt Isa Inlier, Australia. *Australian Journal of Earth Sciences*, **56(7)**, 965-983.

Nordsvan, A.R., Collins, W.J., Li, Z.X., Spencer, C.J., Pourteau, A., Withnall, I.W., Betts, P.G. & Volante, S. (2018). Laurentian crust in northeast Australia: Implications for the assembly of the supercontinent Nuna. *Geology*, **46(3)**: 251–254.

Page, R.W. & Sun, S.S. (1998). Aspects of geochronology and crustal evolution in the Eastern Fold Belt, Mt Isa Inlier. *Australian Journal of Earth Sciences*, **45(3)**, 343-361.

Park, H.U., Zhai, M.G., Yang, J.K., Peng, P., Kim, J.N., Zhang, Y.B., Kim, M.G., Park, U. & Feng, L.J. (2016). Deposition age of the Sangwon Supergroup in the Pyongnam basin (Korea) and the Early Tonian negative carbon isotope interval. *Acta Petrologica Sinica,* **32(07)**, 2181-2195 (in Chinese with English abstract).

Paton, C., Hellstrom, J., Paul, B., Woodhead, J. & Hergt, J. (2011). Iolite: Freeware for the visualisation and processing of mass spectrometric data. *Journal of Analytical Atomic Spectrometry*, **26(12)**, 2508-2518.

Payne, J.L., Pearson, N.J., Grant, K.J. & Halverson, G.P. (2013). Reassessment of relative oxide formation rates and molecular interferences on in situ lutetium–hafnium analysis with laser ablation MC-ICP-MS. *Journal of Analytical Atomic Spectrometry,* **28(7)**, 1068-1079.

Pietsch, B.A., Rawlings, D.J., Creaser, P.M., Kruse, P.D., Ahmad, M., Ferenczi, P.A. & Findhammer, T.L.R., 1991. *Bauhinia Downs, Northern Territory. 1:250 000 geological map series explanatory notes, SE 53-03*. Northern Territory Geological Survey, Darwin.

Pisarevsky, S.A., Elming, S.Å., Pesonen, L.J. & Li, Z.X. (2014). Mesoproterozoic paleogeography: supercontinent and beyond. *Precambrian Research,* **244(1)**, 207-225.

Plumb, K.A. & Wellman, P. (1987). McArthur Basin, Northern Territory: mapping of deep troughs using gravity and magnetic anomalies. *BMR Journal of Australian Geology & Geophysics,* **10**, 243-251.

Pourteau, A., Smit, M.A., Li, Z.X., Collins, W.J., Nordsvan, A.R. & Volante, S. (2018). 1.6 Ga crustal thickening along the final Nuna suture. Geology, **46**, 959-962.

Powell, T.G., Jackson, M.J., Sweet, I.P., Crick, I.H., Boreham, C.J. & Summons, R.E., 1987. *Petroleum geology and geochemistry, middle Proterozoic McArthur Basin*. *Bureau of Mineral Resources, Australia, Record* 1987/048.

Rasmussen, B., Fletcher, I.R., Brocks, J.J. & Kilburn, M.R. (2008). Reassessing the first appearance of eukaryotes and cyanobacteria. *Nature,* **455(7216)**, 1101-1104.

Rawlings, D.J. (1999). Stratigraphic resolution of a multiphase intracratonic basin system: The McArthur Basin, northern Australia. *Australian Journal of Earth Sciences*, **46(5)**, 703-723.

Reid, A.J. & Payne, J.L. (2017). Magmatic zircon Lu-Hf isotopic record of juvenile addition and crustal reworking in the Gawler Craton, Australia. *Lithos*, **292**, 294-306.

Revie, D. (2017).Volumetric resource assessment of the lower Kyalla and middle Velkerri formations of the McArthur Basin. *Annual Geoscience Exploration Seminar (AGES) Proceedings, Alice Springs, Northern Territory 28–29 March 2017*. Northern Territory Geological Survey, Darwin. pp. 86-90.

Ross, G.M. & Villeneuve, M. (2003). Provenance of the Mesoproterozoic (1.45 Ga) belt basin (western North America): another piece in the pre-Rodinia paleogeographic puzzle. *Geological Society of America Bulletin,* **115(10)**, 1191-1217.

Saha, D., Bhowmik, S.K., Bose, S. & Sajeev, K. (2016). Proterozoic tectonics and trans-Indian mobile belts: a status report. *Proceedings of the Indian National Science Academy*, **82(3)**, 445-460.

Sandiford, M., Hand, M. & Mclaren, S. (2001). Tectonic feedback, intraplate orogeny and the geochemical structure of the crust: a central Australian perspective. *Geological Society London Special Publications*, **184(1)**, 195-218.

Scherer, E., Münker, C. & Mezger, K. (2001). Calibration of the lutetium-hafnium clock. *Science,* **293(5530)**, 683-687.

Sheridan, M., Johns, D.R., Johnson, H.D. & Menpes, S. (2018). The stratigraphic architecture, distribution and hydrocarbon potential of the organic-rich Kyalla and Velkerri shales of the Upper Roper Group (McArthur Basin). The APPEA Journal, **58**, 858-864.

Silverman, M.R., Landon, S.M., Leaver, J.S., Mather, T.J. & Berg, E. (2007). No fuel like an old fuel: Proterozoic oil and gas potential in the Beetaloo Basin, Northern Territory, Australia: in Munson TJ and Ambrose GJ (editors)'. In Proceedings of the Central Australian Basins Symposium (CABS), Alice Springs, Northern Territory, 16–18 August, 2005.*'Northern Territory Geological Survey, Special Publication (Vol. 2).*

Silverman, M. & Ahlbrandt, T. (2011). Mesoproterozoic Unconventional Plays in the Beetaloo Basin, Australia: The World's Oldest Petroleum Systems. *AAPG International Conference and Exhibition, Calgary, Alberta, 2011,* 1-41.

Sláma, J., Košler, J., Condon, D.J., Crowley, J.L., Gerdes, A., Hanchar, J.M., Horstwood, M.S.A., Morris, G.A., Nasdala, L., Norberg, N., Schaltegger, U., Schoene, B., Tubrett, M. N. & Whitehouse, M. J. (2008). Plešovice zircon—a new natural reference material for U–Pb and Hf isotopic microanalysis. *Chemical Geology,* **249(1–2)**, 1-35.

Smithies, R.H., Howard, H.M., Evins, P.M., Kirkland, C.L., Kelsey, D.E., Hand, M., Wingate, M.T.D., Collins, A.S. & Belousova, E. (2011). High-temperature granite magmatism, crust–mantle interaction and the Mesoproterozoic intracontinental evolution of the Musgrave Province, Central, Australia. *Journal of Petrology,* **52(5)**, 931-958.

Smits, R.G., Collins, W.J., Hand, M., Dutch, R. & Payne, J. (2014). A Proterozoic Wilson cycle identified by Hf isotopes in central Australia: implications for the assembly of Proterozoic Australia and Rodinia. *Geology*, **42(3)**, 231-234.

Southgate, P.N., Bradshaw, B.E., Domagala, J., Jackson, M.J., Idnurm, M., Krassay, A.A., Page, R.W., Sami, T.T., Scott, D.L., Lindsay, J.F. & McConachie, B. A. (2000). Chronostratigraphic basin framework for Palaeoproterozoic rocks (1730–1575 Ma) in northern Australia and implications for base-metal mineralisation. *Australian Journal of Earth Sciences*, **47(3)**, 461-483.

Spaggiari, C.V., Kirkland, C.L., Smithies, R.H., Wingate, M.T.D. & Belousova, E.A. (2015). Transformation of an Archean craton margin during Proterozoic basin formation and magmatism: The Albany–Fraser Orogen, Western Australia. *Precambrian Research*, **226**, 440-466.

Spencer, C.J., Cawood, P.A., Hawkesworth, C.J., Prave, A.R., Roberts, N.M.W., Horstwood, M.S.A., Whitehouse, M.J. & EIMF. (2015). Generation and preservation of continental crust in the Grenville orogeny. *Geoscience Frontiers,* **6(3)**, 357-372.

Spikings, R.A., Foster, D.A., Kohn, B.P. & Lister, G.S. (2001). Post-orogenic (< 1500 Ma) thermal history of the Proterozoic Eastern Fold Belt, Mount Isa Inlier, Australia. *Precambrian Research*, **109(1)**, 103-144.

Spikings, R.A., Foster, D.A., Kohn, B.P. & Lister, G.S. (2002). Post-orogenic (< 1500 Ma) thermal history of the Palaeo-Mesoproterozoic, Mt. Isa province, NE Australia. *Tectonophysics*, **349(1)**, 327-365.

Szpunar, M., Hand, M., Barovich, K., Belousova, E., Jagodzinski, E.A. (2011). Isotopic and geochemical constraints on the Paleoproterozoic Hutchison Group, southern Australia: implications for Paleoproterozoic continental reconstructions. *Precambrian Research,* **187**, 99-126.

Vermeesch, P. (2013). Multi-sample comparison of detrital age distributions. *Chemical Geology*, **341**, 140-146.

Vermeesch, P. (2014). Corrigendum to "Multi-sample comparison of detrital age distributions" [Chem. Geol. 341 (11 March 2013)—140-146]. *Chemical Geology*, **380**, 191.

Wade, B.P. (2006). Unravelling the tectonic framework of the Musgrave Province, central Australia. PhD Thesis. University of Adelaide.

Walter, M.R., Veevers, J.J., Calver, C.R. & Grey, K. (1995). Neoproterozoic Stratigraphy of the Centralian Superbasin, Australia. *Precambrian Research*, **73**, 173-195.

Warren, J.K., George, S.C., Hamilton, P.J. & Tingate, P. (1998). Proterozoic source rocks: sedimentology and organic characteristics of the Velkerri formation, Northern Territory, Australia. *AAPG Bulletin,* **82(3)**, 442-463.

Wingate, M.T.D., Pirajno, F. & Morris, P.A. (2004). Warakurna large igneous province: A new Mesoproterozoic large igneous province in west-central Australia. *Geology,* **32**, 105-108.

Wong, B.L., Morrissey, L.J., Hand, M., Fields, C.E. & Kelsey, D.E. (2015). Grenvillian-aged reworking of late Paleoproterozoic crust of the southern North Australian Craton, central Australia: implications for the assembly of Mesoproterozoic Australia. *Precambrian Research,* **270**, 100-123.

Woodhead, J., Hergt, J., Shelley, M., Eggins, S. & Kemp, R. (2004). Zircon Hf-isotope analysis with an excimer laser, depth profiling, ablation of complex geometries, and concomitant age estimation. *Chemical Geology,* **209(1–2)**, 121-135.

Woodhead, J.D. & Hergt, J.M. (2005). A preliminary appraisal of seven natural zircon reference materials for in situ Hf isotope determination. *Geostandards & Geoanalytical Research,* **29(2)**, 183–195.

Worden, K.E., Claoué-Long, J.C., Scrimgeour, I.R. & Doyle, N. (2006a). Summary of results. Joint NTGS-GA geochronology project: Pine Creek Orogen and Arunta Region, January–June 2004. *Northern Territory Geological Survey, Record 2006-005.*

Worden, K.E., Claoué-Long, J.C. & Scrimgeour, I.R. (2006b). Summary of results. Joint NTGS-GA geochronology project: Pine Creek Orogen, Tanami Region, Arunta Region and Amadeus Basin, July–December 2004. *Northern Territory Geological Survey, Record 2006-006.*

Worden, K.E., Carson, C.J., Close, D.F., Donnellan, N. & Scrimgeour, I.R. (2008). Summary of results. Joint NTGS-GA geochronology project: Tanami Region, Arunta Region, Pine Creek Orogen and Halls Creek January 2005–March 2007. *Northern Territory Geological Survey, Record 2008-003.*

Xu, H., Yang, Z., Peng, P., Meert, J.G. & Zhu, R. (2014). Paleo-position of the North China Craton within the supercontinent Columbia: constraints from new paleomagnetic results. *Precambrian Research*, **255**, 276–293.

Yang, B., Smith, T.M., Collins, A.S., Munson, T.J., Schoemaker, B., Nicholls, D., Cox, G., Farkas, J. & Glorie, S. (2018). Spatial and temporal detrital zircon U–Pb provenance of the hydrocarbon-bearing upper Roper Group, Beetaloo Sub-Basin, Northern Territory, Australia. *Precambrian Research*, **304**, 140-155.

Yang, D.B., Xu, W.L., Xu, Y.G., Wang, Q.H., Pei, F.P. & Wang, F. (2012). U–Pb ages and Hf isotope data from detrital zircons in the Neoproterozoic sandstones of northern Jiangsu and southern Liaoning provinces, China: implications for the late Precambrian evolution of the southeastern North China Craton. *Precambrian Research,* **216-219(9)**, 162-176.

Yang, J.H., Peng, P., Jong, C.S., Park, U., Mun, J.G., Kin, C.H. & K, H.C. (2016). Comparison on ages of detrital zircons from the Paleoproterozoic to lower Paleozoic sedimentary rocks in the Pyongnam basin, Korea. *Acta Petrologica Sinica,* **32(10)**, 3155-3179 (in Chinese with English abstract).

Zhang, S.H., Zhao, Y., Yang, Z.Y., He, Z.F. & Wu, H. (2009). The 1.35 Ga diabase sills from the northern North China Craton: implications for breakup of the Columbia (Nuna) supercontinent. *Earth & Planetary Science Letters,* **288(3)**, 588-600.

Zhang, S., Li, Z. X., Evans, D.A.D., Wu, H., Li, H. & Dong, J. (2012). Pre-Rodinia supercontinent Nuna shaping up: a global synthesis with new paleomagnetic results from north China. *Earth & Planetary Science Letters*, **353-354**, 145-155.

Zhang, S.H., Zhao, Y., Li, X.H., Ernst, R.E. & Yang, Z.Y. (2017). The 1.33–1.30 Ga Yanliao large igneous province in the North China Craton: implications for reconstruction of the Nuna (Columbia) supercontinent, and specifically with the North Australian Craton. *Earth & Planetary Science Letters,* **465**, 112-125.

Zhang, K., Zhu, X., Wood, R.A., Shi, Y., Gao, Z. & Poulton, S.W. (2018). Oxygenation of the Mesoproterozoic Ocean and the evolution of complex eukaryotes. *Nature Geoscience*, **11**, 345-350.

Chapter 4

Sedimentary geochemical record of the middle Mesoproterozoic —early Neoproterozoic tectonic geography of Northern Australia

---

Submitted as:

Yang, B., Collins, A.S., Cox, G.M., Jarrett, A.J.M., Denyszyn, S., Blades, M.L., Farkaš, J., Glorie, S. Sedimentary geochemical record of the middle Mesoproterozoic—early Neoproterozoic tectonic geography of Northern Australia.

Statement of Authorship

Title of Paper	Sedimentary geochemical record of the middle Mesoproterozoic —early Neoproterozoic tectonic geography of Northern Australia
Publication Status	☐ Published ☐ Accepted for Publication ☑ Submitted for Publication ☐ Unpublished and Unsubmitted w ork w ritten in manuscript style
Publication Details	Yang, B., Collins, A.S., Cox, M.G., Jarrett, J.M.A., Denyszyn, S., Blades, M.L., Farkaš, J., Glorie, S. Submitted. Sedimentary geochemical record of the middle Mesoproterozoic —early Neoproterozoic tectonic geography of Northern Australia.

Principal Author

Name of Principal Author (Candidate)	Bo Yang		
Contribution to the Paper	Sample preparation, data collection and processing, data interpretation, manuscript composition.		
Overall percentage (%)	80		
Certification:	This paper reports on original research I conducted during the period of my Higher Degree by Research candidature and is not subject to any obligations or contractual agreements with a third party that would constrain its inclusion in this thesis. I am the primary author of this paper.		
Signature		Date	21/06/2019

Co-Author Contributions

By signing the Statement of Authorship, each author certifies that:

i. the candidate's stated contribution to the publication is accurate (as detailed above);

ii. permission is granted for the candidate in include the publication in the thesis; and

iii. the sum of all co-author contributions is equal to 100% less the candidate's stated contribution.

Name of Co-Author	Alan S. Collins		
Contribution to the Paper	Guidance on data interpretation, manuscript review.		
Signature		Date	22/06/2019

Name of Co-Author	Grant M. Cox		
Contribution to the Paper	Sample preparation, guidance on data interpretation, manuscript review.		
Signature		Date	22/06/2019

Name of Co-Author	Amber J. M. Jarrett		
Contribution to the Paper	Sample preparation, data collection, manuscript review.		
Signature		Date	11/06/2019

Name of Co-Author	Steven Denyszyn		
Contribution to the Paper	Data collection, guidance on data interpretation, manuscript review.		
Signature		Date	12/06/2019

Name of Co-Author	Morgan L. Blades		
Contribution to the Paper	Manuscript review.		
Signature		Date	21/06/2019

Name of Co-Author	Juraj Farkaš		
Contribution to the Paper	Manuscript review.		
Signature		Date	22/06/2019

Name of Co-Author	Stijn Glorie		
Contribution to the Paper	Manuscript review.		
Signature		Date	22/06/2019

Chapter 4

Sedimentary geochemical record of the middle Mesoproterozoic —early Neoproterozoic tectonic geography of Northern Australia

Abstract

The Beetaloo Sub-basin, northern Australia, is considered the main depocentre of the 1000 km-scale Mesoproterozoic Wilton package of the greater McArthur Basin. The *ca.* 1.40–1.31 Ga upper Roper Group and the latest Mesoproterozoic to early Neoproterozoic unnamed group of the Beetaloo Sub-basin, together, record *ca.* 500-million-years of depositional history within the North Australia Craton. Whole-rock shale Sm–Nd and Pb isotope data reveal a dynamic interaction between sedimentary provenance and ancient tectonic geography. The *ca.* 1.35–1.31 Ga Kyalla Formation of the upper Roper Group is composed of isotopically evolved sedimentary detritus, whereas the upper portions of this formation contain more isotopically juvenile compositions. The increase in juvenile compositions also coincides with elevated total organic carbon (TOC) and phosphorous (P) content of these sediments, which are thought to reflect an increase in nutrient supply associated with the weathering of basaltic sources. Possible, relatively juvenile, basaltic sources include the Wankanki Supersuite in the western Musgraves and the Derim Derim–Galiwinku large igneous province (LIP). The transition into juvenile, basaltic sources directly before a supersequence-bounding unconformity, is here interpreted to reflect uplift and erosion of the Derim Derim–Galiwinku LIP, rather than an influx of southern, Musgrave sources. A new baddeleyite crystallization age of 1312.9 ± 0.7 Ma provides both a tight constraint on the age of this LIP, along with its associated magmatic uplift, as well as providing a minimum age constraint for Roper Group deposition. The supra-Roper Group lower and upper Jamison sandstones were both sourced from the Musgrave Province, at least 300 million years after deposition of the Kyalla Formation. An up-section increase in isotopically juvenile compositions seen in these rocks, are interpreted to document the continuous exhumation of the western Musgrave Province. The overlying Hayfield mudstone received detritus from both the Musgrave and Arunta regions, and its isotopic geochemistry reveals affinities with other early

Neoproterozoic basins (e.g. Amadeus, Victoria and Officer basins), indicating the potential for inter-basin correlations.

1. Introduction

The geochemistry of fine-grained sedimentary rocks provides a wealth of information central to interpreting sedimentary processes and reconstructing the tectonic geography of an area, including sediment provenance, sediment transportation pathways, deposition and organic matter preservation (*Sageman & Lyons, 2003; Piper & Calvert, 2009; Cox et al., 2016a*). Theoretically, an integrated understanding of Earth's sedimentary archive can help elucidate the complex interactions between the climate, biosphere, geography, tectonic evolution, and crust-mantle interactions (e.g. *Anbar & Knoll, 2002; Horton, 2015; Lyons et al., 2015; Cox et al., 2016b; Merdith et al., 2017; Mukherjee et al., 2018*).

One of the best archives of Mesoproterozoic fine-grained sedimentary successions is the greater McArthur Basin (*Close, 2014*) of northern Australia. The basin covers an area over 145,000 km^2, forms a temporal record spanning nearly 1 billion years (from *ca.* 1820 Ma to the early Neoproterozoic), and records the detailed tectonic and sedimentation history of the North Australia Craton (*Rawlings, 1999; Ahmad & Munson, 2013; Cox et al., 2016a; Munson, 2016; Munson et al., 2018; Chapters 1 & 2*). The subsurface Beetaloo Sub-basin, towards the centre of the greater McArthur Basin, is the depocentre of the upper part of the greater McArthur Basin, represented here by the Roper Group (*Lanigan et al., 1994; Ahmad & Munson, 2013*).

This study focuses on the sedimentary geochemistry of the *ca.* 1.35–1.31 Ga Kyalla Formation of the upper Roper Group and three informally named formations (the lower and upper Jamison sandstones and the Hayfield mudstone) that unconformably overlie the Roper Group and are constrained to be deposited after *ca.* 1.09 Ga and before the Cambrian. We have focussed on these units, to investigate the provenance and tectono-geographic changes at the end of the greater McArthur Basin. Shale whole-rock Sm–Nd and Pb isotope data, in combination with new U–Pb isotope dilution thermal ionization mass spectrometry (ID-TIMS) baddeleyite dating, provide a record of the sedimentary history of the basin, as well as a minimum age constraint for deposition. They further reveal the dynamic evolution of the tectonic geography of northern Australia, from the middle Mesoproterozoic to the early Neoproterozoic.

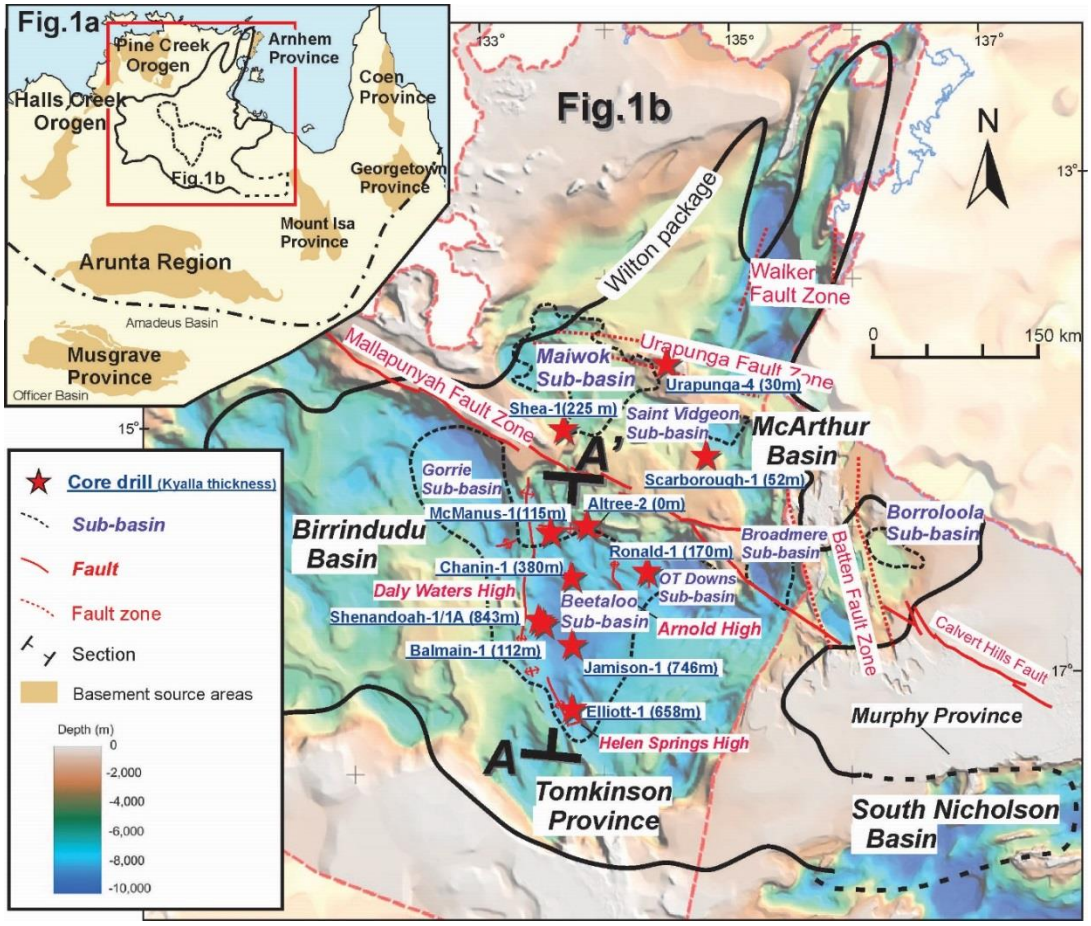

Figure 1 (a) tectonic frame of the North Australia Craton and the McArthur Basin; (b) the extent of the Wilton Package (SEEBASE™ basement surface image after *Frogtech Geoscience (2018)*) modified after *Munson (2016)* and *Chapter 3*.

2. Geological Setting

2.1 Roper Group, Kyalla Formation

The greater McArthur Basin covers most of the northern North Australia Craton and it is surrounded by exposed basement areas and orogens (*Rawlings, 1999*; *Ahmad & Munson, 2013; Munson et al., 2016; Munson et al., 2018;* Figure 1a). The greater McArthur Basin has been sub-divided into five sedimentary packages separated by regional unconformities (*Rawlings, 1999; Ahmad & Munson, 2013; Munson et al., 2016; Munson et al., 2018*). The Wilton Package is the name given to the broad grouping of coeval sedimentary successions deposited in geographically separated basins or sub-basins, including the Roper Group of the McArthur Basin (*sensu strictu*) and the subsurface Beetaloo Sub-basin, the Renner Group of the Tomkinson Province and the Tijunna Group of the Birrindudu Basin (Figure 1b; *Close, 2014; Munson, 2016; Munson et al., 2018*), and potentially the South Nicholson Group of the South Nicholson Basin (*Munson, 2016*). The Beetaloo Sub-basin is where the thickest succession of these sediments has been found and

is considered to be the depocentre of the basin (*Lanigan et al., 1994; Ahmad & Munson, 2013; Munson, 2016; Munson et al., 2018*). The Roper Group has been sub-divided into two subgroups—the lower Collara Subgroup and the upper Maiwok Subgroup (*Rawlings, 1999; Ahmad & Munson, 2013*). These two subgroups were both deposited in a stable shelf environment. The Collara Subgroup is dominated by sandstones with less voluminous mudrocks, while the Maiwok Subgroup is characterised by fine-grained sedimentary formations with minor sandstones (*Rawlings, 1999; Abbott et al., 2001; Ahmad & Munson, 2013; Munson, 2016; Munson et al., 2018*).

The Kyalla Formation is the uppermost shale-dominated formation of the Maiwok Subgroup in the Beetaloo Sub-basin, and is a principle focus of this research. The Kyalla Formation conformably overlies the Moroak Sandstone and comprises interbedded siltstone and mudstone with minor fined-grained sandstone intervals, and is suggested to have been deposited in a storm-dominated shallow-marine shelf environment (*Abbott et al., 2001; Ahmad & Munson, 2013; Munson, 2016; Munson et al., 2018*). The Kyalla Formation is poorly exposed in the McArthur Basin (mainly in the Urapunga Region; *Munson, 2016*), but well preserved in the Beetaloo Sub-basin, where this formation is prospective for both oil and gas (*Revie, 2017; Munson & Revie, 2018; Revie & Normington, 2018*). The Kyalla Formation has been informally sub-divided into three units (lower, middle and upper members) according to geophysical logs. The middle member is slightly coarser-grained (*Gorter & Grey, 2012; Munson, 2016*). The Kyalla Formation exhibits remarkable lateral continuity and thins towards the north–northeast of the basin (*Munson, 2016*; Figures 1b and 2). In the southern and central parts of the basin, the thickness of the Kyalla Formation varies in cores from about 660 m (Elliott-1 – Figures 1b and 2) to about 840 m (Shenandoah-1/1A – Figures 1b and 2), whereas in the north, the upper two members are missing and the thickness drops to about 220 m in McManus-1 (Figures 1b and 2), and the formation is totally missing in Altree-2 (Figures 1b and 2). A sandstone interval (informally named the Elliott sandstone member; *Munson et al., 2016*) within the top of the lower Kyalla member can be identified within the south and central parts of the basin (e.g. cores Elliott-1, Jamison-1, Chanin-1 and Ronald-1; Figure 2), but is absent in the north of the basin (e.g. cores McManus-1 and Altree-2; Figure 2). The absence of this sandstone member in the north is interpreted to suggest its removal by erosion. In the Urapunga Region, the Kyalla Formation shows a variable thickness from *ca.* 30 m in core Urapunga-4, *ca.* 52 m in core Scarborough-1 and about 225 m in core Shea-1 (Figure 1b).

The maximum depositional age of the Kyalla Formation is constrained to be younger than 1308 ± 41 Ma (*Chapter 2*), while the minimum depositional age is constrained by dolerite sills of the

Derim Derim–Galiwinku LIP that cross-cut the Kyalla Formation with a revised age of 1312.9 ± 0.7 Ma (this study). Together these maximum and minimum depositional age constraints bracket deposition between 1349 Ma and 1312.2 Ma (at 2 standard deviations). Sandstone samples collected from the Kyalla Formation of the Beetaloo Sub-basin contain detrital zircon age populations and hafnium isotope signatures that show significant similarities to rocks exposed in the Arunta Region, indicating that this formation was sourced from north-flowing rivers from this area (*Chapters 2 & 3*).

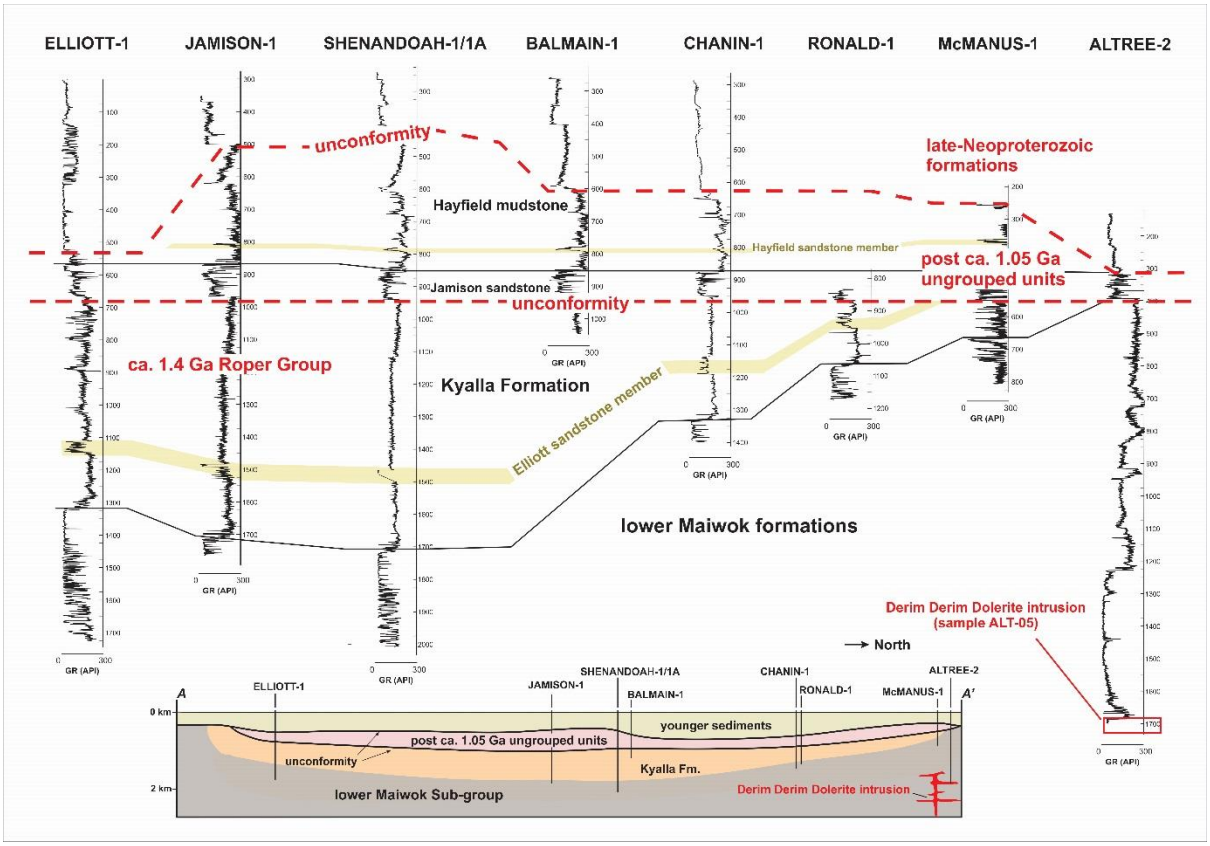

Figure 2 Beetaloo Sub-basin N–S fence diagram with gamma-ray (GR) logs. The Kyalla Formation thins towards the north, which is interpreted to be due to progressive increased pre-Jamison sandstone uplift and erosion towards the north (modified after *Gorter & Grey, 2013*).

2.2 Latest Mesoproterozoic to Neoproterozoic unnamed group

In the Beetaloo Sub-basin, the Kyalla Formation is unconformably overlain by a set of late Mesoproterozoic to early Neoproterozoic sandstone to mudstone successions comprising three formations/units, informally named the lower Jamison sandstone, the upper Jamison sandstone and the Hayfield mudstone (*Munson, 2016*). The lower and upper Jamison sandstone units both contain dominantly medium to coarse quartz sandstone successions with minor siltstone/shale intervals, deposited in a high-energy shoreline to shallow-marine inner shelf setting (*Ahmad &*

Munson, 2013; Lanigan et al., 1994; Munson, 2016; Munson et al., 2018). The Hayfield mudstone conformably overlies the upper Jamison sandstone and is characterised by a set of mudrock-rich organic-poor sediments with minor sandstones, indicative of a subtidal shallow-marine shelf setting (*Munson et al., 2018*). This mudstone unit is unconformably overlain by a set of late Neoproterozoic to early Cambrian sedimentary basins (e.g. the Georgina Basin; Figure 2) as well as by the Kalkarindji LIP. The maximum depositional ages for these three formations are constrained by detrital zircon U–Pb isotopic ages, suggesting that the lower Jamison sandstone was deposited after 1092 ± 16 Ma, and the upper Jamison sandstone and Hayfield mudstone have been constrained to be deposited after 959 ± 18 Ma (*Chapter 2*). The three formations of the unnamed group have been only observed in the Beetaloo Sub-basin. The lower and upper Jamison sandstones show consistent thickness of *ca.* 100 m, whereas significant thickness variations have been observed for the Hayfield mudstone, from ~450m in the central portion of the basin (e.g. Shenandoah-1/1A—Figure 2), but pinching out towards both the south and north (Figure 2). Detrital zircon U–Pb age and hafnium isotope data collected from these three formations show affinities to those of the Musgrave Province (*Munson, 2016; Munson et al., 2018; Chapter 2 & 3*).

3. Shale whole-rock isotopic composition

Shale samples for whole-rock Sm–Nd and Pb isotope analysis were collected from the core Balmain-1 (Figures 1b and 2). A total of fifteen bulk shale samples were analysed, including five samples from the Kyalla Formation, two samples from the lower Jamison sandstone, one from the upper Jamison sandstone and seven from the Hayfield mudstone. Bulk shale samples for the lower and upper Jamison sandstone were collected from shale-component intervals. Details of the sample information and analytical methods and results are provided in the Appendix 3 and the isotope results are presented in Table 1.

Samples from the Kyalla Formation yield whole-rock $\varepsilon_{Nd(t)}$ values ranging from -4.76 to -3.29 (Table 1; Figure 3). Two bulk shale samples from the lower Jamison sandstone yield $\varepsilon_{Nd(t)}$ values of -6.22 and -5.23, showing more evolved characteristics than the sample from the upper Jamison sandstone ($\varepsilon_{Nd(t)}$: -3.63), while $\varepsilon_{Nd(t)}$ values of the samples from the Hayfield mudstone range from -7.83 to -5.09 (Table 1; Figure 3).

The Pb isotopic compositions of the Kyalla Formation are characterised by a large range in $^{206}Pb/^{204}Pb$ (13.983 to 16.957), $^{207}Pb/^{204}Pb$ (14.276 to 15.766) and $^{208}Pb/^{204}Pb$ (35.105 to 39.698) ratios. The samples of the lower Jamison sandstone return $^{206}Pb/^{204}Pb$ ratios of 17.207 and 15.886, $^{207}Pb/^{204}Pb$ ratios of 15.831 and 15.616, and $^{208}Pb/^{204}Pb$ ratios of 40.993 and 39.398.

The upper Jamison sample yields a $^{206}Pb/^{204}Pb$ ratio of 17.474, a $^{207}Pb/^{204}Pb$ ratio of 15.639 and a $^{208}Pb/^{204}Pb$ ratio of 41.565. The $^{206}Pb/^{204}Pb$ ratios of samples from the Hayfield mudstone range from 15.677 to 17.133, and the $^{207}Pb/^{204}Pb$ and $^{208}Pb/^{204}Pb$ ratios range from 15.626 to 15.740 and 40.026 to 42.752, respectively (Table 1).

Table 1 Sm–Nd and Pb-isotopic compositions of the analysed formations from the core Balmain-1.

Formation	Sample	Depth (m)	Age (Ma)	Nd (ppm)	Sm (ppm)	$^{143}Nd/^{144}Nd(t)$	$\varepsilon_{Nd(t)}$	2s.e	T_{DM} (Ga)	$^{206}Pb/^{204}Pb$	2s.e	$^{207}Pb/^{204}Pb$	2s.e	$^{208}Pb/^{204}Pb$	2s.e
Kyalla Fm.	Bal-by-1	1050	1320	53.686	0.192	0.51073	-3.98	0.05	2.18	16.121	0.043	15.676	0.048	39.090	0.053
	Bal-by-2	1016	1320	44.967	0.197	0.51069	-4.76	0.05	2.27	16.083	0.034	15.712	0.036	39.400	0.036
	Bal-by-3	985	1320	52.200	0.197	0.51069	-4.74	0.05	2.27	16.957	0.061	15.766	0.072	39.698	0.086
	Bal-by-4	953	1320	43.914	0.171	0.51077	-3.29	0.05	2.03	14.253	0.415	14.276	0.356	35.105	0.415
	Bal-by-5	940	1320	61.016	0.233	0.51071	-4.31	0.05	2.51	13.983	0.020	15.205	0.021	37.300	0.023
lower Jamison sandstone	Bal-by-6	911	950	121.63	0.204	0.51109	-6.22	0.04	2.15	17.207	0.078	15.831	0.079	40.993	0.074
	Bal-by-7	888	950	79.571	0.191	0.51115	-5.23	0.05	2.06	15.886	0.117	15.616	0.124	39.398	0.123
upper Jamison sandstone	Bal-by-8	869	950	34.217	0.202	0.51123	-3.63	0.08	1.93	17.474	0.174	15.639	0.177	41.565	0.171
Hayfield mudstone	Bal-by-9	838	950	37.016	0.218	0.51101	-7.83	0.04	2.41	16.889	0.006	15.659	0.005	41.518	0.005
	Bal-by-10	807	950	73.866	0.177	0.51115	-5.09	0.05	1.88	17.010	0.127	15.626	0.128	42.317	0.131
	Bal-by-11	775	950	45.492	0.186	0.51113	-5.51	0.03	1.96	15.677	0.104	15.707	0.107	42.752	0.109
	Bal-by-12	746	950	56.289	0.200	0.51106	-6.89	0.04	2.16	17.133	0.194	15.740	0.204	42.204	0.204
	Bal-by-13	706	950	36.155	0.176	0.51112	-5.71	0.05	1.92	17.026	0.051	15.723	0.064	40.571	0.083
	Bal-by-14	675	950	60.726	0.188	0.51110	-6.14	0.06	2.02	16.173	0.049	15.631	0.050	40.156	0.049
	Bal-by-15	646	950	52.287	0.195	0.51109	-6.38	0.05	2.09	16.594	0.106	15.688	0.113	40.026	0.119

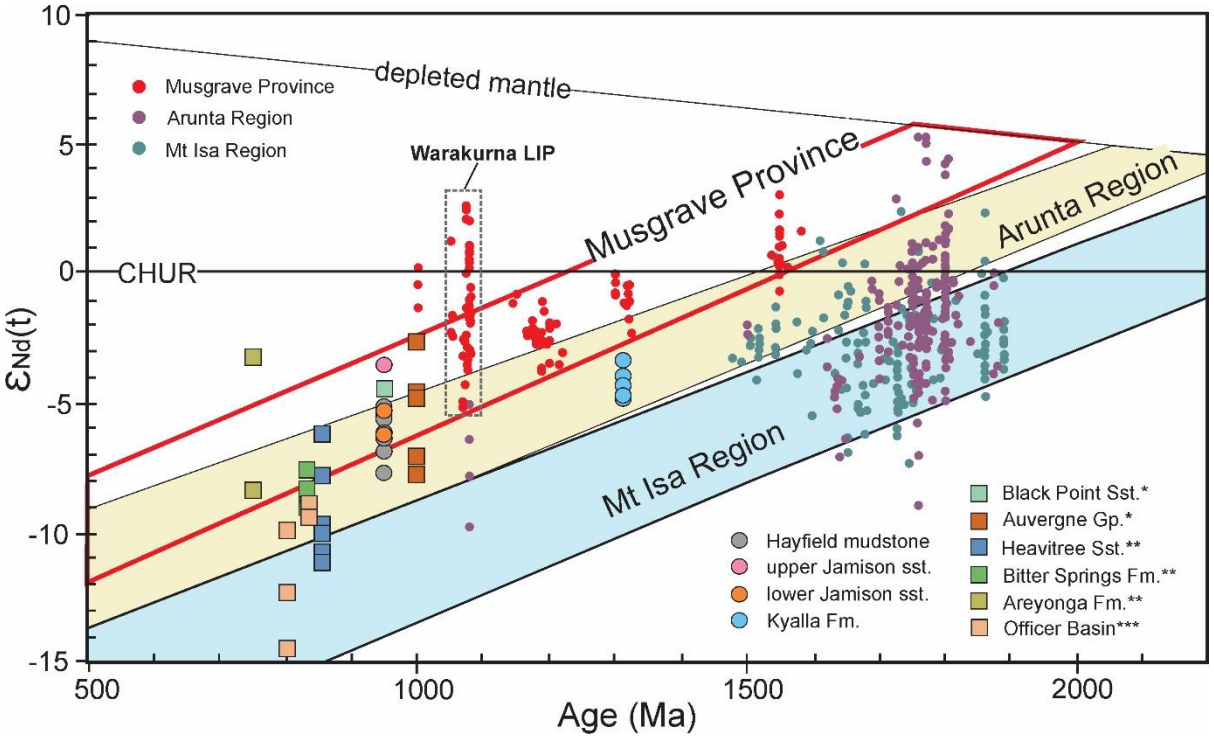

Figure 3 Shale whole-rock εNd vs age diagram illustrating potential provenance regions. Nd data from potential provenance areas are from *Champion (2013) and references therein*. *Data of Black Point Sandstone and Auvergne Group (Victoria Basin) are from *Carson (2013)*. **Data of Amadeus Basin (Heavitree Sandstone, Bitter Springs Formation and Areyonga Formation) are from *Zhao et al. (1994)*. ***Data of Officer Basin are from *Wade et al. (2005)*. CHUR: chondrite reservoir.

4. Isotope dilution thermal ionization mass spectrometry (ID-TIMS) U–Pb baddeleyite geochronology

A Derim Derim sill sample (ALT-05) was collected from the core Altree-2 at the depth of 1154 m (Figure 2) for ID-TIMS U–Pb dating. Detailed sample and analytical information and dating results are presented in the Appendix 3 and Table 2.

Six fractions of one baddeleyite crystal were analysed for U–Pb geochronology after isolation using the Wilfley table (see Appendix 3, Figure 4). The grains were generally small (0.1–0.2 µg, calculated from photomicrographs), without any correlation with age or degree of discordance. Calculated U concentrations were between 100 and 200 ppm U, and Th/U ratios were low (~0.1 or lower). Common lead is less than 0.3 pg for all analyses. All analyses except one (#6) were concordant, with #6 being less than 1% discordance but still resolvably outside of the coherent, concordant grouping of the other data (Figure 4; Table 2). The coherence of the $^{207}Pb/^{206}Pb$ dates of all data indicates that any possible Pb loss was recent, and supports our interpretation of the age presented here as the magmatic emplacement age for the sill.

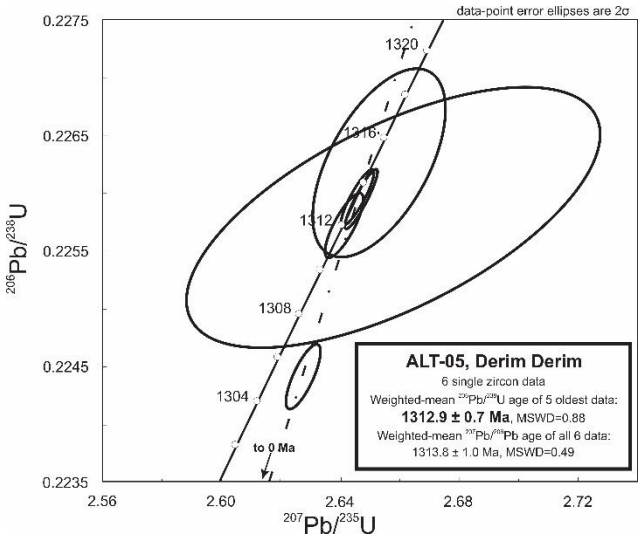

Figure 4 TIMS U–Pb baddeleyite concordia plot of the dolerite sample collected from Altree-2 borehole at a depth of 1154m.

The weighted-mean $^{207}Pb/^{206}Pb$ age of all data is 1313.8 ± 1.0 Ma (2SD, MSWD = 0.49, N = 6) while the weighted-mean $^{206}Pb/^{238}U$ age of the five concordant analyses is 1312.9 ± 0.7 Ma (2SD, MSWD = 0.88, N = 5). These calculated ages overlap within 2σ uncertainty, though for samples of this age the $^{207}Pb/^{206}Pb$ age will always be somewhat older. We consider the weighted-mean $^{206}Pb/^{238}U$ age of the coherent cluster of the five concordant analyses to be the most robust determination of the age of the Derim Derim sample.

Table 2: U–Pb isotopic data for baddeleyites from the Derim Derim sills (ALT-05).

Sample	Wt. (µg)	U (ppm)	Pb_c (pg)	mol% Pb*	Th U	$^{206}Pb/^{204}Pb$	$^{207}Pb/^{206}Pb$	± (%)	$^{207}Pb/^{235}U$	± (%)	$^{206}Pb/^{238}U$	± (%)	ρ	$^{206}Pb/^{238}U$ Age (Ma)	± (Ma)	$^{207}Pb/^{206}Pb$ Age (Ma)	± (Ma)	Conc (%)
1	0.1	118	0.2	85	0.03	122	0.08503	0.58	2.6528	0.70	0.226262	0.29	.58	1314.88	3.85	1316	11.3	99.91
2	0.2	109	0.2	99	0.12	1181	0.08496	0.09	2.6468	0.17	0.225953	0.09	.92	1313.25	1.23	1315	1.8	99.87
3	0.2	196	0.2	98	0.06	1133	0.08492	0.10	2.6455	0.17	0.225949	0.09	.89	1313.23	1.22	1314	1.9	99.94
4	0.1	115	0.3	77	0.08	71	0.08537	1.89	2.6578	2.12	0.225794	0.41	.64	1312.42	5.37	1324	36.6	99.12
5	0.2	151	0.2	98	0.07	610	0.08487	0.12	2.6414	0.18	0.225718	0.10	.80	1312.02	1.32	1313	2.3	99.93
6	0.1	196	0.2	97	0.06	592	0.08491	0.12	2.6274	0.19	0.224415	0.10	.79	1305.16	1.33	1314	2.4	99.32

* Pbc = Total common Pb including analytical blank (0.8 ± 0.3 pg per analysis). ρ = error correlation coefficient of radiogenic $^{207}Pb/^{235}U$ vs. $^{206}Pb/^{238}U$. All uncertainties given at 2σ. Concordance (Conc) was calculated as (1-($^{206}Pb/^{238}U$-$^{207}Pb/^{206}Pb$)/ $^{206}Pb/^{238}U$)*100%.

5. Provenance analysis

5.1 Kyalla Formation

Neodymium isotopic data from five Kyalla Formation mudstone samples overlap with similar data sourced from basement rocks exposed in the Arunta Region (Figure 3), indicating that this formation might have received detritus from this area. This is consistent with the detrital zircon provenance analysis, which revealed zircon U–Pb age and Hf isotope affinities between the Kyalla Formation and the Arunta Region (*Chapters 2 & 3*). Besides that, in stratigraphic scale, a small $\varepsilon_{Nd(t)}$ variation is seen, characterised by an up-section excursion to more positive values, indicative of greater contribution from juvenile sources at the top section of this formation (Figure 5). The positive $\varepsilon_{Nd(t)}$ excursion is mirrored by the covariation in Pb isotopic ratios that show lower radiogenic Pb (^{206}Pb, ^{207}Pb and ^{208}Pb) concentrations at the top of the Kyalla Formation (Figure 5). The Nd and Pb isotope data both support greater contribution from juvenile sources towards the top of the Kyalla Formation. The La/Sm ratio mirrors the Pb isotopic ratios, with an up-section negative excursion (Figure 5). This suggests that the juvenile sources

are also mafic. This is because, the lower crust and upper mantle are LREE-depleted whereas the upper continent is LREE-enriched, and thus more mafic detrital input will lead to lower La/Sm ratios. The upper Kyalla Formation samples have relative lower La/Sm ratios whereas the others stay closer to the average for the average upper continental crust (AUCC) value (Figure 5; *Taylor & McLennan, 1995*), suggesting a higher percentage of basaltic-derived components within this section.

We suggest that the Kyalla Formation was mainly sourced from the Arunta Region, whereas the up-section variation of Nd and Pb isotopes along with La/Sm ratios indicates that the upper Kyalla Formation received detritus from more juvenile basaltic sources. The emergence of juvenile basaltic sources could be conceivably due to a return to the erosion of the Wankanki Supersuite of ca. 1345–1293 Ma plutons in the western Musgrave Province (*Howard et al., 2015*). However, although these are relatively juvenile, they are dominantly granitoids. Alternatively, emplacement of the Derim Derim–Galiwinku LIP is broadly coeval with deposition of the Kyalla Formation and the rocks of this LIP are ubiquitously mafic. The feeder sills and dykes of the Derim Derim–Galiwinku LIP are largely exposed in the Urapunga region in the northeast of the Beetaloo Sub-basin, whereas the relevant volcanic rocks are absent (*Abbott et al., 2001*). We suggest that these volcanic rocks may have been eroded and deposited in the Beetaloo Sub-basin, resulting in a more juvenile, mafic-sourced, component of the uppermost Kyalla Formation.

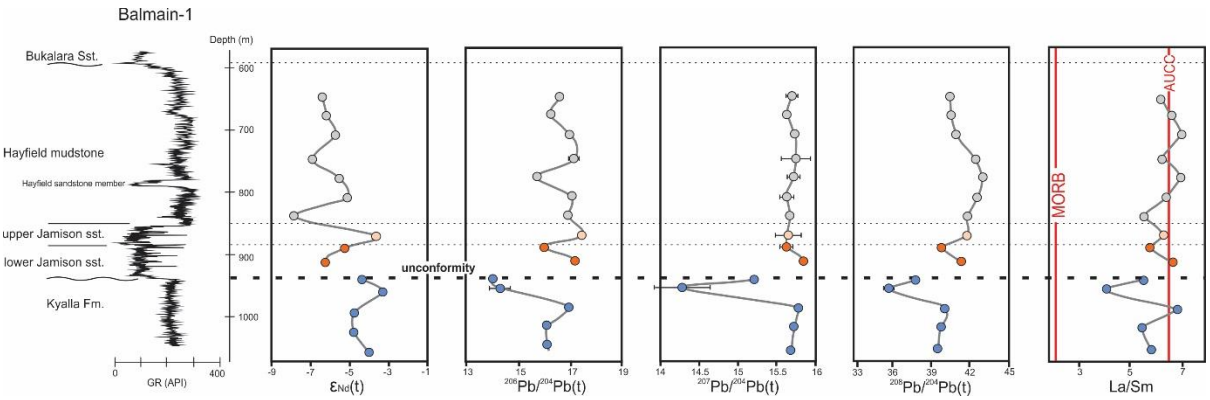

Figure 5 Stratigraphy versus chemistry diagrams in borehole Balmain-1 illustrating the up-section variation of selected isotopes and trace element ratios. Average upper continental crust (AUCC) values from *Taylor & McLennan (1995)*. Mid-ocean ridge basalt (MORB) data from *Sun & McDonough (1989)*. Trace elements data from *Jarrett et al. (2017)*. Most analysed errors are smaller than the plotted points.

5.2 Latest Mesoproterozoic to Neoproterozoic group

Whole-rock Sm–Nd isotope analysis shows that three samples, including two from the lower Jamison sandstone and one from the upper Jamison sandstone, plot in the Musgrave Province domain (Figure 3), indicating that they plausibly received detritus from Musgrave Province

sources. This is consistent with previous detrital zircon provenance studies that demonstrated significant U–Pb age and Hf isotope similarities between the two sandstone units and the Musgrave Province (*Munson et al., 2016, 2018; Chapter 2 & 3*). Stratigraphically, these three samples show an up-section, more positive, $\varepsilon_{Nd(t)}$ trend (Figure 5), indicating a temporal increase of juvenile material. Potential sources for such juvenile detritus are largely exposed in the western Musgrave Province, in which voluminous juvenile magmas were emplaced during the *ca.* 1.1 to 1.05 Ga Giles Event (e.g. Warakurna Supersuite; *Wingate et al., 2004; Champion, 2013; Howard et al., 2015;* Figures 3), that occurred during the time represented by the sub-Jamison unconformity. The up-section, more juvenile trend of the lower and upper Jamison sandstone, is interpreted to suggest that the western Musgrave Province progressively became the dominant source for the upper Jamison sandstone, resulting in more juvenile rocks eroded and then deposited in the Beetaloo Sub-basin.

Compared to the lower and upper Jamison sandstones, the Hayfield mudstone samples yield more negative $\varepsilon_{Nd(t)}$ values, indicating that this formation received detritus from more evolved crustal sources (Figures 3 and 5). In Figure 3, six out of seven samples plot in the overlapping domain of the Musgrave Province and the Arunta Region. Additionally, stratigraphic variations of $\varepsilon_{Nd(t)}$ are seen in this formation, characterised by a positive excursion at the depth of 820m to 770m (Figure 5). The section with higher $\varepsilon_{Nd(t)}$ values is where a sandstone interval (also informally named Hayfield sandstone member; *Gorter & Grey, 2013; Munson, 2016)* is located (Figure 5). *Silverman et al. (2007)* interpreted this sandstone interval to represent a shallowing event or a period of flood or higher flow rate. *Munson et al. (2018)* presented detrital zircon U–Pb age and Hf isotope data and suggested that this sandstone-rich unit shares significant similarities with the upper and lower Jamison sandstone, indicating they might receive detritus from the same sources (e.g. Musgrave Province). The similarities between this sandstone interval and the underlying sandstone units are further demonstrated here by our Nd isotope data. These show that the two shale samples bounding the sandstone interval, yield similar $\varepsilon_{Nd(t)}$ values to the lower Jamison sandstone samples (Figure 5). We suggest that the Hayfield mudstone probably received detritus from both juvenile sources (e.g. Musgrave Province) and evolved sources (e.g. Arunta Region). Basin-margin progradation, or possibly a major flood event, bought more Musgrave Province detritus into the Beetaloo Sub-basin in middle Hayfield mudstone times.

6. Discussion

6.1 Emplacement of the Derim Derim–Galiwinku LIP

The Derim Derim–Galiwinku LIP mafic intrusives are distributed in the northern North Australia Craton from the northern margin of the McArthur Basin (*sensu stricto*) to the northern Beetaloo Sub-basin (*Abbott et al., 2001; Ahmad & Munson, 2013; Whelan et al., 2016*). The Derim Derim–Galiwinku LIP intrudes the Maiwok Subgroup up to the top of the Kyalla Formation in the Beetaloo Sub-basin and the Bukalorkmi Sandstone in the Urapunga Fault Zone, and is therefore considered to constrain the end of the deposition of the Roper Group (*Abbott et al., 2001; Ahmad & Munson, 2013*). The new Derim Derim age of 1312.9 ± 0.7 Ma obtained in this study (Figure 4) is approximately 10 million years younger than a poorly documented secondary ionization mass spectrometry (SIMS) U–Pb baddeleyite age of 1324 ± 4 Ma from a sill within the Urapunga Fault Zone (*Abbott et al., 2001*). Furthermore, the new date is slightly older than the unnamed dolerite intrusions within the Tomkinson Province, to the south of the Beetaloo Sub-basin that yielded a SIMS $^{207}Pb/^{206}Pb$ baddeleyite age of 1295 ± 14 Ma (*Melville, 2010*). In addition, a SIMS $^{207}Pb/^{206}Pb$ baddeleyite age of 1329 ± 55 Ma was reported by *Whelan et al. (2016)* from the Galiwinku Dolerite. Although correlations between these mafic intrusions remain unclear, these ages together, support a period of intraplate mafic magmatism in the North Australian Craton at *ca*. 1313 Ma.

6.2 Uplift of the greater McArthur Basin

The Kyalla Formation, represents the final stage of deposition of the Mesoproterozoic Roper Group in the Beetaloo Sub-basin of the greater McArthur Basin. The Beetaloo Sub-basin subsequently experienced a long period (over 300 Ma) of erosion and non-deposition, which is reflected by the regional unconformity separating the Kyalla Formation from the post *ca.* 1090 Ma lower Jamison sandstone (*Chapter 2*). The lateral stratigraphic continuity of the Kyalla Formation suggests that the original extent of this formation was larger than its present distribution (*Munson, 2016*). Besides that, the progressively northward thinning of this formation and the absence of the upper members in the northern Beetaloo Sub-basin suggests that the northern margin of the basin was uplifted into a broad dome and eroded. A possible explanation for this basin uplift could be folding due to a regional compressional event. The Roper Group in the Urapunga Region, north of the major Mallapunyah Fault, is folded at some time after the ca. 1313 Ma Derim Derim intrusions (*Abbott et al., 2001*). However, we suggest that compression is unlikely as an originator of topography that may have been eroded to form the sub-Jamison unconformity, because a) no macroscopic folds are reported from the Beetlaoo

Basin, and, b) the sub-Jamison unconformity is seen throughout the region, suggesting a broad large wavelength doming to create topography. Intraplate mafic magmatism is also a feature of extensional plume-settings, where such broad domal uplift is expected (*Ernst et al., 2008*). We suggest that the broad upward flexure of the northern Kyalla Formation is associated with magmatic uplift during the emplacement of the Derim Derim–Galiwinku LIP, which progressively inflated the basin from north to south as the plume evolved (Figure 6).

This model explains the change from southerly sources (e.g. the Arunta Region) for the majority of the Kyalla Formation to northerly-sourced detritus, from the Derim Derim–Galiwinku LIP, at the top of the formation (i.e. Urapunga Region; Figure 6a). The subsequent continuous plume emplacement ultimately resulted in the uplift of the whole Beetaloo Sub-basin resulting in the cessation of deposition within the basin (Figure 6b).

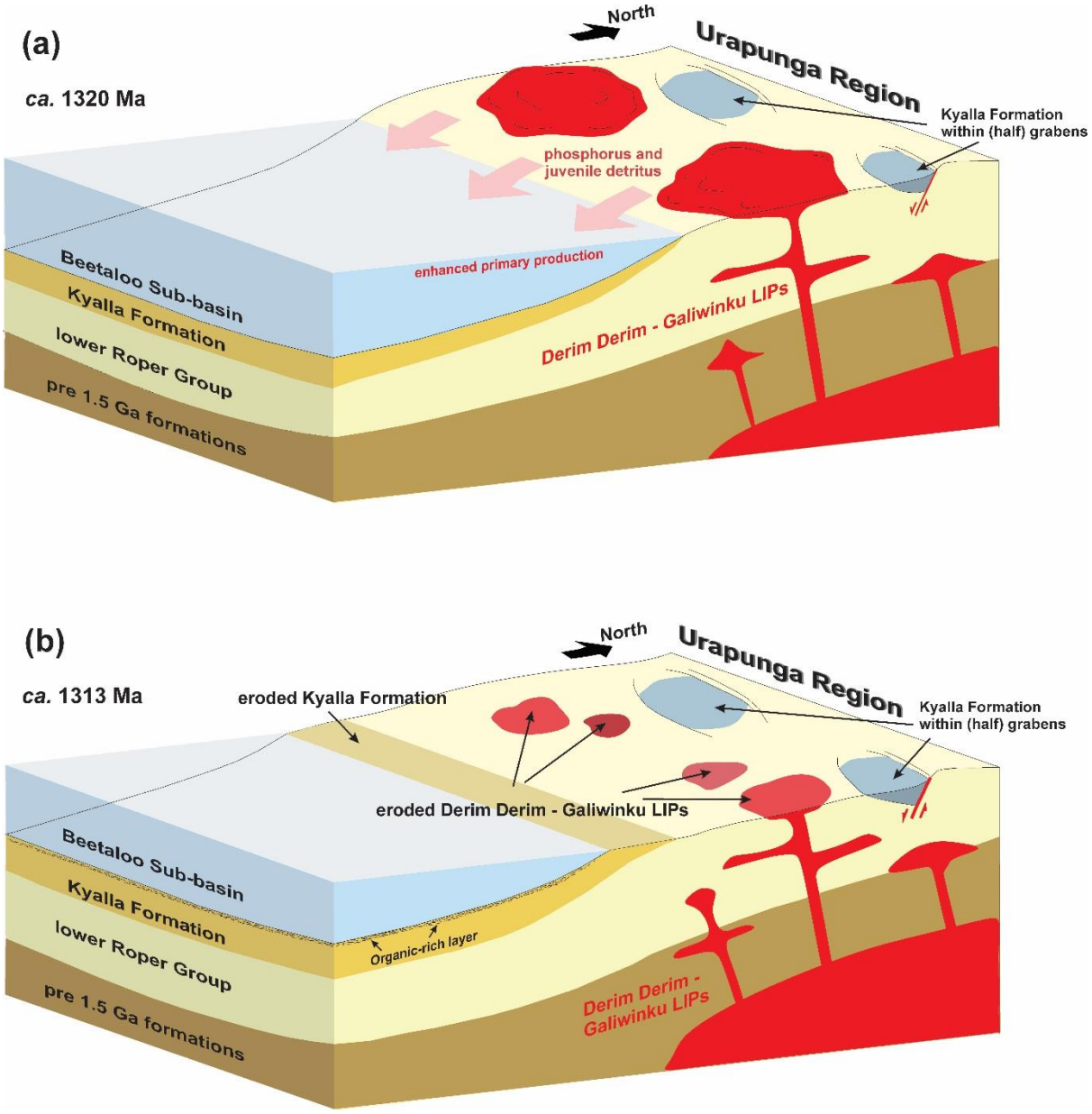

Figure 6 Simplified geographic cartoon showing the envisaged paleogeography during the emplacement of the Derim Derim–Galiwinku LIP: (a) the weathering of the Derim Derim–Galiwinku LIP transported more phosphorus to the basin, which enhanced primary production in the ocean surface waters and resulted in organic carbon enrichment in the sediments; (b) the basin was uplifted from the north during continued plume-related uplift, resulting in the Kyalla Formation being preferentially eroded towards to the north.

Sedimentary rocks of the Kyalla Formation are also observed, from both core and outcrop, in the Urapunga Region, and show a considerable variation in thickness from meters, up to about two-hundred meters (*Munson, 2016;* Figure 1a). We suggest that, during the magmatic uplift, a series of faults may have developed in the Urapunga Region, resulting in Kyalla sediments being deposited within grabens and (or) half-grabens and separated from the Kyalla Formation in the Beetaloo Sub-basin (Figures 6a and 6b). This separation could have resulted in a distinct depositional system in which the overlying Bukalorkmi Sandstone and Chambers River Formation locally developed in the Urapunga Region, but were never deposited in the Beetaloo Sub-basin.

The Derim Derim–Galiwinku magmatism is consistent with the emplacement of the *ca.* 1.33-1.30 Ga Yanliao LIP in the North China Craton (NCC; *Zhang et al., 2017*). *Zhang et al. (2017)* suggested that the co-occurrence of these intraplate mafic magmatism in both northern Australia and the NCC might indicate that these two cratons were juxtaposed at *ca.* 1.3 Ga. This reconstruction is further supported by the recent palaeomagnetic study revealing that the NAC and NCC were at the similar latitudes at *ca.* 1.3 Ga (*Kirscher et al., 2018*). The emplacement of the Yanliao diabase sills was accompanied by a significant magmatic uplift that resulted a regional unconformity separating the ca. 1.34 Ga Xiamaling Formation and the early Neoproterozoic Qingbaikou Group (*Zhang et al., 2017*). Whilst, in the North Australia Craton, we suggest that the Roper Group was also uplifted in a similar manner during the Derim Derim–Galiwinku magmatism. The coeval intraplate mafic magmatism and magmatic uplift suggests that the plume head was located between the northern margin of NAC and northern-northeastern margin of NCC. The plume uplifted both these cratons from their north, simultaneously (*Zhang et al., 2017*).

6.3 Trigger for organic carbon enrichment

The timing of eruption and erosion of the Derim Derim—Galiwinku LIP coincides with the timing of influx of juvenile basaltic detritus and elevated TOC concentrations at the top section of the Kyalla Formation (Figure 7; *Jarrett et al., 2017; Revie & Normington, 2018*). In core Balmain-1, the TOC enriched section of the Kyalla Formation also contains a marked enrichment of magnesium, with a smaller increase in calcium—elements that are commonly enriched in

basaltic rocks (Figure 8). The coincidence of an increased basaltic component to the weathering flux and elevated TOC is in agreement with many recent studies that have noted the increased nutrient delivery (e.g. phosphorus; Figure 8) associated with basaltic weathering and an increase in biological productivity (*Horton, 2015; Cox et al., 2016a, b; 2019*).

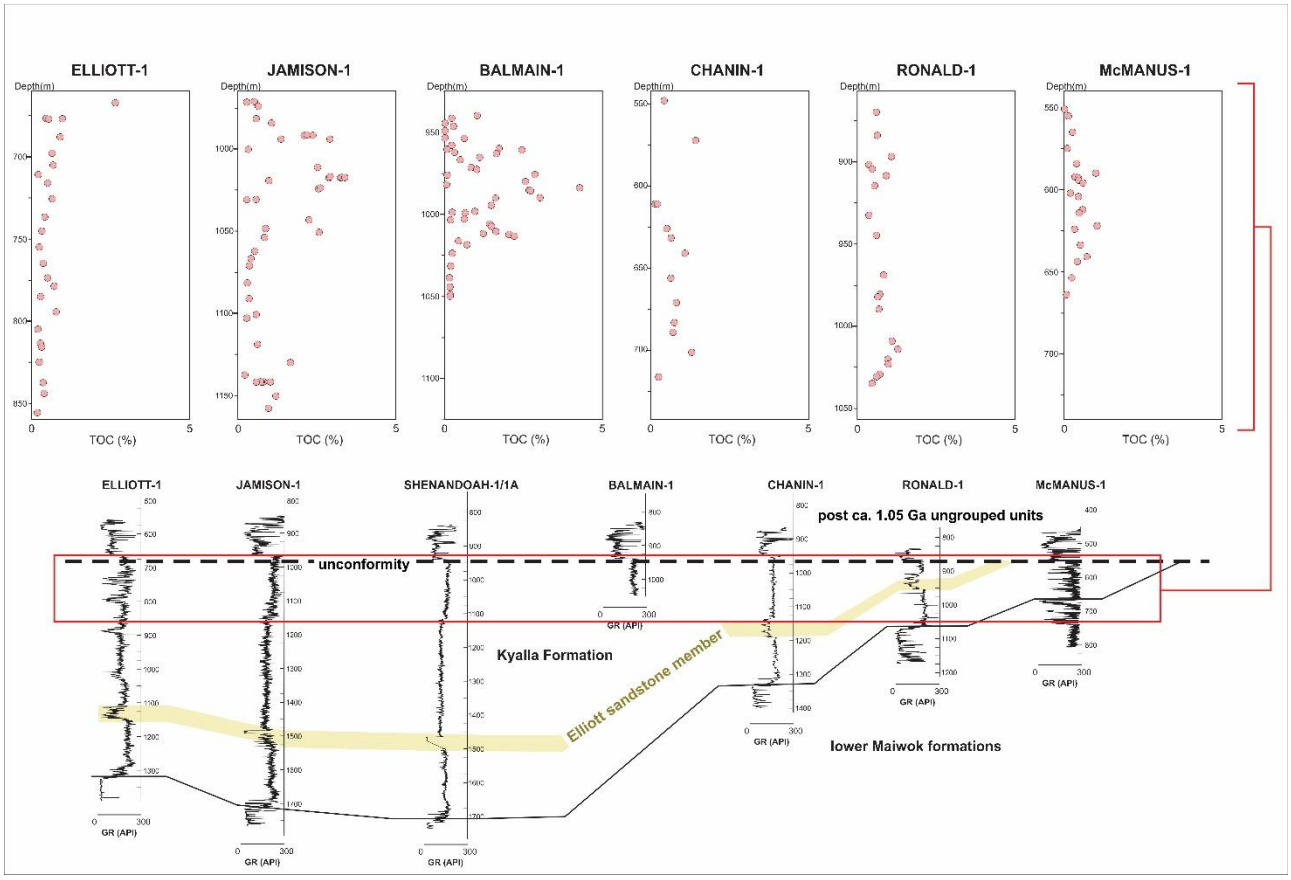

Figure 7 Stratigraphic-Total Organic Carbon (TOC) plots illustrating TOC enrichment in the upper section of the Kyalla Formation. The upper parts of the Kyalla Formation are interpreted to have been eroded from Chanin-1, Ronald-1 and McManus-1. TOC data from *Revie & Normington, (2018)*.

Nitrogen and phosphorus are commonly thought to be bio-limiting nutrients, while nitrogen limits marine bio-productivity on an ecological timescale and phosphorous on a more geological timescale (*Tyrrell, 1999; Sageman & Lyons, 2003*). Terrestrial rocks and soils are thought to be the ultimate sources for phosphorous, which is weathered and delivered to the ocean by rivers (*Piper & Calvert, 2009*). Mafic rocks, compared to other types of terrestrial rocks, are phosphorus enriched (*Horton, 2015)*, so the weathering of this type of rock will deliver more nutrients to sedimentary basins, compared to typical felsic or granitic rocks, resulting in higher primary productivity (*Horton, 2015; Cox et al., 2016a, b*).

Provenance analysis in this study shows a geochemical link between mafic volcanism and sedimentation of organic-rich shales. Our hypothesis is that during the rapid weathering of

Derim Derim–Galiwinku basaltic rocks, more phosphorus was transported to the Beetaloo Sub-basin than previously (Figure 6a). With increased nutrient delivery, more primary organic matter was generated in the ocean surface waters. Higher primary production would increase the likelihood that more organic matter would be exported to bottom waters and then preserved within the sediments, as seen in upper part of the Kyalla Formation where phosphorus and TOC are coherently enriched (Figure 8). A similar model has recently been proposed for the underlying hydrocarbon-prone Velkerri Formation (*Cox et al., 2016a, 2019; Mukherjee & Large, 2016*). The covariance between isotopic ratios, major and trace elements ratios and TOC concentrations within the Kyalla Formation suggests that the Derim Derim–Galiwinku LIP is likely be the cause of the TOC enrichment within this formation.

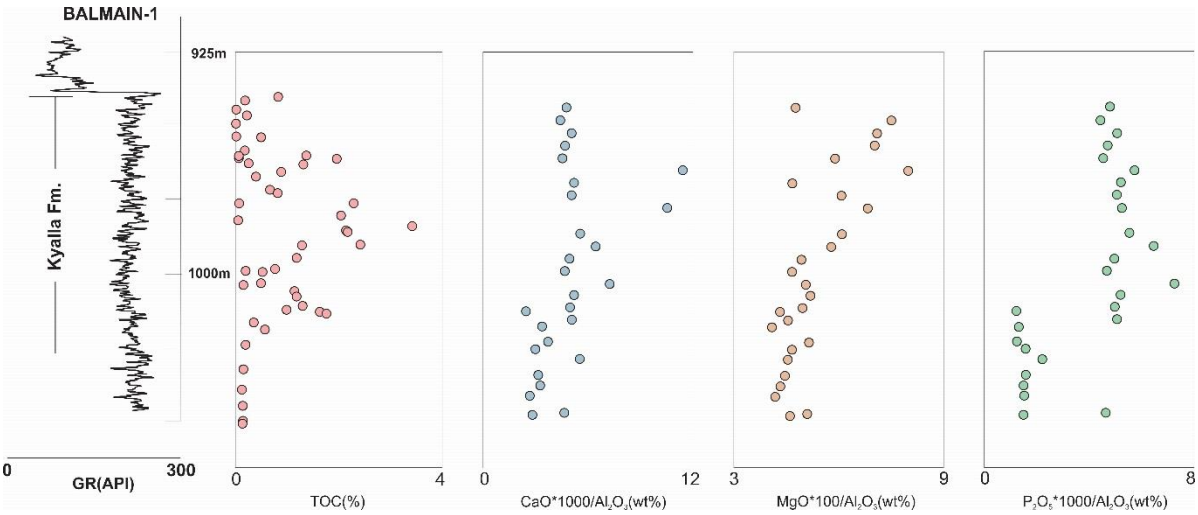

Figure 8 Stratigraphic-Total Organic Carbon (TOC) and major elements plot illustrating the TOC enriched section is consistent higher component of Ca, Mg and P that are enriched in basaltic rocks. TOC data and major element data from *Jarrett et al. (2017).*

6.4 Early Neoproterozoic tectonic geography

Whole-rock shale Sm–Nd isotope provenance analysis in this study suggests that the two sandstone units of the latest Mesoproterozoic to early Neoproterozoic unnamed group, the lower and upper Jamison sandstones, were sourced from the Musgrave province. We further suggest that the significant up-section, increase in juvenile compositions, may be coeval with the *ca.* 1090 to 1040 Ma Giles event (*Howard et al., 2015; Glorie et al., 2017*). During the Giles event, voluminous mafic-ultramafic and juvenile felsic plutons were intruded and accompanied by widespread volcanism (e.g. the Warakurna LIP) and high temperature metamorphism in central Australia (*Smithies et al., 2011; Kirkland et al., 2013; Howard et al., 2015*). These are mainly exposed in the western Musgrave Province (Figure 9a). The Warakurna LIP has been linked to a deep mantle plume system located beneath the Ngaanyatjarra Rift, in the western Musgrave

Province (*Wingate et al., 2004*). We suggest that the lower Jamison sandstone was predominantly sourced from the central Musgrave Province. During the emplacement of the Warakurna LIP, the western Musgrave gradually uplifted and became the dominant source, thus more juvenile detritus were transported and deposited in the Beetaloo Sub-basin. This resulted in the up-section trend to more juvenile compositions within the lower and upper Jamison sandstone. This provenance variation is also coeval with detrital zircon U–Pb provenance analysis, suggesting that the upper Jamison sandstone samples contain higher proportions of *ca.* 1.1 Ga detrital zircon grains than the lower Jamison sandstone (*Munson et al., 2018; Chapter 2*). Hafnium isotope analysis shows that these *ca.* 1.1 Ga detrital zircon grains are juvenile and that many show Pb-loss trends (*Chapter 3*), which are similar to those from the western Musgrave Province (e.g. *Smithies et al., 2011*).

We suggest that the fine-grained early Neoproterozoic unit of the unnamed group, the Hayfield mudstone, received mixed detritus from the Musgrave Province and the Arunta Region. This is consistent with the sedimentary formations of the Amadeus Basin in the central Australia. *Zhao et al. (1992)* suggested that the older units in the Amadeus Basin were sourced from the Musgrave Province as well as the Arunta Region according to the whole-rock Sm–Nd data. In the ε_{Nd} against age plot (Figure 3), analyses from the basal sandstone and mudstone units (the Heavitree Sandstone and Bitter Springs Formation) of the Amadeus Basin all plot in a region overlapping the Musgrave Province and the Arunta Region, similar to those of the Hayfield mudstone, as well as formations from the Officer Basin (*Wade et al., 2005*). Additionally, Sm–Nd isotopic consistency has also been found in the Auvergne Group of the Victoria Basin in the northwest (Figures 3 and 9a). *Carson (2013)* presented Sm–Nd isotope data from the Victoria Basin and illustrated a potential connection with the Amadeus Basin. This dataset is also coeval with the latest Mesoproterozoic to early Neoproterozoic unnamed group, indicating a potential connection to the Beetaloo Sub-basin (Figure 9a). The correlations amongst these basins have been further supported by detrital zircon U–Pb data. Consistent detrital zircon U–Pb age spectra, with dominant age populations centred at *ca.* 1.59 Ga and two minor peaks clustered at *ca.* 1.1 Ga and *ca.* 1.77 Ga, have been found among the basal sandstone unit of the Amadeus Basin (Heavitree Sandstone), the basal sandstone unit of the Victoria Basin (Jasper Gorge Sandstone), the Munyu Sandstone of the Murraba Basin and the unnamed group of the Beetaloo Sub-basin (*Maidment et al., 2007; Kirkland et al., 2009; Carson, 2013; Haines and Allen, 2016; Munson et al., 2018; Chapter 2;* Figure 9b). The potential sources for *ca.* 1.59 Ga and *ca.* 1.1 Ga zircon grains are largely exposed in the Musgrave Province, and those zircon grains with *ca.* 1.77 Ga ages were probably sourced from the Arunta Region (*Chapter 2*; Figure 9b).

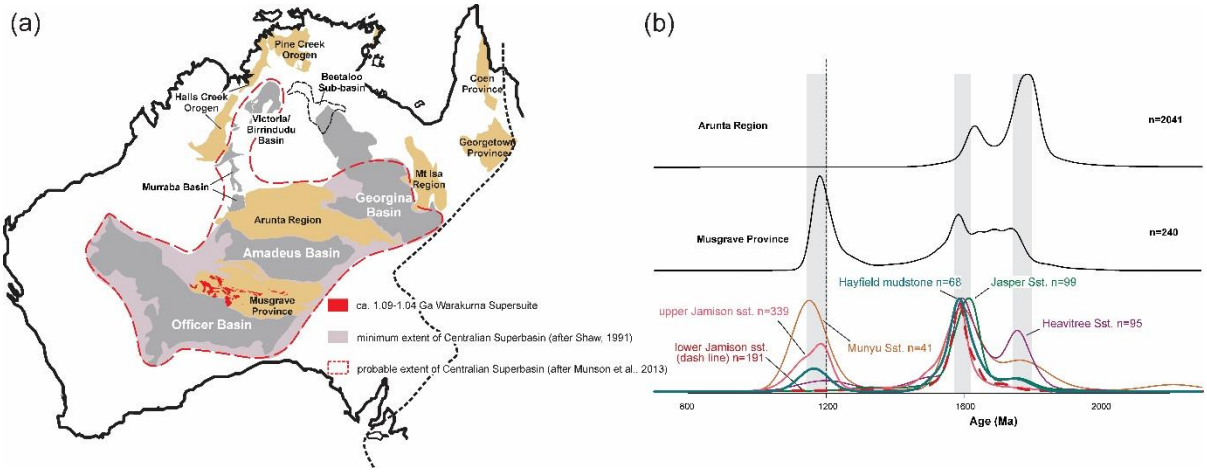

Figure 9 (a) Geological map showing the distribution of Neoproterozoic basins within Australia; (b) Detrital zircon U–Pb age kernel density distribution plots illustrating the provenance consistency among the Jasper Gorge Sandstone (Victoria Basin), Munyu sandstone (Murraba Basin), Heavitree Sandstone (Amadeus Basin), lower and upper Jamison sandstone and Hayfield mudstone (Beetaloo Sub-basin), and their interpreted provenances (Arunta Region and Musgrave Province). Detrital zircon U–Pb age data are from *Maidment et al. (2007), Kirkland et al. (2009), Carson (2013), Haines & Allen (2016), Munson et al. (2018), Chapter 2 and references therein*.

Neoproterozoic central Australia is characterized by the formation of a series of intracontinental sedimentary basins that show considerable stratigraphic similarities, including the Officer, Amadeus, Ngalia and Georgina basins (Figure 9a; *Shaw et al., 1991;* Zhao et al., 1994). *Walter et al. (1995)* suggested that the sedimentary rocks of these basins are separated remnants from a once-continuous depositional system, the Centralian Superbasin (Figure 9a). *Carson (2013)* demonstrated that the Victoria Basin might be another correlative of this super basin in the northwest. Further, data collected from the unnamed group in the Beetaloo Sub-basin show consistency with the sedimentary rocks of these basins, suggesting that the Centralian Superbasin probably covered the Beetaloo Sub-basin and is considerably more extensive than previous thought.

7. Conclusions

Stratigraphic variation of shale whole-rock isotopes reveals a dynamic provenance history of the Beetaloo Sub-basin and records *ca.* 500 million years tectonic geography evolution of the North Australia Craton.

We suggest that the Kyalla Formation was mainly sourced from the Arunta Region, whereas the upper section of this formation contains higher juvenile compositions that is interpreted as the weathering of the Derim Derim–Galiwinku LIP. Simultaneously, the weathering of these basaltic rocks also led to higher nutrient levels supplied to the basin, fuelling higher primary production, as shown by the concurrence of more juvenile detritus, phosphorus and TOC enrichment within

the upper section of Kyalla Formation. The arrival of the Derim Derim–Galiwinku LIP uplifted the Urapunga Region, and with progressively greater uplift, the whole Beetaloo Sub-basin was exhumed and exposed. The new TIMS U–Pb baddeleyite age of 1312 ± 0.7 Ma (2s), for a dolerite sill in the north Beetaloo Sub-basin, provides a new precise age constraint for the age of erosion of the Derim Derim–Galiwinku LIP and interpreted basin uplift event and termination of deposition of the Kyalla Formation as well as the Mesoproterozoic Roper Group.

We suggest that the provenance changed to the Musgrave Province during the deposition of the lower and upper Jamison sandstones. More specifically, the lower Jamison sandstone received detritus from the central Musgrave Province, whereas the western Musgrave Province became the dominant source for the upper Jamison sandstone. This provenance variation is interpreted to be related to the emplacement of Warakurna LIP. The Hayfield mudstone received detritus from both juvenile sources (e.g. Musgrave Province) and evolved sources (e.g. Arunta Region) and share isotopic similarities with the Heavitree–Bitter Springs formations of the Amadeus Basin and the Auvergne Group of the Victoria Basin. The whole-rock geochemical consistency among these early Neoproterozoic basins/strata indicates an extensive super basin with multiple depocentres.

Acknowledgements

This research was funded by an Australian Research Council Linkage Project LP160101353, which is partnered by the Northern Territory Geological Survey, SANTOS Ltd., Origin Energy and Imperial Oil and Gas. David Bruce and Tony Hall are thanked for help collecting geochemical data. AJ publishes with the permission of the CEO, Geoscience Australia. This manuscript forms MGC Record and is a contribution to IGCP Projects 628 (Gondwana Map) and #648 (Supercontinents and Earth Evolution).

References

Abbott, S.T., Sweet, I.P., Plumb, K.A., Young, D.N., Cutovinos, A., Ferenczi, P.A., Pietsch, B.A., 2001. Roper Region: Urapunga and Roper River Special, Northern Territory (Second Edition). 1:250 000 geological map series explanatory notes, SD 53-10, 11. *Northern Territory Geological Survey and Geoscience Australia (National Geoscience Mapping Accord)*. https://geoscience.nt.gov.au/ gemis/ntgsjspui/handle/1/81859.

Ahmad, M., Munson, T.J., 2013. Northern Territory Geological Survey, Geology and mineral resources of the Northern Territory, Special Publication 5. Northern Territory Geological Survey. https://geoscience.nt.gov.au/gemis/ntgsjspui/handle/1/81446.

Anbar, A.D., Knoll, A.H., 2002. Proterozoic ocean chemistry and evolution: a bioinorganic bridge? *Science*, **297(5584)**, 1137-42. https://doi.org/10.1126/science.1069651.

Carson, C.J., 2013. The Victoria and Birrindudu Basins, Victoria River Region, Northern Territory, Australia: a SHRIMP U–Pb detrital zircon and Sm–Nd study. *Journal of the Geological Society of Australia,* **60(2)**, 175-196. https://doi.org/10.1080/08120099.2013.772920.

Champion, D.C., 2013. Neodymium depleted mantle model age map of Australia: explanatory notes and user guide. *Record, 2013/44*. Geoscience Australia, Canberra. https://doi.org/ 10.11636/Record.2013.044.

Close, D.F., 2014. The McArthur Basin: NTGS' approach to a frontier petroleum basin with known base metal prospectivity. *Annual Geoscience Exploration Seminar (AGES) Proceedings, Alice Springs, Northern Territory 15–16 March 2014*. Northern Territory Geological Survey, Darwin. pp. 85–89. https://geoscience.nt.gov.au/gemis/ntgsjspui/handle/1/82357.

Cox, G.M., Jarrett, A., Edwards, D., Crockford, P.W., Halverson, G.P., Collins, A.S., Poirier, A., Li, Z.X., 2016a. Basin redox and primary productivity within the Mesoproterozoic Roper Seaway. *Chemical Geology*, **440**, 101-114. https://doi.org/10.1016/j.chemgeo.2016.06.025.

Cox, G.M., Halverson, G.P., Stevenson, R.K., Vokaty, M., Poirier, A., Kunzmann, M., Li, Z.X., Denyszyn, S.W., Strauss, J.V., Macdonald, F.A., 2016b. Continental flood basalt weathering as a trigger for Neoproterozoic snowball earth. *Earth & Planetary Science Letters,* **446**, 89-99. https://doi.org/ 10.1016/j.epsl.2016.04.016.

Cox, G.M., Sansjofre, P., Blades, M.L., Farkas, J., Collins, A.S., 2019. Dynamic interaction between basin redox and the biogeochemical nitrogen cycle in an unconventional Proterozoic petroleum system. *Scientific Reports*, 9:5200. https://doi.org/10.1038/s41598-019-40783-4.

Ernst, R.E., Wingate, M.T.D., Buchan, K.L., Li, Z.X., 2008. Global record of 1600–700 Ma Large Igneous Provinces (LIPS): Implications for the reconstruction of the proposed Nuna (Columbia) and Rodinia supercontinents. *Precambrian Research,* **160(1)**, 159-178. https://doi.org/ 10.1016 /j.precamres.2007.04.019.

Frogtech Geoscience, 2018. SEEBASE® study and GIS for greater McArthur Basin. *Northern Territory Geological Survey, Digital Information Package DIP 017*. https://geoscience.nt.gov.au/ gemis/ ntgsjspui/handle/1/87064.

Glorie, S., Agostino, K., Dutch, R., Pawley, M., Hall, J., Danišík, M., Evans, N.J., Collins, A.S., 2017. Thermal history and differential exhumation across the eastern Musgrave Province, South Australia: insights from low-temperature thermochronology. *Tectonophysics,* **703–704**, 23-41, https://doi.org/10.1016/j.tecto.2017.03.003.

Gorter, J.D., Grey, K., 2013. Middle Proterozoic biostratigraphy and log correlations of the Kyalla and Chambers River Formations Beetaloo Sub-basin, Northern Territory, Australia. West Australian Basins Symposium (WABS) III. Poster. *Petroleum Exploration Society of Australia*.

Haines, P.W., Allen, H.J., 2016. The Murraba Basin: another piece of the Centralian Superbasin jigsaw puzzle falls into place. *GSWA 2016 extended abstracts: promoting the prospectivity of Western Australia*.

Horton, F., 2015. Did phosphorus derived from the weathering of Large Igneous Provinces fertilize the Neoproterozoic ocean?. *Geochemistry Geophysics Geosystems*, **16(6)**, 1723-1738. https://doi.org/10.1002/ 2015GC005792.

Howard, H.M., Smithies, R.H., Kirkland, C.L., Kelsey, D.E., Aitken, A. Wingate, M.T.D., Quentin de Gromard, R., Spaggiari, C.V., Maier, W.D., 2015. The burning heart — the Proterozoic geology and geological evolution of the west Musgrave Region, central Australia. *Gondwana Research,* **27(1)**, 64-94. https://doi.org /10.1016/j.gr.2014.09.001.

Jarrett, A. J. M., Edwards, D. S., Hong, Z., Palatty, P., Byass, J., Webster, T., 2017. Geochemistry of drillcore Balmain 1, Beetaloo Sub-basin, McArthur Basin, NT. *Geoscience Australia, Record, 2013/44*.

Kirkland, C.L., Wingate, M.T.D., Spaggiari C.V., Tyler I.M., 2009.184339: sandstone, Pollock Hills. Geochronology Record 817, *Geological Survey of Western Australia, Record 2011/4*, pp. 349.

Kirkland, C.L., Smithies, R.H., Woodhouse, A.J., Howard, H.M., Wingate, M.T.D., Belousova, E.A., Cliff, J.B., Murphy, R.C., Spaggiari, C.V., 2013. Constraints and deception in the isotopic record; the crustal evolution of the west Musgrave Province, central Australia. *Gondwana Research,* **23(2)**, 759-781. https://doi.org/10.1016/ j.gr.2012.06.001.

Kirscher, U., Mitchell, R., Liu, Y., Li, Z.X., Cox, G.M., Nordsvan, A., Wang, C., Pisarevsky, S., 2018. Long lived supercontinent Nuna - updated paleomagnetic constraints from Australia. *2018, AGU Fall Meeting*, abstract #GP21B-0647.

Lanigan, K., Hibbird, S., Menpes, S., Torkinton, J., 1994. Petroleum exploration in the Proterozoic Beetaloo sub-basin, Northern Territory. *APEA JOURNAL*, **34**, 674-674. https://doi.org/ 10.1071/ AJ93050.

Lyons, T.W., Reinhard, C.T., Planavsky, N.J., 2015. The rise of oxygen in earth's early ocean and atmosphere. *Nature*, **506(7488)**, 307-315. https://doi.org/10.1038/nature13068.

Maidment, D.W., Williams, I.S., Hand, M., 2010. Testing long-term patterns of basin sedimentation by detrital zircon geochronology, Centralian Superbasin, Australia. *Basin Research,* **19(3)**, 335-360. https://doi.org/10.1111/ j.1365-2117.2007.00326.x.

Melville, P.M., 2010. Geophysics and drilling collaboration final report for drilling program, Lake Woods Project, EL23687, EL24520, EL25631, EL27317, EL27318. *Northern Territory Geological Survey, Open File Report CR2010-0226*. https://geoscience.nt.gov.au/gemis/ntgsjspui/handle/1/75769.

Merdith, A.S., Collins, A.S., Williams, S.E., Pisarevsky, S., Foden, J.F., Archibald, D., Blades, M.L., Alessio, B.L., Armistead, S., Plavsa, D., Clark, C., Müller, R.D., 2017. A full-plate global reconstruction of the Neoproterozoic. *Gondwana Research*, **50**, 84-134. https://doi.org/10.1016/j.gr.2017.04.001.

Mukherjee I., Large, R.R., 2016. Pyrite trace element chemistry of the Velkerri Formation, Roper Group, McArthur Basin: Evidence for atmospheric oxygenation during the Boring Billion. *Precambrian Research*. **281**, 13-26. https://doi.org/10.1016/j.precamres.2016.05.003

Mukherjee I., Large, R.R., Corkrey, R., Danyushevsky, L.V., 2018. The Boring Billion, a slingshot for Complex Life on Earth. *Scientific Reports*, 8:4432. https://doi.org/10.1038/s41598-018-22695-x.

Munson, T.J, Kruse, P.D., Ahmad, M., 2013. Chapter 22 Centralian Superbasin, in Geology and mineral resources of the Northern Territory compiled by M Ahmad and TJ Munson: Northern Territory Geological Survey, Darwin, *Northern Territory, Special Publication 5*, p. 22.1–22.19. https://geoscience.nt.gov.au/gemis/ntgsjspui/ handle/1/81502.

Munson, T.J., 2016. Sedimentary characterisation of the Wilton package, greater McArthur Basin. Northern Territory. *Northern Territory Geological Survey, Record 2016-003*. https://geoscience.nt.gov.au/gemis/ntgsjspui/ handle/1/82741.

Munson, T.J., Revie, D., 2018. Stratigraphic subdivision of Velkerri Formation, Roper Group, McArthur Basin, Northern Territory. *Northern Territory Geological Survey, Record 2018-006***.** https://geoscience.nt.gov.au/gemis/ntgsjspui/handle/1/87322.

Munson, T.J, Thompson, J.M, Zhukova, I., Meffre, S., Beyer, E.E., Woodhead, J.D., Whelan, J.A., 2018. Summary of results. NTGS laser ablation ICP—MS U–Pb and Lu–Hf geochronology project: Roper Group and overlying ungrouped units (McArthur Basin), Renner Group (Tomkinson Province), Tijunna Group (Birrindudu Basin). *Northern Territory Geological Survey, Record 2018-007*. https://geoscience.nt.gov.au/gemis/ntgsjspui/handle/1/87656.

Piper, D.Z., Calvert, S.E., 2009. A marine biogeochemical perspective on black shale deposition. *Earth Science Reviews*, **95(1–2)**, 63-96. https://doi.org/10.1016/j.earscirev.2009.03.001.

Rawlings, D.J., 1999. Stratigraphic resolution of a multiphase intracratonic basin system: The McArthur Basin, northern Australia. *Australian Journal of Earth Sciences*, **46(5)**, 703-723. https://doi.org/ 10.1046/j.1440-0952.1999.00739.x.

Revie, D., 2017.Volumetric resource assessment of the lower Kyalla and middle Velkerri formations of the McArthur Basin. *Annual Geoscience Exploration Seminar (AGES) Proceedings, Alice Springs, Northern Territory 28–29 March 2017*. Northern Territory Geological Survey, Darwin. pp. 86-90. https://geoscience.nt.gov.au/gemis/ntgsjspui/handle/1/85107.

Revie, D., Normington, V., 2018. Shale resource data from the greater McArthur Basin. Northern Territory Geological Survey, *Digital Information Package DIP 014*. https://geoscience.nt.gov.au /gemis/ntgsjspui/handle/1/82595.

Sageman, B.B., Lyons, T.W., 2003. Geochemistry of fine-grained sediments and sedimentary rocks. *Treatise on Geochemistry*, **7**, 115-158. https://doi.org/10.1016/B0-08-043751-6/07157-7.

Shaw, R. D., 1991. The tectonic development of the Amadeus Basin, central Australia. In: Korsch, R.J., Kennard, J.M. (Eds.), Geological and Geophysical Studies in the Amadeus Basin, Central Australia. Bureau of Mineral Resources, Australia, pp.429–461.

Silverman, M.R., Landon, S.M., Leaver, J.S., Mather, T.J., Berg, E., 2007. No fuel like an old fuel: Proterozoic oil and gas potential in the Beetaloo Basin, Northern Territory, Australia: in Munson TJ and Ambrose GJ (editors)'. In Proceedings of the Central Australian Basins Symposium (CABS), Alice Springs, Northern Territory, 16–18 August, 2005.*'Northern Territory Geological Survey, Special Publication (Vol. 2).*

Smithies, R.H., Howard, H.M., Evins, P.M., Kirkland, C.L., Kelsey, D.E., Hand, M., Wingate, M.T.D., Collins, A.S., Belousova, E.A., 2011. High-temperature granite magmatism, crust–mantle interaction and the Mesoproterozoic intracontinental evolution of the Musgrave Province, central, Australia. *Journal of Petrology,* **52(5)**, 931-958. https://doi.org/10.1093/petrology/egr010.

Sun, S.S., McDonough, W.F., 1989. Chemical and isotopic systematics of oceanic basalts: implications for mantle composition and processes. *Geological Society London Special Publications*, **42(1)**, 314-345. https://doi.org/10.1144/GSL.SP.1989.042.01.19.

Taylor, S.R., Mclennan, S.M., 1995. The geochemical evolution of the continental crust. *Reviews of Geophysics,* **33(2)**, 241-265. https://doi.org/10.1029/95RG00262.

Tyrrell, T., 1999. The relative influences of nitrogen and phosphorus on oceanic primary production. *Nature,* **400(6744)**, 525-531. https://doi.org/10.1038/22941.

Wade, B.P., 2005. Nd isotopic and geochemical constraints on provenance of sedimentary rocks in the eastern Officer Basin, Australia: implications. *Journal of Geological Society London,* **162**, 513-530. https://doi.org/10.1144/0016-764904-001.

Walter, M.R., Veevers, J.J., Calver, C.R., Grey, K., 1995. Neoproterozoic stratigraphy of the Centralian Superbasin, Australia. *Precambrian Research,* **73(1–4)**, 173-195. https://doi.org/10.1016/0301-9268(94)00077-5.

Whelan, J.A., Beyer, E.E., Donnellan, N., Bleeker, W., Chamberlin, K.R., Soderlund, U., Ernst, R.E., 2016. 1.4 billion years of Northern Territory geology: Insights from collaborative U–Pb zircon and baddeleyite dating. *Annual Geoscience Exploration Seminar (AGES) Proceedings, Alice Springs, Northern Territory 15–16 March 2016*. Northern Territory Geological Survey, Darwin. pp. 115–123. https://geoscience.nt.gov.au/gemis/ntgsjspui/handle/1/82750.

Wingate, M.T.D., Pirajno, F., Morris, P.A., 2004. Warakurna large igneous province: a new Mesoproterozoic large igneous province in west-central Australia. *Geology,* **32(2)**, 105-108. https://doi.org/10.1130/G20171.1.

Yang, B., Smith, T.M., Collins, A.S., Munson, T.J., Schoemaker, B., Nicholls, D., Cox, G., Farkas, J., Glorie, S., 2018. Spatial and temporal detrital zircon U–Pb provenance of the hydrocarbon-bearing upper Roper Group, Beetaloo Sub-Basin, Northern Territory, Australia. *Precambrian Research*, **304**, 140-155. https://doi.org/10.1016/j.precamres.2017.10.025.

Yang, B., Collins, A.S., Blades, M.L., Capogreco, N., Payne, J.L., Munson, T.J., Cox, G.M., Glorie, S., 2019. Middle-late Mesoproterozoic tectonic geography of the North Australia Craton: U–Pb and Hf isotopes of detrital zircons in the Beetaloo Sub-basin, Northern Territory, Australia. *Journal of the Geological Society, London*. https://doi.org/10.1144/jgs2018-159.

Zhang, S.H., Zhao, Y., Li, X.H., Ernst, R.E., Yang, Z.Y, 2017. The 1.33–1.30 Ga Yanliao large igneous province in the North China Craton: Implications for reconstruction of the Nuna (Columbia) supercontinent, and specifically with the North Australian Craton. *Earth and Planetary Science Letters*, **465**, 122–125. https://doi.org/10.1016/j.epsl.2017.02.034.

Zhao, J.X., McCulloch, M.T., Bennett, V.C., 1992. Sm–Nd and U–Pb zircon isotopic constraints on the provenance of sediments from the Amadeus Basin, central Australia: evidence for REE fractionation. *Geochimica Et Cosmochimica Acta*, **56(3)**, 921-940. https://doi.org/10.1016/0016-7037(92)90037-J.

Zhao, J.X., Mcculloch, M.T., Korsch, R.J., 1994. Characterisation of a plume-related ~ 800 Ma magmatic event and its implications for basin formation in central-southern Australia. *Earth & Planetary Science Letters,* **121(3–4)**, 349-367. https://doi.org/10.1016/0012-821X(94)90077-9.

Chapter 5

Intra basin correlations and tectonic geography of the Mesoproterozoic North Australia Craton: detrital zircon U–Pb age and Hf isotope provenance analysis

In prep as:

Yang, B., Collins, A.S., Cox, Munson, T.J., Blades, M.L., Payne, J.L., Glorie, S, Farkas, J., Intra basin correlations and tectonic geography of the Mesoproterozoic North Australia Craton: detrital zircon U–Pb age and Hf isotope provenance analysis

Statement of Authorship

Title of Paper	Middle–late Mesoproterozoic tectonic geography of the North Australia Craton: U–Pb and Hf isotopes of detrital zircon grains in the Beetaloo Sub-basin, Northern Territory, Australia
Publication Status	☐ Published ☐ Accepted for Publication ☐ Submitted for Publication ☑ Unpublished and Unsubmitted work written in manuscript style
Publication Details	

Principal Author

Name of Principal Author (Candidate)	Bo Yang		
Contribution to the Paper	Field work, sample preparation, data collection and processing, data interpretation, manuscript composition.		
Overall percentage (%)	80		
Certification:	This paper reports on original research I conducted during the period of my Higher Degree by Research candidature and is not subject to any obligations or contractual agreements with a third party that would constrain its inclusion in this thesis. I am the primary author of this paper.		
Signature		Date	23/06/2019

Co-Author Contributions

By signing the Statement of Authorship, each author certifies that:

i. the candidate's stated contribution to the publication is accurate (as detailed above);

ii. permission is granted for the candidate in include the publication in the thesis; and

iii. the sum of all co-author contributions is equal to 100% less the candidate's stated contribution.

Name of Co-Author	Alan S. Collins		
Contribution to the Paper	Guidance on data interpretation, manuscript composition and review.		
Signature		Date	23/06/2019

Name of Co-Author	Tim J. Munson		
Contribution to the Paper	Guidance on data, manuscript review.		
Signature		Date	23/06/2019

Name of Co-Author	Morgan L. Blades		
Contribution to the Paper	Manuscript review		
Signature		Date	23/06/2019

Name of Co-Author	Justin L. Payne		
Contribution to the Paper	Data collection and processing, data interpretation, manuscript review.		
Signature		Date	23/06/2019

Name of Co-Author	Stijn Glorie		
Contribution to the Paper	Manuscript review.		
Signature		Date	23/06/2019

Name of Co-Author	Juraj Farkaš		
Contribution to the Paper	Manuscript review.		
Signature		Date	23/06/2019

Chapter 5

Intra basin correlations and tectonic geography of the Mesoproterozoic North Australia Craton: detrital zircon U–Pb age and Hf isotope provenance analysis

Abstract

The Wilton package of the "greater McArthur Basin", Australia, comprises a series of shallow marine siliciclastic successions that were deposited in several geographically separated basins. Sedimentary rocks of the Wilton package, covers an area over 145 000 Km^2 of the North Australia Craton, and records over 200 million years of tectonic and depositional history, from ca. 1.5 Ga to 1.3 Ga. New detrital zircon U–Pb age and Lu–Hf isotope data were collected from various formations within the Wilton package across multiple basins that make up the greater McArthur Basin. These data were compiled with previously published data in order to provide integral constraints on the basin provenance and intra-basin correlations. Further, these data are used to illustrate the ancient basin geography and its dynamic interactions with the tectonic evolution of the middle Mesoproterozoic North Australia Craton.

Data from the Collara Subgroup (lower Roper Group) suggest provenance from the Mt Isa Province and Arunta Region. Whereas, the overlying Maiwok Subgroup (upper Roper Group) received more detritus from eastern sources (e.g. the Mount Isa Province and the palinspastically adjacent Curnamona and Georgetown provinces; Figure 1). This provenance variation is interpreted to be resultant of the eastern source regions being uplifted after deposition of the Collara Subgroup. The South Nicholson Group exhibits significant provenance consistent to both the Maiwok and Collara subgroups and is interpreted as correlative to the Roper Group. Moreover, another potential correlative is the Inorunie Group of the Croydon Province in the far-east of the interpreted Wilton package. This potential correlation with the Roper Group as well as the South Nicholson Group suggests the Wilton package might be more extensive than previously thought. The Bulita Group of the Birrindudu Basin received detritus from north-eastern and northern sources (e.g. the Halls Creek and Pine Creek orogens). The younger Tijuna Group recorded inundation of the basin by detritus from southerly sources (e.g. the Tanami Region). Neither the Bulita Group nor Tijuna Group show provenance similar to the Roper Group and the South Nicholson Group. However, the mirrored southward provenance changes that are

coincidentally seen in both the Bulita-Tijuna groups and the Maiwok Subgroup, is interpreted to be associated with a consistent tectonic event—the amalgamation of the combined North Australia and South Australia cratons and the West Australia Craton, at ca. 1.3 Ga. During this amalgamation, the southern margin of the North Australia Craton was uplifted and southern sources (e.g. the Arunta and Tanami regions) became the topographic highs and shed detritus to the basins. The consistent provenance evolution correlates the McArthur-Beetaloo and Birrindudu basins temporally, despite the differing detritus source regions. Whereas, the provenance inconsistency between the Birrindudu Basin and the Beetaloo Sub-basin is interpreted to relate to underwater bathymetries (e.g. the Daly Waters High and Mallapunyah Fault Zone) that blocked transportation of sediment.

1. Introduction

The Mesoproterozoic North Australia Craton (NAC) is characterised by the formation of a series of shallow marine siliciclastic successions that deposited in several geographically separated basins (Figure 1; *Abbott & Sweet, 2000; Close, 2014; Ahmad & Munson, 2013; Munson, 2016; Munson et al., 2018*). The coherent lithology and significant undercover continuity amongst these sedimentary rocks has been used to refer the existence of a super basin, informally named the "Wilton package" (*Abbott & Sweet, 2000; Close, 2014; Ahmad & Munson, 2013; Munson, 2016; Munson et al., 2018*). Sedimentary rocks of the Wilton package cover the NAC in 1000 km-scale and form a temporal depositional record spanning about 200 million years, from ca. 1.5 to 1.3 Ga (*Abbott & Sweet, 2000; Close, 2014; Ahmad & Munson, 2013; Munson et al., 2018*). For this long-lived and spatially extensive deposition system, its formation, distribution and drainage patterns are strongly linked to the ancient geography (*Cox et al., 2016, 2019; Morrissey et al., 2018; Chapters 2 & 3*). The NAC was involved in multiple phases of global tectonic framework in the era of Mesoproterozoic, including the break-up of the super-continent Nuna and the amalgamation of the super-continent Rodinia (*Betts & Giles, 2006; Li et al., 2008; Pisarevsky et al., 2014; Smits et al., 2014; Mulder et al., 2015; Merdith et al., 2017, 2019; Chapters 2 & 3*).

In this contribution, we present core samples collected from multiple boreholes covering a large area of the Wilton package (Figure 1). Coupled detrital zircon U–Pb and hafnium isotope data, compiled with previous published data, were used to provide integral assessments on the basin provenance and correlation, and further, reveal a dynamic interactions among the tectonic, ancient geography and basin sedimentation of the middle Mesoproterozoic NAC.

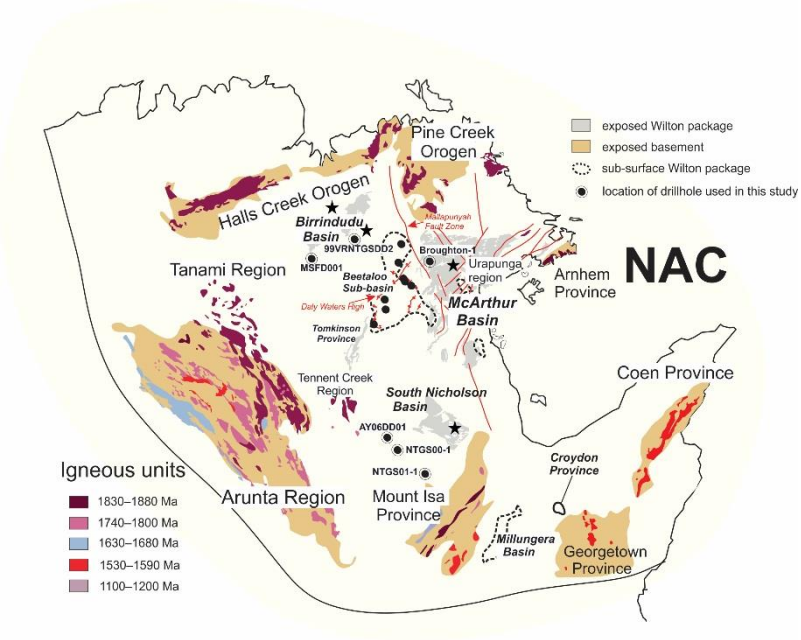

Figure 1 Geological framework of the Mesoproterozoic North Australia Craton (NAC) after *Chapter 2*. Black stars represent the outcrop sample locations of the data from *Carson (2013), Krositcin & Carson (2017),* and *Munson et al (2018)*; solid dots represent the sample locations of the Beetaloo Sub-basin data from *Chapters 2 & 3*.

2. Geological setting

The greater McArthur Basin, northern Australia, is a regionally extensive Paleoproterozoic to Mesoproterozoic basin, covering a large area of the North Australia Craton (*Rawlings, 1999; Ahmad & Munson, 2013; Close, 2014*). It unconformably overlies Archaean to Palaeoproterozoic aged crystalline basements/orogens, and unconformably underlies Neoproterozoic and Phanerozoic successions (*Rawlings, 1999; Ahmad & Munson, 2013; Carson, 2013; Munson, 2016; Munson et al., 2018; Chapter 2*). The greater McArthur Basin contains several coherent lithostratigraphic components and has been sub-divided into five sedimentary packages (*Rawlings, 1999; Ahmad & Munson, 2013; Munson, 2016; Munson et al., 2018*). The uppermost Wilton package is characterized by a group of Mesoproterozoic siliciclastic successions that are distinguishable from the underlying carbonaceous successions—the Favenc package (Figure 2; *Rawlings, 1999; Ahmad & Munson, 2013; Munson, 2016; Munson et al., 2018*). The Wilton package successions exhibit significant undercover continuity and have been suggest to be deposited in several geographically separated basins, including the Roper Group of the McArthur Basin and the Beetaloo Sub-basin, the Renner Group of the Tomkinson Province, the Tijunna Group of the Birrindudu Basin, and potentially the South Nicholson Group of the South Nicholson Basin (Figure 1; *Rawlings, 1999; Ahmad & Munson, 2013; Close, 2014; Munson, 2016; Munson et al., 2018*). Sedimentary rocks of the Wilton package are dominated by sandstone and mudstone units and were likely to be deposited in a range of depositional environments from

shoreline to shallow-marine shelf (*Rawlings, 1999; Ahmad & Munson, 2013; Munson, 2016; Munson et al., 2018*).

2.1 Roper Group

Sedimentary rocks of the Roper Group are largely exposed in the McArthur Basin and buried in the Beetaloo Sub-basin (Figure 1; *Ahmad & Munson, 2013; Munson, 2016*). The Roper Group is interpreted to be deposited in a stable shelf environment and is sub-divided into two subgroups—the lower Collara Subgroup and the upper Maiwok Subgroup (Figure 2; *Rawlings, 1999; Abbott & Sweet, 2000; Ahmad & Munson, 2013*). The Collara Subgroup is dominated by sandstones with less voluminous mudrocks (*Jackson et al., 1988; Rawlings, 1999; Abbott & Sweet, 2000; Abbott et al., 2001; Ahmad & Munson, 2013; Munson, 2016; Munson et al., 2018*). The Collara Subgroup is comprised of eight units, from the bottom to the top, including the Phelp Sandstone, the Mantungula Formation, the Limmen Sandstone, the Mainoru Formation, the Arnold Sandstone, Jalboi Formation and the Hodgson Sandstone (Figure 2; *Jackson et al., 1988; Rawlings, 1999; Abbott & Sweet, 2000; Abbott et al., 2001; Ahmad & Munson, 2013*). The Maiwok Subgroup, however, is more shale-rich with less abundant sandstones, and generally deposited in deeper shelf environments (*Jackson et al., 1988; Abbott & Sweet, 2000; Abbott et al., 2001; Ahmad & Munson, 2013*). Seven sedimentary units are included in this subgroup, which are, in ascending stratigraphic order, the Corcoran Formation, the Bessie Creek Sandstone, the Velkerri Formation, the Moroak Sandstone, the Kyalla Foramtion, the Bukalorkmi Sandstone and the Chambers River Formation (Figure 2; *Ahmad & Munson, 2013*). Two detrital zircon Sensitive High Resolution Ion Microprobe (SHRIMP) U–Pb ages of 1492 ± 29 Ma (2SD; *Jackson et al., 1999*) and 1492 ± 4 Ma (2SD; *Southgate et al., 2000*), from the lower Mainoru Formation, provide maximum depositional age constraints of the Roper Group (Figure 2). Whereas the minimum depositional age is constrained by the Derim Derim Dolerite intrusions that intruded the Roper Group up to the Bukalorkmi Sandstone. A secondary ionization mass spectrometry (SIMS) U–Pb baddeleyite age of 1324 ± 4 Ma is reported by *Abbott et al. (2001)* from the Urapunga Region. An isotope dilution thermal ionization mass spectrometry (ID-TIMS) baddeleyite age of 1312.9 ± 0.9 Ma is obtained from the northern Beetaloo Sub-basin (*Chapter 4*).

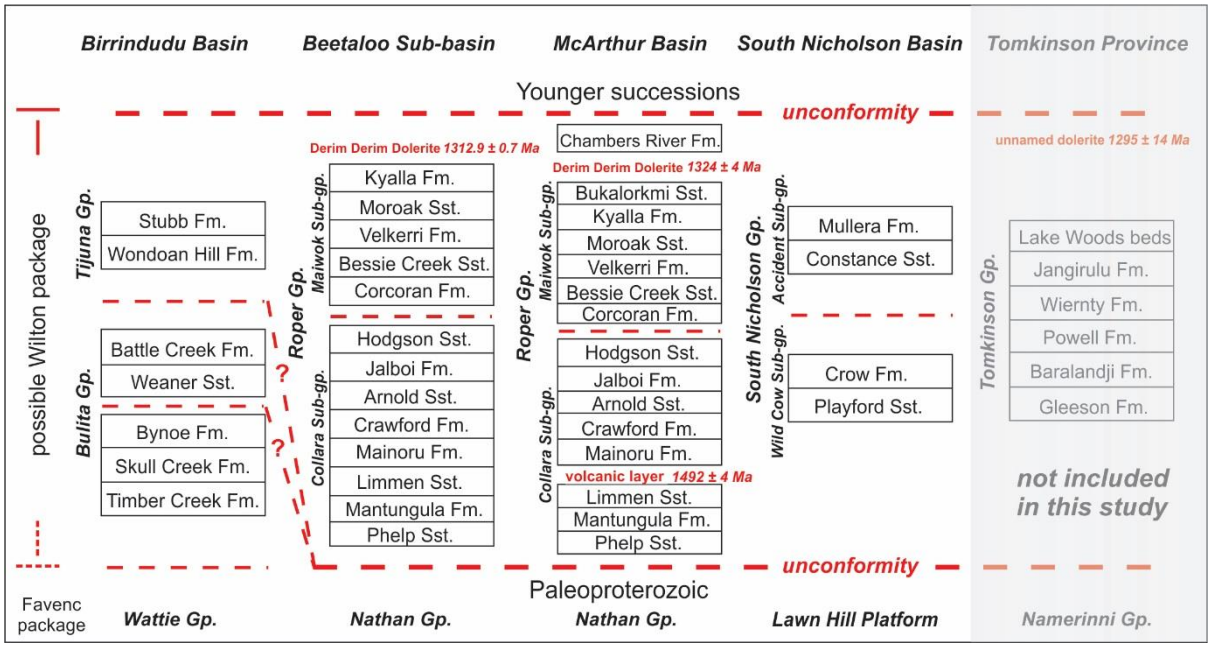

Figure 2 Stratigraphic chart of the Wilton package and its potential equivalents after *Ahamd & Munson (2013), Munson (2016)* and *Munson et al. (2018)*. Gp: Group; Sub-gp: subgroup.

2.2. Bulita Group and Tijuna Group

The Birrindudu Basin is located in the western part of the greater McArthur Basin (Figure 1). The two uppermost sedimentary groups are the Bulita Group and the Tijuna Group. The Bulita Group is unconformably overlain by the Tijuna Group, and contains five formations, in ascending stratigraphic order, the Timber Creek Formation, the Skull Creek Formation, the Bynoe Formation, the Weaner Sandstone and the Battle Creek Formation (Figure 2; *Ahmad & Munson, 2013*). The three lower formations, are characterized by stromatolitic, carbonate dominated successions, whereas the upper formations, the Weaner Sandstone and the Battle Creek Formation, contain more siliciclastic components (*Ahmad & Munson, 2013*). These rocks, together, indicate a shoaling, shallow-marine platform depositional environment (*Ahmad & Munson, 2013*). Sedimentary package classification of the Bulita Group remains unclear, as the lower formations exhibit lithological similarities to the Favenc package and the upper formations show affinities to the Wilton package (Figure 2; *Munson et al., 2018*). Depositional age constraint for this group is limited. The youngest detrital zircon analyse from the underlying Wattie Group (1550 ± 48 Ma, 2SD; *Krositcin & Carson, 2017*) might provide a maximum depositional age constraint for the lower Bulita Group formations. Whereas, the maximum depositional age of the Weaner Sandstone and the Battle Creek are more tightly constrained by the youngest single grain analysed from the Weaner Sandstone (1550 ± 36 Ma, 2SD; *Krositcin & Carson, 2017*).

The Tijuna Group contains a set of siliciclastic succession that are divided into two formations—the Wondoan Hill Formation and the Stubb Formation (Figure 2; *Ahmad & Munson, 2013;*

Munson, 2016). The Wondoan Hill Formation comprises a set of interbedded sandstone and mudstone with minor dolostone and the Stubb Formation is a mudstone dominated succession with minor sandstone. Age constraint for the Tijuna Group is limited. The youngest analysed detrital zircon with a $^{207}Pb/^{206}Pb$ age of 1452 ± 48 Ma obtained from the Wondoan Hill Formation (*Munson et al., 2018*), might provide the maximum deposition age constraint for this group. The Tijuna Group is unconformably overlain by a set of early Neoproterozoic successions—Auvergne Group (*Ahmad & Munson, 2013; Carson, 2013; Munson et al., 2018*).

2.3. South Nicholson Group

The South Nicholson Group of the South Nicholson Basin is located on the southeast of the Beetaloo Sub-basin (Figure 1). It unconformably overlies the Murphy Province and the Western Fold Belt of the Mt Isa Province, and is overlain by a series of Neoproterozoic to Cambrian successions, such as the Georgina Basin and the Helen Spring Volcanics (*Ahmad and Munson, 2013*). The South Nicholson Group is dominated by quartz sandstone interstratified with siltstone and shale, indicating a range of depositional environments from fluvial to shallow-marine shelf (*Ahmad & Munson, 2013*). The South Nicholson Group has been sub-divided into two subgroups. The Wild Cow Subgroup, in the lower part, includes the Playford Sandstone and the Crow Formation (Figure 2). The upper, Accident Subgroup, contains the Constance Sandstone and the Mullera Formation (Figure 2). The South Nicholson Group is poorly age constrained. A recently published $^{207}Pb/^{206}Pb$ age of 1483 ± 12 Ma (weighted mean age of the youngest group, 95% confidence, n=43, MWSD=1.38) from the Crow Formation has been suggested to be used as the maximum depositional constraint for this formation, while the youngest analysed zircon grain returned a $^{207}Pb/^{206}Pb$ age of 1371 ± 94 Ma (2SD; *Kositcin & Carson, 2019*).

3. Detrital zircon U–Pb age and Hf isotope

3.1. Method

3.1.1. U–Pb dating

Twelve sandstone core samples were collected, including two from the Roper Group of the McArthur Basin, three from the undifferentiated South Nicholson Group of the South Nicholson Basin, three from the Bulita Group and four from the Tijuna Group of the Birrindudu Basin. Detailed sampling information is listed in Table 1. Zircon grains were separated from crushed rock powder. Conventional magnetic methods and heavy liquids (LST 2.85 ± 0.02 g/mL) were used for further separation. Individual zircon grains were handpicked and mounted in non-

reactive epoxy resin. Preference to grain sizes, or shapes, or colours was avoided during zircon selection.

Cathodoluminescence (CL) images were obtained using a Phillips XL20 scanning electron microscope with attached Gatan CL (working distance: 15 mm; accelerating voltage: 12 kV) at Adelaide Microscopy, The University of Adelaide, to illustrate zircon internal structures and determine suitable domains for further analysis. A New Wave 213 nm Nd-YAG laser coupled with an Agilent 7900cs inductively-coupled-plasma–mass-spectrometer (ICP–MS) at Adelaide Microscopy, The University of Adelaide, was used for zircon chronological data collection. Zircon cores were mainly targeted. A spot size of 30 μm with frequency of 5 Hz was used. Laser intensity was set to 70% with fluence varying from ~5 to 7 J/cm^2. Instrumental fractionation correction was conducted by GEMOC GJ-1 zircon standard (^{207}Pb/^{206}Pb age of 607.7 ± 4.3 Ma, ^{206}Pb/^{238}U age of 600.7 ± 1.1 Ma and ^{207}Pb/^{235}U age of 602.0 ± 1.0 Ma; *Jackson et al., 2004*), and the Plešovice zircon standard with a published ^{206}Pb/^{238}U age of 337.13 ± 0.37 Ma (*Sláma et al., 2008*) was used to monitor accuracy. Analysis of the Plešovice internal standards yielded a weighted average ^{206}Pb/^{238}U age of 336.49 ± 0.35 Ma (95% confidence, MSWD=1.4, n=133). Data were reduced using Iolite (*Paton et al., 2011*) and plotted using the Excel add-in Isoplot (*Ludwig, 2003*).

3.1.2. Hafnium isotope analysis

Hafnium isotope analyses were done at The University of Adelaide using a New Wave UP-193 ArF excimer laser attached to a Thermo-Scientific Neptune Multi-Collector ICP–MS, following the methods of *Payne et al. (2013)*. Zircon grains, with less than 10% age discordance, were ablated using a spot size of 50 μm or 35 μm (depending on the grain size), frequency of 5 Hz, 4 ns pulse length and an intensity of ~4.5 J/cm^2. The acquisition time of each analyse was about 70 seconds and included about 20 seconds of background measurement. Raw data were reduced using HfTRAX Excel macro (*Payne et al., 2013*). Hafnium mass bias was corrected using a stable ^{179}Hf/^{177}Hf ratio of 0.7325. Correction of the Yb and Lu isobaric interferences on ^{176}Hf was following the methods of *Woodhead et al. (2004)*. The Mudtank zircon standard was used to monitor the instrument stability and data quality. Analysis of Mudtank standard yielded a weighted mean ^{176}Hf/^{177}Hf ratio of 0.282499 ± 14 (2SD, n=10), which is in accordance with the published value of 0.282507 ± 6 (*Woodhead & Hergt, 2005*). A ^{176}Lu decay constant of 1.865 × 10^{-11} year^{-1} after *Scherer et al. (2001)* was used for initial ^{176}Hf/^{177}Hf values calculation. Epsilon hafnium values were calculated using Chondrite reservoir (CHUR) values of ^{176}Hf/^{177}Hf = 0.282785 and ^{176}Lu/^{177}Hf = 0.0336 after *Bouvier et al. (2008)*.

Table 1 Details of samples collected for this study.

Basin	Borehole	Coordinate	Sample	Group	Formation	Lithology
McArthur Basin	Broughton-1	E: 133.62607° S: -14.35995°	Bro-07	Collara Sub-gp.	Arnold Sst.	coarse grained sandstone
			Bro-06	Collara Sub-gp.	Crawford Fm.	fine-medium grained sandstone
Birrindudu Basin	99VRNTGSDD2	E: 131.38248° S: -16.04131°	D57	Tijuna Gp.	Wondoan Hill Fm.	medium grained sandstone
			D24	Bulita Gp.	Weaner Sst.	coarse grained sandstone
			D02	Bulita Gp	Bynoe Fm.	fine grained sandstone/siltstone
	MSFD001	E: 130.44231° S: -17.04630°	MS-03	Tijuna Gp.	Stubb Fm.	medium grained sandstone
			MS-05	Tijuna Gp.	Wondoan Hill Fm.	fine-medium grained sandstone
			MS-06	Bulita Gp.	Battle Creek Sst.	medium grained sandstone
			MS-09	Bulita Gp.	Weaner Sst.	coarse grained sandstone
South Nicholson Basin	AY06DD01	E: 136.30152° S: -19.83585°	AY-01	South Nicholson Gp.	undifferentiated	coarse grained sandstone
	NTGS00-1	E: 136.82621° S: -19.85399°	SOU-01	South Nicholson Gp.	undifferentiated	coarse grained sandstone
	NTGS01-1	E: 137.62108° S: -19.85684°	JR-01	South Nicholson Gp.	undifferentiated	coarse grained sandstone

Gp: gourp; Fm: formation; Sst: sandstone.

3.2. Results

A total of 615 detrital zircon concordant U–Pb analyses and 253 hafnium isotope analyses were collected and discussed. All U–Pb age data are reported as 2SD level. Detailed analysis results are listed in Appendix 4.

3.2.1. U–Pb ages

Collara Subgroup

Two samples from the Collara Subgroup were analysed, including one from the Crawford Formation (Bro-06) and one from the Arnold Sandstone (Bro-07). Sample Bro-06 yielded eighty-seven concordant analyses, ranging from 2838 Ma to 1565 Ma with a dominated cluster centring at ca. 1780 Ma (Figure 3). Fifty three concordant analyses were obtained from the sample Bro-07. All except one yielded $^{207}Pb/^{206}Pb$ ages between 2821 Ma and 1601 Ma. The isolated one returned a Mesoproterozoic age of 1492 ± 50 Ma. The age spectrum of this sample is characterized by a major peak at ca. 1745 Ma and two minor peaks clustering at ca. 1810 Ma and 1895 Ma, respectively (Figure 3).

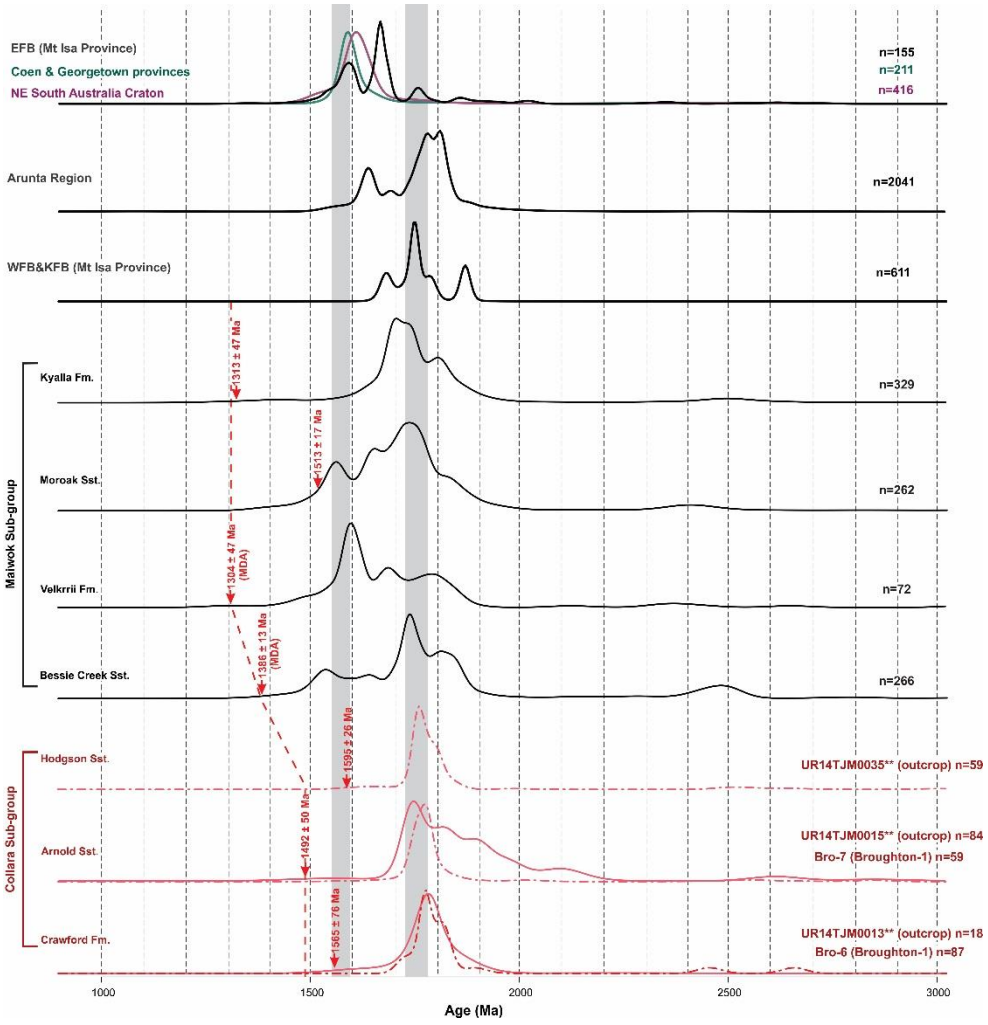

Figure 3 Kernel distribution estimates (KDE) of detrital zircon $^{207}Pb/^{206}Pb$ age spectra of the Roper Group formations and potential sources. Collara Subgroup data are from this study (solid lines) and **Munson et al. (2018)* (dash-dot lines). Maiwok Subgroup data are from *Chapters 2 & 3*, **Munson et al. (2018)* and ***Fanning (2012).* Published $^{207}Pb/^{206}Pb$ ages from both magmatic and detrital zircon grains are included from potential source areas, including Arunta Region (*Cross et al., 2005a, b, c ; Carson et al., 2009; Bodorkos et al., 2013; Kositcin et al., 2013a, b; 2014a, b; 2015b; Beyer et al., 2013, 2015, 2016*); Mount Isa Province (*Page & Sun, 1998; Neumann et al., 2006, 2009; Cross et al., 2015*); NE SAC (*Kromkhun et al., 2013; Armit et al., 2014*); Coen and Georgetown Provinces (*Blewett et al., 1998; Hoskin & Black, 2000; Kositcin et al., 2009*). Red arrows: the youngest detrital zircon $^{207}Pb/^{206}Pb$ age (with >95% concordance) for each formation. MDA: the youngest detrital zircon $^{207}Pb/^{206}Pb$ age used as maximum deposition age constraint. Red dash line represent assigned maximum deposition age for each formation.

Bulita Group

Samples were collected from the Bynoe Formation (sample D02), the Weaner Sandstone (samples D24 and MS-09) and the Battle Creek Formation (sample MS-06). Forty-eight analyses from the sample D02 yielded concordant $^{207}Pb/^{206}Pb$ ages ranging from 2946 Ma to 1538 Ma, forming a major cluster at ca. 1835 Ma (Figure 4). Sample D24 yielded twenty-three concordant analyses. These analyses yielded $^{207}Pb/^{206}Pb$ ages ranging from 2450—1659 Ma, and formed a

major peak at ca. 1830 Ma and two minor peaks at ca. 1730 Ma and ca. 1940 Ma (Figure 4). Forty-three concordant analyses have been obtained from the other Weaner Sandstone sample (sample MS-09). The age spectrum of this sample is characterized by a dominated peak and a minor peak centring at ca. 1830 Ma and ca. 1910 Ma, respectively (Figure 4). The Battle Creek sample (MS-06) yielded concordant $^{207}Pb/^{206}Pb$ ages ranging from 2517 Ma to 1628 Ma that formed a dominated age peak centring at ca. 1810 Ma (Figure 4).

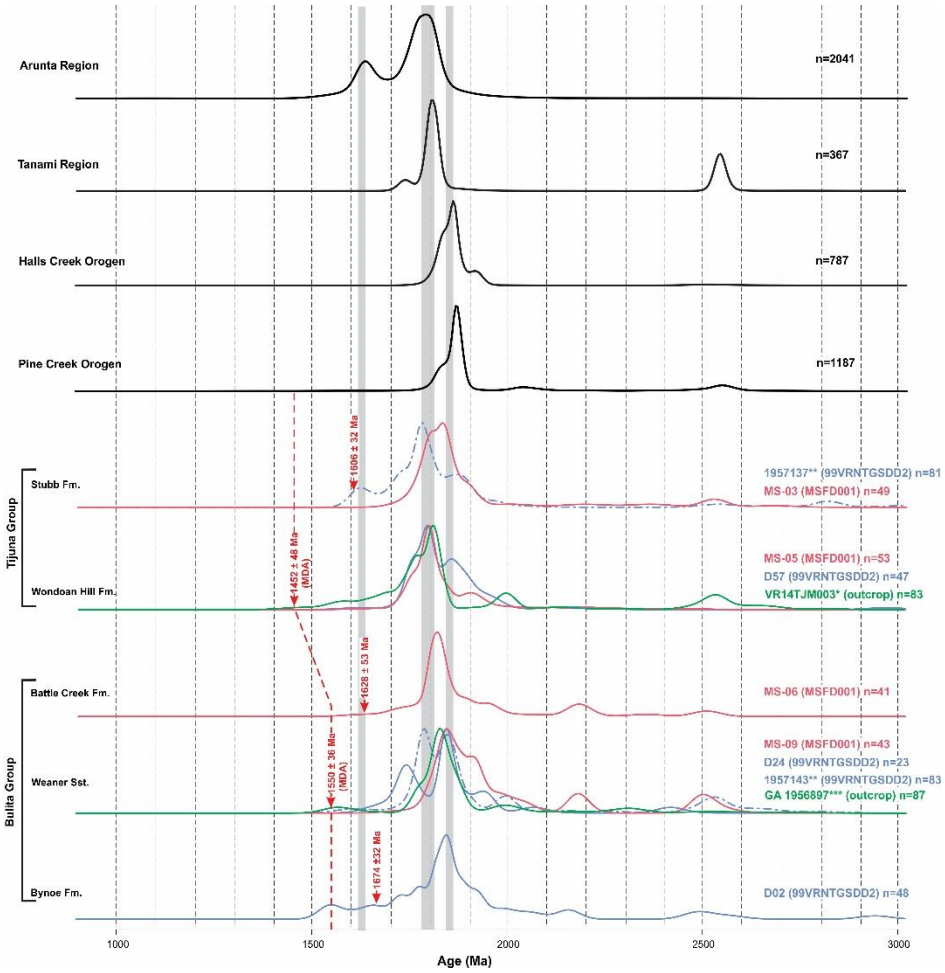

Figure 4 Kernel distribution estimates (KDE) of detrital zircon $^{207}Pb/^{206}Pb$ age spectra of the Bulita and Tijuna groups and potential sources. Data from this study are compiled with published $^{207}Pb/^{206}Pb$ age data from *Munson et al (2018), **Carson (2013) and ***Kositcin & Carson (2017). Published $^{207}Pb/^{206}Pb$ ages from both magmatic and detrital zircon grains are included from potential source areas, including Arunta Region (*Cross et al., 2005a, b, c; Carson et al., 2009; Bodorkos et al., 2013; Kositcin et al., 2013a, b; 2014a, b; 2015b; Beyer et al., 2013, 2015, 2016*); Pine Creek Orogen (*Worden et al., 2006a, b, 2008; Carson et al., 2009; Hollis et al., 2010; Kositcin et al., 2013a; Beyer et al., 2013*); Halls Creek Orogen (*Worden et al., 2008; Hollis et al., 2014*); Tanami Region (*Kositcin et al., 2013a; Kromkhun et al., 2013a*). Red arrows: the youngest detrital zircon $^{207}Pb/^{206}Pb$ age (with >95% concordance) for each formation. MDA: the youngest detrital zircon $^{207}Pb/^{206}Pb$ age used as maximum deposition age constraint. Red dash line represent assigned maximum deposition age for each formation.

Tijuna Group

Two samples from the Wondoan Hill Formation (samples D57 and MS-05) and one from the Stubb Formation (sample MS-03) were analysed. The dating results reveal that the sample D57 contains concordant $^{207}Pb/^{206}Pb$ ages ranging from 2969 Ma to 1619 Ma. Forty-seven analyses formed a major age peak at ca. 1795 Ma and a secondary cluster at 1840 Ma (Figure 4). The concordant analyses from the sample MS-05 are dominated by Paleoproterozoic $^{207}Pb/^{206}Pb$ ages ranging from 2282 Ma to 1647 Ma with a dominated age peak at ca. 1795 Ma (Figure 4). The Stubb Formation sample is also dominated by Paleoproterozoic analyses (2345-1723 Ma), with three isolated analyses yielded Neoarchean ages between 2685 Ma and 2527 Ma. A major peak at ca. 1810 Ma is identifiable in the age spectrum of this sample (Figure 4).

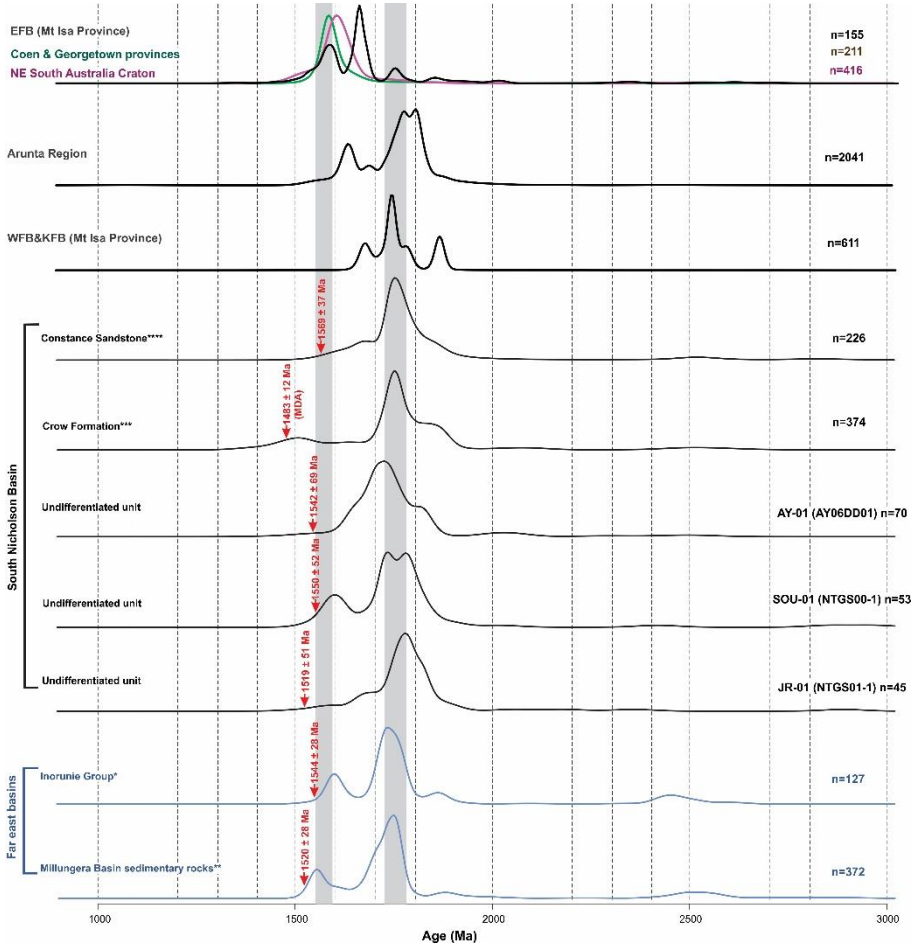

Figure 5 Kernel distribution estimates (KDE) of detrital zircon $^{207}Pb/^{206}Pb$ age spectra of the South Nicholson Group, possible Wilton package equivalents and potential sources. Data used for comparison are from this study and from **Nordsvan et al. (2018), **Neumann & Kositcin (2011), ***Kositcin & Carson (2019) and ****Anderson et al. (2019)*. Published magmatic and detrital zircon age data are included from potential source areas (*Blewett et al., 1998; Page and Sun, 1998; Hoskin & Black, 2000; Condie et al., 2005; Cross et al., 2005a, b, c, 2015; Griffin et al., 2006; Neumann*

et al., 2006, 2009; Murgulov et al., 2007; Kositcin et al., 2009, 2013b, 2014a, b, 2015a, b; Hollis et al., 2010; Beyer et al., 2015, 2016; Bodorkos et al., 2013; Armit et al., 2014). Red arrows: the youngest detrital zircon $^{207}Pb/^{206}Pb$ age (with >95% concordance) for each sample.

South Nicholson Group

Three samples were analysed. Sample AY-01 contains zircon grains dated between 2500 Ma and 1540 Ma. Seventy concordant analyses from this sample exhibited a major peak at ca. 1715 Ma and a minor peak at ca. 1810 Ma (Figure 5). Detrital zircon grains from the sample SOU-01 yielded concordant $^{207}Pb/^{206}Pb$ ages broadly spread between 2939 Ma and 1550 Ma, with two major peaks at ca. 1780 Ma and ca. 1720 Ma, and one minor peak centring at ca. 1600 Ma (Figure 5). Sample JR-01 yielded concordant analyses with $^{207}Pb/^{206}Pb$ ages ranging from 2865 Ma to 1519 Ma (n=45). The age spectrum of this sample shows unimodal signature with a dominated cluster peaking at ca. 1770 Ma (Figure 5).

3.2.2. Lu-Hf isotope results

Collara Subgroup

Hafnium isotopic data from the Crawford Formation sample (sample Bro-06) exhibit $^{176}Hf/^{177}Hf_i$ ratios ranging from 0.280926 to 0.281864. One Mesoarchean analyse with a $^{207}Pb/^{206}Pb$ age of 2838 Ma yielded an $\varepsilon_{Hf}(t)$ value of -1.15 (Figure 6). Zircon grains dated between 1830 Ma and 1769 Ma all returned negative $\varepsilon_{Hf}(t)$ values (from -3.01 to -0.38), indicating radiogenically depleted crystallization environments. Five late Paleoproterozoic to early Mesoproterozoic analyses yielded predominately positive $\varepsilon_{Hf}(t)$ values ranging from -0.87 to +3.73 (Figure 6). Twenty-four analyses were collected from the sample Bro-07 (Arnold Formation). These analyses show $^{176}Hf/^{177}Hf_i$ ratios ranging from 0.281083 to 0.281805. One Neoarchean grain yielded a $\varepsilon_{Hf}(t)$ value of -1.44. Zircon grains dated between 1922 Ma and 1712 Ma returned $\varepsilon_{Hf}(t)$ values ranging from -5.62 to +4.40 (Figure 6).

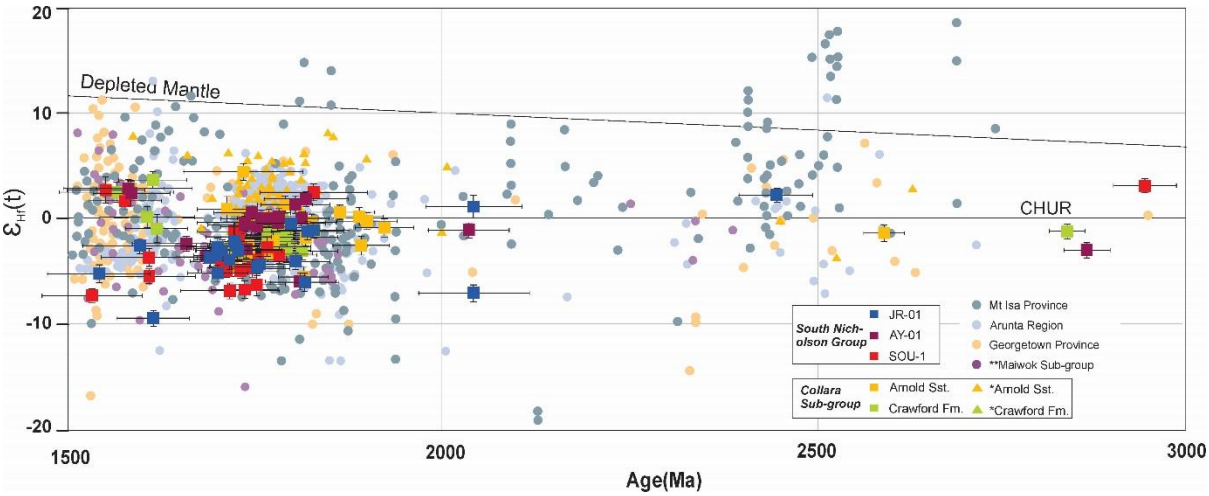

Figure 6 Epsilon hafnium values against $^{207}Pb/^{206}Pb$ ages plot of the measured samples from the Collora Subgroup, the South Nicholson Group and the published data from potential sources. Published data are potential sources, including Mt Isa Province (*Condie et al., 2005; Griffin et al., 2006; Bierlein et al., 2008*); Arunta Region (*Beyer et al., 2013, 2015*); Georgetown Province (*Murgulov et al., 2007*). CHUR: chondrite reservoir. *data from Munson et al. (2018). **data from *Chapter 3*.

Bulita Group

Sample D-02, from the Bynoe Formation, yielded $^{176}Hf/^{177}Hf_i$ ratios ranging from 0.281200 to 0.281730. Two analyses, with late Neoarchean and early Paleoproterozoic ages, both yielded positive $\varepsilon_{Hf}(t)$ values (+2.38 and +11.97; Figure 7). Zircon grains dated between 1931 Ma and 1778 Ma returned $\varepsilon_{Hf}(t)$ values ranging from -8.67 to +0.23 (Figure 7). Five late Paleoproterozoic to early Mesoproterozoic zircon grains, aged between 1638 Ma and 1538 Ma, all returned negative $\varepsilon_{Hf}(t)$ values (from -16.30 to -1.08; Figure 7).

Thirty-seven analyses from the two Weaner Sandstone samples show $^{176}Hf/^{177}Hf_i$ ratios ranging from 0.280942 to 0.281700. Three late Neoarchean and early Paleoproterozoic analyses yielded both positive and negative $\varepsilon_{Hf}(t)$ values ranging from -9.84 to +1.78 (Figure 7). Zircon grains dated between 1949 Ma and 1803 Ma, are dominated by negative $\varepsilon_{Hf}(t)$ values (from -12.94 to -0.14; n=23), except that four returned positive values (from +0.19 to +3.73; Figure 7). Analyses with $^{207}Pb/^{206}Pb$ ages between 1750 Ma and 1729 Ma all returned negative $\varepsilon_{Hf}(t)$ values (from -3.71 to -0.74; Figure 7).

The Battle Creek Formation sample, sample MS-06, exhibits zircon $^{176}Hf/^{177}Hf_i$ ratios ranging from 0.281037 to 0.281696. Two late Neoarchean analyses returned $\varepsilon_{Hf}(t)$ values of +2.64 and -0.43, respectively. Zircon grains dated between 2205 Ma and 1937 Ma returned $\varepsilon_{Hf}(t)$ values ranging from -12.66 to +2.51 (Figure 7). Twelve analyses, with $^{207}Pb/^{206}Pb$ ages between 1852 Ma and 1802 Ma, yielded predominately negative $\varepsilon_{Hf}(t)$ values (-6.09 to -0.20) except two that returned positive values (+1.79 and +2.13; Figure 7).

Tijuna Group

Forty-two zircon grains, from the Wondoan Hill Formation samples (samples MS-05 and D-57), were analysed, exhibiting a range of $^{176}Hf/^{177}Hfi$ ratios from 0.28918 to 0.281857. Two older grains with $^{207}Pb/^{206}Pb$ ages of 2969 Ma and 2282 Ma returned $\varepsilon_{Hf}(t)$ values of +1.61 and -5.15, respectively (Figure 7). For zircon grains aged between 2205 Ma and 1937 Ma, thirty-six yielded negative $\varepsilon_{Hf}(t)$ values ranging from -6.81 to -0.02, and four analyses returned positive values (+1.47 to 6.87; Figure 7).

The Stubb Formation sample, sample MS-03, shows $^{176}Hf/^{177}Hf_i$ ratios from 0.281156 to 0.281679. Two late Neoarchean analyses both returned positive $\varepsilon_{Hf}(t)$ values (+3.42 and +5.90). Whereas, zircon grains aged between 1850 Ma and 1784 Ma yielded predominately negative $\varepsilon_{Hf}(t)$ values ranging from -6.24 to -0.01 with three analyses returned positive $\varepsilon_{Hf}(t)$ values (Figure 7).

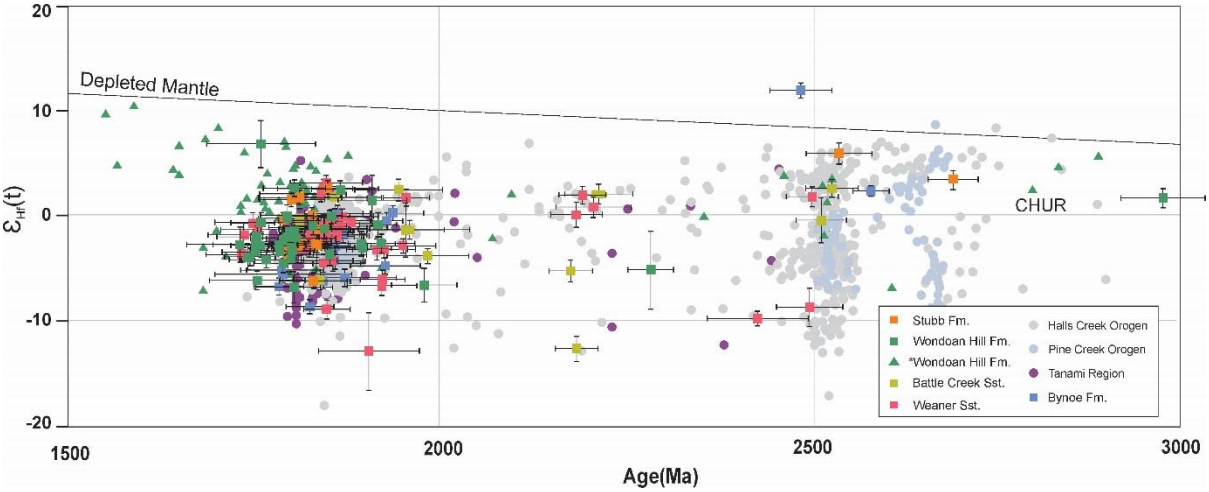

Figure 7 Epsilon hafnium values against $^{207}Pb/^{206}Pb$ ages plot of the measured samples from the Buliita Group, the Tijuna Group and the published data from potential sources. Published data are potential sources, including Tanami Region (*Kositcin et al., 2013a; Kromkhun et al., 2013a*); Halls Creek Orogen (*Hollis et al., 2010;*); Pine Creek Orogen (*Worden et al., 2006a, 2006b; Worden et al., 2008; Carson et al., 2009 Beyer et al., 2013*). CHUR: chondrite reservoir. *data from *Munson et al. (2018)*.

South Nicholson Group

Twenty-two analyses were collected form the sample AY-01, yielding $^{176}Hf/^{177}Hf_i$ ratios from 0.281278 to 0.281694. A single early Paleoarchean grain with a $^{207}Pb/^{206}Pb$ age of 3443 Ma yielded an $\varepsilon_{Hf}(t)$ value of -0.2 (Figure 6). Two zircon grains, with $^{207}Pb/^{206}Pb$ ages of 2042 Ma and 2041 Ma, yielded $\varepsilon_{Hf}(t)$ values of -7.14 and 1.11 (Figure 6). Zircon grains dated between 1828 Ma and 1615 Ma returned dominantly negative $\varepsilon_{Hf}(t)$ values, from -9.54 to -0.51, indicating radiogenically depleted crystallization environments. Two early Mesoproterozoic grains, dated at

1597 Ma and 1542 Ma, also yielded negative $\varepsilon_{Hf}(t)$ values (-2.67 and -5.29; Figure 6). The $^{176}Hf/^{177}Hf_i$ ratios of the sample JR-01 ranges from 0.280857 to 0.281860 (n=20). A single Mesoarchean zircon with a $^{207}Pb/^{206}Pb$ age of 2862 Ma returned a negative $\varepsilon_{Hf}(t)$ value of -3.07 (Figure 6). A middle Paleoproterozoic zircon grain (dated at 2036 Ma) also yielded a negative $\varepsilon_{Hf}(t)$ value (-1.15; Figure 6). Zircon grains with $^{207}Pb/^{206}Pb$ ages between 1818 Ma and 1659 Ma yielded $\varepsilon_{Hf}(t)$ values between -6.02 and +1.83. Two analyses with early Mesoproterozoic ages (1585 Ma and 1580 Ma) returned positive $\varepsilon_{Hf}(t)$ values of +2.38 and +2.85 (Figure 6). Sample SOU-01 yielded $^{176}Hf/^{177}Hf_i$ ratios ranging from 0.280979 to 0.281875. One Mesoarchean zircon grain yielded positive $\varepsilon_{Hf}(t)$ values of +3.10. Fifteen Paleoproterozoic analyses except one yielded negative values (-6.92 to -1.27). The isolated analysis, with a $^{207}Pb/^{206}Pb$ age of 1828 Ma, returned an $\varepsilon_{Hf}(t)$ value of +2.47. Three early Mesoproterozoic analyses dated between 1576 to 1533 Ma yielded both negative and positive $\varepsilon_{Hf}(t)$ values, between -7.34 and +1.63 (Figure 6).

4. Provenance analysis

Coupled detrital zircon U–Pb and Hf data from this research (Table 1), compiled with previous published data from *Fanning (2012), Carson (2013), Kositcin & Carson (2017), Munson et al. (2018), Chapters 2 & 3*, are compared with the data from exposed orogens/basements around the basin, in order to identify the possible source regions for each sedimentary unit.

4.1. Collara Subgroup of McArthur Basin

Two core samples from this study and three published outcrop samples from *Munson et al. (2018)*, including samples UR14TJM0013 (Crawford Formation), UR14TJM0015 (Arnold Sandstone) and UR14TJM0035 (Hodgson Sandstone), were compared and discussed together.

Sample Bro-06 and sample UR14TJM0013, from the Crawford Formation, both show unimodal zircon age spectra with dominant peaks centring at ca. 1780 Ma (Figure 5). This is consistent with the overlying Arnold Sandstone. Two Arnold Sandstone samples, sample Bro-07 and sample UR14TJM0035, are both dominated by zircon grains dated between ca. 1720 Ma and ca. 1800 Ma, with major clusters centring at ca. 1745 Ma and ca. 1780 Ma, respectively (Figure 5). Also, similar age spectrum, with a dominant cluster peaking at ca. 1760 Ma, is seen in the Hodgson Sandstone sample (Figure 5; *Munson et al., 2018*). The consistent detrital zircon age compositions of these samples indicate that the three formations of the Collara Subgroup were likely sourced from similar source regions. The dominant ca. 1740 to 1770 Ma zircon grains are comparable to the ubiquitous ca. 1720 to 1780 Ma magmatic rocks seen in the Mt Isa Province and the Arunta Region (Figure 3; *Condie et al., 2005; Griffin et al., 2006; Murgulov et al., 2007; Bierlein et al., 2008; Beyer et al., 2013, 2015; Armit et al., 2014*). Additionally, the hafnium

isotope data also shows overlapping $\varepsilon_{Hf}(t)$ values of the Collara Subgroup and the Mt Isa-Arunta regions (Figure 6; *Condie et al., 2005; Griffin et al., 2006; Murgulov et al., 2007; Bierlein et al., 2008; Beyer et al., 2013, 2015; Kositcin et al., 2013a; Kromkhun et al., 2013*), indicating potential source regions for the basin.

4.2. Bulita and Tijuna groups of the Birrindudu Basin

4.2.1. Bulita Group

Three formations from the Bulita Group were analysed, including the Bynoe Formation, the Weaner Sandstone and the Battle Creek Sandstone. Six samples, including four core samples from this research (samples D02, D24, MS-09 and MS-06; Table 1), one core sample (sample 1957143, the Weaner Sandstone) from *Carson (2013)* and one outcrop sample (sample GA 1956897, the Weaner Sandstone) from *Kositcin & Carson (2017)*, are discussed.

Sample D02 contains a large portion of zircon grains aged ca. 1830 Ma (Figure 4). Potential sources for these grains might be the Halls Creek and Pine Creek orogens, in which ca. 1820-1840 Ma magmatic rocks are frequently reported (*Worden et al., 2006a, 2008; Carson et al., 2009; Hollis et al., 2010*; Figure 4). The dominant ca. 1830 Ma zircon age populations are also observed in the Weaner Sandstone samples. Age spectra of the four samples all exhibit primary peaks centring at ca. 1830 Ma, showing similarity to the Halls Creek and Pine Creek orogens as well as the underlying Bynoe Formation (Figure 4). Further, in the $\varepsilon_{Hf}(t)$ against age plot, those ca. 1830 Ma zircon grains from the Bynoe Formation and Weaner Sandstone, yielded moderately enriched $\varepsilon_{Hf}(t)$ values, overlapping well with those of the Halls Creek and Pine Creek orogens (Figure 7; *Worden et al., 2006a, 2008; Carson et al., 2009; Hollis et al., 2010*). The consistent zircon age and hafnium isotope similarities indicate that the Bynoe Formation and Weaner Sandstone might be sourced from Halls Creek and Pine Creek orogens. In addition, although the four Weaner Sandstone samples all have dominant ca. 1830 Ma zircon grains, they show inconsistency in the secondary age populations. This is characterized by a minor peak at ca. 1735 Ma in sample D24, a cluster peaking at ca. 1780 Ma in sample 1957143 and a secondary peak ca. 1905 Ma in sample MS-09 (Figure 4). The variation of the secondary zircon populations might be because of varied local sources that locally sourced the basin, resulting the spatial inconsistency within this formation.

Detrital zircon grains obtained from the Battle Creek Formation sample (MS-06) yielded U–Pb ages forming a major peak centring ca. 1810 Ma (Figure 4). Potential source regions for these ca. 1810 Ma zircon grains include the Halls Creek and Pine Creek orogens in the north and northwest (*Worden et al., 2006a, 2008; Carson et al., 2009; Hollis et al., 2010*). Circa 1810 Ma

magmatic rocks are also seen in the Tanami Region in the south of the basin (*Bagas et al., 2008, 2010; Li et al., 2013*). In the $\varepsilon_{Hf}(t)$ against age plot, the Battle Creek Formation analyses overlap well with the Halls Creek and Pine Creek orogens and the Tanami Region as well (Figure 7; *Worden et al., 2006a, 2008; Carson et al., 2009; Hollis et al., 2010; Li et al., 2013*), suggesting the these regions might be the potential source regions for the Battle Creek Formation.

4.2.2. Tijuna Group

Five samples from the Tijuna Group were analysed, including three core samples from this study (samples D57, MS-05 and MS-03; Table 1), one published core sample (sample 1957137, the Stubb Formation) from *Carson (2013)* and one published outcrop sample (sample VR14TJM0003, the Wondoan Hill Formation) from *Munson et al. (2018)*.

Three samples of the Wondoan Hill Formation exhibit consistent age spectra with dominant peaks centring at ca. 1800 Ma (Figure 4). Potential sources for these ca. 1800 Ma zircon grains might be the Tanami Region where ca. 1810 Ma to 1790 Ma magmatic rocks are largely exposed (*Bagas et al., 2008, 2010; Li et al., 2013*). This is also supported by the zircon hafnium isotope data, which show overlapping $\varepsilon_{Hf}(t)$ values of the Wondoan Hill Formation and the Tanami Region (Figure 7). Additionally, the consistent zircon age spectra of three Wondoan Hill samples indicate little spatial variation within this formation, which suggests that sediments were well sorted and mixed, and probably deposited in a uniform depositional system with low bathymetric relief and few local sources.

Spatial provenance consistency, is however, absent in the two Stubb Formation samples. Sample 1957131 is characterised by a major peak at ca. 1780 Ma and two minor peaks at ca. 1615 Ma and ca. 1870 Ma, whereas sample MS-03 is dominated by zircon grains dated between ca. 1800 and 1830 Ma. Potential sources for sample 1957131 are the Arunta Region in which ca. 1770 to 1790 Ma magmatic rocks are ubiquitously exposed (Figure 4). Sample MS-02, however, exhibits a zircon age spectrum that is comparable to the Halls Creek and Pine Creek orogens as well as the Tanami Region (Figure 4).

4.3. South Nicholson Group of the South Nicholson Basin

Three core samples were collected from the undifferentiated South Nicholson Group. The detrital zircon age spectra of these samples, along with the published data from *Kositcin & Crason (2019)* and *Anderson et al. (2019)*, are all dominated by ca. 1700 to 1790 Ma aged zircon grains. The age spectra of the South Nicholson Group samples are comparable to those seen in the Mt Isa and the Arunta regions (Figure 5; *Blewett et al., 1998; Page & Sun, 1998; Hoskin & Black, 2000;*

Condie et al., 2005; Griffin et al., 2006; Neumann et al., 2006, 2009; Murgulov et al., 2007; Bierlein et al., 2008; Kositcin et al., 2009; Armit et al., 2014; Cross et al., 2015). Further, hafnium isotope analysis reveals that these ca. 1700 to 1790 Ma aged zircon grains yielded predominately slightly evolved signatures, showing significant similarity to the data from the Mt Isa and the Arunta regions (Figure 6; *Blewett et al., 1998; Page & Sun, 1998; Hoskin & Black, 2000; Condie et al., 2005; Griffin et al., 2006; Neumann et al., 2006, 2009; Murgulov et al., 2007; Bierlein et al., 2008; Kositcin et al., 2009; Armit et al., 2014; Cross et al., 2015*). In addition, zircon grains aged from ca. 1600 to 1550 Ma are seen in the South Nicholson samples. These grains yielded a spread of $\varepsilon_{Hf}(t)$ values forming a vertical array (ranging from -9.5 to +2.8). This is comparable to those seen in the eastern Mt Isa Province, the Georgetown Province and the northeast South Australia Craton sources (Figure 6; *Blewett et al., 1998; Page & Sun, 1998; Hoskin & Black, 2000; Condie et al., 2005; Griffin et al., 2006; Neumann et al., 2006, 2009; Murgulov et al., 2007; Bierlein et al., 2008; Kositcin et al., 2009; Armit et al., 2014; Cross et al., 2015*). We suggest the South Nicholson Group mainly received detritus from the Mt Isa Province and the Arunta Region, whereas other sources, such as Georgetown Province and the northeast South Australia Craton regions, probably also contributed to a lesser extent.

5. Discussion

5.1. Tectonic geography of Roper Group

Detrital zircon U–Pb and hafnium isotope data suggest that the three formations of the Collara Subgroup, the Crawford Formation, the Arnold Sandstone and the Hodgson Sandstone, were mainly sourced from the Mt Isa Province and the Arunta Region. Their consistent zircon age spectra indicate little variation of provenance. However, the provenance changed after their deposition, which is characterised by the prominent ca. 1.61 to 1.55 Ga zircon grains that are seen in overlying Maiwok Subgroup formations (the Bessie Creek Sandstone, the Velkerri Formation and the Moroak Sandstone; Figure 3). *Chapters 2 & 3* suggest that these ca. 1.6 Ga zircon grains are likely to be sourced from eastern sources, including the Eastern Fold Belt (EFB) of the Mt Isa Province, Georgetown Province and NE South Australia Craton (SAC) regions. These regions are mainly distributed along the eastern margin of the combined North Australia Craton (NAC) and South Australia Craton (Figure 8), following the Proterozoic plate-reconstruction model proposed by *Li & Evans (2011)*. This provenance variation, from the Collara Subgroup to the Maiwok Subgroup, is coeval with the exhumation of these ca. 1.6 Ga zircon source regions, which is evidenced by a series of low temperature mineral cooling ages, including the white mica and biotite Ar-Ar ages (ca.1.46-1.38 Ga) from the Eastern Fold Belt (*Spiking et al., 2001*), the apatite U–Pb ages (ca. 1.47-1.40 Ga) from the northern Gawler Craton (*Hall et al., 2018*), the

biotite Ar-Ar ages (ca. 1530 Ga) from the north-eastern Gawler Craton (*Forbes et al., 2012*), and the hornblende and biotite Ar-Ar ages (ca. 1.43-1.42 Ga) from the south-eastern Gawler Craton (*Foster & Ehlers, 1998*). *Chapters 2 & 3* suggest that this exhumation might be related to the separating of the combined NAC and SAC and the Laurentia at about ca. 1.45 Ga, during which the eastern margin of the combined NAC and SAC was exhumed as a rift shoulder highs. We suggest that this exhumation event probably started after the deposition of the Collara Subgroup, but during or before the deposition of the Maiwok Subgroup.

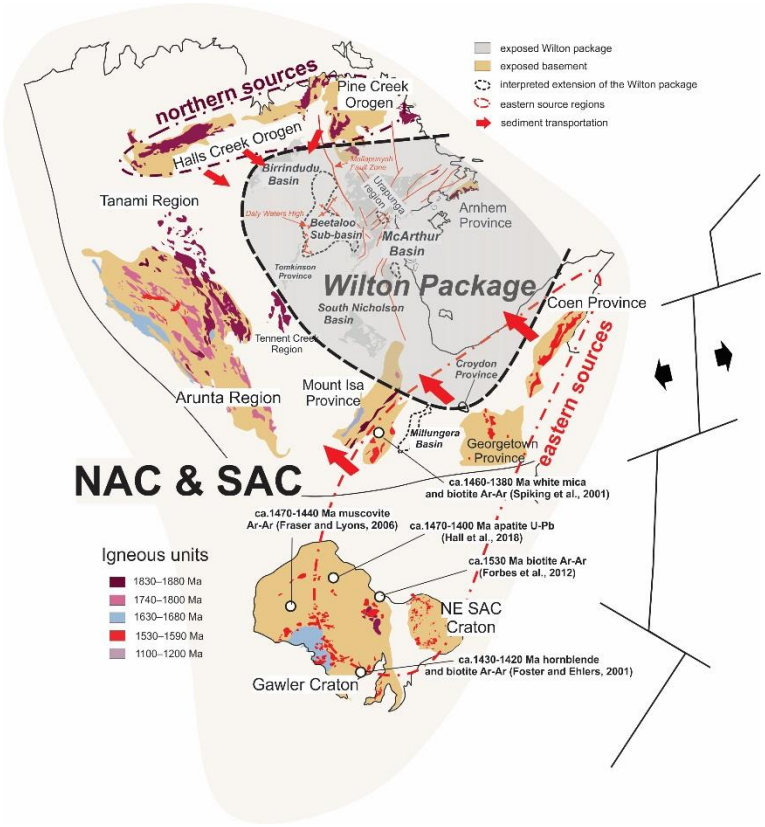

Figure 8 Geological map of the Mesoproterozoic North Australia Craton (NAC) and South Australia Craton (SAC) and the possible exhumation of the eastern source regions during the separation between the NAC-SAC and Laurentia modified after *Chapters 2 & 3*.

5.2. Tectonic geography of Bulita-Tijuna groups

The stratigraphic provenance evolution of the Bulita-Tijuna groups is well reflected in the multi-dimensional scaling (MDS) plot. The Bulita samples are all plotted close to the Halls Creek and Pine Creek orogens (Figure 9). Whereas, the overlying Wondoan Hill Formation samples are closer to the Tanami Region (Figure 9). The Bulita and Tijuna samples together show, stratigraphically up-section, increased affinities to the Tanami Region (Figure 9). This is particularly characterized by the two core sample groups—the 99VRNTGSDD2 group (including samples D02, D24, 1957143, D57 and 1957137) and the MSFD001 group (including samples

MS-09, MS-06, MS-05 and MS-03), both of which exhibit similar up-section trends from the Halls Creek and Pine Creek orogens to the Tanami Region in the MDS plot (Figure 9). Additionally, the spatial provenance inconsistency within the Weaner Sandstone, characterized by the dissimilarities among the four samples (Figure 9), is interpreted as the existence of local sources. Whereas, three Wondoan Hill samples are grouped tightly in the MDS plot (Figure 9), indicating the absence of local sources and provenance consistence. We interpret that the spatial provenance consistence within the Wondoan Hill Formation might represent a significant uplift of the source regions that swamped all the once existing local sources, resulting in the Tanami Region becoming the monopolistic source for the whole basin.

Provenance consistency, however, is absent in the Stubb Formation. Two Stubb Formation samples exhibit obvious dissimilarities, characterized by sample 1957137 plotting close to the Wondoan Hill sample group, whereas sample MS-03 is closer to the Bulita Group formations (Figure 9). A possible explanation is that the sample 1957137 was sourced from the Tanami Region (and Arunta Region), similar to the underlying Wondoan Hill Formation. Whereas, the sample MS-03 probably received more recycled detritus from the exposed older sedimentary rocks (e.g. the Bulita Group). During the uplift of the southern sources, older sedimentary rocks probably got locally exposed and recycled, resulting in the inconsistency seen in the Stubb Formation

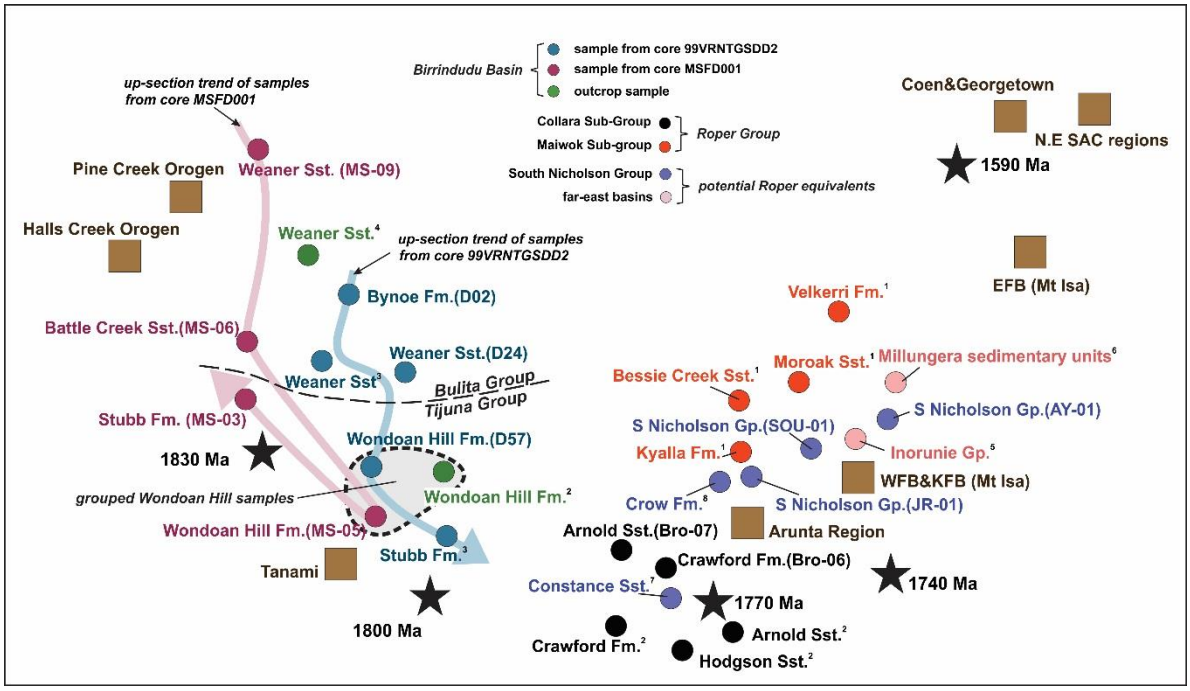

Figure 8 Joint non-parametric multidimensional scaling (MDS) plot (after *Vermeesch, 2013*) showing the relationships amongst analysed formations. Detrital zircon $^{207}Pb/^{206}Pb$ age data include this study, [1]*Chapter 2*, [2]*Munson et al. (2018)*, [3]*Carson (2013)*, [4]*Kositcin & Carson (2017)*, [5]*Nordsvan et al. (2018)*, [6]*Neumann & Kositcin (2011)*, [7]*Anderson et al. (2019)* and [8]Kositcin *& Carson (2019)*. SAC: South Australia Craton; WFB: Western Fold Belt

(Mt Isa Province); KFB: Kathleen Fold Belt (Mt Isa Province); EFB: Eastern Fold Belt (Mt Isa Province); Fm: formation; Sst: sandstone; Gp: Group. Black stars are implanted age peaks following the methods after *Spencer & Kirkland (2016)*.

Sedimentary rocks from the Bulita and Tijuna groups record a provenance change from the northern and north-western sources (e.g. the Halls Creek and Pine Creek orogens) to the southern and south-eastern sources (e.g. the Tanami and Arunta regions). Coincidentally, a similar southward provenance change is also seen in the Maiwok Subgroup of the Roper Group. *Chapters 2 & 3* present detrital zircon U–Pb and Hf data and suggest that the lower Maiwok Subgroup formations (e.g. Bessie Creek Sandstone, Velkerri Formation and Moroak Sandstone) were sourced from the south-eastern and eastern sources (e.g. Mt Isa Region, Coen-Georgetown provinces and Curnamona Province), whereas the Kyalla Formation, in the upper, mainly received detritus from the Arunta Region in the south of the basin. *Chapters 2 & 3* suggest that this provenance change is related to the amalgamation of the West Australia Craton (WAC) and combined North Australia-South Australia cratons (NAC&SAC), during which the southern margin of NAC was uplifted and the southern sources (e.g. the Arunta Region) became the topographic highs and sourced the basin through north-flowing drainage system (Figure 10). This amalgamation event is evidenced by a series of subduction-related magmatism (*Kirkland et al., 2015; Spaggiari et al., 2015; Morrissey et al., 2017*), orogeny (*Howard et al., 2011; Johnson et al., 2013*) and metamorphism (*Anderson et al., 2016*) that happened along the boundary of WAC and the combined NAC and SAC (Figure 10). The amalgamation event is temporally coeval with the deposition of the Tijuna Group. The co-occurrence of the mirrored provenance shifts in the Tijuna Group and the upper Maiwok Group might be related to the same amalgamation event. The consistent tectono-sedimentation interactions demonstrate a temporal correlation of these two basins.

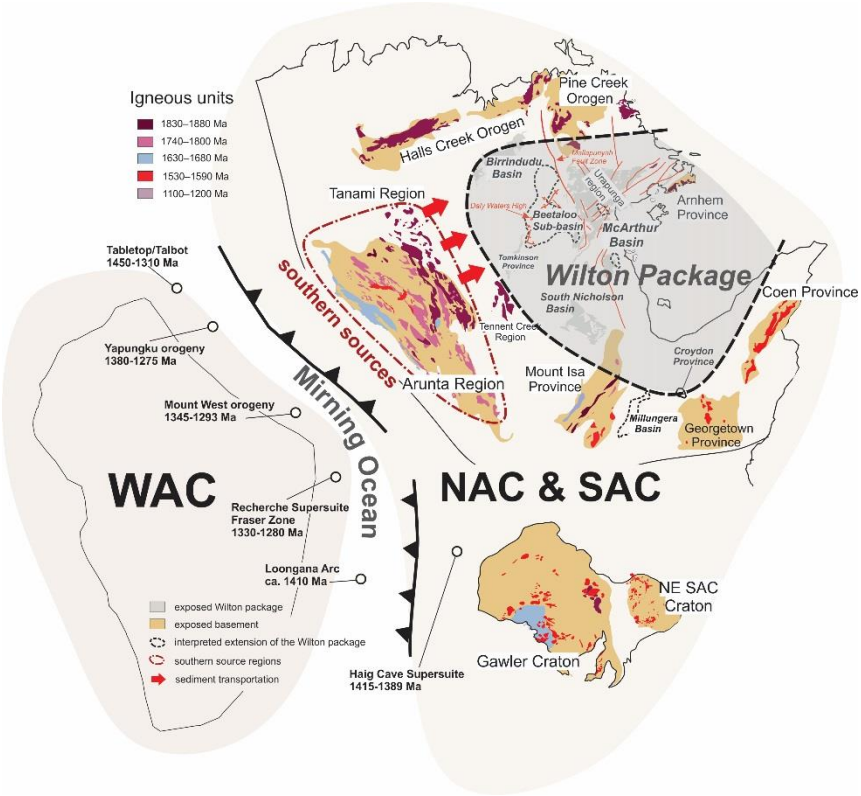

Figure 10 Tectonic sketch showing the closure of the Mirning Ocean between the West Australia Craton (WAC) and an already combined North Australia Craton (NAC) and South Australia Craton (SAC) at 1.32 Ga, uplifting and exposing southern sources (e.g. the Arunta Region and Tanami Region) and allowing them to become sources for the upper Maiwok Group and the Tijuna Group (modified after *Chapters 2 & 3*).

5.3. Spatial basin correlations

The youngest detrital zircon grains obtained from the three South Nicholson Group samples yielded $^{207}Pb/^{206}Pb$ ages of 1519 ± 51 Ma (sample JR-01), 1550 ± 51 Ma (sample SOU-01) and 1542 ± 69 Ma (sample AY-01), respectively. Although these ages were from undifferentiated samples, they are temporally consistent with the maximum depositional age constraint of the Crow Formation (1483 ± 12 Ma; *Kositcin & Carson, 2019*). The deposition of the South Nicholson Group is also consistent the Collara Subgroup that is constrained to be deposited after 1492 ± 4 Ma (*Southgate et al., 1999*). We suggest that the South Nicholson Group and the Collara Subgroup received detritus from similar sources. In the MDS plot, the Collara samples and the South Nicholson sample are grouped, and both of them show affinities to the Mt Isa Province and the Arunta Region (Figure 9). Further, in the $\varepsilon_{Hf}(t)$ against age plots, analyses from the South Nicholson Group and the Collara Subgroup yielded overlapped $\varepsilon_{Hf}(t)$ values (Figure 6). The significant provenance consistence indicates potential correlations between the McArthur-Beetaloo basins and the South Nicholson Basin. However, the South Nicholson Group also shows

provenance similarities to the Maiwok Subgroup (Figures 6 and 9), therefore whether the South Nicholson Group can be correlated to the Collara Subgroup or the Maiwok Subgroup is not yet clear, due to the lack of the minimum depositional age constraint.

Additionally, other potential equivalents of the Wilton package might exist in the far-east of the interpreted Wilton package. The Inorunie Group of the Croydon Province (Figures 1 and 8), a set of ca. 1500 Ma siliciclastic successions (*Budd et al., 2002; Withnall & Hutton, 2013*), are also interpreted to be mainly sourced from the Mt Isa Province (*Nordsvan et al., 2018*), which is consistent with the Roper Group and the South Nicholson Group. This provenance consistency is well reflected in the MDS plot, characterized by the Inorunie sample, South Nicholson samples and Roper samples plotting together (Figure 9). Moreover, another sample collected from the unnamed sedimentary rocks from the sub-surface Millungera Basin (*Neumann & Kositcin, (2011)*; Figures 1 and 8), also shows affinity to the Roper Group and the South Nicholson Group (Figures 5 and 9). However, extra care has to be taken as successions within the Millungera Basin are poorly age constrained and might have sourced from recycled sedimentary rocks.

We suggest provenance consistency and correlations amongst the Roper Group, the South Nicholson Group, and potentially, the Inorunie Group and the unnamed sedimentary rocks from the Millungera Basin. Whereas, the sedimentary formations within the Birrindudu Basin, however, show little provenance similarity to these basins. Provenance analysis suggests the Bulita Group mainly received detritus from the Halls Creek and Pine Creek orogens, whereas the Tijuna Group was sourced from the Tanami and Arunta regions. In the MDS plot, the Bulita and Tijuna samples are plotted close to these source regions, and show dissimilarities to the samples from other basins (Figure 9). A possible explanation for this provenance inconsistency is the existence of under-water paleo-bathymetric reliefs, such as Daly Waters High and Mallapunyah Fault Zone (Figure 1). They might block the transportation and(or) the mixture of sediments, isolating the Birrindudu Basin in the west. This explanation is further supported by the geophysics data that reveal significant variations of sedimentary rock thicknesses, from the both sides of the Daly Waters High (*Frogtech Geosciences, 2018*).

6. Conclusions

Coupled detrital zircon U–Pb age and Hf isotope data presented in this study provide new constraints on the sedimentary provenance and basin correlations, and further illustrate dynamic interactions between sedimentation, ancient geography and tectonic evolution of North Australia Craton, from ca. 1.5 to 1.3 Ga.

We suggest that the Collara Subgroup was mainly sourced from the Mt Isa Province and Arunta Region. After the deposition of the Collara Subgroup, the separating of NAC-SAC and Laurentia resulted the eastern sources (e.g. the Eastern Fold Belt (EFB) of the Mt Isa Province, Georgetown Province and NE South Australia Craton regions) exhumed as rift shoulders and started to shed more detritus to the Maiwok Subgroup formations.

Provenance consistency between the South Nicholson Group and the Roper Group indicates that they were sourced from similar sources with significant spatial correlations. Further, another possible correlative might be the ca. 1.5 Ga Inorunie Group of the Croydon Province, in the far east of the Wilton package. This might suggest the Wilton package is more extensive than previously thought, although more data are needed.

Two groups from the Birrindudu Basin, the Bulita and Tijuna groups, however, show little provenance similarity to the Roper Group and South Nicholson Group. Provenance analysis shows that the Bulita Group was sourced from the north-eastern and northern sources (e.g. Halls Creek Orogen and Pine Creek Orogen), whereas the Tijuna Group received more detritus from the southern sources (e.g. Tanami Region and Arunta Region). Despite the provenance inconsistency, the upper Roper Group and the Bulita-Tijuna groups recorded consistent southward shifting provenance. We suggest these two provenance changes were both related to the amalgamation of the NAC-SAC and the WAC, at ca. 1.35 to 1.28 Ga, resulting in the southern margin of the NAC being uplifted and southern sources became the topographic highs. The coeval tectono-sedimentation interactions correlate these two basins temporally. Whereas their inconsistent detrital zircon age compositions are interpreted to be related to underwater bathymetries that might have blocked sediments transportation.

Acknowledgements

This research was funded by an Australian Research Council Linkage Project LP160101353, which is partnered by the Northern Territory Geological Survey, SANTOS Ltd., Origin Energy and Imperial Oil and Gas. This manuscript forms MGC Record and is a contribution to IGCP Projects 628 (Gondwana Map) and #648 (Supercontinents and Earth Evolution).

References

Abbott, S.T. & Sweet, I.P. (2000). Tectonic control on third-order sequences in a siliciclastic ramp-style basin: An example from the Roper Superbasin (Mesoproterozoic), northern Australia. *Australian Journal of Earth Sciences,* **47(3)**, 637-657.

Abbott, S.T., Sweet, I.P., Plumb, K.A., Young, D.N., Cutovinos, A., Ferenczi, P.A. & Pietsch, B.A. (2001). Roper Region: Urapunga and Roper River Special, Northern Territory (Second Edition). 1:250 000 geological map series

explanatory notes, SD 53-10, 11. *Northern Territory Geological Survey and Geoscience Australia (National Geoscience Mapping Accord)*.

Ahmad, M. & Munson, T.J. (2013). Northern Territory Geological Survey, Geology and mineral resources of the Northern Territory, Special Publication 5. *Northern Territory Geological Survey*.

Anderson, J.R., Kelsey, D.E., Hand, M. & Collins, W.J. (2016). Mesoproterozoic metamorphism in the Rudall Province: revising the timeline of the Yapungku Orogeny and implications for cratonic Australia assembly. *AESC 2016 – Australian Earth Sciences Convention abstract volume*, 227.

Anderson, J.R., Lewis, C.J., Jarrett, A.J.M., Carr, L., Henson, P., Carson, C., Southby, C. & Munson, T. (2019). New SHRIMP U-Pb zircon ages from the South Nicholson Basin, Mout Isa Orogen, and Georgina Basin, Northern Territory and Queensland. *Geoscience Australia, Record 2019/10*. http://dx.doi.org/10.11636/Record.2019.010

Bagas, L., Bierlein, F.P., English, L., Anderson, J.A.C., Maidment, D. & Huston, D.L. (2008). An example of a Palaeoproterozoic back-arc basin: petrology and geochemistry of the ca. 1864 Ma Stubbins Formation as an aid towards an improved understanding of the Granites–Tanami Orogen, Western Australia. *Precambrian Research*, **166(1-4)**, 0-184.

Bagas, L., Bierlein, F.P., Anderson, J.A.C. & Maas, R. (2010). Collision-related granitic magmatism in the Granites–Tanami Orogen, Western Australia. *Precambrian Research,* **177**, 212-226.

Betts, P.G. & Giles, D. (2006). The 1800–1100 Ma tectonic evolution of Australia. *Precambrian Research*, **144(1)**, 92-125.

Beyer, E.E., Hollis, J.A., Whelan, J.A., Glass, L.M., Donnellan, N., Yaxley, G., Armstrong, R., Allen, C. & Scherstén, A., (2013). Summary of results. NTGS laser ablation ICPMS and SHRIMP U-Pb, Hf and O geochronology project: Pine Creek Orogen, Arunta Region, Georgina Basin and McArthur Basin, July 2008–May 2011. *Northern Territory Geological Survey, Record 2012-007*.

Beyer, E.E., Allen, C.M., Armstrong, R. & Woodhead, J.D. (2015). Summary of results. NTGS laser ablation ICPMS U-Pb and Hf geochronology project: selected samples from NAPPERBY 1:250 000 mapsheet area, Arunta Region, July 2010–January 2012. *Northern Territory Geological Survey, Record 2015-009*.

Beyer, E.E., Donnellan, N., Meffre, S. & Thompson, J.M. (2016). Summary of results. NTGS laser ablation ICP-MS in situ zircon and baddeleyite geochronology project: Mount Peake Gabbro, Arunta Region. *Northern Territory Geological Survey, Record 2016-002*.

Blewett, R.S., Black, L.P., Sun, S.S., Knutson, J., Hutton, L.J. & Bain, J.H.C. (1998). U-Pb zircon and Sm-Nd geochronology of the Mesoproterozoic of North Queensland: implications for a Rodinian connection with the Belt Supergroup of North America. *Precambrian Research*, **89**, 101-127.

Bierlein, F.P., Black, L.P., Hergt, J. & Mark, G. (2008). Evolution of pre-1.8 Ga basement rocks in the Western Mt Isa Inlier, northeastern Australia—insights from SHRIMP U—Pb dating and in-situ, Lu—Hf analysis of zircons. *Precambrian Research*, **163(1)**, 159-173.

Bodorkos, S., Beyer, E.E., Edgoose, C.J., Whelan, J.A., Webb, G., Vandenberg, L.C. & Hallett, L. (2013). Summary of results. Joint NTGS–GA geochronology project: Central and eastern Arunta Region, January 2008 – June 2011. *Northern Territory Geological Survey, Record 2013-003*.

Bouvier, A., Vervoort, J.D. & Patchett, P.J. (2008). The Lu—Hf and Sm—Nd isotopic composition of CHUR: constraints from unequilibrated chondrites and implications for the bulk composition of terrestrial planets. *Earth and Planetary Science Letters*, **273(1-2)**, 0-57.

Budd, A.R., Wyborn, L.A.I. & Bastrakova, I.V. (2002) The metallogenic potential of Australian Proterozoic granites [Summary Volume], *Geoscience Australia. Record*, **2001/12**, 152.

Carson, C.J., Claoué-Long, J., Stern, R., Close, D.F., Scrimgeour, I.R. & Glass, L.M. (2009). Summary of results. Joint NTGS-GA geochronology project: Central and eastern Arunta Region and Pine Creek Orogen, July 2006–May 2007. *Northern Territory Geological Survey, Record 2009-001*.

Carson, C.J. (2013). The Victoria and Birrindudu Basins, Victoria River Region, Northern Territory, Australia: a SHRIMP U–Pb detrital zircon and Sm–Nd study. *Journal of the Geological Society of Australia,* **60(2)**, 175-196. https://doi.org/10.1080/08120099.2013.772920.

Close D.F. (2014). The McArthur Basin: NTGS ' approach to a frontier petroleum basin with known base metal prospectivity. *Annual Geoscience Exploration Seminar (AGES) Proceedings, Alice Springs, Northern Territory 15–16 March 2016.* Northern Territory Geological Survey, Darwin. pp. 85–89.

Cox, G.M., Jarrett, A., Edwards, D., Crockford, P.W., Halverson, G.P., Collins, A.S., Poirier, A. & Li, Z.X. (2016). Basin redox and primary productivity within the Mesoproterozoic Roper Seaway. *Chemical Geology*, **440**, 101-114.

Cox, G.M., Sansjofre, P., Blades, M.L., Collins, A.S. & Farkas, J. (2019). Dynamic interaction between basin redox and the biogeochemical nitrogen cycle in an unconventional Proterozoic petroleum system. *Nature Scientific Reports*, 9:5200.

Cross, A.J., Claoué-Long, J.C., Scrimgeour, I.R., Close, D.F. & Edgoose, C.J. (2005a). Summary of results. Joint NTGS-GA geochronology project: southern Arunta Region. *Northern Territory Geological Survey, Record 2004-003*.

Cross, A.J., Claoué-Long, J.C., Scrimgeour, I.R., Crispe, A. & Donnellan, N. (2005b). Summary of results. Joint NTGS-GA geochronology project: northern Arunta and Tanami regions, 2000–2003. *Northern Territory Geological Survey, Record 2005-003*.

Cross, A.J., Claoué-Long, J.C., Scrimgeour, I.R., Ahmad, M. & Kruse, P.D. (2005c). Summary of results. Joint NTGS-GA geochronology project: Rum Jungle, basement to southern Georgina Basin and eastern Arunta Region 2001–2003. *Northern Territory Geological Survey, Record 2005-006*.

Cross, A.J., Purdy, D.J., Bultitude, R.J., Brown, D.D. & Carr, P.A., (2015). Summary of results. Joint GSQ–GA geochronology project: Thomson Orogen, New England Orogen, Mossman Orogen and Mount Isa region, 2011–2013. *Queensland Geological Record 2016/03*.

Fanning, C.M. (2012). SHRIMP U–Pb zircon age determinations on detrital zircons from drill core sample ALT-051. ANU Research School of Earth Sciences, PRISE Report 12-260. Esso Australia. *Northern Territory Geological Survey, Core Sampling Report CSR0211*.

Forbes, C.J., Giles, D., Jourdan, F., Sato, K., Omori, S. & Bunch, M. (2012). Cooling and exhumation history of the northeastern Gawler Craton, South Australia. *Precambrian Research*, **200–203**, 209–238.

Foster, D.A. & Ehlers, K. (1998). ^{40}Ar-^{39}Ar thermochronology of the southern Gawler Craton, Australia: implications for Mesoproterozoic and Neoproterozoic tectonics of East Gondwana and Rodinia. *Journal of Geophysical Research: Solid Earth*, **103(B5)**, 10177-10193.

Frogtech Geoscience, 2018. SEEBASE® study and GIS for greater McArthur Basin. *Northern Territory Geological Survey, Digital Information Package DIP 017*.

Griffin, W.L., Belousova, E.A., Walters, S.G. & O''Reilly, S.Y. (2006). Archaean and Proterozoic crustal evolution in the eastern succession of the Mt Isa district, Australia: U–Pb and Hf–isotope studies of detrital zircons. *Journal of the Geological Society of Australia,* **53(1)**, 125-149.

Hall, J.W., Glorie, S., Reid, A.J., Boone, S.C., Collins, A.S. (2018). An apatite U–Pb thermal history map for the northern Gawler Craton, South Australia. *Geoscience Frontiers*, **9(5)**, 1293-1308. https://doi.org/10.1016/j.gsf.2017.12.010.

Hollis, J.A., Beyer, E.E., Whelan, J.A., Kemp, A.I.S., Scherstén, A. & Greig, A. (2010). Summary of results. NTGS laser U–Pb and Hf geochronology project: Pine Creek Orogen, Murphy Inlier, McArthur Basin and Arunta Region, July 2007–June 2008. *Northern Territory Geological Survey, Record 2010-001*.

Hoskin, P.W.O. & Black, L.P. (2000). Metamorphic zircon formation by solid-state recrystallization of protolith igneous zircon. *Journal of metamorphic Geology*, **18(4)**, 423-439.

Howard, H.M., Werner, M., Smithies, R.H., Kirkland, C.L., Kelsey, D.E., Hand, M., Collins, A., Pirajno, F., Wingate, M.T.D., Maier, W.D. & Raimondo, Y. (2011). The geology of the west Musgrave Province and the Bentley Supergroup–a field guide. *Geological Survey of Western Australia, Record 2011/4*, pp.116.

Jackson, M.J., Sweet, I.P. & Powell, T.G. (1988). Studies on petroleum geology and geochemistry, middle Proterozoic, McArthur Basin Northern Australia I: Petroleum potential. *APEA J*, **28(1)**, 283-302.

Jackson, M.J., Sweet, I.P., Page, R.W. & Bradshaw, B.E. (1999). The South Nicholson and Roper Groups: evidence for the early Mesoproterozoic Roper Superbasin. Integrated Basin Analysis of the Isa Superbasin using Seismic, Well-log, and Geopotential Data: An Evaluation of the Economic Potential of the Northern Lawn Hill Platform: Canberra, Australia, *Australian Geological Survey Organisation Record*, *19*.

Jackson, S.E., Pearson, N.J., Griffin, W.L. & Belousova, E.A. (2004). The application of laser ablation-inductively coupled plasma-mass spectrometry to in situ U–Pb zircon geochronology. *Chemical Geology*, **211(1)**, 47-69.

Johnson, S.P., Thorne, A.M., Tyler, I.M., Korsch, R.J., Kennett, B.L. N., Cutten, H.N., Goodwin, J., Blay, O., Blewett, R.S., Joly, A., Dentith, M.C., Aitken, A.R.A., Holzschuh, J., Salmom, M., Reading, A., Heinson, G., Boren, G., Ross, J., Costelloe, R.D. & Fomim, T. (2013). Crustal architecture of the Capricorn Orogen, Western Australia and associated metallogeny. *Australian Journal of Earth Sciences*, **60**, 681–705.

Kirkland, C.L., Smithies, R.H., Spaggiari, C.V. (2015). Foreign contemporaries – Unravelling disparate isotopic signatures from Mesoproterozoic Central and Western Australia. *Precambrian Research*, **265**, 218-231.

Kositcin, N., Champion, D.C. & Huston, D.L. (2009). Geodynamic synthesis of the North Queensland Region and implications for metallogeny. *Geoscience Australia Record 2009/30*, pp 196.

Kositcin, N., Carson, C.J., Hollis, J.A., Glass, L.M., Close, D.F., Whelan, J.A., Webb, G. & Donnellan, N. (2013a). Summary of results. Joint NTGS–GA geochronology project: Arunta Region, Davenport Province and Pine Creek Orogen July 2009–June 2011. *Northern Territory Geological Survey, Record 2012-008*.

Kositcin, N., Beyer, E.E., Whelan, J.A., Close, D.F., Hallett, L. & Dunkley, D.J. (2013b). Summary of results. Joint NTGS–GA geochronology project: Arunta Region, Ngalia Basin, Tanami Region and Murphy Province, July 2011–June 2012. *Northern Territory Geological Survey, Record 2013-004*.

Kositcin, N., Whelan, J.A., Hallett, L. & Beyer, E.E., (2014a). Summary of results. Joint NTGS–GA geochronology project: Amadeus Basin, Arunta Region and Murphy Province, July 2012–June 2013. *Northern Territory Geological Survey, Record 2014-005*.

Kositcin, N., Beyer, E.E. & Whelan, J.A., (2014b). Summary of results. Joint NTGS–GA SHRIMP geochronology project: Arunta Region, July 2013–June 2014. *Northern Territory Geological Survey, Record 2014 -008*.

Kositcin, N., Kraus, S. & Whelan, J.A. (2015a). Summary of results. Joint NTGS–GA SHRIMP geochronology project: Arnhem Province, July 2014–June 2015. *Northern Territory Geological Survey, Record 2015-010.*

Kositcin, N., Reno, B.L. & Whelan, J.A. (2015b). Summary of results. Joint NTGS–GA geochronology project: Arunta Region, July 2014–June 2015. *Northern Territory Geological Survey, Record 2015-007*.

Kositcin, N. & Carson, C.J. (2017). New SHRIMP U–Pb zircon ages from the Birrindudu and Victoria Basins, Northern Territory: July 2016 – June 2017. *Geoscience Australia Record 2017/16.* http://dx.doi.org/10.11636/Record.2017.016

Kositcin, N. & Carson, C.J. (2019). New SHRIMP U-Pb zircon ages from the South Nicholson and Carrara Range regions, Northern Territory: July 2017–June 2018. *Geoscience Australia Record 2019/09*. http://dx.doi.org/10.11636/Record.2019.009

Kromkhun, K., Foden, J., Hore, S. & Baines, G. (2013). Geochronology and Hf isotopes of the bimodal mafic–felsic high heat producing igneous suite from Mt Painter Province, south Australia. *Gondwana Research*, **24(3-4)**, 1067-1079.

Li, Z.X., Bogdanova, S.V., Collins, A.S., Davidson, A., Waele, B.D., Ernst, R.E., Fitzsimons, I.C.W., Fuck, R.A., Gladkochub, D.P., Jacobs, J., Karlstrom, K.E., Lu, S., Natapov, L.M., Pease, V., Pisarevsky, S.A., Thrane, K. & Vernikovsky, V. (2008). Assembly, configuration, and break-up history of Rodinia: a synthesis. *Precambrian Research, **160*(1)**, 179-210.

Li, Z.X. & Evans, D.A.D. (2011). Late Neoproterozoic 40° intraplate rotation within Australia allows for a tighter-fi tting and longer-lasting Rodinia. *Geology*, **39**, 39-42.

Li, B., Bagas, L., Gallardo, L.A., Said, N., Diwu, C. & Mccuaig, T.C. (2013). Back-arc and post-collisional volcanism in the Palaeoproterozoic Granites-Tanami Orogen, Australia. *Precambrian Research,* **224**, 570-587.

Ludwig, K.R. (2003). User's manual for Isoplot 3.00: a geochronological toolkit for Microsoft Excel (No. 4). Kenneth R. Ludwig.

Mark, G. & Pollard, P. (2006). Episodic, potassic, 'A-type' Mesoproterozoic magmatism in the Mount Isa Inlier, NE Australia: a syn-tectonic origin?. *Geochimica Et Cosmochimica Acta,* **70(18)**, A393-A393.

Merdith, A.S., Collins, A.S., Williams, S.E., Pisarevsky, S., Foden, J.F., Archibald, D., Blades, M.L., Alessio, B.L., Armistead, S., Plavsa, D., Clark, C. & Müller, R.D. (2017). A full-plate global reconstruction of the Neoproterozoic. *Gondwana Research*, **50**, 84-134.

Merdith, A.S., Williams, S.E., Brune, S., Collins, A.S. & Müller, R.D. (2019). Rift and plate boundary evolution across two supercontinent cycles. *Global and Planetary Change*, **173**, 1-14.

Morrissey, L.J., Payne, J.L., Hand, M., Clark, C., Taylor, R., Kirkland, C.L. & Kylander-Clark, A. (2017). Linking the Windmill Islands, east Antarctica and the Albany–Fraser Orogen: insights from U–Pb zircon geochronology and Hf isotopes. *Precambrian Research,* **293,** 131–149.

Morrissey, L.J., Barovich, K.M., Hand, M., Howard, K.E. & Payne, J.L. (2018). Magmatism and metamorphism at c. 1.45 Ga in the northern Gawler Craton: the Australian record of rifting within Nuna (Columbia). *Geoscience Frontiers.* **10(1)**, 175-194.

Mulder, J.A., Halpin, J.A. & Daczko. N.R. (2015). Mesoproterozoic Tasmania: Witness to the East Antarctica–Laurentia connection within Nuna. *Geology*, **43**, 759-769.

Munson, T.J. (2016). Sedimentary characterisation of the Wilton package, greater McArthur Basin. Northern Territory. *Northern Territory Geological Survey, Record 2016-003*.

Munson, T.J, Thompson, J.M, Zhukova, I., Meffre, S., Beyer, E.E., Woodhead, J.D. & Whelan, J.A. (2018). Summary of results. NTGS laser ablation ICP-MS U–Pb and Lu–Hf geochronology project: Roper Group and overlying ungrouped units (McArthur Basin), Renner Group (Tomkinson Province), Tijunna Group (Birrindudu Basin). *Northern Territory Geological Survey, Record* 2018-007.

Murgulov, V., Beyer, E., Griffin, W.L., O'Reilly, S.Y., Walters, S.G. & Stephens, D. (2007). Crustal evolution in the Georgetown Inlier, north Queensland, Australia: a detrital zircon grain study. *Chemical Geology,* **245(3)**, 198-218.

Neumann, N.L., Southgate, P.N., Gibson, G.M. & McIntyre, A. (2006). New SHRIMP geochronology for the Western Fold Belt of the Mt Isa Inlier: developing a 1800–1650 Ma event framework. *Australian Journal of Earth Sciences*, **53(6)**, 1023-1039.

Neumann, N.L., Gibson, G.M. & Southgate, P.N. (2009). New SHRIMP age constraints on the timing and duration of magmatism and sedimentation in the Mary Kathleen Fold Belt, Mt Isa Inlier, Australia. *Australian Journal of Earth Sciences*, **56(7)**, 965-983.

Neumann, N.L. & Kositcin, N. (2011). New SHRIMP U-Pb zircon ages from north Queensland, 2007–2010. *Geoscience Australia, Record*, **2011/38**, 82 p.

Nordsvan, A.R., Collins, W.J., Li, Z.X., Spencer, C.J., Pourteau, A., Withnall, I.W., Betts, P.G. & Volante, S. (2018). Laurentian crust in northeast Australia: Implications for the assembly of the supercontinent Nuna. *Geology*, **46(3)**: 251–254.

Page, R.W. & Sun, S.S. (1998). Aspects of geochronology and crustal evolution in the Eastern Fold Belt, Mt Isa Inlier. *Australian Journal of Earth Sciences*, **45(3)**, 343-361.

Paton, C., Hellstrom, J., Paul, B., Woodhead, J. & Hergt, J. (2011). Iolite: Freeware for the visualisation and processing of mass spectrometric data. *Journal of Analytical Atomic Spectrometry*, **26(12)**, 2508-2518.

Payne, J.L., Pearson, N.J., Grant, K.J. & Halverson, G.P. (2013). Reassessment of relative oxide formation rates and molecular interferences on in situ lutetium–hafnium analysis with laser ablation MC-ICP-MS. *Journal of Analytical Atomic Spectrometry,* **28(7)**, 1068-1079.

Pisarevsky, S.A., Elming, S.Å., Pesonen, L.J. & Li, Z.X. (2014). Mesoproterozoic paleogeography: supercontinent and beyond. *Precambrian Research,* **244(1)**, 207-225.

Rawlings, D.J. (1999). Stratigraphic resolution of a multiphase intracratonic basin system: The McArthur Basin, northern Australia. *Australian Journal of Earth Sciences*, **46(5)**, 703-723.

Reid, A.J. & Payne, J.L. (2017). Magmatic zircon Lu-Hf isotopic record of juvenile addition and crustal reworking in the Gawler Craton, Australia. *Lithos*, **292**, 294-306.

Scherer, E., Münker, C. & Mezger, K. (2001). Calibration of the lutetium-hafnium clock. *Science,* **293(5530)**, 683-687.

Sláma, J., Košler, J., Condon, D.J., Crowley, J.L., Gerdes, A., Hanchar, J.M., Horstwood, M.S.A., Morris, G.A., Nasdala, L., Norberg, N., Schaltegger, U., Schoene, B., Tubrett, M. N. & Whitehouse, M. J. (2008). Plešovice zircon—a new natural reference material for U–Pb and Hf isotopic microanalysis. *Chemical Geology,* **249(1–2)**, 1-35.

Smits, R.G., Collins, W.J., Hand, M., Dutch, R. & Payne, J. (2014). A Proterozoic Wilson cycle identified by Hf isotopes in central Australia: implications for the assembly of Proterozoic Australia and Rodinia. *Geology*, **42(3)**, 231-234.

Southgate, P.N., Bradshaw, B.E., Domagala, J., Jackson, M.J., Idnurm, M., Krassay, A.A., Page, R.W., Sami, T.T., Scott, D.L., Lindsay, J.F. & McConachie, B. A. (2000). Chronostratigraphic basin framework for Palaeoproterozoic rocks (1730–1575 Ma) in northern Australia and implications for base-metal mineralisation. *Australian Journal of Earth Sciences*, **47(3)**, 461-483.

Spaggiari, C.V., Kirkland, C.L., Smithies, R.H., Wingate, M.T.D. & Belousova, E.A. (2015). Transformation of an Archean craton margin during Proterozoic basin formation and magmatism: The Albany–Fraser Orogen, Western Australia. *Precambrian Research*, **226**, 440-466.

Spencer, C.J. & Kirkland, C. L. (2016). Visualizing the sedimentary response through the orogenic cycle: A multidimensional scaling approach. *Lithosphere*, **8(1)**, 29-37.

Spikings, R.A., Foster, D.A., Kohn, B.P. & Lister, G.S. (2001). Post-orogenic (< 1500 Ma) thermal history of the Proterozoic Eastern Fold Belt, Mount Isa Inlier, Australia. *Precambrian Research*, **109(1)**, 103-144.

Vermeesch, P. (2013). Multi-sample comparison of detrital age distributions. *Chemical Geology*, **341**, 140-146.

Withnall, I.W. & Hutton, L.J. (2013). Chapter 2. North Australian Craton. In Jell, P. A., (eds) *Geology of Queensland, Geological Survey of Queensland*, 23-112

Woodhead, J., Hergt, J., Shelley, M., Eggins, S. & Kemp, R. (2004). Zircon Hf-isotope analysis with an excimer laser, depth profiling, ablation of complex geometries, and concomitant age estimation. *Chemical Geology,* **209(1–2)**, 121-135.

Woodhead, J.D. & Hergt, J.M. (2005). A preliminary appraisal of seven natural zircon reference materials for in situ Hf isotope determination. *Geostandards & Geoanalytical Research,* **29(2)**, 183–195.

Worden, K.E., Claoué-Long, J.C., Scrimgeour, I.R. & Doyle, N. (2006a). Summary of results. Joint NTGS-GA geochronology project: Pine Creek Orogen and Arunta Region, January–June 2004. *Northern Territory Geological Survey, Record 2006-005*.

Worden, K.E., Claoué-Long, J.C. & Scrimgeour, I.R. (2006b). Summary of results. Joint NTGS-GA geochronology project: Pine Creek Orogen, Tanami Region, Arunta Region and Amadeus Basin, July–December 2004. *Northern Territory Geological Survey, Record 2006-006*.

Worden, K.E., Carson, C.J., Close, D.F., Donnellan, N. & Scrimgeour, I.R. (2008). Summary of results. Joint NTGS-GA geochronology project: Tanami Region, Arunta Region, Pine Creek Orogen and Halls Creek January 2005–March 2007. *Northern Territory Geological Survey, Record 2008-003*.

Chapter 6

Summary and discussion

Chapter 6

Summary and discussion

The main aim of this research is to investigate the spatial and temporal provenance evolution of the Wilton package, and the tectono-sedimentation interactions and processes within the Mesoproterozoic depositional systems of the North Australia Craton. A better understanding of these systems, local basin provenance and tectonic history of the North Australia Craton, in turn provides new constraints on the Mesoproterozoic paleogeography configuration and its evolution through geological time.

1. Sedimentation and tectonic history of the Roper Group

The sub-surface Beetaloo Sub-basin is in the centre of the interpreted Wilton package distribution, and represents a depo-centre of this complex Mesoproterozoic depositional system (Figure 1), which thus preserves the stratigraphically thickest successions of the Wilton package (*Plumb & Wellman, 1987; Lanigan et al., 1994; Ahmad & Munson, 2013; Munson, 2016; Munson et al., 2018*). The Roper Group of the Beetaloo Sub-basin is the primary focus of *Chapters 2 & 3*. In these chapters, coupled detrital zircon U–Pb and Hf isotope data were used together to get integrated assessments on the basin provenance and tectonic evolution.

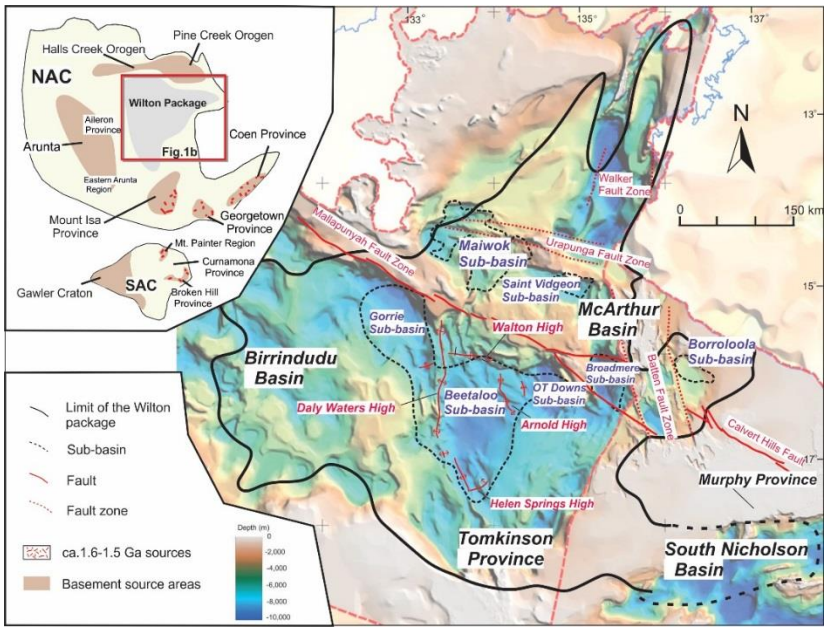

Figure 1 Extent of the Wilton Package (SEEBASE™ basement surface image after *Frogtech Geoscience (2018)*) modified after *Munson (2016)* and *Chapter 3*.

As to sources and sediment pathways, the data from the Collara Subgroup (lower Roper Group) suggest provenance from the Mt Isa Province and Arunta Region. Whereas, the overlying Maiwok Subgroup (upper Roper Group) received more detritus from eastern sources (e.g. the eastern Mount Isa Province and the palinspastically adjacent Curnamona and Georgetown provinces; see Figure 2). These eastern source regions are interpreted as uplifted rift-shoulder highs, formed by contemporaneous extension between Proterozoic Australia and Laurentia. The uplifting of the eastern source regions is evidenced and also age constrained by a series of low temperature mineral dating results, yielding cooling ages ranging from ca. 1.47 to 1.38 Ga (Figure 2).

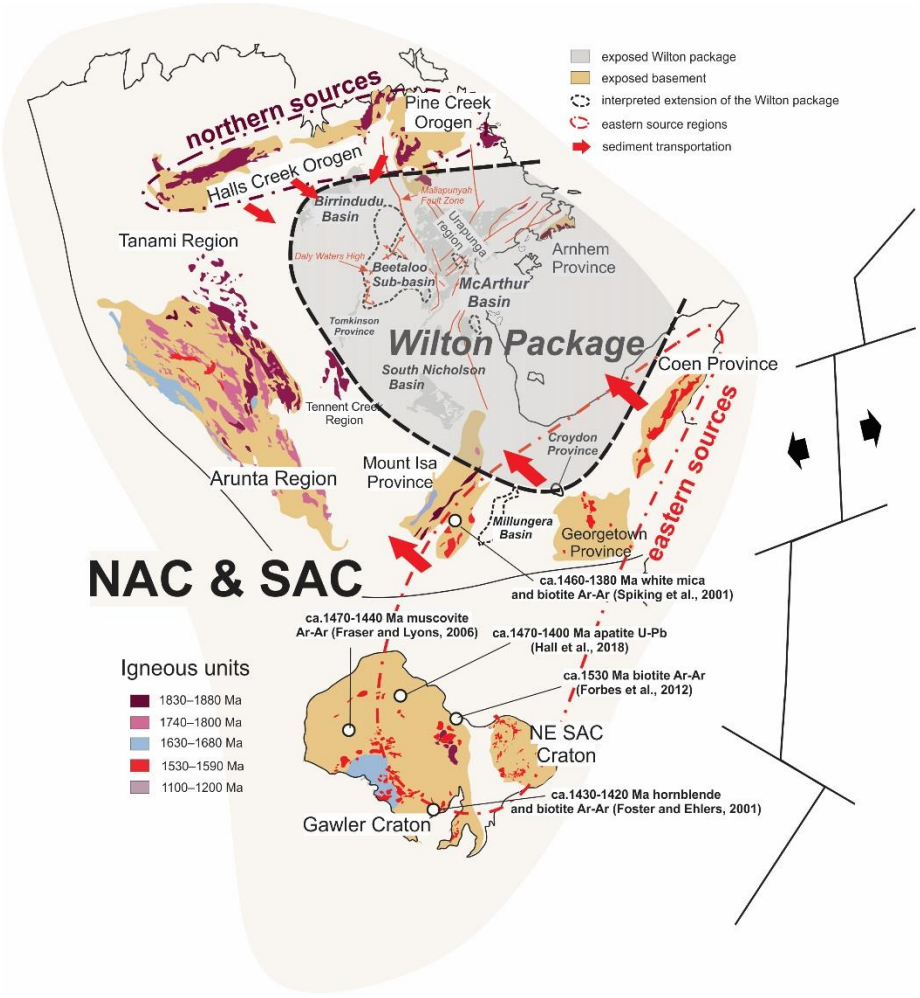

Figure 2. Tectonic sketch showing separation of North Australia Craton and Laurentia at ca. 1.45 Ga, resulting the eastern sources exhumed and started to source the Wilton package (after *Chapter 5*). NAC: North Australia Craton; SAC: South Australia Craton.

The Maiwok Subgroup is constrained to be deposited between ca. 1.38 to 1.31 Ga. Formations within this subgroup demonstrate another provenance changing event, characterized by a rapid swamping of the basin by detritus from southerly sources (e.g. the Arunta Region; Figure 3). Detrital zircon data revealed that the progressively younger formations (the Velkerri Formation,

the Moroak Sandstone and the Kyalla Formation) received less detritus from the eastern sources but more detritus from the southern sources. This change in provenance is temporally coeval with a series of subduction-related magmatism (*Kirkland et al., 2015; Spaggiari et al., 2015; Morrissey et al., 2017*), orogeny (*Howard et al., 2011; Johnson et al., 2013*) and metamorphism (*Anderson et al., 2016*) along the boundaries separating the North Australia Craton and the West Australia Craton. This is interpreted to relate to closure of an ocean basin (e.g. Mirning Ocean; Figure 3) at ca. 1.35 to 1.25 Ga, during which the southern margin of North Australia Craton was uplifted and southern sources started to source the basin.

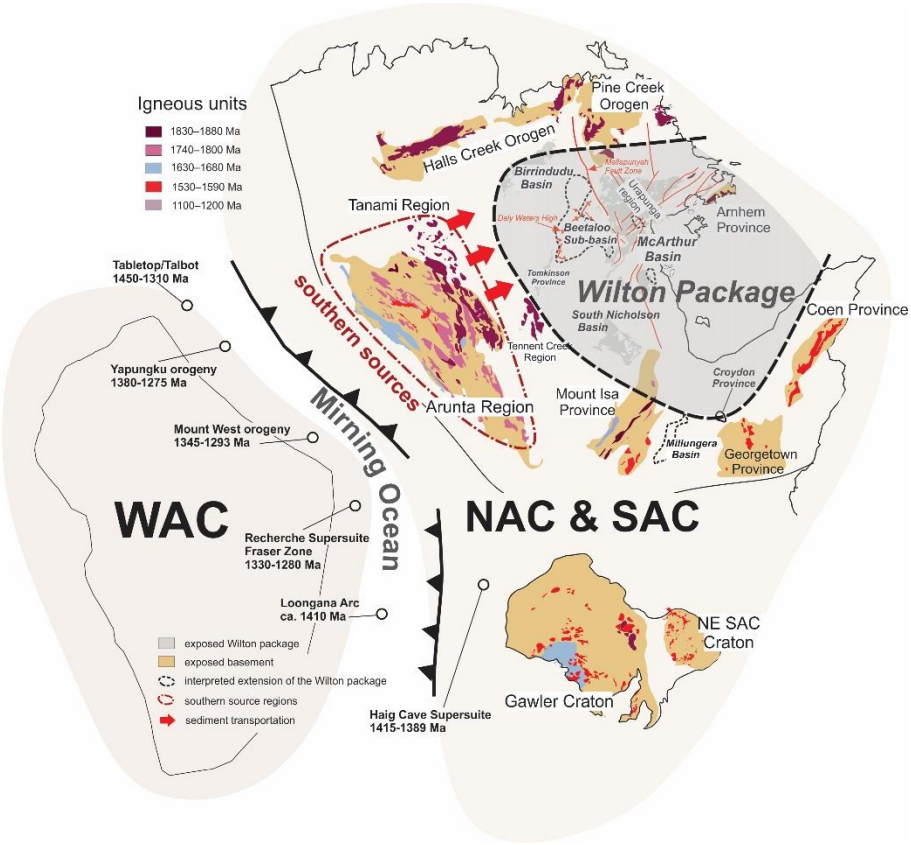

Figure 3 Tectonic sketch showing the closure of the Mirning Ocean between the West Australia Craton (WAC) and an already combined North Australia Craton (NAC) and South Australia Craton (SAC) at 1.32 Ga, uplifting and exposing the southern sources and allowing them to become sources for the Wilton package (after *Chapter 5*).

The end of the deposition of the Roper Group is marked by the Derim Derim–Galiwinku LIP mafic intrusives that penetrated the Roper Group up to the top formations (*Abbott et al., 2001; Ahmad & Munson, 2013; Whelan et al., 2016*). A new Isotope dilution thermal ionization mass spectrometry (ID-TIMS) U–Pb baddeleyite age (1312.9 ± 0.7 Ma), discussed in *Chapter 4*, provides an updated and tighter age constraint for this magmatic event as well as the minimal depositional age constraint for the Roper Group. In addition, the shale whole-rock isotopic and geochemical data reveal that the Derim Derim–Galiwinku LIP not only intruded the basin but

also shed volcanic detritus to the basin. A basin uplift model is proposed in *Chapter 4*, suggesting that the emplacement of the Derim Derim–Galiwinku LIP domal uplifted the basin from the north. The domal uplift resulted the top formation of the Roper Group in the Beetaloo Sub-basin eroded and thinning towards to the north. Simultaneously, the increased weathering of basaltic sources presumably enhanced the nutrient supply and the primary production in the shallow marine settings, resulting in the observed TOC enrichment in the top section of the Kyalla Formation.

2. Intra basin correlation of the Wilton package

The Wilton package successions is widespread throughout northern Australia and have been suggest to be deposited in several geographically separated basins. The sub-surface Roper Group within the Beetaloo Sub-basin, in the centre, links its possible equivalents in the west—the Tijuna Groups of the Birrindudu Basin, in the northeast—the outcropping Roper Group of the McArthur Basin, in the south—the Renner Group of the Timkinson Province, and in the southeast—the South Nicholson Group of the South Nicholson Basin. In *Chapter 5*, the study focus is extended to the wider Wilton package. Specifically, new detrital zircon U–Pb and Hf isotope data were collected from the Bulita-Tijuna Groups of the Birrindudu Basin, the Roper Group of the McArthur Basin and the South Nicholson Group of the South Nicholson Basin. These data were compiled with the Beetaloo Sub-basin data from *Chapters 2 & 3* to build a detailed zircon U–Pb and Hf isotope dataset for the Wilton package. This dataset is used to reveal the intra basin correlations within the Wilton package, and also, to rebuild the basin geography of the Mesoproterozoic North Australia Craton in a wider scale.

Detrital zircon provenance analysis demonstrates that the South Nicholson Group exhibits significant provenance consistence to both of the Maiwok and Collara subgroups, and is therefore being interpreted as a correlative of the Roper Group. Moreover, another possible equivalent might be the Inorunie Group of the Croydon Province in the far-east. Its potential correlation with the Roper Group as well as the South Nicholson Group indicates the Wilton package might be more extensive than previous thoughts.

Provenance analysis illustrates that the Bulita Group of the Birrindudu Basin received detritus from the north-eastern and northern sources (e.g. the Halls Creek Orogen and Pine Creek Orogen). Whereas, the younger Tijuna Group recorded a swamping of the basin by detritus from southerly sources (e.g. the Tanami Region). Neither the Bulita Group nor Tijuna Group shows provenance consistence to the other basins of the Wilton package. However, similar south-ward provenance shifts are seen in both of the Bulita-Tijuna groups and the Maiwok Subgroup. The

consistent provenance changes are interpreted to be related to the same ocean basin closure event, during which the southern margin of the North Australia Craton uplifted and the Arunta Region and the Tanami Region in the south became the topographic highs and started to shed detritus to the Wilton package through north-flowing rivers (Figure 3). Despite the dissimilar provenance in spatial scale, the consistent provenance evolution correlated the Bulita-Tijuna groups and the Maiwok Subgroup in temporal scale. Whereas, their inconsistent detrital zircon age compositions are interpreted to be related to underwater bathymetries that blocked transportation of sediment.

3. Paleogeography configuration, the McArthur-Yanliao Gulf

The Wilton package is interpreted to have been deposited in an enclosed marine basin (*Munson, 2016; Cox et al., 2016; Revie, 2017; Munson & Revie, 2018*). However, the location of the basin's depositional margins are unknown, especially to the present-day north. A potential corollary of the Wilton package might be the succession of the Yanshan Basin (*Zhang et al., 2012; Xu et al., 2014*). The recent palaeomagnetic study places the North Australia Craton and the North China Craton at the similar latitudes at ca. 1.3 Ga, indicating the juxtaposition of these two cratons (*Kirscher et al., 2018*). Additionally, the coeval deposition of the consistent marine successions, particularly characterized by the stratigraphic and geochemical similarities between the Yanshan Basin successions and the Roper Group (*Chu et al., 2007; Luo et al., 2015; Zhang et al., 2017*), indicates a consistent boarder and presumably inter-connected marine depositional system (i.e. the McArthur-Yanliao Gulf (also named the Greater McArthur Gulf); Figure 4).

Further, the Derim Derim–Galiwinku LIP magmatism, constrained at ca. 1.31 Ga, is consistent with the emplacement of the ca. 1.33-1.30 Ga Yanliao LIP in the North China Craton (*Zhang et al., 2017*). Besides that, the emplacement of the Yanliao diabase sills was also accompanied by a significant magmatic uplift that resulted a regional unconformity separating the ca. 1.34 Ga Xiamaling Formation and the early Neoproterozoic Qingbaikou Group (*Zhang et al., 2017*). Whilst, in the North Australia Craton, we suggest that the Roper Group was also uplifted in a similar manner during the Derim Derim–Galiwinku magmatism. The coeval intraplate mafic magmatism and magmatic uplift suggests that the plume head was located between the northern margin of NAC and northern-northeastern margin of North China Craton (Figure 4). The plume uplifted both these cratons from their (present-day) north, simultaneously (*Zhang et al., 2017*).

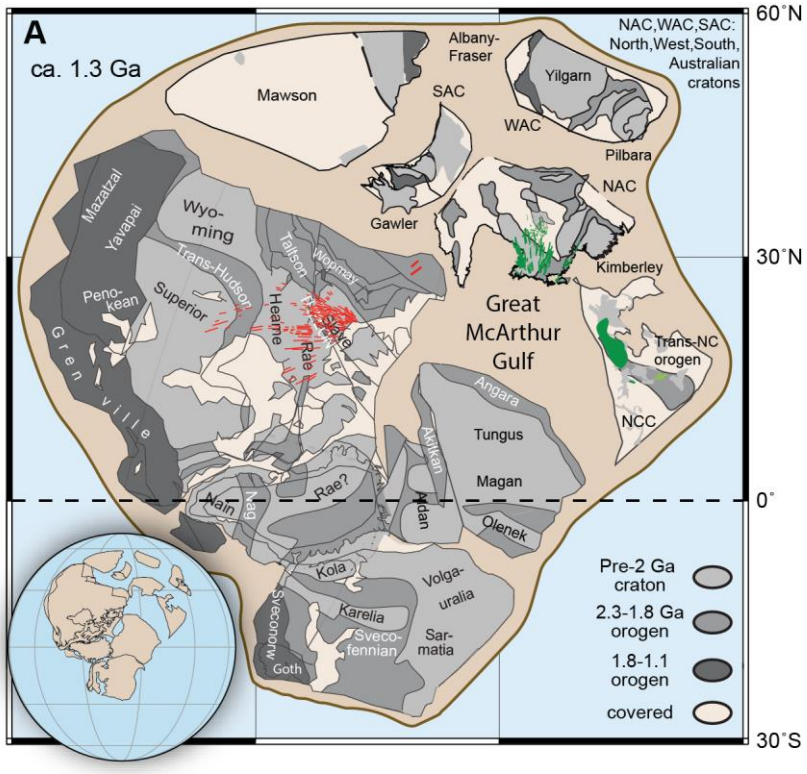

Figure 4 Paleogeography configuration at ca.1.3 Ga after *Kirscher et al. (2018).*Green lines are dykes and sills associated with the ca. 1.3 Ga Derim Derim – Galiwinku and the Yanliao Large Igneous Province. Red lines are the ca. 1.27 Ga Mackenzie dykes.

4. Post Wilton package tectonic geography

The post Wilton North Australia Craton is characterized by the formation of a set of late Mesoproterozoic to early Neoproterozoic sandstone to mudstone successions in the Beetaloo Sub-basin. These successions unconformably overly the Roper Group and comprises three formations/units, informally named the lower Jamison sandstone, the upper Jamison sandstone and the Hayfield mudstone (*Munson, 2016*).

The lower Jamison sandstone is constrained to be deposited after 1092 ± 16 Ma, whereas the deposition of the upper Jamison and Hayfield mudstone has been constrained to be after 959 ± 18 Ma, indicating an over 200 million years of non-deposition after the deposition of the Wilton package (*Chapter 2*). Besides that, these three sedimentary units have markedly contrasting detrital zircon U–Pb ages and hafnium isotope to those of the underlying Roper Group, indicating a significant provenance change associated with the deposition of these rocks (*Munson et al., 2018; Chapters 2 & 3*). Detrital zircon U–Pb ages and hafnium isotope data suggest that the lower and the upper Jamison sandstones both received detritus from the Musgrave Province (*Chapters 2 & 3*). This is consistent with the shale whole-rock Sm-Nd and Pb

isotope data from the *Chapter 4*. Moreover, the whole-rock isotopic data also reveal that the lower Jamison sandstone received detritus from the central Musgrave Province, whereas the western Musgrave Province became the dominant source for the upper Jamison sandstone. This provenance variation is interpreted to be related to the emplacement of Warakurna LIP, which resulted an uplift of the western Musgrave Province. The detrital zircon U–Pb ages and hafnium isotope compositions of the Hayfield mudstone exhibit similarities to the lower and the upper Jamison sandstones, indicating consistent provenance (e.g. the Musgrave Province). Further, the shale whole-rock Sm-Nd and Pb isotope data suggest that this formation also received detritus from evolved sources (e.g. the Arunta Region).

In general, the Neoproterozoic central Australia is characterized by the formation of a series of intracontinental sedimentary basins that show considerable stratigraphic similarities, including the Officer, Amadeus, Ngalia and Georgina basins (Figure 5; *Shaw et al., 1991; Zhao et al., 1994*). As suggested by *Walter et al. (1995)*, the sedimentary records of these basins represent remnants of a once-continuous large depositional system (i.e. the Centralian Superbasin). Importantly, new and combined detrital zircon and shale whole-rock data from *Chapters 2, 3 & 4* demonstrate that the three unnamed sedimentary units in the Beetaloo Sub-basin show obvious consistence and similarities with those deposited in central Australian basins/strata. We therefore suggest that the Centralian Superbasin probably also covered the Beetaloo Sub-basin and is thus considerably more extensive than previous thought (Figure 5).

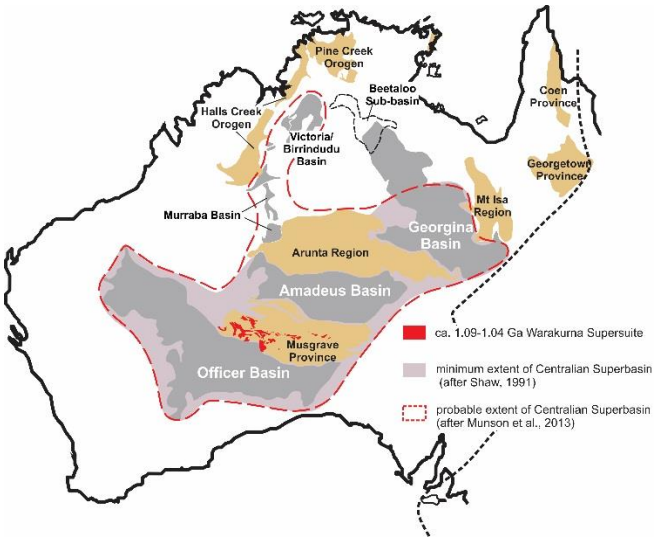

Figure 5 Geological map showing the distribution of Neoproterozoic basins within Australia

In conclusion, the above summaries of individual thesis chapters and their relevant findings and provides new interpretations for the sedimentation and tectonic history of the North Australia Craton, from ca. 1.55 to 0.85 Ga. These new constraints thus contribute to regional tectonic

history and a better understanding of the Mesoproterozoic paleogeography of the North Australia Craton.

References

Abbott, S.T., Sweet, I.P., Plumb, K.A., Young, D.N., Cutovinos, A., Ferenczi, P.A. & Pietsch, B.A. (2001). Roper Region: Urapunga and Roper River Special, Northern Territory (Second Edition). 1:250 000 geological map series explanatory notes, SD 53-10, 11. Northern Territory Geological Survey and Geoscience Australia (National Geoscience Mapping Accord).

Ahmad, M. & Munson, T.J. (2013). Northern Territory Geological Survey, Geology and mineral resources of the Northern Territory, Special Publication 5. Northern Territory Geological Survey.

Anderson, J.R., Kelsey, D.E., Hand, M. & Collins, W.J. (2016). Mesoproterozoic metamorphism in the Rudall Province: revising the timeline of the Yapungku Orogeny and implications for cratonic Australia assembly. *AESC 2016 – Australian Earth Sciences Convention abstract volume*, 227.

Chu, X., Zhang, T., Zhang, Q. & Lyons, T.W. (2007). Sulfur and carbon isotope records from 1700 to 800 Ma carbonates of the Jixian section, northern China: implications for secular isotope variations in Proterozoic seawater and relationships to global supercontinental events. *Geochimica Et Cosmochimica Acta,* ***71*****(19)**, 4668-4692.

Cox, G.M., Jarrett, A., Edwards, D., Crockford, P.W., Halverson, G.P., Collins, A.S., Poirier, A. & Li, Z.X. (2016). Basin redox and primary productivity within the Mesoproterozoic Roper Seaway. *Chemical Geology*, **440**, 101-114.

Frogtech Geoscience, 2018. SEEBASE® study and GIS for greater McArthur Basin. *Northern Territory Geological Survey, Digital Information Package DIP 017*.

Howard, H.M., Werner, M., Smithies, R.H., Kirkland, C.L., Kelsey, D.E., Hand, M., Collins, A., Pirajno, F., Wingate, M.T.D., Maier, W.D. & Raimondo, Y. (2011). The geology of the west Musgrave Province and the Bentley Supergroup–a field guide. *Geological Survey of Western Australia, Record 2011/4*, pp.116.

Johnson, S.P., Thorne, A.M., Tyler, I.M., Korsch, R.J., Kennett, B.L. N., Cutten, H.N., Goodwin, J., Blay, O., Blewett, R.S., Joly, A., Dentith, M.C., Aitken, A.R.A., Holzschuh, J., Salmom, M., Reading, A., Heinson, G., Boren, G., Ross, J., Costelloe, R.D. & Fomim, T. (2013). Crustal architecture of the Capricorn Orogen, Western Australia and associated metallogeny. *Australian Journal of Earth Sciences*, **60**, 681–705.

Kirkland, C.L., Smithies, R.H. & Spaggiari, C.V. (2015). Foreign contemporaries–Unravelling disparate isotopic signatures from Mesoproterozoic Central and Western Australia. *Precambrian Research*, **265**, 218-231.

Kirscher, U., Mitchell, R., Liu, Y., Li, Z.X., Cox, G.M., Nordsvan, A., Wang, C., Pisarevsky, S., 2018. Long lived supercontinent Nuna - updated paleomagnetic constraints from Australia. *2018, AGU Fall Meeting*, abstract #GP21B-0647.

Lanigan, K., Hibbird, S., Menpes, S. & Torkinton, J. (1994). Petroleum exploration in the Proterozoic Beetaloo sub-basin, Northern Territory. *APEA JOURNAL*, **34**, 674-674.

Luo, G., Junium, C.K., Kump, L.R., Huang, J., Li, C., Feng, Q., Shi, X., Bai, X. & Xie, S. (2014). Shallow stratification prevailed for ~1700 to ~1300 Ma ocean: evidence from organic carbon isotopes in the North China Craton. *Earth & Planetary Science Letters*, **400**, 219-232.

Morrissey, L.J., Payne, J.L., Hand, M., Clark, C., Taylor, R., Kirkland, C.L. & Kylander-Clark, A. (2017). Linking the Windmill Islands, east Antarctica and the Albany–Fraser Orogen: insights from U–Pb zircon geochronology and Hf isotopes. *Precambrian Research,* **293,** 131–149.

Munson, T.J. (2016). Sedimentary characterisation of the Wilton package, greater McArthur Basin. Northern Territory. *Northern Territory Geological Survey, Record 2016-003*.

Munson T.J. & Revie, D. (2018). Stratigraphic subdivision of Velkerri Formation, Roper Group, McArthur Basin, Northern Territory. *Northern Territory Geological Survey, Record 2018-006***.**

Munson, T.J, Thompson, J.M, Zhukova, I., Meffre, S., Beyer, E.E., Woodhead, J.D. & Whelan, J.A. (2018). Summary of results. NTGS laser ablation ICP-MS U–Pb and Lu–Hf geochronology project: Roper Group and overlying ungrouped units (McArthur Basin), Renner Group (Tomkinson Province), Tijunna Group (Birrindudu Basin). *Northern Territory Geological Survey, Record* 2018-007.

Plumb, K.A. & Wellman, P. (1987). McArthur Basin, Northern Territory: mapping of deep troughs using gravity and magnetic anomalies. *BMR Journal of Australian Geology & Geophysics,* **10**, 243-251.

Revie, D. (2017).Volumetric resource assessment of the lower Kyalla and middle Velkerri formations of the McArthur Basin. *Annual Geoscience Exploration Seminar (AGES) Proceedings, Alice Springs, Northern Territory 28–29 March 2017.* Northern Territory Geological Survey, Darwin. pp. 86-90.

Shaw, R. D., 1991. The tectonic development of the Amadeus Basin, central Australia. In: Korsch, R.J., Kennard, J.M. (Eds.), Geological and Geophysical Studies in the Amadeus Basin, Central Australia. Bureau of Mineral Resources, Australia, pp.429–461.

Spaggiari, C.V., Kirkland, C.L., Smithies, R.H., Wingate, M.T.D. & Belousova, E.A. (2015). Transformation of an Archean craton margin during Proterozoic basin formation and magmatism: The Albany–Fraser Orogen, Western Australia. *Precambrian Research*, **226**, 440-466.

Walter, M.R., Veevers, J.J., Calver, C.R., Grey, K., 1995. Neoproterozoic stratigraphy of the Centralian Superbasin, Australia. *Precambrian Research,* **73(1–4)**, 173-195. https://doi.org/10.1016/0301-9268(94)00077-5.

Whelan, J.A., Beyer, E.E., Donnellan, N., Bleeker, W., Chamberlin, K.R., Soderlund, U., Ernst, R.E., 2016. 1.4 billion years of Northern Territory geology: Insights from collaborative U–Pb zircon and baddeleyite dating. *Annual Geoscience Exploration Seminar (AGES) Proceedings, Alice Springs, Northern Territory 15–16 March 2016.* Northern Territory Geological Survey, Darwin. pp. 115–123. https://geoscience.nt.gov.au/gemis/ntgsjspui/handle/1/82750.

Xu, H., Yang, Z., Peng, P., Meert, J.G. & Zhu, R. (2014). Paleo-position of the North China Craton within the supercontinent Columbia: constraints from new paleomagnetic results. *Precambrian Research*, **255**, 276–293.

Zhao, J.X., Mcculloch, M.T., Korsch, R.J., 1994. Characterisation of a plume-related ~ 800 Ma magmatic event and its implications for basin formation in central-southern Australia. *Earth & Planetary Science Letters,* **121(3–4)**, 349-367. https://doi.org/10.1016/0012-821X(94)90077-9.

Zhang, S., Li, Z. X., Evans, D.A.D., Wu, H., Li, H. & Dong, J. (2012). Pre-Rodinia supercontinent Nuna shaping up: a global synthesis with new paleomagnetic results from north China. *Earth & Planetary Science Letters*, **353-354**, 145-155.

Zhang, S.H., Zhao, Y., Li, X.H., Ernst, R.E. & Yang, Z.Y. (2017). The 1.33–1.30 Ga Yanliao large igneous province in the North China Craton: implications for reconstruction of the Nuna (Columbia) supercontinent, and specifically with the North Australian Craton. *Earth & Planetary Science Letters,* **465**, 112-12

Appendix 1

Appendix for Chapter 2

Appendix 1

Appendix for Chapter 2

Table 1 Sample information

Formation	Sample name	Core name	Latitude	Longitude	Depth(m)	Formation
upper Jamsion sst.	A-Uj1	Altree 2	-15.9236	133.7866	334.90- 335.49	upper Jamison sst
	A-UJ2	Altree 2	-15.9236	133.7866	349.13- 349.53	upper Jamison sst
	J-UJ3	Jamison 1	-16.7749	133.7672	903.9- 904.43	upper Jamison sst
	W-UJ9	Walton 2	-15.9051	133.6388	227.05- 227.29	upper Jamison sst
lower Jamison sst	E-LJ2	Elliott 1	-17.4025	133.7551	643.69- 644	lower Jamison sst
	M-LJ3	McManus 1	-15.919	133.6242	550.02- 550.27	lower Jamison sst
	E-Ky7	Elliott 1	-17.4025	133.7551	887.27- 887.66	Kyalla Fm.
Kyalla Fm.	J-Ky8	Jamison 1	-16.7749	133.7672	1490.38- 1490.84	Kyalla Fm.
	BirC-Ky1	Birdum Creek 1	-15.625	133.1395	887.40- 887.55	Kyalla Fm.
	J-Mo13	Jamison 1	-16.7749	133.7672	621.57- 621.89	Moroak Sst.
Moroak Sst.	E-Mo13	Elliott 1	-17.4025	133.7551	1518.16- 1518.44	Moroak Sst.
	M-Mo8	McManus 1	-15.919	133.6242	670.82- 671.01	Moroak Sst.
	M-Mo10	McManus 1	-15.919	133.6242	724.34- 724.56	Moroak Sst.
Velkerri Fm.	E-Vel18	Elliott 1	-17.4025	133.7551	1697.41- 1697.71	Velkerri Fm.
	S-BC1	Sever 1	-15.2465	132.844	1167.11- 1167.53	Bessie Creek Sst
Bessie Creek Sst.	W-BC1	Walton 2	-15.9051	133.6388	1013.29- 1013.6	Bessie Creek Sst
	A-BC13	Altree 2	-15.9236	133.7866	1467.79- 1468.19	Bessie Creek Sst

Table 2 Detrital zircon U–Pb dating results of analysed samples

Analysis No.	$^{207}Pb/^{235}U$	2 S.E.	$^{206}Pb/^{238}U$	2 S.E.	Rho	$^{207}Pb/^{235}U$ age (Ma)	2 S.E.	$^{206}Pb/^{238}U$ age (Ma)	2 S.E.	$^{207}Pb/^{206}Pb$ age (Ma)	2 S.E.	Conc (%)
E-LJ2												
Spot1	4.02	0.16	0.2897	0.0083	0.0027	1633	31	1635	42	1643	48	99.5
Spot4	4.15	0.13	0.2941	0.007	0.0035	1670	26	1659	35	1641	63	101.1
Spot5	4.016	0.076	0.2903	0.0045	0.0019	1633	15	1643	23	1594	36	103.1
Spot6	3.869	0.073	0.2895	0.0044	0.002	1610	15	1638	22	1559	39	105.1
Spot7	3.65	0.071	0.2739	0.0039	0.0017	1559	16	1561	20	1525	33	102.4
Spot8	3.905	0.078	0.2859	0.0049	0.0022	1617	16	1621	24	1578	40	102.7
Spot9	4.143	0.092	0.2959	0.0048	0.0021	1663	18	1669	24	1619	41	103.1
Spot10	4.14	0.13	0.2968	0.0073	0.0035	1662	25	1671	36	1635	63	102.2
Spot12	3.693	0.082	0.2754	0.0049	0.0019	1569	18	1568	25	1564	37	100.3
Spot13	3.8	0.1	0.2694	0.0064	0.0025	1593	22	1535	33	1660	47	92.5
Spot14	3.799	0.096	0.281	0.0053	0.0025	1592	20	1597	26	1629	46	98
Spot16	3.719	0.066	0.2806	0.0037	0.0018	1578	14	1595	18	1579	35	101
Spot17	2.098	0.071	0.1933	0.0042	0.0031	1139	23	1147	47	1165	77	98.5
Spot18	3.853	0.082	0.2818	0.0049	0.0023	1606	18	1599	25	1595	45	100.3
Spot19	3.69	0.072	0.2757	0.0048	0.0022	1571	16	1568	24	1605	43	97.7
Spot20	3.554	0.073	0.2688	0.0037	0.0023	1540	17	1536	19	1546	44	99.4
Spot21	3.602	0.079	0.2688	0.0049	0.0022	1552	18	1534	25	1590	41	96.5
Spot22	3.795	0.069	0.2707	0.004	0.002	1591	14	1543	20	1648	37	93.6

Table 2 Detrital zircon U–Pb dating results of analysed samples

Spot23	3.58	0.079	0.2669	0.0038	0.0023	1550	18	1526	19	1589	43	96
Spot24	3.749	0.06	0.2727	0.0033	0.0015	1584	13	1554	17	1612	28	96.4
Spot25	3.583	0.064	0.2615	0.0039	0.002	1545	15	1499	20	1594	37	94
Spot26	3.476	0.073	0.2568	0.0048	0.0026	1518	17	1472	25	1548	51	95.1
Spot28	3.59	0.079	0.2669	0.0042	0.0022	1550	17	1524	21	1574	42	96.8
Spot29	3.675	0.086	0.2656	0.0045	0.0026	1569	18	1520	23	1598	47	95.1
Spot30	3.817	0.074	0.2803	0.0042	0.0021	1595	16	1592	21	1553	39	102.5
Spot31	3.94	0.12	0.2802	0.0061	0.0033	1613	25	1593	31	1631	61	97.7
Spot32	3.571	0.069	0.2608	0.0048	0.0014	1544	15	1494	24	1620	27	92.2
Spot34	3.345	0.071	0.2559	0.0048	0.0027	1489	16	1469	25	1480	55	99.3
Spot35	4.03	0.085	0.2813	0.005	0.0026	1639	17	1601	25	1654	45	96.8
Spot36	3.659	0.087	0.2679	0.0045	0.0026	1563	19	1532	23	1544	50	99.2
Spot38	7.693	0.099	0.3959	0.0047	0.0019	2196	12	2149	22	2186	24	98.3
Spot40	3.464	0.098	0.2474	0.0046	0.0028	1513	23	1424	24	1579	54	90.2
Spot41	3.81	0.074	0.2752	0.0042	0.0019	1591	16	1568	22	1579	37	99.3
Spot42	3.539	0.068	0.2536	0.0034	0.0018	1535	15	1458	18	1608	33	90.7
Spot43	3.764	0.069	0.2712	0.0037	0.0019	1586	14	1548	19	1604	34	96.5
Spot44	3.834	0.094	0.2727	0.0056	0.0024	1595	20	1553	28	1598	44	97.2
Spot45	3.777	0.088	0.2746	0.0047	0.0025	1592	19	1562	24	1567	48	99.7
Spot46	3.736	0.082	0.2764	0.0051	0.0022	1579	17	1574	26	1511	44	104.2
Spot47	4.65	0.076	0.3137	0.0053	0.0018	1756	14	1762	26	1731	30	101.8
Spot48	3.807	0.076	0.2889	0.0042	0.0022	1595	16	1636	21	1567	41	104.4
Spot49	3.697	0.096	0.2701	0.005	0.0029	1571	21	1540	26	1630	52	94.5
Spot50	3.85	0.1	0.2813	0.0059	0.0032	1604	22	1599	30	1628	61	98.2
Spot51	3.586	0.061	0.2645	0.0033	0.0015	1548	14	1512	17	1638	29	92.3
Spot52	1.942	0.048	0.1848	0.003	0.0019	1096	17	1092	16	1142	47	95.6
Spot53	3.85	0.11	0.2774	0.0064	0.0033	1603	22	1576	32	1673	57	94.2
Spot54	3.945	0.094	0.2886	0.0057	0.0027	1630	20	1635	28	1635	49	100
Spot55	3.609	0.071	0.2689	0.0041	0.0018	1551	15	1534	21	1594	34	96.2
Spot56	3.506	0.086	0.2637	0.0049	0.0026	1522	19	1510	25	1569	50	96.2
Spot57	3.674	0.078	0.2738	0.0037	0.0022	1564	17	1559	19	1579	44	98.7
Spot58	4.03	0.11	0.288	0.0056	0.0028	1638	21	1633	28	1646	51	99.2
Spot59	3.656	0.085	0.2743	0.0056	0.0025	1560	19	1561	28	1577	50	99
Spot60	3.727	0.081	0.2756	0.0038	0.0022	1574	18	1571	19	1584	42	99.2
Spot61	1.92	0.12	0.1765	0.006	0.0046	1088	41	1050	34	1130	120	92.9
Spot62	3.253	0.093	0.2506	0.0049	0.0026	1474	23	1440	25	1490	54	96.6
Spot64	3.78	0.1	0.278	0.0059	0.0028	1588	21	1586	31	1584	53	100.1
Spot65	3.66	0.058	0.2741	0.0037	0.0016	1565	13	1561	19	1551	31	100.6
Spot66	3.705	0.059	0.2761	0.0043	0.0018	1575	13	1571	22	1592	36	98.7
Spot68	3.352	0.097	0.2515	0.0064	0.0036	1496	23	1444	33	1577	70	91.6
Spot69	3.68	0.13	0.2758	0.0067	0.0038	1569	27	1568	34	1571	77	99.8
Spot70	3.734	0.084	0.2765	0.005	0.0024	1575	18	1576	25	1589	45	99.2
Spot72	3.672	0.083	0.274	0.0051	0.0022	1564	18	1560	26	1613	42	96.7
Spot73	3.71	0.12	0.2746	0.0052	0.0031	1566	26	1563	27	1578	59	99
Spot74	3.804	0.085	0.2799	0.0046	0.0024	1593	19	1589	23	1618	45	98.2
Spot75	3.767	0.083	0.2789	0.0051	0.0023	1588	18	1586	25	1614	45	98.3
Spot76	4.093	0.079	0.2861	0.0049	0.0017	1653	16	1625	25	1713	31	94.9
Spot77	3.085	0.071	0.2387	0.0041	0.002	1429	18	1379	21	1524	39	90.5
		Rejected analysis										
Spot2	2.955	0.06	0.2064	0.0038	0.0017	1394	16	1210	20	1651	31	73.3
Spot3	1.097	0.034	0.0807	0.0025	0.0018	754	17	499	15	1575	35	31.7
Spot11	1.741	0.03	0.1298	0.002	0.0016	1026	11	787	12	1532	32	51.4
Spot15	1.569	0.037	0.0901	0.0015	0.0022	962	14	555.8	9	2015	30	27.6
Spot27	1.077	0.024	0.0856	0.0015	0.0017	740	12	529.5	8.9	1427	37	37.1
Spot33	1.127	0.027	0.0836	0.0017	0.0016	765	13	517	10	1590	29	32.5
Spot37	0.635	0.017	0.0489	0.0012	0.0023	500	10	307.7	7.4	1505	44	20.4

Table 2 Detrital zircon U–Pb dating results of analysed samples

Spot39	1.539	0.025	0.1146	0.0018	0.0015	946.3	9.7	699	11	1574	29	44.4
Spot63	2.817	0.055	0.2081	0.0034	0.0021	1359	15	1218	18	1607	39	75.8
Spot67	2.313	0.052	0.1761	0.0034	0.0021	1218	15	1045	18	1585	40	65.9
M-LJ3												
Spot2	3.831	0.06	0.2807	0.0045	0.0017	1599	12	1594	23	1577	33	101
Spot6	3.654	0.072	0.2646	0.0045	0.0025	1563	16	1512	23	1658	44	91
Spot7	4.042	0.094	0.2798	0.0047	0.0023	1643	19	1589	24	1702	40	93
Spot9	3.916	0.093	0.275	0.005	0.0026	1617	19	1565	25	1654	49	95
Spot12	3.622	0.082	0.2717	0.0047	0.0023	1556	18	1551	24	1571	44	99
Spot14	2.207	0.077	0.1976	0.0041	0.0029	1177	24	1168	23	1193	79	98
Spot16	3.654	0.073	0.2654	0.0041	0.0019	1557	16	1516	21	1618	35	94
Spot17	2.401	0.041	0.2089	0.003	0.0014	1243	13	1224	16	1287	33	95
Spot18	4.14	0.12	0.2957	0.0063	0.0034	1674	23	1668	31	1706	58	98
Spot19	4.33	0.12	0.285	0.0051	0.0028	1696	24	1615	26	1612	55	100
Spot24	3.95	0.095	0.2572	0.0052	0.0021	1621	19	1478	26	1640	37	90
Spot28	3.703	0.084	0.2653	0.0051	0.0021	1579	18	1518	26	1555	40	98
Spot29	2.14	0.057	0.1838	0.0032	0.002	1159	19	1087	17	1206	53	90
Spot34	3.603	0.082	0.2651	0.0049	0.0025	1548	18	1520	25	1535	49	99
Spot36	4.71	0.1	0.2939	0.0044	0.0028	1769	19	1660	22	1751	48	95
Spot41	6.49	0.16	0.341	0.0065	0.0032	2044	23	1890	31	2044	46	92
Spot42	3.141	0.089	0.2273	0.005	0.003	1439	22	1319	26	1430	66	92
Spot43	3.52	0.072	0.2486	0.0034	0.0021	1529	16	1431	17	1489	43	96
Spot44	3.431	0.064	0.2351	0.0038	0.002	1513	15	1362	20	1604	37	85
Spot45	3.92	0.1	0.2704	0.005	0.0028	1617	21	1542	25	1592	54	97
Spot48	3.757	0.076	0.2669	0.0037	0.0019	1582	17	1525	19	1575	36	97
Spot52	3.6	0.1	0.2567	0.005	0.0028	1548	23	1476	26	1575	52	94
Spot54	3.401	0.098	0.2519	0.0047	0.0026	1503	23	1447	24	1566	51	92
Spot61	4.736	0.08	0.3088	0.0047	0.0022	1771	14	1734	23	1799	36	96
Spot65	3.171	0.068	0.2446	0.0042	0.0023	1448	17	1410	22	1526	45	92
Spot67	3.767	0.096	0.2721	0.0042	0.0024	1579	21	1552	21	1597	47	97
Spot68	3.502	0.058	0.2608	0.0034	0.0015	1526	13	1493	17	1542	29	97
Spot70	3.64	0.1	0.2633	0.0055	0.0031	1560	22	1505	28	1618	59	93
Spot72	2.097	0.051	0.2057	0.003	0.002	1149	17	1205	16	1285	47	94
Spot73	3.272	0.059	0.266	0.0034	0.0016	1475	14	1519	17	1620	31	94
Spot74	3.12	0.11	0.2569	0.0066	0.0039	1439	27	1470	34	1541	78	95
Spot76	3.463	0.07	0.2641	0.0043	0.0021	1516	16	1513	22	1609	38	94
	Rejected analysis											
Spot1	2.865	0.098	0.2093	0.006	0.0039	1366	26	1223	32	1774	64	89.5
Spot3	1.721	0.051	0.1365	0.004	0.0024	1020	19	827	23	1655	44	81.1
Spot4	0.834	0.011	0.06754	0.0007	0.0013	614.8	6.3	421.3	4	1579	23	68.5
Spot5	2.104	0.057	0.1671	0.004	0.0019	1151	19	996	22	1584	35	86.5
Spot8	1.38	0.023	0.1051	0.0015	0.0018	879.8	9.9	644.1	8.5	1645	34	73.2
Spot10	0.363	0.009	0.03169	0.0007	0.0024	314.2	6.7	201.1	4.6	1404	54	64
Spot11	3.099	0.062	0.2019	0.0032	0.0021	1431	15	1185	17	1786	35	82.8
Spot13	2.352	0.038	0.1812	0.0021	0.0014	1228	11	1073	11	1663	24	87.4
Spot15	1.568	0.028	0.1243	0.0021	0.0021	956	11	755	12	1683	37	79
Spot20	2.399	0.074	0.1775	0.004	0.0029	1238	22	1053	22	1589	56	85.1
Spot21	3.101	0.065	0.2009	0.0042	0.0021	1433	17	1179	22	1677	40	82.3
Spot22	2.551	0.049	0.1609	0.0029	0.002	1286	14	961	16	1707	35	74.7
Spot23	1.801	0.061	0.1214	0.0032	0.0026	1049	23	738	18	1563	54	70.4
Spot25	2.162	0.054	0.161	0.0037	0.003	1167	18	962	20	1591	54	82.4
Spot26	2.959	0.058	0.2109	0.003	0.0018	1398	15	1233	16	1676	35	88.2
Spot27	0.929	0.017	0.05402	0.0007	0.0025	666.1	9.2	339.1	4.1	2046	34	50.9
Spot30	2.204	0.06	0.1646	0.003	0.0028	1181	19	982	17	1539	54	83.1

Table 2 Detrital zircon U–Pb dating results of analysed samples

Spot31	1.524	0.024	0.1089	0.0016	0.0016	940.3	9.5	667	9.2	1665	29	70.9
Spot32	2.112	0.037	0.04377	0.0009	0.0065	1151	12	276.1	5.5	3719	28	24
Spot33	1.942	0.075	0.1477	0.0045	0.0039	1097	27	887	25	1549	72	80.9
Spot35	2.733	0.064	0.2026	0.0042	0.0025	1339	17	1189	23	1584	48	88.8
Spot37	2.057	0.043	0.1505	0.0029	0.0021	1136	14	903	16	1629	39	79.5
Spot38	2.277	0.05	0.1683	0.0036	0.0023	1203	16	1002	20	1599	44	83.3
Spot39	2.03	0.1	0.1376	0.0069	0.0015	1107	36	829	39	1710	26	74.9
Spot40	2.704	0.045	0.1847	0.0026	0.0017	1330	12	1092	14	1730	30	82.1
Spot46	1.266	0.059	0.0798	0.0022	0.0033	828	26	495	13	1877	53	59.8
Spot47	1.668	0.04	0.1342	0.0026	0.0019	997	15	813	15	1434	40	81.5
Spot49	2.719	0.06	0.1977	0.0033	0.0022	1338	16	1164	18	1618	43	87
Spot50	0.742	0.015	0.05545	0.0009	0.0016	563.9	8.9	347.8	5.5	1561	32	61.7
Spot51	2.012	0.099	0.152	0.005	0.0048	1114	33	912	28	1550	110	81.9
Spot53	1.915	0.042	0.118	0.002	0.0019	1088	15	719	11	1931	28	66.1
Spot55	2.111	0.048	0.1517	0.0027	0.002	1149	16	910	15	1635	38	79.2
Spot56	0.918	0.073	0.0679	0.0049	0.0025	647	40	422	29	1573	49	65.2
Spot57	2.567	0.061	0.1929	0.0036	0.0027	1288	18	1137	19	1535	51	88.3
Spot58	3.069	0.066	0.2192	0.0039	0.0024	1423	17	1277	20	1631	46	89.7
Spot59	2.852	0.07	0.2078	0.0046	0.0025	1368	19	1216	24	1618	51	88.9
Spot60	3.251	0.091	0.2385	0.005	0.0027	1465	22	1381	26	1616	51	85.5
Spot62	2.775	0.046	0.2085	0.003	0.0019	1348	12	1220	16	1556	37	78.4
Spot63	3.433	0.078	0.2361	0.0038	0.0019	1516	18	1368	19	1586	38	86.3
Spot64	3.121	0.052	0.2307	0.0041	0.0019	1442	13	1338	21	1557	37	85.9
Spot66	2.835	0.069	0.2239	0.0045	0.002	1367	18	1302	23	1506	38	86.5
Spot69	2.698	0.068	0.2032	0.0043	0.0026	1325	19	1195	23	1546	51	77.3
Spot71	4.096	0.074	0.2702	0.0042	0.0021	1655	16	1541	21	1767	37	87.2
Spot75	3.589	0.087	0.252	0.004	0.0027	1545	19	1448	20	1637	50	88.5
Spot77	2.7	0.059	0.2055	0.0044	0.0029	1328	16	1204	23	1718	50	70.1
Spot78	2.585	0.041	0.222	0.0028	0.0016	1296	12	1292	15	1517	31	85.2
Spot79	2.28	0.06	0.1872	0.004	0.0024	1208	19	1105	22	1589	46	69.5
Spot80	2.125	0.057	0.1804	0.0031	0.0029	1164	18	1074	17	1534	57	70
Spot81	3.061	0.049	0.2469	0.0034	0.0018	1421	12	1423	18	1655	33	86
Spot82	3.115	0.074	0.2428	0.004	0.0025	1439	18	1400	20	1584	47	88.4
Spot83	2.585	0.041	0.222	0.0028	0.0016	1296	12	1292	15	1517	31	85.2
W-UJ9												
Spot6	3.376	0.07	0.2598	0.004	0.0022	1498	16	1488	21	1562	41	95.3
Spot7	3.519	0.094	0.2656	0.0052	0.0032	1531	22	1518	27	1591	61	95.4
Spot8	4.278	0.098	0.2979	0.0059	0.0026	1695	20	1680	29	1778	44	94.5
Spot9	2.159	0.097	0.1972	0.0056	0.0037	1160	31	1158	30	1155	96	100.3
Spot10	2.028	0.073	0.1893	0.0039	0.0027	1119	25	1117	21	1140	71	98
Spot11	3.125	0.078	0.2369	0.0045	0.0028	1439	20	1370	23	1554	55	88.2
Spot12	3.553	0.081	0.2691	0.005	0.0025	1539	18	1538	25	1563	47	98.4
Spot15	2.169	0.05	0.1989	0.0035	0.0021	1173	16	1169	19	1169	53	100
Spot16	3.311	0.085	0.2581	0.0069	0.0024	1482	20	1478	35	1556	46	95
Spot17	2.184	0.068	0.1997	0.0034	0.0025	1178	22	1173	18	1164	61	100.8
Spot18	1.949	0.087	0.1809	0.0048	0.0044	1096	31	1073	26	1170	110	91.7
Spot20	2.252	0.058	0.2056	0.0044	0.002	1199	18	1204	24	1213	49	99.3
Spot21	3.847	0.097	0.2808	0.0051	0.0026	1600	21	1594	26	1666	48	95.7
Spot22	2.107	0.067	0.1935	0.0049	0.0025	1151	22	1146	26	1181	65	97
Spot23	3.309	0.083	0.2576	0.0042	0.0022	1481	20	1480	22	1541	42	96
Spot24	3.001	0.077	0.2314	0.0058	0.003	1405	19	1341	30	1486	63	90.2
Spot25	3.89	0.25	0.28	0.016	0.0082	1614	54	1606	76	1750	140	91.8
Spot26	3.377	0.066	0.2595	0.0038	0.0019	1496	15	1489	19	1561	37	95.4
Spot27	1.961	0.086	0.1851	0.0045	0.0039	1100	30	1093	25	1120	100	97.6

Table 2 Detrital zircon U–Pb dating results of analysed samples

Spot28	4.12	0.12	0.2918	0.0063	0.003	1656	24	1649	32	1689	53	97.6
Spot29	2.11	0.11	0.1939	0.0062	0.0046	1145	39	1145	33	1170	110	97.9
Spot31	3.503	0.095	0.266	0.0046	0.0028	1525	22	1519	23	1554	53	97.7
Spot32	2.076	0.06	0.1931	0.0037	0.0023	1142	20	1139	20	1127	60	101.1
Spot33	1.963	0.072	0.1827	0.0039	0.0032	1095	25	1086	21	1158	85	93.8
Spot34	2.099	0.05	0.1907	0.0032	0.0022	1144	17	1126	17	1174	55	95.9
Spot35	3.25	0.11	0.2487	0.0074	0.0028	1471	28	1431	38	1572	56	91
Spot36	2.314	0.049	0.2052	0.0037	0.0021	1215	15	1204	20	1243	50	96.9
Spot38	2.911	0.099	0.239	0.0056	0.0028	1380	26	1381	29	1433	56	96.4
Spot40	2.01	0.085	0.1883	0.0054	0.0037	1106	29	1110	30	1107	96	100.3
Spot41	4.604	0.075	0.3119	0.004	0.0018	1751	14	1749	20	1759	30	99.4
Spot42	3.697	0.084	0.2742	0.0041	0.0023	1570	18	1566	21	1583	45	98.9
Spot43	2.088	0.078	0.1926	0.0051	0.0032	1142	26	1137	27	1122	84	101.3
Spot45	4.364	0.088	0.3019	0.0064	0.0024	1704	17	1700	32	1746	39	97.4
Spot47	3.629	0.063	0.2725	0.0042	0.0019	1556	14	1555	21	1559	37	99.7
Spot48	2.192	0.048	0.2003	0.0035	0.0021	1180	15	1176	19	1197	54	98.2
Spot50	3.611	0.098	0.2701	0.0052	0.0029	1548	22	1541	26	1599	55	96.4
Spot52	2.054	0.077	0.1827	0.0029	0.0031	1128	25	1081	16	1195	74	90.5
Spot53	1.849	0.06	0.1805	0.0035	0.0026	1065	21	1069	19	1090	72	98.1
Spot54	2.109	0.054	0.1963	0.0033	0.0024	1158	17	1155	18	1197	62	96.5
Spot55	3.47	0.12	0.265	0.0053	0.0029	1518	28	1514	27	1559	59	97.1
Spot56	2.085	0.058	0.1931	0.0051	0.002	1141	19	1137	28	1196	50	95.1
Spot57	3.495	0.066	0.2621	0.0049	0.0025	1524	15	1503	25	1583	47	94.9
Spot59	1.853	0.048	0.1758	0.0033	0.0021	1062	17	1051	19	1149	51	91.5
Spot60	1.94	0.087	0.1844	0.0039	0.0038	1097	30	1090	21	1138	99	95.8
Spot61	1.828	0.087	0.1812	0.0051	0.004	1052	31	1072	28	1040	100	103.1
Spot62	3.328	0.06	0.2528	0.004	0.0018	1485	14	1454	21	1585	35	91.7
Spot64	2.272	0.072	0.2063	0.0039	0.0024	1208	22	1208	21	1158	64	104.3
Spot65	4.59	0.11	0.3097	0.0073	0.0016	1749	19	1742	36	1773	28	98.3
Spot66	3.851	0.051	0.2704	0.0033	0.0017	1602	11	1542	17	1701	30	90.7
Spot67	3.57	0.11	0.2726	0.0059	0.0026	1556	23	1552	30	1548	53	100.3
Spot68	3.743	0.071	0.2771	0.0052	0.0018	1576	15	1575	27	1597	36	98.6
Spot69	3.775	0.087	0.2786	0.0052	0.0024	1590	18	1582	26	1624	43	97.4
Spot71	2.262	0.05	0.2039	0.0032	0.0019	1197	16	1195	17	1207	48	99
Spot72	3.532	0.083	0.2693	0.0059	0.0026	1536	19	1536	30	1568	49	98
Spot73	2.016	0.045	0.1893	0.0031	0.0018	1122	15	1177	45	1119	17	95.1
Spot74	1.997	0.063	0.1877	0.0036	0.0027	1112	22	1108	20	1108	74	100
Spot75	3.834	0.082	0.2824	0.0046	0.0022	1598	17	1602	23	1560	42	102.7
Spot77	2.169	0.05	0.1978	0.0033	0.0022	1169	17	1165	18	1217	54	95.7
Spot78	2.151	0.07	0.204	0.0036	0.0027	1161	22	1196	19	1140	69	104.9
Spot79	3.497	0.082	0.2671	0.0044	0.002	1522	19	1525	22	1558	38	97.9
Spot82	3.428	0.086	0.2575	0.0055	0.0027	1508	20	1484	27	1574	51	94.3
Spot83	3.634	0.076	0.2716	0.0059	0.0019	1552	17	1547	30	1614	36	95.8
Spot85	3.446	0.059	0.2641	0.0039	0.0018	1516	13	1512	20	1568	36	96.4
Spot87	3.422	0.081	0.2604	0.0044	0.0022	1511	17	1493	23	1564	41	95.5
Spot88	3.584	0.085	0.269	0.0045	0.0024	1545	19	1542	23	1596	47	96.6
Spot89	3.298	0.085	0.2552	0.0044	0.0026	1482	20	1464	22	1548	51	94.6
		Rejected analysis										
Spot1	3.521	0.076	0.252	0.0042	0.0022	1531	17	1448	22	1652	39	88
Spot2	2.554	0.048	0.1905	0.0027	0.0022	1287	14	1123	15	1605	41	70
Spot3	2.218	0.051	0.1637	0.0038	0.0024	1185	16	977	21	1633	44	60
Spot4	0.994	0.027	0.072	0.0014	0.0026	701	14	447.8	8.6	1573	51	28
Spot5	4.65	0.2	0.2136	0.0053	0.0065	1757	36	1247	28	2347	75	53
Spot13	0.895	0.014	0.07233	0.001	0.0016	648.6	7.5	450.1	5.9	1464	33	31
Spot14	3.351	0.081	0.1831	0.0042	0.0035	1493	19	1083	23	2159	43	50
Spot19	3.301	0.077	0.0855	0.0015	0.0054	1483	18	529	9.2	3350	31	16

Table 2 Detrital zircon U–Pb dating results of analysed samples

Spot30	2.019	0.034	0.1312	0.0023	0.0021	1122	11	794	13	1870	34	42
Spot37	2.09	0.069	0.1615	0.0057	0.0032	1147	22	964	32	1572	61	61
Spot39	1.359	0.042	0.1151	0.0022	0.0029	871	18	702	12	1333	66	53
Spot44	2.606	0.041	0.1714	0.0028	0.0019	1305	11	1019	15	1777	32	57
Spot46	2.543	0.096	0.181	0.0056	0.0045	1283	28	1075	30	1638	83	66
Spot49	2.194	0.071	0.1618	0.0044	0.002	1175	22	969	24	1643	36	59
Spot51	2.571	0.076	0.1878	0.0044	0.0025	1289	22	1109	24	1606	45	69
Spot58	1.379	0.04	0.125	0.0033	0.0025	880	17	759	19	1243	61	61
Spot63	1.72	0.021	0.1237	0.0015	0.0015	1015.9	8	753.6	8.3	1652	27	46
Spot70	1.008	0.02	0.0801	0.0011	0.0018	708	10	496.9	6.7	1501	37	33
Spot76	2.69	0.15	0.2018	0.0077	0.0047	1313	39	1183	41	1612	83	73
Spot80	1.678	0.03	0.1155	0.0016	0.0018	1001	11	704.3	9.4	1750	31	40
Spot81	1.796	0.053	0.1514	0.0035	0.0031	1047	20	908	19	1319	71	69
Spot84	3.001	0.053	0.1911	0.0035	0.0022	1406	14	1127	19	1916	33	59
Spot86	2.59	0.24	0.211	0.01	0.0081	1275	55	1231	54	1430	170	86
Spot90	1.925	0.047	0.1727	0.0026	0.0018	1088	16	1026	14	1218	44	84
J-UJ3												
Spot1	3.142	0.059	0.2533	0.0042	0.0016	1444	15	1456	22	1398	35	104.1
Spot2	3.98	0.12	0.287	0.0063	0.0033	1625	25	1624	32	1597	62	101.7
Spot3	4.038	0.09	0.2826	0.0056	0.0023	1641	19	1603	28	1637	43	97.9
Spot4	3.891	0.072	0.2808	0.0039	0.0019	1610	15	1594	20	1592	36	100.1
Spot5	3.962	0.073	0.2792	0.0041	0.0016	1623	15	1586	20	1604	29	98.9
Spot7	3.97	0.21	0.2704	0.0051	0.0042	1587	28	1543	26	1602	57	96.3
Spot9	2.314	0.056	0.2052	0.0036	0.002	1215	17	1202	19	1147	49	104.8
Spot10	2.167	0.058	0.1968	0.0033	0.0022	1170	18	1157	18	1117	57	103.6
Spot11	3.83	0.1	0.2793	0.0056	0.0024	1597	22	1590	28	1523	49	104.4
Spot12	3.705	0.073	0.268	0.0044	0.0018	1568	16	1529	23	1529	35	100
Spot13	2.38	0.057	0.1974	0.0037	0.0022	1236	17	1160	20	1274	51	91.1
Spot14	3.777	0.073	0.2688	0.0043	0.0018	1590	15	1535	22	1604	35	95.7
Spot15	4.09	0.1	0.2811	0.0047	0.0028	1648	20	1597	24	1622	51	98.5
Spot16	2.046	0.079	0.1868	0.0047	0.0031	1132	27	1102	26	1084	83	101.7
Spot17	2.188	0.071	0.1925	0.0042	0.003	1174	23	1133	23	1182	75	95.9
Spot18	3.862	0.075	0.2844	0.0046	0.0018	1606	15	1615	23	1611	32	100.2
Spot19	2.309	0.059	0.2079	0.0038	0.0021	1214	18	1220	21	1176	53	103.7
Spot20	2.231	0.055	0.2029	0.0037	0.0022	1192	18	1191	20	1207	53	98.7
Spot22	2.116	0.048	0.2006	0.0031	0.0016	1158	15	1178	17	1100	42	107.1
Spot23	2.29	0.051	0.203	0.0033	0.0019	1211	16	1190	18	1195	48	99.6
Spot24	3.686	0.079	0.2732	0.0045	0.0022	1566	18	1558	23	1552	43	100.4
Spot26	3.797	0.085	0.2687	0.0043	0.0021	1591	18	1533	22	1598	39	95.9
Spot27	2.19	0.058	0.1904	0.0037	0.0023	1177	18	1126	20	1194	56	94.3
Spot28	3.757	0.085	0.2685	0.0048	0.0023	1579	18	1532	24	1578	42	97.1
Spot30	3.71	0.088	0.2588	0.0048	0.0018	1575	18	1484	24	1603	34	92.6
Spot31	3.786	0.08	0.2692	0.0045	0.0022	1590	17	1537	23	1588	43	96.8
Spot33	2.224	0.048	0.1924	0.0034	0.0016	1187	15	1186	40	1135	18	95.7
Spot34	3.62	0.088	0.2614	0.0044	0.0022	1560	19	1496	23	1569	42	95.3
Spot35	4.177	0.084	0.3037	0.006	0.002	1671	16	1708	30	1639	36	104.2
Spot36	2.308	0.058	0.2134	0.0033	0.0021	1218	18	1251	18	1161	53	107.8
Spot37	3.901	0.078	0.2917	0.0051	0.0024	1610	16	1653	26	1607	45	102.9
Spot38	2.19	0.057	0.2016	0.0038	0.0021	1177	18	1183	20	1173	52	100.9
Spot39	3.584	0.085	0.2679	0.0041	0.0023	1543	19	1532	21	1563	44	98
Spot40	3.591	0.071	0.257	0.0048	0.0018	1545	16	1473	25	1591	35	92.6
Spot41	2.071	0.066	0.1864	0.0044	0.0025	1145	22	1101	24	1182	63	93.1
Spot42	2.256	0.085	0.2049	0.0052	0.0031	1204	26	1200	28	1172	79	102.4
Spot43	2.17	0.14	0.1917	0.0086	0.0051	1166	44	1129	47	1190	130	94.9

Table 2 Detrital zircon U–Pb dating results of analysed samples

Spot44	3.749	0.084	0.2707	0.0044	0.0023	1583	18	1543	22	1580	43	97.7
Spot47	3.9	0.11	0.2731	0.0058	0.0035	1611	23	1558	30	1614	65	96.5
Spot49	2.141	0.076	0.1942	0.0051	0.0031	1156	25	1146	27	1135	79	101
Spot50	3.79	0.084	0.2707	0.0052	0.0021	1594	17	1547	26	1632	40	94.8
Spot51	4.057	0.075	0.3082	0.0044	0.0017	1644	15	1731	22	1595	33	108.5
Spot52	2.254	0.082	0.2061	0.0043	0.0035	1203	25	1207	23	1251	80	96.5
Spot53	3.829	0.081	0.2858	0.0046	0.0016	1606	17	1619	23	1612	31	100.4
Spot55	2.026	0.087	0.1909	0.0054	0.0029	1125	28	1126	29	1231	70	91.5
Spot56	2.253	0.059	0.2096	0.0033	0.0023	1200	18	1228	17	1180	56	104.1
Spot58	3.775	0.087	0.2706	0.0049	0.0022	1585	18	1543	25	1596	41	96.7
Spot59	5.173	0.098	0.3325	0.0058	0.0022	1846	16	1854	28	1866	35	99.4
Spot60	3.992	0.085	0.2886	0.0045	0.0022	1632	17	1633	22	1642	40	99.5
Spot62	3.63	0.11	0.2666	0.0063	0.0032	1557	24	1523	32	1590	61	95.8
Spot65	4.02	0.14	0.2849	0.0067	0.0041	1634	29	1613	34	1622	77	99.4
Spot66	4.048	0.083	0.2891	0.0049	0.0021	1642	17	1638	24	1614	40	101.5
Spot67	2.379	0.079	0.2143	0.0047	0.0035	1237	24	1252	25	1227	83	102
Spot68	2.174	0.052	0.194	0.0039	0.0022	1170	16	1146	21	1195	53	95.9
Spot69	3.891	0.096	0.2813	0.0055	0.0022	1611	20	1598	28	1583	43	100.9
Spot70	2.205	0.076	0.1989	0.0045	0.0025	1180	23	1171	24	1167	66	100.3
Spot73	3.75	0.072	0.2726	0.0039	0.0021	1579	15	1555	19	1591	38	97.7
Spot76	3.365	0.085	0.257	0.0054	0.0024	1492	20	1473	28	1501	48	98.1
Spot77	2.165	0.052	0.1943	0.0036	0.0019	1168	17	1145	20	1205	46	95
Spot78	3.33	0.081	0.246	0.0044	0.0022	1488	19	1417	23	1531	43	92.6
Spot79	3.585	0.094	0.2674	0.0048	0.0027	1547	22	1528	24	1548	52	98.7
Spot81	3.708	0.082	0.2688	0.0047	0.0024	1576	18	1538	24	1606	45	95.8
Spot82	1.966	0.079	0.18	0.0036	0.0036	1095	27	1066	20	1147	88	92.9
Spot83	4.03	0.089	0.2974	0.0047	0.0021	1637	18	1677	23	1556	42	107.8
Spot84	3.89	0.12	0.2874	0.0065	0.0031	1615	25	1626	32	1602	58	101.5
Spot86	2.297	0.058	0.2068	0.0036	0.0022	1213	18	1211	19	1242	51	97.5
Spot87	3.71	0.12	0.2866	0.0065	0.0038	1573	27	1624	32	1525	75	106.5
Spot88	3.651	0.078	0.2602	0.0053	0.0023	1561	17	1490	27	1635	41	91.1
Spot91	3.631	0.06	0.2697	0.0046	0.0017	1556	13	1538	23	1583	31	97.2
Spot92	3.838	0.078	0.2805	0.0049	0.0024	1600	17	1592	25	1612	43	98.8
Spot93	3.478	0.054	0.2544	0.0041	0.0013	1523	12	1462	21	1597	26	91.5
Spot94	3.187	0.07	0.2479	0.0047	0.0021	1454	17	1429	24	1545	40	92.5
Spot96	3.646	0.088	0.2748	0.0057	0.0028	1563	20	1565	28	1580	53	99.1
Spot97	1.998	0.047	0.1877	0.003	0.0016	1111	16	1108	16	1104	42	100.4
Spot98	3.581	0.094	0.2669	0.0055	0.0025	1537	21	1523	28	1567	49	97.2
Spot99	3.46	0.11	0.2601	0.0057	0.0033	1516	26	1489	29	1613	58	92.3
Spot100	2.315	0.069	0.2072	0.0038	0.0026	1212	21	1213	20	1206	62	100.6
Spot101	3.922	0.076	0.2862	0.0046	0.0019	1616	16	1621	23	1607	37	100.9
Spot103	2.279	0.059	0.2041	0.0033	0.0025	1204	18	1196	18	1185	58	100.9
Spot105	4.01	0.071	0.284	0.0042	0.002	1635	15	1612	21	1662	38	97
Spot107	2.122	0.099	0.194	0.006	0.0044	1152	32	1140	33	1140	100	100
Spot108	3.95	0.11	0.2738	0.006	0.0026	1620	23	1564	30	1678	47	93.2
Spot110	3.745	0.068	0.2636	0.0039	0.0016	1579	15	1509	20	1594	26	94.7
		Rejected analysis										
Spot6	1.256	0.037	0.0883	0.0019	0.0024	827	16	545	12	1661	42	33
Spot8	3.195	0.053	0.1785	0.0032	0.002	1456	13	1058	17	2048	28	52
Spot21	2.672	0.054	0.1635	0.0032	0.0021	1319	15	975	18	1872	33	52
Spot25	1.741	0.045	0.1132	0.0018	0.0028	1020	16	691	10	1743	40	40
Spot29	1.74	0.036	0.1051	0.0025	0.0018	1022	13	644	14	1884	29	34
Spot32	2.057	0.077	0.053	0.0024	0.014	1140	24	332	15	3241	79	10
Spot45	1.934	0.056	0.1259	0.0038	0.0013	1087	20	763	22	1754	24	44
Spot46	1.106	0.019	0.0724	0.0014	0.0014	755.5	9	450.4	8.6	1761	24	26
Spot48	3.485	0.081	0.2288	0.0048	0.0026	1524	19	1329	26	1774	44	75

Table 2 Detrital zircon U–Pb dating results of analysed samples

Spot54	3.508	0.072	0.2425	0.0042	0.002	1531	17	1399	22	1637	35	85
Spot57	1.272	0.038	0.0934	0.0043	0.0063	834	17	573	26	1679	87	34
Spot61	2.111	0.057	0.1532	0.0042	0.003	1153	18	918	23	1617	58	57
Spot63	3.273	0.085	0.2204	0.0034	0.0027	1471	20	1285	18	1741	44	74
Spot64	2.492	0.041	0.17	0.0033	0.002	1272	11	1012	18	1693	36	60
Spot71	4.28	0.1	0.2683	0.0047	0.0029	1687	19	1531	24	1854	46	83
Spot72	1.082	0.018	0.0723	0.0012	0.0017	744	9	449.8	7.3	1775	29	25
Spot74	3.221	0.065	0.2255	0.0044	0.0019	1461	15	1311	23	1692	33	77
Spot75	2.147	0.074	0.1816	0.0037	0.0033	1167	24	1075	20	1331	73	81
Spot80	0.944	0.017	0.0661	0.0012	0.0017	676.2	8.6	412.4	7.1	1669	32	25
Spot85	3.811	0.095	0.2327	0.0045	0.003	1600	20	1347	23	1952	45	69
Spot89	1.857	0.032	0.1178	0.0026	0.0021	1066	11	718	15	1877	34	38
Spot90	2.72	0.057	0.1977	0.0038	0.002	1334	16	1164	20	1606	36	72
Spot95	1.031	0.026	0.0808	0.0018	0.0018	718	13	501	11	1451	38	35
Spot102	1.932	0.048	0.1753	0.0035	0.0016	1092	17	1042	19	1177	39	89
Spot104	3.3	0.069	0.2443	0.0034	0.0022	1477	16	1408	18	1566	43	89.9
Spot106	3.383	0.084	0.2486	0.0055	0.0028	1498	19	1432	29	1594	26	89.8
A-UJ1												
Spot1	3.88	0.078	0.2907	0.0044	0.002	1609	16	1644	22	1546	38	106.3
Spot2	3.53	0.12	0.2746	0.0056	0.0031	1534	27	1562	28	1476	64	105.8
Spot4	3.53	0.12	0.2713	0.0055	0.0037	1527	29	1553	27	1472	76	105.5
Spot5	3.18	0.15	0.2652	0.0091	0.0047	1447	36	1514	46	1438	97	105.3
Spot6	3.469	0.095	0.2753	0.0052	0.0027	1524	21	1565	26	1492	55	104.9
Spot8	2.28	0.19	0.202	0.012	0.0085	1191	59	1185	64	1130	230	104.9
Spot10	2.047	0.063	0.1942	0.0039	0.0027	1130	21	1143	21	1093	75	104.6
Spot11	2.012	0.079	0.1919	0.0044	0.0029	1116	26	1131	24	1095	77	103.3
Spot15	2.082	0.06	0.1972	0.0036	0.0025	1137	20	1161	20	1126	66	103.1
Spot17	3.559	0.078	0.2721	0.0041	0.0023	1540	17	1550	21	1505	46	103
Spot19	3.676	0.074	0.2832	0.0054	0.0023	1564	16	1606	27	1561	45	102.9
Spot20	2.096	0.077	0.1962	0.0045	0.0031	1149	24	1154	24	1132	78	101.9
Spot22	3.482	0.091	0.2692	0.0054	0.003	1520	21	1537	27	1515	59	101.5
Spot25	3.449	0.095	0.2627	0.0054	0.0029	1511	22	1502	27	1497	58	100.3
Spot27	3.967	0.077	0.2866	0.0037	0.002	1629	16	1623	19	1618	37	100.3
Spot28	3.696	0.096	0.2797	0.0046	0.0027	1570	20	1591	24	1587	51	100.3
Spot30	3.77	0.12	0.2808	0.0066	0.0031	1578	25	1593	33	1591	56	100.1
Spot31	3.524	0.075	0.2664	0.0041	0.0022	1534	17	1523	21	1524	41	99.9
Spot32	2.032	0.067	0.1893	0.0036	0.0026	1126	22	1117	20	1126	66	99.2
Spot33	3.72	0.25	0.271	0.01	0.0058	1554	54	1549	54	1570	120	98.7
Spot34	3.305	0.081	0.2583	0.0054	0.0025	1481	19	1483	28	1514	52	98
Spot39	1.938	0.055	0.1803	0.0034	0.0021	1095	19	1068	19	1092	55	97.8
Spot40	3.25	0.1	0.2521	0.0056	0.0029	1467	24	1451	29	1484	61	97.8
Spot41	3.24	0.11	0.2552	0.0068	0.0031	1465	29	1463	35	1498	67	97.7
Spot42	8.92	0.31	0.439	0.012	0.0051	2327	33	2344	53	2402	55	97.6
Spot43	3.399	0.073	0.2566	0.004	0.002	1505	17	1471	21	1508	40	97.5
Spot44	2.03	0.061	0.1849	0.0041	0.003	1125	21	1095	22	1124	74	97.4
Spot46	3.46	0.31	0.264	0.016	0.0063	1508	71	1506	79	1550	120	97.2
Spot47	3.69	0.16	0.27	0.0067	0.0041	1556	34	1542	34	1591	77	96.9
Spot48	3.594	0.093	0.2683	0.005	0.0027	1546	21	1530	25	1583	51	96.7
Spot49	3.65	0.13	0.2673	0.0065	0.0041	1557	30	1531	33	1589	76	96.3
Spot50	3.522	0.092	0.2685	0.0045	0.0025	1531	21	1532	23	1592	49	96.2
Spot51	3.49	0.11	0.2603	0.0066	0.0033	1527	26	1490	34	1552	65	96
Spot53	3.506	0.091	0.2656	0.005	0.0027	1524	20	1517	25	1588	50	95.5
Spot56	3.973	0.069	0.2779	0.0044	0.0019	1627	14	1580	22	1654	33	95.5
Spot58	3.9	0.18	0.267	0.01	0.0048	1605	39	1523	51	1599	94	95.2

Table 2 Detrital zircon U–Pb dating results of analysed samples

Spot59	3.16	0.1	0.2424	0.0055	0.0032	1448	24	1402	29	1481	68	94.7
Spot60	2.82	0.27	0.244	0.014	0.011	1352	69	1408	75	1500	200	93.9
Spot61	6.35	0.13	0.353	0.0065	0.0023	2021	18	1947	31	2092	32	93.1
Spot62	3.274	0.09	0.2457	0.0053	0.0029	1468	21	1414	27	1529	57	92.5
Spot66	4.017	0.084	0.2761	0.0049	0.002	1634	17	1570	25	1698	36	92.5
Spot67	3.045	0.06	0.2348	0.0036	0.0017	1417	15	1360	19	1484	33	91.6
Spot68	2.42	0.11	0.2123	0.0094	0.0066	1243	31	1249	47	1370	150	91.2
Spot72	3.65	0.21	0.263	0.012	0.0063	1579	43	1506	58	1660	120	90.7
Spot73	3.23	0.1	0.2431	0.0053	0.0032	1462	24	1408	26	1552	62	90.7
Spot78	2.86	0.11	0.2239	0.0064	0.0046	1375	32	1301	34	1439	92	90.4
Spot79	3.239	0.097	0.2454	0.005	0.0028	1465	23	1414	26	1569	49	90.1
		Rejected analysis										
Spot3	3.07	0.1	0.2275	0.0064	0.0032	1426	26	1321	34	1578	61	83.7
Spot7	3.47	0.11	0.2424	0.0048	0.0036	1514	25	1398	25	1691	64	82.7
Spot9	2.695	0.087	0.215	0.0047	0.0035	1327	23	1255	25	1524	72	82.3
Spot12	1.718	0.041	0.1595	0.0028	0.0021	1015	15	953	15	1173	53	81.2
Spot13	2.217	0.057	0.1872	0.0042	0.0022	1185	18	1106	23	1388	48	79.7
Spot14	3.17	0.1	0.2267	0.0056	0.0033	1448	25	1319	29	1668	62	79.1
Spot16	2.54	0.13	0.1996	0.0073	0.0052	1275	38	1172	39	1502	97	78
Spot18	1.755	0.058	0.1594	0.0044	0.0024	1034	22	952	24	1224	59	77.8
Spot21	2.585	0.069	0.1995	0.0037	0.0026	1296	19	1172	20	1509	50	77.7
Spot23	2.748	0.05	0.2035	0.0028	0.0018	1340	14	1193	15	1551	34	76.9
Spot24	2.574	0.053	0.1935	0.0035	0.0023	1291	15	1140	19	1498	45	76.1
Spot26	1.477	0.06	0.1418	0.004	0.0028	920	25	854	23	1125	78	75.9
Spot29	2.666	0.082	0.2028	0.0063	0.0038	1315	23	1189	34	1610	67	73.9
Spot35	1.583	0.03	0.144	0.0023	0.0015	964	12	867	13	1186	36	73.1
Spot36	2.556	0.09	0.1925	0.0056	0.0027	1283	26	1134	31	1553	50	73
Spot37	2.504	0.08	0.1923	0.0062	0.0031	1270	23	1133	33	1553	59	73
Spot38	2.36	0.16	0.1823	0.0056	0.0071	1214	47	1084	30	1550	140	69.9
Spot45	3.013	0.059	0.2078	0.0041	0.0022	1411	15	1219	21	1775	37	68.7
Spot52	2.52	0.13	0.1878	0.0079	0.0048	1274	39	1106	43	1624	91	68.1
Spot54	2.459	0.085	0.1837	0.0041	0.0032	1261	27	1091	21	1612	60	67.7
Spot55	2.298	0.089	0.1729	0.0045	0.0038	1207	27	1027	25	1537	75	66.8
Spot57	2.35	0.1	0.1781	0.0049	0.0034	1226	31	1056	27	1589	63	66.5
Spot63	2.68	0.17	0.1869	0.0073	0.0074	1311	47	1102	40	1680	140	65.6
Spot64	4.74	0.33	0.25	0.012	0.012	1753	60	1436	65	2260	140	63.5
Spot65	2.51	0.33	0.182	0.018	0.011	1292	97	1075	99	1760	180	61.1
Spot69	2	0.16	0.1517	0.0096	0.006	1102	54	908	54	1490	130	60.9
Spot70	2.3	0.2	0.164	0.011	0.0098	1219	62	977	60	1640	210	59.6
Spot71	2.85	0.12	0.1736	0.0045	0.0052	1367	29	1031	25	1854	82	55.6
Spot74	1.881	0.074	0.1456	0.0042	0.0028	1078	26	876	23	1589	55	55.1
Spot75	3.92	0.14	0.2057	0.009	0.0072	1626	29	1203	48	2270	86	53
Spot76	1.856	0.067	0.1371	0.0039	0.0037	1063	23	828	22	1614	70	51.3
Spot77	1.92	0.12	0.1372	0.0065	0.008	1088	43	828	37	1650	150	50.2
Spot80	102	28	1.02	0.21	0.091	4720	270	4450	720	4960	210	89.7
A-UJ2												
Spot1	2.002	0.088	0.1855	0.0047	0.0031	1123	30	1096	26	1173	79	93
Spot2	2.114	0.079	0.2023	0.0056	0.0033	1146	27	1185	30	1109	86	107
Spot3	3.68	0.14	0.2659	0.0068	0.0045	1564	29	1519	35	1576	82	96
Spot5	4.831	0.096	0.3235	0.0056	0.0026	1795	17	1808	28	1756	44	103
Spot6	2.222	0.069	0.2036	0.0041	0.0026	1191	22	1195	21	1140	66	105
Spot8	3.58	0.11	0.2621	0.0059	0.003	1540	23	1498	30	1593	57	94
Spot9	3.246	0.078	0.2445	0.0055	0.0028	1475	18	1411	29	1559	56	91
Spot11	3.91	0.11	0.284	0.0048	0.0031	1616	22	1614	24	1619	56	100

Table 2 Detrital zircon U–Pb dating results of analysed samples

Spot17	3.724	0.094	0.2759	0.0056	0.0026	1570	20	1568	29	1585	52	99
Spot20	2.05	0.11	0.1904	0.006	0.005	1126	39	1121	32	1130	130	99
Spot22	3.83	0.11	0.2795	0.0063	0.0031	1604	23	1586	32	1591	60	100
Spot23	0.724	0.031	0.061	0.0023	0.003	549	18	381	14	1358	64	28
Spot24	3.4	0.12	0.2568	0.0062	0.0037	1501	26	1476	32	1543	68	96
Spot25	3.9	0.12	0.265	0.0055	0.0033	1610	24	1516	28	1693	60	90
Spot26	4	0.21	0.2842	0.0089	0.0062	1629	41	1610	45	1650	110	98
Spot27	3.26	0.21	0.2508	0.0097	0.0062	1454	48	1446	48	1460	120	99
Spot28	3.71	0.11	0.2689	0.0057	0.0032	1566	24	1533	29	1587	62	97
Spot30	3.632	0.098	0.2779	0.0056	0.0026	1553	22	1579	28	1534	49	103
Spot31	3.98	0.15	0.2753	0.0068	0.0043	1613	29	1564	34	1680	72	93
Spot33	2.1	0.13	0.1919	0.0086	0.006	1151	44	1129	46	1170	150	96
Spot34	3.85	0.14	0.2761	0.0073	0.0043	1601	30	1568	37	1627	82	96
Spot35	3.84	0.24	0.283	0.012	0.0077	1611	50	1608	63	1620	140	99
Spot37	3.58	0.11	0.2711	0.0065	0.0035	1546	25	1543	33	1558	66	99
Spot39	3.568	0.097	0.2745	0.0054	0.0027	1538	21	1561	27	1489	53	105
Spot40	4.28	0.32	0.302	0.017	0.0091	1675	61	1697	82	1650	170	103
Spot41	3.556	0.08	0.2645	0.004	0.0023	1537	18	1511	20	1542	44	98
Spot42	2.184	0.051	0.2012	0.0035	0.0023	1175	17	1180	19	1145	57	103
Spot43	2.234	0.062	0.2062	0.0039	0.0027	1195	19	1207	21	1169	67	103
Spot44	2.098	0.077	0.1912	0.0044	0.003	1159	25	1128	24	1205	76	94
Spot47	3.37	0.15	0.247	0.01	0.0039	1485	34	1420	52	1566	76	91
Spot48	3.38	0.1	0.2597	0.0061	0.003	1500	24	1486	31	1511	58	98
Spot49	3.76	0.11	0.2775	0.0063	0.0033	1581	24	1579	32	1537	65	103
Spot50	3.66	0.13	0.2762	0.0063	0.0036	1557	29	1569	32	1530	68	103
Spot52	3.78	0.12	0.2759	0.0054	0.0033	1585	27	1573	28	1599	61	98
Spot53	3.845	0.099	0.278	0.0055	0.0026	1605	21	1579	28	1600	50	99
Spot55	2.07	0.14	0.1875	0.0076	0.0059	1124	48	1106	41	1100	150	101
Spot57	3.73	0.11	0.2877	0.0064	0.0031	1571	23	1630	31	1508	63	108
Spot59	3.22	0.14	0.2476	0.0078	0.0047	1471	34	1425	40	1535	90	93
Spot61	3.331	0.082	0.2503	0.0047	0.0025	1484	20	1443	24	1525	50	95
Spot62	2.185	0.082	0.2002	0.0049	0.0031	1168	26	1179	26	1145	79	103
Spot63	10.03	0.19	0.4509	0.0081	0.003	2436	18	2395	36	2455	32	98
Spot64	3.45	0.11	0.2482	0.0046	0.0032	1510	23	1432	24	1593	58	90
Spot65	2.17	0.1	0.1911	0.0043	0.0041	1156	31	1126	23	1163	95	97
Spot68	3.89	0.15	0.288	0.01	0.0045	1608	30	1633	52	1569	86	104
Spot69	1.822	0.06	0.1775	0.0057	0.0028	1062	23	1052	31	1106	71	95
Spot70	3.47	0.075	0.2738	0.0051	0.0023	1517	17	1558	26	1475	49	106
Spot72	4.63	0.13	0.3123	0.0071	0.0032	1754	23	1748	35	1742	55	100
Spot73	4.91	0.1	0.3243	0.0066	0.0023	1808	17	1811	33	1814	38	100
Spot74	3.527	0.088	0.2678	0.0049	0.0029	1537	19	1528	25	1538	55	99
Spot76	3.73	0.1	0.2808	0.0054	0.0029	1579	22	1596	28	1535	55	104
Spot77	3.861	0.077	0.28	0.0051	0.0023	1606	16	1590	26	1597	44	100
Spot79	3.55	0.079	0.2667	0.0052	0.0023	1537	18	1524	27	1524	45	100
Spot80	3.95	0.13	0.2922	0.0072	0.0036	1625	26	1659	35	1554	71	107
Spot81	3.72	0.12	0.2792	0.0055	0.0032	1578	25	1585	28	1577	61	101
Spot82	3.045	0.074	0.2588	0.0049	0.0019	1417	19	1485	25	1371	41	108
Spot83	1.809	0.055	0.1863	0.0041	0.0025	1049	20	1100	22	1045	67	105
Spot84	3.92	0.15	0.28	0.0096	0.0032	1611	31	1589	48	1546	63	103
Spot85	2.842	0.088	0.2409	0.0051	0.003	1356	24	1393	26	1357	66	103
Spot86	2.653	0.079	0.2308	0.0048	0.0025	1316	21	1337	25	1323	55	101
Spot87	3.327	0.077	0.2468	0.0061	0.002	1490	18	1423	31	1445	45	98
Spot88	1.909	0.055	0.1672	0.004	0.0024	1084	19	995	22	1014	65	98
Spot89	2.011	0.073	0.1719	0.0043	0.0031	1111	25	1021	23	1042	85	98
Spot90	3.083	0.066	0.2284	0.004	0.0016	1427	17	1329	21	1359	37	98
Spot91	2.87	0.076	0.2361	0.0042	0.0023	1378	20	1365	22	1396	52	98

Table 2 Detrital zircon U–Pb dating results of analysed samples

Spot92	2.306	0.089	0.2074	0.0051	0.003	1207	28	1214	27	1248	70	97
Spot93	1.856	0.055	0.1605	0.0033	0.0023	1062	19	959	18	987	68	97
Spot94	1.9	0.1	0.1718	0.0054	0.0046	1080	36	1019	29	1070	120	95
Spot95	3.107	0.079	0.2404	0.0043	0.0026	1432	20	1389	22	1463	54	95
Spot96	3.05	0.15	0.245	0.011	0.004	1420	38	1408	57	1502	82	94
Spot98	2.595	0.069	0.2221	0.005	0.0027	1296	19	1297	26	1385	60	94
Spot99	3.08	0.11	0.2246	0.0077	0.0023	1423	28	1304	40	1396	57	93
Spot100	3.82	0.1	0.2652	0.0055	0.0027	1594	22	1514	28	1659	50	91
Spot101	3.129	0.06	0.2333	0.0042	0.0022	1441	15	1351	22	1492	46	91
		Rejected analysis										
Spot4	1.56	0.061	0.1381	0.0033	0.0025	955	23	833	19	1013	72	82
Spot7	0.393	0.018	0.0385	0.0014	0.003	333	13	243.5	8.9	298	77	82
Spot10	2.356	0.078	0.1911	0.0045	0.0032	1230	24	1126	24	1395	71	81
Spot12	1.955	0.069	0.163	0.0047	0.0032	1097	24	972	26	1206	79	81
Spot13	0.661	0.024	0.0602	0.0015	0.0015	515	15	378.7	9.4	474	59	80
Spot14	2.109	0.087	0.2121	0.0049	0.0031	1145	28	1238	26	1011	84	122
Spot15	0.694	0.032	0.0885	0.002	0.0026	527	16	546	12	467	79	117
Spot16	1.981	0.049	0.1929	0.0033	0.0017	1114	17	1136	18	979	49	116
Spot19	0.896	0.031	0.1032	0.0019	0.0022	647	16	634	11	548	75	116
Spot18	0.966	0.025	0.0754	0.0019	0.0021	685	13	469	11	1492	42	31
Spot21	3.51	0.23	0.239	0.012	0.0066	1525	54	1381	63	1690	110	82
Spot29	1.559	0.044	0.1183	0.0029	0.0032	955	18	720	17	1529	62	47
Spot32	1.63	0.048	0.0988	0.0024	0.0031	978	19	607	14	1939	46	31
Spot36	2.79	0.13	0.2085	0.0072	0.0037	1343	34	1219	38	1520	77	80
Spot38	2.703	0.09	0.2064	0.0054	0.003	1323	25	1208	29	1529	61	79
Spot45	2.91	0.13	0.2171	0.0064	0.005	1383	33	1265	34	1548	93	82
Spot46	1.057	0.073	0.0808	0.0033	0.0066	721	36	500	20	1510	120	33
Spot51	3.08	0.11	0.2238	0.0065	0.0037	1428	28	1304	33	1566	70	83
Spot54	1.132	0.041	0.1059	0.003	0.0026	765	20	648	17	1152	63	56
Spot56	2.25	0.14	0.1726	0.0085	0.0047	1194	44	1029	46	1500	99	69
Spot58	0.582	0.028	0.043	0.0017	0.0029	460	18	271	11	1560	56	17
Spot60	1.739	0.085	0.0881	0.0048	0.0084	1020	31	543	28	2270	110	24
Spot66	1.405	0.047	0.1056	0.003	0.0038	893	21	649	17	1538	72	42
Spot67	1.738	0.096	0.1533	0.0064	0.0049	1024	38	922	35	1240	120	74
Spot71	2.101	0.099	0.165	0.0058	0.0046	1156	32	983	32	1435	96	69
Spot75	0.724	0.031	0.061	0.0023	0.003	549	18	381	14	1358	64	28
Spot78	3.112	0.081	0.2287	0.0061	0.0028	1437	21	1326	32	1579	53	84
Spot97	0.708	0.018	0.0543	0.001	0.0023	545	11	340.7	6.4	1521	46	22
BirC-Ky1												
Spot1	2.761	0.056	0.2395	0.0037	0.0019	1342	15	1385	19	1280	45	108.2
Spot2	2.998	0.094	0.2474	0.0059	0.0034	1411	25	1423	31	1435	69	99.2
Spot3	4.257	0.066	0.2887	0.0041	0.0015	1684	13	1636	20	1734	26	94.3
Spot4	4.382	0.076	0.3053	0.0043	0.0016	1709	14	1716	21	1757	28	97.7
Spot10	4.26	0.1	0.3102	0.0056	0.0028	1684	20	1742	27	1682	51	103.6
Spot11	4.002	0.061	0.2831	0.0035	0.0015	1633	12	1606	18	1694	26	94.8
Spot13	9.48	0.13	0.4204	0.0056	0.002	2385	13	2260	25	2491	21	90.7
Spot15	4.44	0.1	0.298	0.006	0.0026	1714	19	1685	30	1748	44	96.4
Spot16	4.211	0.093	0.2896	0.0056	0.0027	1677	17	1638	28	1737	45	94.3
Spot17	4.197	0.075	0.2807	0.0043	0.0017	1672	15	1594	22	1755	29	90.8
Spot21	4.448	0.085	0.2978	0.0048	0.002	1720	16	1682	24	1753	33	95.9
Spot29	4.272	0.071	0.3013	0.0046	0.0017	1687	14	1696	23	1747	29	97.1
Spot31	4.177	0.066	0.2851	0.0037	0.0015	1672	13	1616	19	1748	26	92.4
Spot34	3.918	0.064	0.2814	0.005	0.002	1617	14	1600	26	1637	36	97.7
Spot35	4.275	0.067	0.293	0.0041	0.0015	1687	13	1655	21	1722	27	96.1

Table 2 Detrital zircon U–Pb dating results of analysed samples

Spot38	4.498	0.08	0.3024	0.0053	0.0018	1729	15	1706	26	1777	30	96
Spot40	4.302	0.085	0.2975	0.0052	0.0022	1696	17	1680	25	1713	37	98.1
Spot41	5.02	0.08	0.3289	0.0046	0.0017	1823	13	1832	22	1824	27	100.4
Spot42	4.932	0.076	0.3295	0.0049	0.0015	1807	13	1840	24	1771	25	103.9
Spot43	4.893	0.097	0.3172	0.0047	0.002	1807	17	1775	23	1819	33	97.6
Spot45	4.62	0.11	0.3047	0.0077	0.0024	1757	21	1713	38	1778	40	96.3
Spot46	4.315	0.068	0.2981	0.0048	0.0015	1693	13	1682	24	1726	26	97.5
Spot47	4.231	0.079	0.2941	0.0048	0.0021	1677	15	1663	24	1698	35	97.9
Spot48	4.358	0.068	0.2954	0.0041	0.0015	1707	13	1669	20	1737	26	96.1
Spot51	4.57	0.11	0.2989	0.0053	0.0029	1743	20	1684	26	1802	47	93.5
Spot52	4.572	0.093	0.3145	0.0054	0.0025	1740	17	1761	26	1745	43	100.9
Spot53	11.23	0.17	0.5056	0.0097	0.0026	2543	15	2636	42	2480	27	106.3
Spot55	4.23	0.08	0.2854	0.0047	0.002	1678	16	1617	24	1696	35	95.3
Spot56	4.55	0.091	0.287	0.0048	0.0024	1737	17	1628	24	1773	40	91.8
Spot59	4.6	0.1	0.292	0.0058	0.0025	1749	19	1652	29	1735	43	95.2
Spot61	4.08	0.11	0.2654	0.0046	0.0023	1647	21	1520	23	1679	44	90.5
Spot66	4.331	0.091	0.278	0.0047	0.0023	1698	18	1585	24	1696	41	93.5
Spot68	4.3	0.12	0.2998	0.008	0.0026	1689	23	1688	40	1769	42	95.4
Spot71	4.526	0.099	0.3199	0.0063	0.002	1744	19	1788	31	1747	34	102.3
Spot72	4.784	0.095	0.314	0.0066	0.0024	1780	17	1763	33	1871	39	94.2
Spot73	3.901	0.048	0.2821	0.0034	0.001	1614.7	9.8	1603	17	1709	17	93.8
Spot74	4.656	0.088	0.3075	0.005	0.0022	1759	16	1727	25	1890	33	91.4
Spot76	3.995	0.071	0.2829	0.0045	0.0015	1632	14	1609	23	1757	25	91.6
Spot78	3.599	0.093	0.2649	0.0052	0.0023	1544	21	1516	27	1651	43	91.8
Spot79	3.422	0.062	0.267	0.0041	0.0018	1507	14	1524	21	1617	34	94.2
Spot80	4.399	0.072	0.304	0.0046	0.0017	1709	14	1709	23	1750	28	97.7
Spot81	2.843	0.066	0.2417	0.0041	0.0021	1366	17	1398	22	1400	43	99.9
Spot82	5.346	0.096	0.338	0.0054	0.0018	1876	15	1875	26	1955	25	95.9
Spot83	3.6	0.074	0.2667	0.0047	0.0018	1546	16	1523	24	1680	32	90.7
Spot86	4.243	0.087	0.298	0.0057	0.0021	1682	17	1682	28	1781	34	94.4
Spot88	3.743	0.07	0.2874	0.0049	0.002	1578	15	1627	25	1661	36	98
Spot89	3.49	0.1	0.2597	0.0065	0.0027	1521	24	1487	33	1651	50	90.1
Spot96	4.67	0.11	0.3092	0.0053	0.0018	1760	19	1735	26	1831	29	94.8
		Rejected analysis										
Spot5	3.395	0.089	0.2294	0.0041	0.0022	1498	21	1333	21	1775	36	75.1
Spot6	3.938	0.062	0.2751	0.0046	0.0018	1629	13	1565	23	1747	31	89.6
Spot7	2.985	0.051	0.2054	0.0035	0.0017	1403	13	1206	19	1763	28	68.4
Spot8	3.322	0.061	0.2447	0.0037	0.0016	1482	14	1410	19	1633	30	86.3
Spot9	2.57	0.058	0.2004	0.0036	0.0016	1290	17	1178	19	1550	32	76
Spot12	3.055	0.059	0.2114	0.0034	0.0015	1423	14	1236	18	1743	27	70.9
Spot14	3.571	0.08	0.2263	0.0036	0.0016	1541	18	1315	19	1931	24	68.1
Spot18	6.01	0.13	0.3027	0.0059	0.002	1974	18	1703	29	2360	23	72.2
Spot19	3.774	0.056	0.2698	0.0038	0.0015	1588	12	1538	19	1724	27	89.2
Spot20	2.854	0.075	0.2063	0.0054	0.0021	1370	20	1212	29	1729	36	70.1
Spot22	3.688	0.065	0.2555	0.0045	0.002	1567	14	1466	23	1756	34	83.5
Spot23	3.514	0.064	0.2546	0.0043	0.0016	1527	14	1461	22	1713	29	85.3
Spot24	3.439	0.074	0.241	0.0051	0.002	1515	17	1391	26	1768	33	78.7
Spot25	2.821	0.048	0.2026	0.0033	0.0017	1360	13	1189	18	1670	31	71.2
Spot26	3.32	0.054	0.233	0.0037	0.0016	1488	12	1349	19	1717	28	78.6
Spot27	1250	350	11.7	4.5	0.12	7140	320	######	#####	4970	270	311.9
Spot28	2.271	0.032	0.1643	0.0021	0.0012	1203	10	982	11	1592	24	61.7
Spot30	8.45	0.15	0.3745	0.0068	0.0027	2283	16	2048	32	2374	30	86.3
Spot32	3.51	0.1	0.207	0.0055	0.0027	1527	23	1212	29	1831	43	66.2
Spot33	#####	#####	10.3	4.3	0.11	7020	520	######	#####	4700	270	353.2
Spot36	2.45	0.04	0.1786	0.0024	0.0012	1257	12	1059	13	1641	22	64.5
Spot37	2.93	0.082	0.2272	0.0062	0.0028	1393	19	1319	32	1577	56	83.6

Table 2 Detrital zircon U–Pb dating results of analysed samples

Spot39	2.729	0.055	0.2181	0.0041	0.0016	1335	15	1271	22	1510	32	84.2
Spot44	3.389	0.066	0.2473	0.0045	0.0015	1500	15	1423	23	1738	25	81.9
Spot49	3.55	0.063	0.2569	0.0045	0.0015	1535	14	1473	23	1724	26	85.4
Spot50	3.809	0.085	0.2669	0.0055	0.0018	1596	19	1524	28	1750	32	87.1
Spot54	1.918	0.047	0.1496	0.0031	0.0018	1091	16	898	17	1581	35	56.8
Spot57	3.808	0.08	0.2655	0.0055	0.0018	1589	17	1516	28	1739	30	87.2
Spot58	3.657	0.059	0.2559	0.004	0.0015	1559	13	1468	21	1733	27	84.7
Spot60	3.78	0.1	0.2563	0.0057	0.0022	1586	22	1469	29	1744	38	84.2
Spot62	3.157	0.054	0.2291	0.004	0.0017	1446	13	1328	21	1666	32	79.7
Spot63	3.019	0.059	0.2024	0.0032	0.0015	1410	15	1188	17	1774	26	67
Spot64	3.233	0.057	0.2227	0.0034	0.0015	1464	13	1295	18	1727	27	75
Spot65	7.65	0.2	0.378	0.01	0.003	2200	22	2066	47	2335	35	88.5
Spot67	3.869	0.061	0.2628	0.0038	0.0015	1606	12	1506	19	1786	25	84.3
Spot69	4.37	0.13	0.2645	0.0063	0.0018	1704	25	1511	32	2024	27	74.7
Spot70	1.763	0.031	0.1566	0.002	0.0011	1031	11	937	11	1353	25	69.3
Spot75	2.765	0.055	0.2117	0.0036	0.0014	1345	15	1241	20	1622	26	76.5
Spot77	8.04	0.13	0.374	0.0052	0.0021	2237	14	2049	25	2508	21	81.7
Spot84	4.856	0.073	0.3125	0.0047	0.0016	1794	12	1751	23	1972	23	88.8
Spot85	3.324	0.067	0.2151	0.0045	0.0021	1483	16	1257	24	1926	32	65.3
Spot87	3.848	0.089	0.2751	0.007	0.0018	1603	19	1564	35	1757	34	89
Spot91	3.643	0.052	0.2482	0.0036	0.0016	1561	11	1428	19	1815	26	78.7
J-Ky8												
Spot2	10.46	0.14	0.4271	0.0056	0.0019	2476	13	2291	25	2521	19	90.9
Spot5	3.92	0.13	0.2695	0.0067	0.0036	1612	27	1537	34	1597	65	96.2
Spot6	5.498	0.097	0.3385	0.0042	0.0018	1897	15	1880	20	1835	30	102.5
Spot7	5.229	0.082	0.3275	0.004	0.0018	1856	13	1827	20	1811	30	100.9
Spot8	4.877	0.071	0.3069	0.0046	0.002	1796	12	1728	23	1827	32	94.6
Spot9	3.016	0.074	0.229	0.0042	0.0021	1411	19	1328	22	1469	47	90.4
Spot10	3.983	0.049	0.2716	0.003	0.0013	1629	10	1548	15	1694	22	91.4
Spot11	4.305	0.07	0.2878	0.0041	0.0019	1694	13	1629	20	1745	33	93.4
Spot12	4.73	0.12	0.3108	0.0042	0.0026	1759	16	1747	20	1789	40	97.7
Spot13	4.511	0.07	0.3132	0.0037	0.0016	1733	13	1755	18	1745	27	100.6
Spot14	3.648	0.06	0.2612	0.004	0.0013	1561	13	1497	21	1646	23	90.9
Spot15	3.917	0.077	0.2919	0.0042	0.0021	1615	16	1650	21	1593	40	103.6
Spot16	4.775	0.078	0.3167	0.005	0.0018	1781	14	1772	25	1805	29	98.2
Spot17	9.25	0.13	0.4207	0.0064	0.0021	2362	13	2261	29	2479	23	91.2
Spot18	4.906	0.069	0.3288	0.0041	0.0018	1803	12	1832	20	1804	30	101.6
Spot19	8.99	0.28	0.4142	0.0099	0.003	2332	28	2236	44	2415	34	92.6
Spot20	5.244	0.088	0.3254	0.004	0.0019	1863	15	1815	19	1925	29	94.3
Spot23	4.208	0.065	0.2939	0.004	0.0016	1679	13	1662	20	1705	28	97.5
Spot25	4.233	0.076	0.2889	0.0047	0.0018	1683	15	1635	24	1698	31	96.3
Spot26	4.109	0.099	0.2787	0.005	0.0019	1653	20	1584	25	1737	33	91.2
Spot28	3.82	0.12	0.28	0.01	0.0026	1595	25	1590	51	1648	47	96.5
Spot30	4.24	0.11	0.2981	0.0061	0.0027	1683	21	1687	29	1695	47	99.5
Spot31	3.991	0.072	0.2813	0.0038	0.0014	1631	15	1599	19	1706	25	93.7
Spot33	5.29	0.11	0.3233	0.0071	0.0023	1864	18	1808	34	1932	36	93.6
Spot34	2.499	0.074	0.2183	0.0036	0.0027	1271	19	1272	19	1324	59	96.1
Spot36	4.91	0.1	0.3255	0.0052	0.0026	1806	18	1816	25	1784	42	101.8
Spot38	4.42	0.11	0.3036	0.0064	0.0034	1712	22	1714	33	1756	57	97.6
Spot41	4.78	0.11	0.3052	0.0056	0.0036	1785	19	1716	28	1897	55	90.5
Spot42	5.024	0.095	0.309	0.0053	0.002	1822	16	1735	26	1888	32	91.9
Spot43	4.194	0.076	0.2907	0.0048	0.0017	1678	15	1644	24	1686	31	97.5
Spot44	4.368	0.057	0.299	0.0038	0.0014	1706	11	1685	19	1715	24	98.3
Spot45	3.487	0.071	0.2594	0.0042	0.0021	1521	16	1487	21	1558	41	95.4

Table 2 Detrital zircon U–Pb dating results of analysed samples

Spot48	4.121	0.099	0.2942	0.0052	0.0026	1656	19	1665	25	1607	49	103.6
Spot50	4.081	0.06	0.278	0.004	0.0016	1652	12	1580	20	1699	28	93
Spot51	4.413	0.076	0.2862	0.0056	0.0017	1718	14	1625	28	1756	30	92.5
Spot52	3.892	0.089	0.268	0.0051	0.002	1609	18	1530	26	1670	37	91.6
Spot54	3.872	0.091	0.2735	0.0047	0.0026	1608	19	1562	25	1618	47	96.5
Spot56	4.246	0.073	0.287	0.0038	0.0017	1680	14	1625	19	1761	28	92.3
Spot58	4.531	0.076	0.311	0.0043	0.0019	1737	13	1744	21	1739	32	100.3
Spot62	3.775	0.087	0.263	0.0047	0.002	1592	18	1507	23	1671	36	90.2
Spot63	4.403	0.074	0.3027	0.0046	0.002	1713	14	1703	23	1690	27	100.8
Spot64	4.99	0.1	0.3165	0.0049	0.0023	1816	17	1778	24	1860	36	95.6
Spot65	4.281	0.07	0.2842	0.0044	0.0016	1689	14	1614	22	1727	27	93.5
Spot66	4.94	0.073	0.3091	0.0039	0.0016	1812	12	1735	19	1861	26	93.2
Spot68	11.08	0.18	0.4776	0.0083	0.0036	2529	15	2516	36	2611	33	96.4
Spot69	10.78	0.21	0.4718	0.008	0.0035	2503	18	2488	35	2593	33	96
Spot70	4.6	0.078	0.3037	0.0046	0.0018	1747	14	1708	23	1878	29	90.9
Spot71	3.704	0.068	0.2763	0.0058	0.0018	1572	15	1571	29	1684	32	93.3
Spot72	4.353	0.077	0.3	0.0038	0.0021	1701	15	1691	19	1731	34	97.7
Spot73	4.33	0.11	0.2958	0.0058	0.003	1697	20	1668	29	1692	54	98.6
Spot74	4.74	0.11	0.3134	0.0061	0.0027	1776	21	1760	30	1796	42	98
		Rejected analysis										
Spot1	5.33	0.11	0.2345	0.004	0.0036	1871	18	1357	21	2400	39	56.5
Spot3	5.337	0.071	0.3061	0.0038	0.0017	1873	11	1721	19	1947	25	88.4
Spot4	3.387	0.055	0.2279	0.0036	0.0014	1502	13	1322	19	1743	25	75.8
Spot21	2.431	0.033	0.1609	0.0022	0.0015	1251.7	9.8	962	12	1744	25	55.2
Spot22	4.38	0.12	0.2795	0.0049	0.0022	1710	22	1588	25	1910	33	83.1
Spot24	8.21	0.15	0.3787	0.006	0.0024	2257	17	2068	28	2482	25	83.3
Spot27	3.152	0.064	0.2419	0.0042	0.0022	1444	16	1395	22	1569	42	88.9
Spot29	3.69	0.1	0.2677	0.0056	0.0032	1569	22	1530	28	1708	59	89.6
Spot32	2.892	0.063	0.212	0.0043	0.0017	1380	16	1238	23	1699	31	72.9
Spot35	3.9	0.12	0.2331	0.009	0.0039	1615	27	1348	47	1959	60	68.8
Spot37	2.523	0.094	0.2131	0.0049	0.0033	1278	27	1249	25	1443	70	86.6
Spot39	3.13	0.13	0.1779	0.0043	0.0064	1437	29	1060	23	2121	84	50
Spot40	7.21	0.14	0.3069	0.0053	0.0033	2139	17	1724	26	2625	31	65.7
Spot46	4.67	0.26	0.2667	0.0085	0.0071	1724	41	1519	43	2131	82	71.3
Spot47	2.499	0.067	0.2038	0.0041	0.0025	1269	19	1195	22	1467	56	81.5
Spot49	5.36	0.12	0.3077	0.0055	0.0029	1878	19	1728	27	2080	41	83.1
Spot53	2.148	0.029	0.18	0.0024	0.0012	1164.8	9.6	1067	13	1374	27	77.7
Spot55	3.809	0.079	0.242	0.0049	0.0022	1594	17	1396	25	1840	35	75.9
Spot57	5.65	0.11	0.2599	0.004	0.0021	1920	16	1489	20	2372	23	62.8
Spot59	6.54	0.15	0.2804	0.0054	0.0028	2053	21	1592	27	2437	31	65.3
Spot60	4.399	0.067	0.2778	0.0037	0.0019	1710	13	1579	19	1827	31	86.4
Spot61	9.22	0.14	0.4088	0.0055	0.0024	2359	14	2208	25	2464	26	89.6
Spot67	4.398	0.067	0.2541	0.0036	0.0019	1712	13	1460	18	1950	28	74.9
Spot75	3.352	0.056	0.2261	0.0027	0.0017	1491	13	1315	15	1707	29	77
E-Ky7												
Spot1	4.302	0.069	0.2957	0.0043	0.0019	1693	13	1671	22	1697	34	98.5
Spot2	3.606	0.099	0.261	0.0033	0.0026	1550	22	1494	17	1576	48	94.8
Spot3	4.423	0.084	0.306	0.0042	0.0019	1714	15	1719	21	1687	33	101.9
Spot4	4.277	0.08	0.2888	0.0042	0.002	1690	15	1634	21	1724	34	94.8
Spot5	4.397	0.09	0.2995	0.0048	0.0025	1710	17	1690	24	1700	44	99.4
Spot6	4.377	0.074	0.3065	0.0033	0.0016	1705	14	1723	16	1679	30	102.6
Spot7	4.259	0.076	0.2922	0.0041	0.0018	1685	15	1651	20	1717	33	96.2
Spot8	5.9	0.12	0.3431	0.0055	0.0025	1958	18	1900	26	2013	36	94.4
Spot9	3.787	0.06	0.2713	0.0036	0.0018	1589	13	1547	18	1648	33	93.9

Table 2 Detrital zircon U–Pb dating results of analysed samples

Spot11	4.376	0.076	0.2914	0.0049	0.0019	1707	14	1647	24	1764	31	93.4
Spot12	5.103	0.093	0.3219	0.0045	0.0021	1836	16	1798	22	1872	34	96.0
Spot13	4.46	0.067	0.3041	0.0035	0.0015	1723	13	1714	18	1728	25	99.2
Spot14	4.446	0.075	0.2891	0.0046	0.0018	1720	14	1639	23	1821	29	90.0
Spot16	4.755	0.079	0.3064	0.004	0.0018	1778	14	1722	20	1833	29	93.9
Spot17	4.124	0.085	0.2838	0.0043	0.0022	1658	18	1610	22	1696	38	94.9
Spot18	3.985	0.087	0.2736	0.0042	0.0024	1635	18	1560	21	1696	43	92.0
Spot19	4.177	0.077	0.2898	0.0042	0.0022	1668	15	1639	21	1701	38	96.4
Spot20	9.92	0.15	0.4241	0.006	0.0026	2425	14	2278	27	2529	26	90.1
Spot21	4.435	0.094	0.2993	0.0056	0.0025	1718	17	1686	28	1769	41	95.3
Spot23	8.12	0.13	0.4043	0.006	0.0024	2246	15	2187	28	2264	30	96.6
Spot24	3.906	0.078	0.2701	0.0039	0.0021	1617	17	1544	20	1705	38	90.6
Spot25	4.63	0.13	0.3063	0.0063	0.0034	1757	24	1726	30	1753	58	98.5
Spot26	13.12	0.24	0.4974	0.0083	0.0037	2695	17	2599	36	2730	33	95.2
Spot27	4.95	0.1	0.3184	0.0051	0.0027	1808	18	1783	25	1828	44	97.5
Spot28	9.44	0.17	0.4181	0.0063	0.0031	2378	16	2253	29	2471	32	91.2
Spot29	4.415	0.069	0.3054	0.0041	0.0016	1721	13	1719	20	1708	29	100.6
Spot30	4.24	0.089	0.2899	0.0051	0.0016	1682	18	1640	25	1690	29	97.0
Spot31	4.38	0.08	0.3016	0.004	0.0015	1706	16	1700	20	1690	27	100.6
Spot32	4.533	0.076	0.2905	0.0044	0.0019	1734	14	1643	22	1817	31	90.4
Spot33	5.443	0.085	0.3445	0.0043	0.0015	1893	13	1907	21	1868	25	102.1
Spot34	4.62	0.094	0.318	0.0053	0.0022	1754	17	1785	26	1711	39	104.3
Spot35	2.594	0.069	0.216	0.0038	0.0025	1292	20	1259	20	1322	57	95.2
Spot36	4.291	0.081	0.2951	0.0039	0.0017	1687	16	1668	20	1698	29	98.2
Spot37	4.498	0.093	0.3093	0.0043	0.0022	1727	17	1736	21	1706	38	101.8
Spot38	4.466	0.088	0.3078	0.0049	0.002	1722	17	1730	25	1697	35	101.9
Spot39	9.1	0.2	0.4356	0.0098	0.0044	2348	20	2335	45	2385	48	97.9
Spot40	4.881	0.09	0.3166	0.0045	0.002	1798	15	1773	22	1814	32	97.7
Spot41	2.637	0.062	0.2228	0.0034	0.002	1307	18	1296	18	1313	47	98.7
Spot42	4.138	0.094	0.2778	0.0048	0.0023	1664	18	1579	24	1736	39	91.0
Spot44	5.44	0.13	0.3325	0.0061	0.0031	1894	20	1848	29	1934	47	95.6
Spot45	4.44	0.11	0.2973	0.0052	0.0027	1713	21	1678	26	1758	47	95.4
Spot47	5.13	0.1	0.3323	0.0049	0.0024	1844	17	1848	24	1829	39	101.0
Spot48	4.281	0.084	0.2954	0.0042	0.0023	1690	16	1668	21	1708	40	97.7
Spot49	4.471	0.076	0.3048	0.0043	0.002	1725	14	1714	21	1704	34	100.6
Spot50	4.17	0.12	0.2931	0.0062	0.0033	1665	25	1660	30	1663	59	99.8
Spot52	4.944	0.094	0.3094	0.0046	0.0021	1809	16	1739	22	1873	33	92.8
Spot53	4.315	0.094	0.3007	0.0057	0.0025	1695	18	1697	28	1722	44	98.5
Spot55	3.063	0.09	0.2447	0.0051	0.0027	1421	22	1412	26	1423	57	99.2
Spot56	4.67	0.12	0.3082	0.0062	0.0034	1758	22	1735	30	1794	56	96.7
Spot57	3.5	0.11	0.2568	0.005	0.0033	1525	24	1472	26	1570	64	93.8
Spot58	3.235	0.083	0.2448	0.0045	0.0029	1464	19	1410	23	1548	56	91.1
Spot60	4.182	0.085	0.2834	0.0044	0.0018	1673	16	1607	22	1744	30	92.1
Spot61	4.648	0.085	0.3027	0.0048	0.0021	1760	15	1706	24	1826	34	93.4
Spot62	4.6	0.1	0.3028	0.0051	0.0022	1748	19	1704	25	1796	37	94.9
Spot63	4.28	0.1	0.2881	0.0064	0.0034	1688	19	1634	31	1726	57	94.7
Spot64	4.34	0.1	0.2942	0.0053	0.0028	1694	20	1665	26	1727	48	96.4
Spot65	4.226	0.074	0.2906	0.0045	0.0022	1680	15	1643	23	1733	38	94.8
Spot66	6.31	0.14	0.3719	0.0079	0.003	2016	20	2035	37	2060	41	98.8
Spot68	5.4	0.1	0.3388	0.0053	0.0016	1885	16	1879	25	1849	25	101.6
Spot70	5.167	0.093	0.3228	0.007	0.0025	1847	15	1801	34	1906	39	94.5
Spot72	4.807	0.095	0.3303	0.0048	0.0018	1791	16	1843	23	1698	32	108.5
Spot73	4.5	0.092	0.3043	0.0044	0.0017	1729	17	1711	22	1723	30	99.3
Spot74	4.473	0.098	0.3012	0.0046	0.0023	1728	18	1696	23	1821	38	93.1
Spot75	2.976	0.063	0.2419	0.0047	0.0022	1397	16	1397	24	1425	46	98.0
Spot77	4.58	0.14	0.3105	0.0056	0.0035	1741	25	1741	28	1853	55	94.0

Table 2 Detrital zircon U–Pb dating results of analysed samples

Spot78	4.089	0.08	0.2898	0.0062	0.0019	1650	16	1639	31	1811	31	90.5
Spot79	5.13	0.11	0.3299	0.0057	0.0027	1845	18	1842	28	1987	40	92.7
Spot80	4.397	0.093	0.3091	0.0055	0.0022	1711	18	1735	27	1672	39	103.8
Spot81	4.91	0.12	0.322	0.0051	0.002	1802	21	1800	24	1714	35	105.0
Spot82	5.04	0.11	0.3279	0.0057	0.0023	1827	18	1826	28	1711	42	106.7
Spot83	4.76	0.099	0.3177	0.0051	0.002	1779	18	1779	25	1714	34	103.8
Spot84	5.365	0.093	0.3382	0.0048	0.0017	1879	15	1877	23	1821	28	103.1
Spot85	5.48	0.11	0.341	0.0058	0.0025	1897	17	1892	28	1849	39	102.3
Spot86	5.033	0.093	0.3264	0.0056	0.0019	1821	16	1822	27	1818	29	100.2
Spot87	3.6	0.15	0.263	0.0081	0.0051	1554	33	1502	41	1606	94	93.5
Spot88	4.972	0.094	0.323	0.0061	0.0023	1814	16	1803	30	1807	38	99.8
Spot89	4.91	0.11	0.3222	0.0061	0.0023	1803	20	1802	30	1861	37	96.8
Spot90	10.55	0.23	0.4425	0.0066	0.0027	2484	20	2360	29	2612	25	90.4
Spot91	4.223	0.08	0.2971	0.0055	0.002	1677	15	1675	27	1700	37	98.5
Spot93	5.091	0.073	0.3276	0.0054	0.0016	1832	12	1828	26	1849	26	98.9
Spot94	10.74	0.2	0.4729	0.0079	0.0033	2501	17	2498	35	2573	31	97.1
Spot96	4.291	0.081	0.3015	0.0045	0.0021	1691	15	1697	22	1688	36	100.5
Spot97	14.42	0.23	0.5242	0.0085	0.0032	2775	15	2717	36	2817	26	96.5
Spot98	4.433	0.086	0.3056	0.0047	0.0018	1720	16	1718	23	1699	31	101.1
Spot99	4.483	0.093	0.3051	0.0051	0.0021	1723	18	1717	25	1701	37	100.9
Spot100	4.416	0.089	0.3028	0.0055	0.0023	1714	17	1711	27	1720	41	99.5
Spot101	4.5	0.091	0.3063	0.0049	0.0019	1727	17	1723	24	1739	34	99.1
Spot103	4.7	0.12	0.3002	0.006	0.0028	1759	21	1692	30	1837	45	92.1
Spot106	5.1	0.082	0.3371	0.0059	0.002	1838	14	1870	29	1820	33	102.7
Spot107	4.41	0.12	0.3143	0.0058	0.0025	1711	23	1763	29	1726	43	102.1
Spot108	4.446	0.089	0.288	0.0045	0.0018	1721	16	1630	22	1723	32	94.6
Spot109	4.135	0.066	0.2938	0.0043	0.0019	1662	13	1660	21	1719	35	96.6
Spot110	4.878	0.089	0.315	0.0044	0.002	1797	16	1766	22	1830	34	96.5
Spot111	5.09	0.12	0.3261	0.0067	0.0028	1830	20	1817	33	1865	45	97.4
Spot112	3.24	0.082	0.2481	0.0045	0.0025	1464	19	1427	23	1536	43	92.9
Spot113	4.654	0.094	0.3069	0.0059	0.0023	1758	17	1723	29	1804	38	95.5
Spot115	4.353	0.091	0.3026	0.0048	0.0017	1706	17	1703	24	1701	29	100.1
Spot116	4.57	0.075	0.3112	0.0046	0.0017	1741	14	1747	22	1714	31	101.9
Spot117	4.205	0.09	0.2955	0.0054	0.0024	1670	17	1667	27	1701	41	98.0
Spot118	4.31	0.11	0.2906	0.0054	0.0027	1695	21	1643	27	1811	44	90.7
Spot120	4.579	0.092	0.31	0.0052	0.002	1747	17	1739	26	1735	34	100.2
		Rejected analysis										
Spot10	3.678	0.071	0.2549	0.0047	0.0021	1563	15	1464	25	1676	37	87.4
Spot15	0.39	0.01	0.05444	0.0009	0.0014	333.6	7	342.1	5.2	275	58	124.4
Spot22	0.808	0.024	0.0953	0.0018	0.0021	601	13	586	11	656	73	89.3
Spot43	1.672	0.034	0.1132	0.0019	0.0017	1000	13	691	11	1733	28	39.9
Spot46	2.17	0.11	0.1535	0.0075	0.0019	1157	38	916	42	1691	32	54.2
Spot51	3.347	0.096	0.2467	0.005	0.0032	1490	22	1422	26	1596	60	89.1
Spot54	5.503	0.099	0.2675	0.0038	0.0024	1900	15	1528	19	2331	26	65.6
Spot59	2.032	0.057	0.1445	0.0033	0.0023	1123	19	870	18	1682	44	51.7
Spot67	2.483	0.053	0.1687	0.0036	0.0026	1268	16	1004	20	1684	46	59.6
Spot69	1.662	0.036	0.1352	0.0029	0.0018	995	14	817	16	1613	34	50.7
Spot71	3.97	0.11	0.2703	0.0056	0.0023	1626	22	1545	28	1769	38	87.3
Spot76	6.23	0.11	0.2913	0.0052	0.0018	2010	16	1646	26	2518	19	65.4
Spot92	3.566	0.061	0.2602	0.0045	0.0016	1545	14	1490	23	1714	28	86.9
Spot95	3.717	0.06	0.2504	0.0047	0.0016	1573	13	1439	24	1716	29	83.9
Spot102	3.903	0.075	0.2575	0.0057	0.0024	1614	15	1479	29	1903	37	77.7
Spot104	5.72	0.1	0.3201	0.0044	0.0022	1931	15	1792	22	2108	30	85.0
Spot105	12.05	0.49	0.3109	0.0083	0.011	2589	37	1742	41	3214	63	54.2
Spot114	4.26	0.14	0.261	0.0081	0.0031	1684	27	1499	42	1695	54	88.4
Spot119	3.227	0.083	0.2421	0.0056	0.0026	1467	20	1401	30	1730	44	81.0

Table 2 Detrital zircon U–Pb dating results of analysed samples

E-Mo13												
Spot1	10.69	0.14	0.5022	0.0068	0.0014	2494	12	2626	29	2407	15	109.1
Spot2	10.94	0.17	0.4987	0.0068	0.0021	2518	15	2609	29	2445	23	106.7
Spot3	3.337	0.05	0.2474	0.0035	0.0014	1490	12	1424	18	1586	29	90.1
Spot4	3.647	0.058	0.2769	0.0041	0.0014	1561	13	1575	21	1562	27	100.8
Spot5	3.095	0.045	0.2564	0.0033	0.0008	1430	11	1470	17	1383	18	106.3
Spot8	4.245	0.098	0.3069	0.005	0.0025	1688	19	1724	25	1640	46	105.1
Spot9	5.52	0.1	0.3545	0.0056	0.0019	1903	16	1960	26	1866	29	105
Spot10	11.75	0.16	0.5086	0.007	0.0017	2584	13	2649	30	2526	18	104.9
Spot11	4.695	0.061	0.3228	0.0038	0.0012	1768	11	1802	19	1729	21	104.2
Spot12	9.44	0.14	0.4598	0.0067	0.002	2382	14	2437	29	2340	22	104.1
Spot16	3.97	0.12	0.2918	0.006	0.0033	1630	24	1651	31	1611	61	102.5
Spot17	4.016	0.074	0.2917	0.0045	0.0017	1640	15	1650	22	1620	32	101.9
Spot18	5.403	0.095	0.3405	0.0068	0.0017	1883	15	1887	33	1854	27	101.8
Spot21	4.803	0.072	0.324	0.0044	0.0013	1787	13	1808	21	1777	21	101.7
Spot22	9.9	0.13	0.462	0.0056	0.0019	2423	12	2447	25	2415	20	101.3
Spot23	3.67	0.12	0.2757	0.0068	0.0036	1560	25	1570	35	1574	66	99.7
Spot25	4.204	0.07	0.2969	0.0036	0.0014	1675	14	1677	18	1669	26	100.5
Spot26	4.519	0.087	0.3066	0.0058	0.0018	1732	16	1726	29	1728	20	99.9
Spot28	4.147	0.082	0.2871	0.0052	0.0017	1665	16	1629	26	1747	28	93.2
Spot29	21.16	0.27	0.63	0.0096	0.0028	3147	13	3146	38	3159	18	99.6
Spot30	4.69	0.076	0.3156	0.004	0.0013	1762	14	1769	19	1777	21	99.5
Spot31	7.44	0.12	0.3986	0.0056	0.0016	2161	14	2161	26	2172	21	99.5
Spot32	14.18	0.24	0.5349	0.0086	0.0031	2766	16	2760	36	2780	27	99.3
Spot33	4.279	0.072	0.2979	0.0038	0.0013	1689	13	1680	19	1694	24	99.2
Spot36	3.65	0.17	0.2733	0.0084	0.005	1560	37	1559	43	1573	97	99.1
Spot37	4.73	0.15	0.3159	0.0068	0.0037	1776	28	1767	34	1784	62	99
Spot38	4.361	0.074	0.3008	0.0051	0.002	1703	14	1694	25	1714	35	98.8
Spot39	9.23	0.15	0.4391	0.0067	0.0018	2362	14	2345	30	2379	21	98.6
Spot40	4.511	0.058	0.3068	0.004	0.0015	1731	11	1728	20	1755	26	98.5
Spot41	4.277	0.076	0.2984	0.0044	0.0017	1688	15	1682	22	1709	30	98.4
Spot43	4.176	0.069	0.2941	0.0046	0.0015	1667	13	1661	23	1689	28	98.3
Spot44	3.961	0.062	0.2865	0.004	0.0013	1628	12	1625	20	1653	23	98.3
Spot45	3.476	0.091	0.2639	0.0056	0.0028	1518	21	1512	28	1550	57	97.5
Spot46	3.521	0.072	0.2659	0.0045	0.0017	1535	16	1522	23	1561	32	97.5
Spot47	4.306	0.073	0.2968	0.004	0.0016	1695	14	1675	20	1720	28	97.4
Spot48	3.478	0.063	0.2656	0.004	0.0014	1519	14	1517	20	1558	29	97.4
Spot49	4.403	0.081	0.2995	0.0048	0.0015	1714	15	1688	24	1744	26	96.8
Spot51	3.92	0.11	0.2801	0.0052	0.0027	1615	22	1590	26	1643	52	96.8
Spot52	4.188	0.084	0.2961	0.0055	0.0017	1675	16	1671	27	1735	28	96.3
Spot53	4.278	0.071	0.2938	0.0044	0.0018	1689	14	1661	22	1731	33	96
Spot54	3.95	0.11	0.2813	0.0058	0.0031	1620	23	1596	29	1664	58	95.9
Spot55	3.932	0.091	0.2821	0.005	0.0019	1620	19	1601	25	1692	33	94.6
Spot56	4.06	0.084	0.2841	0.0054	0.002	1648	16	1614	28	1714	34	94.2
Spot57	3.972	0.096	0.2808	0.0053	0.0027	1629	20	1595	27	1697	47	94
Spot61	5.44	0.11	0.3269	0.0054	0.0022	1888	17	1824	27	1941	33	94
Spot62	3.05	0.061	0.237	0.0038	0.0017	1419	15	1371	20	1469	37	93.3
Spot63	4.118	0.064	0.3031	0.0042	0.0015	1657	13	1706	21	1586	29	107.6
Spot64	4.316	0.07	0.2924	0.0047	0.0016	1694	13	1653	24	1776	27	93.1
Spot65	4.03	0.063	0.2791	0.0037	0.0016	1638	13	1588	18	1707	28	93
Spot66	4.463	0.058	0.2942	0.0035	0.0014	1725	11	1662	17	1796	23	92.5
Spot69	3.847	0.074	0.2758	0.0051	0.0019	1602	15	1572	26	1700	33	92.5
Spot70	3.549	0.042	0.2614	0.0027	0.0009	1538.8	9.1	1496	14	1620	18	92.3
Spot71	6.74	0.13	0.3645	0.0057	0.0015	2080	17	2004	27	2174	20	92.2

Table 2 Detrital zircon U–Pb dating results of analysed samples

Spot72	5.47	0.083	0.3279	0.0052	0.0017	1894	13	1827	25	1987	24	91.9
Spot73	4.44	0.11	0.2964	0.008	0.0026	1718	20	1672	40	1820	39	91.9
Spot74	3.931	0.082	0.2751	0.004	0.0021	1623	17	1570	21	1711	37	91.8
Spot75	3.261	0.07	0.2483	0.0048	0.0018	1469	17	1429	25	1558	35	91.7
Spot78	3.827	0.056	0.2702	0.0032	0.0012	1599	12	1541	16	1685	22	91.5
Spot80	3.268	0.07	0.2477	0.0044	0.0022	1469	17	1427	22	1561	44	91.4
Spot82	4.664	0.072	0.3009	0.0051	0.0014	1759	13	1694	25	1855	22	91.3
Spot83	4.593	0.069	0.2969	0.0042	0.0018	1748	13	1675	21	1837	29	91.2
Spot84	8.39	0.11	0.3987	0.0051	0.0018	2275	12	2162	24	2386	20	90.6
Spot85	3.947	0.068	0.2733	0.0037	0.0017	1622	14	1558	19	1720	29	90.6
Spot86	3.195	0.059	0.2433	0.0039	0.0016	1454	14	1403	20	1551	31	90.5
Spot88	8.51	0.12	0.4002	0.0063	0.0021	2285	13	2168	29	2398	23	90.4
Spot89	5.254	0.077	0.3163	0.004	0.0018	1859	12	1770	19	1958	27	90.4
Spot91	3.282	0.092	0.2463	0.0048	0.0025	1473	22	1418	25	1572	50	90.2
Spot92	5.099	0.087	0.3436	0.005	0.0018	1834	14	1902	24	1773	29	107.3
		Rejected analysis										
Spot6	3.724	0.064	0.2605	0.0033	0.0018	1574	14	1493	17	1717	34	87
Spot7	3.635	0.069	0.2551	0.0036	0.0017	1558	15	1464	18	1690	30	86.6
Spot13	3.564	0.088	0.2458	0.0056	0.0022	1542	20	1415	29	1726	39	82
Spot14	3.692	0.069	0.2395	0.0037	0.0017	1568	15	1383	19	1826	27	75.7
Spot15	2.871	0.037	0.198	0.0024	0.0011	1372.5	9.6	1164	13	1738	18	67
Spot19	2.898	0.097	0.197	0.0057	0.0027	1377	25	1158	30	1768	46	65.5
Spot20	2.19	0.044	0.1602	0.0027	0.0016	1179	14	959	15	1600	30	59.9
Spot24	1.518	0.049	0.1194	0.0029	0.0025	937	20	727	17	1497	54	48.6
Spot27	4.193	0.095	0.2819	0.0052	0.0019	1670	19	1600	26	1805	30	88.6
Spot34	4.151	0.086	0.2756	0.0056	0.0026	1665	17	1572	29	1785	43	88.1
Spot35	4.19	0.081	0.2793	0.0044	0.0023	1672	16	1587	22	1804	37	88
Spot42	9.25	0.14	0.4065	0.0056	0.0016	2361	14	2199	26	2516	16	87.4
Spot50	9.42	0.17	0.4057	0.0063	0.002	2377	16	2194	29	2539	20	86.4
Spot58	3.633	0.088	0.2578	0.0051	0.0016	1557	19	1482	26	1717	28	86.3
Spot59	4.075	0.061	0.2699	0.0034	0.0012	1650	12	1543	18	1788	19	86.3
Spot60	5.91	0.1	0.3275	0.0045	0.0017	1961	15	1825	22	2116	22	86.2
Spot67	3.888	0.065	0.2656	0.0051	0.0017	1611	14	1517	26	1768	28	85.8
Spot68	2.996	0.087	0.2119	0.0049	0.0023	1408	21	1238	26	1680	41	73.7
Spot76	2.964	0.065	0.2137	0.0044	0.0024	1398	17	1247	23	1701	42	73.3
Spot77	2.819	0.037	0.2027	0.0025	0.001	1360.8	9.8	1189	13	1640	18	72.5
Spot79	4.326	0.076	0.3276	0.0053	0.0015	1696	15	1827	25	1572	29	116.2
Spot81	6.09	0.077	0.3929	0.0046	0.0014	1987	11	2135	21	1857	23	115
Spot87	4.695	0.091	0.3329	0.0055	0.0019	1763	16	1850	26	1645	35	112.5
Spot90	4.58	0.11	0.3311	0.0057	0.0023	1743	19	1842	27	1639	43	112.4
M-Mo8												
Spot1	4.74	0.13	0.3108	0.0076	0.0033	1771	24	1741	37	1778	54	98
Spot2	3.804	0.078	0.2874	0.006	0.0021	1593	16	1631	30	1538	40	106
Spot3	4.07	0.1	0.2842	0.006	0.0031	1647	21	1613	30	1686	57	96
Spot5	4.671	0.089	0.3139	0.0056	0.0021	1760	16	1758	27	1738	38	101
Spot11	4.35	0.31	0.291	0.022	0.011	1704	59	1650	100	1820	170	91
Spot14	8.92	0.16	0.4115	0.0087	0.0031	2328	16	2223	39	2391	35	93
Spot15	4.36	0.16	0.2883	0.0091	0.0041	1706	31	1629	45	1757	72	93
Spot17	4.429	0.091	0.2923	0.0046	0.0021	1717	17	1652	23	1780	35	93
Spot26	4.76	0.1	0.311	0.0067	0.0025	1777	19	1743	33	1775	43	98
Spot27	3.565	0.079	0.2655	0.0047	0.002	1545	17	1518	24	1572	41	97
Spot29	4.181	0.095	0.2848	0.0051	0.0026	1673	18	1614	26	1732	43	93
Spot43	4.54	0.12	0.2992	0.0055	0.0029	1733	22	1688	28	1788	48	94
Spot47	3.879	0.074	0.2793	0.0038	0.0022	1613	16	1589	20	1667	40	95

Table 2 Detrital zircon U–Pb dating results of analysed samples

Spot48	4.65	0.12	0.312	0.0072	0.0028	1757	22	1747	36	1745	49	100
Spot53	3.96	0.16	0.28	0.01	0.0034	1619	32	1589	52	1649	61	96
Spot56	3.668	0.099	0.2692	0.0064	0.0033	1564	22	1540	33	1597	63	96
Spot59	3.51	0.1	0.2612	0.0068	0.0029	1522	24	1499	34	1569	57	96
Spot60	4.3	0.23	0.278	0.015	0.0071	1690	43	1582	74	1750	120	90
Spot65	3.47	0.11	0.2525	0.0067	0.0044	1522	25	1449	35	1589	84	91
Spot66	15.16	0.36	0.527	0.011	0.0041	2817	23	2725	44	2871	33	95
Spot68	4.52	0.1	0.3043	0.0056	0.0025	1742	19	1710	28	1763	42	97
Spot70	5.03	0.096	0.3255	0.0053	0.0021	1824	16	1819	26	1821	35	100
		Rejected analysis										
Spot7	3.86	0.15	0.2592	0.0097	0.0043	1600	33	1482	49	1727	78	86
Spot4	1.758	0.037	0.1148	0.0021	0.0022	1030	14	701	12	1776	36	39
Spot6	2.158	0.045	0.1374	0.0028	0.0019	1166	14	829	16	1858	31	45
Spot8	64.1	6.6	0.828	0.083	0.05	4130	100	3760	280	4420	140	85
Spot9	0.442	0.013	0.03154	0.0009	0.0024	372.3	8.9	200.1	5.5	1619	43	12
Spot10	0.536	0.026	0.0382	0.002	0.0016	430	17	241	12	1706	30	14
Spot12	3.612	0.094	0.2521	0.0043	0.0028	1552	20	1448	22	1703	49	85
Spot13	3.48	0.15	0.2316	0.007	0.0043	1520	34	1341	37	1786	71	75
Spot16	1.406	0.023	0.1125	0.0018	0.0014	890.7	9.7	688	10	1398	31	49
Spot18	3.411	0.09	0.2215	0.0054	0.0027	1504	21	1290	28	1825	45	71
Spot19	3.46	0.13	0.209	0.0068	0.0044	1518	32	1222	36	1922	68	64
Spot20	40	14	0.48	0.24	0.96	3420	310	1860	540	######	####	-6
Spot21	3.703	0.082	0.2581	0.0052	0.002	1573	17	1479	27	1709	35	87
Spot22	2.188	0.046	0.1238	0.0033	0.0031	1177	15	755	19	2079	42	36
Spot23	3.004	0.098	0.2201	0.0057	0.0032	1411	26	1281	30	1604	59	80
Spot24	3.36	0.15	0.2358	0.0078	0.0041	1496	34	1369	40	1636	75	84
Spot25	1.73	0.12	0.0776	0.0018	0.0089	989	42	482	11	2328	95	21
Spot28	2.726	0.084	0.1878	0.0054	0.0032	1331	23	1108	29	1704	58	65
Spot30	1.475	0.031	0.1051	0.0016	0.0021	920	12	643.9	9.5	1654	38	39
Spot31	2.58	0.11	0.1491	0.0032	0.0048	1283	32	895	18	1959	69	46
Spot32	1.75	0.12	0.1125	0.0048	0.0055	1010	41	689	28	1857	75	37
Spot33	1.75	0.039	0.119	0.0027	0.0025	1027	15	724	16	1740	42	42
Spot34	8.95	0.31	0.343	0.011	0.0075	2332	30	1908	53	2704	67	71
Spot35	2.05	0.088	0.1303	0.005	0.0036	1124	29	788	28	1831	62	43
Spot36	2.13	0.083	0.1422	0.0057	0.0019	1151	27	857	32	1751	34	49
Spot37	0.714	0.018	0.0511	0.001	0.0019	546	11	321.2	6.1	1617	37	20
Spot38	0.9	0.013	0.05807	0.0009	0.0019	651.9	7.3	363.8	5.4	1824	32	20
Spot39	3.911	0.094	0.2487	0.006	0.0031	1610	20	1430	31	1840	51	78
Spot40	3.03	0.11	0.2231	0.0065	0.0041	1416	28	1296	34	1623	75	80
Spot41	2.944	0.093	0.2046	0.0063	0.0031	1389	24	1203	33	1712	54	70
Spot42	3.02	0.078	0.2128	0.0045	0.0027	1410	20	1243	24	1701	44	73
Spot44	0.729	0.027	0.0505	0.0023	0.0019	553	15	317	14	1706	33	19
Spot45	4.39	0.52	0.2302	0.0071	0.014	1707	91	1338	36	2110	150	63
Spot46	2.454	0.084	0.1593	0.005	0.0027	1259	25	951	28	1839	42	52
Spot49	3.516	0.094	0.2503	0.0055	0.0029	1534	21	1441	29	1652	53	87
Spot50	1.089	0.026	0.0864	0.0019	0.0018	747	12	534	11	1410	37	38
Spot51	0.513	0.02	0.0372	0.0017	0.0027	422	14	235	10	1680	47	14
Spot52	3.07	0.11	0.2218	0.0081	0.0045	1429	28	1295	42	1603	84	81
Spot54	1.586	0.026	0.105	0.0018	0.0017	964	10	644	10	1777	29	36
Spot55	3.199	0.098	0.2162	0.0053	0.0038	1458	25	1260	28	1706	65	74
Spot57	1.953	0.045	0.1307	0.0029	0.0021	1099	16	793	16	1769	35	45
Spot58	1.756	0.058	0.1159	0.0032	0.0031	1027	22	706	18	1769	51	40
Spot61	2.678	0.097	0.1369	0.0044	0.0039	1317	27	826	25	2272	48	36
Spot62	6.35	0.2	0.2683	0.0087	0.0031	2022	27	1535	45	2555	31	60
Spot63	2.28	0.13	0.1728	0.007	0.0066	1201	41	1027	39	1730	120	59
Spot64	2.213	0.08	0.1431	0.0051	0.0034	1183	24	865	28	1833	55	47

Table 2 Detrital zircon U–Pb dating results of analysed samples

Spot67	2.44	0.074	0.1702	0.0044	0.0026	1262	22	1016	25	1687	45	60
Spot69	1.42	0.085	0.1016	0.005	0.003	900	35	626	30	1658	54	38
Spot71	2.525	0.062	0.1575	0.0039	0.0022	1275	18	943	22	1884	35	50
Spot72	2.599	0.056	0.1705	0.0034	0.0023	1296	16	1014	19	1757	37	58
Spot73	0.745	0.02	0.0503	0.0014	0.0026	561	11	316.3	8.4	1729	43	18
M-Mo11												
Spot78	4.7	0.12	0.3177	0.0068	0.0032	1766	22	1778	33	1745	55	102
Spot22	4.61	0.11	0.3116	0.0067	0.0031	1748	20	1752	33	1728	51	101
Spot79	4.02	0.13	0.2887	0.0063	0.0032	1641	25	1636	32	1627	60	101
Spot66	3.92	0.12	0.2829	0.0074	0.0033	1616	24	1604	37	1600	61	100
Spot67	3.476	0.076	0.2615	0.0048	0.0022	1520	17	1496	25	1527	45	98
Spot37	4.9	0.1	0.3172	0.0049	0.002	1800	17	1774	24	1823	31	97
Spot3	4.63	0.16	0.3048	0.0074	0.0044	1755	30	1712	36	1790	74	96
Spot42	3.68	0.15	0.27	0.011	0.0056	1562	33	1539	57	1610	110	96
Spot19	4.24	0.24	0.283	0.013	0.0054	1678	49	1615	68	1697	97	95
Spot47	3.784	0.099	0.2701	0.0059	0.0029	1587	22	1545	31	1625	54	95
Spot8	4.72	0.13	0.306	0.0064	0.003	1772	22	1724	31	1817	48	95
Spot50	5.62	0.14	0.3334	0.0055	0.0035	1917	22	1855	26	1978	50	94
Spot68	3.355	0.086	0.2506	0.0054	0.003	1493	21	1439	28	1550	57	93
Spot33	11.78	0.29	0.463	0.01	0.0046	2584	23	2450	44	2654	42	92
Spot53	4.24	0.13	0.2851	0.006	0.0032	1674	24	1614	30	1750	56	92
Spot61	4.13	0.11	0.2816	0.0063	0.0036	1657	22	1598	32	1733	60	92
Spot5	4.29	0.11	0.2883	0.0056	0.0028	1690	21	1631	28	1777	49	92
Spot12	4.21	0.14	0.2831	0.0084	0.003	1672	26	1604	42	1759	54	91
		Rejected analysis										
Spot4	3.09	0.13	0.2289	0.0071	0.0049	1432	30	1340	38	1578	91	85
Spot27	3.831	0.092	0.259	0.0058	0.0029	1605	19	1486	30	1760	48	84
Spot58	3.86	0.18	0.253	0.01	0.0063	1607	39	1457	52	1800	100	81
Spot51	3.38	0.14	0.2365	0.009	0.0049	1510	34	1374	49	1762	87	78
Spot29	3.497	0.074	0.2356	0.0042	0.0026	1523	17	1364	22	1762	43	77
Spot25	3.159	0.076	0.2167	0.0038	0.0024	1445	19	1265	20	1719	41	74
Spot60	3.26	0.13	0.2204	0.0085	0.0046	1467	32	1282	45	1805	78	71
Spot44	2.86	0.1	0.1997	0.0075	0.0036	1376	26	1172	40	1706	72	69
Spot15	2.42	0.12	0.1793	0.0068	0.0036	1248	37	1075	40	1653	63	65
Spot49	2.924	0.067	0.1937	0.004	0.0024	1386	18	1140	22	1769	40	64
Spot48	2.31	0.054	0.1697	0.0031	0.0023	1221	16	1011	17	1577	45	64
Spot81	2.96	0.16	0.1944	0.007	0.0065	1413	41	1144	37	1790	110	64
Spot35	2.422	0.082	0.1731	0.0057	0.003	1249	25	1028	31	1663	53	62
Spot23	2.692	0.068	0.1793	0.0035	0.0026	1324	19	1063	19	1755	45	61
Spot54	2.354	0.084	0.1705	0.0059	0.0033	1223	26	1013	32	1677	59	60
Spot17	2.449	0.097	0.172	0.0049	0.0042	1254	29	1022	27	1699	74	60
Spot16	2.618	0.076	0.1756	0.0047	0.0032	1299	21	1041	25	1744	56	60
Spot40	2.165	0.047	0.1546	0.0026	0.0027	1172	15	926	14	1640	47	56
Spot13	4.54	0.31	0.2179	0.006	0.0088	1719	51	1270	32	2291	94	55
Spot80	2.557	0.064	0.1657	0.004	0.0026	1288	18	987	22	1792	44	55
Spot46	1.807	0.044	0.1348	0.0028	0.0021	1049	16	814	16	1570	41	52
Spot52	2.357	0.058	0.1565	0.0034	0.0025	1232	18	936	19	1809	42	52
Spot64	2.111	0.063	0.1446	0.0035	0.0032	1151	20	870	19	1717	56	51
Spot70	2.53	0.14	0.1582	0.0077	0.0059	1269	41	951	42	1896	89	50
Spot75	2.307	0.085	0.1461	0.0049	0.0029	1210	26	881	27	1863	46	47
Spot39	1.819	0.057	0.1283	0.0025	0.0027	1053	20	778	14	1649	50	47
Spot38	2.038	0.039	0.1373	0.0023	0.002	1129	13	829	13	1785	34	46
Spot20	1.586	0.045	0.118	0.0029	0.0028	961	18	719	17	1596	54	45
Spot72	1.6	0.045	0.1175	0.0032	0.0034	967	18	715	18	1598	63	45

Table 2 Detrital zircon U–Pb dating results of analysed samples

Spot65	1.932	0.069	0.1295	0.0039	0.0026	1083	24	783	22	1767	43	44
Spot55	1.815	0.063	0.1235	0.0034	0.0038	1051	23	750	19	1696	64	44
Spot56	1.759	0.051	0.1214	0.0029	0.0026	1024	19	738	17	1704	46	43
Spot74	1.237	0.076	0.0941	0.0043	0.0055	825	35	578	25	1430	120	40
Spot43	1.125	0.033	0.0907	0.0023	0.002	769	15	559	13	1395	45	40
Spot18	1.374	0.045	0.1027	0.0026	0.0031	881	19	630	15	1580	62	40
Spot77	1.97	0.13	0.1204	0.0061	0.0077	1091	42	738	33	1910	120	39
Spot73	1.79	0.04	0.1148	0.0021	0.0027	1041	15	700	12	1820	45	38
Spot71	1.459	0.059	0.1027	0.0035	0.0041	919	26	629	20	1658	79	38
Spot32	1.368	0.025	0.0988	0.0015	0.0018	876	11	607.3	8.7	1606	34	38
Spot6	1.602	0.096	0.1054	0.0042	0.0073	965	36	645	25	1740	120	37
Spot41	1.62	0.034	0.1072	0.0017	0.0023	977	13	656	10	1778	36	37
Spot31	1.628	0.044	0.105	0.0024	0.0027	979	16	643	14	1816	46	35
Spot14	0.768	0.053	0.068	0.0029	0.0056	573	30	423	17	1210	130	35
Spot34	1.995	0.066	0.1129	0.0031	0.0026	1106	23	690	18	2002	37	34
Spot7	2.675	0.092	0.1311	0.0036	0.0042	1316	25	793	20	2320	47	34
Spot82	1.19	0.031	0.0872	0.002	0.0026	794	14	539	12	1584	49	34
Spot26	1.195	0.048	0.0866	0.0026	0.0028	795	22	536	16	1589	52	34
Spot36	1.018	0.019	0.0788	0.0014	0.0018	712.8	9.7	488.6	8.1	1477	36	33
Spot62	1.105	0.029	0.082	0.0017	0.0022	754	14	508	10	1591	40	32
Spot57	1.013	0.055	0.0755	0.0018	0.0034	697	24	469	11	1492	62	31
Spot2	1.159	0.027	0.0831	0.0016	0.0026	781	12	514.4	9.3	1641	49	31
Spot69	1.128	0.039	0.0817	0.0024	0.0023	768	19	506	14	1630	44	31
Spot30	0.935	0.023	0.0727	0.0015	0.0023	668	12	452.4	9.3	1468	50	31
Spot24	1.79	0.11	0.1007	0.0045	0.0028	1012	39	617	26	2012	42	31
Spot21	0.518	0.019	0.0412	0.0012	0.0018	421	12	260.3	7.7	1406	38	19
Spot1	0.567	0.02	0.0436	0.0013	0.0025	455	13	275.3	7.7	1507	52	18
Spot9	0.551	0.013	0.04187	0.0009	0.0016	444.4	8.5	264.3	5.5	1481	34	18
Spot11	17	17	0.15	0.15	0.83	######	#####	880	880	######	####	18
Spot76	0.82	0.21	0.0495	0.0088	0.031	660	130	310	53	1970	540	16
Spot45	0.611	0.024	0.0408	0.0014	0.0044	484	15	257.7	8.9	1745	73	15
Spot59	0.533	0.086	0.0342	0.0026	0.014	417	48	216	16	1530	310	14
Spot10	0.287	0.013	0.02417	0.0009	0.0033	256	10	153.9	5.6	1323	73	12
Spot28	0.441	0.041	0.0298	0.0021	0.01	369	28	189	13	1870	160	10
Spot63	7.5	4.5	0.117	0.075	1.8	2070	530	670	410	######	####	-1
J-Mo13												
Spot2	5.304	0.076	0.353	0.0045	0.0016	1868	12	1948	21	1774	26	109.8
Spot8	4.453	0.054	0.302	0.0029	0.0012	1720	10	1701	14	1728	20	98.4
Spot10	4.451	0.062	0.2979	0.0041	0.0016	1720	12	1680	20	1758	27	95.6
Spot13	5.78	0.067	0.3599	0.0039	0.001	1943	10	1982	18	1879	16	105.5
Spot14	4.48	0.13	0.3064	0.0072	0.0031	1721	24	1721	35	1641	57	104.9
Spot15	4.823	0.063	0.3275	0.0031	0.0012	1790	11	1826	15	1749	20	104.4
Spot16	4.876	0.06	0.3268	0.0036	0.0012	1798	10	1824	17	1752	19	104.1
Spot17	3.644	0.066	0.2742	0.0047	0.0014	1559	15	1561	24	1502	28	103.9
Spot18	4.8	0.091	0.3194	0.0044	0.0019	1782	16	1786	22	1736	32	102.9
Spot19	4.736	0.059	0.3208	0.0038	0.0011	1774	11	1793	18	1748	18	102.6
Spot20	4.959	0.078	0.3239	0.0046	0.0016	1812	14	1808	22	1765	27	102.4
Spot22	4.54	0.1	0.2996	0.0046	0.0023	1742	19	1688	23	1800	38	93.8
Spot24	4.505	0.056	0.2955	0.0035	0.001	1735	10	1670	18	1793	16	93.1
Spot26	3.905	0.069	0.2685	0.0038	0.0016	1612	14	1532	19	1693	29	90.5
Spot27	5.47	0.1	0.3467	0.0045	0.0021	1894	17	1918	22	1886	32	101.7
Spot29	5.133	0.096	0.3318	0.0051	0.0015	1842	16	1848	25	1820	25	101.5
Spot33	3.566	0.064	0.2707	0.0039	0.0015	1540	14	1543	20	1520	30	101.5
Spot34	4.8	0.099	0.3175	0.0065	0.0016	1783	17	1777	32	1767	26	100.6

Table 2 Detrital zircon U–Pb dating results of analysed samples

Spot36	3.66	0.049	0.2751	0.0032	0.0011	1564	11	1566	16	1562	21	100.3
Spot37	3.684	0.066	0.2743	0.0036	0.0014	1568	15	1564	19	1564	26	100
Spot38	4.34	0.07	0.2997	0.0042	0.0011	1699	13	1689	21	1690	19	99.9
Spot39	4.565	0.088	0.3087	0.0048	0.002	1740	16	1733	24	1738	34	99.7
Spot42	5.02	0.1	0.334	0.0049	0.0015	1825	17	1857	24	1738	25	106.8
Spot43	2.916	0.045	0.2379	0.0029	0.0013	1385	12	1375	15	1404	28	97.9
Spot45	5.136	0.06	0.3241	0.0033	0.0012	1840	10	1813	16	1865	19	97.2
Spot47	4.418	0.077	0.3	0.004	0.0015	1714	14	1694	20	1757	25	96.4
Spot48	5.012	0.082	0.3391	0.0047	0.0018	1820	14	1881	23	1756	30	107.1
Spot49	3.961	0.049	0.2778	0.0029	0.001	1625.8	9.9	1581	15	1655	18	95.5
Spot53	3.627	0.046	0.2623	0.0029	0.0011	1554	10	1503	15	1576	20	95.4
Spot54	4.377	0.083	0.2937	0.0046	0.0014	1707	16	1659	23	1745	25	95.1
Spot56	4.94	0.1	0.3169	0.0058	0.0021	1814	19	1773	28	1879	31	94.4
Spot57	4.103	0.058	0.2757	0.0032	0.0011	1654	12	1570	16	1721	21	91.2
Spot58	4.03	0.062	0.2753	0.004	0.0012	1639	12	1567	20	1720	21	91.1
Spot59	3.453	0.052	0.2551	0.0029	0.0013	1516	12	1464	15	1575	26	93
Spot63	4.47	0.06	0.2936	0.004	0.0013	1728	11	1659	20	1798	22	92.3
Spot66	3.994	0.056	0.2885	0.004	0.0014	1632	12	1633	20	1596	26	102.3
Spot67	3.991	0.06	0.2738	0.0034	0.0015	1631	12	1560	17	1703	27	91.6
Spot68	4.114	0.064	0.2787	0.0034	0.0013	1654	13	1585	17	1733	22	91.5
Spot71	4.681	0.08	0.3144	0.0056	0.0012	1762	14	1762	27	1721	19	102.4
Spot72	4	0.053	0.2764	0.0031	0.001	1633	11	1572	16	1715	18	91.7
Spot73	3.578	0.065	0.2712	0.0036	0.0018	1543	15	1546	18	1519	35	101.8
Spot76	3.311	0.067	0.245	0.0033	0.0022	1483	16	1412	17	1568	40	90.1
		Rejected analysis										
Spot62	7.55	0.38	0.514	0.018	0.0044	2173	45	2669	78	1744	83	153
Spot52	3.957	0.046	0.2697	0.0029	0.0014	1624	9.4	1539	15	1721	24	89.4
Spot40	3.995	0.069	0.2671	0.0043	0.0022	1633	14	1526	22	1727	38	88.4
Spot35	3.903	0.062	0.2657	0.0034	0.0017	1615	13	1518	17	1724	31	88.1
Spot60	4.271	0.062	0.2776	0.0031	0.0017	1688	12	1579	16	1801	28	87.7
Spot51	3.789	0.038	0.262	0.0024	0.001	1589.3	8	1500	12	1713	17	87.6
Spot25	3.458	0.066	0.2472	0.0041	0.0013	1518	15	1423	21	1643	22	86.6
Spot30	3.708	0.049	0.2553	0.003	0.0011	1572	11	1465	15	1706	19	85.9
Spot65	3.698	0.052	0.2545	0.0028	0.0014	1570	11	1463	14	1706	24	85.8
Spot21	4.264	0.058	0.2724	0.0035	0.001	1686	11	1552	18	1810	16	85.7
Spot70	3.795	0.051	0.2594	0.0027	0.0015	1592	11	1486	14	1734	25	85.7
Spot1	3.78	0.053	0.2559	0.0029	0.0016	1589	11	1468	15	1727	28	85
Spot4	3.455	0.053	0.2429	0.0034	0.0016	1516	12	1402	18	1660	28	84.5
Spot74	2.709	0.026	0.1985	0.0017	0.001	1330	7.2	1167.9	9.3	1581	19	73.9
Spot6	6.47	0.12	0.3058	0.0051	0.0024	2043	16	1719	25	2339	27	73.5
Spot61	2.507	0.051	0.1864	0.003	0.0016	1275	14	1105	16	1529	32	72.3
Spot50	2.88	0.032	0.2032	0.0019	0.001	1375.8	8.3	1192	10	1655	19	72
Spot9	2.343	0.072	0.1817	0.0045	0.001	1227	22	1076	25	1497	21	71.9
Spot12	2.485	0.037	0.1826	0.0025	0.001	1271	11	1081	14	1574	20	68.7
Spot32	1.873	0.019	0.1526	0.0016	0.0009	1070.9	6.6	915.4	9.1	1380	19	66.3
Spot23	2.871	0.086	0.196	0.0049	0.0031	1379	22	1153	26	1750	55	65.9
Spot55	5.01	0.074	0.2559	0.0036	0.0016	1819	13	1468	18	2250	19	65.2
Spot64	3.144	0.083	0.2026	0.0038	0.0028	1445	19	1189	20	1852	43	64.2
Spot69	2.112	0.028	0.1581	0.0019	0.0014	1151.8	9.1	946	11	1525	28	62
Spot44	1.979	0.048	0.1494	0.0027	0.0016	1106	16	897	15	1536	31	58.4
Spot11	2.155	0.056	0.1506	0.003	0.0022	1164	18	904	17	1646	41	54.9
Spot7	4.87	0.1	0.225	0.003	0.0032	1797	17	1308	16	2402	35	54.5
Spot46	7.41	0.38	0.2538	0.0035	0.01	2145	47	1458	18	2867	85	50.9
Spot3	1.356	0.017	0.1079	0.0013	0.001	869.6	7.6	660.3	7.5	1427	22	46.3
Spot28	2.57	0.17	0.1448	0.0027	0.0078	1271	43	871	15	1957	99	44.5
Spot75	1.528	0.038	0.1124	0.0024	0.0008	941	15	686	14	1566	16	43.8

Table 2 Detrital zircon U–Pb dating results of analysed samples

Spot5	1.292	0.019	0.1018	0.0014	0.0009	841.3	8.6	624.7	8.4	1465	18	42.6
Spot31	80	130	0.3	0.13	4.1	######	#####	1630	630	######	####	9.6
Spot41	9.48	0.14	0.4172	0.0048	0.0021	2386	13	2247	22	2498	21	90
E-Vel18												
Spot1	3.8	0.056	0.281	0.0037	0.0014	1593	12	1599	19	1744	24	91.7
Spot2	4.074	0.081	0.2849	0.0048	0.002	1653	16	1614	24	1760	36	91.7
Spot3	3.604	0.074	0.2679	0.0043	0.0016	1550	16	1531	22	1631	29	93.9
Spot5	3.69	0.088	0.2772	0.0045	0.0025	1566	19	1576	23	1628	46	96.8
Spot6	8.94	0.18	0.4209	0.0081	0.002	2330	19	2266	37	2435	22	93.1
Spot7	3.526	0.07	0.2615	0.0056	0.0018	1531	16	1499	29	1611	32	93
Spot8	4.13	0.093	0.2965	0.0056	0.0021	1664	18	1672	28	1686	38	99.2
Spot9	4.38	0.11	0.3033	0.0057	0.0026	1710	21	1707	28	1740	44	98.1
Spot11	4.612	0.097	0.3097	0.0063	0.0019	1751	18	1737	31	1674	33	103.8
Spot12	3.96	0.1	0.2844	0.0056	0.0021	1622	21	1611	28	1539	42	104.7
Spot14	5.162	0.094	0.3277	0.0059	0.0017	1845	16	1826	29	1766	28	103.4
Spot15	4.36	0.12	0.2865	0.0071	0.0027	1700	22	1624	35	1683	50	96.5
Spot17	5.107	0.094	0.3107	0.005	0.0016	1836	15	1743	25	1800	26	96.8
Spot19	2.721	0.068	0.2202	0.0037	0.002	1331	18	1282	20	1298	47	98.8
Spot19£¨1£©	2.67	0.11	0.2259	0.0082	0.0043	1327	28	1318	42	1348	95	97.8
Spot20	5.05	0.7	0.329	0.028	0.02	1840	110	1840	140	1820	280	101.1
Spot21	3.908	0.075	0.2642	0.0043	0.0016	1620	16	1510	22	1659	29	91
Spot22	3.201	0.072	0.2546	0.0045	0.0021	1458	18	1465	24	1488	44	98.5
Spot24	3.62	0.19	0.2734	0.0073	0.0049	1518	36	1557	38	1430	100	108.9
Spot28	4.68	0.097	0.3134	0.0048	0.0026	1763	17	1760	24	1786	42	98.5
Spot32	4.986	0.068	0.3186	0.0042	0.0016	1818	12	1782	20	1834	25	97.2
Spot33	3.33	0.078	0.2531	0.0046	0.0022	1485	19	1453	24	1505	44	96.5
Spot34	4.06	0.17	0.2918	0.0081	0.005	1637	35	1653	40	1621	93	102
Spot36	4.419	0.085	0.3014	0.0053	0.0016	1712	16	1696	26	1786	27	95
Spot38	4.23	0.12	0.296	0.0077	0.0032	1683	23	1675	39	1684	59	99.5
Spot39	4.24	0.11	0.2963	0.0062	0.0031	1682	22	1676	32	1770	50	94.7
Spot41	4.456	0.068	0.293	0.0049	0.0016	1722	12	1655	24	1797	26	92.1
Spot43	4.13	0.066	0.2909	0.0046	0.0015	1658	13	1646	23	1722	27	95.6
Spot44	4.073	0.076	0.2978	0.0047	0.0018	1648	15	1681	23	1623	32	103.6
Spot46	8.12	0.21	0.398	0.0079	0.0033	2242	24	2158	36	2340	39	92.2
Spot47	3.163	0.051	0.2443	0.0038	0.0016	1448	12	1414	19	1553	30	91
Spot50	3.69	0.17	0.274	0.01	0.0059	1556	37	1556	50	1590	120	97.9
Spot51	4.84	0.15	0.3029	0.0077	0.004	1795	27	1702	38	1886	63	90.2
Spot52	3.66	0.21	0.2685	0.0064	0.0068	1522	31	1530	32	1468	86	104.2
Spot54	4.06	0.1	0.2956	0.0048	0.0027	1635	20	1670	24	1608	49	103.9
Spot55	4	0.37	0.282	0.016	0.011	1608	82	1602	80	1600	200	100.1
Spot57	3.89	0.2	0.2828	0.0094	0.0064	1595	39	1603	47	1600	110	100.2
Spot58	4.859	0.099	0.3197	0.0057	0.0025	1791	17	1786	28	1812	41	98.6
Spot60	4.08	0.65	0.274	0.024	0.023	1610	130	1600	130	1700	340	94.1
Spot61	3.572	0.085	0.2699	0.0045	0.0025	1543	19	1539	23	1560	48	98.7
Spot62	3.335	0.075	0.2543	0.0047	0.002	1486	17	1460	24	1596	37	91.5
Spot63	4.08	0.23	0.293	0.01	0.0062	1653	46	1650	51	1590	120	103.8
Spot64	4.23	0.3	0.296	0.012	0.0091	1661	60	1671	59	1600	160	104.4
Spot66	4.8	0.071	0.3236	0.0049	0.0015	1782	13	1808	24	1806	25	100.1
Spot70	4.62	0.43	0.305	0.017	0.014	1713	81	1706	82	1700	200	100.4
Spot71	3.53	0.16	0.2573	0.0082	0.0045	1527	36	1483	42	1568	87	94.6
Spot72	3.58	0.14	0.2727	0.0089	0.0048	1548	33	1560	45	1602	93	97.4
Spot75	4.31	0.09	0.2853	0.0055	0.002	1693	17	1616	28	1710	35	94.5
Spot76	3.89	0.18	0.2825	0.0074	0.005	1594	38	1603	37	1614	95	99.3
Spot78	4.431	0.074	0.2952	0.0045	0.0019	1721	14	1666	23	1718	34	97

Table 2 Detrital zircon U–Pb dating results of analysed samples

	Rejected analysis											
Spot4	1.962	0.059	0.1869	0.005	0.003	1099	20	1103	27	1462	61	75.4
Spot10	2.644	0.069	0.2557	0.0056	0.0021	1322	20	1466	29	1712	38	85.6
Spot13	2.293	0.034	0.2282	0.0032	0.0015	1210	11	1326	17	1722	25	77.0
Spot18	1.287	0.027	0.1604	0.0028	0.0018	839	12	958	15	1421	36	67.4
Spot23	4.474	0.072	0.3211	0.0053	0.0019	1725	13	1794	26	2480	20	72.3
Spot25	1.296	0.028	0.1729	0.0038	0.0017	842	12	1030	21	1467	35	70.2
Spot26	0.832	0.02	0.124	0.0022	0.0014	615	11	754	12	1313	31	57.4
Spot29	1.418	0.058	0.1989	0.0062	0.0041	890	24	1172	34	1428	89	82.1
Spot30	1.863	0.044	0.2305	0.0045	0.0027	1067	16	1338	24	1775	47	75.4
Spot31	1.465	0.032	0.1859	0.0035	0.0017	914	13	1099	19	1753	29	62.7
Spot37	0.986	0.023	0.1497	0.0027	0.0017	696	12	899	15	1428	35	63.0
Spot40	1.133	0.027	0.1691	0.0043	0.002	770	13	1010	24	1449	41	69.7
Spot42	1.436	0.026	0.1889	0.0037	0.0017	903	11	1117	21	1686	31	66.3
Spot45	1.402	0.039	0.189	0.0045	0.0018	892	17	1115	24	1614	35	69.1
Spot48	1.928	0.039	0.2218	0.0046	0.0015	1089	14	1290	24	1725	25	74.8
Spot49	1.67	0.032	0.2101	0.004	0.0016	995	12	1228	21	1490	34	82.4
Spot53	2.536	0.048	0.1931	0.0038	0.0014	1282	14	1140	20	1554	28	73.4
Spot56	1.977	0.052	0.1598	0.0029	0.0019	1109	18	955	16	1449	40	65.9
Spot59	2.88	0.11	0.2026	0.0069	0.0033	1382	28	1188	37	1751	57	67.8
Spot65	1.771	0.029	0.161	0.0027	0.001	1036	11	962	15	1248	24	77.1
Spot67	2.126	0.067	0.1779	0.005	0.0027	1162	23	1055	27	1413	55	74.7
Spot68	2.562	0.053	0.1749	0.0034	0.0017	1287	15	1038	19	1792	28	57.9
Spot69	1.957	0.048	0.1581	0.0032	0.002	1104	16	946	18	1463	42	64.7
Spot73	3.7	0.13	0.2636	0.0071	0.0024	1570	28	1507	36	1738	41	86.7
Spot74	2.451	0.048	0.1886	0.0039	0.0015	1256	14	1113	21	1542	29	72.2
Spot79	2.725	0.075	0.1972	0.0052	0.0014	1337	20	1159	28	1632	26	71.0
Spot27	2.815	0.079	0.2067	0.0054	0.0026	1358	22	1210	29	1665	48	72.7
A-BC13												
Spot66	4.17	0.13	0.3065	0.0063	0.0037	1680	25	1722	31	1575	67	109.3
Spot20	3.68	0.081	0.2843	0.0044	0.0021	1562	18	1612	22	1511	41	106.7
Spot5	3.669	0.053	0.288	0.0032	0.0013	1562	12	1631	16	1539	26	106
Spot72	4.212	0.067	0.3089	0.0053	0.0015	1675	13	1734	26	1642	29	105.6
Spot63	4.1	0.059	0.298	0.0039	0.0013	1652	12	1680	19	1601	25	104.9
Spot42	4.336	0.065	0.3083	0.0041	0.0013	1699	12	1732	20	1668	24	103.8
Spot40	3.071	0.069	0.2519	0.0041	0.002	1423	18	1447	21	1409	42	102.7
Spot4	3.445	0.058	0.268	0.0034	0.0015	1515	13	1530	17	1493	30	102.5
Spot36	3.574	0.055	0.2711	0.0033	0.0015	1545	12	1546	17	1513	31	102.2
Spot68	3.586	0.05	0.273	0.0026	0.0014	1548	12	1556	13	1524	29	102.1
Spot32	4.266	0.097	0.3062	0.0063	0.002	1685	19	1721	31	1692	35	101.7
Spot59	3.094	0.053	0.25	0.0036	0.0014	1431	13	1440	18	1421	32	101.3
Spot71	4.803	0.089	0.3208	0.0048	0.0021	1785	15	1792	24	1780	36	100.7
Spot46	3.563	0.074	0.2696	0.0046	0.0023	1539	16	1538	23	1532	44	100.4
Spot23	4.338	0.066	0.3014	0.004	0.0016	1701	13	1697	20	1692	29	100.3
Spot17	18.18	0.2	0.5904	0.0069	0.0025	2999	11	2989	28	2987	18	100.1
Spot11	4.392	0.077	0.3035	0.004	0.0018	1711	15	1711	19	1710	33	100.1
Spot1	3.566	0.071	0.271	0.004	0.0019	1541	16	1545	21	1555	39	99.4
Spot62	4.411	0.099	0.3044	0.0055	0.0026	1717	18	1714	27	1726	45	99.3
Spot56	10.19	0.17	0.464	0.0077	0.0027	2453	15	2455	34	2475	28	99.2
Spot6	3.35	0.083	0.2622	0.0045	0.0024	1491	19	1503	23	1519	47	98.9
Spot29	3.144	0.051	0.2516	0.0036	0.0015	1443	13	1446	18	1466	31	98.6
Spot67	4	0.41	0.286	0.023	0.0093	1627	86	1640	110	1670	160	98.2
Spot35	4.335	0.066	0.2975	0.004	0.0014	1701	13	1680	19	1712	24	98.1
Spot26	3.272	0.065	0.2576	0.0045	0.0017	1479	15	1479	23	1510	34	97.9

Table 2 Detrital zircon U–Pb dating results of analysed samples

Spot53	3.172	0.072	0.2557	0.0049	0.0023	1452	18	1467	25	1498	49	97.9
Spot38	9.43	0.16	0.4437	0.0074	0.0025	2384	16	2369	33	2422	27	97.8
Spot65	3.708	0.05	0.2773	0.0047	0.0015	1572	11	1577	24	1616	27	97.6
Spot30	4.178	0.069	0.2937	0.005	0.0019	1669	14	1659	25	1708	32	97.1
Spot49	3.065	0.052	0.2449	0.0038	0.0015	1424	13	1411	20	1454	31	97
Spot9	3.04	0.1	0.2468	0.0055	0.003	1419	25	1421	29	1475	64	96.3
Spot74	4.163	0.078	0.2935	0.0051	0.0019	1669	16	1658	25	1725	33	96.1
Spot75	10.04	0.12	0.4459	0.0048	0.0018	2439	11	2378	21	2476	18	96
Spot18	4.499	0.072	0.3064	0.0046	0.0016	1729	13	1722	23	1805	27	95.4
Spot22	3.429	0.063	0.2557	0.0039	0.0018	1511	14	1467	20	1539	34	95.3
Spot14	3.45	0.19	0.267	0.011	0.0052	1510	44	1522	56	1598	96	95.2
Spot2	4.304	0.076	0.2961	0.0045	0.0018	1694	14	1671	22	1763	32	94.8
Spot37	3.62	0.21	0.273	0.012	0.0045	1553	45	1550	63	1636	81	94.7
Spot52	4.232	0.054	0.2895	0.0033	0.0013	1680	11	1639	16	1730	23	94.7
Spot7	7.618	0.099	0.3917	0.0056	0.0017	2186	12	2132	26	2255	21	94.5
Spot51	3.883	0.051	0.2754	0.0032	0.0013	1610	11	1567	16	1663	24	94.2
Spot34	3.785	0.05	0.2701	0.0032	0.0014	1588	11	1540	16	1645	26	93.6
Spot8	3.48	0.12	0.2631	0.0086	0.0033	1518	29	1503	44	1606	65	93.6
Spot19	4.266	0.079	0.2877	0.0042	0.0017	1686	16	1631	21	1743	28	93.6
Spot10	3.705	0.073	0.2699	0.0046	0.0021	1570	16	1539	23	1648	37	93.4
Spot25	3.947	0.077	0.2789	0.0039	0.0018	1623	15	1588	20	1706	30	93.1
Spot13	3.291	0.055	0.2488	0.0036	0.0019	1477	13	1431	19	1539	36	93
Spot69	4.03	0.1	0.2879	0.0069	0.0027	1643	20	1630	34	1759	44	92.7
Spot16	3.145	0.076	0.2475	0.0053	0.0019	1441	19	1428	28	1547	37	92.3
Spot28	3.287	0.072	0.2446	0.004	0.002	1477	17	1412	21	1540	40	91.7
Spot15	3.72	0.9	0.263	0.038	0.03	1650	140	1490	190	1640	610	90.9
Spot48	2.801	0.047	0.2223	0.0032	0.0017	1354	13	1294	17	1433	36	90.3
Spot44	3.448	0.07	0.2606	0.0052	0.0021	1514	16	1492	27	1654	37	90.2
		Rejected analysis										
Spot31	4.211	0.073	0.2804	0.0039	0.0011	1674	14	1592	20	1779	19	89.5
Spot47	3.736	0.078	0.2688	0.0061	0.0025	1578	16	1534	31	1725	43	88.9
Spot21	3.45	0.13	0.2584	0.0071	0.0034	1521	31	1483	36	1670	62	88.8
Spot60	3.077	0.054	0.2358	0.0041	0.0016	1425	14	1364	21	1537	32	88.7
Spot58	3.77	0.22	0.2705	0.009	0.0058	1587	49	1542	46	1740	100	88.6
Spot57	3.156	0.061	0.232	0.0034	0.0021	1446	15	1344	18	1546	41	86.9
Spot54	3.37	0.1	0.2478	0.0088	0.0043	1495	23	1426	45	1664	76	85.7
Spot73	2.438	0.026	0.2007	0.0021	0.001	1252.8	7.7	1179	11	1379	22	85.5
Spot64	2.719	0.045	0.2163	0.0034	0.0013	1335	12	1261	18	1476	26	85.4
Spot45	2.697	0.046	0.2126	0.0033	0.0016	1327	13	1242	17	1457	34	85.2
Spot27	3.402	0.05	0.2418	0.0029	0.0016	1502	12	1396	15	1653	30	84.5
Spot24	2.312	0.04	0.1933	0.0026	0.0013	1216	12	1139	14	1361	30	83.7
Spot3	3.397	0.087	0.245	0.0048	0.0022	1501	20	1412	25	1693	39	83.4
Spot33	2.634	0.092	0.2143	0.0051	0.0035	1314	23	1252	26	1503	63	83.3
Spot12	3.12	0.044	0.23	0.0023	0.0011	1440	11	1334	12	1602	21	83.3
Spot70	6.89	0.19	0.342	0.0058	0.0017	2099	24	1900	28	2282	20	83.3
Spot43	7.46	0.11	0.3539	0.004	0.0013	2166	13	1956	19	2372	14	82.5
Spot50	6.63	0.11	0.3383	0.0047	0.0019	2065	14	1880	22	2288	22	82.2
Spot61	3.054	0.055	0.2285	0.0041	0.0018	1421	14	1326	21	1616	32	82.1
Spot39	3.16	0.069	0.238	0.0063	0.0021	1446	17	1375	33	1678	39	81.9
Spot55	2.864	0.055	0.2192	0.004	0.0015	1374	14	1277	21	1564	29	81.6
Spot41	2.709	0.038	0.2097	0.0027	0.0013	1333	10	1227	15	1503	25	81.6
S-BC1												
Spot79	5.05	0.11	0.3439	0.006	0.0018	1830	19	1903	29	1739	31	109
Spot76	31.88	0.33	0.7883	0.0076	0.0025	3546	10	3745	27	3443	13	109

Table 2 Detrital zircon U–Pb dating results of analysed samples

Spot46	5.812	0.085	0.3682	0.0047	0.0013	1946	13	2020	22	1869	20	108
Spot65	4.986	0.088	0.3386	0.0051	0.0017	1814	15	1878	25	1741	30	108
Spot4	21.58	0.31	0.672	0.01	0.0018	3166	14	3312	40	3078	12	108
Spot69	5.162	0.049	0.3433	0.0031	0.0008	1846.7	8.1	1902	15	1779	14	107
Spot5	10.95	0.11	0.4943	0.0054	0.0014	2519.1	9.4	2588	23	2464	15	105
Spot92	3.683	0.032	0.2798	0.0023	0.0008	1568.3	6.8	1590	12	1527	15	104
Spot55	9.99	0.11	0.4681	0.0061	0.0016	2433	9.9	2474	27	2393	18	103
Spot73	4.547	0.058	0.3138	0.0032	0.0014	1739	11	1759	16	1713	25	103
Spot10	4.752	0.081	0.3226	0.0049	0.0017	1775	14	1804	24	1744	29	103
Spot89	2.907	0.028	0.2399	0.0025	0.0007	1383	7.3	1386	13	1354	14	102
Spot52	3.847	0.053	0.2843	0.0032	0.0014	1602	11	1612	16	1578	28	102
Spot56	3.488	0.078	0.2681	0.0043	0.0023	1521	18	1532	22	1513	46	101
Spot45	4.749	0.071	0.3185	0.0038	0.0013	1775	13	1782	19	1766	21	101
Spot14	4.483	0.075	0.3088	0.004	0.0016	1725	14	1733	20	1728	29	100
Spot61	3.667	0.062	0.2718	0.0038	0.0017	1564	13	1549	19	1550	34	100
Spot29	5.536	0.09	0.3426	0.0057	0.0021	1906	14	1898	28	1902	33	100
Spot47	4.606	0.06	0.3123	0.0034	0.0012	1752	11	1751	17	1760	21	99
Spot16	4.6	0.11	0.3117	0.0064	0.0017	1743	21	1747	32	1759	28	99
Spot66	10.68	0.12	0.4701	0.0045	0.0015	2495	11	2488	20	2506	16	99
Spot22	5.466	0.07	0.3386	0.004	0.0012	1894	11	1879	19	1901	18	99
Spot3	6.544	0.09	0.3708	0.0043	0.0018	2050	12	2032	20	2060	25	99
Spot60	5.174	0.098	0.3295	0.0049	0.0017	1847	16	1835	24	1865	26	98
Spot64	4.383	0.087	0.2962	0.0039	0.0021	1708	17	1672	19	1702	38	98
Spot12	9.6	0.12	0.4458	0.0053	0.0017	2396	11	2375	24	2423	18	98
Spot36	25.36	0.21	0.6599	0.0057	0.0015	3322.4	8.3	3266	22	3338.8	8.3	98
Spot71	4.437	0.055	0.2998	0.0038	0.0015	1719	10	1690	19	1737	25	97
Spot13	5.101	0.062	0.3215	0.0033	0.0012	1836	10	1798	16	1875	19	96
Spot27	4.309	0.089	0.2945	0.0047	0.0022	1695	17	1666	23	1740	38	96
Spot72	4.346	0.06	0.2977	0.0037	0.0016	1703	11	1679	18	1754	29	96
Spot21	4.242	0.072	0.2921	0.0039	0.0015	1683	14	1651	19	1725	26	96
Spot78	4.68	0.13	0.3046	0.0049	0.0031	1765	23	1713	24	1794	50	95
Spot51	3.396	0.05	0.2553	0.0028	0.0012	1504	12	1465	15	1535	24	95
Spot40	4.592	0.057	0.3013	0.0041	0.0015	1748	10	1697	20	1790	25	95
Spot75	4.662	0.064	0.3044	0.0037	0.0016	1760	12	1712	18	1817	26	94
Spot30	4.839	0.073	0.3109	0.0038	0.0017	1791	13	1744	18	1852	27	94
Spot95	3.4	0.045	0.256	0.0029	0.0012	1508	11	1469	15	1562	23	94
Spot41	4.057	0.065	0.2807	0.0038	0.0017	1647	13	1596	19	1700	30	94
Spot54	4.235	0.05	0.2887	0.0033	0.0013	1682	9.8	1634	17	1743	22	94
Spot11	4.201	0.065	0.2878	0.0042	0.0023	1676	13	1630	21	1740	39	94
Spot20	4.984	0.07	0.312	0.0033	0.0016	1817	12	1752	16	1876	25	93
Spot1	4.605	0.084	0.2963	0.0043	0.0019	1755	15	1672	22	1827	31	92
Spot85	4.177	0.063	0.2834	0.0037	0.0015	1669	12	1608	19	1723	26	93
Spot43	4.688	0.059	0.3031	0.0031	0.0015	1766	11	1707	15	1843	24	93
Spot86	9.905	0.093	0.4312	0.0037	0.0014	2424.7	8.7	2310	16	2505	15	92
Spot23	4.015	0.063	0.2776	0.0036	0.0016	1637	13	1578	18	1713	27	92
Spot32	4.471	0.058	0.2946	0.0032	0.0013	1725	11	1665	16	1809	22	92
Spot49	4.013	0.048	0.2807	0.0029	0.0011	1638.4	9.5	1594	15	1707	19	93
Spot42	3.62	0.13	0.2645	0.0061	0.0038	1554	28	1510	31	1651	69	91
Spot81	13.1	0.18	0.4863	0.0059	0.0019	2687	12	2554	26	2797	16	91
Spot93	11.55	0.17	0.456	0.0059	0.0023	2567	14	2421	26	2662	21	91
Spot88	3.899	0.049	0.2706	0.0031	0.0012	1615	10	1543	16	1699	23	91
Spot18	8.93	0.18	0.4097	0.0088	0.0037	2331	19	2212	40	2438	38	91
Spot67	4.559	0.055	0.2946	0.0031	0.001	1741	10	1666	15	1838	16	91
Spot25	4.145	0.079	0.2799	0.0039	0.0017	1663	16	1592	19	1761	28	90
Spot50	4.03	0.056	0.2753	0.0035	0.0013	1639	11	1570	17	1738	23	90
Spot26	3.072	0.043	0.2345	0.003	0.0013	1426	11	1358	16	1505	25	90

Table 2 Detrital zircon U–Pb dating results of analysed samples

Spot38	3.43	0.072	0.2505	0.0035	0.002	1512	17	1440	18	1598	38	90
Spot82	3.963	0.055	0.2723	0.003	0.0014	1625	11	1552	15	1724	23	90
Spot2	6.53	0.19	0.3516	0.0092	0.0045	2044	26	1941	44	2157	60	90
Spot19	9.64	0.13	0.4204	0.005	0.0019	2401	12	2261	23	2516	20	90
Spot62	4.552	0.049	0.293	0.0028	0.0011	1739.9	9.1	1656	14	1845	18	90
Spot87	3.277	0.038	0.242	0.0024	0.0008	1474.4	9	1397	13	1557	15	90
Spot59	9.3	0.13	0.4146	0.0051	0.0021	2367	13	2234	23	2490	22	90
Spot77	4.484	0.055	0.2925	0.0034	0.0013	1727	10	1653	17	1845	21	90
		Rejected analysis										
Spot33	5.987	0.086	0.4105	0.0052	0.0014	1974	13	2218	24	1726	24	129
Spot90	5.76	0.1	0.396	0.0055	0.0016	1944	15	2149	25	1702	29	126
Spot35	7	0.11	0.4398	0.0049	0.0016	2111	14	2349	22	1868	26	126
Spot34	6.464	0.081	0.4172	0.0051	0.0012	2040	11	2252	23	1836	20	123
Spot37	14.22	0.23	0.612	0.0082	0.0017	2764	16	3076	33	2543	17	121
Spot15	5.811	0.091	0.3907	0.005	0.0017	1947	14	2125	23	1759	29	121
Spot28	5.709	0.091	0.3839	0.0046	0.0017	1931	14	2095	22	1758	29	119
Spot44	5.95	0.11	0.3887	0.0063	0.0022	1966	16	2119	29	1788	37	119
Spot91	6.608	0.087	0.4121	0.005	0.002	2063	12	2226	23	1888	31	118
Spot48	3.789	0.079	0.2593	0.0041	0.0022	1587	17	1485	21	1701	38	87
Spot80	3.751	0.058	0.2618	0.0033	0.0018	1583	13	1498	17	1720	30	87
Spot58	3.084	0.052	0.2319	0.0035	0.0013	1429	13	1346	18	1546	25	87
Spot63	3.974	0.05	0.2679	0.003	0.0013	1629	10	1530	15	1759	22	87
Spot9	4.39	0.056	0.282	0.003	0.0013	1710	10	1601	15	1849	21	87
Spot53	3.078	0.058	0.232	0.0033	0.0018	1427	14	1344	17	1556	34	86
Spot94	3.716	0.058	0.2559	0.0031	0.0017	1572	13	1472	16	1706	30	86
Spot7	4.076	0.048	0.2708	0.0028	0.0011	1648.7	9.5	1544	14	1792	18	86
Spot17	4.374	0.081	0.2788	0.0037	0.002	1705	15	1585	19	1847	31	86
Spot74	3.732	0.051	0.2556	0.003	0.0013	1576	11	1468	15	1712	22	86
Spot70	3.627	0.066	0.2511	0.0031	0.0019	1552	14	1445	16	1703	34	85
Spot31	3.728	0.06	0.2556	0.003	0.0015	1578	13	1467	15	1730	25	85
Spot84	4.12	0.05	0.2692	0.003	0.0016	1657	10	1538	15	1818	26	85
Spot39	3.601	0.057	0.2493	0.0027	0.0013	1548	13	1436	14	1698	22	85
Spot57	2.1	0.02	0.1409	0.0013	0.0009	1148.3	6.7	849.7	7.3	1762	16	48
Spot83	2.07	0.051	0.1359	0.0029	0.0021	1137	17	821	16	1803	33	46
Spot6	0.915	0.016	0.0638	0.0011	0.0014	659.5	8.2	398.4	6.8	1681	24	24
Spot24	3.939	0.063	0.2519	0.0037	0.0015	1617	13	1450	19	1825	23	79
Spot68	2.605	0.04	0.2007	0.0029	0.0013	1301	11	1178	16	1492	27	79
W-BC1												
Spot63	5.223	0.086	0.3467	0.0045	0.0015	1862	14	1919	22	1808	24	106
Spot87	5.388	0.073	0.3496	0.0041	0.0016	1883	12	1932	20	1853	25	104
Spot60	4.746	0.05	0.3257	0.0031	0.0011	1776.4	8.6	1817	15	1748	18	104
Spot2	5.229	0.084	0.3399	0.0054	0.0015	1856	14	1885	26	1830	25	103
Spot50	4.632	0.057	0.3187	0.0037	0.0013	1754	10	1782	18	1741	22	102
Spot109	4.538	0.068	0.3123	0.0037	0.0014	1737	12	1751	18	1747	25	100
Spot84	10.92	0.14	0.4788	0.0059	0.0025	2518	12	2523	26	2539	25	99
Spot47	8.58	0.11	0.4256	0.0063	0.0015	2294	11	2288	28	2327	19	98
Spot108	4.403	0.061	0.3026	0.0041	0.0013	1714	11	1705	20	1735	22	98
Spot90	9.5	0.13	0.4423	0.0063	0.0023	2387	13	2362	28	2420	24	98
Spot94	9.8	0.11	0.4501	0.0046	0.0016	2414.5	9.9	2395	21	2454	17	98
Spot53	26.01	0.3	0.6699	0.0096	0.0032	3346	11	3304	37	3394	17	97
Spot34	4.898	0.054	0.3196	0.0033	0.001	1805.8	9.8	1787	16	1839	17	97
Spot103	4.314	0.054	0.2987	0.0032	0.0013	1698	10	1686	16	1740	23	97
Spot42	4.685	0.051	0.311	0.0028	0.0013	1764	8.9	1745	14	1805	21	97
Spot74	4.272	0.049	0.2951	0.0027	0.0011	1687.5	9.3	1667	13	1730	19	96

Table 2 Detrital zircon U–Pb dating results of analysed samples

Spot31	4.289	0.06	0.2958	0.0032	0.0011	1693	12	1670	16	1736	18	96
Spot1	10.35	0.16	0.4555	0.0068	0.0024	2468	14	2421	30	2517	24	96
Spot57	3.526	0.049	0.2648	0.0032	0.0014	1533	11	1515	16	1579	27	96
Spot41	7.049	0.081	0.3805	0.0041	0.0014	2118	10	2078	19	2167	18	96
Spot98	5.528	0.066	0.3349	0.0035	0.0015	1906	10	1862	17	1942	22	96
Spot99	4.325	0.061	0.2951	0.0037	0.0012	1697	11	1668	19	1741	20	96
Spot16	4.74	0.055	0.3125	0.0035	0.0009	1772.8	9.8	1754	18	1833	15	96
Spot61	5.147	0.062	0.3253	0.0033	0.001	1843	10	1815	16	1898	16	96
Spot38	4.302	0.056	0.2969	0.0038	0.0015	1694	11	1675	19	1754	26	95
Spot20	10.12	0.18	0.4478	0.0065	0.0026	2447	16	2384	29	2498	27	95
Spot54	7.774	0.099	0.3958	0.0046	0.0013	2207	11	2152	21	2281	16	94
Spot62	4.003	0.053	0.2809	0.0035	0.0013	1635	11	1595	17	1697	23	94
Spot70	4.168	0.054	0.2871	0.0033	0.0014	1667	11	1626	16	1738	25	94
Spot19	4.192	0.082	0.2871	0.005	0.002	1675	16	1626	25	1742	35	93
Spot106	4.73	0.082	0.3029	0.0049	0.0022	1773	14	1707	24	1840	36	93
Spot49	4.294	0.062	0.2897	0.0039	0.0016	1691	12	1641	19	1770	27	93
Spot92	4.712	0.09	0.3028	0.0057	0.0022	1767	16	1704	28	1846	36	92
Spot39	9.49	0.14	0.4276	0.0064	0.0022	2387	13	2293	29	2485	22	92
Spot26	4.755	0.05	0.3046	0.0034	0.001	1776.8	9.1	1715	17	1860	15	92
Spot36	4.103	0.094	0.2814	0.005	0.0022	1653	19	1598	25	1735	37	92
Spot81	9.1	0.1	0.4174	0.0046	0.002	2348	10	2250	21	2444	21	92
Spot91	4.111	0.048	0.2826	0.0027	0.0013	1655.6	9.7	1604	13	1751	22	92
Spot21	26.91	0.24	0.6451	0.0068	0.0022	3379.1	8.8	3210	27	3505	11	92
Spot65	4.189	0.055	0.2839	0.0034	0.0013	1671	11	1610	17	1764	22	91
Spot17	3.507	0.047	0.2576	0.0029	0.0013	1527	11	1477	15	1621	24	91
Spot76	4.073	0.061	0.2798	0.0033	0.001	1648	12	1590	17	1747	17	91
Spot69	3.934	0.048	0.2744	0.0034	0.0011	1620	10	1563	17	1728	18	90
Spot93	4.859	0.071	0.3192	0.0049	0.0015	1793	12	1786	24	1809	24	99
Spot52	5.396	0.089	0.3395	0.0052	0.0018	1884	14	1882	25	1906	28	99
Spot58	11.33	0.17	0.5064	0.0067	0.0024	2552	14	2639	29	2464	26	107
Spot30	4.964	0.073	0.3292	0.0037	0.0014	1813	12	1834	18	1768	24	104
Spot64	5.807	0.085	0.3551	0.0045	0.0017	1947	13	1957	21	1933	25	101
Spot8	4.614	0.069	0.3123	0.0038	0.0013	1749	12	1751	18	1739	22	101
Spot59	4.901	0.07	0.321	0.0037	0.0012	1803	12	1794	18	1798	20	100
Spot46	11.06	0.16	0.479	0.0057	0.0017	2526	13	2522	25	2532	17	100
Spot96	5.312	0.053	0.3325	0.0029	0.0011	1869.6	8.5	1850	14	1869	17	99
Spot67	20.72	0.25	0.6132	0.0066	0.0019	3126	12	3082	27	3158	12	98
Spot4	4.287	0.054	0.2947	0.0035	0.0011	1691	10	1665	17	1723	19	97
Spot82	5.049	0.071	0.3165	0.0036	0.0019	1826	12	1772	18	1854	30	96
Spot100	3.973	0.043	0.2805	0.0025	0.0011	1628.2	8.7	1594	13	1669	19	96
Spot66	5.678	0.073	0.3391	0.0038	0.0015	1930	11	1882	18	1972	22	95
Spot28	4.744	0.068	0.3072	0.0039	0.0018	1778	12	1728	19	1820	29	95
Spot88	4.284	0.063	0.2898	0.0033	0.0014	1689	12	1642	17	1739	25	94
Spot23	4.453	0.061	0.295	0.0036	0.0016	1722	11	1669	18	1777	27	94
Spot35	4.886	0.094	0.3101	0.0055	0.0026	1797	16	1740	27	1856	42	94
Spot78	3.54	0.064	0.2599	0.0032	0.0017	1533	14	1488	16	1598	32	93
Spot72	23.94	0.31	0.6207	0.0074	0.003	3268	12	3114	29	3351	17	93
Spot3	4.29	0.057	0.2876	0.0035	0.0015	1691	11	1631	18	1761	27	93
Spot10	6.657	0.09	0.3601	0.0039	0.0018	2069	12	1984	18	2147	23	92
Spot85	4.531	0.059	0.2944	0.0032	0.0013	1735	11	1664	16	1808	21	92
Spot45	3.255	0.052	0.2458	0.0027	0.0014	1468	13	1416	14	1539	26	92
Spot89	4.136	0.052	0.2826	0.0031	0.0011	1662	11	1604	16	1745	18	92
Spot14	4.212	0.064	0.2839	0.0029	0.0016	1677	12	1611	15	1755	27	92
Spot56	4.628	0.044	0.2973	0.0026	0.0009	1753.3	7.9	1678	13	1843	14	91
Spot6	4.189	0.075	0.2822	0.0042	0.0014	1671	15	1604	21	1784	24	90
Spot12	9.307	0.077	0.4161	0.004	0.0015	2368.4	7.5	2243	18	2493	16	90

Table 2 Detrital zircon U–Pb dating results of analysed samples

	Rejected analysis											
Spot5	6.3	0.11	0.417	0.0058	0.0018	2021	14	2245	26	1811	29	124
Spot79	11.26	0.2	0.5532	0.0088	0.0024	2542	17	2841	36	2306	28	123
Spot55	6.71	0.12	0.4264	0.0063	0.0018	2074	15	2288	29	1892	28	121
Spot44	5.119	0.085	0.3572	0.0053	0.0012	1839	14	1972	26	1683	22	117
Spot101	5.813	0.071	0.3831	0.0044	0.0012	1947	11	2090	21	1806	19	116
Spot51	5.191	0.09	0.3558	0.005	0.0017	1853	15	1961	24	1731	29	113
Spot71	6.486	0.077	0.3979	0.0041	0.0012	2044	10	2161	19	1935	18	112
Spot25	12.41	0.15	0.546	0.0065	0.0018	2635	11	2807	27	2524	18	111
Spot95	16.18	0.43	0.612	0.013	0.0033	2886	26	3090	55	2787	27	111
Spot11	4.182	0.076	0.2797	0.0039	0.0014	1672	15	1589	20	1787	24	89
Spot33	3.766	0.057	0.2627	0.0032	0.0012	1586	12	1505	16	1704	22	88
Spot27	3.616	0.048	0.2574	0.0027	0.0013	1551	11	1476	14	1685	23	88
Spot86	4.067	0.061	0.2717	0.0043	0.0013	1648	12	1549	22	1808	22	86
Spot13	8.05	0.13	0.3727	0.0069	0.0021	2236	15	2041	32	2429	21	84
Spot73	3.459	0.062	0.2451	0.0043	0.0019	1517	14	1413	22	1682	35	84
Spot97	8.026	0.073	0.3689	0.0034	0.0015	2233.5	8.1	2023	16	2457	16	82
Spot80	4.039	0.069	0.2644	0.0054	0.0025	1641	14	1512	28	1838	39	82
Spot83	4.332	0.068	0.2707	0.0035	0.0014	1698	13	1544	18	1913	22	81
Spot9	3.725	0.059	0.2488	0.0031	0.0013	1578	12	1432	16	1782	22	80
Spot77	3.29	0.045	0.2299	0.0028	0.0009	1477	11	1333	15	1710	16	78
Spot7	3.383	0.034	0.2309	0.0021	0.001	1499.4	7.9	1339	11	1751	17	76
Spot68	5.291	0.066	0.2823	0.0028	0.0012	1867	11	1602	14	2190	15	73
Spot102	2.856	0.036	0.196	0.0023	0.0012	1369.2	9.5	1154	12	1744	21	66
Spot24	4.878	0.081	0.2556	0.0034	0.0026	1799	14	1467	17	2224	32	66
Spot110	2.461	0.039	0.1761	0.0023	0.0011	1259	11	1047	13	1659	21	63
Spot32	3.399	0.037	0.2249	0.002	0.0008	1503	8.4	1308	11	1774	14	74
Spot43	5.334	0.075	0.2826	0.0035	0.0013	1876	12	1604	18	2186	16	73
Spot75	4.12	0.1	0.2428	0.0056	0.0031	1661	21	1400	29	1994	48	70
Spot37	7.25	0.14	0.3124	0.0048	0.0036	2140	18	1752	23	2549	32	69
Spot104	2.806	0.06	0.1887	0.0036	0.0018	1359	17	1114	20	1778	30	63
Spot105	2.124	0.03	0.1546	0.0025	0.0011	1155.6	9.9	928	14	1595	21	58
Spot48	2.639	0.041	0.1663	0.002	0.0014	1312	12	992	11	1879	23	53
Spot15	1.965	0.02	0.1351	0.0012	0.0006	1103	7	816.9	6.8	1715	11	48
Spot29	1.75	0.029	0.1183	0.0018	0.0012	1026	11	720	10	1756	20	41
Spot107	76	38	0.43	0.21	0.43	4100	480	2100	880	######	####	34
Spot18	1.371	0.027	0.0839	0.0012	0.0017	876	11	519.4	7.2	1939	25	27
Spot40	7.503	0.063	0.4271	0.0039	0.001	2173.2	7.4	2293	18	2081	13	110
Spot22	3.833	0.083	0.2682	0.0039	0.0024	1604	17	1531	20	1705	42	90

Appendix 2

Appendix for Chapter 3

Appendix 2

Appendix for Chapter 3

1. U–Pb dating samples and results

Three sandstone samples were selected for U–Pb analysis and the sample information is presented in Table 1. Detrital Zircon U–Pb discordance was calculated by dividing the $^{206}Pb/^{238}U$ age by the $^{207}Pb/^{206}Pb$ age and multiplying by 100. The $^{207}Pb/^{206}Pb$ ages are used and results were plotted using Excel add-in Isoplot (*Ludwig 2003*).

Table 1 Summary of detrital zircon U–Pb samples

Core drill	Coordinate	Sample	Depth (m)	Formation	concordant/total analyses	Lithology
Elliott-1	E: 133.7551° S:17.4025°	EN-Ky4	1021.5	Kyalla Fm	92/127	fine-grained sandstone with interlaminated siltstone/shale
		EN-Mo8	1367.3	Moroak Sst.	59/113	quartz-granule-rich medium to coarse-grained sandstone
Jamison-1	E: 133.7672° S: 16.7749°	JN-Ky6	1587.0	Kyalla Fm	36/57	fine-grained sandstone

Kyalla Formation (EN-Ky4)

One hundred and sixteen zircons were analysed from EN-Ky4 and of these, ninety one are within 10% of concordance. These zircons range in Pb^{207}/Pb^{206} age from 2991 Ma to 1517 Ma. A major peak is identified on the kernel density plot at 1727 Ma, with majority of the analyses sitting between 2073–1571 Ma. Minor peaks are seen at 1781 and 1622 Ma. The youngest near concordant grain within EN-Ky4 is 1517 ± 58 Ma.

Moroak Sandstone (EN-Mo8)

One hundred and thirteen zircons were analysed. Of these seventy seven are within 10% of concordance and have a range of Pb^{207}/Pb^{206} ages between 3073–1502 Ma. The kernel density plot highlights one major peak at 1697 Ma, with majority of the data sitting between 1823–1502 Ma. A minor peak is seen at 1561 Ma, with one solitary grain at 3073 ± 26 Ma. The youngest analysis yielded a Pb^{207}/Pb^{206} age of 1502 Ma ± 75 Ma.

Kyalla Formation (JN-Ky6)

Thirty six, less than 10% discordant analyses (n=57), yielded Pb^{207}/Pb^{206} ages between 1883 and 1360 Ma. A majority of the data sit between 1794–1647 Ma, with a dominated peak and a minor peak highlighted in the kernel density estimates at 1723 Ma and 1795 Ma, respectively. The youngest grain analysed in this sample yielded a Pb^{207}/Pb^{206} age of 1360 ± 47 Ma.

Table 2 Detrital zircon U–Pb dating results

Analysis No.	$^{207}Pb/^{235}U$	2 S.E.	$^{206}Pb/^{238}U$	2 S.E.	Rho	$^{207}Pb/^{235}U$ age (Ma)	2 S.E.	$^{206}Pb/^{238}U$ age (Ma)	2 S.E.	$^{207}Pb/^{206}Pb$ age (Ma)	2 S.E.	Conc (%)
EN-Ky4												
9-EN4-1	4.37	0.13	0.3006	0.0087	0.67084	1705	25	1691	43	**1732**	**45**	97.6
10-EN4-2	5.11	0.1	0.3191	0.008	0.73606	1835	17	1783	39	**1898**	**30**	93.6
12-EN4-4	3.91	0.13	0.277	0.0071	0.64938	1615	30	1578	37	**1699**	**50**	92.3
13-EN4-5	5.02	0.17	0.312	0.011	0.6474	1817	29	1750	53	**1898**	**52**	91.5
15-EN4-7	4.95	0.14	0.3147	0.009	0.74859	1815	23	1762	44	**1890**	**36**	92.7
16-EN4-8	9.64	0.24	0.442	0.012	0.76041	2410	22	2371	54	**2451**	**29**	96.6
18-EN4-10	4.45	0.2	0.3	0.011	0.58409	1743	37	1687	53	**1793**	**62**	93.7
20-EN4-12	4.27	0.12	0.288	0.011	0.62804	1685	22	1629	55	**1751**	**56**	92.5
23-EN4-15	4.13	0.13	0.2848	0.009	0.73447	1656	27	1614	45	**1702**	**47**	94.5
32-EN4-16	4.54	0.13	0.3107	0.0095	0.70493	1739	25	1745	47	**1755**	**39**	99.4
34-EN4-18	4.37	0.13	0.299	0.011	0.72221	1703	25	1685	52	**1748**	**38**	96.3
37-EN4-21	3.78	0.11	0.2714	0.0074	0.33123	1588	25	1546	38	**1639**	**60**	94.0
38-EN4-22	3.65	0.15	0.275	0.011	0.53699	1568	33	1562	54	**1599**	**86**	97.6
39-EN4-23	4.32	0.13	0.2969	0.0089	0.58568	1703	26	1674	44	**1775**	**49**	94.0
41-EN4-25	4.58	0.23	0.303	0.012	0.79287	1739	42	1703	62	**1787**	**60**	95.1
43-EN4-27	4.29	0.15	0.289	0.01	0.66926	1687	29	1641	49	**1732**	**49**	94.5
44-EN4-28	4.6	0.17	0.3044	0.0088	0.60099	1742	31	1711	43	**1790**	**56**	95.4
45-EN4-29	5.01	0.14	0.3263	0.0099	0.71708	1822	25	1827	48	**1844**	**43**	99.1
46-EN4-30	4.92	0.14	0.3184	0.0084	0.61062	1801	24	1785	40	**1819**	**37**	98.1
58-EN4-34	8.39	0.32	0.399	0.015	0.81588	2270	35	2178	65	**2356**	**34**	91.8
59-EN4-35	4.05	0.11	0.2819	0.0082	0.74801	1640	23	1604	42	**1655**	**37**	96.8
60-EN4-36	4.82	0.16	0.311	0.01	0.4517	1787	28	1742	50	**1803**	**64**	96.5
63-EN4-39	4.87	0.13	0.3229	0.0099	0.77496	1798	21	1809	47	**1747**	**35**	103.4
64-EN4-40	4.14	0.12	0.2776	0.0092	0.76815	1659	24	1578	47	**1711**	**44**	91.6
65-EN4-41	4.478	0.097	0.3046	0.0073	0.70858	1728	18	1712	36	**1684**	**30**	101.6
66-EN4-42	5.22	0.13	0.3277	0.0088	0.44345	1857	20	1826	43	**1806**	**53**	101.1
67-EN4-43	4.7	0.12	0.3146	0.0092	0.44302	1771	20	1768	46	**1700**	**50**	103.8
68-EN4-44	5.05	0.13	0.326	0.0079	0.63407	1824	22	1817	38	**1791**	**43**	101.4
69-EN4-45	4.42	0.12	0.302	0.008	0.72437	1715	22	1699	40	**1680**	**36**	101.1
78-EN4-46	4.87	0.13	0.3074	0.0094	0.60034	1795	24	1725	47	**1810**	**48**	95.1
79-EN4-47	3.85	0.15	0.26	0.011	0.76528	1604	33	1487	56	**1631**	**54**	90.3
80-EN4-48	5.1	0.15	0.3234	0.0091	0.64554	1831	25	1810	45	**1761**	**41**	102.7
81-EN4-49	4.92	0.22	0.314	0.016	0.81487	1810	35	1759	79	**1754**	**54**	100.3
82-EN4-50	4.44	0.17	0.307	0.012	0.62592	1723	30	1728	59	**1641**	**57**	105.0

Table 2 Detrital zircon U–Pb dating results

83-EN4-51	4.02	0.11	0.2778	0.0074	0.76591	1634	21	1578	37	**1620**	**35**	97.3
84-EN4-52	4.48	0.12	0.3081	0.0092	0.742	1724	22	1729	45	**1650**	**35**	104.6
85-EN4-53	4.56	0.13	0.2996	0.0084	0.75409	1745	22	1693	43	**1692**	**31**	100.1
88-EN4-56	9.13	0.25	0.413	0.012	0.62641	2352	25	2226	53	**2367**	**36**	93.7
92-EN4-60	4.204	0.094	0.2922	0.0073	0.74654	1671	19	1651	37	**1640**	**30**	100.7
102-EN4-61	5.11	0.17	0.33	0.012	0.57979	1838	29	1835	60	**1781**	**62**	102.9
103-EN4-62	4.84	0.13	0.3215	0.008	0.63564	1790	22	1795	39	**1757**	**40**	102.1
105-EN4-64	5.57	0.17	0.3459	0.0093	0.64968	1911	26	1913	45	**1851**	**43**	103.2
106-EN4-65	4.58	0.1	0.3099	0.0075	0.8078	1745	18	1747	37	**1714**	**23**	101.9
108-EN4-67	3.67	0.13	0.267	0.012	0.58213	1562	29	1525	61	**1517**	**58**	100.5
109-EN4-68	3.67	0.15	0.2683	0.0082	0.63381	1561	31	1531	42	**1553**	**54**	98.6
111-EN4-70	5.02	0.11	0.324	0.0078	0.62075	1822	19	1807	38	**1795**	**37**	100.7
112-EN4-71	4.55	0.12	0.3026	0.0085	0.46199	1741	22	1702	42	**1720**	**47**	98.9
113-EN4-72	4.83	0.11	0.3121	0.0073	0.46717	1787	19	1749	36	**1784**	**39**	98.0
114-EN4-73	4.22	0.16	0.282	0.013	0.68419	1675	31	1601	63	**1725**	**47**	92.3
116-EN4-75	11.03	0.37	0.478	0.018	0.72622	2524	32	2522	75	**2517**	**43**	100.2
126-EN4-77	4.4	0.13	0.304	0.011	0.66204	1710	24	1708	54	**1707**	**51**	100.1
127-EN4-78	5.29	0.14	0.337	0.01	0.58299	1869	22	1859	50	**1824**	**48**	101.9
128-EN4-79	4.22	0.1	0.2965	0.008	0.59543	1678	21	1676	39	**1693**	**42**	99.0
129-EN4-80	4.66	0.13	0.305	0.011	0.45911	1757	24	1715	52	**1846**	**57**	92.4
131-EN4-82	16.61	0.31	0.542	0.013	0.75695	2912	19	2801	54	**2991**	**24**	93.2
132-EN4-83	4.58	0.19	0.309	0.01	0.47874	1736	36	1735	51	**1737**	**68**	99.9
136-EN4-87	4.18	0.11	0.2906	0.0076	0.68843	1667	21	1643	38	**1743**	**37**	93.9
137-EN4-88	4.63	0.22	0.314	0.012	0.33628	1751	40	1757	61	**1732**	**79**	101.4
138-EN4-89	4.43	0.15	0.309	0.011	0.593	1722	28	1735	53	**1722**	**50**	100.7
148-EN4-91	5.09	0.12	0.3345	0.0084	0.71681	1835	20	1857	40	**1866**	**31**	99.5
149-EN4-92	4.73	0.15	0.313	0.011	0.45177	1771	26	1753	52	**1816**	**60**	96.4
150-EN4-93	4.08	0.24	0.281	0.017	0.50537	1643	50	1592	84	**1720**	**110**	92.0
151-EN4-94	10.22	0.22	0.457	0.01	0.63459	2454	20	2422	46	**2500**	**31**	96.8
152-EN4-95	5.08	0.13	0.3296	0.0095	0.749	1834	23	1834	46	**1835**	**34**	99.9
156-EN4-99	6.09	0.3	0.354	0.015	0.59377	1991	45	1953	70	**2073**	**68**	93.9
157-EN4-100	3.95	0.17	0.285	0.011	0.47147	1620	35	1612	55	**1739**	**77**	92.1
158-EN4-101	4.67	0.1	0.3132	0.0083	0.69371	1758	19	1754	41	**1814**	**29**	96.6
159-EN4-102	4.46	0.13	0.312	0.0092	0.57626	1723	23	1749	45	**1746**	**43**	100.2
161-EN4-104	10.56	0.27	0.461	0.015	0.81842	2484	24	2437	68	**2540**	**32**	95.8
162-EN4-105	4.33	0.11	0.3039	0.008	0.45037	1699	21	1708	40	**1748**	**48**	97.7
172-EN4-107	4.2	0.15	0.284	0.011	0.80073	1671	29	1608	57	**1764**	**46**	90.3
173-EN4-108	4.512	0.092	0.304	0.0071	0.60634	1733	17	1709	35	**1798**	**33**	94.8
181-EN4-116	4.68	0.12	0.3203	0.0079	0.53732	1769	21	1789	38	**1787**	**40**	100.1
182-EN4-117	4.6	0.13	0.3167	0.0084	0.48818	1750	24	1771	41	**1767**	**46**	100.2
184-EN4-119	4.29	0.12	0.2942	0.0085	0.71126	1688	23	1661	42	**1741**	**31**	95.2
195-EN4-122	5.53	0.12	0.345	0.0083	0.72234	1905	19	1908	40	**1928**	**30**	99.0
196-EN4-123	15.6	1.1	0.535	0.028	0.679	2868	60	2760	120	**2986**	**96**	91.8
197-EN4-124	5.15	0.11	0.3308	0.0085	0.70468	1843	17	1839	41	**1861**	**27**	98.8
199-EN4-126	7.78	0.19	0.396	0.012	0.67251	2203	22	2148	56	**2204**	**34**	97.4

Table 2 Detrital zircon U–Pb dating results

200-EN4-127	3.95	0.12	0.2852	0.0084	0.64208	1626	27	1616	42	**1657**	**40**	97.5
201-EN4-128	3.77	0.11	0.2695	0.0076	0.63756	1582	24	1537	39	**1622**	**43**	94.5
202-EN4-129	10.44	0.3	0.462	0.013	0.68094	2473	26	2445	56	**2498**	**38**	97.8
205-EN4-132	4.65	0.17	0.316	0.015	0.72076	1755	32	1767	75	**1774**	**57**	99.6
206-EN4-133	5.77	0.16	0.353	0.01	0.80511	1940	25	1948	49	**1939**	**30**	100.5
207-EN4-134	4.45	0.14	0.301	0.01	0.65117	1722	26	1696	49	**1718**	**44**	98.7
219-EN4-138	4.724	0.094	0.3173	0.0084	0.71203	1769	17	1774	41	**1747**	**32**	101.5
221-EN4-140	4.28	0.12	0.286	0.011	0.61025	1687	23	1618	54	**1760**	**59**	91.2
222-EN4-141	4.45	0.14	0.296	0.018	0.8074	1721	26	1670	92	**1750**	**70**	95.2
224-EN4-143	5.37	0.3	0.337	0.019	0.72102	1874	48	1870	90	**1914**	**63**	97.6
226-EN4-145	4.23	0.12	0.291	0.011	0.79777	1677	24	1644	54	**1698**	**41**	96.7
228-EN4-147	4.03	0.24	0.272	0.017	0.40034	1636	47	1549	86	**1673**	**66**	92.0
229-EN4-148	4.21	0.13	0.294	0.011	0.85396	1673	25	1658	53	**1680**	**34**	98.7
					Rejected disconcordant analyses							
011-EN4-3	3.93	0.11	0.2529	0.0081	0.54829	1617	24	1452	42	1857	42	72.1
014-EN4-6	3.066	0.082	0.2155	0.0078	0.49814	1422	21	1257	41	1727	40	62.6
019-EN4-11	3.95	0.12	0.2528	0.0077	0.72578	1620	24	1452	40	1876	40	70.8
021-EN4-13	2.563	0.063	0.1738	0.0064	0.73708	1293	19	1033	35	1814	47	24.4
035-EN4-19	3.24	0.12	0.218	0.0072	0.69286	1461	30	1270	38	1791	53	59.0
040-EN4-24	2.58	0.078	0.1747	0.006	0.71906	1300	22	1037	33	1726	46	33.6
042-EN4-26	3.27	0.11	0.2187	0.0074	0.68623	1477	26	1274	39	1746	46	63.0
057-EN4-33	2.785	0.083	0.2038	0.0074	0.65518	1349	22	1195	39	1532	62	71.8
061-EN4-37	3.46	0.15	0.227	0.01	0.65057	1515	34	1316	54	1778	46	64.9
062-EN4-38	2.61	0.13	0.1788	0.0082	0.69484	1301	36	1060	45	1715	62	38.2
086-EN4-54	3.47	0.18	0.2329	0.0088	0.73547	1526	39	1349	46	1712	62	73.1
090-EN4-58	3.36	0.15	0.2141	0.0097	0.82154	1492	34	1250	52	1778	43	57.8
107-EN4-66	3.67	0.12	0.2331	0.0083	0.66446	1563	26	1349	44	1785	54	67.7
110-EN4-69	3.23	0.12	0.2156	0.0096	0.72656	1462	29	1257	51	1699	35	64.8
125-EN4-76	3.67	0.14	0.244	0.011	0.6227	1562	30	1407	55	1757	63	75.1
134-EN4-85	2.7	0.11	0.1857	0.0074	0.82388	1325	31	1097	40	1671	48	47.7
139-EN4-90	3.9	0.19	0.242	0.016	0.73573	1610	40	1395	85	1888	69	64.7
160-EN4-103	2.75	0.092	0.1905	0.008	0.81405	1344	26	1123	43	1743	46	44.8
171-EN4-106	3.6	0.2	0.243	0.013	0.40851	1546	45	1400	65	1840	80	68.6
174-EN4-109	3.63	0.1	0.237	0.01	0.87139	1555	22	1369	53	1851	42	64.8
176-EN4-111	3.3	0.13	0.229	0.011	0.74626	1478	31	1328	57	1710	68	71.2
178-EN4-113	3.6	0.1	0.2309	0.0078	0.78392	1546	23	1338	41	1851	42	61.7
198-EN4-125	3.77	0.16	0.246	0.018	0.68283	1586	34	1415	93	1791	54	73.4
203-EN4-130	3.43	0.1	0.2341	0.0098	0.53266	1509	23	1355	51	1739	43	71.7
208-EN4-135	0.302	0.019	0.1649	0.0099	0.70076	267	14	983	54	1520	56	45.4
EN-Mo8												
240-EN8-1	4.3	0.17	0.292	0.01	0.62924	1693	32	1649	51	**1691**	**50**	97.5
241-EN8-2	4.57	0.16	0.3059	0.0097	0.64495	1738	29	1732	48	**1705**	**51**	101.6

Table 2 Detrital zircon U–Pb dating results

243-EN8-4	4.119	0.099	0.2891	0.0097	0.61624	1665	22	1635	49	**1682**	**54**	97.1
248-EN8-9	4.2	0.15	0.285	0.0095	0.64246	1673	27	1614	48	**1676**	**54**	96.2
249-EN8-10	4.73	0.13	0.3109	0.009	0.7292	1770	24	1742	44	**1726**	**35**	100.9
250-EN8-11	4.9	0.15	0.328	0.01	0.64902	1799	26	1827	49	**1692**	**43**	107.4
252-EN8-13	3.71	0.11	0.2564	0.0095	0.7343	1571	23	1470	49	**1667**	**35**	86.6
253-EN8-14	4.52	0.14	0.3093	0.0092	0.77992	1737	24	1735	46	**1697**	**33**	102.2
254-EN8-15	4.65	0.11	0.3156	0.0078	0.59934	1763	19	1766	38	**1682**	**35**	104.8
264-EN8-17	4.18	0.13	0.3082	0.0092	0.74767	1665	25	1730	45	**1567**	**42**	109.4
265-EN8-18	4.92	0.13	0.3328	0.0089	0.62364	1804	22	1849	43	**1776**	**33**	103.9
266-EN8-19	5.01	0.12	0.3324	0.0085	0.69658	1824	22	1857	40	**1786**	**34**	103.8
267-EN8-20	4.77	0.28	0.323	0.013	0.68171	1771	50	1807	66	**1710**	**140**	105.4
268-EN8-21	3.81	0.12	0.2886	0.0084	0.76858	1606	26	1633	42	**1561**	**43**	104.4
269-EN8-22	4.37	0.13	0.3047	0.0087	0.80432	1711	24	1712	43	**1709**	**33**	100.2
270-EN8-23	4.32	0.12	0.2988	0.0095	0.80685	1696	23	1683	47	**1697**	**34**	99.2
271-EN8-24	4.09	0.12	0.2914	0.0072	0.64115	1655	23	1647	36	**1710**	**29**	96.2
273-EN8-26	4.57	0.12	0.3073	0.0081	0.5521	1740	22	1725	40	**1742**	**38**	99.0
274-EN8-27	4.21	0.11	0.2886	0.0085	0.83437	1676	22	1632	43	**1701**	**43**	95.8
275-EN8-28	4.5	0.15	0.314	0.01	0.75342	1734	27	1758	51	**1658**	**60**	105.7
276-EN8-30	10.58	0.25	0.469	0.012	0.38478	2485	23	2489	52	**2467**	**22**	100.9
286-EN8-32	4.77	0.14	0.3012	0.008	0.31994	1784	26	1700	39	**1823**	**31**	92.8
287-EN8-33	4.59	0.18	0.3016	0.0096	0.54611	1745	32	1704	46	**1700**	**61**	100.2
288-EN8-34	4.72	0.14	0.3035	0.0086	0.54262	1768	26	1706	42	**1775**	**61**	96.0
289-EN8-35	4.27	0.17	0.285	0.012	0.51585	1684	32	1627	60	**1696**	**74**	95.8
293-EN8-39	4.69	0.14	0.311	0.008	0.59274	1759	26	1743	40	**1718**	**48**	101.4
295-EN8-41	4.7	0.14	0.3157	0.0089	0.43688	1765	26	1771	43	**1738**	**38**	101.9
296-EN8-42	3.75	0.11	0.277	0.0066	0.39021	1587	22	1575	33	**1580**	**42**	99.7
299-EN8-45	3.34	0.13	0.2497	0.0086	0.54219	1489	32	1435	45	**1550**	**83**	92.0
313-EN8-51	3.75	0.15	0.278	0.01	0.28194	1584	33	1581	51	**1502**	**75**	105.0
317-EN8-55	3.8	0.11	0.2689	0.0083	0.66012	1586	25	1533	42	**1616**	**44**	94.6
320-EN8-58	3.63	0.16	0.26	0.011	0.74626	1557	34	1499	54	**1527**	**50**	98.1
335-EN8-65	3.8	0.16	0.2993	0.0073	0.79805	1591	33	1686	36	**1613**	**73**	104.3
336-EN8-66	3.644	0.086	0.2938	0.007	0.80953	1556	19	1658	35	**1558**	**46**	106.0
338-EN8-68	18.85	0.48	0.615	0.016	0.60625	3033	25	3084	63	**3073**	**26**	100.4
341-EN8-71	3.62	0.13	0.2879	0.0079	0.73268	1561	29	1634	39	**1565**	**62**	104.2
343-EN8-73	4.67	0.13	0.326	0.01	0.78187	1759	23	1826	50	**1707**	**31**	106.5
344-EN8-74	4.43	0.17	0.315	0.012	0.71045	1721	31	1763	58	**1696**	**46**	103.8
345-EN8-75	4.56	0.19	0.308	0.011	0.78061	1738	36	1729	56	**1700**	**50**	101.7
354-EN8-76	4.32	0.14	0.2899	0.0084	0.6643	1700	26	1639	42	**1769**	**51**	92.1
357-EN8-79	4.4	0.15	0.2998	0.0089	0.75732	1705	28	1688	44	**1702**	**63**	99.2
358-EN8-80	4.9	0.13	0.3307	0.0097	0.64511	1798	22	1839	47	**1742**	**39**	105.3
359-EN8-81	3.67	0.15	0.2638	0.0088	0.78579	1561	32	1507	45	**1607**	**33**	93.4
361-EN8-83	4.31	0.11	0.2918	0.008	0.63841	1691	21	1653	40	**1717**	**30**	96.1
364-EN8-86	4.95	0.17	0.321	0.011	0.71655	1805	30	1797	57	**1738**	**59**	103.3
365-EN8-87	4.46	0.16	0.312	0.0094	0.88573	1722	29	1748	46	**1678**	**60**	104.0
366-EN8-88	3.67	0.13	0.2661	0.0074	0.80102	1562	27	1519	37	**1600**	**44**	94.7

Table 2 Detrital zircon U–Pb dating results

367-EN8-89	4.6	0.12	0.3195	0.0083	0.63491	1757	24	1785	40	**1715**	**31**	103.9
368-EN8-90	3.83	0.12	0.2802	0.0079	0.62712	1593	25	1590	40	**1563**	**37**	101.7
388-EN8-102	3.473	0.084	0.2769	0.0073	0.79654	1521	20	1579	37	**1551**	**33**	101.8
390-EN8-104	8.52	0.27	0.442	0.014	0.67786	2284	29	2358	61	**2342**	**31**	100.7
391-EN8-105	5.034	0.092	0.3394	0.0073	0.77278	1825	15	1882	35	**1818**	**25**	103.4
400-EN8-106	4.76	0.15	0.3013	0.0088	0.65828	1776	28	1695	44	**1705**	**43**	99.4
401-EN8-107	10.66	0.33	0.449	0.012	0.80183	2489	29	2388	55	**2476**	**32**	96.3
403-EN8-109	4.85	0.2	0.309	0.011	0.74977	1791	35	1733	54	**1714**	**34**	101.1
405-EN8-111	4.83	0.13	0.3119	0.0082	0.81434	1786	23	1748	40	**1729**	**36**	101.1
412-EN8-118	4.41	0.13	0.302	0.0083	0.61862	1721	26	1699	41	**1748**	**39**	97.1
413-EN8-119	4.052	0.087	0.2955	0.008	0.46038	1645	18	1667	40	**1598**	**46**	104.1
414-EN8-120	3.59	0.18	0.279	0.011	0.74763	1548	37	1584	58	**1555**	**72**	101.8
					Rejected disconcordant analyses							
242-EN8-3	3.21	0.1	0.2199	0.0056	0.63347	1460	25	1281	30	1671	46	69.6
244-EN8-5	2.643	0.086	0.1979	0.0066	0.14989	1313	23	1163	35	1473	34	73.3
245-EN8-6	2.292	0.087	0.1741	0.0062	0.62996	1211	28	1034	34	1506	64	54.4
247-EN8-8	3.081	0.083	0.2047	0.0065	0.5177	1428	21	1199	35	1730	44	55.7
251-EN8-12	10.72	0.3	0.349	0.011	0.76775	2502	25	1933	49	2958	24	47.0
263-EN8-16	2.402	0.089	0.188	0.0083	0.52296	1239	27	1115	44	1520	61	63.7
285-EN8-31	2.252	0.079	0.1468	0.0053	0.51468	1194	25	882	30	1727	42	4.2
290-EN8-36	4.69	0.18	0.2614	0.0086	0.71655	1764	33	1495	44	1702	57	86.2
292-EN8-38	3.417	0.084	0.2261	0.0065	0.88573	1513	18	1312	34	1736	36	67.7
297-EN8-43	2.418	0.088	0.1669	0.0067	0.54452	1249	27	994	37	1653	39	33.7
309-EN8-47	2.657	0.079	0.1744	0.0044	0.5359	1315	22	1035	24	1803	34	25.8
310-EN8-48	2.179	0.064	0.1293	0.0032	0.7461	1179	20	784	19	1676	35	-13.8
311-EN8-49	7.22	0.24	0.3239	0.0083	0.79941	2137	30	1808	40	2484	23	62.6
312-EN8-50	2.217	0.065	0.1424	0.0041	0.65378	1185	21	858	23	1812	20	-11.2
314-EN8-52	2.014	0.054	0.1512	0.0042	0.70645	1117	18	907	24	1484	31	36.4
315-EN8-53	3.063	0.072	0.2048	0.0055	0.6522	1423	18	1203	30	1692	41	59.4
319-EN8-57	3.71	0.11	0.2152	0.0063	0.77186	1573	25	1255	33	1961	45	43.7
321-EN8-59	2.305	0.069	0.1684	0.005	0.52827	1214	21	1002	27	1561	55	44.2
337-EN8-67	2.044	0.052	0.1568	0.0042	0.78342	1130	17	941	23	1644	36	25.3
340-EN8-70	1.402	0.052	0.1084	0.0034	0.53363	889	22	663	20	1546	50	-33.2
342-EN8-72	1.972	0.066	0.1332	0.0052	0.52518	1108	21	811	31	1483	34	17.1
355-EN8-77	2.75	0.16	0.1587	0.0075	0.73117	1344	41	949	42	1646	76	26.6
356-EN8-78	3.614	0.073	0.236	0.0052	0.73547	1550	16	1365	27	1800	27	68.1
360-EN8-82	2.934	0.095	0.2069	0.0061	0.82154	1387	25	1211	33	1649	37	63.8
362-EN8-84	2.89	0.14	0.188	0.011	0.66446	1373	37	1106	58	1777	47	39.3
379-EN8-93	3.407	0.097	0.2289	0.0079	0.47317	1506	23	1327	41	1791	34	65.0
382-EN8-96	3.67	0.18	0.2149	0.0084	0.59215	1567	41	1252	44	2144	29	28.8
385-EN8-99	9.86	0.34	0.405	0.015	0.64282	2417	32	2190	69	2695	34	76.9
386-EN8-100	2.666	0.081	0.1967	0.0074	0.48283	1317	23	1156	40	1673	45	55.3
389-EN8-103	2.824	0.09	0.2078	0.0067	0.60423	1358	24	1216	36	1688	30	61.2
404-EN8-110	3.88	0.16	0.252	0.01	0.79941	1607	34	1446	52	1753	68	78.8

Table 2 Detrital zircon U–Pb dating results

406-EN8-112	2.74	0.11	0.195	0.0079	0.75048	1337	31	1147	43	1542	61	65.6
407-EN8-113	1.952	0.045	0.1418	0.0041	0.83831	1097	15	854	23	1519	32	22.1
408-EN8-114	1.881	0.074	0.1428	0.006	0.67802	1072	26	860	34	1460	44	30.2
410-EN8-116	2.352	0.07	0.1763	0.0055	0.73708	1237	22	1046	30	1578	40	49.1
411-EN8-117	1.745	0.045	0.1326	0.0027	0.69286	1022	17	803	15	1527	34	9.8
272-EN8-25	3.395	0.082	0.2367	0.0068	0.53284	1502	19	1368	36	**1768**	**37**	70.8
291-EN8-37	3.82	0.11	0.2572	0.0076	0.62597	1596	23	1474	39	**1678**	**39**	86.2
308-EN8-46	3.53	0.12	0.2419	0.0086	0.79399	1534	27	1395	45	**1704**	**48**	77.8
316-EN8-54	3.26	0.1	0.2306	0.0067	0.37576	1467	25	1344	33	**1578**	**50**	82.6
318-EN8-56	3.55	0.11	0.2454	0.0091	0.6433	1541	26	1413	47	**1583**	**44**	88.0
322-EN8-60	3.55	0.12	0.2478	0.0083	0.78392	1541	26	1426	43	**1685**	**56**	81.8
331-EN8-61	2.888	0.082	0.2239	0.009	0.68283	1377	21	1301	48	**1690**	**51**	70.1
332-EN8-62	2.506	0.07	0.2	0.0068	0.53266	1271	20	1174	36	**1611**	**32**	62.8
333-EN8-63	3.232	0.098	0.2435	0.0084	0.70076	1464	23	1403	43	**1691**	**45**	79.5
339-EN8-69	2.827	0.066	0.2213	0.006	0.45117	1367	17	1287	32	**1539**	**34**	80.4
363-EN8-85	3.5	0.11	0.2504	0.0071	0.73477	1531	25	1439	36	**1636**	**39**	86.3
377-EN8-91	3.075	0.097	0.2327	0.007	0.56882	1429	26	1347	37	**1562**	**49**	84.0
380-EN8-94	3.648	0.099	0.2638	0.006	0.6669	1567	22	1508	31	**1721**	**38**	85.9
383-EN8-97	2.584	0.066	0.2066	0.0056	0.74763	1296	18	1210	30	**1560**	**41**	71.1
384-EN8-98	3.48	0.13	0.2602	0.0094	0.79783	1524	31	1489	48	**1697**	**49**	86.0
387-EN8-101	2.98	0.12	0.219	0.0088	0.72495	1396	32	1275	46	**1661**	**47**	69.7
402-EN8-108	3.265	0.085	0.2318	0.0062	0.65144	1471	21	1342	32	**1549**	**30**	84.6
409-EN8-115	4.13	0.12	0.265	0.0089	0.82605	1660	23	1519	44	**1817**	**34**	80.4
JN-Ky6												
9-JN6-1	4.16	0.18	0.294	0.013	0.64024	1664	35	1661	64	**1719**	**49**	96.5
10-JN6-2	5.14	0.14	0.302	0.01	0.63347	1840	23	1698	51	**1794**	**180**	94.3
11-JN6-3	3.51	0.3	0.262	0.012	0.01499	1502	67	1497	61	**1360**	**47**	109.2
12-JN6-4	4.47	0.15	0.28	0.01	0.62996	1728	29	1588	51	**1712**	**52**	92.2
15-JN6-7	4.91	0.11	0.3034	0.0093	0.47317	1803	19	1706	46	**1811**	**34**	93.8
19-JN6-11	4.31	0.1	0.2914	0.0078	0.59215	1699	18	1647	39	**1718**	**53**	95.7
204-JN6-03	4.26	0.12	0.3001	0.0088	0.52296	1687	23	1690	44	**1710**	**30**	98.8
205-JN6-04	5.048	0.094	0.3301	0.0049	0.51468	1827	15	1838	24	**1811**	**33**	101.5
206-JN6-05	4.311	0.099	0.2956	0.0046	0.40769	1697	18	1669	23	**1775**	**55**	93.6
208-JN6-07	4.12	0.15	0.2924	0.0074	0.41878	1654	29	1652	37	**1737**	**47**	94.9
220-JN6-11	4.91	0.16	0.323	0.01	0.6407	1808	26	1805	49	**1745**	**47**	103.3
221-JN6-12	4.04	0.14	0.279	0.0071	0.69232	1639	29	1586	36	**1671**	**63**	94.6
226-JN6-17	2.93	0.18	0.233	0.01	0.63916	1398	43	1351	54	**1428**	**56**	94.3
241-JN6-23	4.15	0.19	0.286	0.01	0.75642	1660	37	1622	52	**1718**	**120**	94.1
242-JN6-24	3.06	0.26	0.242	0.017	0.5177	1425	66	1394	86	**1420**	**49**	98.1
243-JN6-25	4.28	0.19	0.287	0.01	0.76775	1688	38	1628	51	**1740**	**38**	93.1
244-JN6-26	4.55	0.1	0.3093	0.006	0.5064	1738	18	1736	29	**1702**	**40**	102.0
247-JN6-29	4.99	0.14	0.3136	0.008	0.57491	1819	24	1757	39	**1883**	**87**	92.8
248-JN6-30	4.72	0.28	0.316	0.014	0.6351	1765	49	1768	69	**1795**	**73**	98.5
254-JN6-36	4.11	0.17	0.2833	0.0068	0.36485	1652	34	1607	34	**1727**	**51**	92.5

Table 2 Detrital zircon U–Pb dating results

265-JN6-39	4.37	0.15	0.3028	0.0094	0.43711	1708	30	1704	47	**1742**	**40**	97.8
267-JN6-41	4.56	0.11	0.3068	0.009	0.60858	1740	21	1724	44	**1813**	**96**	94.8
274-JN6-48	4.2	0.24	0.289	0.01	0.42549	1668	47	1635	51	**1748**	**84**	93.1
278-JN6-52	3.85	0.16	0.281	0.01	0.43224	1608	31	1596	52	**1663**	**61**	95.8
290-JN6-56	3.84	0.14	0.275	0.0076	0.45086	1598	29	1565	38	**1653**	**38**	94.4
321-JN6-79	4.52	0.1	0.3028	0.0077	0.66305	1732	19	1703	38	**1749**	**56**	97.3
325-JN6-83	4.17	0.13	0.2857	0.0065	0.42774	1664	25	1619	33	**1724**	**67**	93.5
340-JN6-90	4.38	0.17	0.2947	0.009	0.61022	1710	33	1663	45	**1699**	**110**	97.8
343-JN6-93	4.44	0.27	0.293	0.012	0.40471	1716	53	1655	59	**1750**	**39**	94.3
357-JN6-99	4.56	0.12	0.3038	0.0078	0.65131	1741	22	1709	39	**1768**	**43**	96.5
371-JN6-113	4.596	0.097	0.3114	0.0079	0.46221	1747	18	1746	39	**1804**	**55**	96.7
380-JN6-114	4.3	0.13	0.2907	0.0073	0.50126	1689	25	1644	37	**1753**	**74**	93.4
381-JN6-115	4.44	0.23	0.294	0.015	0.17473	1716	42	1658	75	**1792**	**81**	91.9
385-JN6-119	4.32	0.18	0.2989	0.0096	0.14576	1694	34	1683	48	**1766**	**72**	95.1
390-JN6-124	3.98	0.14	0.298	0.01	0.26815	1628	28	1681	50	**1647**	**43**	102.0
394-JN6-128	5.26	0.16	0.3516	0.0081	0.59752	1868	24	1941	39	**1847**	**47**	104.8
					Rejected disconcordant analyses							
13-JN6-5	3.678	0.071	0.2549	0.0047	0.54344	1563	15	1404	25	1676	37	80.6
14-JN6-6	1.672	0.034	0.1132	0.0019	0.85838	1000	13	691	11	1733	28	-50.8
16-JN6-8	2.17	0.11	0.1535	0.0075	0.33134	1257	38	916	42	1691	32	15.4
20-JN6-12	3.347	0.096	0.2467	0.005	0.47794	1490	22	1352	26	1596	60	82.0
21-JN6-13	5.503	0.099	0.2675	0.0038	0.67306	1900	15	1528	19	2331	26	47.4
22-JN6-14	2.032	0.057	0.1445	0.0033	0.55	1123	19	870	18	1682	44	6.7
219-JN6-10	2.483	0.053	0.1687	0.0036	0.34855	1268	16	1004	20	1684	46	32.3
227-JN6-18	4.43	0.11	0.28	0.0047	0.16277	1757	19	1591	24	1836	43	84.6
251-JN6-33	3.478	0.066	0.2387	0.0036	0.55459	1522	15	1379	19	1718	33	75.4
252-JN6-34	2.257	0.074	0.1535	0.0044	0.50211	1198	22	920	24	1669	50	18.6
269-JN6-43	3.781	0.075	0.2533	0.005	0.80388	1589	15	1414	25	1758	39	75.7
270-JN6-44	3.41	0.069	0.2309	0.0037	0.33093	1505	16	1339	20	1751	34	69.2
279-JN6-53	2.085	0.044	0.1503	0.0025	0.49335	1142	15	902	14	1655	37	16.5
280-JN6-54	5.37	0.16	0.2572	0.0058	0.20318	1879	26	1477	29	2346	42	41.2
298-JN6-64	4.196	0.095	0.2749	0.0046	0.18341	1691	18	1534	23	1825	43	81.0
299-JN6-65	3.537	0.085	0.2242	0.0066	0.48988	1537	19	1302	34	1828	56	59.6
300-JN6-66	9.6	0.15	0.3878	0.0056	0.36485	2394	14	2111	26	2640	20	74.9
328-JN6-86	4.57	0.19	0.2818	0.0078	0.43711	1749	34	1579	39	1909	83	79.1
341-JN6-91	2.203	0.048	0.1583	0.0033	0.60858	1182	15	947	18	1650	31	25.8
359-JN6-101	3.38	0.11	0.2147	0.006	0.42549	1499	25	1257	31	1821	54	55.1
363-JN6-105	2.517	0.039	0.1768	0.0023	0.43224	1276	11	1049	13	1675	26	40.3

2. Lu–Hf isotope samples and results

Detrital zircon hafnium data were collected from fourteen samples that previously published by *Yang et al. (2018)*. Individual zircon initial $^{176}Hf/^{177}Hf$ value ($^{176}Hf/^{177}Hf_i$) and epsilon hafnium

($\varepsilon_{Hf}(t)$) was calculated and plotted according to the published age. Detailed sample information is presented in Table 2.

Table 3 Summary of detrital zircon Lu–Hf samples

Core drill	Coordinate	Sample	Formation	Number of analyses	Rock type
Elliott-1	E: 133.7551° S:17.4025°	E-LJ2	lower Jamison sst.	13	coarse-grained sandstone
		E-Ky7	Kyalla Fm	24	medium-grained sandstone
		E-Mo13	Moroak Sst.	15	coarse-grained sandstone
		E-Vel18	Velkerri Fm.	17	fine-grained siltstone
Jamison-1	E: 133.7672° S: 16.7749°	J-UJ3	upper Jamison sst.	16	coarse-grained sandstone
		J-Ky8	Kyalla Fm	16	fine to medium- grained sandstone
		J-Mo13	Moroak Sst.	16	coarse-grained sandstone
Walton-2	E: 133.6388° S: 15.9051°	W-UJ9	upper Jamison sst.	16	coarse-grained sandstone
		W-BC1	Bessie Creek Sst.	15	coarse-grained sandstone
McManus-1	E: 133.6242° S: 15.919°	M-LJ3	lower Jamison sst.	11	coarse-grained sandstone
Altree-2	E: 133.786592° S:15.923645°	A-UJ1	upper Jamison sst.	15	coarse-grained sandstone
		A-BC13	Bessie Creek Sst.	12	coarse-grained sandstone
Sever-1	E: 132.843963° S:15.24646°	S-BC1	Bessie Creek Sst.	19	coarse-grained sandstone
Birdum Creek-1	E: 133.1395° S: 15.625°	BirC-Ky1	Kyalla Fm	16	fine to medium- grained siltstone

Table 4 Detrital zircon hafnium isotope analytical results

Analysis	$^{207}Pb/^{206}Pb$ age (Ma)	Lu^{176}/Hf^{177}	Hf^{176}/Hf^{177}	2 S.E.	Hf/Hf(t)	eHf(t)	2 S.E.	T(DM)
J-UJ3								
BY J3-102	1602	0.0005	0.281871	0.000018	0.281855	3.15	0.62	2.10
BY J3-106	1583	0.0012	0.281940	0.000026	0.281903	4.41	0.90	2.01
BY J3-12	1157	0.0013	0.281940	0.000022	0.281913	-4.95	0.77	2.25
BY J3-122	1607	0.0005	0.281887	0.000019	0.281870	3.82	0.65	2.07
BY J3-123	1196	0.0005	0.282117	0.000018	0.282105	2.76	0.62	1.81
BY J3-22	1220	0.0006	0.282101	0.000020	0.282087	2.68	0.68	1.83
BY J3-33	1135	0.0006	0.282120	0.000016	0.282108	1.47	0.57	1.84
BY J3-36	1588	0.0008	0.281938	0.000019	0.281914	4.95	0.65	1.98
BY J3-4	1597	0.0006	0.281743	0.000017	0.281724	-1.61	0.59	2.39
BY J3-44	1183	0.0006	0.282107	0.000020	0.282094	2.06	0.69	1.84
BY J3-51	1200	0.0005	0.282104	0.000017	0.282093	2.42	0.61	1.83
BY J3-58	1596	0.0019	0.281948	0.000029	0.281892	4.34	1.00	2.03
BY J3-64	1612	0.0010	0.281898	0.000023	0.281869	3.89	0.81	2.07
BY J3-67	1607	0.0007	0.281919	0.000019	0.281898	4.81	0.67	2.01

Table 4 Detrital zircon hafnium isotope analytical results

BY J3-8	1592	0.0017	0.281911	0.000023	0.281859	3.08	0.82	2.10
BY J3-90	1591	0.0009	0.281898	0.000022	0.281869	3.41	0.77	2.08
E-LJ2								
BY E2-08	1594	0.0009	0.281920	0.000021	0.281894	4.35	0.73	2.02
BY E2-103	1579	0.0019	0.281953	0.000027	0.281897	4.13	0.96	2.03
BY E2-107	1577	0.0018	0.281918	0.000034	0.281864	2.90	1.18	2.10
BY E2-111	1050	0.0006	0.282103	0.000018	0.282091	-1.06	0.62	1.93
BY E2-131	1578	0.0006	0.281913	0.000018	0.281895	4.03	0.64	2.03
BY E2-29	1142	0.0007	0.282090	0.000021	0.282075	0.47	0.72	1.91
BY E2-30	1595	0.0019	0.281925	0.000028	0.281868	3.47	0.99	2.08
BY E2-32	1605	0.0007	0.281886	0.000021	0.281864	3.54	0.75	2.08
BY E2-34	1590	0.0013	0.281948	0.000030	0.281908	4.77	1.06	1.99
BY E2-39	1612	0.0009	0.281929	0.000018	0.281902	5.04	0.64	2.00
BY E2-54	1589	0.0007	0.281905	0.000018	0.281883	3.86	0.63	2.05
BY E2-67	2186	0.0009	0.281268	0.000029	0.281230	-5.56	1.03	3.08
BY E2-69	1579	0.0008	0.281908	0.000023	0.281886	3.72	0.79	2.05
M-LJ3								
BY M3-105	1620	0.0014	0.281908	0.000030	0.281864	3.88	1.06	2.07
BY M3-118	1609	0.0013	0.281789	0.000023	0.281748	-0.48	0.80	2.33
BY M3-12	1571	0.0007	0.281934	0.000021	0.281915	4.57	0.73	1.99
BY M3-2	1577	0.0014	0.281949	0.000024	0.281906	4.38	0.82	2.01
BY M3-31	1618	0.0008	0.281933	0.000020	0.281907	5.38	0.70	1.98
BY M3-44	1612	0.0009	0.281796	0.000022	0.281770	0.36	0.76	2.28
BY M3-56	1087	0.0006	0.282088	0.000018	0.282077	-0.72	0.62	1.94
BY M3-77	1575	0.0010	0.281946	0.000022	0.281917	4.75	0.76	1.98
BY M3-79	1575	0.0011	0.281927	0.000022	0.281894	3.91	0.78	2.04
BY M3-83	1566	0.0006	0.281919	0.000017	0.281900	3.95	0.60	2.03
BY M3-90	1597	0.0007	0.281936	0.000021	0.281915	5.18	0.75	1.98
W-UJ9								
BY W9-06	1155	0.0009	0.282114	0.000019	0.282094	1.45	0.65	1.86
BY W9-09	1563	0.0008	0.281969	0.000025	0.281944	5.42	0.86	1.93
BY W9-101	1560	0.0010	0.281934	0.000023	0.281905	3.99	0.82	2.02
BY W9-107	1558	0.0008	0.281966	0.000025	0.281941	5.21	0.87	1.94
BY W9-111	1568	0.0009	0.281932	0.000019	0.281906	4.20	0.65	2.01
BY W9-114	1564	0.0010	0.281915	0.000021	0.281887	3.41	0.74	2.06
BY W9-14	1556	0.0017	0.281768	0.000027	0.281718	-2.77	0.95	2.43
BY W9-19	1073	0.0008	0.282064	0.000034	0.282048	-2.06	1.21	2.01
BY W9-27	1561	0.0012	0.281906	0.000027	0.281869	2.72	0.95	2.10
BY W9-36	1145	0.0006	0.282079	0.000022	0.282066	0.22	0.76	1.93
BY W9-37	1554	0.0009	0.281898	0.000020	0.281872	2.68	0.70	2.09
BY W9-42	1126	0.0008	0.282108	0.000020	0.282092	0.71	0.69	1.88
BY W9-48	1086	0.0007	0.282033	0.000021	0.282018	-2.81	0.72	2.07
BY W9-55	1559	0.0015	0.281940	0.000026	0.281896	3.64	0.89	2.04
BY W9-74	1119	0.0007	0.282117	0.000017	0.282103	0.94	0.61	1.86
BY W9-75	1051	0.0007	0.282102	0.000019	0.282087	-1.16	0.66	1.94
A-UJ1								
BY_A1-10	1497	0.0007	0.281919	0.000019	0.281899	2.31	0.66	2.07
BY_A1-101	1515	0.0012	0.281924	0.000032	0.281888	2.35	1.14	2.08
BY_A1-15	1092	0.0011	0.282024	0.000028	0.282003	-3.23	0.99	2.10
BY_A1-21	2402	0.0001	0.281136	0.000012	0.281133	-4.00	0.41	3.16
BY_A1-34	1618	0.0008	0.281743	0.000017	0.281717	-1.37	0.58	2.39
BY_A1-39	1154	0.0010	0.282107	0.000036	0.282085	1.10	1.27	1.88
BY_A1-40	1550	0.0014	0.282045	0.000077	0.282006	7.32	2.68	1.81
BY_A1-45	1095	0.0005	0.282095	0.000017	0.282085	-0.22	0.58	1.91
BY_A1-56	1481	0.0013	0.281960	0.000020	0.281923	2.81	0.69	2.03
BY_A1-58	1587	0.0013	0.281789	0.000026	0.281750	-0.91	0.91	2.34
BY_A1-68	1161	0.0006	0.282102	0.000016	0.282090	1.42	0.56	1.86
BY_A1-73	1438	0.0009	0.281947	0.000022	0.281922	1.79	0.78	2.06
BY_A1-77	1589	0.0007	0.281942	0.000019	0.281923	5.27	0.65	1.96
BY_A1-87	1484	0.0012	0.281914	0.000019	0.281881	1.37	0.67	2.12
BY_A1-96	1131	0.0006	0.282107	0.000019	0.282094	0.91	0.67	1.87
E-Ky7								
BY E7-106	1690	0.0009	0.281605	0.000018	0.281578	-4.66	0.64	2.65
BY E7-110	1711	0.0008	0.281593	0.000023	0.281568	-4.52	0.81	2.65
BY E7-114	1698	0.0010	0.281698	0.000022	0.281667	-1.31	0.77	2.45
BY E7-116	1706	0.0007	0.281670	0.000018	0.281648	-1.81	0.62	2.49
BY E7-117	1697	0.0008	0.281614	0.000019	0.281589	-4.11	0.66	2.62
BY E7-119	1704	0.0009	0.281630	0.000017	0.281602	-3.48	0.61	2.58
BY E7-120	1814	0.0009	0.281602	0.000020	0.281570	-2.10	0.70	2.59
BY E7-126	1829	0.0010	0.281608	0.000018	0.281575	-1.57	0.64	2.57
BY E7-21	1714	0.0005	0.281619	0.000018	0.281602	-3.25	0.63	2.58
BY E7-22	1711	0.0005	0.281619	0.000018	0.281602	-3.32	0.63	2.58
BY E7-23	1714	0.0005	0.281685	0.000020	0.281668	-0.92	0.70	2.44
BY E7-24	1821	0.0007	0.281551	0.000019	0.281527	-3.46	0.68	2.67
BY E7-26	1818	0.0007	0.281551	0.000019	0.281527	-3.53	0.68	2.68
BY E7-32	1700	0.0008	0.281624	0.000021	0.281600	-3.64	0.73	2.59

Table 4 Detrital zircon hafnium isotope analytical results

BY E7-34	2573	0.0007	0.281277	0.000019	0.281240	3.81	0.66	2.83
BY E7-39	1720	0.0006	0.281591	0.000016	0.281573	-4.15	0.57	2.64
BY E7-42	1820	0.0007	0.281577	0.000019	0.281553	-2.55	0.65	2.62
BY E7-49	1830	0.0011	0.281616	0.000020	0.281577	-1.48	0.69	2.56
BY E7-55	1701	0.0009	0.281621	0.000019	0.281593	-3.88	0.67	2.61
BY E7-61	1697	0.0011	0.281615	0.000022	0.281580	-4.42	0.76	2.64
BY E7-66	1700	0.0010	0.281597	0.000024	0.281563	-4.94	0.84	2.67
BY E7-89	1833	0.0009	0.281541	0.000022	0.281511	-3.75	0.76	2.70
BY E7-90	1696	0.0008	0.281630	0.000019	0.281604	-3.58	0.65	2.58
BY E7-96	2264	0.0006	0.281256	0.000019	0.281229	-3.81	0.67	3.04
J-Ky8								
BY J8-01	2521	0.0006	0.280960	0.000017	0.280930	-8.45	0.60	3.51
BY J8-10	1811	0.0004	0.281520	0.000017	0.281506	-4.43	0.59	2.72
BY J8-19	1694	0.0010	0.281693	0.000026	0.281659	-1.68	0.92	2.47
BY J8-20	1745	0.0008	0.281599	0.000023	0.281573	-3.55	0.79	2.62
BY J8-30	1805	0.0006	0.281532	0.000019	0.281513	-4.34	0.66	2.71
BY J8-31	2479	0.0007	0.281124	0.000021	0.281092	-3.66	0.72	3.20
BY J8-33	1804	0.0009	0.281590	0.000019	0.281560	-2.69	0.66	2.61
BY J8-38	1705	0.0012	0.281580	0.000025	0.281542	-5.58	0.88	2.71
BY J8-41	1698	0.0010	0.281625	0.000019	0.281592	-3.99	0.66	2.61
BY J8-47	1695	0.0005	0.281605	0.000016	0.281589	-4.14	0.57	2.62
BY J8-48	1706	0.0013	0.281636	0.000026	0.281594	-3.73	0.91	2.60
BY J8-57	1756	0.0008	0.281702	0.000025	0.281677	0.36	0.88	2.39
BY J8-63	1690	0.0008	0.281788	0.000019	0.281762	1.88	0.66	2.25
BY J8-67	1699	0.0013	0.281676	0.000026	0.281634	-2.45	0.91	2.52
BY J8-71	1756	0.0012	0.281618	0.000025	0.281579	-3.09	0.89	2.60
BY J8-89	1739	0.0008	0.281634	0.000021	0.281607	-2.51	0.75	2.55
BirC-Ky1								
BY_BirC-10	1757	0.0016	0.281639	0.000026	0.281586	-2.84	0.89	2.59
BY_BirC-102	1750	0.0009	0.281718	0.000029	0.281687	0.60	1.03	2.37
BY_BirC-21	1694	0.0004	0.281621	0.000016	0.281607	-3.53	0.57	2.58
BY_BirC-23	2491	0.0006	0.281175	0.000017	0.281148	-1.40	0.61	3.07
BY_BirC-24	1748	0.0004	0.281512	0.000023	0.281499	-6.11	0.79	2.78
BY_BirC-26	1755	0.0009	0.281738	0.000025	0.281707	1.42	0.89	2.33
BY_BirC-30	1748	0.0017	0.281678	0.000028	0.281622	-1.76	0.99	2.52
BY_BirC-38	1777	0.0022	0.281640	0.000033	0.281565	-3.13	1.17	2.62
BY_BirC-48	1771	0.0012	0.281582	0.000024	0.281543	-4.03	0.85	2.67
BY_BirC-56	1698	0.0010	0.281665	0.000030	0.281634	-2.49	1.06	2.52
BY_BirC-61	1748	0.0007	0.281775	0.000027	0.281752	2.87	0.94	2.24
BY_BirC-62	2480	0.0005	0.281150	0.000027	0.281129	-2.34	0.94	3.12
BY_BirC-70	1696	0.0007	0.281709	0.000021	0.281687	-0.66	0.74	2.41
BY_BirC-83	1769	0.0013	0.281755	0.000025	0.281712	1.92	0.89	2.31
BY_BirC-84	1747	0.0011	0.281739	0.000029	0.281703	1.09	1.03	2.34
BY_BirC-91	1757	0.0011	0.281705	0.000038	0.281669	0.11	1.34	2.41
E-Mo13								
BY_E13-002	1740	0.0005	0.281195	0.000018	0.281177	-17.73	0.62	3.46
BY_E13-003	1586	0.0003	0.281825	0.000014	0.281817	1.43	0.47	2.20
BY_E13-004	1562	0.0009	0.281789	0.000022	0.281762	-1.05	0.77	2.33
BY_E13-024	1720	0.0008	0.281631	0.000020	0.281606	-2.95	0.70	2.57
BY_E13-026	1728	0.0011	0.281603	0.000021	0.281566	-4.21	0.75	2.65
BY_E13-036	1837	0.0017	0.281606	0.000023	0.281547	-2.37	0.81	2.62
BY_E13-044	2398	0.0008	0.281256	0.000022	0.281222	-0.94	0.76	2.97
BY_E13-055	1550	0.0008	0.281807	0.000021	0.281784	-0.56	0.75	2.29
BY_E13-063	1581	0.0004	0.281766	0.000019	0.281755	-0.88	0.66	2.33
BY_E13-066	3159	0.0007	0.280756	0.000021	0.280712	-1.22	0.74	3.59
BY_E13-069	1561	0.0011	0.281839	0.000023	0.281805	0.46	0.82	2.23
BY_E13-078	2415	0.0006	0.281066	0.000017	0.281040	-7.02	0.61	3.35
BY_E13-084	2340	0.0002	0.281188	0.000017	0.281178	-3.83	0.60	3.10
BY_E13-114	1729	0.0007	0.281634	0.000016	0.281612	-2.55	0.56	2.55
BY_E13-134	2526	0.0010	0.280963	0.000021	0.280915	-8.85	0.75	3.54
J-Mo13								
BY_J13-002	1728	0.0010	0.281652	0.000022	0.281619	-2.34	0.75	2.53
BY_J13-007	1733	0.0007	0.281676	0.000021	0.281653	-0.99	0.73	2.46
BY_J13-014	1738	0.0011	0.281780	0.000023	0.281744	2.34	0.82	2.26
BY_J13-021	1655	0.0007	0.281668	0.000014	0.281645	-3.06	0.51	2.52
BY_J13-023	1564	0.0012	0.281731	0.000023	0.281696	-3.37	0.82	2.47
BY_J13-027	1568	0.0006	0.281622	0.000019	0.281605	-6.50	0.65	2.66
BY_J13-028	1693	0.0005	0.281587	0.000016	0.281569	-4.90	0.55	2.66
BY_J13-053	2498	0.0009	0.281106	0.000018	0.281065	-4.18	0.64	3.24
BY_J13-066	1404	0.0005	0.281578	0.000019	0.281564	-11.69	0.67	2.85
BY_J13-071	1562	0.0010	0.282044	0.000021	0.282013	7.86	0.72	1.78
BY_J13-072	1774	0.0006	0.281696	0.000022	0.281676	0.74	0.76	2.38
BY_J13-075	1575	0.0017	0.281927	0.000026	0.281877	3.31	0.91	2.07
BY_J13-099	1798	0.0006	0.281553	0.000017	0.281532	-3.80	0.58	2.68
BY_J13-108	1765	0.0003	0.281541	0.000015	0.281532	-4.56	0.54	2.70
BY_J13-110	1736	0.0006	0.281626	0.000019	0.281607	-2.58	0.65	2.56
BY_J13-114	1738	0.0007	0.281613	0.000017	0.281592	-3.07	0.61	2.59

Table 4 Detrital zircon hafnium isotope analytical results

E-Vel18								
BY E18-115	1628	0.0003	0.281564	0.000021	0.281553	-6.96	0.75	2.74
BY E18-122	1611	0.0013	0.281633	0.000028	0.281592	-5.97	0.99	2.66
BY E18-123	1722	0.0017	0.281653	0.000046	0.281597	-3.25	1.61	2.58
BY E18-125	2435	0.0006	0.281180	0.000025	0.281151	-2.58	0.88	3.10
BY E18-126	2340	0.0015	0.281349	0.000035	0.281280	-0.21	1.23	2.89
BY E18-29	1631	0.0012	0.281805	0.000024	0.281766	0.68	0.85	2.28
BY E18-39	1684	0.0009	0.281667	0.000030	0.281639	-2.64	1.04	2.52
BY E18-42	1797	0.0008	0.281580	0.000022	0.281554	-3.05	0.76	2.63
BY E18-45	1623	0.0013	0.281651	0.000030	0.281610	-5.05	1.04	2.62
BY E18-47	1686	0.0007	0.281694	0.000026	0.281671	-1.46	0.90	2.45
BY E18-61	1674	0.0005	0.281604	0.000027	0.281590	-4.59	0.93	2.63
BY E18-66	1683	0.0006	0.281575	0.000026	0.281557	-5.57	0.90	2.69
BY E18-71	1800	0.0005	0.281625	0.000022	0.281609	-1.01	0.77	2.51
BY E18-76	1710	0.0006	0.281614	0.000026	0.281593	-3.65	0.91	2.60
BY E18-83	1596	0.0006	0.281514	0.000032	0.281495	-9.76	1.11	2.88
BY E18-87	1806	0.0007	0.281455	0.000026	0.281432	-7.16	0.90	2.88
BY E18-99	1718	0.0005	0.281611	0.000023	0.281593	-3.47	0.80	2.60
S-BC1								
BY_S1-004	3443	0.0007	0.280596	0.000017	0.280550	-0.23	0.61	3.73
BY_S1-011	1513	0.0011	0.282081	0.000025	0.282051	8.09	0.87	1.73
BY_S1-046	1759	0.0006	0.281692	0.000019	0.281673	0.32	0.67	2.40
BY_S1-047	1741	0.0007	0.281628	0.000020	0.281606	-2.49	0.69	2.55
BY_S1-049	1707	0.0008	0.281633	0.000021	0.281607	-3.25	0.72	2.57
BY_S1-04s	1695	0.0012	0.281665	0.000024	0.281627	-2.79	0.83	2.54
BY_S1-052	1838	0.0006	0.281572	0.000017	0.281552	-2.19	0.60	2.61
BY_S1-057	1845	0.0007	0.281470	0.000021	0.281445	-5.82	0.73	2.83
BY_S1-058	1699	0.0007	0.281478	0.000019	0.281457	-8.76	0.65	2.90
BY_S1-091	1651	0.0007	0.281815	0.000024	0.281792	2.05	0.83	2.21
BY_S1-113	1852	0.0007	0.281474	0.000019	0.281450	-5.47	0.65	2.82
BY_S1-115	1535	0.0009	0.281746	0.000020	0.281719	-3.20	0.69	2.44
BY_S1-122	1527	0.0007	0.281621	0.000018	0.281602	-7.54	0.63	2.69
BY_S1-127	1740	0.0006	0.281560	0.000022	0.281540	-4.84	0.77	2.69
BY_S1-128	1702	0.0008	0.281628	0.000019	0.281604	-3.47	0.66	2.58
BY_S1-143	1827	0.0005	0.281493	0.000018	0.281474	-5.20	0.63	2.78
BY_S1-20s	1688	0.0009	0.281630	0.000025	0.281603	-3.81	0.86	2.59
BY_S1-22s	1692	0.0008	0.281625	0.000020	0.281599	-3.85	0.69	2.60
BY_S1_06s	1695	0.0006	0.281533	0.000017	0.281514	-6.82	0.61	2.78
W-BC1								
BY_W1-03	1748	0.0014	0.281655	0.000025	0.281609	-2.24	0.88	2.54
BY_W1-04	1853	0.0006	0.281458	0.000020	0.281436	-5.95	0.69	2.85
BY_W1-08	2534	0.0004	0.281029	0.000017	0.281010	-5.28	0.60	3.34
BY_W1-09	1805	0.0011	0.281607	0.000022	0.281568	-2.38	0.77	2.60
BY_W1-12	1751	0.0008	0.281653	0.000020	0.281625	-1.59	0.70	2.51
BY_W1-14	2444	0.0010	0.281342	0.000023	0.281297	2.81	0.81	2.79
BY_W1-19	1741	0.0004	0.281616	0.000017	0.281603	-2.59	0.60	2.56
BY_W1-26	1860	0.0011	0.281544	0.000021	0.281504	-3.38	0.73	2.70
BY_W1-27	2493	0.0007	0.281122	0.000021	0.281088	-3.47	0.74	3.20
BY_W1-35	2454	0.0005	0.281296	0.000017	0.281274	2.24	0.60	2.83
BY_W1-50	1735	0.0014	0.281585	0.000025	0.281539	-5.02	0.86	2.70
BY_W1-67	1728	0.0019	0.281655	0.000023	0.281592	-3.27	0.82	2.59
BY_W1-68	1846	0.0004	0.281486	0.000020	0.281471	-4.85	0.70	2.78
BY_W1-71	1742	0.0005	0.281632	0.000024	0.281614	-2.17	0.85	2.53
BY_W1-73	1840	0.0005	0.281570	0.000019	0.281554	-2.04	0.66	2.60
A-BC13								
BY_A13-107	1421	0.0017	0.282015	0.000055	0.281969	3.05	1.93	1.97
BY_A13-29b	1535	0.0011	0.281957	0.000029	0.281925	4.12	1.02	1.99
BY_A13-30	1435	0.0010	0.281759	0.000039	0.281730	-5.08	1.36	2.47
BY_A13-33	1650	0.0009	0.281646	0.000034	0.281617	-4.18	1.19	2.59
BY_A13-49	1454	0.0014	0.282032	0.000034	0.281993	4.66	1.20	1.89
BY_A13-52	2987	0.0006	0.280794	0.000018	0.280758	-3.62	0.63	3.59
BY_A13-54	1648	0.0013	0.281698	0.000024	0.281659	-2.75	0.86	2.50
BY_A13-55	2476	0.0010	0.280999	0.000022	0.280953	-8.69	0.78	3.49
BY_A13-64	1540	0.0014	0.282031	0.000023	0.281991	6.55	0.80	1.85
BY_A13-72	1555	0.0015	0.281889	0.000045	0.281846	1.77	1.57	2.15
BY_A13-78	2255	0.0008	0.281418	0.000023	0.281385	1.54	0.81	2.71
BY_A13-88	1539	0.0010	0.281941	0.000020	0.281911	3.71	0.71	2.02

Appendix 3

Appendix for Chapter 4

Appendix 3

Appendix for Chapter 4

1. Sm–Nd and Pb–Pb isotopes

A total of 15 shale samples, taken at approximately 30 metres intervals, covering the core length of the Balmain-1, were crushed for both Sm–Nd and Pb–Pb isotopic analysis. Approximately 80 mg rock powder of each sample was combined with a spike of ^{150}Nd and ^{147}Sm, was dissolved with a mixture solution of nitric acid (2 mL, 7 N) and hydrofluoric acid (4 mL, 48 wt.%). Samples were over-heated at a constant temperature (140 °C) in sealed Teflon cups for two days. The samples were then evaporated to dry, with nitric acid (6 N) reconcentration. The dried samples were redissolved with hydrochloric acid (6 N) and heated at 160°C for two days. Each sample was separated to two portions for Sm–Nd and Pb–Pb analysis, respectively.

For Sm–Nd analysis, the rare earth element concentration was obtained by passing samples through columns filled with 200-400 mesh AGW X8 anion exchange resin in Polyprep columns to removal free iron. Then the subsequent isolation of both Sm and Nd was carried out by using glass columns filled with 1 mL Eichrom Ln ion exchange resin. After the purification, samples were loaded onto outgassed rhenium filaments and the $^{143}Nd/^{144}Nd$ and $^{147}Sm/^{144}Nd$ ratios were measured on an Isotopx Pheonix TIMS at the University of Adelaide. Mass bias corrections were performed using $^{146}Nd/^{144}Nd=0.721903$. Repeated measurement of JNdi-1 (n=4) and SCo-1 (n=2) standards returned $^{143}Nd/^{144}Nd$ values of 0.512107 ± 2 (2σ) and 0.512157 ± 2 (2σ). Nd and Sm corrections were corrected for 200 pg and 150 pg blanks.

Pb extraction was conducted by using standard miniaturised HBr–HCl chemistry on columns charged with AG1x8, 200–400 mesh resin after *Reuer et al. (2003)*. The samples were then eluted by with 1 N HBr, 2 N HCl and 6 N HCl to achieve the required purity for analysis. Samples were loaded onto outgassed rhenium filaments and Pb isotopic compositions were measured on an Isotopx Pheonix TIMS at the University of Adelaide. The reported uncertainties are better than ± 1.1% (2σ, $^{206}Pb/^{204}Pb$), ± 1.3% (2σ, $^{207}Pb/^{204}Pb$) and ± 0.5% (2σ, $^{208}Pb/^{204}Pb$). The SRM-981 standard was analysed to correct the instrumental mass fractionation, using the values of 16.9412 ($^{206}Pb/^{204}Pb$), 15.4988 ($^{207}Pb/^{204}Pb$) and 36.7233 ($^{208}Pb/^{204}Pb$) after *Taylor et al. (2015)*. Two SCo-1 standard analyses returned $^{206}Pb/^{204}Pb = 19.240 \pm 0.16$, $^{207}Pb/^{204}Pb = 15.695 \pm 0.018$

and $^{208}Pb/^{204}Pb$ = 38.933 ± 0.38. The procedural blanks during the measurement were less than 100 pg.

2. U–Pb TIMS dating

Baddeleyite crystals were separated using the Wilfley water-shaking table in a technique modified after *Söderlund and Johansson (2002)*. This method, using a pipette to remove a concentrate of small, dense, flat minerals off the Wilfley table, yielded several small baddeleyite grains. No pre-treatment methods were used beyond cleaning the grains with concentrated distilled HNO_3 and HCl and, due to their small size, no chemical separation methods were required. For ID-TIMS analysis, the samples were spiked with an in-house ^{205}Pb-^{235}U tracer solution, which has been calibrated against SRM981, SRM 982 (for Pb), and CRM 115 (for U), as well as an externally-calibrated U–Pb solution (the JMM solution from the EarthTime consortium).

Dissolution and equilibration of spiked single crystals was by vapour transfer of HF, using Teflon microcapsules in a Parr pressure vessel placed in a 200°C oven for six days. The resulting residue was re-dissolved in HCl and H_3PO_4 and placed on an outgassed, zone-refined rhenium single filament with 5µL of silicic acid gel. U–Pb isotope analyses were carried out using a Thermo Triton T1 mass spectrometer at the John de Laeter Centre of Curtin University, in peak-jumping mode using a secondary electron multiplier. Uranium was measured as an oxide (UO_2). Fractionation and deadtime were monitored using SRM981 and SRM 982. Mass fractionation was 0.03 ± 0.06 %/amu. Data were reduced and plotted using the software packages Tripoli (from CIRDLES.org) and Isoplot (*Ludwig, 2009*). All uncertainties are reported at 2σ. Sample weights are calculated from crystal dimensions and are associated with as much as 50% uncertainty (estimated). Blank composition is: $^{206}Pb/^{204}Pb$ = 18.55 ± 0.63, $^{207}Pb/^{204}Pb$ = 15.50 ± 0.55, $^{208}Pb/^{204}Pb$ = 38.07 ± 1.56 (all 2σ), and a $^{206}Pb/^{204}Pb$ – $^{207}Pb/^{204}Pb$ correlation of 0.9. Th/U calculated from radiogenic $^{208}Pb/^{206}Pb$ and age. Measured isotopic ratios corrected for tracer contribution and mass fractionation (0.03 ± 0.06 %/amu). Ratios involving ^{206}Pb are corrected for initial disequilibrium in $^{230}Th/^{238}U$ using Th/U = 4 in the crystallization environment. Dating results are listed in Table 1.

References

Ludwig, K.R., 2003. User's manual for Isoplot 3.00: a geochronological toolkit for Microsoft Excel (No. 4). Kenneth R. Ludwig.

Reuer, M.K., Boyle, E.A. & Grant, B.C., 2003. Lead isotope analysis of marine carbonates and seawater by multiple collector ICP—MS. *Chemical Geology,* **200(1)**, 137-153.

Söderlund, U., Johansson, L., 2002. A simple way to extract baddeleyite (ZrO_2). *Geochemistry Geophysics Geosystems,* **3(2)**, 1-7.

Taylor, R.N., Ishizuka, O., Michalik, A., Milton, J. A., Croudace, I.W., 2015. Evaluating the precision of Pb isotope measurement by mass spectrometry. *J. Anal. At. Spectrom.*, **30(1)**, 198-213.

Appendix 4

Appendix for Chapter 5

Appendix 4

Appendix for Chapter 5

1. U–Pb dating results

Table 1 Detrital zircon U–Pb analytical data.

Analysis No.	$^{207}Pb/^{235}U$	2 S.E.	$^{206}Pb/^{238}U$	2 S.E.	Rho	$^{207}Pb/^{235}U$ age (Ma)	2 S.E.	$^{206}Pb/^{238}U$ age (Ma)	2 S.E.	$^{207}Pb/^{206}Pb$ age (Ma)	2 S.E.	Conc (%)
Bro-06												
9-Bro-6-002	4.539	0.077	0.2996	0.004	0.419	1736	14	1689	22	1781	31	-5.4
12-Bro-6-005	4.606	0.084	0.3076	0.004	0.442	1750	16	1731	20	1784	30	-3.1
19-Bro-6-012	4.18	0.12	0.2872	0.007	0.45	1677	25	1632	33	1710	53	-4.8
22-Bro-6-015	4.659	0.093	0.3122	0.006	0.528	1762	17	1750	30	1771	33	-1.2
34-Bro-6-020	4.58	0.1	0.301	0.005	0.518	1745	18	1696	22	1812	35	-6.8
39-Bro-6-025	4.746	0.084	0.306	0.005	0.346	1774	15	1724	24	1830	40	-6.1
42-Bro-6-028	4.99	0.12	0.3158	0.006	0.411	1816	20	1769	28	1894	45	-7.1
44-Bro-6-030	4.438	0.074	0.2998	0.004	0.487	1720	13	1693	22	1749	30	-3.3
54-Bro-6-033	4.56	0.11	0.3001	0.005	0.24	1739	20	1691	23	1801	48	-6.5
55-Bro-6-034	4.578	0.088	0.3041	0.004	0.167	1745	17	1711	21	1789	39	-4.6
60-Bro-6-039	4.306	0.089	0.29	0.004	0.562	1694	17	1644	20	1745	32	-6.1
62-Bro-6-041	4.64	0.14	0.3041	0.006	0.493	1759	26	1717	28	1809	46	-5.4
63-Bro-6-042	4.535	0.086	0.3067	0.004	0.302	1745	17	1724	21	1771	38	-2.7
64-Bro-6-043	4.622	0.08	0.3085	0.005	0.501	1751	14	1733	22	1766	33	-1.9
66-Bro-6-045	4.703	0.084	0.3124	0.006	0.366	1766	15	1752	29	1773	42	-1.2
67-Bro-6-046	4.611	0.088	0.3059	0.005	0.273	1749	16	1720	23	1782	38	-3.6
76-Bro-6-048	4.153	0.092	0.2899	0.005	0.095	1668	18	1640	25	1691	51	-3.1
79-Bro-6-051	4.9	0.19	0.3206	0.01	0.207	1801	32	1790	48	1818	67	-1.6
80-Bro-6-052	15.37	0.25	0.5569	0.009	0.597	2838	16	2856	39	2838	24	0.6
84-Bro-6-056	4.14	0.2	0.2825	0.009	0.42	1660	40	1604	45	1748	90	-9.0
86-Bro-6-058	4.47	0.17	0.3041	0.008	0.67	1725	33	1710	38	1763	59	-3.1
87-Bro-6-059	4.78	0.092	0.3145	0.006	0.606	1780	16	1762	31	1788	37	-1.5
97-Bro-6-062	5.05	0.15	0.3254	0.007	0.768	1824	25	1815	36	1845	39	-1.7
98-Bro-6-063	4.55	0.12	0.3054	0.006	0.435	1737	23	1722	28	1736	48	-0.8
100-Bro-6-065	4.644	0.084	0.3078	0.004	0.552	1755	15	1729	21	1790	28	-3.5
101-Bro-6-066	4.63	0.16	0.3046	0.005	0.365	1751	28	1713	26	1833	61	-7.0
103-Bro-6-068	4.7	0.14	0.3109	0.008	0.494	1762	24	1743	37	1801	44	-3.3
104-Bro-6-069	4.443	0.099	0.2963	0.006	0.498	1721	19	1672	29	1778	38	-6.3
107-Bro-6-072	4.42	0.11	0.3059	0.006	0.39	1717	21	1723	30	1718	45	0.3
110-Bro-6-075	5.29	0.1	0.3364	0.005	0.404	1868	17	1868	25	1847	38	1.1
119-Bro-6-076	4.667	0.098	0.3107	0.005	0.305	1760	18	1746	23	1759	39	-0.7
121-Bro-6-078	3.86	0.096	0.2819	0.005	0.407	1604	21	1600	25	1613	46	-0.8
122-Bro-6-079	4.616	0.098	0.3081	0.005	0.519	1755	18	1731	26	1745	35	-0.8

Table 1 Detrital zircon U–Pb analytical data.

124-Bro-6-081	4.46	0.12	0.2938	0.005	0.138	1723	22	1660	24	1803	52	-8.6
127-Bro-6-084	4.39	0.11	0.3019	0.005	0.364	1707	22	1700	24	1711	49	-0.6
131-Bro-6-088	4.67	0.1	0.31	0.005	0.449	1766	20	1740	22	1783	39	-2.5
133-Bro-6-090	4.53	0.11	0.3021	0.005	0.232	1736	21	1704	26	1773	51	-4.0
141-Bro-6-091	4.444	0.095	0.2942	0.005	0.594	1719	18	1662	23	1793	32	-7.9
146-Bro-6-096	4.383	0.088	0.3037	0.006	0.603	1710	17	1709	29	1703	32	0.4
148-Bro-6-098	5.15	0.11	0.3287	0.006	0.298	1848	18	1831	27	1882	41	-2.8
150-Bro-6-100	4.687	0.09	0.3166	0.005	0.477	1767	17	1775	25	1769	36	0.3
152-Bro-6-102	5.13	0.13	0.326	0.007	0.464	1844	23	1818	35	1896	50	-4.3
154-Bro-6-104	4.63	0.11	0.3136	0.006	0.422	1754	20	1757	31	1777	45	-1.1
155-Bro-6-105	4.54	0.1	0.318	0.004	0.533	1742	18	1782	21	1683	33	5.6
164-Bro-6-107	4.519	0.081	0.3149	0.005	0.415	1735	15	1764	23	1724	31	2.3
165-Bro-6-108	6.74	0.2	0.3733	0.008	0.421	2082	25	2047	40	2109	51	-3.0
167-Bro-6-110	4.425	0.074	0.3002	0.005	0.628	1716	14	1692	23	1746	26	-3.2
168-Bro-6-111	4.625	0.076	0.3143	0.004	0.435	1752	14	1761	20	1737	30	1.4
170-Bro-6-113	4.703	0.086	0.3176	0.005	0.192	1765	15	1781	24	1761	36	1.1
171-Bro-6-114	4.591	0.082	0.3135	0.005	0.255	1749	15	1757	24	1751	34	0.3
173-Bro-6-116	5.233	0.087	0.3319	0.005	0.361	1859	15	1847	23	1861	36	-0.8
174-Bro-6-117	4.79	0.12	0.3176	0.005	0.36	1785	20	1777	26	1778	47	-0.1
175-Bro-6-118	4.68	0.092	0.3115	0.005	0.2	1761	16	1747	25	1793	40	-2.6
185-Bro-6-121	4.715	0.081	0.3134	0.005	0.285	1768	14	1756	22	1787	35	-1.8
186-Bro-6-122	4.205	0.073	0.2958	0.004	0.552	1676	15	1670	21	1669	30	0.1
188-Bro-6-124	3.84	0.16	0.2799	0.005	0.287	1589	34	1590	26	1565	76	1.6
189-Bro-6-125	4.844	0.089	0.3276	0.005	0.384	1792	16	1826	23	1751	32	4.1
192-Bro-6-128	5.391	0.083	0.3418	0.005	0.432	1884	13	1895	26	1871	32	1.3
193-Bro-6-129	4.49	0.18	0.3095	0.005	0.423	1733	31	1738	25	1724	65	0.8
195-Bro-6-131	3.787	0.09	0.2815	0.004	0.305	1589	19	1598	21	1584	46	0.9
198-Bro-6-134	3.943	0.084	0.2864	0.003	0.202	1621	17	1626	16	1619	41	0.4
199-Bro-6-135	4.904	0.091	0.3254	0.005	0.436	1807	15	1816	22	1779	34	2.0
202-Bro-6-138	4.428	0.092	0.2971	0.004	0.285	1719	17	1676	20	1769	35	-5.5
203-Bro-6-139	4.49	0.081	0.305	0.005	0.318	1727	15	1715	23	1735	37	-1.2
212-Bro-6-141	4.591	0.081	0.3111	0.005	0.694	1747	14	1748	23	1763	24	-0.9
214-Bro-6-143	4.517	0.087	0.2987	0.004	0.409	1732	16	1684	22	1773	35	-5.3
215-Bro-6-144	4.841	0.086	0.3245	0.005	0.458	1790	15	1814	25	1751	31	3.5
216-Bro-6-145	4.779	0.089	0.3185	0.005	0.208	1783	16	1781	23	1762	37	1.1
217-Bro-6-146	4.75	0.11	0.3174	0.006	0.396	1779	20	1776	27	1770	41	0.3
218-Bro-6-147	4.73	0.12	0.3087	0.005	0.264	1772	21	1734	26	1814	47	-4.6
15-Bro-6-008	4.138	0.074	0.2975	0.005	0.563	1662	14	1681	25	1771	29	-5.4
17-Bro-6-010	4.601	0.097	0.3109	0.005	0.355	1748	18	1746	24	1871	42	-7.2
31-Bro-6-017	3.7	0.13	0.2712	0.005	0.612	1569	28	1544	28	1745	53	-13.0
32-Bro-6-018	3.3	0.1	0.2592	0.005	0.401	1479	24	1502	25	1644	56	-9.5
33-Bro-6-019	4.237	0.085	0.2925	0.004	0.453	1679	17	1653	22	1831	37	-10.8
36-Bro-6-022	4.207	0.083	0.3005	0.004	0.623	1673	16	1693	22	1790	28	-5.7
38-Bro-6-024	3.93	0.14	0.2814	0.008	0.773	1615	29	1646	41	1774	48	-7.8

Table 1 Detrital zircon U–Pb analytical data.

77-Bro-6-049	4.49	0.12	0.3029	0.008	0.654	1731	21	1715	38	1883	34	-9.8
123-Bro-6-080	3.9	0.13	0.2815	0.008	0.499	1612	26	1627	40	1776	53	-9.2
125-Bro-6-082	3.96	0.11	0.284	0.005	0.327	1625	23	1613	22	1761	50	-9.2
126-Bro-6-083	4.604	0.095	0.3169	0.005	0.365	1748	17	1695	27	1845	43	-8.8
142-Bro-6-092	4.156	0.075	0.2964	0.004	0.343	1665	15	1622	21	1780	39	-9.7
169-Bro-6-112	4.402	0.091	0.2998	0.005	0.3	1711	17	1697	23	1874	37	-10.4
172-Bro-6-115	4.49	0.11	0.3138	0.009	0.706	1733	22	1659	44	1831	44	-10.4
187-Bro-6-123	3.36	0.11	0.2662	0.005	0.028	1491	25	1518	24	1606	64	-5.8
194-Bro-6-130	4.01	0.11	0.2946	0.006	0.462	1633	22	1593	33	1735	51	-8.9
196-Bro-6-132	4.63	0.11	0.3171	0.006	0.441	1753	20	1696	31	1851	44	-9.1
120-Bro-6-077	4.33	0.14	0.3033	0.009	0.768	1702	28	1657	45	1822	38	-10.0
						Rejected analysis						
106-Bro-6-071	*7.37*	*0.17*	*0.3603*	*0.01*	*0.798*	*2166*	*24*	*1982*	*46*	*2303*	*35*	*-16.2*
144-Bro-6-094	*2.97*	*0.15*	*0.2361*	*0.007*	*0.571*	*1388*	*40*	*1265*	*35*	*1569*	*84*	*-24.0*
151-Bro-6-101	*3.697*	*0.093*	*0.2685*	*0.006*	*0.325*	*1568*	*20*	*1430*	*28*	*1765*	*38*	*-23.4*
8-Bro-6-001	*3.54*	*0.13*	*0.212*	*0.008*	*0.717*	*1532*	*30*	*1238*	*40*	*1970*	*47*	*-59.1*
10-Bro-6-003	*1.939*	*0.062*	*0.1059*	*0.004*	*0.774*	*1092*	*21*	*648*	*23*	*2145*	*39*	*-231.0*
11-Bro-6-004	*3.72*	*0.077*	*0.248*	*0.004*	*0.351*	*1575*	*17*	*1427*	*21*	*1787*	*42*	*-25.2*
13-Bro-6-006	*3.714*	*0.072*	*0.2461*	*0.004*	*0.436*	*1573*	*15*	*1418*	*22*	*1808*	*36*	*-27.5*
14-Bro-6-007	*2.56*	*0.088*	*0.1664*	*0.005*	*0.553*	*1287*	*25*	*992*	*28*	*1762*	*67*	*-77.6*
16-Bro-6-009	*4.1*	*0.11*	*0.2505*	*0.01*	*0.815*	*1657*	*23*	*1439*	*48*	*1939*	*38*	*-34.7*
18-Bro-6-011	*3.263*	*0.071*	*0.2054*	*0.004*	*0.565*	*1471*	*17*	*1204*	*21*	*1903*	*47*	*-58.1*
20-Bro-6-013	*3.974*	*0.074*	*0.2467*	*0.004*	*0.481*	*1628*	*15*	*1421*	*22*	*1905*	*36*	*-34.1*
21-Bro-6-014	*2.947*	*0.075*	*0.2057*	*0.004*	*0.508*	*1396*	*19*	*1208*	*21*	*1711*	*42*	*-41.6*
30-Bro-6-016	*2.52*	*0.11*	*0.1615*	*0.008*	*0.859*	*1275*	*33*	*964*	*46*	*1855*	*68*	*-92.4*
35-Bro-6-021	*3.1*	*0.096*	*0.2108*	*0.006*	*0.637*	*1430*	*24*	*1233*	*29*	*1769*	*41*	*-43.5*
37-Bro-6-023	*2.21*	*0.12*	*0.1443*	*0.004*	*0.692*	*1181*	*37*	*869*	*25*	*1854*	*53*	*-113.3*
40-Bro-6-026	*2.48*	*0.2*	*0.163*	*0.012*	*0.922*	*1273*	*55*	*973*	*65*	*1786*	*61*	*-83.6*
41-Bro-6-027	*2.173*	*0.056*	*0.147*	*0.003*	*0.621*	*1174*	*19*	*884*	*18*	*1778*	*40*	*-101.1*
43-Bro-6-029	*2.296*	*0.059*	*0.146*	*0.004*	*0.684*	*1212*	*18*	*878*	*20*	*1877*	*40*	*-113.8*
52-Bro-6-031	*4.09*	*0.15*	*0.2508*	*0.008*	*0.724*	*1651*	*29*	*1441*	*39*	*1968*	*47*	*-36.6*
53-Bro-6-032	*3.26*	*0.12*	*0.1867*	*0.006*	*0.86*	*1468*	*29*	*1103*	*35*	*2033*	*34*	*-84.3*
56-Bro-6-035	*3.76*	*0.14*	*0.2366*	*0.006*	*0.573*	*1581*	*30*	*1368*	*31*	*1893*	*55*	*-38.4*
57-Bro-6-036	*2.898*	*0.059*	*0.1737*	*0.003*	*0.687*	*1380*	*15*	*1032*	*19*	*1958*	*28*	*-89.7*
58-Bro-6-037	*2.775*	*0.061*	*0.1676*	*0.006*	*0.895*	*1348*	*16*	*998*	*30*	*1949*	*39*	*-95.3*
59-Bro-6-038	*3.353*	*0.086*	*0.195*	*0.005*	*0.755*	*1492*	*20*	*1148*	*29*	*2041*	*30*	*-77.8*
61-Bro-6-040	*2.823*	*0.067*	*0.1871*	*0.004*	*0.705*	*1359*	*18*	*1105*	*22*	*1785*	*31*	*-61.5*
65-Bro-6-044	*2.066*	*0.052*	*0.1167*	*0.003*	*0.68*	*1138*	*18*	*711*	*19*	*2080*	*34*	*-192.5*
75-Bro-6-047	*2.397*	*0.082*	*0.167*	*0.005*	*0.471*	*1239*	*25*	*995*	*27*	*1689*	*70*	*-69.7*
78-Bro-6-050	*1.811*	*0.039*	*0.0954*	*0.002*	*0.708*	*1048*	*14*	*587*	*13*	*2194*	*34*	*-273.8*
81-Bro-6-053	*3.109*	*0.09*	*0.2019*	*0.006*	*0.559*	*1432*	*22*	*1185*	*29*	*1831*	*50*	*-54.5*
82-Bro-6-054	*6.75*	*0.45*	*0.3176*	*0.005*	*0.275*	*2064*	*59*	*1777*	*27*	*2394*	*97*	*-34.7*
83-Bro-6-055	*2.9*	*0.11*	*0.1645*	*0.006*	*0.93*	*1380*	*28*	*981*	*33*	*2078*	*24*	*-111.8*
85-Bro-6-057	*2.729*	*0.069*	*0.176*	*0.005*	*0.712*	*1337*	*18*	*1045*	*25*	*1855*	*35*	*-77.5*

Table 1 Detrital zircon U–Pb analytical data.

88-Bro-6-060	*3.83*	*0.11*	*0.2501*	*0.006*	*0.658*	*1598*	*22*	*1438*	*33*	*1812*	*36*	*-26.0*
96-Bro-6-061	*3.787*	*0.078*	*0.2241*	*0.006*	*0.748*	*1588*	*16*	*1303*	*30*	*1970*	*27*	*-51.2*
99-Bro-6-064	*6.87*	*0.28*	*0.2981*	*0.009*	*0.298*	*2091*	*36*	*1681*	*45*	*2530*	*70*	*-50.5*
102-Bro-6-067	*3.685*	*0.09*	*0.2462*	*0.008*	*0.695*	*1569*	*19*	*1418*	*40*	*1785*	*44*	*-25.9*
108-Bro-6-073	*3.393*	*0.097*	*0.2193*	*0.008*	*0.681*	*1505*	*21*	*1277*	*40*	*1821*	*46*	*-42.6*
109-Bro-6-074	*2.752*	*0.08*	*0.1568*	*0.004*	*0.678*	*1340*	*22*	*943*	*21*	*2005*	*39*	*-112.6*
128-Bro-6-085	*2.84*	*0.12*	*0.1749*	*0.007*	*0.872*	*1367*	*30*	*1038*	*36*	*1920*	*33*	*-85.0*
129-Bro-6-086	*2.581*	*0.095*	*0.161*	*0.005*	*0.78*	*1291*	*27*	*962*	*28*	*1880*	*38*	*-95.4*
130-Bro-6-087	*2.215*	*0.054*	*0.1343*	*0.003*	*0.808*	*1184*	*17*	*812*	*19*	*1852*	*28*	*-128.1*
132-Bro-6-089	*3.046*	*0.07*	*0.2201*	*0.003*	*0.371*	*1417*	*18*	*1285*	*18*	*1633*	*40*	*-27.1*
143-Bro-6-093	*2.761*	*0.05*	*0.1791*	*0.003*	*0.471*	*1350*	*13*	*1062*	*14*	*1869*	*27*	*-76.0*
145-Bro-6-095	*4.09*	*0.13*	*0.1946*	*0.007*	*0.873*	*1650*	*26*	*1145*	*39*	*2374*	*21*	*-107.3*
147-Bro-6-097	*1.376*	*0.038*	*0.0726*	*0.002*	*0.525*	*877*	*16*	*452*	*12*	*2181*	*46*	*-382.5*
149-Bro-6-099	*2.304*	*0.058*	*0.1421*	*0.004*	*0.573*	*1216*	*19*	*856*	*20*	*1931*	*43*	*-125.6*
153-Bro-6-103	*3.42*	*0.11*	*0.2292*	*0.005*	*0.552*	*1507*	*26*	*1330*	*26*	*1779*	*61*	*-33.8*
163-Bro-6-106	*3.757*	*0.058*	*0.2343*	*0.003*	*0.541*	*1584*	*12*	*1357*	*15*	*1888*	*28*	*-39.1*
166-Bro-6-109	*3.29*	*0.1*	*0.1828*	*0.005*	*0.671*	*1479*	*25*	*1082*	*30*	*2107*	*42*	*-94.7*
Bro-07												
220-Bro-7-002	4.71	0.13	0.3201	0.006	0.675	1765	23	1789	30	1740	52	2.7
225-Bro-7-007	4.6	0.13	0.3114	0.006	0.083	1748	23	1747	31	1767	60	-1.1
235-Bro-7-010	4.559	0.098	0.3179	0.005	0.453	1746	18	1778	25	1712	39	3.7
236-Bro-7-011	4.436	0.08	0.3067	0.005	0.546	1719	15	1723	26	1719	30	0.2
242-Bro-7-017	4.61	0.12	0.3057	0.006	0.284	1749	22	1719	31	1793	53	-4.3
244-Bro-7-019	4.12	0.18	0.285	0.006	0.37	1647	34	1615	31	1734	79	-7.4
246-Bro-7-021	4.71	0.11	0.3195	0.006	0.488	1769	19	1786	31	1742	42	2.5
262-Bro-7-030	5.14	0.11	0.3224	0.007	0.662	1840	18	1805	34	1889	32	-4.7
264-Bro-7-032	4.84	0.11	0.3253	0.005	0.365	1795	18	1814	24	1733	40	4.5
266-Bro-7-034	3.77	0.15	0.2785	0.006	0.322	1583	31	1583	28	1601	73	-1.1
278-Bro-7-039	5.29	0.11	0.3287	0.008	0.516	1866	18	1836	39	1909	42	-4.0
281-Bro-7-042	4.99	0.11	0.3275	0.006	0.417	1815	18	1825	27	1790	36	1.9
284-Bro-7-045	4.42	0.11	0.3107	0.006	0.441	1715	20	1743	28	1695	45	2.8
285-Bro-7-046	4.78	0.11	0.3136	0.006	0.635	1783	19	1757	29	1825	33	-3.9
288-Bro-7-049	4.686	0.094	0.32	0.006	0.508	1763	17	1789	30	1731	38	3.2
291-Bro-7-052	4.94	0.11	0.326	0.009	0.479	1810	19	1817	41	1817	43	0.0
292-Bro-7-053	4.67	0.12	0.3177	0.006	0.48	1765	22	1778	29	1728	42	2.8
305-Bro-7-059	4.8	0.11	0.3121	0.007	0.525	1788	19	1749	32	1834	41	-4.9
308-Bro-7-062	4.986	0.096	0.3108	0.006	0.316	1817	17	1743	29	1899	40	-9.0
310-Bro-7-064	5.38	0.11	0.3358	0.007	0.414	1882	18	1865	33	1891	37	-1.4
313-Bro-7-067	4.663	0.094	0.3187	0.005	0.232	1760	17	1782	27	1726	39	3.1
314-Bro-7-068	4.777	0.089	0.3248	0.005	0.501	1779	16	1812	24	1726	29	4.7
323-Bro-7-070	5.19	0.17	0.3168	0.008	0.586	1846	29	1780	39	1945	47	-9.3
324-Bro-7-071	4.795	0.097	0.3127	0.005	0.382	1783	17	1753	25	1819	38	-3.8
326-Bro-7-073	15.3	0.31	0.553	0.013	0.628	2837	19	2834	56	2821	28	0.5

Table 1 Detrital zircon U–Pb analytical data.

331-Bro-7-078	12.16	0.19	0.504	0.01	0.63	2615	15	2635	44	2588	27	1.8
332-Bro-7-079	4.66	0.15	0.3003	0.008	0.6	1759	26	1691	38	1867	49	-10.4
333-Bro-7-080	10.83	0.23	0.4655	0.009	0.589	2510	18	2462	40	2586	25	-5.0
336-Bro-7-083	5.26	0.13	0.3314	0.007	0.592	1858	21	1844	35	1876	33	-1.7
347-Bro-7-087	4.991	0.095	0.3241	0.006	0.525	1821	16	1809	29	1814	33	-0.3
350-Bro-7-090	5.44	0.14	0.3306	0.008	0.516	1894	23	1839	38	1966	46	-6.9
353-Bro-7-093	5.16	0.14	0.3322	0.009	0.557	1843	23	1847	46	1863	46	-0.9
354-Bro-7-094	5.26	0.13	0.3167	0.007	0.639	1859	21	1776	37	1960	34	-10.4
355-Bro-7-095	4.97	0.11	0.3319	0.007	0.486	1812	18	1846	33	1761	36	4.6
356-Bro-7-096	4.99	0.17	0.3244	0.006	0.463	1816	29	1810	30	1815	52	-0.3
359-Bro-7-099	4.76	0.14	0.3189	0.007	0.558	1775	24	1789	34	1774	46	0.8
360-Bro-7-100	4.89	0.11	0.335	0.007	0.667	1797	19	1861	32	1737	30	6.7
369-Bro-7-102	4.83	0.13	0.3326	0.008	0.43	1788	23	1849	37	1742	47	5.8
370-Bro-7-103	5.58	0.14	0.3453	0.008	0.529	1910	22	1916	38	1922	39	-0.3
371-Bro-7-104	4.54	0.14	0.3113	0.007	0.443	1739	25	1750	33	1717	49	1.9
375-Bro-7-108	4.86	0.11	0.3249	0.007	0.56	1794	20	1812	33	1783	39	1.6
377-Bro-7-110	4.83	0.15	0.3247	0.008	0.33	1790	26	1817	38	1789	66	1.5
378-Bro-7-111	6.62	0.21	0.357	0.013	0.79	2059	29	1965	60	2126	60	-8.2
379-Bro-7-112	3.7	0.13	0.2887	0.007	0.645	1566	27	1633	33	1492	50	8.6
381-Bro-7-114	4.97	0.14	0.3161	0.009	0.651	1815	24	1769	44	1860	44	-5.1
257-Bro-7-025	4.88	0.16	0.3126	0.006	0.412	1796	27	1743	31	1884	53	-8.1
270-Bro-7-038	4.19	0.14	0.2822	0.008	0.597	1669	27	1651	40	1818	52	-10.1
287-Bro-7-048	5.44	0.12	0.3178	0.006	0.338	1893	19	1929	30	2102	46	-9.0
300-Bro-7-054	5.34	0.13	0.3153	0.005	0.45	1875	21	1917	23	2066	39	-7.8
303-Bro-7-057	5.19	0.1	0.3205	0.005	0.331	1849	17	1842	25	1981	37	-7.5
306-Bro-7-060	5.77	0.22	0.331	0.01	0.319	1943	34	1891	49	2083	68	-10.2
327-Bro-7-074	5.4	0.19	0.3225	0.009	0.521	1898	31	1872	44	2054	57	-9.7
373-Bro-7-106	5.12	0.18	0.3164	0.008	0.06	1836	30	1822	39	1960	63	-7.6
						Rejected analysis						
219-Bro-7-001	*7.39*	*0.46*	*0.1372*	*0.006*	*0.86*	*2157*	*57*	*828*	*31*	*3864*	*48*	*-366.7*
221-Bro-7-003	*7.22*	*0.45*	*0.2771*	*0.008*	*0.347*	*2130*	*56*	*1576*	*40*	*2710*	*130*	*-72.0*
223-Bro-7-005	*7.48*	*0.2*	*0.3078*	*0.008*	*0.47*	*2167*	*25*	*1728*	*40*	*2610*	*44*	*-51.0*
224-Bro-7-006	*5.86*	*0.25*	*0.1715*	*0.005*	*0.293*	*1954*	*36*	*1020*	*25*	*3171*	*70*	*-210.9*
226-Bro-7-008	*11.36*	*0.18*	*0.2141*	*0.004*	*0.835*	*2551*	*15*	*1250*	*22*	*3847*	*16*	*-207.8*
234-Bro-7-009	*11.65*	*0.32*	*0.428*	*0.011*	*0.572*	*2574*	*25*	*2297*	*49*	*2839*	*41*	*-23.6*
237-Bro-7-012	*6.52*	*0.98*	*0.1977*	*0.004*	*0.088*	*2000*	*140*	*1163*	*21*	*2980*	*250*	*-156.2*
239-Bro-7-014	*10.98*	*0.32*	*0.403*	*0.012*	*0.781*	*2519*	*28*	*2193*	*54*	*2777*	*35*	*-26.6*
240-Bro-7-015	*10.33*	*0.14*	*0.1406*	*0.002*	*0.678*	*2464*	*12*	*848*	*14*	*4338*	*17*	*-411.6*
241-Bro-7-016	*6.71*	*0.22*	*0.1697*	*0.004*	*0.666*	*2069*	*29*	*1010*	*24*	*3376*	*38*	*-234.3*
243-Bro-7-018	*13.89*	*0.29*	*0.2996*	*0.008*	*0.73*	*2740*	*19*	*1688*	*37*	*3630*	*25*	*-115.0*
245-Bro-7-020	*10.25*	*0.3*	*0.2582*	*0.007*	*0.435*	*2452*	*28*	*1479*	*38*	*3357*	*55*	*-127.0*
247-Bro-7-022	*11.06*	*0.32*	*0.2122*	*0.005*	*0.688*	*2524*	*27*	*1240*	*26*	*3809*	*32*	*-207.2*
248-Bro-7-023	*4.87*	*0.13*	*0.2846*	*0.005*	*0.391*	*1796*	*22*	*1614*	*26*	*2039*	*47*	*-26.3*
256-Bro-7-024	*5.24*	*0.15*	*0.28*	*0.005*	*0.168*	*1857*	*24*	*1590*	*27*	*2172*	*57*	*-36.6*

Table 1 Detrital zircon U–Pb analytical data.

258-Bro-7-026	*4.97*	*0.15*	*0.2823*	*0.009*	*0.22*	*1812*	*26*	*1603*	*44*	*2071*	*66*	*-29.2*
259-Bro-7-027	*5.84*	*0.36*	*0.2832*	*0.006*	*0.056*	*1943*	*52*	*1611*	*28*	*2340*	*110*	*-45.3*
260-Bro-7-028	*4.94*	*0.26*	*0.2876*	*0.004*	*0.136*	*1815*	*46*	*1629*	*21*	*2010*	*93*	*-23.4*
263-Bro-7-031	*5.93*	*0.16*	*0.201*	*0.006*	*0.693*	*1963*	*24*	*1180*	*31*	*2954*	*31*	*-150.3*
267-Bro-7-035	*5.002*	*0.096*	*0.287*	*0.005*	*0.378*	*1820*	*17*	*1626*	*27*	*2059*	*39*	*-26.6*
268-Bro-7-036	*5.63*	*0.38*	*0.1936*	*0.007*	*0.48*	*1910*	*59*	*1140*	*35*	*2870*	*100*	*-151.8*
269-Bro-7-037	*4.99*	*0.11*	*0.2884*	*0.004*	*0.523*	*1819*	*20*	*1633*	*22*	*2030*	*35*	*-24.3*
279-Bro-7-040	*5.59*	*0.13*	*0.2648*	*0.008*	*0.439*	*1916*	*19*	*1513*	*41*	*2393*	*48*	*-58.2*
280-Bro-7-041	*9.33*	*0.2*	*0.1822*	*0.004*	*0.733*	*2370*	*20*	*1079*	*20*	*3778*	*23*	*-250.1*
282-Bro-7-043	*8.68*	*0.19*	*0.2695*	*0.006*	*0.485*	*2302*	*20*	*1537*	*33*	*3079*	*39*	*-100.3*
283-Bro-7-044	*5.485*	*0.096*	*0.2985*	*0.005*	*0.551*	*1898*	*15*	*1683*	*26*	*2156*	*29*	*-28.1*
286-Bro-7-047	*9.56*	*0.15*	*0.2919*	*0.004*	*0.458*	*2394*	*14*	*1650*	*21*	*3096*	*21*	*-87.6*
289-Bro-7-050	*8.37*	*0.33*	*0.2736*	*0.009*	*0.685*	*2277*	*32*	*1558*	*47*	*2952*	*59*	*-89.5*
290-Bro-7-051	*14.94*	*0.29*	*0.462*	*0.017*	*0.598*	*2811*	*18*	*2446*	*73*	*3071*	*47*	*-25.6*
301-Bro-7-055	*5.71*	*0.15*	*0.297*	*0.007*	*0.343*	*1930*	*22*	*1675*	*36*	*2235*	*43*	*-33.4*
302-Bro-7-056	*5.73*	*0.13*	*0.2458*	*0.007*	*0.103*	*1933*	*19*	*1416*	*35*	*2544*	*52*	*-79.7*
304-Bro-7-058	*9.01*	*0.24*	*0.1748*	*0.006*	*0.852*	*2341*	*24*	*1038*	*30*	*3802*	*24*	*-266.3*
307-Bro-7-061	*7.19*	*0.49*	*0.2396*	*0.004*	*0.072*	*2138*	*63*	*1387*	*23*	*2950*	*130*	*-112.7*
309-Bro-7-063	*3.158*	*0.06*	*0.1828*	*0.004*	*0.797*	*1446*	*14*	*1082*	*22*	*2054*	*26*	*-89.8*
311-Bro-7-065	*10.82*	*0.18*	*0.2482*	*0.006*	*0.627*	*2509*	*16*	*1428*	*29*	*3530*	*27*	*-147.2*
312-Bro-7-066	*6.13*	*0.19*	*0.2852*	*0.006*	*0.652*	*1989*	*28*	*1617*	*31*	*2389*	*37*	*-47.7*
322-Bro-7-069	*5.9*	*0.14*	*0.2937*	*0.006*	*0.492*	*1961*	*20*	*1659*	*30*	*2296*	*38*	*-38.4*
325-Bro-7-072	*5.58*	*0.19*	*0.3053*	*0.005*	*0.145*	*1912*	*28*	*1722*	*21*	*2100*	*57*	*-22.0*
328-Bro-7-075	*6.18*	*0.34*	*0.2829*	*0.008*	*0.097*	*2000*	*50*	*1605*	*41*	*2440*	*120*	*-52.0*
329-Bro-7-076	*9.11*	*0.25*	*0.2981*	*0.01*	*0.113*	*2346*	*25*	*1680*	*48*	*2988*	*75*	*-77.9*
330-Bro-7-077	*7.91*	*0.17*	*0.2613*	*0.007*	*0.589*	*2221*	*19*	*1500*	*33*	*2990*	*29*	*-99.3*
334-Bro-7-081	*5.26*	*0.14*	*0.2961*	*0.007*	*0.607*	*1860*	*20*	*1670*	*35*	*2073*	*39*	*-24.1*
344-Bro-7-084	*6.57*	*0.13*	*0.2546*	*0.007*	*0.465*	*2053*	*18*	*1461*	*34*	*2712*	*40*	*-85.6*
346-Bro-7-086	*6.03*	*0.16*	*0.3073*	*0.01*	*0.547*	*1977*	*23*	*1726*	*48*	*2249*	*45*	*-30.3*
348-Bro-7-088	*7*	*0.2*	*0.3331*	*0.008*	*0.676*	*2107*	*26*	*1852*	*39*	*2381*	*31*	*-28.6*
349-Bro-7-089	*5.25*	*0.17*	*0.2654*	*0.007*	*0.36*	*1859*	*27*	*1516*	*38*	*2277*	*57*	*-50.2*
351-Bro-7-091	*4.91*	*0.2*	*0.2451*	*0.006*	*0.019*	*1805*	*33*	*1413*	*31*	*2271*	*77*	*-60.7*
352-Bro-7-092	*5*	*0.1*	*0.2533*	*0.005*	*0.533*	*1817*	*18*	*1455*	*23*	*2263*	*32*	*-55.5*
357-Bro-7-097	*8.35*	*0.34*	*0.3297*	*0.007*	*0.457*	*2269*	*39*	*1845*	*32*	*2677*	*62*	*-45.1*
358-Bro-7-098	*6.3*	*0.26*	*0.324*	*0.01*	*0.226*	*2012*	*37*	*1806*	*49*	*2253*	*72*	*-24.8*
368-Bro-7-101	*9.12*	*0.35*	*0.3155*	*0.008*	*0.32*	*2348*	*35*	*1766*	*40*	*2905*	*60*	*-64.5*
376-Bro-7-109	*7.06*	*0.18*	*0.2495*	*0.007*	*0.659*	*2116*	*23*	*1434*	*38*	*2864*	*35*	*-99.7*
382-Bro-7-115	*5.74*	*0.15*	*0.2988*	*0.008*	*0.171*	*1934*	*23*	*1684*	*40*	*2226*	*64*	*-32.2*
383-Bro-7-116	*3.3*	*0.16*	*0.1712*	*0.008*	*0.814*	*1485*	*35*	*1018*	*46*	*2266*	*47*	*-122.6*
MS-03												
187-MS-03-007	5.26	0.12	0.3298	0.005	0.507	1860	20	1837	22	1881	37	-2.4
192-MS-03-012	4.9	0.12	0.328	0.005	0.471	1803	20	1828	25	1768	40	3.3
195-MS-03-015	4.67	0.14	0.3123	0.006	0.472	1767	27	1751	29	1804	57	-3.0

Table 1 Detrital zircon U–Pb analytical data.

209-MS-03-023	5.6	0.12	0.3445	0.006	0.536	1912	18	1911	30	1904	36	0.4
234-MS-03-042	4.77	0.1	0.3286	0.006	0.443	1780	18	1830	27	1739	39	5.0
237-MS-03-045	11.28	0.22	0.491	0.01	0.698	2544	18	2577	44	2527	25	1.9
249-MS-03-051	8.93	0.17	0.435	0.009	0.696	2328	18	2326	40	2346	31	-0.9
251-MS-03-053	4.829	0.095	0.3246	0.006	0.604	1790	17	1811	27	1754	32	3.1
253-MS-03-055	5.05	0.12	0.3385	0.007	0.514	1830	21	1878	33	1806	40	3.8
254-MS-03-056	5.13	0.13	0.3363	0.006	0.554	1840	22	1868	27	1802	44	3.5
255-MS-03-057	5.23	0.14	0.3349	0.006	0.481	1855	23	1865	31	1833	44	1.7
258-MS-03-060	4.9	0.19	0.3211	0.009	0.794	1797	33	1794	42	1812	56	-1.0
266-MS-03-062	11.5	0.53	0.492	0.018	0.844	2552	44	2573	78	2534	44	1.5
267-MS-03-063	4.49	0.11	0.3136	0.005	0.184	1734	19	1758	23	1723	50	2.0
270-MS-03-066	4.6	0.14	0.305	0.008	0.18	1747	25	1766	41	1846	57	-4.5
272-MS-03-068	5.03	0.11	0.3274	0.005	0.428	1824	19	1825	23	1853	37	-1.5
275-MS-03-071	4.78	0.11	0.3156	0.006	0.55	1779	19	1767	27	1784	34	-1.0
287-MS-03-077	11.9	0.26	0.467	0.01	0.484	2601	20	2477	43	2685	32	-8.4
290-MS-03-080	5.16	0.24	0.326	0.013	0.793	1851	37	1819	63	1889	57	-3.8
312-MS-03-096	5.19	0.18	0.335	0.011	0.562	1849	30	1861	52	1835	60	1.4
314-MS-03-098	5.37	0.12	0.3348	0.005	0.381	1879	19	1861	23	1914	34	-2.8
321-MS-03-105	5.13	0.16	0.3147	0.006	0.379	1838	26	1763	29	1901	47	-7.8
330-MS-03-108	4.61	0.14	0.2971	0.009	0.412	1749	26	1676	46	1797	66	-7.2
334-MS-03-112	4.93	0.1	0.324	0.005	0.337	1804	18	1808	25	1813	41	-0.3
335-MS-03-113	6.32	0.16	0.3727	0.007	0.323	2021	21	2044	32	2029	43	0.7
349-MS-03-121	5.21	0.15	0.3415	0.008	0.576	1853	26	1892	36	1830	45	3.3
350-MS-03-122	5.07	0.15	0.3359	0.005	0.312	1833	23	1866	26	1808	53	3.1
353-MS-03-125	7.64	0.15	0.3934	0.006	0.52	2195	16	2138	29	2221	28	-3.9
355-MS-03-127	5.15	0.11	0.3349	0.006	0.421	1840	18	1861	29	1828	40	1.8
356-MS-03-128	4.89	0.19	0.3056	0.009	0.475	1795	32	1718	42	1850	67	-7.7
362-MS-03-134	5.3	0.13	0.3406	0.006	0.512	1869	21	1888	28	1856	38	1.7
369-MS-03-135	5.17	0.13	0.3346	0.006	0.31	1850	23	1860	30	1833	49	1.5
371-MS-03-137	5.05	0.12	0.3351	0.007	0.678	1825	20	1862	33	1786	40	4.1
372-MS-03-138	4.8	0.1	0.3194	0.006	0.485	1787	19	1785	29	1791	36	-0.3
373-MS-03-139	4.88	0.17	0.328	0.012	0.78	1794	30	1825	58	1775	48	2.7
374-MS-03-140	4.8	0.16	0.3137	0.009	0.611	1788	25	1757	44	1810	52	-3.0
382-MS-03-148	4.67	0.12	0.2994	0.005	0.496	1757	22	1687	26	1838	40	-9.0
184-MS-03-004	4.56	0.17	0.3013	0.007	0.319	1739	31	1697	33	1861	71	-9.7
213-MS-03-027	4.33	0.16	0.303	0.007	0.407	1694	31	1706	33	1858	62	-8.9
246-MS-03-048	4.111	0.092	0.2969	0.005	0.367	1654	18	1675	27	1770	44	-5.7
271-MS-03-067	4.17	0.13	0.2947	0.009	0.406	1666	25	1694	44	1853	67	-9.4
274-MS-03-070	4.186	0.092	0.2946	0.005	0.431	1673	18	1663	26	1806	36	-8.6
294-MS-03-084	3.951	0.071	0.2849	0.005	0.363	1625	14	1644	25	1790	40	-8.9
300-MS-03-090	4.22	0.13	0.2954	0.008	0.585	1674	25	1677	38	1835	51	-9.4
310-MS-03-094	4.33	0.12	0.2928	0.007	0.724	1703	24	1715	33	1880	36	-9.6
370-MS-03-136	4.37	0.18	0.3075	0.007	0.516	1702	33	1728	37	1834	58	-6.1
352-MS-03-124	4.56	0.15	0.3047	0.009	0.686	1742	26	1814	42	1909	42	-5.2

Table 1 Detrital zircon U–Pb analytical data.

361-MS-03-133	4.69	0.18	0.303	0.011	0.697	1763	32	1805	57	1986	55	-10.0
381-MS-03-147	4.39	0.12	0.3002	0.008	0.456	1713	21	1691	39	1835	44	-8.5
					Rejected analysis							
206-MS-03-020	*6.48*	*0.22*	*0.3475*	*0.008*	*0.52*	*2039*	*31*	*1922*	*39*	*2174*	*55*	*-13.1*
214-MS-03-028	*9.53*	*0.45*	*0.415*	*0.017*	*0.515*	*2386*	*42*	*2235*	*80*	*2531*	*75*	*-13.2*
291-MS-03-081	*8.16*	*0.23*	*0.383*	*0.012*	*0.333*	*2247*	*25*	*2088*	*55*	*2392*	*60*	*-14.6*
181-MS-03-001	*2.138*	*0.063*	*0.1194*	*0.004*	*0.876*	*1159*	*20*	*727*	*24*	*2082*	*30*	*-186.4*
182-MS-03-002	*3.8*	*0.15*	*0.246*	*0.011*	*0.777*	*1597*	*30*	*1414*	*56*	*1820*	*36*	*-28.7*
183-MS-03-003	*1.359*	*0.036*	*0.081*	*0.003*	*0.652*	*870*	*16*	*502*	*16*	*2031*	*44*	*-304.6*
185-MS-03-005	*2.382*	*0.062*	*0.1414*	*0.003*	*0.707*	*1241*	*20*	*852*	*18*	*2016*	*31*	*-136.6*
186-MS-03-006	*3.145*	*0.096*	*0.1754*	*0.004*	*0.291*	*1442*	*24*	*1041*	*23*	*2085*	*56*	*-100.3*
188-MS-03-008	*3.337*	*0.066*	*0.1868*	*0.003*	*0.545*	*1488*	*15*	*1104*	*19*	*2088*	*33*	*-89.1*
190-MS-03-010	*3.53*	*0.17*	*0.2142*	*0.01*	*0.833*	*1530*	*37*	*1250*	*51*	*1928*	*50*	*-54.2*
191-MS-03-011	*2.186*	*0.099*	*0.1254*	*0.005*	*0.863*	*1172*	*32*	*761*	*31*	*2017*	*39*	*-165.0*
193-MS-03-013	*3.829*	*0.078*	*0.2055*	*0.004*	*0.426*	*1601*	*16*	*1205*	*22*	*2179*	*35*	*-80.8*
194-MS-03-014	*1.079*	*0.024*	*0.0527*	*0.001*	*0.599*	*743*	*12*	*330.8*	*7.8*	*2331*	*29*	*-604.7*
202-MS-03-016	*3.94*	*0.24*	*0.233*	*0.012*	*0.406*	*1616*	*49*	*1348*	*61*	*1990*	*120*	*-47.6*
203-MS-03-017	*1.541*	*0.031*	*0.0887*	*0.002*	*0.655*	*947*	*12*	*548*	*10*	*2041*	*28*	*-272.4*
204-MS-03-018	*1.271*	*0.039*	*0.0751*	*0.003*	*0.731*	*832*	*17*	*470*	*19*	*2016*	*41*	*-328.9*
205-MS-03-019	*2.509*	*0.088*	*0.1491*	*0.005*	*0.766*	*1272*	*26*	*895*	*30*	*1981*	*42*	*-121.3*
207-MS-03-021	*1.347*	*0.05*	*0.0727*	*0.003*	*0.79*	*867*	*21*	*452*	*15*	*2131*	*39*	*-371.5*
208-MS-03-022	*4.22*	*0.17*	*0.257*	*0.011*	*0.737*	*1681*	*31*	*1475*	*55*	*1934*	*48*	*-31.1*
210-MS-03-024	*2.136*	*0.079*	*0.1223*	*0.004*	*0.741*	*1157*	*25*	*743*	*23*	*2014*	*39*	*-171.1*
211-MS-03-025	*2.545*	*0.073*	*0.1456*	*0.005*	*0.684*	*1290*	*23*	*876*	*29*	*2075*	*52*	*-136.9*
212-MS-03-026	*2.946*	*0.079*	*0.1663*	*0.006*	*0.602*	*1392*	*20*	*991*	*32*	*2053*	*47*	*-107.2*
215-MS-03-029	*4.13*	*0.12*	*0.26*	*0.008*	*0.5*	*1657*	*23*	*1489*	*43*	*1901*	*52*	*-27.7*
216-MS-03-030	*4.13*	*0.14*	*0.2613*	*0.009*	*0.456*	*1664*	*28*	*1496*	*47*	*1889*	*60*	*-26.3*
223-MS-03-031	*5.108*	*0.085*	*0.2904*	*0.005*	*0.535*	*1842*	*15*	*1643*	*22*	*2064*	*31*	*-25.6*
224-MS-03-032	*5.96*	*0.4*	*0.316*	*0.018*	*0.841*	*1980*	*50*	*1769*	*91*	*2244*	*56*	*-26.9*
225-MS-03-033	*3.41*	*0.1*	*0.2132*	*0.005*	*0.646*	*1510*	*25*	*1245*	*28*	*1921*	*44*	*-54.3*
226-MS-03-034	*3.79*	*0.27*	*0.189*	*0.012*	*0.888*	*1584*	*56*	*1116*	*67*	*2316*	*56*	*-107.5*
227-MS-03-035	*3.94*	*0.11*	*0.2279*	*0.006*	*0.658*	*1620*	*22*	*1323*	*33*	*2061*	*41*	*-55.8*
228-MS-03-036	*1.632*	*0.045*	*0.0911*	*0.003*	*0.782*	*984*	*17*	*561*	*19*	*2127*	*38*	*-279.1*
229-MS-03-037	*1.669*	*0.083*	*0.0944*	*0.006*	*0.478*	*995*	*32*	*581*	*38*	*2023*	*87*	*-248.2*
230-MS-03-038	*5.06*	*0.24*	*0.267*	*0.011*	*0.414*	*1830*	*38*	*1523*	*54*	*2217*	*77*	*-45.6*
231-MS-03-039	*1.879*	*0.081*	*0.1021*	*0.004*	*0.826*	*1071*	*29*	*626*	*24*	*2175*	*43*	*-247.4*
232-MS-03-040	*2.56*	*0.046*	*0.144*	*0.003*	*0.566*	*1290*	*13*	*867*	*19*	*2103*	*36*	*-142.6*
233-MS-03-041	*0.969*	*0.037*	*0.0477*	*0.002*	*0.865*	*690*	*20*	*300*	*14*	*2320*	*38*	*-673.3*
235-MS-03-043	*1.164*	*0.05*	*0.0628*	*0.003*	*0.877*	*787*	*25*	*392*	*19*	*2198*	*43*	*-460.7*
236-MS-03-044	*3.453*	*0.083*	*0.2071*	*0.006*	*0.111*	*1516*	*19*	*1213*	*30*	*1971*	*55*	*-62.5*
244-MS-03-046	*1.578*	*0.041*	*0.0929*	*0.003*	*0.706*	*960*	*16*	*572*	*17*	*2012*	*39*	*-251.7*
245-MS-03-047	*2.557*	*0.07*	*0.1508*	*0.004*	*0.665*	*1286*	*20*	*905*	*22*	*2018*	*36*	*-123.0*
247-MS-03-049	*1.27*	*0.058*	*0.074*	*0.004*	*0.923*	*837*	*27*	*464*	*23*	*2009*	*34*	*-333.0*
248-MS-03-050	*1.276*	*0.027*	*0.0672*	*0.002*	*0.751*	*834*	*12*	*419*	*11*	*2182*	*32*	*-420.8*

Table 1 Detrital zircon U–Pb analytical data.

250-MS-03-052	*1.916*	*0.051*	*0.1063*	*0.003*	*0.752*	*1086*	*18*	*651*	*17*	*2104*	*33*	*-223.2*
252-MS-03-054	*3.27*	*0.24*	*0.196*	*0.013*	*0.883*	*1464*	*59*	*1151*	*71*	*1993*	*67*	*-73.2*
256-MS-03-058	*2.438*	*0.081*	*0.1361*	*0.005*	*0.796*	*1252*	*24*	*822*	*28*	*2084*	*38*	*-153.5*
257-MS-03-059	*6.55*	*0.18*	*0.3319*	*0.008*	*0.665*	*2050*	*24*	*1855*	*41*	*2239*	*42*	*-20.7*
265-MS-03-061	*2.83*	*0.11*	*0.1653*	*0.006*	*0.764*	*1363*	*30*	*985*	*34*	*2017*	*52*	*-104.8*
268-MS-03-064	*3.09*	*0.13*	*0.204*	*0.01*	*0.772*	*1433*	*31*	*1196*	*55*	*1875*	*54*	*-56.8*
269-MS-03-065	*3.12*	*0.18*	*0.1855*	*0.008*	*0.506*	*1433*	*46*	*1096*	*45*	*1981*	*87*	*-80.7*
273-MS-03-069	*2.84*	*0.11*	*0.1475*	*0.005*	*0.781*	*1363*	*29*	*886*	*28*	*2210*	*37*	*-149.4*
276-MS-03-072	*3.425*	*0.091*	*0.213*	*0.006*	*0.683*	*1511*	*20*	*1244*	*32*	*1918*	*33*	*-54.2*
277-MS-03-073	*3.93*	*0.12*	*0.2559*	*0.006*	*0.516*	*1622*	*27*	*1468*	*33*	*1841*	*62*	*-25.4*
278-MS-03-074	*4.77*	*0.12*	*0.2755*	*0.007*	*0.809*	*1781*	*21*	*1567*	*34*	*2041*	*26*	*-30.2*
279-MS-03-075	*4.32*	*0.21*	*0.216*	*0.01*	*0.877*	*1692*	*41*	*1262*	*55*	*2291*	*51*	*-81.5*
286-MS-03-076	*3.27*	*0.14*	*0.2071*	*0.009*	*0.902*	*1470*	*32*	*1222*	*51*	*1878*	*36*	*-53.7*
288-MS-03-078	*3.51*	*0.2*	*0.22*	*0.014*	*0.846*	*1523*	*45*	*1282*	*74*	*1900*	*59*	*-48.2*
289-MS-03-079	*2.538*	*0.06*	*0.1393*	*0.003*	*0.739*	*1285*	*17*	*840*	*19*	*2119*	*30*	*-152.3*
292-MS-03-082	*1.674*	*0.064*	*0.0975*	*0.003*	*0.791*	*1000*	*23*	*599*	*20*	*2021*	*42*	*-237.4*
293-MS-03-083	*11.57*	*0.34*	*0.409*	*0.014*	*0.919*	*2570*	*29*	*2220*	*62*	*2885*	*21*	*-30.0*
295-MS-03-085	*5.87*	*0.37*	*0.314*	*0.011*	*0.634*	*1944*	*54*	*1758*	*52*	*2144*	*86*	*-22.0*
296-MS-03-086	*1.639*	*0.062*	*0.0861*	*0.003*	*0.868*	*982*	*24*	*532*	*19*	*2257*	*38*	*-324.2*
297-MS-03-087	*2.779*	*0.057*	*0.1764*	*0.003*	*0.446*	*1347*	*15*	*1047*	*17*	*1853*	*34*	*-77.0*
298-MS-03-088	*2.602*	*0.047*	*0.1612*	*0.004*	*0.808*	*1299*	*13*	*963*	*19*	*1922*	*24*	*-99.6*
299-MS-03-089	*2.49*	*0.15*	*0.1434*	*0.009*	*0.883*	*1252*	*42*	*866*	*51*	*2041*	*38*	*-135.7*
307-MS-03-091	*3.89*	*0.14*	*0.2423*	*0.01*	*0.639*	*1609*	*28*	*1398*	*51*	*1927*	*54*	*-37.8*
308-MS-03-092	*2.364*	*0.09*	*0.1273*	*0.004*	*0.859*	*1228*	*27*	*772*	*25*	*2107*	*30*	*-172.9*
309-MS-03-093	*3.79*	*0.13*	*0.2296*	*0.007*	*0.733*	*1594*	*26*	*1331*	*36*	*1972*	*39*	*-48.2*
311-MS-03-095	*3.057*	*0.072*	*0.1568*	*0.004*	*0.711*	*1424*	*17*	*939*	*20*	*2246*	*29*	*-139.2*
313-MS-03-097	*4.145*	*0.099*	*0.2634*	*0.007*	*0.488*	*1661*	*20*	*1506*	*35*	*1853*	*52*	*-23.0*
315-MS-03-099	*3.13*	*0.18*	*0.1865*	*0.009*	*0.768*	*1435*	*45*	*1101*	*49*	*1994*	*79*	*-81.1*
316-MS-03-100	*1.531*	*0.043*	*0.0868*	*0.002*	*0.748*	*944*	*18*	*536*	*14*	*2062*	*35*	*-284.7*
317-MS-03-101	*3.53*	*0.16*	*0.221*	*0.011*	*0.582*	*1531*	*35*	*1285*	*60*	*1931*	*84*	*-50.3*
318-MS-03-102	*3.59*	*0.15*	*0.2151*	*0.009*	*0.703*	*1544*	*33*	*1254*	*50*	*1976*	*62*	*-57.6*
319-MS-03-103	*1.376*	*0.045*	*0.073*	*0.003*	*0.85*	*876*	*19*	*454*	*17*	*2224*	*36*	*-389.9*
320-MS-03-104	*2.83*	*0.093*	*0.1601*	*0.006*	*0.359*	*1362*	*25*	*957*	*35*	*2070*	*80*	*-116.3*
328-MS-03-106	*1.627*	*0.087*	*0.101*	*0.006*	*0.883*	*976*	*34*	*620*	*34*	*1932*	*54*	*-211.6*
329-MS-03-107	*3.56*	*0.2*	*0.229*	*0.012*	*0.44*	*1536*	*46*	*1330*	*64*	*1878*	*93*	*-41.2*
331-MS-03-109	*2.305*	*0.047*	*0.136*	*0.004*	*0.696*	*1212*	*14*	*821*	*21*	*2020*	*32*	*-146.0*
332-MS-03-110	*1.718*	*0.041*	*0.0876*	*0.003*	*0.804*	*1014*	*15*	*541*	*16*	*2242*	*34*	*-314.4*
333-MS-03-111	*3.334*	*0.095*	*0.2054*	*0.006*	*0.598*	*1486*	*22*	*1207*	*31*	*1940*	*41*	*-60.7*
336-MS-03-114	*2.967*	*0.055*	*0.1783*	*0.004*	*0.494*	*1398*	*14*	*1057*	*21*	*1980*	*46*	*-87.3*
337-MS-03-115	*1.937*	*0.04*	*0.1145*	*0.003*	*0.734*	*1096*	*14*	*700*	*16*	*2012*	*30*	*-187.4*
338-MS-03-116	*2.78*	*0.1*	*0.1524*	*0.006*	*0.774*	*1347*	*27*	*913*	*33*	*2120*	*42*	*-132.2*
339-MS-03-117	*2.342*	*0.086*	*0.1373*	*0.005*	*0.911*	*1221*	*26*	*828*	*27*	*2011*	*26*	*-142.9*
340-MS-03-118	*2.624*	*0.076*	*0.1383*	*0.007*	*0.801*	*1306*	*21*	*842*	*35*	*2183*	*46*	*-159.3*

Table 1 Detrital zircon U–Pb analytical data.

MS-05												
393-MS-05-003	3.7	0.28	0.265	0.02	0.83	1566	60	1660	100	1760	74	-6.0
398-MS-05-008	3.9	0.16	0.269	0.009	0.788	1610	33	1683	44	1799	50	-6.9
400-MS-05-010	4.92	0.1	0.3192	0.006	0.375	1807	17	1784	28	1827	38	-2.4
401-MS-05-011	5.28	0.14	0.3312	0.007	0.348	1870	23	1842	35	1921	44	-4.3
402-MS-05-012	6.39	0.14	0.3599	0.007	0.595	2031	19	1980	34	2065	33	-4.3
413-MS-05-017	4.95	0.16	0.311	0.01	0.653	1808	28	1744	49	1893	47	-8.5
415-MS-05-019	5.03	0.12	0.3167	0.006	0.49	1824	21	1807	32	1978	44	-9.5
416-MS-05-020	4.68	0.11	0.3102	0.006	0.468	1759	21	1740	30	1784	39	-2.5
419-MS-05-023	4.62	0.1	0.3063	0.006	0.402	1751	19	1721	27	1770	40	-2.8
422-MS-05-026	3.44	0.15	0.2509	0.006	0.613	1508	34	1591	30	1716	68	-7.9
423-MS-05-027	4.5	0.19	0.3003	0.008	0.718	1725	35	1689	40	1843	48	-9.1
436-MS-05-034	4.44	0.13	0.2944	0.006	0.369	1721	24	1666	30	1800	49	-8.0
441-MS-05-039	4.88	0.11	0.3223	0.007	0.635	1802	18	1799	33	1799	33	0.0
442-MS-05-040	4.88	0.11	0.3219	0.006	0.457	1800	19	1798	29	1807	40	-0.5
443-MS-05-041	4.567	0.094	0.3112	0.006	0.581	1747	17	1745	27	1745	33	0.0
446-MS-05-044	5.32	0.1	0.3188	0.006	0.7	1872	15	1783	29	1967	28	-10.3
455-MS-05-047	4.08	0.13	0.2807	0.008	0.67	1651	28	1643	41	1803	51	-9.7
460-MS-05-052	4.71	0.11	0.3107	0.005	0.386	1767	19	1743	25	1797	43	-3.1
465-MS-05-057	4.366	0.088	0.2938	0.007	0.681	1713	17	1659	35	1784	35	-7.5
478-MS-05-064	7.82	0.39	0.395	0.016	0.9	2233	45	2145	73	2282	31	-6.4
483-MS-05-069	4.94	0.15	0.3155	0.01	0.596	1808	25	1768	49	1927	56	-9.0
486-MS-05-072	4	0.12	0.2714	0.007	0.685	1633	23	1665	37	1788	38	-7.4
488-MS-05-074	4.59	0.18	0.3003	0.008	0.528	1748	34	1692	39	1808	69	-6.9
498-MS-05-078	5.59	0.11	0.34	0.006	0.619	1915	17	1886	27	1917	25	-1.6
501-MS-05-081	4.66	0.12	0.314	0.006	0.613	1766	21	1759	29	1760	35	-0.1
504-MS-05-084	4.704	0.098	0.3158	0.007	0.682	1765	17	1768	32	1741	31	1.5
506-MS-05-086	4.65	0.16	0.307	0.011	0.573	1761	30	1697	53	1872	65	-10.3
507-MS-05-087	4.69	0.1	0.3171	0.007	0.628	1763	18	1782	33	1763	33	1.1
509-MS-05-089	4.18	0.16	0.2819	0.009	0.85	1666	31	1658	46	1807	37	-9.0
521-MS-05-095	4.79	0.11	0.3108	0.006	0.44	1786	18	1744	28	1838	38	-5.4
522-MS-05-096	4.69	0.12	0.3076	0.006	0.447	1765	21	1728	28	1788	40	-3.5
523-MS-05-097	4.76	0.1	0.3158	0.005	0.467	1779	18	1772	27	1764	34	0.5
525-MS-05-099	5.3	0.17	0.3323	0.007	0.465	1866	29	1848	36	1843	61	0.3
527-MS-05-101	4.273	0.08	0.3001	0.005	0.526	1688	16	1641	23	1795	35	-9.4
531-MS-05-105	4.06	0.17	0.28	0.01	0.783	1643	34	1590	51	1738	60	-9.3
540-MS-05-108	4.38	0.13	0.2976	0.008	0.689	1710	25	1668	42	1808	41	-8.4
541-MS-05-109	3.64	0.18	0.264	0.011	0.65	1553	39	1579	55	1732	72	-9.7
543-MS-05-111	4.89	0.12	0.3254	0.006	0.508	1804	20	1815	30	1793	41	1.2
544-MS-05-112	5.18	0.11	0.3233	0.006	0.385	1849	18	1805	29	1890	39	-4.7
547-MS-05-115	7.03	0.12	0.3874	0.007	0.558	2115	15	2114	32	2105	28	0.4
552-MS-05-120	4.16	0.11	0.2883	0.007	0.72	1668	22	1632	37	1796	41	-10.0
560-MS-05-122	4.829	0.093	0.3182	0.004	0.338	1790	17	1783	22	1798	35	-0.8
563-MS-05-125	4.203	0.092	0.2843	0.006	0.6	1676	19	1672	29	1817	31	-8.7
568-MS-05-130	4.53	0.12	0.2938	0.006	0.448	1736	22	1659	28	1800	46	-8.5

Table 1 Detrital zircon U–Pb analytical data.

569-MS-05-131	4.38	0.12	0.3008	0.007	0.566	1706	22	1710	37	1835	46	-7.3
580-MS-05-136	5.27	0.12	0.3267	0.005	0.434	1864	21	1822	24	1908	46	-4.7
581-MS-05-137	3.5	0.13	0.2644	0.008	0.654	1526	29	1536	47	1647	61	-7.2
582-MS-05-138	4.36	0.14	0.289	0.01	0.727	1702	27	1634	51	1787	47	-9.4
586-MS-05-142	4.88	0.14	0.3146	0.006	0.155	1801	25	1766	28	1829	59	-3.6
588-MS-05-145	4.76	0.17	0.305	0.01	0.619	1774	29	1716	51	1839	50	-7.2
589-MS-05-146	4.63	0.13	0.3094	0.006	0.49	1754	24	1737	30	1757	47	-1.2
590-MS-05-147	3.981	0.086	0.2887	0.005	0.104	1628	17	1593	26	1753	53	-10.0
591-MS-05-148	5.31	0.11	0.3317	0.006	0.358	1868	18	1846	26	1896	37	-2.7
					Rejected analysis							
395-MS-05-005	*8.72*	*0.18*	*0.3947*	*0.008*	*0.699*	*2309*	*18*	*2143*	*35*	*2461*	*27*	*-14.8*
550-MS-05-118	*6.77*	*0.25*	*0.355*	*0.013*	*0.593*	*2084*	*35*	*1957*	*63*	*2211*	*64*	*-13.0*
391-MS-05-001	*3.623*	*0.073*	*0.2382*	*0.004*	*0.561*	*1554*	*16*	*1377*	*20*	*1808*	*33*	*-31.3*
394-MS-05-004	*2.666*	*0.098*	*0.1732*	*0.005*	*0.647*	*1316*	*27*	*1029*	*29*	*1759*	*48*	*-70.9*
396-MS-05-006	*4.7*	*0.15*	*0.2186*	*0.007*	*0.834*	*1763*	*27*	*1273*	*36*	*2427*	*32*	*-90.7*
397-MS-05-007	*2.545*	*0.088*	*0.157*	*0.007*	*0.755*	*1288*	*24*	*940*	*40*	*1946*	*62*	*-107.0*
399-MS-05-009	*2.61*	*0.15*	*0.1541*	*0.007*	*0.765*	*1298*	*42*	*923*	*40*	*1984*	*64*	*-115.0*
403-MS-05-013	*2.318*	*0.042*	*0.1464*	*0.003*	*0.646*	*1223*	*12*	*880*	*18*	*1878*	*32*	*-113.4*
404-MS-05-014	*3.21*	*0.1*	*0.1971*	*0.007*	*0.701*	*1462*	*26*	*1159*	*38*	*1923*	*48*	*-65.9*
405-MS-05-015	*1.27*	*0.054*	*0.0842*	*0.005*	*0.884*	*835*	*23*	*521*	*27*	*1817*	*45*	*-248.8*
412-MS-05-016	*3.247*	*0.082*	*0.2147*	*0.005*	*0.59*	*1469*	*19*	*1257*	*27*	*1825*	*32*	*-45.2*
414-MS-05-018	*3.206*	*0.061*	*0.2145*	*0.003*	*0.614*	*1459*	*14*	*1252*	*17*	*1753*	*30*	*-40.0*
417-MS-05-021	*1.951*	*0.05*	*0.1337*	*0.003*	*0.539*	*1100*	*17*	*808*	*16*	*1723*	*39*	*-113.2*
418-MS-05-022	*2.217*	*0.061*	*0.1438*	*0.004*	*0.568*	*1184*	*19*	*866*	*23*	*1815*	*39*	*-109.6*
420-MS-05-024	*2.34*	*0.11*	*0.1591*	*0.007*	*0.82*	*1221*	*34*	*960*	*43*	*1739*	*43*	*-81.1*
421-MS-05-025	*2.89*	*0.093*	*0.1644*	*0.004*	*0.693*	*1381*	*23*	*981*	*23*	*2040*	*42*	*-108.0*
424-MS-05-028	*2.164*	*0.074*	*0.1407*	*0.005*	*0.845*	*1166*	*24*	*848*	*26*	*1804*	*34*	*-112.7*
425-MS-05-029	*2.233*	*0.072*	*0.1351*	*0.006*	*0.633*	*1190*	*23*	*816*	*32*	*1919*	*59*	*-135.2*
426-MS-05-030	*2.156*	*0.072*	*0.1441*	*0.005*	*0.658*	*1164*	*23*	*867*	*26*	*1811*	*45*	*-108.9*
433-MS-05-031	*3.583*	*0.07*	*0.2199*	*0.005*	*0.596*	*1546*	*16*	*1284*	*24*	*1914*	*31*	*-49.1*
434-MS-05-032	*1.705*	*0.044*	*0.113*	*0.003*	*0.741*	*1008*	*16*	*690*	*16*	*1809*	*33*	*-162.2*
435-MS-05-033	*2.285*	*0.053*	*0.1317*	*0.003*	*0.752*	*1207*	*17*	*799*	*19*	*2028*	*30*	*-153.8*
437-MS-05-035	*2.144*	*0.067*	*0.0993*	*0.003*	*0.806*	*1168*	*22*	*613*	*19*	*2437*	*35*	*-297.6*
438-MS-05-036	*2.43*	*0.11*	*0.1503*	*0.005*	*0.881*	*1258*	*32*	*902*	*30*	*1937*	*36*	*-114.7*
439-MS-05-037	*2.17*	*0.13*	*0.1459*	*0.008*	*0.871*	*1164*	*42*	*885*	*44*	*1754*	*50*	*-98.2*
440-MS-05-038	*3.703*	*0.092*	*0.2463*	*0.005*	*0.69*	*1568*	*20*	*1418*	*26*	*1776*	*28*	*-25.2*
444-MS-05-042	*1.355*	*0.064*	*0.0788*	*0.004*	*0.937*	*865*	*27*	*488*	*23*	*2019*	*34*	*-313.7*
445-MS-05-043	*1.57*	*0.032*	*0.1031*	*0.002*	*0.746*	*957*	*13*	*632*	*14*	*1780*	*28*	*-181.6*
447-MS-05-045	*2.393*	*0.071*	*0.1354*	*0.004*	*0.846*	*1236*	*21*	*818*	*20*	*2073*	*29*	*-153.4*
454-MS-05-046	*0.767*	*0.022*	*0.0477*	*0.001*	*0.767*	*578*	*12*	*300.4*	*8.1*	*1902*	*36*	*-533.2*
456-MS-05-048	*1.431*	*0.03*	*0.0961*	*0.002*	*0.746*	*901*	*13*	*591*	*14*	*1763*	*30*	*-198.3*
457-MS-05-049	*2.834*	*0.089*	*0.1637*	*0.005*	*0.77*	*1362*	*24*	*982*	*30*	*2030*	*41*	*-106.7*
458-MS-05-050	*2.081*	*0.063*	*0.1381*	*0.005*	*0.78*	*1140*	*21*	*833*	*28*	*1778*	*38*	*-113.4*
459-MS-05-051	*5.46*	*0.35*	*0.276*	*0.017*	*0.925*	*1894*	*59*	*1566*	*87*	*2298*	*45*	*-46.7*

Table 1 Detrital zircon U–Pb analytical data.

461-MS-05-053	*3.84*	*0.11*	*0.234*	*0.007*	*0.758*	*1599*	*24*	*1354*	*37*	*1923*	*38*	*-42.0*
462-MS-05-054	*3.284*	*0.09*	*0.1627*	*0.005*	*0.841*	*1474*	*21*	*971*	*27*	*2310*	*27*	*-137.9*
463-MS-05-055	*2.123*	*0.068*	*0.1467*	*0.004*	*0.784*	*1162*	*21*	*881*	*24*	*1705*	*35*	*-93.5*
466-MS-05-058	*4.03*	*0.11*	*0.2471*	*0.006*	*0.755*	*1650*	*23*	*1422*	*32*	*1931*	*32*	*-35.8*
467-MS-05-059	*3.76*	*0.13*	*0.2162*	*0.008*	*0.796*	*1580*	*27*	*1260*	*42*	*2062*	*40*	*-63.7*
468-MS-05-060	*2.141*	*0.083*	*0.1425*	*0.005*	*0.888*	*1156*	*26*	*858*	*27*	*1791*	*32*	*-108.7*
475-MS-05-061	*3.17*	*0.22*	*0.139*	*0.01*	*0.955*	*1452*	*52*	*837*	*59*	*2522*	*36*	*-201.3*
476-MS-05-062	*1.643*	*0.036*	*0.1135*	*0.002*	*0.684*	*987*	*14*	*693*	*14*	*1721*	*31*	*-148.3*
477-MS-05-063	*3.31*	*0.11*	*0.2191*	*0.007*	*0.624*	*1484*	*26*	*1276*	*38*	*1766*	*52*	*-38.4*
479-MS-05-065	*1.694*	*0.067*	*0.1175*	*0.004*	*0.888*	*1000*	*25*	*715*	*23*	*1708*	*38*	*-138.9*
480-MS-05-066	*2.381*	*0.061*	*0.1444*	*0.004*	*0.758*	*1234*	*18*	*872*	*21*	*1930*	*34*	*-121.3*
481-MS-05-067	*2.99*	*0.073*	*0.1977*	*0.005*	*0.769*	*1404*	*19*	*1162*	*26*	*1803*	*33*	*-55.2*
482-MS-05-068	*1.577*	*0.041*	*0.1045*	*0.004*	*0.749*	*960*	*16*	*643*	*23*	*1780*	*40*	*-176.8*
484-MS-05-070	*3.37*	*0.12*	*0.164*	*0.007*	*0.891*	*1497*	*27*	*978*	*36*	*2346*	*32*	*-139.9*
485-MS-05-071	*1.843*	*0.058*	*0.119*	*0.003*	*0.847*	*1062*	*22*	*724*	*20*	*1824*	*30*	*-151.9*
487-MS-05-073	*2.63*	*0.092*	*0.1704*	*0.007*	*0.846*	*1312*	*27*	*1017*	*37*	*1836*	*36*	*-80.5*
489-MS-05-075	*9.12*	*0.2*	*0.3912*	*0.008*	*0.666*	*2351*	*21*	*2127*	*36*	*2548*	*27*	*-19.8*
496-MS-05-076	*2.469*	*0.07*	*0.1686*	*0.004*	*0.521*	*1260*	*20*	*1004*	*20*	*1732*	*48*	*-72.5*
497-MS-05-077	*2.246*	*0.084*	*0.132*	*0.004*	*0.787*	*1191*	*26*	*799*	*24*	*2004*	*43*	*-150.8*
499-MS-05-079	*3.96*	*0.13*	*0.2543*	*0.009*	*0.629*	*1625*	*26*	*1460*	*44*	*1860*	*57*	*-27.4*
502-MS-05-082	*3.55*	*0.11*	*0.1738*	*0.006*	*0.837*	*1534*	*25*	*1032*	*35*	*2350*	*37*	*-127.7*
503-MS-05-083	*2.062*	*0.077*	*0.1332*	*0.006*	*0.809*	*1133*	*26*	*806*	*31*	*1817*	*45*	*-125.4*
505-MS-05-085	*4.48*	*0.2*	*0.2304*	*0.009*	*0.881*	*1731*	*35*	*1335*	*49*	*2220*	*35*	*-66.3*
508-MS-05-088	*2.247*	*0.064*	*0.1467*	*0.004*	*0.821*	*1192*	*20*	*882*	*22*	*1824*	*29*	*-106.8*
510-MS-05-090	*2.345*	*0.092*	*0.1438*	*0.006*	*0.781*	*1222*	*29*	*865*	*34*	*1924*	*43*	*-122.4*
517-MS-05-091	*2.217*	*0.068*	*0.1418*	*0.006*	*0.666*	*1184*	*22*	*854*	*32*	*1850*	*50*	*-116.6*
518-MS-05-092	*2.242*	*0.061*	*0.1343*	*0.004*	*0.752*	*1196*	*18*	*812*	*20*	*1974*	*31*	*-143.1*
519-MS-05-093	*2.105*	*0.064*	*0.1387*	*0.003*	*0.629*	*1148*	*21*	*837*	*19*	*1793*	*48*	*-114.2*
520-MS-05-094	*1.554*	*0.07*	*0.0925*	*0.004*	*0.838*	*948*	*27*	*570*	*23*	*2002*	*41*	*-251.2*
524-MS-05-098	*2.092*	*0.044*	*0.1348*	*0.003*	*0.674*	*1144*	*14*	*815*	*15*	*1819*	*32*	*-123.2*
526-MS-05-100	*1.98*	*0.11*	*0.1191*	*0.003*	*0.382*	*1112*	*36*	*725*	*15*	*1979*	*83*	*-173.0*
MS-06												
609-MS-06-008	7.46	0.14	0.3958	0.006	0.583	2168	17	2149	30	2176	28	-1.3
613-MS-06-012	5.05	0.2	0.315	0.011	0.704	1825	34	1783	52	1947	52	-9.2
616-MS-06-015	8.97	0.15	0.4269	0.008	0.53	2333	15	2290	35	2354	27	-2.8
626-MS-06-019	4.87	0.17	0.3136	0.008	0.781	1799	30	1757	40	1826	49	-3.9
627-MS-06-020	10.93	0.25	0.4755	0.008	0.539	2521	21	2506	34	2503	34	0.1
629-MS-06-022	4.86	0.11	0.3183	0.006	0.414	1798	19	1785	28	1817	39	-1.8
633-MS-06-026	4.78	0.092	0.3133	0.006	0.511	1783	15	1759	28	1806	34	-2.7
634-MS-06-027	5.55	0.21	0.333	0.012	0.29	1910	35	1862	60	1952	80	-4.8
635-MS-06-028	5.45	0.16	0.3352	0.007	0.228	1890	24	1862	35	1937	60	-4.0
636-MS-06-029	4.65	0.2	0.301	0.011	0.761	1753	38	1696	55	1822	56	-7.4
672-MS-06-053	4.79	0.12	0.303	0.008	0.707	1781	22	1712	40	1823	47	-6.5

Table 1 Detrital zircon U–Pb analytical data.

674-MS-06-055	4.424	0.099	0.2979	0.006	0.43	1714	19	1730	28	1830	39	-5.8
677-MS-06-058	4.96	0.14	0.3257	0.008	0.655	1808	24	1816	40	1772	41	2.4
688-MS-06-063	6.57	0.2	0.3748	0.009	0.602	2056	26	2050	44	2064	41	-0.7
691-MS-06-066	5	0.14	0.3258	0.005	0.166	1817	24	1820	24	1803	51	0.9
696-MS-06-071	4.58	0.11	0.3028	0.007	0.547	1742	20	1704	32	1802	36	-5.8
700-MS-06-075	7.69	0.2	0.406	0.01	0.803	2190	23	2192	46	2168	29	1.1
769-MS-06-078	4.39	0.16	0.2903	0.009	0.778	1709	31	1721	47	1886	42	-9.6
770-MS-06-079	4.67	0.16	0.305	0.01	0.627	1761	28	1713	50	1832	45	-6.9
772-MS-06-081	4.59	0.12	0.3114	0.006	0.459	1749	22	1746	31	1728	47	1.0
777-MS-06-086	4.87	0.16	0.3179	0.008	0.415	1799	27	1777	40	1805	56	-1.6
780-MS-06-089	4.31	0.1	0.2866	0.007	0.571	1693	19	1630	34	1749	44	-7.3
789-MS-06-091	6.13	0.18	0.3646	0.008	0.411	1991	27	2002	38	1975	55	1.3
806-MS-06-108	4.704	0.089	0.3213	0.007	0.484	1768	16	1795	32	1711	37	4.7
821-MS-06-116	5.04	0.13	0.3306	0.006	0.509	1824	21	1840	30	1804	42	2.0
822-MS-06-117	5.22	0.14	0.3342	0.008	0.419	1854	23	1862	35	1810	50	2.8
825-MS-06-120	4.1	0.13	0.2943	0.008	0.424	1659	23	1662	38	1628	53	2.0
840-MS-06-128	5.15	0.2	0.3237	0.007	0.565	1835	32	1807	32	1850	53	-2.4
842-MS-06-130	4.95	0.15	0.3127	0.008	0.511	1808	25	1756	37	1879	49	-7.0
844-MS-06-132	4.21	0.17	0.2878	0.009	0.329	1673	33	1729	48	1893	77	-9.5
847-MS-06-135	7.77	0.2	0.4051	0.01	0.601	2199	23	2190	45	2205	46	-0.7
850-MS-06-138	4.77	0.13	0.305	0.009	0.435	1776	22	1734	40	1832	53	-5.7
851-MS-06-139	5.29	0.12	0.3328	0.008	0.527	1863	19	1850	37	1851	40	-0.1
852-MS-06-140	4.09	0.15	0.2785	0.008	0.606	1657	32	1682	40	1843	64	-9.6
860-MS-06-141	10.85	0.26	0.4766	0.009	0.507	2508	23	2515	42	2517	36	-0.1
862-MS-06-143	4.12	0.11	0.275	0.006	0.51	1658	21	1729	29	1830	43	-5.8
865-MS-06-146	4.89	0.18	0.322	0.01	0.739	1806	34	1796	51	1852	63	-3.1
867-MS-06-148	5	0.16	0.326	0.011	0.833	1813	27	1816	55	1810	39	0.3
868-MS-06-149	5.5	0.17	0.3396	0.008	0.599	1897	27	1882	38	1895	48	-0.7
869-MS-06-150	3.76	0.18	0.267	0.011	0.812	1588	39	1671	55	1786	76	-6.9
871-MS-06-152	7.5	0.41	0.397	0.023	0.584	2169	48	2150	110	2190	100	-1.9
					Rejected analysis							
602-MS-06-001	*1.785*	*0.05*	*0.1154*	*0.003*	*0.512*	*1042*	*19*	*704*	*18*	*1806*	*55*	*-156.5*
603-MS-06-002	*3.734*	*0.089*	*0.1872*	*0.004*	*0.256*	*1577*	*19*	*1106*	*22*	*2299*	*47*	*-107.9*
604-MS-06-003	*5.36*	*0.26*	*0.2357*	*0.01*	*0.938*	*1875*	*43*	*1363*	*52*	*2485*	*50*	*-82.3*
605-MS-06-004	*2.207*	*0.071*	*0.1277*	*0.004*	*0.738*	*1182*	*23*	*774*	*25*	*1987*	*44*	*-156.7*
606-MS-06-005	*5.04*	*0.13*	*0.2874*	*0.006*	*0.632*	*1831*	*24*	*1636*	*34*	*2027*	*34*	*-23.9*
607-MS-06-006	*1.773*	*0.056*	*0.1077*	*0.004*	*0.676*	*1039*	*23*	*659*	*25*	*1958*	*62*	*-197.1*
608-MS-06-007	*8.53*	*0.2*	*0.3797*	*0.007*	*0.312*	*2287*	*21*	*2074*	*32*	*2442*	*40*	*-17.7*
610-MS-06-009	*3.89*	*0.19*	*0.2466*	*0.01*	*0.726*	*1614*	*42*	*1420*	*51*	*1840*	*68*	*-29.6*
611-MS-06-010	*1.485*	*0.065*	*0.0745*	*0.003*	*0.605*	*928*	*25*	*463*	*18*	*2264*	*61*	*-389.0*
612-MS-06-011	*2.258*	*0.072*	*0.1311*	*0.003*	*0.085*	*1197*	*23*	*794*	*19*	*2002*	*59*	*-152.1*
614-MS-06-013	*1.933*	*0.036*	*0.1167*	*0.002*	*0.485*	*1095*	*13*	*711*	*14*	*1930*	*31*	*-171.4*
615-MS-06-014	*2.082*	*0.051*	*0.1147*	*0.002*	*0.6*	*1141*	*17*	*700*	*13*	*2150*	*36*	*-207.1*
623-MS-06-016	*2.399*	*0.092*	*0.1496*	*0.004*	*0.427*	*1240*	*28*	*899*	*24*	*1942*	*47*	*-116.0*
624-MS-06-017	*2.796*	*0.068*	*0.1641*	*0.003*	*0.701*	*1354*	*18*	*979*	*18*	*1984*	*32*	*-102.7*

Table 1 Detrital zircon U–Pb analytical data.

625-MS-06-018	*1.596*	*0.035*	*0.0908*	*0.002*	*0.736*	*969*	*14*	*560*	*12*	*2077*	*30*	*-270.9*
628-MS-06-021	*3.45*	*0.13*	*0.2076*	*0.01*	*0.654*	*1524*	*34*	*1215*	*52*	*1944*	*83*	*-60.0*
630-MS-06-023	*1.881*	*0.044*	*0.1136*	*0.003*	*0.577*	*1073*	*16*	*693*	*17*	*1958*	*46*	*-182.5*
631-MS-06-024	*2.059*	*0.064*	*0.1293*	*0.003*	*0.706*	*1132*	*21*	*783*	*19*	*1887*	*38*	*-141.0*
637-MS-06-030	*1.649*	*0.029*	*0.1062*	*0.002*	*0.458*	*989*	*11*	*651*	*11*	*1825*	*34*	*-180.3*
644-MS-06-031	*3.58*	*0.18*	*0.215*	*0.011*	*0.938*	*1550*	*43*	*1252*	*60*	*1957*	*36*	*-56.3*
645-MS-06-032	*1.59*	*0.068*	*0.0928*	*0.004*	*0.834*	*963*	*27*	*571*	*25*	*1987*	*41*	*-248.0*
646-MS-06-033	*3.28*	*0.12*	*0.2049*	*0.007*	*0.689*	*1472*	*30*	*1200*	*39*	*1867*	*54*	*-55.6*
647-MS-06-034	*3.127*	*0.087*	*0.2*	*0.007*	*0.359*	*1438*	*22*	*1175*	*35*	*1915*	*58*	*-63.0*
648-MS-06-035	*3.84*	*0.19*	*0.243*	*0.012*	*0.727*	*1597*	*39*	*1402*	*62*	*1853*	*68*	*-32.2*
649-MS-06-036	*1.699*	*0.039*	*0.0961*	*0.002*	*0.695*	*1008*	*14*	*591*	*11*	*2066*	*29*	*-249.6*
650-MS-06-037	*2.53*	*0.11*	*0.1627*	*0.009*	*0.143*	*1279*	*32*	*971*	*51*	*1868*	*94*	*-92.4*
652-MS-06-039	*2.135*	*0.077*	*0.1311*	*0.006*	*0.63*	*1158*	*25*	*793*	*31*	*1921*	*52*	*-142.2*
653-MS-06-040	*3.448*	*0.077*	*0.2289*	*0.004*	*0.392*	*1514*	*18*	*1328*	*19*	*1807*	*43*	*-36.1*
654-MS-06-041	*2.521*	*0.07*	*0.145*	*0.004*	*0.599*	*1277*	*20*	*873*	*23*	*2010*	*43*	*-130.2*
655-MS-06-042	*5.18*	*0.21*	*0.2512*	*0.007*	*0.253*	*1847*	*34*	*1444*	*37*	*2358*	*62*	*-63.3*
656-MS-06-043	*1.667*	*0.039*	*0.0977*	*0.002*	*0.788*	*994*	*15*	*601*	*14*	*1998*	*30*	*-232.4*
657-MS-06-044	*2.257*	*0.077*	*0.137*	*0.004*	*0.716*	*1201*	*25*	*827*	*22*	*1948*	*40*	*-135.6*
658-MS-06-045	*1.51*	*0.037*	*0.084*	*0.002*	*0.647*	*933*	*15*	*520*	*13*	*2064*	*37*	*-296.9*
665-MS-06-046	*1.145*	*0.046*	*0.0577*	*0.002*	*0.896*	*770*	*21*	*361*	*13*	*2261*	*30*	*-526.3*
666-MS-06-047	*4.41*	*0.11*	*0.2379*	*0.006*	*0.591*	*1717*	*21*	*1375*	*32*	*2208*	*37*	*-60.6*
667-MS-06-048	*4.26*	*0.2*	*0.249*	*0.014*	*0.812*	*1683*	*38*	*1430*	*74*	*1970*	*59*	*-37.8*
668-MS-06-049	*2.96*	*0.081*	*0.1794*	*0.005*	*0.744*	*1400*	*23*	*1063*	*27*	*1955*	*49*	*-83.9*
669-MS-06-050	*2.7*	*0.11*	*0.1452*	*0.005*	*0.653*	*1324*	*29*	*874*	*27*	*2149*	*51*	*-145.9*
670-MS-06-051	*4.06*	*0.14*	*0.2351*	*0.007*	*0.542*	*1649*	*26*	*1361*	*34*	*2052*	*44*	*-50.8*
671-MS-06-052	*1.53*	*0.11*	*0.1032*	*0.009*	*0.924*	*938*	*44*	*632*	*50*	*1735*	*60*	*-174.5*
673-MS-06-054	*2.879*	*0.085*	*0.125*	*0.004*	*0.776*	*1374*	*22*	*759*	*22*	*2496*	*36*	*-228.9*
675-MS-06-056	*3.014*	*0.08*	*0.1419*	*0.004*	*0.84*	*1409*	*20*	*855*	*20*	*2303*	*33*	*-169.4*
676-MS-06-057	*1.794*	*0.055*	*0.1011*	*0.003*	*0.734*	*1040*	*20*	*621*	*15*	*2005*	*37*	*-222.9*
678-MS-06-059	*5.23*	*0.16*	*0.2961*	*0.007*	*0.556*	*1853*	*26*	*1677*	*33*	*2067*	*45*	*-23.3*
679-MS-06-060	*2.78*	*0.13*	*0.1386*	*0.006*	*0.929*	*1357*	*34*	*836*	*34*	*2278*	*29*	*-172.5*
686-MS-06-061	*0.3447*	*0.009*	*0.01526*	*5E-04*	*0.738*	*300.2*	*7*	*97.6*	*3.1*	*2526*	*35*	*-2488.1*
687-MS-06-062	*2.416*	*0.068*	*0.1407*	*0.004*	*0.655*	*1249*	*19*	*848*	*24*	*1982*	*41*	*-133.7*
689-MS-06-064	*2.31*	*0.16*	*0.141*	*0.011*	*0.851*	*1209*	*49*	*850*	*61*	*1841*	*78*	*-116.6*
690-MS-06-065	*3.081*	*0.075*	*0.1849*	*0.005*	*0.712*	*1427*	*18*	*1096*	*24*	*1941*	*33*	*-77.1*
692-MS-06-067	*2.233*	*0.057*	*0.1357*	*0.004*	*0.723*	*1196*	*18*	*819*	*20*	*1950*	*33*	*-138.1*
693-MS-06-068	*3.92*	*0.11*	*0.2298*	*0.006*	*0.857*	*1613*	*22*	*1336*	*31*	*1987*	*25*	*-48.7*
694-MS-06-069	*1.765*	*0.087*	*0.1062*	*0.004*	*0.837*	*1036*	*30*	*650*	*22*	*1941*	*42*	*-198.6*
695-MS-06-070	*3.48*	*0.44*	*0.216*	*0.024*	*0.874*	*1500*	*100*	*1250*	*130*	*1850*	*110*	*-48.0*
698-MS-06-073	*1.823*	*0.056*	*0.106*	*0.003*	*0.759*	*1050*	*20*	*649*	*16*	*2006*	*35*	*-209.1*
699-MS-06-074	*7.46*	*0.24*	*0.345*	*0.011*	*0.602*	*2171*	*27*	*1908*	*53*	*2400*	*47*	*-25.8*
767-MS-06-076	*1.182*	*0.051*	*0.0684*	*0.003*	*0.921*	*792*	*25*	*429*	*19*	*2002*	*28*	*-366.7*
768-MS-06-077	*3.25*	*0.14*	*0.222*	*0.007*	*0.723*	*1466*	*33*	*1292*	*37*	*1769*	*51*	*-36.9*
771-MS-06-080	*2.24*	*0.12*	*0.1348*	*0.008*	*0.847*	*1198*	*34*	*814*	*46*	*1985*	*56*	*-143.9*
773-MS-06-082	*2.96*	*0.12*	*0.1305*	*0.004*	*0.459*	*1390*	*31*	*790*	*24*	*2530*	*66*	*-220.3*

Table 1 Detrital zircon U–Pb analytical data.

774-MS-06-083	*3.11*	*0.11*	*0.1715*	*0.005*	*0.581*	*1432*	*28*	*1020*	*27*	*2119*	*48*	*-107.7*
775-MS-06-084	*7.18*	*0.23*	*0.321*	*0.011*	*0.391*	*2131*	*29*	*1793*	*55*	*2394*	*64*	*-33.5*
776-MS-06-085	*2.036*	*0.038*	*0.108*	*0.002*	*0.711*	*1126*	*13*	*661*	*14*	*2192*	*28*	*-231.6*
778-MS-06-087	*2.721*	*0.061*	*0.1649*	*0.004*	*0.693*	*1332*	*17*	*983*	*21*	*1973*	*29*	*-100.7*
779-MS-06-088	*1.03*	*0.027*	*0.0662*	*0.002*	*0.862*	*717*	*14*	*413*	*13*	*1834*	*30*	*-344.1*
781-MS-06-090	*3.005*	*0.076*	*0.1874*	*0.005*	*0.689*	*1408*	*20*	*1113*	*25*	*1874*	*34*	*-68.4*
790-MS-06-092	*5.65*	*0.23*	*0.296*	*0.012*	*0.688*	*1924*	*35*	*1667*	*58*	*2147*	*58*	*-28.8*
791-MS-06-093	*1.538*	*0.063*	*0.0936*	*0.004*	*0.883*	*947*	*26*	*576*	*24*	*1931*	*31*	*-235.2*
792-MS-06-094	*2.259*	*0.05*	*0.1365*	*0.003*	*0.632*	*1197*	*16*	*824*	*15*	*1920*	*34*	*-133.0*
793-MS-06-095	*1.139*	*0.022*	*0.0693*	*0.002*	*0.676*	*771*	*11*	*432*	*11*	*1934*	*32*	*-347.7*
794-MS-06-096	*2.007*	*0.054*	*0.1229*	*0.004*	*0.642*	*1116*	*18*	*747*	*23*	*1908*	*42*	*-155.4*
795-MS-06-097	*2.617*	*0.09*	*0.1609*	*0.007*	*0.738*	*1309*	*27*	*961*	*39*	*1946*	*47*	*-102.5*
796-MS-06-098	*1.402*	*0.047*	*0.0999*	*0.004*	*0.848*	*889*	*20*	*614*	*24*	*1699*	*41*	*-176.7*
797-MS-06-099	*1.714*	*0.074*	*0.1076*	*0.004*	*0.218*	*1012*	*28*	*659*	*23*	*1914*	*91*	*-190.4*
798-MS-06-100	*3.27*	*0.12*	*0.1925*	*0.006*	*0.812*	*1473*	*30*	*1134*	*35*	*1982*	*39*	*-74.8*
799-MS-06-101	*2.65*	*0.079*	*0.1568*	*0.004*	*0.627*	*1316*	*23*	*938*	*21*	*2025*	*43*	*-115.9*
800-MS-06-102	*1.807*	*0.041*	*0.113*	*0.003*	*0.784*	*1048*	*15*	*690*	*16*	*1890*	*31*	*-173.9*
801-MS-06-103	*2.29*	*0.11*	*0.1266*	*0.009*	*0.592*	*1206*	*33*	*768*	*49*	*2050*	*100*	*-166.9*
802-MS-06-104	*3.156*	*0.092*	*0.1842*	*0.006*	*0.831*	*1453*	*22*	*1089*	*30*	*1974*	*31*	*-81.3*
803-MS-06-105	*2.543*	*0.086*	*0.1647*	*0.006*	*0.638*	*1286*	*26*	*982*	*32*	*1795*	*53*	*-82.8*
804-MS-06-106	*2.912*	*0.069*	*0.1573*	*0.005*	*0.721*	*1383*	*18*	*941*	*28*	*2126*	*31*	*-125.9*
805-MS-06-107	*2.959*	*0.095*	*0.189*	*0.005*	*0.772*	*1396*	*24*	*1115*	*29*	*1826*	*37*	*-63.8*
807-MS-06-109	*2.083*	*0.068*	*0.12*	*0.004*	*0.694*	*1142*	*23*	*730*	*23*	*2016*	*45*	*-176.2*
808-MS-06-110	*1.594*	*0.04*	*0.0991*	*0.002*	*0.608*	*966*	*16*	*611*	*13*	*1894*	*37*	*-210.0*
MS-09												
873-MS-09-002	4.8	0.16	0.3194	0.01	0.345	1792	23	1786	48	1819	69	-1.8
882-MS-09-004	4.76	0.11	0.3113	0.005	0.565	1777	19	1746	23	1807	36	-3.5
884-MS-09-006	4.89	0.12	0.3067	0.007	0.665	1797	21	1723	33	1844	40	-7.0
888-MS-09-010	4.02	0.15	0.2752	0.009	0.547	1636	30	1695	47	1793	64	-5.8
890-MS-09-012	4.59	0.22	0.3049	0.01	0.779	1741	40	1714	47	1742	76	-1.6
891-MS-09-013	4.98	0.12	0.3265	0.006	0.573	1814	20	1820	27	1803	35	0.9
893-MS-09-015	5.2	0.12	0.3328	0.006	0.43	1850	19	1851	30	1873	42	-1.2
904-MS-09-019	4.7	0.15	0.3037	0.008	0.338	1764	26	1717	41	1856	59	-8.1
906-MS-09-021	4.51	0.14	0.2922	0.005	0.499	1731	27	1746	25	1925	48	-10.3
907-MS-09-022	5.96	0.13	0.3405	0.006	0.312	1978	21	1888	30	2041	45	-8.1
908-MS-09-023	5.84	0.29	0.342	0.013	0.602	1947	43	1892	65	1968	62	-4.0
910-MS-09-025	7.65	0.21	0.3962	0.009	0.337	2188	25	2154	42	2199	51	-2.1
914-MS-09-029	10.81	0.29	0.464	0.011	0.643	2515	24	2457	50	2559	32	-4.2
915-MS-09-030	4.93	0.14	0.3177	0.006	0.616	1809	23	1778	31	1851	43	-4.1
928-MS-09-036	10.28	0.23	0.453	0.01	0.644	2463	21	2404	46	2507	32	-4.3
931-MS-09-039	5.91	0.14	0.3481	0.007	0.438	1962	21	1928	36	1976	41	-2.5
932-MS-09-040	4.74	0.15	0.3039	0.008	0.72	1771	26	1717	43	1834	39	-6.8
934-MS-09-042	5.1	0.14	0.3137	0.008	0.539	1834	24	1758	41	1916	47	-9.0
935-MS-09-043	10.49	0.29	0.4701	0.01	0.629	2494	26	2482	43	2491	35	-0.4

Table 1 Detrital zircon U–Pb analytical data.

936-MS-09-044	7.42	0.16	0.3991	0.006	0.48	2160	19	2168	28	2176	35	-0.4
939-MS-09-047	5.12	0.16	0.3225	0.007	0.445	1834	26	1800	36	1846	55	-2.6
948-MS-09-049	4.98	0.14	0.326	0.008	0.489	1820	26	1817	41	1834	52	-0.9
951-MS-09-052	5.39	0.14	0.328	0.007	0.526	1879	22	1827	33	1918	42	-5.0
956-MS-09-057	5.02	0.19	0.3248	0.009	0.147	1826	33	1810	46	1818	78	-0.4
957-MS-09-058	4.77	0.13	0.3086	0.006	0.554	1775	22	1783	28	1910	40	-7.1
958-MS-09-059	5.84	0.19	0.346	0.014	0.4	1958	27	1916	67	1988	79	-3.8
959-MS-09-060	9.68	0.22	0.432	0.01	0.506	2403	21	2369	47	2524	37	-6.5
962-MS-09-063	5.25	0.14	0.3323	0.007	0.351	1860	22	1853	33	1862	48	-0.5
971-MS-09-065	4.31	0.14	0.2897	0.008	0.629	1692	28	1719	38	1888	51	-9.8
973-MS-09-067	5.58	0.14	0.3402	0.007	0.599	1908	22	1890	34	1918	34	-1.5
978-MS-09-072	6.34	0.16	0.3608	0.008	0.538	2024	23	1984	39	2050	43	-3.3
979-MS-09-073	5	0.13	0.3247	0.007	0.617	1819	22	1811	33	1838	39	-1.5
983-MS-09-077	4.46	0.1	0.2927	0.007	0.605	1721	19	1723	33	1888	35	-9.6
992-MS-09-079	5.01	0.12	0.3221	0.006	0.677	1828	20	1799	30	1835	34	-2.0
996-MS-09-083	5.16	0.19	0.3249	0.009	0.494	1837	31	1817	44	1861	63	-2.4
997-MS-09-084	4.8	0.16	0.3038	0.01	0.73	1780	27	1758	48	1877	45	-6.8
1000-MS-09-087	6.06	0.23	0.3472	0.01	0.287	1975	34	1931	45	2012	76	-4.2
1001-MS-09-088	4.89	0.22	0.31	0.011	0.562	1801	39	1739	56	1898	67	-9.1
1002-MS-09-089	5.36	0.13	0.3205	0.007	0.447	1874	21	1791	32	1936	46	-8.1
1014-MS-09-094	6.47	0.2	0.3549	0.009	0.79	2042	29	2016	44	2173	39	-7.8
1015-MS-09-095	5.9	0.25	0.352	0.018	0.704	1957	37	1938	85	1941	52	-0.2
1022-MS-09-102	5.39	0.12	0.3416	0.009	0.51	1883	19	1897	46	1879	51	0.9
1023-MS-09-103	7.73	0.15	0.4115	0.009	0.632	2202	17	2219	41	2184	31	1.6
1026-MS-09-106	9.77	0.39	0.43	0.018	0.778	2409	37	2303	81	2488	45	-8.0
					Rejected analysis							
872-MS-09-001	*2.433*	*0.069*	*0.1272*	*0.003*	*0.434*	*1251*	*20*	*772*	*16*	*2228*	*46*	*-188.6*
874-MS-09-003	*2.23*	*0.1*	*0.1237*	*0.006*	*0.843*	*1187*	*32*	*751*	*36*	*2106*	*49*	*-180.4*
883-MS-09-005	*1.971*	*0.054*	*0.111*	*0.003*	*0.534*	*1107*	*18*	*679*	*20*	*2053*	*48*	*-202.4*
885-MS-09-007	*1.526*	*0.031*	*0.0854*	*0.002*	*0.714*	*941*	*12*	*528*	*12*	*2074*	*29*	*-292.8*
886-MS-09-008	*2.799*	*0.09*	*0.1541*	*0.005*	*0.556*	*1357*	*25*	*924*	*27*	*2148*	*47*	*-132.5*
887-MS-09-009	*4.36*	*0.18*	*0.226*	*0.01*	*0.604*	*1701*	*35*	*1312*	*54*	*2153*	*59*	*-64.1*
889-MS-09-011	*2.152*	*0.042*	*0.1326*	*0.003*	*0.641*	*1169*	*14*	*802*	*18*	*1913*	*30*	*-138.5*
894-MS-09-016	*1.007*	*0.028*	*0.0463*	*0.001*	*0.808*	*706*	*14*	*291.6*	*8.7*	*2420*	*31*	*-729.9*
895-MS-09-017	*1.51*	*0.027*	*0.0964*	*0.002*	*0.647*	*933*	*11*	*594*	*11*	*1837*	*26*	*-209.3*
896-MS-09-018	*1.892*	*0.051*	*0.1091*	*0.003*	*0.639*	*1079*	*18*	*667*	*18*	*2045*	*43*	*-206.6*
905-MS-09-020	*3.92*	*0.11*	*0.2336*	*0.004*	*0.522*	*1614*	*22*	*1353*	*22*	*1948*	*41*	*-44.0*
909-MS-09-024	*2.122*	*0.052*	*0.1144*	*0.004*	*0.729*	*1157*	*17*	*698*	*21*	*2140*	*35*	*-206.6*
911-MS-09-026	*2.306*	*0.051*	*0.1434*	*0.003*	*0.611*	*1214*	*16*	*865*	*15*	*1904*	*33*	*-120.1*
912-MS-09-027	*3.32*	*0.12*	*0.1894*	*0.007*	*0.798*	*1482*	*28*	*1117*	*38*	*2002*	*40*	*-79.2*
913-MS-09-028	*2.899*	*0.079*	*0.1714*	*0.006*	*0.712*	*1380*	*21*	*1019*	*32*	*1992*	*48*	*-95.5*
916-MS-09-031	*2.352*	*0.08*	*0.1292*	*0.005*	*0.659*	*1225*	*25*	*783*	*30*	*2074*	*52*	*-164.9*
917-MS-09-032	*1.501*	*0.055*	*0.0903*	*0.003*	*0.688*	*928*	*22*	*557*	*18*	*1947*	*43*	*-249.6*
918-MS-09-033	*1.702*	*0.046*	*0.0804*	*0.002*	*0.681*	*1006*	*17*	*498*	*11*	*2370*	*30*	*-375.9*
926-MS-09-034	*1.961*	*0.04*	*0.1066*	*0.002*	*0.701*	*1101*	*14*	*653*	*12*	*2130*	*27*	*-226.2*

Table 1 Detrital zircon U–Pb analytical data.

927-MS-09-035	*3.086*	*0.074*	*0.1674*	*0.004*	*0.656*	*1428*	*19*	*997*	*22*	*2197*	*40*	*-120.4*
929-MS-09-037	*2.73*	*0.063*	*0.1277*	*0.003*	*0.79*	*1336*	*17*	*774*	*18*	*2376*	*25*	*-207.0*
930-MS-09-038	*2.115*	*0.053*	*0.1152*	*0.004*	*0.658*	*1158*	*17*	*702*	*20*	*2116*	*43*	*-201.4*
933-MS-09-041	*1.996*	*0.041*	*0.109*	*0.002*	*0.48*	*1112*	*14*	*666*	*12*	*2111*	*35*	*-217.0*
937-MS-09-045	*1.402*	*0.032*	*0.0742*	*0.002*	*0.797*	*890*	*14*	*461*	*12*	*2222*	*27*	*-382.0*
938-MS-09-046	*3.035*	*0.069*	*0.1386*	*0.003*	*0.825*	*1414*	*17*	*838*	*19*	*2448*	*23*	*-192.1*
940-MS-09-048	*3.42*	*0.35*	*0.18*	*0.015*	*0.959*	*1491*	*79*	*1063*	*80*	*2093*	*58*	*-96.9*
949-MS-09-050	*3.7*	*0.13*	*0.241*	*0.013*	*0.688*	*1569*	*27*	*1388*	*69*	*1816*	*73*	*-30.8*
950-MS-09-051	*3.009*	*0.082*	*0.1823*	*0.006*	*0.547*	*1412*	*20*	*1079*	*31*	*1951*	*49*	*-80.8*
952-MS-09-053	*3.23*	*0.1*	*0.1989*	*0.007*	*0.695*	*1467*	*24*	*1168*	*36*	*1925*	*42*	*-64.8*
953-MS-09-054	*3.52*	*0.11*	*0.214*	*0.007*	*0.623*	*1528*	*24*	*1249*	*35*	*1862*	*47*	*-49.1*
954-MS-09-055	*1.481*	*0.03*	*0.0981*	*0.002*	*0.775*	*923*	*13*	*603*	*14*	*1797*	*30*	*-198.0*
955-MS-09-056	*2.312*	*0.084*	*0.13*	*0.003*	*0.492*	*1217*	*27*	*788*	*19*	*2120*	*48*	*-169.0*
960-MS-09-061	*1.914*	*0.051*	*0.0889*	*0.002*	*0.819*	*1085*	*17*	*549*	*14*	*2386*	*30*	*-334.6*
961-MS-09-062	*1.712*	*0.039*	*0.0896*	*0.002*	*0.771*	*1014*	*15*	*553*	*13*	*2196*	*29*	*-297.1*
970-MS-09-064	*3.563*	*0.091*	*0.2188*	*0.007*	*0.761*	*1538*	*20*	*1274*	*35*	*1912*	*39*	*-50.1*
972-MS-09-066	*1.746*	*0.051*	*0.0937*	*0.003*	*0.723*	*1027*	*20*	*577*	*19*	*2105*	*42*	*-264.8*
974-MS-09-068	*1.876*	*0.044*	*0.0997*	*0.003*	*0.577*	*1071*	*16*	*612*	*17*	*2133*	*40*	*-248.5*
975-MS-09-069	*2.98*	*0.13*	*0.1787*	*0.01*	*0.806*	*1400*	*33*	*1058*	*52*	*1934*	*64*	*-82.8*
976-MS-09-070	*2.623*	*0.058*	*0.1531*	*0.004*	*0.684*	*1305*	*16*	*918*	*23*	*1990*	*33*	*-116.8*
977-MS-09-071	*1.689*	*0.077*	*0.0958*	*0.005*	*0.872*	*1000*	*29*	*589*	*27*	*2050*	*41*	*-248.0*
980-MS-09-074	*2.271*	*0.044*	*0.1534*	*0.003*	*0.781*	*1203*	*13*	*920*	*18*	*1759*	*24*	*-91.2*
981-MS-09-075	*2.686*	*0.063*	*0.1523*	*0.004*	*0.701*	*1326*	*17*	*913*	*22*	*2042*	*33*	*-123.7*
984-MS-09-078	*1.899*	*0.038*	*0.1164*	*0.003*	*0.81*	*1079*	*13*	*709*	*20*	*1935*	*28*	*-172.9*
993-MS-09-080	*3.72*	*0.12*	*0.217*	*0.01*	*0.646*	*1574*	*27*	*1265*	*51*	*2019*	*54*	*-59.6*
994-MS-09-081	*1.978*	*0.046*	*0.1083*	*0.003*	*0.736*	*1106*	*16*	*662*	*15*	*2128*	*26*	*-221.5*
999-MS-09-086	*2.092*	*0.058*	*0.146*	*0.004*	*0.77*	*1143*	*19*	*878*	*24*	*1694*	*32*	*-92.9*
1003-MS-09-090	*1.997*	*0.055*	*0.1167*	*0.003*	*0.722*	*1112*	*19*	*711*	*17*	*2005*	*33*	*-182.0*
1004-MS-09-091	*4.5*	*0.31*	*0.274*	*0.018*	*0.721*	*1725*	*56*	*1557*	*92*	*1860*	*110*	*-19.5*
1005-MS-09-092	*4.27*	*0.17*	*0.266*	*0.015*	*0.599*	*1686*	*34*	*1517*	*75*	*1863*	*85*	*-22.8*
1006-MS-09-093	*1.823*	*0.038*	*0.1075*	*0.003*	*0.666*	*1052*	*14*	*658*	*15*	*1988*	*34*	*-202.1*
1017-MS-09-097	*2.821*	*0.073*	*0.1181*	*0.003*	*0.653*	*1359*	*19*	*719*	*19*	*2561*	*37*	*-256.2*
1018-MS-09-098	*2.397*	*0.087*	*0.13*	*0.005*	*0.83*	*1239*	*26*	*787*	*29*	*2147*	*44*	*-172.8*
1019-MS-09-099	*0.963*	*0.025*	*0.0572*	*0.002*	*0.806*	*683*	*13*	*358*	*10*	*1994*	*32*	*-457.0*
1020-MS-09-100	*1.911*	*0.04*	*0.1058*	*0.002*	*0.539*	*1085*	*14*	*651*	*12*	*2105*	*33*	*-223.3*
1021-MS-09-101	*2.026*	*0.049*	*0.1111*	*0.003*	*0.797*	*1122*	*17*	*679*	*17*	*2105*	*28*	*-210.0*
1024-MS-09-104	*5.23*	*0.1*	*0.2956*	*0.006*	*0.648*	*1856*	*17*	*1668*	*32*	*2065*	*29*	*-23.8*
1025-MS-09-105	*4.25*	*0.24*	*0.215*	*0.011*	*0.765*	*1678*	*46*	*1265*	*61*	*2274*	*67*	*-79.8*
1027-MS-09-107	*8.28*	*0.31*	*0.333*	*0.013*	*0.797*	*2257*	*34*	*1852*	*61*	*2652*	*42*	*-43.2*
D02												
D2N01	4.671	0.091	0.3008	0.005	0.454	1765	16	1696	26	1674	32	1.3
D2N03	11.3	0.22	0.4438	0.008	0.774	2545	19	2364	33	2507	22	-6.0
D2N04	4.86	0.13	0.2824	0.005	0.36	1794	22	1602	27	1739	47	-8.6
D2N05	5.66	0.11	0.3202	0.006	0.59	1928	17	1792	27	1816	30	-1.3

Table 1 Detrital zircon U–Pb analytical data.

D2N07	5.99	0.14	0.3188	0.006	0.497	1974	21	1832	30	1931	41	-5.4
D2N102	4.59	0.11	0.3115	0.006	0.498	1746	19	1747	31	1849	39	-5.8
D2N104	3.93	0.14	0.2773	0.007	0.438	1629	28	1624	36	1721	57	-6.0
D2N16	3.422	0.073	0.2469	0.004	0.38	1509	17	1421	22	1547	41	-8.9
D2N18	11.15	0.21	0.4421	0.007	0.648	2533	18	2358	33	2573	25	-9.1
D2N24	4.481	0.098	0.3061	0.006	0.578	1732	18	1725	29	1778	34	-3.1
D2N26	6.06	0.13	0.3519	0.007	0.604	1983	19	1942	33	2045	28	-5.3
D2N28	4.37	0.1	0.2992	0.006	0.613	1704	20	1689	29	1729	31	-2.4
D2N29	5.09	0.11	0.3166	0.006	0.416	1831	19	1822	29	1985	40	-8.9
D2N30	5.13	0.12	0.328	0.006	0.525	1843	20	1826	29	1885	35	-3.2
D2N31	5.86	0.12	0.3461	0.006	0.642	1953	18	1921	26	2075	23	-8.0
D2N32	5.08	0.1	0.3278	0.006	0.68	1831	17	1828	27	1853	25	-1.4
D2N33	3.72	0.14	0.2642	0.008	0.269	1582	27	1509	42	1638	80	-8.5
D2N34	5.21	0.11	0.3157	0.007	0.672	1857	18	1818	33	1993	29	-9.6
D2N35	5.4	0.1	0.3285	0.006	0.496	1884	16	1829	29	1897	31	-3.7
D2N36	3.989	0.088	0.2831	0.006	0.765	1628	18	1600	32	1748	31	-9.3
D2N38	4.6	0.1	0.2995	0.005	0.578	1749	19	1705	26	1837	37	-7.7
D2N39	5.12	0.12	0.3195	0.007	0.444	1837	20	1785	36	1829	42	-2.5
D2N41	5.18	0.2	0.322	0.013	0.637	1846	32	1834	67	1920	48	-4.7
D2N42	5.54	0.2	0.322	0.01	0.512	1904	32	1804	51	1866	68	-3.4
D2N44	5.01	0.11	0.2981	0.006	0.541	1816	20	1683	30	1821	38	-8.2
D2N50	5.04	0.1	0.3058	0.006	0.557	1821	17	1718	29	1819	33	-5.9
D2N51	7.39	0.14	0.3697	0.007	0.675	2159	16	2030	31	2159	27	-6.4
D2N54	5.31	0.11	0.3232	0.007	0.499	1866	18	1807	31	1841	37	-1.9
D2N55	3.186	0.074	0.246	0.005	0.484	1454	18	1499	26	1608	39	-7.3
D2N57	7.39	0.18	0.3884	0.008	0.465	2162	20	2113	36	2165	37	-2.5
D2N58	4.58	0.1	0.2871	0.005	0.649	1743	18	1699	25	1864	32	-9.7
D2N61	5.03	0.15	0.314	0.007	0.541	1822	25	1760	36	1781	46	-1.2
D2N63	4.439	0.084	0.2819	0.006	0.597	1720	16	1602	28	1731	33	-8.1
D2N64	5.27	0.13	0.3039	0.006	0.567	1863	20	1714	32	1822	37	-6.3
D2N66	10.71	0.3	0.42	0.011	0.586	2505	26	2270	45	2479	42	-9.2
D2N69	3.644	0.084	0.2442	0.004	0.426	1556	18	1411	22	1538	42	-9.0
D2N75	4.88	0.16	0.2981	0.007	0.302	1790	28	1684	32	1782	57	-5.8
D2N80	3.6	0.16	0.2508	0.008	0.17	1546	34	1439	41	1568	91	-9.0
D2N81	3.9	0.12	0.2767	0.008	0.637	1609	25	1579	40	1667	47	-5.6
D2N84	4.96	0.21	0.322	0.013	0.341	1807	37	1803	64	1939	87	-7.5
D2N87	4.028	0.081	0.2783	0.004	0.519	1641	16	1732	22	1891	31	-9.2
D2N88	4.65	0.11	0.3142	0.006	0.225	1757	21	1760	31	1881	51	-6.9
D2N89	4.08	0.21	0.2873	0.01	0.272	1650	42	1636	50	1783	93	-9.0
D2N90	13.68	0.28	0.4984	0.009	0.539	2732	19	2691	39	2946	28	-9.5
D2N91	4.929	0.086	0.3204	0.005	0.71	1804	15	1790	26	1923	22	-7.4
D2N92	4.82	0.16	0.334	0.01	0.723	1795	28	1863	45	1853	44	0.5
D2N95	4.024	0.092	0.279	0.005	0.751	1635	19	1735	25	1845	27	-6.3
D2N97	4.98	0.13	0.3259	0.006	0.457	1813	21	1817	30	1856	44	-2.1

Rejected analysis

Table 1 Detrital zircon U–Pb analytical data.

D2N02	*10.99*	*0.2*	*0.4207*	*0.007*	*0.803*	*2519*	*18*	*2264*	*32*	*2557*	*18*	*-12.9*
D2N06	*3.97*	*0.086*	*0.2164*	*0.004*	*0.433*	*1630*	*17*	*1262*	*22*	*1842*	*42*	*-46.0*
D2N08	*8.56*	*0.16*	*0.3404*	*0.007*	*0.413*	*2291*	*17*	*1887*	*32*	*2424*	*34*	*-28.5*
D2N09	*2.711*	*0.04*	*0.1493*	*0.002*	*0.577*	*1332*	*11*	*897*	*12*	*1891*	*22*	*-110.8*
D2N10	*6.78*	*0.16*	*0.2866*	*0.006*	*0.696*	*2082*	*21*	*1626*	*30*	*2376*	*28*	*-46.1*
D2N100	*2.563*	*0.058*	*0.1569*	*0.003*	*0.72*	*1288*	*17*	*939*	*18*	*1947*	*29*	*-107.3*
D2N101	*2.737*	*0.07*	*0.1859*	*0.005*	*0.811*	*1340*	*19*	*1101*	*25*	*1814*	*28*	*-64.8*
D2N103	*3.911*	*0.091*	*0.2317*	*0.005*	*0.701*	*1615*	*19*	*1343*	*23*	*1951*	*31*	*-45.3*
D2N105	*3.427*	*0.074*	*0.2124*	*0.004*	*0.612*	*1510*	*17*	*1241*	*23*	*1852*	*34*	*-49.2*
D2N106	*3.059*	*0.068*	*0.1848*	*0.003*	*0.645*	*1420*	*17*	*1092*	*18*	*1875*	*27*	*-71.7*
D2N107	*2.715*	*0.043*	*0.1702*	*0.003*	*0.659*	*1332*	*12*	*1012*	*14*	*1849*	*23*	*-82.7*
D2N11	*7.62*	*0.17*	*0.3149*	*0.008*	*0.779*	*2187*	*19*	*1763*	*38*	*2451*	*26*	*-39.0*
D2N12	*3.57*	*0.12*	*0.228*	*0.007*	*0.827*	*1537*	*27*	*1328*	*36*	*1733*	*34*	*-30.5*
D2N13	*2.998*	*0.077*	*0.1881*	*0.004*	*0.75*	*1408*	*20*	*1112*	*23*	*1783*	*32*	*-60.3*
D2N14	*2.132*	*0.056*	*0.148*	*0.004*	*0.691*	*1158*	*18*	*889*	*20*	*1609*	*38*	*-81.0*
D2N15	*2.955*	*0.088*	*0.1668*	*0.004*	*0.762*	*1394*	*23*	*996*	*21*	*1995*	*27*	*-100.3*
D2N17	*3.855*	*0.078*	*0.2428*	*0.005*	*0.489*	*1605*	*16*	*1400*	*26*	*1769*	*39*	*-26.4*
D2N19	*3.258*	*0.064*	*0.1893*	*0.004*	*0.446*	*1470*	*16*	*1117*	*20*	*1937*	*38*	*-73.4*
D2N20	*2.432*	*0.074*	*0.1515*	*0.004*	*0.668*	*1250*	*21*	*909*	*25*	*1919*	*44*	*-111.1*
D2N21	*10.5*	*0.23*	*0.3937*	*0.008*	*0.672*	*2478*	*21*	*2138*	*37*	*2795*	*32*	*-30.7*
D2N22	*2.545*	*0.049*	*0.1707*	*0.003*	*0.59*	*1283*	*14*	*1016*	*16*	*1827*	*29*	*-79.8*
D2N23	*3.587*	*0.091*	*0.2391*	*0.005*	*0.528*	*1543*	*20*	*1381*	*24*	*1861*	*43*	*-34.8*
D2N25	*3.39*	*0.11*	*0.2208*	*0.006*	*0.597*	*1506*	*26*	*1289*	*32*	*1848*	*45*	*-43.4*
D2N27	*3.18*	*0.093*	*0.1995*	*0.006*	*0.811*	*1449*	*23*	*1172*	*34*	*1921*	*35*	*-63.9*
D2N37	*3.159*	*0.054*	*0.2012*	*0.003*	*0.587*	*1450*	*13*	*1181*	*18*	*1805*	*28*	*-52.8*
D2N40	*2.86*	*0.042*	*0.1442*	*0.002*	*0.518*	*1372*	*11*	*868*	*14*	*2182*	*27*	*-151.4*
D2N43	*3.51*	*0.096*	*0.1955*	*0.004*	*0.594*	*1533*	*21*	*1151*	*24*	*1909*	*40*	*-65.9*
D2N45	*3.48*	*0.15*	*0.2342*	*0.008*	*0.372*	*1522*	*32*	*1354*	*42*	*1572*	*85*	*-16.1*
D2N46	*3.8*	*0.1*	*0.2249*	*0.005*	*0.49*	*1587*	*21*	*1307*	*24*	*1781*	*37*	*-36.3*
D2N47	*4.75*	*0.23*	*0.26*	*0.012*	*0.612*	*1772*	*41*	*1484*	*62*	*1982*	*72*	*-33.6*
D2N48	*3.048*	*0.073*	*0.207*	*0.004*	*0.462*	*1423*	*18*	*1211*	*21*	*1598*	*44*	*-32.0*
D2N49	*2.602*	*0.058*	*0.1611*	*0.003*	*0.686*	*1298*	*17*	*962*	*19*	*1728*	*30*	*-79.6*
D2N52	*4.369*	*0.08*	*0.2646*	*0.004*	*0.629*	*1705*	*15*	*1514*	*23*	*1849*	*29*	*-22.1*
D2N53	*3.892*	*0.071*	*0.239*	*0.005*	*0.571*	*1613*	*15*	*1381*	*24*	*1801*	*30*	*-30.4*
D2N56	*2.677*	*0.054*	*0.179*	*0.003*	*0.607*	*1320*	*15*	*1061*	*18*	*1778*	*31*	*-67.6*
D2N59	*4.72*	*0.15*	*0.2143*	*0.006*	*0.784*	*1777*	*26*	*1254*	*30*	*2382*	*31*	*-90.0*
D2N60	*3.427*	*0.045*	*0.2185*	*0.003*	*0.523*	*1509*	*10*	*1273*	*17*	*1824*	*24*	*-43.3*
D2N62	*5.01*	*0.19*	*0.2688*	*0.008*	*0.659*	*1815*	*32*	*1533*	*38*	*1974*	*50*	*-28.8*
D2N65	*4.64*	*0.12*	*0.2763*	*0.005*	*0.523*	*1756*	*20*	*1574*	*24*	*1801*	*37*	*-14.4*
D2N67	*3.562*	*0.096*	*0.2082*	*0.006*	*0.422*	*1542*	*22*	*1222*	*32*	*1777*	*52*	*-45.4*
D2N68	*4.6*	*0.14*	*0.2282*	*0.005*	*0.632*	*1750*	*25*	*1324*	*28*	*2086*	*41*	*-57.6*
D2N70	*3.142*	*0.059*	*0.1878*	*0.004*	*0.63*	*1440*	*14*	*1110*	*21*	*1828*	*29*	*-64.7*
D2N71	*18.88*	*0.44*	*0.496*	*0.012*	*0.499*	*3033*	*22*	*2594*	*50*	*3244*	*34*	*-25.1*
D2N72	*4.479*	*0.087*	*0.1917*	*0.004*	*0.6*	*1730*	*17*	*1130*	*23*	*2452*	*30*	*-117.0*
D2N73	*3.65*	*0.12*	*0.1991*	*0.005*	*0.667*	*1554*	*27*	*1170*	*27*	*1945*	*43*	*-66.2*

Table 1 Detrital zircon U–Pb analytical data.

D2N74	*4.201*	*0.098*	*0.2561*	*0.006*	*0.569*	*1676*	*19*	*1468*	*30*	*1801*	*42*	*-22.7*
D2N76	*8.73*	*0.22*	*0.38*	*0.01*	*0.633*	*2310*	*24*	*2079*	*50*	*2382*	*38*	*-14.6*
D2N77	*3.367*	*0.059*	*0.2049*	*0.004*	*0.692*	*1496*	*14*	*1205*	*20*	*1819*	*26*	*-51.0*
D2N78	*2.22*	*0.039*	*0.1497*	*0.003*	*0.6*	*1190*	*12*	*899*	*16*	*1711*	*28*	*-90.3*
D2N79	*3.839*	*0.082*	*0.2374*	*0.004*	*0.473*	*1604*	*17*	*1374*	*23*	*1842*	*35*	*-34.1*
D24												
D22N03	6.18	0.17	0.3489	0.007	0.487	2000	25	1934	32	1944	44	-0.5
D22N06	5.1	0.2	0.339	0.011	0.504	1838	32	1878	51	1885	74	-0.4
D22N17	4.13	0.11	0.2804	0.007	0.417	1658	21	1640	36	1750	50	-6.7
D22N37	4.655	0.076	0.3008	0.005	0.452	1759	13	1800	24	1949	31	-8.3
D22N46	4.03	0.12	0.2785	0.008	0.629	1636	24	1631	42	1729	48	-6.0
D22N48	4.733	0.091	0.3105	0.005	0.551	1775	16	1742	26	1855	30	-6.5
D24N64	4.08	0.1	0.2934	0.006	0.361	1646	21	1764	29	1841	48	-4.4
D24N70	4.44	0.18	0.304	0.01	0.287	1720	32	1715	48	1821	77	-6.2
D24N71	4.488	0.072	0.312	0.005	0.505	1727	13	1749	26	1744	29	0.3
D24N80	4.08	0.12	0.2891	0.006	0.292	1648	24	1641	33	1703	55	-3.8
D24N84	4.185	0.085	0.2953	0.006	0.194	1671	17	1666	27	1780	46	-6.8
D24N88	4.69	0.11	0.324	0.007	0.323	1764	20	1808	33	1838	50	-1.7
D24N101	5.034	0.097	0.3185	0.005	0.362	1822	16	1784	26	1871	36	-4.9
D24N102	5.47	0.11	0.3454	0.007	0.587	1899	17	1910	33	1917	31	-0.4
D24N105	3.94	0.12	0.2856	0.007	0.264	1619	24	1618	36	1659	59	-2.5
D24N107	9.24	0.33	0.442	0.017	0.448	2369	34	2364	73	2419	69	-2.3
D24N108	4.85	0.11	0.3301	0.008	0.687	1797	20	1843	36	1842	31	0.1
D24N113	4.12	0.1	0.3078	0.008	0.422	1662	20	1733	37	1731	48	0.1
D24N117	4.72	0.13	0.3276	0.01	0.366	1770	23	1826	48	1839	54	-0.7
D24N118	4.87	0.11	0.3107	0.006	0.479	1796	19	1894	30	2068	42	-9.2
D24N119	4.441	0.089	0.3145	0.006	0.525	1718	16	1761	29	1770	34	-0.5
D24N122	5.55	0.1	0.3259	0.006	0.317	1911	16	1817	28	1855	36	-2.1
D24N129	10.51	0.16	0.4184	0.006	0.389	2481	14	2252	29	2450	28	-8.8
					Rejected analysis							
D22N01	*3.421*	*0.076*	*0.2016*	*0.005*	*0.649*	*1509*	*18*	*1185*	*25*	*1918*	*28*	*-61.9*
D22N02	*3.287*	*0.063*	*0.194*	*0.004*	*0.677*	*1480*	*15*	*1142*	*21*	*1955*	*28*	*-71.2*
D22N04	*3.728*	*0.088*	*0.2072*	*0.005*	*0.548*	*1585*	*20*	*1213*	*26*	*2028*	*38*	*-67.2*
D22N05	*2.372*	*0.042*	*0.1464*	*0.003*	*0.64*	*1233*	*13*	*880*	*14*	*1848*	*24*	*-110.0*
D22N07	*2.461*	*0.047*	*0.1482*	*0.003*	*0.69*	*1259*	*14*	*890*	*16*	*1882*	*27*	*-111.5*
D22N08	*2.679*	*0.068*	*0.1427*	*0.004*	*0.881*	*1320*	*19*	*859*	*23*	*2109*	*23*	*-145.5*
D22N09	*3.449*	*0.077*	*0.1851*	*0.003*	*0.656*	*1513*	*18*	*1094*	*19*	*2015*	*28*	*-84.2*
D22N10	*2.697*	*0.07*	*0.1683*	*0.004*	*0.543*	*1326*	*19*	*1001*	*23*	*1819*	*46*	*-81.7*
D22N11	*4.99*	*0.13*	*0.2519*	*0.006*	*0.518*	*1816*	*23*	*1446*	*33*	*2174*	*42*	*-50.3*
D22N12	*3.58*	*0.12*	*0.2019*	*0.006*	*0.876*	*1544*	*25*	*1188*	*32*	*1997*	*22*	*-68.1*
D22N13	*3.373*	*0.061*	*0.194*	*0.004*	*0.575*	*1500*	*14*	*1142*	*23*	*1954*	*32*	*-71.1*
D22N14	*1.989*	*0.066*	*0.1268*	*0.004*	*0.685*	*1117*	*23*	*768*	*23*	*1797*	*47*	*-134.0*
D22N15	*3.024*	*0.083*	*0.1677*	*0.005*	*0.771*	*1409*	*22*	*998*	*29*	*2125*	*43*	*-112.9*
D22N16	*4.78*	*0.1*	*0.2547*	*0.006*	*0.628*	*1780*	*18*	*1461*	*30*	*2141*	*35*	*-46.5*

Table 1 Detrital zircon U–Pb analytical data.

D22N18	*3.57*	*0.065*	*0.2351*	*0.006*	*0.331*	*1544*	*14*	*1360*	*29*	*1815*	*44*	*-33.5*
D22N19	*3.981*	*0.077*	*0.2462*	*0.004*	*0.601*	*1629*	*15*	*1421*	*22*	*1839*	*30*	*-29.4*
D22N20	*2.491*	*0.047*	*0.1157*	*0.002*	*0.773*	*1270*	*14*	*705*	*13*	*2377*	*21*	*-237.2*
D22N21	*4.81*	*0.15*	*0.2759*	*0.007*	*0.693*	*1783*	*26*	*1570*	*35*	*1840*	*37*	*-17.2*
D22N22	*7.21*	*0.15*	*0.2959*	*0.005*	*0.744*	*2140*	*19*	*1669*	*26*	*2447*	*23*	*-46.6*
D22N23	*2.806*	*0.08*	*0.1579*	*0.005*	*0.875*	*1356*	*22*	*944*	*29*	*1956*	*30*	*-107.2*
D22N24	*2.169*	*0.04*	*0.1287*	*0.002*	*0.764*	*1171*	*13*	*780*	*14*	*1788*	*22*	*-129.2*
D22N25	*2.948*	*0.096*	*0.1535*	*0.004*	*0.839*	*1389*	*25*	*922*	*23*	*2005*	*28*	*-117.5*
D22N26	*3.76*	*0.1*	*0.2068*	*0.005*	*0.797*	*1585*	*21*	*1210*	*28*	*1952*	*30*	*-61.3*
D22N27	*3.44*	*0.13*	*0.2015*	*0.007*	*0.539*	*1511*	*29*	*1180*	*35*	*1802*	*53*	*-52.7*
D22N28	*8.5*	*0.17*	*0.3563*	*0.007*	*0.576*	*2283*	*18*	*1966*	*32*	*2439*	*28*	*-24.1*
D22N29	*4.94*	*0.11*	*0.2831*	*0.006*	*0.613*	*1807*	*19*	*1609*	*30*	*1900*	*33*	*-18.1*
D22N30	*3.422*	*0.096*	*0.2095*	*0.006*	*0.855*	*1508*	*23*	*1231*	*34*	*1895*	*30*	*-53.9*
D22N31	*2.843*	*0.073*	*0.1755*	*0.004*	*0.508*	*1364*	*19*	*1042*	*21*	*1815*	*48*	*-74.2*
D22N32	*2.399*	*0.084*	*0.1374*	*0.004*	*0.775*	*1238*	*25*	*830*	*23*	*1928*	*39*	*-132.3*
D22N33	*8.12*	*0.2*	*0.2541*	*0.005*	*0.509*	*2243*	*22*	*1463*	*27*	*3052*	*35*	*-108.6*
D22N35	*4.59*	*0.11*	*0.2416*	*0.006*	*0.593*	*1751*	*20*	*1394*	*29*	*2183*	*40*	*-56.6*
D22N36	*2.039*	*0.044*	*0.1214*	*0.002*	*0.672*	*1130*	*15*	*739*	*14*	*1967*	*27*	*-166.2*
D22N38	*5.22*	*0.11*	*0.29*	*0.005*	*0.682*	*1855*	*18*	*1640*	*25*	*2071*	*27*	*-26.3*
D22N39	*2.451*	*0.048*	*0.1552*	*0.003*	*0.605*	*1256*	*14*	*930*	*17*	*1855*	*31*	*-99.5*
D22N40	*2.375*	*0.042*	*0.1429*	*0.003*	*0.599*	*1235*	*13*	*861*	*19*	*1947*	*33*	*-126.1*
D22N41	*2.706*	*0.063*	*0.1888*	*0.004*	*0.573*	*1327*	*17*	*1114*	*23*	*1621*	*43*	*-45.5*
D22N42	*2.441*	*0.073*	*0.1495*	*0.004*	*0.853*	*1253*	*22*	*898*	*24*	*1978*	*35*	*-120.3*
D22N43	*1.845*	*0.036*	*0.1088*	*0.002*	*0.673*	*1062*	*13*	*666*	*12*	*2003*	*27*	*-200.8*
D22N44	*3.301*	*0.056*	*0.2303*	*0.003*	*0.826*	*1483*	*13*	*1336*	*18*	*1710*	*18*	*-28.0*
D22N45	*3.778*	*0.09*	*0.2482*	*0.004*	*0.693*	*1584*	*19*	*1428*	*22*	*1805*	*28*	*-26.4*
D22N47	*2.939*	*0.064*	*0.1884*	*0.005*	*0.502*	*1389*	*16*	*1112*	*25*	*1866*	*44*	*-67.8*
D22N49	*1.867*	*0.038*	*0.1194*	*0.002*	*0.533*	*1071*	*14*	*727*	*13*	*1893*	*34*	*-160.4*
D22N50	*3.8*	*0.1*	*0.2479*	*0.005*	*0.742*	*1589*	*22*	*1427*	*24*	*1835*	*36*	*-28.6*
D22N51	*2.459*	*0.036*	*0.0968*	*0.002*	*0.645*	*1263*	*10*	*595.3*	*9.4*	*2728*	*26*	*-358.3*
D22N52	*2.887*	*0.065*	*0.2034*	*0.004*	*0.421*	*1380*	*17*	*1193*	*19*	*1735*	*42*	*-45.4*
D22N53	*2.773*	*0.091*	*0.1835*	*0.006*	*0.752*	*1353*	*24*	*1085*	*33*	*1921*	*37*	*-77.1*
D22N54	*3.278*	*0.09*	*0.2311*	*0.006*	*0.655*	*1475*	*22*	*1339*	*33*	*1798*	*35*	*-34.3*
D22N56	*1.462*	*0.046*	*0.0762*	*0.001*	*0.256*	*916*	*19*	*473.6*	*7.7*	*2351*	*57*	*-396.4*
D22N57	*1.332*	*0.021*	*0.0878*	*0.002*	*0.793*	*859.6*	*9.1*	*542.6*	*8.8*	*1871*	*17*	*-244.8*
D22N58	*3.984*	*0.083*	*0.2467*	*0.005*	*0.411*	*1632*	*17*	*1425*	*29*	*1929*	*46*	*-35.4*
D22N59	*3.405*	*0.083*	*0.2113*	*0.004*	*0.438*	*1505*	*19*	*1235*	*22*	*1939*	*36*	*-57.0*
D22N60	*3.117*	*0.056*	*0.1816*	*0.004*	*0.743*	*1437*	*14*	*1077*	*19*	*2058*	*23*	*-91.1*
D24N61	*2.909*	*0.046*	*0.2*	*0.003*	*0.521*	*1383*	*12*	*1175*	*15*	*1762*	*25*	*-50.0*
D24N62	*3.457*	*0.066*	*0.2261*	*0.004*	*0.58*	*1515*	*15*	*1313*	*22*	*1850*	*31*	*-40.9*
D24N63	*2.193*	*0.05*	*0.1501*	*0.002*	*0.527*	*1179*	*16*	*903*	*13*	*1807*	*36*	*-100.1*
D24N65	*7.09*	*0.18*	*0.2738*	*0.008*	*0.363*	*2123*	*23*	*1557*	*41*	*2760*	*48*	*-77.3*
D24N66	*2.76*	*0.18*	*0.1582*	*0.008*	*0.703*	*1348*	*51*	*945*	*44*	*2134*	*77*	*-125.8*
D24N67	*2.565*	*0.098*	*0.1798*	*0.006*	*0.555*	*1296*	*26*	*1065*	*30*	*1785*	*59*	*-67.6*
D24N68	*3.252*	*0.085*	*0.2193*	*0.004*	*0.507*	*1471*	*21*	*1277*	*22*	*1818*	*46*	*-42.4*

Table 1 Detrital zircon U–Pb analytical data.

D24N69	*2.14*	*0.029*	*0.1119*	*0.002*	*0.826*	*1161.1*	*9.6*	*684*	*13*	*2264*	*22*	*-231.0*
D24N72	*4.686*	*0.099*	*0.2387*	*0.005*	*0.619*	*1762*	*18*	*1379*	*27*	*2231*	*32*	*-61.8*
D24N73	*2.227*	*0.048*	*0.1337*	*0.003*	*0.658*	*1192*	*14*	*808*	*15*	*2015*	*29*	*-149.4*
D24N74	*3.01*	*0.083*	*0.212*	*0.005*	*0.37*	*1407*	*21*	*1239*	*26*	*1718*	*49*	*-38.7*
D24N75	*5.07*	*0.12*	*0.2581*	*0.007*	*0.783*	*1830*	*20*	*1483*	*38*	*2266*	*31*	*-52.8*
D24N76	*11.9*	*1.5*	*0.185*	*0.023*	*0.967*	*2620*	*110*	*1090*	*120*	*4103*	*53*	*-276.4*
D24N77	*3.77*	*0.13*	*0.2274*	*0.008*	*0.724*	*1582*	*27*	*1319*	*40*	*1923*	*50*	*-45.8*
D24N78	*2.886*	*0.074*	*0.1901*	*0.005*	*0.621*	*1379*	*20*	*1121*	*29*	*1810*	*38*	*-61.5*
D24N79	*2.279*	*0.039*	*0.1435*	*0.002*	*0.555*	*1207*	*13*	*864*	*14*	*1900*	*29*	*-119.9*
D24N81	*1.995*	*0.054*	*0.1338*	*0.004*	*0.708*	*1121*	*18*	*809*	*25*	*1844*	*38*	*-127.9*
D24N82	*2.115*	*0.034*	*0.1324*	*0.002*	*0.673*	*1152*	*11*	*801*	*13*	*1940*	*25*	*-142.2*
D24N83	*2.676*	*0.075*	*0.1804*	*0.006*	*0.8*	*1320*	*21*	*1068*	*30*	*1823*	*38*	*-70.7*
D24N85	*3.218*	*0.058*	*0.2065*	*0.004*	*0.471*	*1459*	*14*	*1209*	*19*	*1931*	*33*	*-59.7*
D24N86	*3.58*	*0.14*	*0.1881*	*0.007*	*0.881*	*1550*	*32*	*1109*	*40*	*2310*	*37*	*-108.3*
D24N87	*2.462*	*0.067*	*0.1566*	*0.004*	*0.594*	*1259*	*20*	*937*	*24*	*1942*	*43*	*-107.3*
D24N89	*4.45*	*0.21*	*0.2327*	*0.006*	*0.24*	*1718*	*37*	*1351*	*30*	*2348*	*75*	*-73.8*
D24N90	*2.92*	*0.14*	*0.1346*	*0.006*	*0.437*	*1384*	*35*	*813*	*32*	*2473*	*73*	*-204.2*
D24N91	*3.017*	*0.05*	*0.2034*	*0.003*	*0.476*	*1410*	*13*	*1195*	*18*	*1886*	*30*	*-57.8*
D24N92	*3.266*	*0.093*	*0.1952*	*0.004*	*0.595*	*1473*	*21*	*1149*	*20*	*2140*	*39*	*-86.2*
D24N93	*3.385*	*0.076*	*0.2111*	*0.003*	*0.34*	*1500*	*18*	*1234*	*18*	*2045*	*41*	*-65.7*
D24N94	*1.974*	*0.032*	*0.1331*	*0.002*	*0.692*	*1107*	*11*	*805*	*12*	*1905*	*23*	*-136.6*
D24N95	*3.248*	*0.059*	*0.2242*	*0.004*	*0.658*	*1466*	*14*	*1305*	*21*	*1845*	*29*	*-41.4*
D24N96	*5.349*	*0.075*	*0.2628*	*0.004*	*0.651*	*1876*	*12*	*1503*	*21*	*2436*	*22*	*-62.1*
D24N97	*2.935*	*0.088*	*0.1765*	*0.005*	*0.602*	*1390*	*23*	*1047*	*25*	*2035*	*48*	*-94.4*
D24N98	*0.312*	*0.02*	*0.0207*	*0.002*	*0.963*	*272*	*16*	*132*	*12*	*2000*	*79*	*-1415.2*
D24N99	*2.11*	*0.089*	*0.1466*	*0.006*	*0.483*	*1149*	*29*	*888*	*33*	*1826*	*69*	*-105.6*
D24N100	*4.68*	*0.12*	*0.2609*	*0.005*	*0.345*	*1761*	*21*	*1493*	*28*	*2170*	*44*	*-45.3*
D57												
D57N003	5.27	0.18	0.311	0.008	0.385	1859	30	1757	39	1843	61	-4.9
D57N013	4.63	0.11	0.2977	0.006	0.28	1758	21	1692	32	1848	47	-9.2
D57N014	4.46	0.089	0.2904	0.005	0.43	1724	17	1692	22	1817	37	-7.4
D57N022	5.26	0.13	0.3324	0.007	0.313	1860	20	1851	35	1886	46	-1.9
D57N025	4.11	0.26	0.284	0.016	0.662	1651	53	1611	78	1740	91	-8.0
D57N028	4.553	0.092	0.3175	0.007	0.485	1739	17	1775	35	1783	40	-0.5
D57N033	3.89	0.079	0.2885	0.006	0.179	1610	16	1646	30	1789	49	-8.7
D57N035	4.172	0.095	0.3125	0.006	0.512	1666	19	1752	29	1795	38	-2.5
D57N038	4.29	0.32	0.321	0.012	0.256	1710	64	1815	66	1850	160	-1.9
D57N039	3.91	0.1	0.2901	0.006	0.146	1610	22	1640	31	1759	62	-7.3
D57N040	4.883	0.094	0.3364	0.006	0.578	1800	16	1875	28	1886	30	-0.6
D57N041	4.39	0.11	0.3136	0.007	0.586	1709	20	1757	35	1804	43	-2.7
D57N042	4.3	0.12	0.3188	0.006	0.253	1694	23	1884	32	1964	57	-4.2
D57N045	15.33	0.52	0.555	0.022	0.152	2836	31	2838	91	2969	58	-4.6
D57N049	5.12	0.14	0.3362	0.007	0.26	1834	24	1867	33	1905	51	-2.0
D57N050	4.391	0.093	0.3096	0.007	0.488	1711	18	1737	33	1802	41	-3.7

Table 1 Detrital zircon U–Pb analytical data.

D57N051	4.77	0.21	0.318	0.013	0.023	1774	37	1779	61	1920	110	-7.9
D57N052	3.97	0.15	0.2884	0.008	0.703	1626	31	1646	46	1752	58	-6.4
D57N053	4.095	0.099	0.2967	0.007	0.448	1655	21	1680	33	1766	50	-5.1
D57N054	4.51	0.1	0.3151	0.006	0.301	1730	19	1764	29	1805	46	-2.3
D57N055	3.8	0.18	0.291	0.011	0.499	1607	36	1791	57	1864	85	-4.1
D57N056	4.66	0.14	0.3197	0.008	0.251	1765	25	1786	37	1853	59	-3.8
D57N059	4	0.18	0.2927	0.01	0.12	1630	38	1659	47	1750	110	-5.5
D57N061	4.09	0.14	0.3022	0.007	0.275	1654	28	1701	37	1755	65	-3.2
D57N063	4.65	0.11	0.311	0.008	0.315	1755	20	1748	36	1874	49	-7.2
D57N066	4.247	0.099	0.3001	0.006	0.42	1689	21	1862	29	1939	46	-4.1
D57N075	5.06	0.094	0.3148	0.005	0.416	1828	15	1765	26	1788	34	-1.3
D57N084	5.71	0.19	0.373	0.01	0.417	1946	29	1983	50	2126	56	-7.2
D57N086	4.72	0.13	0.3098	0.007	0.336	1780	22	1741	32	1795	50	-3.1
D57N087	3.71	0.12	0.2685	0.008	0.283	1573	27	1532	40	1619	70	-5.7
D57N089	5.61	0.27	0.338	0.013	0.644	1913	42	1877	65	1976	66	-5.3
D57N103	5.09	0.1	0.3026	0.004	0.261	1840	17	1703	22	1793	36	-5.3
D57N107	5.04	0.15	0.3107	0.008	0.764	1823	24	1748	39	1760	41	-0.7
D57N111	4.83	0.12	0.2953	0.006	0.323	1790	22	1667	32	1828	45	-9.7
D57N114	4.74	0.11	0.2994	0.005	0.19	1775	20	1687	26	1851	49	-9.7
D57N117	4.68	0.12	0.2942	0.007	0.165	1761	21	1660	35	1784	61	-7.5
D57N119	4.36	0.12	0.284	0.005	0.109	1704	24	1759	27	1832	63	-4.2
D57N147	5.17	0.12	0.3502	0.008	0.242	1851	18	1928	38	1897	54	1.6
D57N148	6.42	0.24	0.3691	0.008	0.257	2023	31	2022	35	2212	60	-9.4
D57N152	4.23	0.073	0.2929	0.004	0.32	1678	14	1655	21	1793	36	-8.3
D57N153	3.989	0.092	0.296	0.006	0.529	1635	19	1690	31	1751	44	-3.6
D57N156	4.2	0.12	0.2791	0.007	0.312	1669	24	1584	34	1730	58	-9.2
D57N158	4.84	0.1	0.306	0.006	0.362	1794	17	1722	28	1893	40	-9.9
D57N94	4.582	0.09	0.3029	0.005	0.296	1746	17	1707	22	1799	37	-5.4
D57N98	5.27	0.11	0.3253	0.008	0.152	1862	18	1818	40	1865	39	-2.6
D57N99	6.17	0.12	0.3458	0.007	0.569	2001	16	1915	34	1946	36	-1.6
					Rejected analysis							
D57N001	*4.59*	*0.12*	*0.27*	*0.005*	*0.385*	*1748*	*21*	*1539*	*25*	*1848*	*49*	*-20.1*
D57N002	*6.17*	*0.15*	*0.2956*	*0.006*	*0.358*	*2007*	*23*	*1668*	*32*	*2230*	*45*	*-33.7*
D57N004	*5.63*	*0.14*	*0.2506*	*0.004*	*0.222*	*1918*	*22*	*1441*	*18*	*2345*	*43*	*-62.7*
D57N005	*3.72*	*0.075*	*0.2435*	*0.004*	*0.337*	*1572*	*16*	*1404*	*22*	*1716*	*40*	*-22.2*
D57N006	*4.5*	*0.11*	*0.2555*	*0.006*	*0.295*	*1730*	*22*	*1469*	*32*	*1996*	*55*	*-35.9*
D57N007	*7.52*	*0.15*	*0.2908*	*0.006*	*0.514*	*2173*	*18*	*1650*	*30*	*2686*	*33*	*-62.8*
D57N009	*4.67*	*0.15*	*0.2654*	*0.006*	*0.271*	*1754*	*26*	*1515*	*30*	*1974*	*63*	*-30.3*
D57N010	*2.26*	*0.15*	*0.129*	*0.01*	*0.924*	*1202*	*46*	*777*	*56*	*2060*	*52*	*-165.1*
D57N011	*2.74*	*0.13*	*0.1732*	*0.007*	*0.723*	*1345*	*34*	*1029*	*38*	*1828*	*61*	*-77.6*
D57N012	*7.17*	*0.25*	*0.3476*	*0.007*	*0.236*	*2124*	*31*	*1922*	*34*	*2299*	*64*	*-19.6*
D57N015	*1.707*	*0.093*	*0.1049*	*0.003*	*0.748*	*991*	*32*	*642*	*20*	*1767*	*40*	*-175.2*
D57N016	*4.112*	*0.095*	*0.2512*	*0.005*	*0.482*	*1653*	*19*	*1443*	*25*	*1945*	*35*	*-34.8*
D57N017	*5.79*	*0.14*	*0.3037*	*0.006*	*0.137*	*1947*	*20*	*1709*	*28*	*2171*	*45*	*-27.0*
D57N018	*5.164*	*0.09*	*0.285*	*0.006*	*0.216*	*1846*	*15*	*1615*	*29*	*2090*	*39*	*-29.4*

Table 1 Detrital zircon U–Pb analytical data.

D57N019	*3.757*	*0.072*	*0.2155*	*0.004*	*0.306*	*1580*	*15*	*1257*	*22*	*2031*	*39*	*-61.6*
D57N020	*3.38*	*0.15*	*0.1933*	*0.007*	*0.732*	*1495*	*34*	*1138*	*36*	*2072*	*53*	*-82.1*
D57N021	*1.521*	*0.04*	*0.0789*	*0.002*	*0.312*	*934*	*16*	*490*	*14*	*2180*	*46*	*-344.9*
D57N023	*6.41*	*0.12*	*0.1715*	*0.002*	*0.674*	*2030*	*16*	*1020*	*13*	*3317*	*23*	*-225.2*
D57N024	*2.695*	*0.06*	*0.1217*	*0.002*	*0.396*	*1326*	*16*	*741*	*10*	*2447*	*34*	*-230.2*
D57N026	*3.93*	*0.24*	*0.215*	*0.012*	*0.855*	*1615*	*48*	*1264*	*67*	*2153*	*47*	*-70.3*
D57N027	*1.936*	*0.033*	*0.1089*	*0.002*	*0.658*	*1095*	*11*	*666*	*11*	*2092*	*24*	*-214.1*
D57N029	*3.52*	*0.14*	*0.2094*	*0.009*	*0.576*	*1528*	*30*	*1224*	*48*	*2088*	*78*	*-70.6*
D57N030	*2.529*	*0.096*	*0.1754*	*0.008*	*0.81*	*1274*	*27*	*1040*	*41*	*1867*	*39*	*-79.5*
D57N031	*2.552*	*0.052*	*0.1834*	*0.004*	*0.587*	*1287*	*15*	*1085*	*19*	*1815*	*31*	*-67.3*
D57N032	*11.75*	*0.63*	*0.3293*	*0.009*	*0.182*	*2565*	*48*	*1833*	*43*	*3359*	*83*	*-83.3*
D57N034	*3.39*	*0.32*	*0.233*	*0.022*	*0.46*	*1523*	*59*	*1350*	*120*	*1940*	*110*	*-43.7*
D57N036	*3.202*	*0.072*	*0.2051*	*0.005*	*0.273*	*1459*	*17*	*1202*	*26*	*2044*	*48*	*-70.0*
D57N037	*5.91*	*0.12*	*0.2602*	*0.007*	*0.457*	*1961*	*18*	*1489*	*36*	*2629*	*38*	*-76.6*
D57N043	*1.668*	*0.024*	*0.1185*	*0.002*	*0.546*	*996.6*	*9.2*	*721.9*	*9.7*	*1795*	*24*	*-148.6*
D57N044	*2.878*	*0.051*	*0.1929*	*0.004*	*0.428*	*1374*	*13*	*1138*	*20*	*1895*	*34*	*-66.5*
D57N046	*4.188*	*0.096*	*0.1756*	*0.004*	*0.612*	*1669*	*19*	*1042*	*22*	*2687*	*34*	*-157.9*
D57N047	*4.84*	*0.16*	*0.2645*	*0.006*	*0.009*	*1791*	*28*	*1515*	*33*	*2141*	*70*	*-41.3*
D57N048	*4.209*	*0.092*	*0.1734*	*0.003*	*0.451*	*1671*	*18*	*1032*	*16*	*2692*	*26*	*-160.9*
D57N057	*4.42*	*0.14*	*0.2261*	*0.007*	*0.339*	*1713*	*26*	*1312*	*36*	*2366*	*68*	*-80.3*
D57N058	*6.23*	*0.1*	*0.161*	*0.004*	*0.641*	*2007*	*14*	*962*	*21*	*3488*	*26*	*-262.6*
D57N060	*7.92*	*0.21*	*0.333*	*0.011*	*0.316*	*2224*	*23*	*1847*	*56*	*2698*	*49*	*-46.1*
D57N062	*3.918*	*0.093*	*0.2316*	*0.006*	*0.382*	*1616*	*20*	*1341*	*33*	*2127*	*49*	*-58.6*
D57N065	*5.111*	*0.093*	*0.1781*	*0.003*	*0.645*	*1839*	*16*	*1058*	*18*	*2974*	*26*	*-181.1*
D57N067	*4.58*	*0.15*	*0.202*	*0.004*	*0.249*	*1736*	*26*	*1187*	*20*	*2523*	*42*	*-112.6*
D57N068	*2.483*	*0.058*	*0.1522*	*0.004*	*0.486*	*1268*	*16*	*913*	*21*	*1960*	*41*	*-114.7*
D57N069	*3.769*	*0.089*	*0.2459*	*0.005*	*0.435*	*1584*	*19*	*1419*	*26*	*1869*	*42*	*-31.7*
D57N070	*2.978*	*0.08*	*0.199*	*0.005*	*0.655*	*1402*	*20*	*1169*	*25*	*1730*	*41*	*-48.0*
D57N071	*4.26*	*0.19*	*0.2649*	*0.009*	*0.62*	*1688*	*35*	*1514*	*48*	*1856*	*70*	*-22.6*
D57N072	*2.896*	*0.092*	*0.149*	*0.005*	*0.603*	*1388*	*21*	*900*	*28*	*2092*	*56*	*-132.4*
D57N073	*6.69*	*0.24*	*0.2771*	*0.008*	*0.252*	*2071*	*31*	*1575*	*40*	*2503*	*71*	*-58.9*
D57N074	*2.886*	*0.073*	*0.134*	*0.002*	*0.569*	*1375*	*19*	*812*	*14*	*2299*	*31*	*-183.1*
D57N076	*6.09*	*0.12*	*0.274*	*0.006*	*0.482*	*1987*	*17*	*1559*	*28*	*2390*	*30*	*-53.3*
D57N077	*9.24*	*0.14*	*0.3158*	*0.006*	*0.568*	*2362*	*13*	*1767*	*29*	*2833*	*25*	*-60.3*
D57N078	*2.523*	*0.098*	*0.1347*	*0.005*	*0.671*	*1269*	*27*	*812*	*28*	*2042*	*32*	*-151.5*
D57N079	*8.51*	*0.26*	*0.2776*	*0.008*	*0.426*	*2283*	*28*	*1582*	*38*	*2960*	*45*	*-87.1*
D57N080	*5.76*	*0.12*	*0.1696*	*0.005*	*0.612*	*1936*	*18*	*1009*	*25*	*3099*	*28*	*-207.1*
D57N081	*7.65*	*0.19*	*0.2843*	*0.006*	*0.463*	*2187*	*23*	*1612*	*28*	*2743*	*39*	*-70.2*
D57N082	*8.56*	*0.33*	*0.2891*	*0.008*	*0.07*	*2287*	*35*	*1636*	*40*	*2895*	*79*	*-77.0*
D57N083	*5.01*	*0.22*	*0.2017*	*0.006*	*0.33*	*1812*	*35*	*1188*	*32*	*2603*	*77*	*-119.1*
D57N085	*3.736*	*0.09*	*0.15*	*0.004*	*0.442*	*1572*	*19*	*900*	*22*	*2600*	*32*	*-188.9*
D57N088	*5.49*	*0.12*	*0.3064*	*0.006*	*0.134*	*1896*	*19*	*1722*	*31*	*2125*	*44*	*-23.4*
D57N90	*3.26*	*0.044*	*0.1434*	*0.002*	*0.552*	*1472*	*10*	*863.7*	*9.2*	*2536*	*19*	*-193.6*
D57N91	*5.52*	*0.24*	*0.2912*	*0.006*	*0.706*	*1893*	*38*	*1645*	*32*	*2213*	*51*	*-34.5*
D57N92	*7.56*	*0.21*	*0.2048*	*0.007*	*0.766*	*2175*	*26*	*1199*	*36*	*3366*	*39*	*-180.7*

Table 1 Detrital zircon U–Pb analytical data.

D57N93	*3.841*	*0.093*	*0.1995*	*0.003*	*0.44*	*1595*	*19*	*1172*	*15*	*2216*	*39*	*-89.1*
D57N95	*2.392*	*0.061*	*0.1483*	*0.003*	*0.609*	*1239*	*18*	*891*	*18*	*1829*	*37*	*-105.3*
D57N96	*4.16*	*0.13*	*0.1942*	*0.004*	*0.427*	*1659*	*26*	*1143*	*21*	*2365*	*46*	*-106.9*
D57N97	*1.704*	*0.027*	*0.1081*	*0.002*	*0.614*	*1009*	*10*	*662*	*11*	*1760*	*25*	*-165.9*
AY-01												
AY001	4.95	0.23	0.312	0.014	0.722	1803	39	1748	67	1805	59	-3.3
AY002	5.8	0.13	0.3561	0.008	0.343	1948	20	1967	36	1804	47	8.3
AY003	4.05	0.21	0.276	0.014	0.364	1636	40	1566	70	1540	140	1.7
AY004	5.74	0.14	0.3579	0.008	0.13	1966	20	1905	39	1759	75	7.7
AY005	5.56	0.13	0.3585	0.007	0.253	1939	19	1889	32	1714	46	9.3
AY009	5.66	0.14	0.3605	0.007	0.543	1956	20	1926	32	1768	42	8.2
AY010	5.73	0.15	0.3571	0.007	0.236	1960	22	1962	34	1777	47	9.4
AY011	5.58	0.21	0.3549	0.01	0.168	1914	32	1954	45	1806	78	7.6
AY013	4.94	0.11	0.3332	0.007	0.373	1806	19	1800	31	1624	46	9.8
AY014	4.24	0.14	0.2937	0.01	0.851	1678	29	1659	49	1666	37	-0.4
AY016	4.186	0.089	0.2838	0.006	0.16	1670	17	1614	30	1661	45	-2.9
AY019	4.43	0.16	0.311	0.01	0.761	1716	30	1747	52	1720	41	1.5
AY020	5.28	0.14	0.3428	0.007	0.314	1862	22	1897	34	1798	47	5.2
AY021	5.81	0.17	0.3544	0.008	0.248	1944	25	1893	38	1727	60	8.8
AY022	3.95	0.47	0.262	0.018	0.318	1585	45	1490	87	1470	410	1.3
AY024	4.422	0.097	0.3024	0.007	0.608	1719	18	1700	34	1691	36	0.5
AY025	4.51	0.34	0.313	0.021	0.48	1699	68	1760	110	1744	57	0.9
AY028	5.76	0.21	0.337	0.012	0.292	1943	32	1871	58	2042	74	-9.1
AY029	4.18	0.13	0.2853	0.008	0.508	1665	26	1617	38	1742	59	-7.7
AY030	4.6	0.14	0.309	0.01	0.623	1737	27	1737	50	1631	52	6.1
AY031	4.2	0.14	0.279	0.011	0.444	1668	27	1583	53	1635	65	-3.3
AY032	5.5	0.11	0.351	0.007	0.477	1936	17	1934	31	1742	38	9.9
AY036	5.13	0.15	0.3367	0.007	0.304	1869	25	1863	34	1677	49	10.0
AY037	4.84	0.19	0.306	0.012	0.798	1773	31	1712	57	1731	41	-1.1
AY038	3.99	0.16	0.2607	0.009	0.45	1631	31	1491	47	1637	70	-9.8
AY039	4.06	0.11	0.2694	0.007	0.514	1647	21	1536	34	1668	46	-8.6
AY043	4.64	0.18	0.323	0.012	0.515	1741	33	1747	58	1844	61	-5.6
AY045	5.34	0.15	0.3417	0.009	0.539	1920	23	1901	43	1721	44	9.5
AY049	4.34	0.13	0.3059	0.01	0.369	1701	25	1715	47	1722	49	-0.4
AY052	10.55	0.82	0.432	0.015	0.379	2427	66	2318	66	2500	110	-7.9
AY054	3.8	0.17	0.276	0.011	0.616	1599	37	1580	54	1729	58	-9.4
AY055	5.16	0.15	0.3246	0.009	0.361	1880	24	1899	43	1766	56	7.0
AY056	5.82	0.24	0.352	0.015	0.638	1948	36	1939	70	2041	64	-5.3
AY057	3.9	0.17	0.288	0.012	0.789	1607	35	1632	59	1639	54	-0.4
AY061	4.36	0.15	0.3012	0.009	0.713	1698	29	1695	45	1702	47	-0.4
AY062	4.63	0.21	0.308	0.015	0.889	1725	41	1721	74	1723	33	-0.1
AY063	4.61	0.16	0.311	0.01	0.802	1755	30	1750	50	1750	39	0.0
AY064	4.01	0.15	0.2866	0.009	0.72	1635	30	1621	44	1615	48	0.4
AY065	6.44	0.45	0.358	0.023	0.364	2035	56	1970	110	1990	110	-1.0

Table 1 Detrital zircon U–Pb analytical data.

AY070	5.18	0.12	0.3537	0.007	0.538	1890	18	1841	31	1684	33	8.5
AY072	4.51	0.17	0.309	0.013	0.888	1730	31	1726	64	1725	30	0.1
AY075	5.11	0.11	0.3379	0.009	0.15	1832	18	1870	43	1685	38	9.9
AY076	4.23	0.17	0.288	0.015	0.736	1686	34	1626	76	1738	57	-6.9
AY077	4.72	0.22	0.311	0.015	0.828	1759	39	1751	77	1757	40	-0.3
AY078	4.31	0.14	0.304	0.01	0.866	1690	27	1703	51	1706	35	-0.2
AY079	4.15	0.26	0.296	0.018	0.919	1621	54	1649	92	1702	39	-3.2
AY082	4.91	0.15	0.3255	0.009	0.762	1794	26	1816	44	1816	46	0.0
AY084	5.53	0.16	0.3731	0.008	0.56	1934	25	1933	38	1764	46	8.7
AY085	4	0.17	0.29	0.012	0.781	1625	35	1631	61	1678	40	-2.9
AY089	3.72	0.23	0.274	0.017	0.904	1552	49	1560	85	1652	42	-5.9
AY090	4.39	0.16	0.315	0.011	0.852	1699	33	1762	53	1699	31	3.6
AY091	4.37	0.18	0.324	0.011	0.377	1763	31	1753	53	1597	76	8.9
AY093	5.23	0.17	0.357	0.01	0.459	1904	26	1892	44	1742	54	7.9
AY094	4.36	0.2	0.291	0.015	0.4	1705	39	1644	73	1722	91	-4.7
AY095	3.97	0.12	0.277	0.007	0.537	1623	23	1574	34	1716	47	-9.0
AY096	4.27	0.11	0.2982	0.008	0.605	1683	21	1685	39	1683	45	0.1
AY099	4.51	0.2	0.305	0.014	0.809	1727	38	1709	67	1736	46	-1.6
AY101	4.65	0.24	0.317	0.015	0.766	1774	40	1771	73	1778	69	-0.4
AY105	5	0.22	0.319	0.013	0.867	1813	38	1775	62	1787	35	-0.7
AY107	5.01	0.1	0.3332	0.006	0.42	1865	16	1803	29	1642	33	8.9
AY108	6.19	0.18	0.3724	0.009	0.372	2030	25	2018	38	1828	48	9.4
AY110	4.8	0.16	0.3089	0.008	0.771	1786	27	1732	41	1753	35	-1.2
AY111	4.99	0.13	0.3344	0.006	0.397	1846	22	1819	28	1655	47	9.0
AY112	4.5	0.12	0.3009	0.008	0.647	1731	24	1696	39	1701	40	-0.3
AY116	4.17	0.1	0.289	0.006	0.526	1671	21	1635	29	1700	42	-4.0
AY117	4.87	0.24	0.331	0.01	0.154	1820	38	1812	50	1642	99	9.4
AY118	4.33	0.12	0.2848	0.006	0.458	1700	23	1619	29	1693	54	-4.6
AY119	5.07	0.12	0.3486	0.007	0.386	1880	18	1836	33	1670	39	9.0
AY120	4.34	0.12	0.2858	0.007	0.412	1703	21	1618	35	1758	51	-8.7
AY122	4.62	0.11	0.3382	0.007	0.408	1791	19	1866	34	1700	42	8.9
AY123	4.22	0.32	0.302	0.026	0.746	1668	61	1690	130	1823	92	-7.9
AY130	4.47	0.14	0.3168	0.01	0.646	1721	27	1768	48	1811	42	-2.4
AY133	5.48	0.12	0.3671	0.007	0.225	1898	18	2001	36	1816	45	9.2
AY134	4.23	0.25	0.296	0.015	0.794	1663	46	1672	78	1689	47	-1.0
AY136	10.28	0.31	0.503	0.014	0.621	2458	30	2618	61	2447	49	6.5
AY138	4.88	0.12	0.3221	0.006	0.196	1824	20	1842	29	1685	45	8.5
AY139	4.2	0.17	0.303	0.012	0.86	1664	35	1700	58	1703	40	-0.2
					Rejected analysis							
AY006	*0.984*	*0.025*	*0.055*	*0.001*	*0.69*	*693*	*13*	*345.2*	*8.5*	*2000*	*29*	*-479.4*
AY007	*2.674*	*0.092*	*0.1674*	*0.006*	*0.386*	*1320*	*26*	*997*	*31*	*1763*	*56*	*-76.8*
AY008	*3.2*	*0.12*	*0.2109*	*0.006*	*0.501*	*1453*	*30*	*1233*	*34*	*1701*	*65*	*-38.0*
AY012	*6.27*	*0.16*	*0.425*	*0.01*	*0.135*	*2009*	*24*	*2269*	*46*	*1833*	*56*	*19.2*
AY015	*2.64*	*0.14*	*0.167*	*0.006*	*0.462*	*1319*	*37*	*994*	*33*	*1770*	*79*	*-78.1*
AY017	*2.659*	*0.083*	*0.176*	*0.005*	*0.524*	*1314*	*23*	*1044*	*27*	*1701*	*56*	*-62.9*

Table 1 Detrital zircon U–Pb analytical data.

AY018	*2.32*	*0.07*	*0.1383*	*0.004*	*0.641*	*1216*	*21*	*835*	*24*	*1933*	*47*	*-131.5*
AY023	*2.92*	*0.16*	*0.2056*	*0.008*	*0.339*	*1383*	*41*	*1205*	*45*	*1650*	*120*	*-36.9*
AY026	*3.66*	*0.12*	*0.228*	*0.007*	*0.478*	*1559*	*26*	*1322*	*39*	*1808*	*58*	*-36.8*
AY027	*4.56*	*0.12*	*0.197*	*0.005*	*0.59*	*1737*	*22*	*1158*	*28*	*2419*	*39*	*-108.9*
AY033	*3.4*	*0.2*	*0.203*	*0.012*	*0.852*	*1501*	*44*	*1186*	*66*	*1968*	*71*	*-65.9*
AY034	*2.31*	*0.11*	*0.1489*	*0.008*	*0.65*	*1210*	*35*	*893*	*42*	*1711*	*73*	*-91.6*
AY035	*1.617*	*0.046*	*0.0912*	*0.003*	*0.662*	*978*	*17*	*562*	*16*	*1928*	*43*	*-243.1*
AY040	*0.892*	*0.035*	*0.0573*	*0.002*	*0.858*	*646*	*19*	*360*	*15*	*1786*	*38*	*-396.1*
AY041	*3.005*	*0.08*	*0.2019*	*0.005*	*0.458*	*1408*	*21*	*1184*	*28*	*1711*	*48*	*-44.5*
AY042	*6.25*	*0.14*	*0.4252*	*0.008*	*0.494*	*2012*	*20*	*2280*	*38*	*1761*	*42*	*22.8*
AY044	*2.6*	*0.13*	*0.1697*	*0.008*	*0.66*	*1297*	*35*	*1008*	*44*	*1785*	*64*	*-77.1*
AY046	*0.62*	*0.028*	*0.0358*	*0.002*	*0.889*	*483*	*17*	*226*	*12*	*2018*	*41*	*-792.9*
AY047	*6.03*	*0.11*	*0.411*	*0.008*	*0.53*	*1981*	*16*	*2216*	*35*	*1721*	*35*	*22.3*
AY048	*5.74*	*0.19*	*0.4097*	*0.009*	*0.318*	*1936*	*28*	*2209*	*43*	*1679*	*65*	*24.0*
AY050	*2.137*	*0.058*	*0.1402*	*0.003*	*0.554*	*1158*	*19*	*845*	*18*	*1750*	*46*	*-107.1*
AY051	*5.7*	*0.13*	*0.4004*	*0.007*	*0.497*	*1929*	*20*	*2168*	*30*	*1684*	*39*	*22.3*
AY053	*3.201*	*0.08*	*0.2088*	*0.005*	*0.339*	*1458*	*20*	*1221*	*29*	*1874*	*52*	*-53.5*
AY058	*2.99*	*0.16*	*0.204*	*0.01*	*0.799*	*1402*	*40*	*1195*	*54*	*1667*	*57*	*-39.5*
AY059	*3.317*	*0.082*	*0.2231*	*0.006*	*0.662*	*1481*	*19*	*1297*	*34*	*1725*	*41*	*-33.0*
AY060	*5.54*	*0.14*	*0.3962*	*0.008*	*0.247*	*1907*	*22*	*2148*	*35*	*1669*	*52*	*22.3*
AY066	*1.061*	*0.025*	*0.0637*	*0.002*	*0.559*	*733*	*12*	*398*	*10*	*1923*	*40*	*-383.2*
AY067	*2.097*	*0.066*	*0.134*	*0.005*	*0.752*	*1145*	*22*	*809*	*26*	*1862*	*41*	*-130.2*
AY068	*5.67*	*0.11*	*0.3941*	*0.008*	*0.56*	*1926*	*17*	*2141*	*35*	*1726*	*33*	*19.4*
AY069	*6.68*	*0.15*	*0.4207*	*0.007*	*0.315*	*2068*	*20*	*2261*	*33*	*1821*	*45*	*19.5*
AY071	*10.62*	*0.28*	*0.53*	*0.012*	*0.358*	*2488*	*25*	*2734*	*49*	*2269*	*46*	*17.0*
AY073	*3.1*	*0.11*	*0.2195*	*0.007*	*0.778*	*1431*	*27*	*1278*	*38*	*1620*	*37*	*-26.8*
AY074	*5.57*	*0.15*	*0.3923*	*0.008*	*0.365*	*1913*	*24*	*2134*	*36*	*1653*	*53*	*22.5*
AY080	*1.14*	*0.051*	*0.0744*	*0.003*	*0.938*	*774*	*25*	*462*	*20*	*1839*	*32*	*-298.1*
AY081	*6.01*	*0.17*	*0.428*	*0.011*	*0.448*	*1975*	*24*	*2287*	*48*	*1716*	*51*	*25.0*
AY083	*5.7*	*0.11*	*0.4056*	*0.007*	*0.422*	*1931*	*17*	*2195*	*33*	*1689*	*38*	*23.1*
AY086	*6.75*	*0.13*	*0.452*	*0.009*	*0.403*	*2079*	*17*	*2399*	*40*	*1825*	*38*	*23.9*
AY087	*5.85*	*0.14*	*0.4235*	*0.009*	*0.414*	*1950*	*21*	*2276*	*40*	*1661*	*42*	*27.0*
AY088	*5.15*	*0.12*	*0.3598*	*0.008*	*0.652*	*1849*	*20*	*1977*	*38*	*1718*	*37*	*13.1*
AY092	*5.88*	*0.14*	*0.4223*	*0.008*	*0.483*	*1957*	*21*	*2268*	*36*	*1666*	*40*	*26.5*
AY097	*3.203*	*0.085*	*0.2161*	*0.005*	*0.618*	*1455*	*21*	*1260*	*28*	*1797*	*39*	*-42.6*
AY098	*7.61*	*0.22*	*0.44*	*0.011*	*0.328*	*2179*	*27*	*2347*	*51*	*1982*	*60*	*15.6*
AY100	*0.409*	*0.017*	*0.0205*	*0.001*	*0.864*	*346*	*12*	*130.8*	*6.7*	*2331*	*46*	*-1682.1*
AY102	*1.025*	*0.025*	*0.0629*	*0.002*	*0.763*	*717*	*12*	*393.1*	*9.5*	*1937*	*30*	*-392.7*
AY103	*2.801*	*0.074*	*0.188*	*0.005*	*0.481*	*1356*	*19*	*1110*	*24*	*1670*	*47*	*-50.5*
AY104	*5.04*	*0.17*	*0.3608*	*0.009*	*0.367*	*1829*	*28*	*1990*	*42*	*1542*	*69*	*22.5*
AY106	*3.59*	*0.15*	*0.2196*	*0.008*	*0.709*	*1537*	*32*	*1277*	*41*	*1791*	*50*	*-40.3*
AY109	*4.3*	*0.22*	*0.2215*	*0.01*	*0.864*	*1690*	*41*	*1294*	*52*	*2096*	*43*	*-62.0*
JR-01												
JR001	5.74	0.17	0.354	0.012	0.683	1936	25	1942	60	2036	54	-4.8

Table 1 Detrital zircon U–Pb analytical data.

JR004	3.802	0.084	0.2814	0.005	0.194	1591	18	1597	25	1585	51	0.8
JR005	3.399	0.099	0.2564	0.006	0.412	1504	24	1569	28	1702	54	-8.5
JR008	4.65	0.12	0.3044	0.007	0.326	1761	21	1714	32	1805	47	-5.3
JR009	3.88	0.1	0.2765	0.006	0.421	1612	21	1670	30	1765	47	-5.7
JR016	3.22	0.15	0.2641	0.008	0.483	1476	40	1607	41	1580	86	1.7
JR020	3.556	0.094	0.2652	0.005	0.198	1543	20	1518	27	1519	51	-0.1
JR024	4.49	0.16	0.3002	0.01	0.511	1721	30	1696	49	1752	62	-3.3
JR028	4.16	0.14	0.2918	0.008	0.338	1658	28	1653	37	1659	73	-0.4
JR031	4.3	0.11	0.2938	0.006	0.468	1695	20	1759	31	1814	46	-3.1
JR035	3.94	0.16	0.2868	0.007	0.28	1614	32	1772	34	1880	75	-6.1
JR040	4.257	0.098	0.289	0.006	0.181	1685	19	1635	31	1746	51	-6.8
JR041	5	0.1	0.3266	0.008	0.348	1826	17	1822	37	1836	45	-0.8
JR051	3.513	0.08	0.2632	0.006	0.402	1529	18	1601	30	1711	49	-6.9
JR052	4.16	0.11	0.2951	0.006	0.426	1667	22	1770	30	1781	45	-0.6
JR053	3.92	0.11	0.2889	0.007	0.395	1621	23	1637	35	1758	56	-7.4
JR054	4.05	0.21	0.2906	0.009	0.006	1635	43	1640	46	1780	120	-8.5
JR056	4.31	0.13	0.2918	0.009	0.484	1694	24	1648	46	1764	57	-7.0
JR057	3.74	0.11	0.2815	0.006	0.324	1578	24	1596	32	1722	61	-7.9
JR060	4.088	0.086	0.2814	0.005	0.426	1652	18	1597	26	1685	41	-5.5
JR067	15.09	0.29	0.5284	0.01	0.462	2818	18	2734	41	2862	31	-4.7
JR069	4.88	0.11	0.3111	0.005	0.4	1799	19	1744	25	1812	37	-3.9
JR073	4.71	0.11	0.307	0.006	0.137	1769	20	1724	27	1754	50	-1.7
JR075	5.1	0.3	0.33	0.013	0.191	1836	51	1839	66	1880	130	-2.2
JR076	4.16	0.16	0.2842	0.007	0.37	1673	31	1611	35	1737	65	-7.8
JR077	4.8	0.17	0.3034	0.009	0.377	1789	29	1705	42	1774	67	-4.0
JR078	4.58	0.14	0.2969	0.007	0.405	1740	27	1676	33	1780	52	-6.2
JR079	4.69	0.14	0.306	0.007	0.227	1764	24	1721	34	1762	60	-2.4
JR085	4.33	0.18	0.2986	0.009	0.341	1698	36	1683	45	1735	87	-3.1
JR093	4.8	0.15	0.3052	0.006	0.266	1783	26	1715	31	1818	57	-6.0
JR094	4.32	0.15	0.304	0.014	0.285	1698	28	1719	65	1805	70	-5.0
JR095	4.742	0.097	0.3131	0.006	0.375	1771	17	1759	27	1782	36	-1.3
JR115	3.39	0.11	0.2639	0.006	0.255	1501	26	1513	30	1653	68	-9.3
JR116	3.68	0.12	0.2692	0.006	0.121	1571	27	1532	32	1677	73	-9.5
JR117	4.51	0.2	0.2938	0.008	0.275	1738	36	1658	39	1750	76	-5.5
JR123	4.74	0.14	0.3011	0.007	0.385	1771	24	1703	35	1825	54	-7.2
JR135	6.91	0.14	0.3576	0.009	0.336	2104	18	1972	43	2165	47	-9.8
JR136	3.71	0.12	0.2722	0.007	0.402	1572	25	1647	37	1791	49	-8.7
JR137	4.6	0.11	0.3015	0.006	0.433	1750	20	1697	29	1769	43	-4.2
JR139	4.7	0.13	0.3111	0.006	0.373	1761	23	1744	31	1736	50	0.5
JR143	4.02	0.16	0.285	0.007	0.649	1639	31	1713	36	1853	54	-8.2
JR144	4.45	0.12	0.2958	0.006	0.258	1718	22	1669	30	1738	49	-4.1
JR145	3.64	0.2	0.269	0.012	0.312	1553	45	1551	60	1660	110	-7.0
JR146	4.53	0.14	0.295	0.008	0.561	1731	25	1664	41	1811	47	-8.8
JR147	4.79	0.12	0.2947	0.007	0.309	1784	21	1667	38	1779	54	-6.7
JR153	4.76	0.18	0.292	0.011	0.303	1772	33	1656	52	1794	78	-8.3

Table 1 Detrital zircon U–Pb analytical data.

Rejected analysis

JR002	*0.643*	*0.012*	*0.03098*	*6E-04*	*0.579*	*504*	*7.3*	*196.9*	*3.6*	*2367*	*28*	*-1102.1*
JR003	*0.688*	*0.017*	*0.04099*	*1E-03*	*0.631*	*530*	*10*	*258.9*	*6*	*2010*	*39*	*-676.4*
JR006	*1.669*	*0.027*	*0.0481*	*0.001*	*0.708*	*997*	*10*	*302.5*	*6.2*	*3193*	*24*	*-955.5*
JR007	*7.34*	*0.22*	*0.3625*	*0.01*	*0.697*	*2153*	*26*	*1999*	*46*	*2338*	*39*	*-17.0*
JR010	*0.86*	*0.023*	*0.0509*	*0.001*	*0.728*	*630*	*13*	*319.7*	*8.1*	*2009*	*38*	*-528.4*
JR011	*1.08*	*0.031*	*0.0675*	*0.001*	*0.575*	*745*	*15*	*420.8*	*8.7*	*1863*	*45*	*-342.7*
JR012	*0.449*	*0.011*	*0.02207*	*5E-04*	*0.503*	*376.2*	*7.6*	*140.7*	*3.1*	*2287*	*37*	*-1525.4*
JR013	*0.458*	*0.013*	*0.02382*	*7E-04*	*0.629*	*380.7*	*8.9*	*151.7*	*4.5*	*2178*	*37*	*-1335.7*
JR014	*0.884*	*0.019*	*0.054*	*0.001*	*0.455*	*641*	*10*	*339.8*	*6.2*	*1875*	*37*	*-451.8*
JR015	*2.64*	*0.11*	*0.1355*	*0.006*	*0.762*	*1307*	*32*	*825*	*31*	*2144*	*53*	*-159.9*
JR017	*8.18*	*0.25*	*0.3398*	*0.009*	*0.655*	*2259*	*28*	*1884*	*43*	*2511*	*37*	*-33.3*
JR018	*4.19*	*0.1*	*0.2553*	*0.006*	*0.378*	*1668*	*20*	*1464*	*31*	*1843*	*50*	*-25.9*
JR019	*0.433*	*0.013*	*0.02526*	*7E-04*	*0.619*	*367.8*	*9.2*	*160.8*	*4.5*	*2008*	*44*	*-1148.8*
JR021	*2.683*	*0.074*	*0.1197*	*0.002*	*0.576*	*1323*	*20*	*729*	*14*	*2400*	*38*	*-229.2*
JR022	*3.077*	*0.085*	*0.189*	*0.006*	*0.578*	*1424*	*22*	*1115*	*32*	*1824*	*48*	*-63.6*
JR023	*0.336*	*0.017*	*0.01864*	*8E-04*	*0.888*	*294*	*13*	*119.5*	*5.3*	*2082*	*36*	*-1642.3*
JR025	*0.412*	*0.01*	*0.02545*	*5E-04*	*0.598*	*350.2*	*7.3*	*162*	*3.2*	*1917*	*36*	*-1083.3*
JR026	*0.593*	*0.013*	*0.03965*	*7E-04*	*0.588*	*473.8*	*8.5*	*250.6*	*4.6*	*1766*	*34*	*-604.7*
JR027	*2.274*	*0.092*	*0.1336*	*0.004*	*0.557*	*1198*	*29*	*811*	*22*	*1957*	*61*	*-141.3*
JR029	*1.478*	*0.058*	*0.0967*	*0.004*	*0.445*	*918*	*24*	*594*	*20*	*1902*	*78*	*-220.2*
JR030	*0.24*	*0.011*	*0.01257*	*6E-04*	*0.842*	*217*	*8.9*	*80.5*	*3.7*	*2242*	*40*	*-2685.1*
JR032	*3.036*	*0.094*	*0.2207*	*0.006*	*0.207*	*1415*	*24*	*1283*	*31*	*1558*	*64*	*-21.4*
JR034	*0.46*	*0.023*	*0.0297*	*0.002*	*0.844*	*382*	*16*	*189*	*11*	*1847*	*46*	*-877.2*
JR036	*2.042*	*0.047*	*0.0683*	*0.002*	*0.518*	*1129*	*15*	*427.1*	*8.6*	*2930*	*35*	*-586.0*
JR037	*3.266*	*0.068*	*0.1795*	*0.003*	*0.45*	*1473*	*17*	*1063*	*19*	*2124*	*37*	*-99.8*
JR039	*1.155*	*0.035*	*0.0725*	*0.003*	*0.658*	*779*	*17*	*451*	*15*	*1882*	*46*	*-317.3*
JR042	*3.585*	*0.065*	*0.0978*	*0.002*	*0.506*	*1545*	*14*	*601*	*11*	*3330*	*35*	*-454.1*
JR043	*2.807*	*0.08*	*0.1287*	*0.003*	*0.657*	*1355*	*22*	*780*	*19*	*2500*	*37*	*-220.5*
JR044	*0.967*	*0.042*	*0.06*	*0.003*	*0.743*	*688*	*21*	*375*	*17*	*1901*	*51*	*-406.9*
JR045	*1.231*	*0.036*	*0.0828*	*0.002*	*0.419*	*814*	*16*	*513*	*11*	*1774*	*47*	*-245.8*
JR046	*0.526*	*0.015*	*0.0306*	*0.001*	*0.548*	*428*	*9.8*	*194.1*	*7*	*2055*	*37*	*-958.7*
JR047	*1.696*	*0.047*	*0.0566*	*0.001*	*0.748*	*1008*	*18*	*354.7*	*8.4*	*2985*	*30*	*-741.6*
JR048	*1.228*	*0.042*	*0.0844*	*0.003*	*0.639*	*819*	*18*	*522*	*17*	*1770*	*52*	*-239.1*
JR050	*2.059*	*0.08*	*0.1564*	*0.005*	*0.505*	*1137*	*25*	*936*	*28*	*1605*	*61*	*-71.5*
JR055	*1.09*	*0.036*	*0.0645*	*0.002*	*0.517*	*746*	*18*	*403*	*9.2*	*2012*	*51*	*-399.3*
JR058	*3.29*	*0.14*	*0.2133*	*0.009*	*0.668*	*1471*	*35*	*1248*	*47*	*1798*	*56*	*-44.1*
JR059	*0.603*	*0.02*	*0.0351*	*0.001*	*0.81*	*477*	*12*	*222.1*	*7.8*	*2023*	*36*	*-810.9*
JR061	*3.64*	*0.12*	*0.2275*	*0.008*	*0.505*	*1554*	*27*	*1319*	*43*	*1822*	*65*	*-38.1*
JR062	*2.46*	*0.14*	*0.1648*	*0.009*	*0.772*	*1252*	*43*	*990*	*47*	*1827*	*66*	*-84.5*
JR063	*3.386*	*0.092*	*0.1646*	*0.004*	*0.404*	*1497*	*21*	*984*	*23*	*2243*	*51*	*-127.9*
JR064	*2.81*	*0.89*	*0.15*	*0.019*	*0.957*	*1217*	*42*	*947*	*32*	*1620*	*110*	*-71.1*
JR065	*3.64*	*0.18*	*0.1548*	*0.007*	*0.864*	*1555*	*41*	*925*	*41*	*2471*	*40*	*-167.1*
JR066	*0.5557*	*0.008*	*0.01647*	*3E-04*	*0.425*	*448.2*	*5.4*	*105.3*	*1.9*	*3144*	*27*	*-2885.8*
JR068	*0.645*	*0.024*	*0.0386*	*0.001*	*0.222*	*505*	*15*	*243.9*	*8.2*	*1871*	*77*	*-667.1*

Table 1 Detrital zircon U–Pb analytical data.

JR070	*7.36*	*0.36*	*0.344*	*0.011*	*0.103*	*2143*	*44*	*1901*	*52*	*2440*	*110*	*-28.4*
JR071	*3.806*	*0.083*	*0.2346*	*0.005*	*0.505*	*1591*	*18*	*1357*	*25*	*1874*	*36*	*-38.1*
JR072	*1.337*	*0.068*	*0.0814*	*0.005*	*0.599*	*858*	*29*	*504*	*29*	*1853*	*84*	*-267.7*
JR074	*2.759*	*0.079*	*0.1483*	*0.005*	*0.278*	*1342*	*21*	*891*	*26*	*2008*	*64*	*-125.4*
JR080	*2.105*	*0.059*	*0.1387*	*0.003*	*0.363*	*1151*	*19*	*837*	*16*	*1721*	*60*	*-105.6*
JR081	*2.31*	*0.15*	*0.1385*	*0.008*	*0.701*	*1215*	*45*	*843*	*45*	*1882*	*81*	*-123.3*
JR082	*4.67*	*0.12*	*0.2766*	*0.006*	*0.282*	*1761*	*22*	*1572*	*29*	*1941*	*54*	*-23.5*
JR083	*1.741*	*0.041*	*0.109*	*0.002*	*0.511*	*1021*	*15*	*667*	*14*	*1837*	*39*	*-175.4*
JR084	*2.04*	*0.11*	*0.1209*	*0.006*	*0.544*	*1129*	*38*	*735*	*36*	*1903*	*77*	*-158.9*
JR086	*0.683*	*0.026*	*0.0236*	*0.002*	*0.933*	*524*	*15*	*150.4*	*9.4*	*2904*	*43*	*-1830.9*
JR087	*1.147*	*0.049*	*0.0712*	*0.003*	*0.914*	*768*	*25*	*442*	*19*	*1913*	*37*	*-332.8*
JR088	*1.095*	*0.064*	*0.067*	*0.004*	*0.95*	*746*	*31*	*416*	*24*	*1941*	*34*	*-366.6*
JR089	*1.087*	*0.057*	*0.0617*	*0.003*	*0.941*	*739*	*28*	*387*	*18*	*2068*	*33*	*-434.4*
JR090	*3.44*	*0.18*	*0.2289*	*0.009*	*0.285*	*1503*	*42*	*1327*	*46*	*1779*	*98*	*-34.1*
JR091	*1.227*	*0.032*	*0.0756*	*0.002*	*0.346*	*811*	*15*	*470*	*13*	*1828*	*58*	*-288.9*
JR092	*2.566*	*0.043*	*0.04605*	*9E-04*	*0.673*	*1288*	*12*	*290.1*	*5.7*	*3904*	*19*	*-1245.7*
JR096	*0.71*	*0.036*	*0.0385*	*0.002*	*0.598*	*543*	*21*	*243*	*12*	*1981*	*85*	*-715.2*
JR097	*0.754*	*0.015*	*0.01508*	*4E-04*	*0.628*	*571.2*	*9.1*	*96.5*	*2.5*	*3691*	*33*	*-3724.9*
JR098	*2.34*	*0.12*	*0.1459*	*0.006*	*0.698*	*1232*	*36*	*877*	*35*	*1818*	*62*	*-107.3*
JR099	*0.837*	*0.025*	*0.04*	*9E-04*	*0.466*	*618*	*14*	*252.8*	*5.4*	*2285*	*42*	*-803.9*
JR100	*2.68*	*0.13*	*0.1667*	*0.007*	*0.659*	*1324*	*35*	*993*	*40*	*1883*	*76*	*-89.6*
JR101	*5.27*	*0.15*	*0.2533*	*0.009*	*0.57*	*1860*	*25*	*1454*	*45*	*2407*	*56*	*-65.5*
JR102	*3.08*	*0.14*	*0.2213*	*0.009*	*0.528*	*1424*	*34*	*1287*	*49*	*1783*	*76*	*-38.5*
JR103	*3.71*	*0.19*	*0.1554*	*0.005*	*0.525*	*1584*	*40*	*930*	*28*	*2581*	*71*	*-177.5*
JR104	*3.43*	*0.1*	*0.2215*	*0.005*	*0.557*	*1505*	*24*	*1288*	*28*	*1786*	*44*	*-38.7*
JR105	*1.902*	*0.079*	*0.1197*	*0.005*	*0.54*	*1078*	*27*	*728*	*29*	*1719*	*69*	*-136.1*
JR106	*0.749*	*0.025*	*0.0396*	*0.001*	*0.468*	*569*	*15*	*250.4*	*7.4*	*2061*	*62*	*-723.1*
JR107	*1.52*	*0.36*	*0.0563*	*0.003*	*0.875*	*725*	*49*	*348*	*17*	*2111*	*84*	*-506.6*
JR108	*2.089*	*0.079*	*0.1519*	*0.005*	*0.525*	*1142*	*26*	*910*	*26*	*1606*	*57*	*-76.5*
JR109	*2.211*	*0.083*	*0.1292*	*0.004*	*0.443*	*1179*	*26*	*782*	*25*	*1915*	*55*	*-144.9*
JR1100	*0.713*	*0.019*	*0.03338*	*8E-04*	*0.496*	*547*	*11*	*211.6*	*4.9*	*2305*	*41*	*-989.3*
SOU-01												
SOU001	4.91	0.14	0.314	0.009	0.736	1806	23	1759	45	1753	39	0.3
SOU002	4.01	0.15	0.2835	0.008	0.636	1628	31	1603	43	1608	62	-0.3
SOU009	4.82	0.2	0.3031	0.009	0.531	1782	34	1703	46	1745	81	-2.5
SOU010	4.08	0.14	0.2731	0.008	0.51	1650	29	1561	37	1642	66	-5.2
SOU011	4.95	0.18	0.3014	0.008	0.426	1809	31	1701	41	1800	56	-5.8
SOU014	3.8	0.15	0.2676	0.007	0.374	1588	31	1525	37	1574	72	-3.2
SOU015	15.22	0.46	0.517	0.016	0.541	2825	27	2664	60	2824	48	-6.0
SOU018	4.75	0.36	0.293	0.014	0.132	1756	55	1651	67	1794	98	-8.7
SOU019	3.86	0.12	0.2629	0.007	0.276	1598	25	1502	34	1608	64	-7.1
SOU021	5.39	0.14	0.3365	0.008	0.469	1880	22	1867	38	1872	50	-0.3
SOU022	4.23	0.15	0.2869	0.01	0.423	1671	29	1630	45	1687	61	-3.5
SOU024	5.02	0.18	0.3109	0.008	0.252	1825	29	1742	41	1828	72	-4.9

Table 1 Detrital zircon U–Pb analytical data.

SOU025	4.9	0.12	0.3131	0.006	0.013	1796	21	1762	29	1776	42	-0.8
SOU026	4.47	0.15	0.301	0.007	0.453	1728	24	1693	35	1723	50	-1.8
SOU027	4.66	0.12	0.3018	0.008	0.332	1758	22	1701	38	1721	55	-1.2
SOU028	3.83	0.15	0.2672	0.008	0.172	1579	28	1522	41	1606	66	-5.5
SOU029	4.77	0.24	0.3211	0.01	0.189	1805	27	1788	47	1790	61	-0.1
SOU030	4.59	0.12	0.3086	0.008	0.441	1749	21	1730	38	1728	44	0.1
SOU032	4.29	0.31	0.284	0.013	0.375	1675	45	1605	67	1681	81	-4.7
SOU035	3.52	0.15	0.2642	0.009	0.513	1516	32	1510	44	1649	66	-9.2
SOU040	3.6	0.17	0.2696	0.01	0.581	1559	38	1583	53	1715	78	-8.3
SOU041	3.82	0.27	0.283	0.02	0.668	1581	45	1690	100	1821	86	-7.8
SOU042	3.63	0.095	0.2664	0.006	0.324	1553	21	1520	30	1576	49	-3.7
SOU043	4.52	0.15	0.3091	0.007	0.681	1727	29	1732	36	1746	51	-0.8
SOU044	3.431	0.082	0.2589	0.005	0.139	1512	19	1482	26	1550	52	-4.6
SOU046	4.53	0.14	0.3	0.008	0.412	1732	28	1688	38	1766	59	-4.6
SOU049	4.51	0.15	0.2905	0.008	0.575	1726	29	1640	40	1765	54	-7.6
SOU052	4.11	0.18	0.278	0.014	0.288	1667	37	1581	72	1710	84	-8.2
SOU054	4.51	0.16	0.2887	0.01	0.43	1737	29	1631	47	1761	69	-8.0
SOU063	9.45	0.33	0.439	0.013	0.481	2376	32	2338	56	2398	51	-2.6
SOU064	3.86	0.15	0.279	0.007	0.496	1608	33	1682	35	1830	48	-8.8
SOU070	4.52	0.12	0.3013	0.007	0.535	1732	22	1699	34	1737	45	-2.2
SOU072	5.09	0.16	0.3223	0.007	0.213	1827	27	1798	35	1808	60	-0.6
SOU073	4.52	0.13	0.2942	0.008	0.396	1728	23	1664	40	1731	53	-4.0
SOU074	3.934	0.089	0.2696	0.006	0.537	1618	19	1537	30	1679	41	-9.2
SOU077	4.89	0.12	0.3107	0.006	0.306	1799	20	1742	29	1782	50	-2.3
SOU078	3.96	0.14	0.2822	0.009	0.477	1620	28	1597	44	1733	49	-8.5
SOU082	4.97	0.19	0.316	0.008	0.389	1798	31	1772	41	1774	58	-0.1
SOU083	4.53	0.13	0.3026	0.007	0.593	1734	23	1701	35	1704	41	-0.2
SOU084	5.58	0.19	0.342	0.009	0.749	1902	30	1898	44	1880	40	0.9
SOU087	3.46	0.12	0.2665	0.007	0.022	1519	28	1518	34	1579	76	-4.0
SOU089	3.98	0.2	0.28	0.01	0.725	1622	42	1627	52	1777	55	-9.2
SOU092	4.52	0.11	0.2984	0.005	0.507	1736	21	1685	25	1713	39	-1.7
SOU096	5.89	0.16	0.33	0.008	0.257	1955	23	1843	35	2001	55	-8.6
SOU097	16.89	0.46	0.541	0.014	0.531	2928	26	2793	59	2939	42	-5.2
SOU111	4.32	0.15	0.2837	0.007	0.571	1691	29	1614	38	1715	47	-6.3
SOU119	4.29	0.15	0.2951	0.007	0.488	1683	28	1669	36	1716	66	-2.8
SOU121	4.92	0.13	0.3043	0.006	0.061	1793	20	1710	30	1755	43	-2.6
SOU125	4.67	0.15	0.2891	0.008	0.341	1752	26	1638	37	1783	65	-8.9
SOU126	4.96	0.15	0.303	0.006	0.357	1816	26	1708	30	1806	56	-5.7
SOU132	3.85	0.13	0.2653	0.007	0.419	1597	28	1515	33	1583	63	-4.5
SOU134	5.01	0.11	0.3134	0.006	0.339	1819	19	1755	29	1767	47	-0.7
SOU135	3.91	0.2	0.2746	0.009	0.082	1637	41	1560	45	1606	99	-2.9
						Rejected analysis						
SOU003	*1.82*	*0.072*	*0.1212*	*0.004*	*0.54*	*1043*	*22*	*736*	*24*	*1695*	*40*	*-130.3*
SOU004	*1.55*	*0.12*	*0.1001*	*0.008*	*0.361*	*940*	*48*	*613*	*43*	*1670*	*100*	*-172.4*
SOU005	*3.47*	*0.11*	*0.2208*	*0.005*	*0.426*	*1513*	*24*	*1285*	*24*	*1712*	*58*	*-33.2*

Table 1 Detrital zircon U–Pb analytical data.

SOU006	*2.341*	*0.099*	*0.1483*	*0.006*	*0.079*	*1235*	*36*	*890*	*35*	*1717*	*72*	*-92.9*
SOU007	*3.75*	*0.2*	*0.244*	*0.013*	*0.661*	*1580*	*40*	*1404*	*68*	*1677*	*99*	*-19.4*
SOU008.	*3.35*	*0.16*	*0.1905*	*0.006*	*0.553*	*1478*	*25*	*1129*	*29*	*1927*	*81*	*-70.7*
SOU012	*2.098*	*0.085*	*0.1273*	*0.005*	*0.804*	*1146*	*29*	*780*	*31*	*1764*	*49*	*-126.2*
SOU013	*2.74*	*0.23*	*0.1452*	*0.007*	*0.796*	*1317*	*60*	*873*	*38*	*2013*	*85*	*-130.6*
SOU016	*3.68*	*0.12*	*0.2321*	*0.006*	*0.37*	*1555*	*22*	*1342*	*32*	*1790*	*49*	*-33.4*
SOU017	*2.319*	*0.046*	*0.1517*	*0.003*	*0.547*	*1216*	*14*	*910*	*15*	*1695*	*31*	*-86.3*
SOU020	*2.719*	*0.075*	*0.1552*	*0.004*	*0.499*	*1333*	*20*	*929*	*24*	*1977*	*48*	*-112.8*
SOU023	*5.86*	*0.4*	*0.2158*	*0.008*	*0.567*	*1931*	*60*	*1257*	*40*	*2800*	*88*	*-122.8*
SOU031	*3.755*	*0.094*	*0.2346*	*0.004*	*0.279*	*1579*	*21*	*1357*	*20*	*1872*	*45*	*-38.0*
SOU033	*2.13*	*0.13*	*0.1556*	*0.008*	*0.008*	*1147*	*40*	*930*	*42*	*1541*	*94*	*-65.7*
SOU061	*4.12*	*0.15*	*0.2402*	*0.007*	*0.279*	*1642*	*30*	*1385*	*35*	*1979*	*49*	*-42.9*
SOU062	*2.121*	*0.046*	*0.1491*	*0.002*	*0.798*	*1152*	*16*	*895*	*14*	*1702*	*31*	*-90.2*
SOU065	*1.63*	*0.033*	*0.114*	*0.002*	*0.367*	*982*	*13*	*696*	*13*	*1682*	*41*	*-141.7*
SOU066	*3.569*	*0.087*	*0.1686*	*0.003*	*0.657*	*1537*	*20*	*1005*	*17*	*2408*	*25*	*-139.6*
SOU067	*3.5*	*0.15*	*0.2219*	*0.01*	*0.357*	*1523*	*33*	*1290*	*52*	*1880*	*82*	*-45.7*
SOU068	*3.36*	*0.14*	*0.2314*	*0.008*	*0.722*	*1491*	*33*	*1340*	*39*	*1694*	*53*	*-26.4*
SOU069	*5.23*	*0.15*	*0.2911*	*0.01*	*0.563*	*1868*	*26*	*1644*	*48*	*2074*	*56*	*-26.2*
SOU071	*4.225*	*0.097*	*0.262*	*0.006*	*0.596*	*1674*	*19*	*1500*	*29*	*1893*	*36*	*-26.2*
SOU122	*2.755*	*0.085*	*0.1795*	*0.005*	*0.549*	*1340*	*23*	*1063*	*29*	*1685*	*50*	*-58.5*
SOU123	*4.37*	*0.15*	*0.27*	*0.009*	*0.583*	*1705*	*27*	*1538*	*44*	*1803*	*56*	*-17.2*
SOU124	*2.726*	*0.072*	*0.183*	*0.004*	*0.457*	*1336*	*21*	*1082*	*23*	*1700*	*43*	*-57.1*
SOU127	*3.53*	*0.1*	*0.2205*	*0.005*	*0.495*	*1531*	*24*	*1283*	*28*	*1781*	*41*	*-38.8*
SOU128	*3.056*	*0.07*	*0.1501*	*0.003*	*0.685*	*1421*	*18*	*901*	*18*	*2209*	*34*	*-145.2*
SOU129	*1.609*	*0.074*	*0.1025*	*0.004*	*0.917*	*970*	*30*	*627*	*24*	*1741*	*30*	*-177.7*
SOU130	*2.732*	*0.067*	*0.1791*	*0.004*	*0.474*	*1337*	*18*	*1064*	*19*	*1675*	*45*	*-57.4*
SOU131	*3.09*	*0.15*	*0.1893*	*0.007*	*0.726*	*1424*	*37*	*1115*	*39*	*1820*	*53*	*-63.2*
SOU133	*3.4*	*0.21*	*0.1946*	*0.01*	*0.338*	*1471*	*49*	*1138*	*52*	*1920*	*110*	*-68.7*
SOU136	*2.3*	*0.066*	*0.1445*	*0.004*	*0.851*	*1210*	*21*	*868*	*22*	*1788*	*28*	*-106.0*
SOU137	*2.7*	*0.16*	*0.1704*	*0.009*	*0.946*	*1305*	*44*	*1010*	*49*	*1778*	*35*	*-76.0*

2. Lu–Hf isotope results

Table 2 Detrital zircon hafnium isotope analytical results.

Sample	Analysis	$^{207}Pb/^{206}Pb$ age (Ma)	Lu^{176}/Hf^{177}	Hf^{176}/Hf^{177}	2 S.E.	Hf/Hf(t)	eHf(t)	2 S.E.	T(DM)
MS-03	BY-MS03_015	1804	0.001386247	0.281622176	2.2767E-05	0.2815747	-2.15	0.7968	2.58
	BY-MS03_056	1802	0.000580718	0.281699303	2.1053E-05	0.2816795	1.52	0.7369	2.36
	BY-MS03_060	1812	0.000886862	0.281708569	1.9574E-05	0.2816781	1.70	0.6851	2.36
	BY-MS03_062	2534	0.001289953	0.281387265	2.8476E-05	0.2813248	5.90	0.9967	2.68
	BY-MS03_066	1846	0.00213808	0.281648529	2.9463E-05	0.2815736	-1.22	1.0312	2.56
	BY-MS03_070	1806	0.001174533	0.281585009	2.5529E-05	0.2815448	-3.17	0.8935	2.65
	BY-MS03_071	1784	0.000829118	0.281592085	1.9595E-05	0.281564	-2.99	0.6858	2.62
	BY-MS03_077	2685	0.000961791	0.281205067	2.5897E-05	0.2811557	3.42	0.9064	2.94
	BY-MS03_084	1790	0.001097536	0.281588169	2.2555E-05	0.2815509	-3.32	0.7894	2.64

Table 2 Detrital zircon hafnium isotope analytical results.

	BY-MS03_090	1835	0.002032167	0.281644181	3.3494E-05	0.2815734	-1.48	1.1723	2.57
	BY-MS03_096	1835	0.001116642	0.281578439	2.4453E-05	0.2815396	-2.69	0.8559	2.64
	BY-MS03_108	1797	0.001306828	0.281563899	3.2442E-05	0.2815194	-4.28	1.1355	2.70
	BY-MS03_112	1813	0.001075093	0.281596691	2.7608E-05	0.2815597	-2.48	0.9663	2.61
	BY-MS03_121	1830	0.000578	0.281462797	2.2228E-05	0.2814427	-6.24	0.778	2.85
	BY-MS03_122	1808	0.000789395	0.28158802	2.2372E-05	0.2815609	-2.55	0.783	2.61
	BY-MS03_127	1828	0.000594578	0.281640168	2.0846E-05	0.2816195	-0.01	0.7296	2.47
	BY-MS03_128	1850	0.000911708	0.281708656	2.3718E-05	0.2816767	2.53	0.8301	2.34
	BY-MS03_138	1791	0.000805702	0.281659341	2.123E-05	0.281632	-0.42	0.743	2.47
	BY-MS03_147	1835	0.001799462	0.281595821	3.1421E-05	0.2815332	-2.91	1.0997	2.65
	BY-MS03_148	1838	0.000973175	0.281610536	2.5127E-05	0.2815766	-1.30	0.8795	2.56
MS-05	BY-MS05_003	1760	0.003271145	0.2819664	6.4512E-05	0.2818572	6.87	2.2579	2.00
	BY-MS05_011	1921	0.000786173	0.281513665	2.6488E-05	0.281485	-2.64	0.9271	2.70
	BY-MS05_017	1893	0.001568727	0.281558859	3.3444E-05	0.2815025	-2.67	1.1706	2.68
	BY-MS05_019	1978	0.002601856	0.281432711	4.5759E-05	0.2813349	-6.66	1.6016	2.99
	BY-MS05_020	1784	0.001085538	0.281589529	2.5405E-05	0.2815528	-3.39	0.8892	2.64
	BY-MS05_039	1799	0.000984183	0.281577206	2.6535E-05	0.2815436	-3.37	0.9287	2.65
	BY-MS05_040	1807	0.001072573	0.281607685	2.8531E-05	0.2815709	-2.22	0.9986	2.59
	BY-MS05_041	1745	0.001003389	0.281596579	2.5037E-05	0.2815634	-3.91	0.8763	2.64
	BY-MS05_047	1803	0.002243918	0.281520794	4.3301E-05	0.2814441	-6.81	1.5155	2.86
	BY-MS05_052	1797	0.001095671	0.281632174	2.3582E-05	0.2815948	-1.60	0.8254	2.54
	BY-MS05_057	1784	0.001127184	0.281605743	2.9249E-05	0.2815676	-2.86	1.0237	2.61
	BY-MS05_064	2282	0.005649666	0.281425024	0.00010607	0.2811794	-5.15	3.7124	3.13
	BY-MS05_078	1917	0.001242622	0.281582362	3.3856E-05	0.2815371	-0.88	1.1849	2.59
	BY-MS05_084	1741	0.001063892	0.281601049	3.5609E-05	0.2815659	-3.91	1.2463	2.64
	BY-MS05_096	1788	0.000945266	0.281548219	2.4337E-05	0.2815162	-4.60	0.8518	2.72
	BY-MS05_101	1795	0.001148237	0.28167493	3.6529E-05	0.2816358	-0.19	1.2785	2.46
	BY-MS05_109	1732	0.001960681	0.281668602	4.7604E-05	0.2816042	-2.76	1.6661	2.56
	BY-MS05_120	1796	0.000842192	0.281609602	3.0884E-05	0.2815809	-2.12	1.0809	2.57
	BY-MS05_130	1800	0.000899983	0.281580437	3.2077E-05	0.2815497	-3.13	1.1227	2.64
	BY-MS05_136	1908	0.002723581	0.281707815	6.819E-05	0.2816092	1.47	2.3866	2.45
	BY-MS05_147	1753	0.000969022	0.281643002	3.2239E-05	0.2816108	-2.04	1.1284	2.54
	BY-MS05_148	1896	0.001666742	0.281547764	4.0757E-05	0.2814878	-3.12	1.4265	2.71
MS-06	BY-MS06_008	2176	0.000691909	0.281065803	3.4082E-05	0.2810371	-12.66	1.1929	3.50
	BY-MS06_012	1947	0.003029733	0.281616573	7.3307E-05	0.2815045	-1.35	2.5658	2.65
	BY-MS06_019	1826	0.002295707	0.281657606	5.3572E-05	0.2815781	-1.53	1.875	2.56
	BY-MS06_020	2503	0.002918125	0.281306723	6.143E-05	0.2811673	-0.43	2.15	3.03
	BY-MS06_022	1817	0.001007194	0.281602599	3.3339E-05	0.2815679	-2.09	1.1669	2.59
	BY-MS06_026	1806	0.001307984	0.281600102	2.5374E-05	0.2815553	-2.79	0.8881	2.62
	BY-MS06_027	1952	0.000342045	0.281515209	2.7187E-05	0.2815025	-1.30	0.9515	2.65
	BY-MS06_028	1937	0.000688726	0.281645102	2.9182E-05	0.2816198	2.51	1.0214	2.41
	BY-MS06_029	1822	0.001405403	0.281586003	2.4427E-05	0.2815374	-3.06	0.855	2.65

Table 2 Detrital zircon hafnium isotope analytical results.

	BY-MS06_053	1823	0.001146596	0.281650614	2.4838E-05	0.281611	-0.43	0.8693	2.49
	BY-MS06_055	1830	0.000940889	0.281601998	2.8153E-05	0.2815693	-1.74	0.9854	2.58
	BY-MS06_066	1803	0.000778741	0.28172266	2.3603E-05	0.281696	2.13	0.8261	2.32
	BY-MS06_071	1802	0.001921707	0.28162794	3.1318E-05	0.2815623	-2.64	1.0961	2.61
	BY-MS06_075	2168	0.001282278	0.281304686	2.9153E-05	0.2812518	-5.22	1.0204	3.05
	BY-MS06_086	1805	0.000900622	0.281659739	2.6672E-05	0.2816289	-0.20	0.9335	2.47
	BY-MS06_091	1975	0.000251961	0.281426786	2.0216E-05	0.2814173	-3.80	0.7076	2.81
	BY-MS06_116	1804	0.000969726	0.28163784	2.4954E-05	0.2816047	-1.09	0.8734	2.52
	BY-MS06_135	2205	0.000781911	0.281466148	2.7036E-05	0.2814333	2.09	0.9463	2.64
	BY-MS06_138	1832	0.001211876	0.281487846	2.7834E-05	0.2814457	-6.09	0.9742	2.84
	BY-MS06_141	2517	0.00054592	0.281270703	2.341E-05	0.2812445	2.64	0.8194	2.86
	BY-MS06_146	1852	0.000761792	0.28168139	2.9823E-05	0.2816546	1.79	1.0438	2.38
MS-09	BY-MS09_004	1807	0.001015952	0.281577753	3.7312E-05	0.2815429	-3.21	1.3059	2.65
	BY-MS09_006	1844	0.000847459	0.281585438	2.8851E-05	0.2815558	-1.90	1.0098	2.60
	BY-MS09_013	1803	0.002503046	0.281632405	3.9774E-05	0.2815468	-3.17	1.3921	2.64
	BY-MS09_015	1873	0.000850317	0.281600661	2.6648E-05	0.2815704	-0.71	0.9327	2.55
	BY-MS09_025	2199	0.000542531	0.281422668	2.8673E-05	0.2814	0.77	1.0036	2.72
	BY-MS09_030	1851	0.001399727	0.281531326	2.807E-05	0.2814822	-4.36	0.9825	2.75
	BY-MS09_040	1834	0.001623934	0.281644563	2.8683E-05	0.2815881	-0.99	1.0039	2.54
	BY-MS09_042	1916	0.001116096	0.281414234	2.6746E-05	0.2813736	-6.71	0.9361	2.94
	BY-MS09_043	2491	0.000556909	0.281263882	2.8113E-05	0.2812374	1.78	0.984	2.89
	BY-MS09_044	2176	0.001586421	0.281461751	3.4204E-05	0.281396	0.09	1.1971	2.74
	BY-MS09_047	1846	0.001093153	0.281631761	2.3418E-05	0.2815935	-0.52	0.8196	2.52
	BY-MS09_049	1834	0.000957743	0.281597088	2.5065E-05	0.2815638	-1.85	0.8773	2.59
	BY-MS09_052	1918	0.000997221	0.281506452	2.3827E-05	0.2814701	-3.24	0.834	2.74
	BY-MS09_057	1818	0.000425211	0.281553227	2.3353E-05	0.2815386	-3.11	0.8174	2.65
	BY-MS09_058	1910	0.001402265	0.281525913	2.9585E-05	0.2814751	-3.25	1.0355	2.73
	BY-MS09_063	1862	0.000714994	0.281618937	2.2035E-05	0.2815937	-0.14	0.7712	2.51
	BY-MS09_073	1838	0.000780941	0.28171339	2.4325E-05	0.2816862	2.59	0.8514	2.32
	BY-MS09_079	1835	0.000680999	0.281694674	1.9903E-05	0.281671	1.98	0.6966	2.36
	BY-MS09_083	1861	0.001312579	0.281613755	2.4377E-05	0.2815674	-1.10	0.8532	2.56
	BY-MS09_088	1898	0.011509658	0.281624445	0.00010535	0.2812097	-12.95	3.6874	3.30
	BY-MS09_103	2184	0.000569186	0.281466466	2.4529E-05	0.2814428	1.94	0.8585	2.63
	BY-MS09_106	2488	0.004206698	0.281141687	5.2543E-05	0.2809419	-8.79	1.839	3.51
DD2	BY_DD2_007	1931	0.000386517	0.281573447	2.0641E-05	0.2815593	0.23	0.7224	2.54
	BY_DD2_016	1547	0.000698408	0.281750215	2.2853E-05	0.2817298	-2.54	0.7999	2.41
	BY_DD2_018	2573	0.000707893	0.281234987	1.4807E-05	0.2812002	2.38	0.5182	2.92
	BY_DD2_024	1778	0.000770712	0.281487783	2.4321E-05	0.2814618	-6.76	0.8512	2.84
	BY_DD2_032	1853	0.000742068	0.281510184	2.2459E-05	0.2814841	-4.24	0.7861	2.75
	BY_DD2_033	1638	0.000830109	0.281738091	2.2006E-05	0.2817123	-1.08	0.7702	2.39
	BY_DD2_038	1837	0.000954046	0.281471832	2.0942E-05	0.2814386	-6.23	0.733	2.85
	BY_DD2_041	1920	0.000936886	0.281460366	2.4026E-05	0.2814262	-4.75	0.8409	2.83
	BY_DD2_042	1866	0.000936886	0.281460366	2.4026E-05	0.2814272	-5.96	0.8409	2.86

Table 2 Detrital zircon hafnium isotope analytical results.

	BY_DD2_044	1821	0.000977364	0.281616132	2.0869E-05	0.2815824	-1.49	0.7304	2.56
	BY_DD2_050	1819	0.000511466	0.281399202	2.0697E-05	0.2813816	-8.67	0.7244	2.98
	BY_DD2_054	1841	0.000384694	0.281569226	1.8138E-05	0.2815558	-1.97	0.6348	2.60
	BY_DD2_055	1608	0.000604604	0.281738293	2.275E-05	0.2817199	-1.50	0.7962	2.39
	BY_DD2_058	1864	0.00086706	0.281576053	2.2166E-05	0.2815454	-1.81	0.7758	2.61
	BY_DD2_061	1781	0.000542313	0.28152291	2.1952E-05	0.2815046	-5.17	0.7683	2.75
	BY_DD2_066	2479	0.000731624	0.281566202	2.0717E-05	0.2815316	11.97	0.7251	2.27
	BY_DD2_069	1538	0.000827625	0.281372086	2.2844E-05	0.281348	-16.30	0.7996	3.23
	BY_DD2_075	1782	0.000288281	0.281512556	2.0556E-05	0.2815028	-5.21	0.7194	2.75
	BY_DD2_080	1568	0.000551927	0.281728291	2.5175E-05	0.2817119	-2.70	0.8811	2.43
	BY_DD2_089	1783	0.000166417	0.281496417	2.2793E-05	0.2814908	-5.61	0.7978	2.77
	BY_DD2_091	1923	0.000990297	0.281579827	2.2588E-05	0.2815437	-0.51	0.7906	2.58
	BY_DD2_092	1853	0.000232104	0.281529378	1.9119E-05	0.2815212	-2.92	0.6692	2.67
	BY_DD2_095	1845	0.000637947	0.281626851	1.9671E-05	0.2816045	-0.15	0.6885	2.49
	BY_DD2_097	1856	0.000819822	0.28163576	2.3396E-05	0.2816069	0.19	0.8188	2.48
DD24	BY_DD24_003	1944	0.000718975	0.281489795	1.9595E-05	0.2814632	-2.88	0.6858	2.74
	BY_DD24_017	1750	0.000717048	0.281655968	1.9192E-05	0.2816322	-1.35	0.6717	2.49
	BY_DD24_037	1949	0.001038088	0.281627191	2.2341E-05	0.2815888	1.69	0.7819	2.46
	BY_DD24_046	1729	0.001300356	0.281621859	2.0497E-05	0.2815792	-3.71	0.7174	2.62
	BY_DD24_048	1855	0.001260349	0.281608923	3.3604E-05	0.2815646	-1.34	1.1761	2.57
	BY_DD24_064	1841	0.000775478	0.281727202	2.0383E-05	0.2817001	3.15	0.7134	2.29
	BY_DD24_070	1821	0.000926303	0.281601327	2.7798E-05	0.2815693	-1.95	0.9729	2.58
	BY_DD24_071	1744	0.000962928	0.281685235	2.898E-05	0.2816534	-0.74	1.0143	2.45
	BY_DD24_088	1838	0.000471916	0.281500547	2.5605E-05	0.2814841	-4.59	0.8962	2.76
	BY_DD24_102	1917	0.000702635	0.281416128	2.4637E-05	0.2813906	-6.09	0.8623	2.91
	BY_DD24_107	2419	0.000472352	0.280979391	2.0718E-05	0.2809576	-9.84	0.7251	3.52
	BY_DD24_108	1842	0.000856944	0.281388566	2.6614E-05	0.2813586	-8.95	0.9315	3.02
	BY_DD24_113	1731	0.001251437	0.281670075	3.3619E-05	0.281629	-1.90	1.1767	2.51
	BY_DD24_117	1839	0.002846904	0.281652312	3.7419E-05	0.281553	-2.12	1.3096	2.61
	BY_DD24_122	1855	0.000894358	0.281574466	2.4379E-05	0.281543	-2.10	0.8533	2.62
DD57	BY_DD57Hf-001	1843	0.002003672	0.281643156	4.0912E-05	0.2815731	-1.31	1.4319	2.56
	BY_DD57Hf-002	1759	0.001004459	0.281679948	2.6404E-05	0.2816465	-0.64	0.9241	2.46
	BY_DD57Hf-003	1804	0.000784275	0.281735615	2.2284E-05	0.2817088	2.61	0.7799	2.29
	BY_DD57Hf-004	2969	0.000614684	0.280953248	2.6526E-05	0.2809183	1.65	0.9284	3.27
	BY_DD57Hf-005	1802	0.000787593	0.281609039	2.5199E-05	0.2815821	-1.93	0.882	2.57
	BY_DD57Hf-006	1752	0.001112741	0.281630042	2.7156E-05	0.2815931	-2.70	0.9505	2.57
	BY_DD57Hf-007	1766	0.000811908	0.281568249	2.1783E-05	0.2815411	-4.22	0.7624	2.68
	BY_DD57Hf-008	1805	0.00075073	0.281618474	2.4152E-05	0.2815928	-1.49	0.8453	2.54
	BY_DD57Hf-009	1853	0.000560238	0.281620181	2.0729E-05	0.2816005	-0.11	0.7255	2.50
	BY_DD57Hf-010	1755	0.000556305	0.281511678	2.4979E-05	0.2814932	-6.17	0.8743	2.79
	BY_DD57Hf-011	1788	0.000889411	0.281606327	2.0005E-05	0.2815762	-2.47	0.7002	2.59
	BY_DD57Hf-012	1795	0.000793925	0.281605705	2.7071E-05	0.2815787	-2.22	0.9475	2.58
	BY_DD57Hf-013	1799	0.001052139	0.281559745	2.8224E-05	0.2815238	-4.07	0.9878	2.69

Table 2 Detrital zircon hafnium isotope analytical results.

	BY_DD57Hf-014	1865	0.000944259	0.281699676	2.4698E-05	0.2816663	2.50	0.8644	2.35
	BY_DD57Hf-015	1760	0.000759313	0.281608279	2.432E-05	0.2815829	-2.87	0.8512	2.59
	BY_DD57Hf-016	1793	0.000806719	0.28161371	2.531E-05	0.2815863	-1.99	0.8858	2.56
	BY_DD57Hf-017	1828	0.000861082	0.281620379	2.7742E-05	0.2815905	-1.04	0.971	2.53
	BY_DD57Hf-018	1851	0.001369292	0.281546868	2.9747E-05	0.2814988	-3.77	1.0412	2.72
	BY_DD57Hf-019	1793	0.001333674	0.281687303	2.908E-05	0.281642	-0.02	1.0178	2.45
	BY_DD57Hf-020	1751	0.00116096	0.281609456	3.1202E-05	0.2815709	-3.50	1.0921	2.62
Bro-6	BY_Bro6_002	1781	0.000607263	0.281631127	2.1873E-05	0.2816106	-1.41	0.7656	2.52
	BY_Bro6_005	1784	0.000776767	0.281600911	2.1183E-05	0.2815746	-2.61	0.7414	2.59
	BY_Bro6_015	1771	0.000730577	0.281641418	1.8119E-05	0.2816169	-1.41	0.6342	2.51
	BY_Bro6_022	1790	0.000869076	0.281622382	1.4905E-05	0.2815929	-1.83	0.5217	2.55
	BY_Bro6_024	1774	0.001346111	0.281666215	2.7689E-05	0.2816209	-1.20	0.9691	2.50
	BY_Bro6_025	1830	0.001163798	0.281629859	2.1011E-05	0.2815895	-1.03	0.7354	2.54
	BY_Bro6_045	1773	0.000766138	0.281603816	1.9139E-05	0.2815781	-2.75	0.6699	2.59
	BY_Bro6_052	2838	0.000514055	0.280954386	1.9832E-05	0.2809264	-1.15	0.6941	3.33
	BY_Bro6_077	1822	0.000757514	0.281615144	2.2169E-05	0.281589	-1.23	0.7759	2.54
	BY_Bro6_078	1613	0.001047806	0.281895859	2.2173E-05	0.2818639	3.73	0.776	2.08
	BY_Bro6_080	1776	0.00129346	0.281686275	2.8382E-05	0.2816427	-0.38	0.9934	2.45
	BY_Bro6_088	1783	0.000676589	0.281650418	2.2169E-05	0.2816275	-0.76	0.7759	2.48
	BY_Bro6_090	1773	0.000434747	0.281617423	2.1028E-05	0.2816028	-1.87	0.736	2.54
	BY_Bro6_091	1793	0.001244339	0.281602391	3.4847E-05	0.2815601	-2.92	1.2197	2.62
	BY_Bro6_118	1793	0.000695892	0.281628489	2.7893E-05	0.2816048	-1.34	0.9763	2.52
	BY_Bro6_123	1606	0.001083338	0.281801798	2.7911E-05	0.2817689	0.19	0.9769	2.29
	BY_Bro6_124	1565	0.000757846	0.281885825	2.6735E-05	0.2818634	2.61	0.9357	2.11
	BY_Bro6_131	1584	0.001107435	0.281893468	2.0274E-05	0.2818603	2.93	0.7096	2.10
	BY_Bro6_134	1619	0.001915241	0.281789275	3.8516E-05	0.2817306	-0.87	1.348	2.36
	BY_Bro6_135	1779	0.000644301	0.281629457	2.5402E-05	0.2816077	-1.55	0.8891	2.53
	BY_Bro6_138	1769	0.000846509	0.281636484	2.6173E-05	0.2816081	-1.77	0.9161	2.53
	BY_Bro6_143	1773	0.000743514	0.281617073	2.255E-05	0.2815921	-2.25	0.7893	2.56
	BY_Bro6_146	1770	0.001065288	0.281637982	3.2868E-05	0.2816022	-1.96	1.1504	2.54
	BY_Bro6_147	1814	0.000492837	0.281561152	2.3784E-05	0.2815442	-3.01	0.8324	2.64
Bro-7	BY_Bro7_002	1740	0.000559741	0.281623039	2.6054E-05	0.2816046	-2.56	0.9119	2.56
	BY_Bro7_007	1767	0.000642819	0.281586453	2.2798E-05	0.2815649	-3.35	0.7979	2.63
	BY_Bro7_010	1712	0.001339809	0.281762302	3.468E-05	0.2817188	0.85	1.2138	2.33
	BY_Bro7_011	1719	0.000490764	0.281575821	2.5586E-05	0.2815598	-4.63	0.8955	2.67
	BY_Bro7_019	1734	0.000528752	0.281822063	2.2722E-05	0.2818047	4.40	0.7953	2.13
	BY_Bro7_021	1742	0.000583308	0.281590253	2.1473E-05	0.281571	-3.71	0.7515	2.63
	BY_Bro7_030	1889	0.000923312	0.281617348	2.4261E-05	0.2815842	0.14	0.8491	2.51
	BY_Bro7_032	1733	0.000567841	0.281611138	2.3309E-05	0.2815925	-3.15	0.8158	2.59
	BY_Bro7_042	1790	0.000875754	0.281710086	2.3344E-05	0.2816804	1.28	0.817	2.36
	BY_Bro7_046	1825	0.000964949	0.281643082	2.2964E-05	0.2816097	-0.43	0.8037	2.49
	BY_Bro7_049	1731	0.000795732	0.281614782	2.3324E-05	0.2815887	-3.33	0.8163	2.60
	BY_Bro7_052	1817	0.00090519	0.281606618	2.4651E-05	0.2815754	-1.83	0.8628	2.57

Table 2 Detrital zircon hafnium isotope analytical results.

	BY_Bro7_062	1899	0.000732365	0.281592256	2.2448E-05	0.2815659	-0.28	0.7857	2.54
	BY_Bro7_064	1891	0.00095625	0.281539565	2.6083E-05	0.2815052	-2.62	0.9129	2.68
	BY_Bro7_067	1726	0.00128154	0.281655086	3.119E-05	0.2816132	-2.58	1.0916	2.55
	BY_Bro7_068	1726	0.000688702	0.281624026	2.4111E-05	0.2816015	-2.99	0.8439	2.57
	BY_Bro7_078	2588	0.000362676	0.281100843	2.252E-05	0.2810829	-1.44	0.7882	3.15
	BY_Bro7_087	1814	0.001296747	0.281515229	2.713E-05	0.2814706	-5.62	0.9496	2.80
	BY_Bro7_093	1863	0.000562561	0.281632378	1.9328E-05	0.2816125	0.55	0.6765	2.47
	BY_Bro7_099	1774	0.00105931	0.281627635	2.5211E-05	0.281592	-2.23	0.8824	2.56
	BY_Bro7_100	1737	0.000704149	0.281605452	2.6072E-05	0.2815823	-3.42	0.9125	2.61
	BY_Bro7_102	1742	0.000590834	0.281604274	2.3282E-05	0.2815848	-3.22	0.8149	2.60
	BY_Bro7_103	1922	0.000756599	0.281559988	2.4274E-05	0.2815324	-0.94	0.8496	2.60
	BY_Bro7_104	1717	0.000811975	0.281636456	2.0387E-05	0.28161	-2.90	0.7136	2.56
JR	BY_JR_001	2036	0.000333967	0.281465279	2.0415E-05	0.2814524	-1.15	0.7145	2.70
	BY_JR_004	1585	0.001814575	0.281898551	3.2439E-05	0.2818441	2.38	1.1353	2.14
	BY_JR_008	1805	0.000719872	0.281695932	2.3731E-05	0.2816713	1.30	0.8306	2.37
	BY_JR_016	1580	0.000970947	0.281889468	2.4556E-05	0.2818604	2.85	0.8595	2.10
	BY_JR_024	1752	0.000600062	0.281665201	2.2823E-05	0.2816453	-0.84	0.7988	2.46
	BY_JR_028	1659	0.000627922	0.28168108	2.0979E-05	0.2816613	-2.41	0.7343	2.48
	BY_JR_040	1746	0.000554675	0.281706046	2.0834E-05	0.2816877	0.53	0.7292	2.38
	BY_JR_053	1758	0.000654636	0.281685203	2.3864E-05	0.2816634	-0.06	0.8352	2.42
	BY_JR_060	1685	0.000678044	0.281632788	2.0385E-05	0.2816111	-3.59	0.7135	2.58
	BY_JR_067	2862	0.000649798	0.28089229	2.0684E-05	0.2808567	-3.07	0.7239	3.46
	BY_JR_069	1812	0.000782437	0.281655285	2.0194E-05	0.2816284	-0.06	0.7068	2.46
	BY_JR_073	1754	0.000740019	0.281668901	2.1233E-05	0.2816443	-0.83	0.7431	2.46
	BY_JR_076	1737	0.000579996	0.281686857	2.382E-05	0.2816678	-0.39	0.8337	2.42
	BY_JR_078	1780	0.000543725	0.281657448	2.4103E-05	0.2816391	-0.42	0.8436	2.46
	BY_JR_093	1818	0.000542327	0.281696482	2.0558E-05	0.2816778	1.83	0.7195	2.35
	BY_JR_095	1782	0.000702273	0.281677199	2.2324E-05	0.2816535	0.14	0.7813	2.43
	BY_JR_095	1769	0.000614871	0.281679069	2.4033E-05	0.2816584	0.02	0.8412	2.42
	BY_JR_139	1736	0.000564413	0.281679324	2.4591E-05	0.2816608	-0.66	0.8607	2.44
	BY_JR_144	1738	0.000975315	0.281625986	2.2426E-05	0.2815939	-2.99	0.7849	2.58
	BY_JR_146	1811	0.00068318	0.281484777	2.3381E-05	0.2814613	-6.02	0.8183	2.82
SOU	BY_SOU_001	1753	0.00086894	0.281518726	2.9411E-05	0.2814898	-6.34	1.0294	2.79
	BY_SOU_002	1608	0.000467946	0.281620031	2.0276E-05	0.2816058	-5.55	0.7097	2.64
	BY_SOU_019	1608	0.001019731	0.281687052	2.3867E-05	0.281656	-3.77	0.8353	2.53
	BY_SOU_024	1828	0.000600551	0.281710223	2.3441E-05	0.2816894	2.47	0.8204	2.32
	BY_SOU_026	1723	0.001163268	0.281690105	2.5184E-05	0.2816521	-1.27	0.8815	2.47
	BY_SOU_030	1728	0.001044165	0.281668475	2.2813E-05	0.2816343	-1.78	0.7985	2.50
	BY_SOU_042	1576	0.000807621	0.281852641	2.402E-05	0.2818286	1.63	0.8407	2.18
	BY_SOU_043	1746	0.000660124	0.281559285	2.3753E-05	0.2815374	-4.81	0.8314	2.70
	BY_SOU_044	1550	0.002581772	0.281951028	3.5945E-05	0.2818753	2.69	1.2581	2.09
	BY_SOU_046	1766	0.000739148	0.281607564	2.6603E-05	0.2815828	-2.74	0.9311	2.59
	BY_SOU_057	1533	0.000738312	0.28162498	1.8428E-05	0.2816036	-7.34	0.645	2.69

Table 2 Detrital zircon hafnium isotope analytical results.

	BY_SOU_070	1737	0.001233781	0.281528175	2.4477E-05	0.2814876	-6.79	0.8567	2.81
	BY_SOU_073	1731	0.000830216	0.281567912	2.0571E-05	0.2815407	-5.04	0.72	2.70
	BY_SOU_077	1782	0.000594814	0.281570633	2.3351E-05	0.2815505	-3.52	0.8173	2.65
	BY_SOU_083	1704	0.001188512	0.281622461	2.2018E-05	0.2815841	-4.12	0.7706	2.62
	BY_SOU_092	1713	0.000609903	0.281572459	1.8531E-05	0.2815527	-5.03	0.6486	2.68
	BY_SOU_097	2939	0.000301075	0.280996043	1.9592E-05	0.2809791	3.10	0.6857	3.16
	BY_SOU_191	1716	0.00054653	0.28151507	2.1384E-05	0.2814973	-6.92	0.7484	2.80
	BY_SOU_121	1755	0.00101657	0.281589217	2.7282E-05	0.2815554	-3.96	0.9549	2.65
AY	BY_AYHf-002	1804	0.000590851	0.281539383	2.3263E-05	0.2815192	-4.12	0.8142	2.70
	BY_AYHf-020	1798	0.000971237	0.281657986	2.9863E-05	0.2816249	-0.51	1.0452	2.48
	BY_AYHf-024	1691	0.001673665	0.281655444	2.7644E-05	0.2816018	-3.79	0.9675	2.59
	BY_AYHf-028	2042	0.000635541	0.281304371	2.2401E-05	0.2812797	-7.14	0.784	3.07
	BY_AYHf-054	1729	0.001812935	0.281655873	2.8062E-05	0.2815965	-3.10	0.9822	2.58
	BY_AYHf-056	2041	0.002044952	0.281591874	3.0497E-05	0.2815125	1.11	1.0674	2.57
	BY_AYHf-062	1723	0.001621415	0.281677636	3.0294E-05	0.2816247	-2.24	1.0603	2.52
	BY_AYHf-064	1615	0.000532605	0.281504945	2.1978E-05	0.2814887	-9.54	0.7692	2.88
	BY_AYHf-073	1725	0.00155117	0.28166204	2.8503E-05	0.2816113	-2.67	0.9976	2.55
	BY_AYHf-069	1821	0.00090087	0.281622449	2.5613E-05	0.2815913	-1.17	0.8964	2.54
	BY_AYHf-077	1757	0.000854429	0.281569606	2.2992E-05	0.2815411	-4.42	0.8047	2.68
	BY_AYHf-078	1706	0.001115279	0.281649157	2.8479E-05	0.2816131	-3.04	0.9968	2.56
	BY_AYHf-082	1816	0.001025394	0.281490649	2.4367E-05	0.2814553	-6.11	0.8528	2.83
	BY_AYHf-090	1699	0.001010238	0.281636071	2.3239E-05	0.2816035	-3.54	0.8134	2.58
	BY_AYHf-091	1597	0.000804231	0.28171831	2.0219E-05	0.281694	-2.67	0.7077	2.45
	BY_AYHf-095	1716	0.001813299	0.281639016	2.9111E-05	0.28158	-3.98	1.0189	2.62
	BY_AYHf-104	1542	0.00131772	0.281694066	2.5031E-05	0.2816556	-5.29	0.8761	2.57
	BY_AYHf-108	1828	0.000604059	0.281608802	2.0881E-05	0.2815879	-1.13	0.7308	2.54
	BY_AYHf-110	1753	0.000645639	0.281558021	2.2761E-05	0.2815366	-4.68	0.7966	2.69
	BY_AYHf-116	1700	0.001324025	0.281668435	2.321E-05	0.2816258	-2.73	0.8123	2.54
	BY_AYHf-122	1701	0.000986119	0.281585215	2.2836E-05	0.2815534	-5.27	0.7993	2.69
	BY_AYHf-136	2447	0.000363163	0.281295017	1.9044E-05	0.2812781	2.20	0.6665	2.83